ISSN 1018-5593

European Commission

nuclear science and technology

Borehole radar trial in Borehole 7A, Sellafield, Cumbria, UK

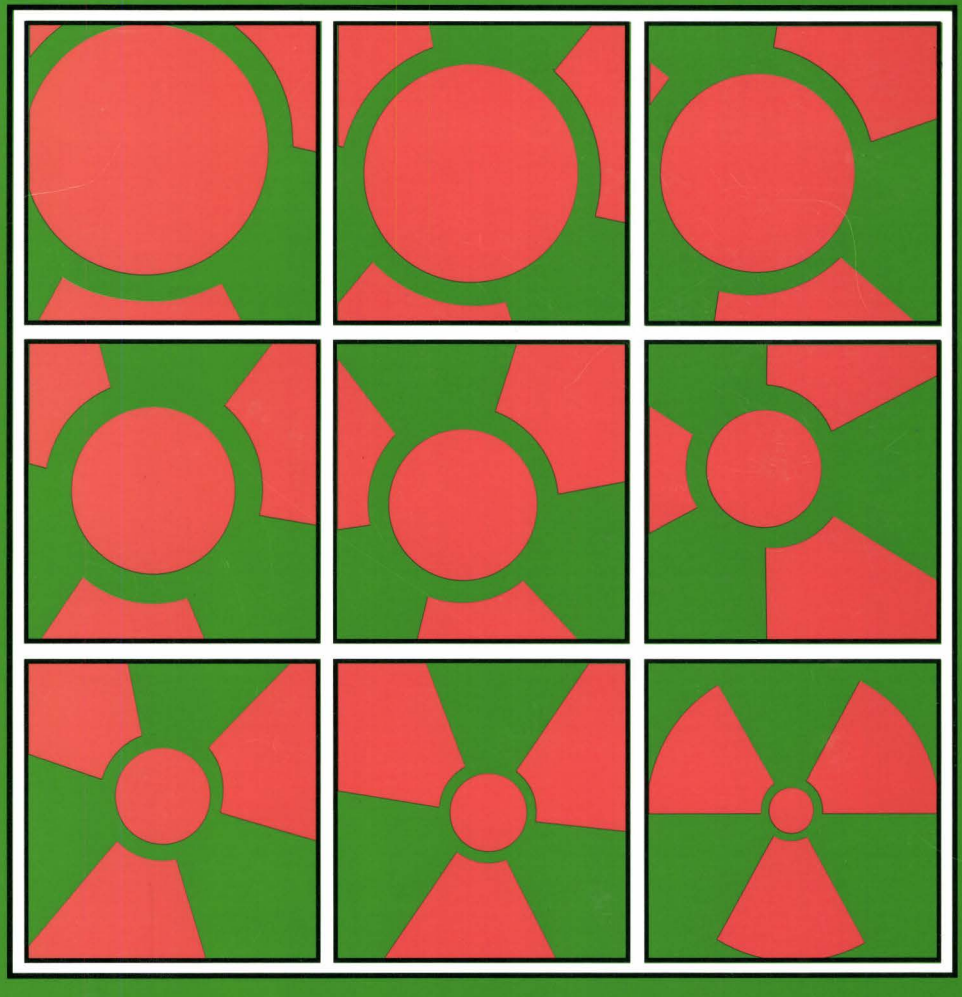

Report

EUR 15974 EN

European Commission

nuclear science and technology

Borehole radar trial in Borehole 7A, Sellafield, Cumbria, UK

S. J. Emsley
United Kingdom NIREX Ltd
Curie Avenue
Harwell, Didcot
Oxfordshire OX11 0RA
United Kingdom

Contract No FI2W/CT91/0114

Topical report

This work has been performed under a cost-sharing contract with the European Atomic Energy Community, in the framework of its fourth R&D programme 'Management and storage of radioactive waste' (1990-94)
Part B 'Underground laboratories'

Directorate-General
Science, Research and Development

1995

EUR 15974 EN

Published by the
EUROPEAN COMMISSION

Directorate-General XIII
Telecommunications, Information Market and Exploitation of Research

L-2920 Luxembourg

LEGAL NOTICE

Cataloguing data can be found at the end of this publication

Luxembourg: Office for Official Publications of the European Communities, 1995

ISBN 92-826-9459-3

Printed in Luxembourg

CONTENTS

		Page No.
CONTENTS		i
LIST OF TABLES		v
LIST OF PLATES		vii
LIST OF FIGURES		viii
ABSTRACT		xxv
EXECUTIVE SUMMARY		xxvi
1.	INTRODUCTION	1-1
2.	OBJECTIVES OF THE BOREHOLE RADAR TRIAL	2-1
3.	EQUIPMENT AND PRINCIPLES OF OPERATION	3-1
	3.1 The RAMAC Borehole Radar System	3-1
	3.2 Principles of Operation	3-6
	3.3 Modifications to the RAMAC System for the Sellafield Survey	3-7
4.	SURVEY DESIGN	4-1
	4.1 Borehole Radar Survey	4-3
5.	DATA ACQUISITION	5-1
	5.1 Introduction to the Data Acquisition Runs	5-1
	5.2 Preliminary Function Test Runs	5-4
	5.2.1 Time Base Determination - Run 1	5-4
	5.2.2 System Function Test 60 MHz Omni-directional System - Run 2	5-5
	5.3 Velocity Determination Runs	5-5

5.4 22 MHz Omni-directional Survey 5-9
5.4.1 System Function Test 22 MHz Omni-directional System - Run 4 5-9
5.4.2 22 MHz Omni-directional Survey - Run 5 5-10
5.5 60 MHz Omni-directional Survey - Runs 6 to 9 5-11
5.6 60 MHz Directional Survey - Runs 11 and 13 5-14

6. PROCESSING OF THE RADAR DATA 6-1
6.1 Initial Processing 6-1
6.1.1 Run 3 - Velocity Determination Run 6-1
6.1.2 Run 5 - 22 MHz Omni-directional Survey 6-2
6.1.3 Runs 6 and 9 - 60 MHz Omni-directional Survey 6-3
6.1.4 Runs 11 and 13 - 60 MHz Directional Survey 6-5
6.2 Further Processing of the Radar Data 6-6
6.2.1 22 MHz Omni-directional Survey 6-6
6.2.2 60 MHz Omni-directional Survey 6-6
6.2.3 60 MHz Directional Survey 6-11
6.3 Reflector Identification 6-12
6.3.1 Principles 6-12
6.3.2 Reflectors 6-13
6.3.3 Radar Range 6-15

7. CORRELATION OF THE RADAR DATA WITH GEOPHYSICAL WIRELINE LOGS 7-1
7.1 Introduction 7-1
7.2 Correlation of Radar Amplitudes with Resistivity Logs 7-3
7.3 Correlation of Radar Reflectors with Resistivity Logs 7-9

8. PROGNOSIS FOR THE USE OF RADAR IN OTHER BOREHOLES AT SELLAFIELD 8-1
8.1 Introduction 8-1
8.2 Prediction of Radar Range for Other Boreholes 8-1
8.3 Estimates of Radar Range 8-4

9. DISCUSSION OF THE RESULTS OF THE RADAR TRIAL 9-1
9.1 Discussion of the Results 9-1
9.1.1 Run 3 - Velocity Determination Run 9-1
9.1.2 Run 5 - 22 MHz Omni-directional Survey 9-2
9.1.3 Runs 6 and 9 - 60 MHz Omni-directional Survey 9-2
9.1.4 Runs 11 and 13 - 60 MHz Directional Survey 9-3
9.2 Discussion of the Radar Trial in Relation to the Objectives 9-3
9.2.1 Objective 1 - Establish Radar Range in the BVG 9-4
9.2.2 Objective 2 - Provide Information on Contrasts in Electrical Properties 9-5
9.2.3 Objective 3 - Assess Whether the Results are Representative of other UK Nirex Ltd Boreholes at Sellafield 9-6
9.2.4 Objective 4 - Assess the Feasibility of the Method and Equipment for Surveys in Boreholes 2 and 4 9-7
9.2.5 Objective 5 - Identify Equipment/Survey Parameters for Further Surveys 9-8
9.2.6 Objectives 6 and 7 - Correlate Reflectors with Fault/Fractures Already Identified 9-9

10. CONCLUSIONS AND RECOMMENDATIONS 10-1

REFERENCES

APPENDIX A

LIST OF TABLES

		Page No.
Table 3-1	Technical specifications of the RAMAC borehole radar system	3-4
Table 5-1	Specifications for borehole radar Run 1	5-4
Table 5-2	Specifications for borehole radar Run 2	5-5
Table 5-3	Specifications for borehole radar Run 3	5-6
Table 5-4	Specifications for borehole radar Run 4	5-10
Table 5-5	Specifications for borehole radar Run 5	5-10
Table 5-6	Specifications for borehole radar Run 6	5-12
Table 5-7	Specifications for borehole radar Run 9	5-13
Table 5-8	Specifications for borehole radar Run 10	5-15
Table 5-9	Specifications for borehole radar Run 12	5-16
Table 5-10	Specifications for borehole radar Run 11	5-17
Table 5-11	Specifications for borehole radar Run 13	5-18
Table 6-1	List of radar reflectors identified from the 60 MHz omni-directional and 60 MHz directional surveys in Borehole 7A	6-17
Table 7-1	List of radar reflectors identified from the 60 MHz omni-directional and 60 MHz directional surveys in Borehole 7A	7-11
Table 8-1	Radar evaluation parameters from Borehole 7A	8-6
Table 8-2	Radar evaluation parameters from Borehole 2	8-7
Table 8-3	Radar evaluation parameters from Borehole 4	8-8
Table 8-4	Radar evaluation parameters from Borehole 5	8-9

Table 8-5 Borehole radar ranges for Borehole 2, Borehole 4 and Borehole 5 8-10

LIST OF PLATES

Plate 1 Components of the RAMAC borehole radar survey equipment

LIST OF FIGURES

Figure 3-1 Schematic diagram of the components of the RAMAC directional borehole radar system and principles of operation.

Figure 5-1 Data summary and plot of recorded traces for Run 1 - Time Base Determination

Figure 5-2 Peak to peak amplitude of the direct wave as a function of depth for an interval which includes the end of the casing (444.7 mbRT)

Figure 5-3 Radar map from Run 3i - Determination of depth accuracy and casing end

Figure 5-4 Radar map from Run 3ii - Preliminary assessment of radar range

Figure 5-5 Radar map from Run 3iii first velocity determination run, transmitter to receiver separation 5.9 metres.

Figure 5-6 Radar map from Run 3iv second velocity determination run, transmitter to receiver separation 11.9 metres.

Figure 5-7 Radar map from Run 3v third velocity determination run, transmitter to receiver separation 7.9 metres.

Figure 5-8 Radar map from Run 5, 22 MHz omni-directional survey (519.76 - 600.00 mbRT)

Figure 5-9 Radar map from Run 5, 22 MHz omni-directional survey (600.00 - 700.00 mbRT)

Figure 5-10 Radar map from Run 5, 22 MHz omni-directional survey (700.00 - 800.00 mbRT)

Figure 5-11 Radar map from Run 5, 22 MHz omni-directional survey (800.00 - 900.00 mbRT)

Figure 5-12 Radar map from Run 5, 22 MHz omni-directional survey (900.00 - 958.76 mbRT)

Figure 5-13 Radar map from Run 6, 60 MHz omni-directional survey (517.64 - 600.00 mbRT)

Figure 5-14 Radar map from Run 6, 60 MHz omni-directional survey (600.00 - 700.00 mbRT)
Figure 5-15 Radar map from Run 6, 60 MHz omni-directional survey (700.00 - 749.14 mbRT)
Figure 5-16 Radar map from Run 9, 60 MHz omni-directional survey (743.08 - 800.00 mbRT)
Figure 5-17 Radar map from Run 9, 60 MHz omni-directional survey (800.00 - 900.00 mbRT)
Figure 5-18 Radar map from Run 9, 60 MHz omni-directional survey (900.00 - 956.08 mbRT)
Figure 5-19 Peak to peak amplitude as a function of depth for the direct wave between transmitter and receiver for the 60 MHz omni-directional survey, Runs 6 and 9
Figure 5-20 Checksum signal obtained from the 60 MHz directional antenna array
Figure 5-21 Dipole signal obtained from the 60 MHz directional antenna array

Figure 6-1 Arrival time of the direct wave propagating along the borehole as a function of depth for the three transmitter-receiver separations
Figure 6-2 Travel time differences for propagation distances of 2, 4 and 6 m
Figure 6-3 Peak to peak amplitude as a function of depth for the direct wave between the transmitter and receiver for the 22 MHz omni-directional survey
Figure 6-4 Peak to peak amplitude as a function of depth for the direct wave between the transmitter and receiver for the 60 MHz directional survey, dipole component
Figure 6-5 Radar signal (upper) recorded by the 60 MHz omni-directional system at a depth of 542.12 mbRT and the spectral content of the siganl (lower)
Figure 6-6 Radar signal (upper) recorded by the 60 MHz omni-directional system at a depth of 710.64 mbRT and the spectral content of the siganl (lower)
Figure 6-7 Radar map from Run 6, 60 MHz omni-directional survey (517.64 - 600.00 mbRT) after band pass filtering

Figure 6-8 Radar map from Run 6, 60 MHz omni-directional survey (600.00 - 700.00 mbRT) after band pass filtering

Figure 6-9 Radar map from Run 6, 60 MHz omni-directional survey (700.00 - 749.14 mbRT) after band pass filtering

Figure 6-10 Radar map from Run 9, 60 MHz omni-directional survey (743.08 - 800.00 mbRT) after band pass filtering

Figure 6-11 Radar map from Run 9, 60 MHz omni-directional survey (800.00 - 900.00 mbRT) after band pass filtering

Figure 6-12 Radar map from Run 9, 60 MHz omni-directional survey (900.00 - 956.08 mbRT) after band pass filtering

Figure 6-13 Radar map from Run 6, 60 MHz omni-directional survey (517.64 - 600.00 mbRT) after the application of a moving average filter to the band pass filtered data

Figure 6-14 Radar map from Run 6, 60 MHz omni-directional survey (600.00 - 700.00 mbRT) after the application of a moving average filter to the band pass filtered data

Figure 6-15 Radar map from Run 6, 60 MHz omni-directional survey (700.00 - 749.14 mbRT) after the application of a moving average filter to the band pass filtered data

Figure 6-16 Radar map from Run 9, 60 MHz omni-directional survey (743.08 - 800.00 mbRT) after the application of a moving average filter to the band pass filtered data

Figure 6-17 Radar map from Run 9, 60 MHz omni-directional survey (800.00 - 900.00 mbRT) after the application of a moving average filter to the band pass filtered data

Figure 6-18 Radar map from Run 9, 60 MHz omni-directional survey (900.00 - 956.08 mbRT) after the application of a moving average filter to the band pass filtered data

Figure 6-19 Static corrections applied to the Run 6 data

Figure 6-20 Static corrections applied to the Run 9 data

Figure 6-21 Radar velocity as a function of borehole depth for Runs 6 and 9

Figure 6-22 Dielectric constant as a function of borehole depth for Runs 6 and 9

Figure 6-23 Moving average filtered data after static corrections for the interval 517.64 - 600.00 mbRT from Run 6, 60 MHz omni-directional survey

Figure 6-24 Radar map after trace equalisation and static corrections for the interval 517.64 - 600.00 mbRT from Run 6, 60 MHz omni-directional survey

Figure 6-25 Radar map of the data (processing sequence) shown in Figure 6-24 after moving average filtering

Figure 6-26 Radar map for the interval 517.64 - 600.00 mbRT from Run 6, 60 MHz omni-directional survey showing the result of deconvolution after static corrections and Automatic Gain Control (AGC)

Figure 6-27 The result of FK-filtering after AGC and static corrections where spatial frequencies corresponding to the direct pulse have been suppressed by 40 dB for the interval 517.64 - 600.00 mbRT from Run 6, 60 MHz omni-directional survey

Figure 6-28 Shows the radar map for the interval 517.64 - 600.00 mbRT from Run 6, 60 MHz omni-directional survey after cross-correlation with the average of 35 traces from the limestone section of the borehole after band-pass filtering

Figure 6-29 Shows the radar map for the interval 517.64 - 600.00 mbRT from Run 6, 60 MHz omni-directional survey after cross-correlation with a synthetic pulse similar to the transmitted pulse

Figure 6-30 The result of adaptive filtering after static corrections and AGC for the interval 517.64 - 600.00 mbRT from Run 6, 60 MHz omni-directional survey

Figure 6-31 Radar map from Run 6, 60 MHz omni-directional survey (517.64 - 600.00 mbRT) after the application of a moving average filter to the data after trace equalisation and static corrections

Figure 6-32 Radar map from Run 6, 60 MHz omni-directional survey (600.00 - 700.00 mbRT) after the application of a moving average filter to the data after trace equalisation and static corrections

Figure 6-33 Radar map from Run 6 and 9, 60 MHz omni-directional survey (700.00 - 800.00 mbRT) after the application of a moving average filter to the data after trace equalisation and static corrections

Figure 6-34 Radar map from Run 9, 60 MHz omni-directional survey (800.00 - 900.00 mbRT) after the application of a moving average filter to the data after trace equalisation and static corrections

Figure 6-35 Radar map from Run 9, 60 MHz omni-directional survey (900.00 - 956.08 mbRT) after the application of a moving average filter to the data after trace equalisation and static corrections

Figure 6-36 Radar map of the dipole component from the 60 MHz directional survey Run 11 after depth correction and band pass filtering for the depth interval 518.80 to 598.80 mbRT at an azimuth of 0°

Figure 6-37 Radar map of the dipole component from the 60 MHz directional survey Run 11 after depth correction and band pass filtering for the depth interval 518.80 to 598.80 mbRT at an azimuth of 10°

Figure 6-38 Radar map of the dipole component from the 60 MHz directional survey Run 11 after depth correction and band pass filtering for the depth interval 518.80 to 598.80 mbRT at an azimuth of 20°

Figure 6-39 Radar map of the dipole component from the 60 MHz directional survey Run 11 after depth correction and band pass filtering for the depth interval 518.80 to 598.80 mbRT at an azimuth of 30°

Figure 6-40 Radar map of the dipole component from the 60 MHz directional survey Run 11 after depth correction and band pass filtering for the depth interval 518.80 to 598.80 mbRT at an azimuth of 40°

Figure 6-41 Radar map of the dipole component from the 60 MHz directional survey Run 11 after depth correction and band pass filtering for the depth interval 518.80 to 598.80 mbRT at an azimuth of 50°

Figure 6-42 Radar map of the dipole component from the 60 MHz directional survey Run 11 after depth correction and band pass filtering for the depth interval 518.80 to 598.80 mbRT at an azimuth of 60°

Figure 6-43 Radar map of the dipole component from the 60 MHz directional survey Run 11 after depth correction and band pass filtering for the depth interval 518.80 to 598.80 mbRT at an azimuth of 70°

Figure 6-44 Radar map of the dipole component from the 60 MHz directional survey Run 11 after depth correction and band pass filtering for the depth interval 518.80 to 598.80 mbRT at an azimuth of 80°

Figure 6-45 Radar map of the dipole component from the 60 MHz directional survey Run 11 after depth correction and band pass filtering for the depth interval 518.80 to 598.80 mbRT at an azimuth of 90°

Figure 6-46 Radar map of the dipole component from the 60 MHz directional survey Run 11 after depth correction and band pass filtering for the depth interval 518.80 to 598.80 mbRT at an azimuth of 100°

Figure 6-47 Radar map of the dipole component from the 60 MHz directional survey Run 11 after depth correction and band pass filtering for the depth interval 518.80 to 598.80 mbRT at an azimuth of 110°

Figure 6-48 Radar map of the dipole component from the 60 MHz directional survey Run 11 after depth correction and band pass filtering for the depth interval 518.80 to 598.80 mbRT at an azimuth of 120°

Figure 6-49 Radar map of the dipole component from the 60 MHz directional survey Run 11 after depth correction and band pass filtering for the depth interval 518.80 to 598.80 mbRT at an azimuth of 130°

Figure 6-50 Radar map of the dipole component from the 60 MHz directional survey Run 11 after depth correction and band pass filtering for the depth interval 518.80 to 598.80 mbRT at an azimuth of 140°

Figure 6-51 Radar map of the dipole component from the 60 MHz directional survey Run 11 after depth correction and band pass filtering for the depth interval 518.80 to 598.80 mbRT at an azimuth of 150°

Figure 6-52 Radar map of the dipole component from the 60 MHz directional survey Run 11 after depth correction and band pass filtering for the depth interval 518.80 to 598.80 mbRT at an azimuth of 160°

Figure 6-53 Radar map of the dipole component from the 60 MHz directional survey Run 11 after depth correction and band pass filtering for the depth interval 518.80 to 598.80 mbRT at an azimuth of 170°

Figure 6-54 Radar map of the dipole component from the 60 MHz directional survey Run 11 after depth correction and band pass filtering for the depth interval 518.80 to 598.80 mbRT at an azimuth of 180°

Figure 6-55 Radar map of the dipole component from the 60 MHz directional survey Run 11 after depth correction and band pass filtering for the depth interval 518.80 to 598.80 mbRT at an azimuth of 190°

Figure 6-56 Radar map of the dipole component from the 60 MHz directional survey Run 11 after depth correction and band pass filtering for the depth interval 518.80 to 598.80 mbRT at an azimuth of 200°

Figure 6-57 Radar map of the dipole component from the 60 MHz directional survey Run 11 after depth correction and band pass filtering for the depth interval 518.80 to 598.80 mbRT at an azimuth of 210°

Figure 6-58 Radar map of the dipole component from the 60 MHz directional survey Run 11 after depth correction and band pass filtering for the depth interval 518.80 to 598.80 mbRT at an azimuth of 220°

Figure 6-59 Radar map of the dipole component from the 60 MHz directional survey Run 11 after depth correction and band pass filtering for the depth interval 518.80 to 598.80 mbRT at an azimuth of 230°

Figure 6-60 Radar map of the dipole component from the 60 MHz directional survey Run 11 after depth correction and band pass filtering for the depth interval 518.80 to 598.80 mbRT at an azimuth of 240°

Figure 6-61 Radar map of the dipole component from the 60 MHz directional survey Run 11 after depth correction and band pass filtering for the depth interval 518.80 to 598.80 mbRT at an azimuth of 250°

Figure 6-62 Radar map of the dipole component from the 60 MHz directional survey Run 11 after depth correction and band pass filtering for the depth interval 518.80 to 598.80 mbRT at an azimuth of 260°

Figure 6-63 Radar map of the dipole component from the 60 MHz directional survey Run 11 after depth correction and band pass filtering for the depth interval 518.80 to 598.80 mbRT at an azimuth of 270°

Figure 6-64 Radar map of the dipole component from the 60 MHz directional survey Run 11 after depth correction and band pass filtering for the depth interval 518.80 to 598.80 mbRT at an azimuth of 280°

Figure 6-65 Radar map of the dipole component from the 60 MHz directional survey Run 11 after depth correction and band pass filtering for the depth interval 518.80 to 598.80 mbRT at an azimuth of 290°

Figure 6-66 Radar map of the dipole component from the 60 MHz directional survey Run 11 after depth correction and band pass filtering for the depth interval 518.80 to 598.80 mbRT at an azimuth of 300°

Figure 6-67 Radar map of the dipole component from the 60 MHz directional survey Run 11 after depth correction and band pass filtering for the depth interval 518.80 to 598.80 mbRT at an azimuth of 310°

Figure 6-68 Radar map of the dipole component from the 60 MHz directional survey Run 11 after depth correction and band pass filtering for the depth interval 518.80 to 598.80 mbRT at an azimuth of 320°

Figure 6-69 Radar map of the dipole component from the 60 MHz directional survey Run 11 after depth correction and band pass filtering for the depth interval 518.80 to 598.80 mbRT at an azimuth of 330°

Figure 6-70 Radar map of the dipole component from the 60 MHz directional survey Run 11 after depth correction and band pass filtering for the depth interval 518.80 to 598.80 mbRT at an azimuth of 340°

Figure 6-71 Radar map of the dipole component from the 60 MHz directional survey Run 11 after depth correction and band pass filtering for the depth interval 518.80 to 598.80 mbRT at an azimuth of 350°

Figure 6-72 Radar map of the dipole component from the 60 MHz directional survey Run 11 after depth correction and the application of a moving average filter for the depth interval 518.80 to 598.80 mbRT at an azimuth of 0°

Figure 6-73 Radar map of the dipole component from the 60 MHz directional survey Run 11 after depth correction and the application of a moving average filter for the depth interval 518.80 to 598.80 mbRT at an azimuth of 10°

Figure 6-74 Radar map of the dipole component from the 60 MHz directional survey Run 11 after depth correction and the application of a moving average filter for the depth interval 518.80 to 598.80 mbRT at an azimuth of 20°

Figure 6-75 Radar map of the dipole component from the 60 MHz directional survey Run 11 after depth correction and the application of a moving average filter for the depth interval 518.80 to 598.80 mbRT at an azimuth of 30°

Figure 6-76 Radar map of the dipole component from the 60 MHz directional survey Run 11 after depth correction and the application of a moving average filter for the depth interval 518.80 to 598.80 mbRT at an azimuth of 40°

Figure 6-77 Radar map of the dipole component from the 60 MHz directional survey Run 11 after depth correction and the application of a moving average filter for the depth interval 518.80 to 598.80 mbRT at an azimuth of 50°

Figure 6-78 Radar map of the dipole component from the 60 MHz directional survey Run 11 after depth correction and the application of a moving average filter for the depth interval 518.80 to 598.80 mbRT at an azimuth of 60°

Figure 6-79 Radar map of the dipole component from the 60 MHz directional survey Run 11 after depth correction and the application of a moving average filter for the depth interval 518.80 to 598.80 mbRT at an azimuth of 70°

Figure 6-80 Radar map of the dipole component from the 60 MHz directional survey Run 11 after depth correction and the application of a moving average filter for the depth interval 518.80 to 598.80 mbRT at an azimuth of 80°

Figure 6-81 Radar map of the dipole component from the 60 MHz directional survey Run 11 after depth correction and the application of a moving average filter for the depth interval 518.80 to 598.80 mbRT at an azimuth of 90°

Figure 6-82 Radar map of the dipole component from the 60 MHz directional survey Run 11 after depth correction and the application of a moving average filter for the depth interval 518.80 to 598.80 mbRT at an azimuth of 100°

Figure 6-83 Radar map of the dipole component from the 60 MHz directional survey Run 11 after depth correction and the application of a moving average filter for the depth interval 518.80 to 598.80 mbRT at an azimuth of 110°

Figure 6-84 Radar map of the dipole component from the 60 MHz directional survey Run 11 after depth correction and the application of a moving average filter for the depth interval 518.80 to 598.80 mbRT at an azimuth of 120°

Figure 6-85 Radar map of the dipole component from the 60 MHz directional survey Run 11 after depth correction and the application of a moving average filter for the depth interval 518.80 to 598.80 mbRT at an azimuth of 130°

Figure 6-86 Radar map of the dipole component from the 60 MHz directional survey Run 11 after depth correction and the application of a moving average filter for the depth interval 518.80 to 598.80 mbRT at an azimuth of 140°

Figure 6-87 Radar map of the dipole component from the 60 MHz directional survey Run 11 after depth correction and the application of a moving average filter for the depth interval 518.80 to 598.80 mbRT at an azimuth of 150°

Figure 6-88 Radar map of the dipole component from the 60 MHz directional survey Run 11 after depth correction and the application of a moving average filter for the depth interval 518.80 to 598.80 mbRT at an azimuth of 160°

Figure 6-89 Radar map of the dipole component from the 60 MHz directional survey Run 11 after depth correction and the application of a moving average filter for the depth interval 518.80 to 598.80 mbRT at an azimuth of 170°

Figure 6-90 Radar map of the dipole component from the 60 MHz directional survey Run 11 after depth correction and the application of a moving average filter for the depth interval 518.80 to 598.80 mbRT at an azimuth of 180°

Figure 6-91 Radar map of the dipole component from the 60 MHz directional survey Run 11 after depth correction and the application of a moving average filter for the depth interval 518.80 to 598.80 mbRT at an azimuth of 190°

Figure 6-92 Radar map of the dipole component from the 60 MHz directional survey Run 11 after depth correction and the application of a moving average filter for the depth interval 518.80 to 598.80 mbRT at an azimuth of 200°

Figure 6-93 Radar map of the dipole component from the 60 MHz directional survey Run 11 after depth correction and the application of a moving average filter for the depth interval 518.80 to 598.80 mbRT at an azimuth of 210°

Figure 6-94 Radar map of the dipole component from the 60 MHz directional survey Run 11 after depth correction and the application of a moving average filter for the depth interval 518.80 to 598.80 mbRT at an azimuth of 220°

Figure 6-95 Radar map of the dipole component from the 60 MHz directional survey Run 11 after depth correction and the application of a moving average filter for the depth interval 518.80 to 598.80 mbRT at an azimuth of 230°

Figure 6-96 Radar map of the dipole component from the 60 MHz directional survey Run 11 after depth correction and the application of a moving average filter for the depth interval 518.80 to 598.80 mbRT at an azimuth of 240°

Figure 6-97 Radar map of the dipole component from the 60 MHz directional survey Run 11 after depth correction and the application of a moving average filter for the depth interval 518.80 to 598.80 mbRT at an azimuth of 250°

Figure 6-98 Radar map of the dipole component from the 60 MHz directional survey Run 11 after depth correction and the application of a moving average filter for the depth interval 518.80 to 598.80 mbRT at an azimuth of 260°

Figure 6-99 Radar map of the dipole component from the 60 MHz directional survey Run 11 after depth correction and the application of a moving average filter for the depth interval 518.80 to 598.80 mbRT at an azimuth of 270°

Figure 6-100 Radar map of the dipole component from the 60 MHz directional survey Run 11 after depth correction and the application of a moving average filter for the depth interval 518.80 to 598.80 mbRT at an azimuth of 280°

Figure 6-101 Radar map of the dipole component from the 60 MHz directional survey Run 11 after depth correction and the application of a moving average filter for the depth interval 518.80 to 598.80 mbRT at an azimuth of 290°

Figure 6-102 Radar map of the dipole component from the 60 MHz directional survey Run 11 after depth correction and the application of a moving average filter for the depth interval 518.80 to 598.80 mbRT at an azimuth of 300°

Figure 6-103 Radar map of the dipole component from the 60 MHz directional survey Run 11 after depth correction and the application of a moving average filter for the depth interval 518.80 to 598.80 mbRT at an azimuth of 310°

Figure 6-104 Radar map of the dipole component from the 60 MHz directional survey Run 11 after depth correction and the application of a moving average filter for the depth interval 518.80 to 598.80 mbRT at an azimuth of 320°

Figure 6-105 Radar map of the dipole component from the 60 MHz directional survey Run 11 after depth correction and the application of a moving average filter for the depth interval 518.80 to 598.80 mbRT at an azimuth of 330°

Figure 6-106 Radar map of the dipole component from the 60 MHz directional survey Run 11 after depth correction and the application of a moving average filter for the depth interval 518.80 to 598.80 mbRT at an azimuth of 340°

Figure 6-107 Radar map of the dipole component from the 60 MHz directional survey Run 11 after depth correction and the application of a moving average filter for the depth interval 518.80 to 598.80 mbRT at an azimuth of 350°

Figure 6-108 Radar map of the dipole component from the 60 MHz directional survey Run 11 after depth correction and the application of a moving average filter for the depth interval 518.80 to 598.80 mbRT at an azimuth of 360°

Figure 6-109 Radar map of the dipole component from the 60 MHz directional survey Run 13 (648.80 to 768.80 mbRT)

Figure 6-110 Radar map of the dipole component from the 60 MHz directional survey Run 13 (840.80 to 875.80 mbRT and 890.80 to 918.90 mbRT)

Figure 6-111 Radar map of the dipole component from the 60 MHz directional survey Run 13 (890.80 to 918.80 mbRT and 943.80 to 954.80 mbRT)

Figure 6-112 Radar map of the moving average filtered dipole component from the 60 MHz directional survey Run 13 (648.80 to 768.80 mbRT)

Figure 6-113 Radar map of the moving average filtered dipole component from the 60 MHz directional survey Run 13 (840.80 to 875.80 mbRT and 890.80 to 918.90 mbRT)

Figure 6-114 Radar map of the moving average filtered dipole component from the 60 MHz directional survey Run 13 (890.80 to 918.80 mbRT and 943.80 to 954.80 mbRT)
Figure 6-115 Radar map of the moving average filtered dipole component from the 60 MHz directional survey Run 13 (648.80 to 768.80 mbRT) at an azimuth of 0°
Figure 6-116 Radar map of the moving average filtered dipole component from the 60 MHz directional survey Run 13 (648.80 to 768.80 mbRT) at an azimuth of 10°
Figure 6-117 Radar map of the moving average filtered dipole component from the 60 MHz directional survey Run 13 (648.80 to 768.80 mbRT) at an azimuth of 20°
Figure 6-118 Radar map of the moving average filtered dipole component from the 60 MHz directional survey Run 13 (648.80 to 768.80 mbRT) at an azimuth of 30°
Figure 6-119 Radar map of the moving average filtered dipole component from the 60 MHz directional survey Run 13 (648.80 to 768.80 mbRT) at an azimuth of 40°
Figure 6-120 Radar map of the moving average filtered dipole component from the 60 MHz directional survey Run 13 (648.80 to 768.80 mbRT) at an azimuth of 50°
Figure 6-121 Radar map of the moving average filtered dipole component from the 60 MHz directional survey Run 13 (648.80 to 768.80 mbRT) at an azimuth of 60°
Figure 6-122 Radar map of the moving average filtered dipole component from the 60 MHz directional survey Run 13 (648.80 to 768.80 mbRT) at an azimuth of 70°
Figure 6-123 Radar map of the moving average filtered dipole component from the 60 MHz directional survey Run 13 (648.80 to 768.80 mbRT) at an azimuth of 80°
Figure 6-124 Radar map of the moving average filtered dipole component from the 60 MHz directional survey Run 13 (648.80 to 768.80 mbRT) at an azimuth of 90°
Figure 6-125 Radar map of the moving average filtered dipole component from the 60 MHz directional survey Run 13 (648.80 to 768.80 mbRT) at an azimuth of 100°
Figure 6-126 Radar map of the moving average filtered dipole component from the 60 MHz directional survey Run 13 (648.80 to 768.80 mbRT) at an azimuth of 110°
Figure 6-127 Radar map of the moving average filtered dipole component from the 60 MHz directional survey Run 13 (648.80 to 768.80 mbRT) at an azimuth of 120°

Figure 6-128 Radar map of the moving average filtered dipole component from the 60 MHz directional survey Run 13 (648.80 to 768.80 mbRT) at an azimuth of 130°
Figure 6-129 Radar map of the moving average filtered dipole component from the 60 MHz directional survey Run 13 (648.80 to 768.80 mbRT) at an azimuth of 140°
Figure 6-130 Radar map of the moving average filtered dipole component from the 60 MHz directional survey Run 13 (648.80 to 768.80 mbRT) at an azimuth of 150°
Figure 6-131 Radar map of the moving average filtered dipole component from the 60 MHz directional survey Run 13 (648.80 to 768.80 mbRT) at an azimuth of 160°
Figure 6-132 Radar map of the moving average filtered dipole component from the 60 MHz directional survey Run 13 (648.80 to 768.80 mbRT) at an azimuth of 170°
Figure 6-133 Radar map of the moving average filtered dipole component from the 60 MHz directional survey Run 13 (648.80 to 768.80 mbRT) at an azimuth of 180°
Figure 6-134 Radar map of the moving average filtered dipole component from the 60 MHz directional survey Run 13 (648.80 to 768.80 mbRT) at an azimuth of 190°
Figure 6-135 Radar map of the moving average filtered dipole component from the 60 MHz directional survey Run 13 (648.80 to 768.80 mbRT) at an azimuth of 200°
Figure 6-136 Radar map of the moving average filtered dipole component from the 60 MHz directional survey Run 13 (648.80 to 768.80 mbRT) at an azimuth of 210°
Figure 6-137 Radar map of the moving average filtered dipole component from the 60 MHz directional survey Run 13 (648.80 to 768.80 mbRT) at an azimuth of 220°
Figure 6-138 Radar map of the moving average filtered dipole component from the 60 MHz directional survey Run 13 (648.80 to 768.80 mbRT) at an azimuth of 230°
Figure 6-139 Radar map of the moving average filtered dipole component from the 60 MHz directional survey Run 13 (648.80 to 768.80 mbRT) at an azimuth of 240°
Figure 6-140 Radar map of the moving average filtered dipole component from the 60 MHz directional survey Run 13 (648.80 to 768.80 mbRT) at an azimuth of 250°
Figure 6-141 Radar map of the moving average filtered dipole component from the 60 MHz directional survey Run 13 (648.80 to 768.80 mbRT) at an azimuth of 260°
Figure 6-142 Radar map of the moving average filtered dipole component from the 60 MHz directional survey Run 13 (648.80 to 768.80 mbRT) at an azimuth of 270°

Figure 6-143 Radar map of the moving average filtered dipole component from the 60 MHz directional survey Run 13 (648.80 to 768.80 mbRT) at an azimuth of 280°
Figure 6-144 Radar map of the moving average filtered dipole component from the 60 MHz directional survey Run 13 (648.80 to 768.80 mbRT) at an azimuth of 290°
Figure 6-145 Radar map of the moving average filtered dipole component from the 60 MHz directional survey Run 13 (648.80 to 768.80 mbRT) at an azimuth of 300°
Figure 6-146 Radar map of the moving average filtered dipole component from the 60 MHz directional survey Run 13 (648.80 to 768.80 mbRT) at an azimuth of 310°
Figure 6-147 Radar map of the moving average filtered dipole component from the 60 MHz directional survey Run 13 (648.80 to 768.80 mbRT) at an azimuth of 320°
Figure 6-148 Radar map of the moving average filtered dipole component from the 60 MHz directional survey Run 13 (648.80 to 768.80 mbRT) at an azimuth of 330°
Figure 6-149 Radar map of the moving average filtered dipole component from the 60 MHz directional survey Run 13 (648.80 to 768.80 mbRT) at an azimuth of 340°
Figure 6-150 Radar map of the moving average filtered dipole component from the 60 MHz directional survey Run 13 (648.80 to 768.80 mbRT) at an azimuth of 350°
Figure 6-151 Radar map of the moving average filtered dipole component from the 60 MHz directional survey Run 13 (648.80 to 768.80 mbRT) at an azimuth of 360°
Figure 6-152 Radar map of the unfiltered dipole component from the 60 MHz directional survey Run 13 (648.80 to 768.80 mbRT) at an azimuth of 0°
Figure 6-153 (a) Principle of single hole reflection radar measurements and (b) the characteristic patterns generated by plane and point reflectors
Figure 6-154 Nomogram for planar and point reflectors used to determine angle of intersection and distance to point reflectors
Figure 6-155 Radar reflectors identified in the interval 518.80 to 600.00 mbRT
Figure 6-156 Radar reflectors identified in the interval 600.00 to 700.00 mbRT
Figure 6-157 Radar reflectors identified in the interval 700.00 to 800.00 mbRT
Figure 6-158 Radar reflectors identified in the interval 800.00 to 900.00 mbRT
Figure 6-159 Radar reflectors identified in the interval 900.00 to 954.80 mbRT

Figure 7-1 Resistivity logs (LLD, LLG, LLS, MSFL) from Borehole 7A

Figure 7-2 Radar amplitude and velocity (60 MHz survey data), neutron porosity (NPHI) and fluid conductivity (ACON) from Borehole 7A

Figure 7-3 Radar peak to peak amplitude and LLD resistivity

Figure 7-4 Radar velocity and neutron porosity (NPHI), (the straight line segments in the radar velocity plot represent borehole sections where no data was acquired)

Figure 7-5 Cross plots of radar amplitude against LLD resistivity and radar velocity against porosity; the cross plots are shown for band pass filtered data (upper) and data averaged at 1m intervals (lower)

Figure 7-6 Cross plots of radar amplitude against LLD, LLS, LLG and MSFL resistivity data averaged at 1m intervals

Figure 7-7 Cross plots of radar velocity against radar amplitude, porosity and LLD resistivity

Figure 7-8 Cross plots of radar amplitude against porosity, MSFL against LLD resistivity and LLD resistivity against porosity

Figure 7-9 Cross plot of radar range against average resistivity (LLD) and regression line based on the three data points in the table on Page 7-8, the figure also shows the regression line obtained under the assumption that radar range is a linear function (solid line) of, or proportional to, the logarithm (dashed line) of the averaged LLD resistivity

Figure 7-10 Plot of the indentified radar reflectors, LLD and MSFL resistivity logs for the interval 500 to 600 mbRT, predicted intersections of the radar reflectors with the borehole are indicated by two horizontal lines.

Figure 7-11 Plot of the indentified radar reflectors, LLD and MSFL resistivity logs for the interval 680 to 780 mbRT, predicted intersections of the radar reflectors with the borehole are indicated by two horizontal lines.

Figure 7-12 Plot of the indentified radar reflectors, LLD and MSFL resistivity logs for the interval 800 to 900 mbRT, predicted intersections of the radar reflectors with the borehole are indicated by two horizontal lines.

Figure 7-13 Plot of the indentified radar reflectors, LLD and MSFL resistivity logs for the interval 900 to 1000 mbRT, predicted intersections of the radar reflectors with the borehole are indicated by two horizontal lines.

Figure 8-1 Predicted 60 MHz ranges for Borehole 2

Figure 8-2 Predicted 60 MHz ranges for Borehole 4

Figure 8-3 Predicted 60 MHz ranges for Borehole 5

ABSTRACT

A trial borehole radar survey was conducted in UK Nirex Ltd Borehole 7A at Sellafield with the objectives of establishing the feasibility of the technique and determining the range and resolution of the system within the Borrowdale Volcanic Group (BVG).

The data acquired with the 22 MHz system provided no information on geological features in the BVG. However, a range of 5-10 metres was achieved with the 60 MHz omni-directional system for 50% of the BVG, whilst a range of approximately 5 metres was obtained with the 60 MHz directional system; with resolutions of approximately 1 metre.

The correlation of the radar results with wireline logs indicated that the resistivity logs could be used to estimate radar ranges for other boreholes and showed a positive correlation between radar reflectors and resistivity anomalies. Further analysis showed that; the radar range was limited by the relatively low resistivities of the formations; and the conductivity of the borehole fluid seemed to be of limited importance. The estimates of radar range made on the basis of the correlations suggested that the technique would only be effective over short intervals of other boreholes at Sellafield and that it would not be possible to undertake a cross-hole radar survey.

EXECUTIVE SUMMARY

This report presents the results of the borehole radar trial conducted in the UK Nirex Ltd Borehole 7A at Sellafield Cumbria, UK. The survey was undertaken as a component of a long term programme of monitoring, testing and experimentation in completed boreholes. The programme, termed Post Completion Testing is being undertaken to decrease uncertainties in the structural and hydrogeological characterisation of the rock volume and will contribute towards establishing sufficient confidence in the characterisation of the site to move towards its validation as a suitable host for the Deep Waste Repository.

Geophysical logging forms an integral component of the programme and it was proposed that a borehole radar survey, undertaken in Borehole 4, would form a component of the logging; additionally a cross-hole radar survey between Boreholes 2 and 4 was also considered. The objectives of these surveys were to provide additional information on the structural environment of the borehole and establish continuity of structural features between boreholes. Initial survey design work was undertaken based on geophysical wireline logging which suggested that the formation resistivities combined with the fluid conductivity and borehole diameter would preclude the acquisition of cross-hole radar data. It was therefore recommended that a trial of the borehole radar technique, in the single hole reflection mode, should be undertaken in Borehole 7A to establish the feasibility of the methodology and determine the potential range which could be obtained in the cross-hole mode.

Consequently the objectives of the survey were to establish the radar range within the Borrowdale Volcanic Group (BVG) in terms of penetration and resolution. The survey was also required to provide information relating to contrasts in the electrical properties of the rock mass and to assess whether the results obtained from the trial in Borehole 7A could be considered to be representative of all other UK Nirex Ltd boreholes at Sellafield. Further objectives were identified which included assessing the feasibility of using both the same methods and equipment and identifying suitable equipment and survey parameters for further single hole reflection surveys. Additional objectives were to compare and, where possible,

correlate reflectors with previously identified features derived from other geophysical methods.

This report presents a discussion of the equipment used and the modifications made to the system. The survey design is also presented along with detailed discussions of the data acquisition phases of the survey and the subsequent data processing undertaken.

The data were acquired using 22 MHz omni-directional, 60 MHz omni-directional and 60 MHz directional systems. The results indicated that the 22 MHz system did not operate in the wave propagation mode and this element of the survey gave no information about geological features and the radar range can be considered to be zero. The data acquired with the 60 MHz omni-directional system achieved a range of between 5-10 metres for 50% of the BVG, whilst the range in the rest of the BVG was effectively 0 metres and within the Carboniferous Limestone the radar range obtained was 10-15 metres. A total of 16 radar reflectors were identified within the BVG and 10 reflectors were identified within the Carboniferous Limestone interval of the borehole which were stronger than those observed in the BVG. The results obtained from the 60 MHz directional survey achieved a range of approximately 5 metres in the BVG although this was over a shorter overall length than for the omni-directional survey. Over the rest of the BVG the directional antenna provided no information. Within the Carboniferous Limestone the range attained was 5-10 metres. From these results it was only possible to determine the azimuth for one of the reflectors in the BVG and for four reflectors in the Carboniferous Limestone. The resolution of the 60 MHz systems was approximately 1 metre.

The radar results were correlated with geophysical wireline logs acquired in the Borehole 7A and the results of the correlation indicated that the resistivity logs could be used to estimate attainable radar ranges for other boreholes, where average resistivities are less than 1000 ohmm and hence indicate where radar surveys could be performed.

The correlation between predicted intersections of radar reflectors with the borehole and the location of resistivity anomalies was evaluated. This showed a positive correlation between 17 of the 26 radar reflectors and resistivity anomalies and indicated that essentially all of the identified reflectors could be attributed to discontinuities in the formation.

The borehole radar trial in Borehole 7A at Sellafield and the subsequent analysis of the data showed that the radar range was limited by the relatively low resistivities of the formations. The limit at which the radar commences to provide useful information is at 200-300 ohmm for the omni-directional system and 500-600 ohmm for the directional antenna and future radar surveys at Sellafield should be restricted to intervals of the boreholes where the average resistivities exceed these values. The conductivity of the borehole fluid seems to be of limited importance, although it had an overall negative effect on the radar results, particularly for the 22 MHz system. It is therefore considered to be essential that the annulus of borehole fluid surrounding the antennas is minimised and it is suggested that the plastic covers used in conjunction with the antennas were reasonably successful in reducing the effects of the borehole fluid for the 60 MHz systems although survey elements were not undertaken without the plastic covers.

The trial survey in Borehole 7A tested a number of parameters to determine the optimum survey parameters and those used are considered to be optimal for the system utilised for the trial survey, however, if further surveys were to be performed at Sellafield the 60 MHz omni-directional and directional systems should be used and the use of higher frequencies should also be considered. Further, the surveys should be confined to those parts of the boreholes where the formations are sufficiently resistive, quantifiable from resistivity wireline logs, for the radar to provide useful results.

Minor modifications could also be made to the radar system in an attempt to improve results for future surveys. These modifications would include increasing the length of the plastic covers and reducing further the separation between transmitter and receiver, although this may adversely affect the radar range.

The results of the borehole radar trial conducted in Borehole 7A were considered, at a Site meeting attended by members of the interpretation and integration teams, to have provided little further information than was already available from other geophysical surveys and geological information. The estimation of radar range which may be attained in Boreholes 2 and 4 suggested that the technique may only be effective over short sections of the boreholes and on this basis it was decided not to conduct further surveys. Furthermore, the estimates of radar range suggested that it would not be possible to undertake a cross-hole radar survey.

1. INTRODUCTION

UK Nirex Ltd is currently undertaking a Site Characterisation Programme to assess the suitability of the geology in the Sellafield area, Cumbria, UK, for the construction of a deep repository for the disposal of solid low and intermediate level radioactive waste.

A component of this investigation is a long term programme of monitoring, testing and experimentation in completed boreholes. This programme, termed Post Completion Testing, will contribute towards establishing sufficient confidence in the characterisation of the site to move towards its validation as a suitable host for the Deep Waste Repository.

The overall objectives of the project are to decrease uncertainties in the structural and hydrogeological characterisation of the rock volume. As an integral part of the overall Post Completion Testing it was proposed that geophysical logging would be undertaken in Borehole 4. Further, it was proposed that the principal technique to be applied would be borehole radar operated in the single borehole reflection mode, although initially a cross-hole radar survey between Boreholes 2 and 4 was also considered. It was also proposed that cross-hole geophysical surveys, seismic tomography, would be undertaken between Boreholes 2 and 4 and potentially between Boreholes 2 and 5.

The data from the geophysical surveys would be utilised to decrease the uncertainties in the three dimensional structural model for the site which forms an input to the hydrogeological modelling.

A full suite of wireline logs were run following completion of drilling of the boreholes which included; dual induction, dual laterolog and microspherically focused resistivity logs; array sonic; dipole shear sonic imager; lithodensity log; compensated

neutron log; natural gamma ray spectroscopy; geochemical logging tool; formation microimager, borehole televiewer and caliper log. Additionally in Borehole 2 an electromagnetic propagation tool was also run specifically to provide information on the formation dielectric constant to be used in the design of the radar surveys and to evaluate whether it would be possible to undertake a cross-hole radar survey. Vertical seismic profiling (VSP), including zero offset and far offset surveys, have also been undertaken.

The specific objectives of the geophysical wireline logging in Borehole 4 was to provide additional information on the structural environment in close proximity to the borehole. Whilst the objective of the cross-hole geophysical surveys was to establish the continuity of structural features through the formations between the boreholes.

Copies of the relevant geophysical wireline logs, including the resistivity logs for Sellafield Boreholes 2 and 4 were forwarded to ABEM to be used in the initial design phase for the borehole radar surveys. ABEM were consulted because of their experience of performing both single borehole radar and cross-hole radar surveys in hard fractured rocks.

The resistivity logs from the two boreholes show similar ranges in the value of resistivity to depths of 800 metres below Rotary Table although the values for Borehole 2 were generally lower than those for Borehole 4. Below depths of 800 metres below Rotary Table resistivity values in both boreholes are observed to decrease.

It was considered that the resistivity values in combination with the fluid conductivity and borehole diameter indicated that a cross-hole radar survey between Boreholes 2 and 4 which are approximately 120 metres apart would not be feasible. Further it was considered, by ABEM, that based on the available information, the maximum distance at which a radar pulse, with a 22 MHz frequency, could be detected was

approximately 100 metres. It was further considered that should a radar survey be conducted in a single hole reflection mode it would be possible to estimate the penetration which may be obtained in the cross-hole mode.

From the initial design phase it was recommended that a trial of the borehole radar should be undertaken in Borehole 7A to establish the feasibility of the methodology. Cross-hole surveys should therefore be restricted, initially, to the seismic tomographic technique.

This report discusses the borehole radar trial conducted in Borehole 7A. The objectives of the radar trial are set out with the emphasis placed on establishing the range of propagation of the radar; providing information on contrasts in the electrical properties of the rock mass; assessing whether the results were representative of all other boreholes at Sellafield and the identification of suitable equipment and survey parameters for further single hole reflection surveys.

The report discusses the radar equipment and principles of operation, the survey design and presents a detailed description of the data acquisition and processing undertaken.

The borehole radar survey was conducted during the period 16 January to 19 January 1993 and consisted of four elements as listed below:

- velocity determination runs
- 22 MHz Omni-directional Survey
- 60 MHz Omni-directional Survey
- 60 MHz Directional Survey

Preceding each survey element, surface testing and function checks were conducted to ensure that the radar equipment was functioning correctly.

The velocity determination run was undertaken using the 60 MHz omni-directional system. Radar measurements were, after depth control checks conducted at the base of the casing, made within a section of the borehole which included the base of the Brockram, the Carboniferous Limestone and the top of the BVG to assess the radar range in the different stratigraphic units represented. Within the Brockram no signals were recorded except for a 7 metre interval just above the limestone. Large amplitude direct waves and reflections were observed through the Carboniferous Limestone, whilst no signal was recorded within the top of the BVG. The radar velocity for the BVG was determined over a 25 metre section within the BVG.

The 22 MHz omni-directional survey was undertaken within the Carboniferous Limestone and the BVG. The results showed that where a signal was recorded it appeared to represent a guided borehole wave reflected from discontinuities in the radar antenna array. Reflectors were not apparent within the data recorded. The 60 MHz omni-directional survey was undertaken over essentially the same section of the borehole and was composed of two runs due to equipment malfunction. The results showed that the radar signal was only recorded over certain intervals of the borehole section surveyed. These sections were targeted for the subsequent 60 MHz directional survey, as the signal amplitudes would generally be lower than the corresponding signal amplitude from the omni-directional system.

Following extensive data processing the radar results were correlated with geophysical wireline logs and the results of the correlations are presented and the prognosis for the use of radar in other boreholes at Sellafield is also discussed. The results of the radar survey are also discussed in terms of the objectives identified for the trial and conclusions and recommendations are presented.

2. OBJECTIVES OF THE BOREHOLE RADAR TRIAL

Following the review of resistivity logs and the subsequent discussions with ABEM discussed in the preceding Section it was decided to conduct a trial of the borehole radar system to assess the potential range of the system which could be attained at Sellafield. The results of the single borehole radar trial would provide a site specific measure of propagation distances within the Borrowdale Volcanic Group, (BVG). From these site specific measurements the ability to conduct a cross-hole radar survey between Boreholes 2 and 4 would be reviewed and further single hole radar surveys would be considered.

The objectives of the borehole radar trial in Borehole 7A were defined as set out below:

(i) establish the range of the radar in the Borrowdale Volcanic Group (BVG) in terms of penetration and resolution within the BVG

(ii) provide information pertaining to the contrast in electrical properties of the rock mass at distances away from the borehole and with increasing depth in the formations

(iii) assess whether the results obtained from Borehole 7A are representative of all UK Nirex Ltd boreholes at Sellafield.

(iv) assess the feasibility of using both the same methods and equipment for surveys in Boreholes 2 and 4.

(v) identify suitable equipment/survey parameters for further single hole reflection surveys at Sellafield

Additional Objectives of the trial survey were to have the option to:

(vi) correlate near borehole reflections with previously identified discontinuities that intersect the borehole and to evaluate the orientation of the features defined by the radar survey against those derived from other geophysical methods

(vii) compare and where possible correlate geometric information of reflectors located at distances away from the borehole, derived from the borehole radar reflection surveys with information derived from other geophysical surveys

The results of the trial conducted in Borehole 7A would be evaluated in terms of the objectives of the trial. The results would be correlated with geophysical wireline logs acquired in Borehole 7A and any relationships identified would be utilised in conjunction with the wireline logs acquired for Boreholes 2, 4 and 5 to make predictions of the radar range which would be expected for these Boreholes. Based upon these predictions a decision on conducting further borehole radar surveys would be taken.

The objectives of further single borehole radar reflection surveys would be:

(a) to provide information pertaining to the contrast in electrical properties of the rock mass at distances away from the borehole and with increasing depth in the formations.

(b) to correlate near borehole reflections with previously identified discontinuities that intersect the borehole and to evaluate the orientation of the features defined by the radar survey against those derived from other geophysical methods.

(c) to compare and where possible correlate geometric information of reflectors located at distances away from the borehole, derived from the borehole radar reflection surveys with information derived from other geophysical surveys.

If the results of the borehole radar surveys produced relevant data it was considered possible that further radar surveys would be undertaken in other UK Nirex Ltd boreholes at Sellafield as they became available.

3. EQUIPMENT AND PRINCIPLES OF OPERATION

3.1 The RAMAC Borehole Radar System

The equipment used for the borehole radar trial, conducted in Borehole 7A at Sellafield, was the RAMAC borehole radar system. The RAMAC system was developed within the framework of the International Stripa Project. The development efforts at Stripa comprised construction of a new radar system, a comprehensive field testing program, and the interpretation of the collected data (Olsson et al., 1987, Sandberg et al., 1991).

The RAMAC borehole radar system is a short pulse radar system; which consists of five major components (Plate 1);

- an IBM-compatible computer for control of measurements, data storage, display of the recorded data, and signal analysis. A beeper, which gives an audio signal, indicating when a measurement is completed during manual operation.

- a control unit for timing control, storage, and stacking of single radar measurements.

- a borehole transmitter, for the generation of short radar pulses, and transmitter battery pack.

- a borehole receiver for detection and digitization of radar pulses, and receiver battery pack. Two different types of receivers are available:

    - an omni-directional dipole antenna receiver
    - a directional antenna receiver

- a motor-driven cable winch with a specially designed optical borehole cable for transmission of trigger signals to the borehole probes; and data transmission from the receiver to the control unit. The movement of the winch is controlled by the computer unit during the measurement cycle when the system is in automatic mode.

A block diagram of the RAMAC borehole radar system is shown in Figure 3-1 and the technical specifications of the system are given in Table 3-1.

The RAMAC system operates by generating a short current pulse which is sent to the dipole transmitter which generates a short pulse of electromagnetic energy which propagates through the rock mass. The pulse is as short as possible to obtain high resolution. The transmitter utilizes a dipole antenna which makes the radiation cylindrically symmetric with respect to the borehole. In the receiver the signal is amplified and recorded as a function of time. From the full wave record of the signal the distance (travel time) to a reflector, the strength of the reflection, and the attenuation and delay of the direct wave between transmitter and receiver may be deduced (Olsson et al., 1992).

The omni-directional dipole receiver has an antenna pattern which is also cylindrically symmetric. Hence, it is possible to determine the distance to a reflecting object from the borehole but not the direction to that object.

The directional receiver antenna consists of an array of four loop antennas which makes it possible to determine the direction of the incoming radiation and hence the absolute location of a reflector (Sandberg et al., 1991). At each measurement location the signal from the four antennas are measured in sequence. Therefore, a measurement, with the directional antenna, takes roughly four times longer than a measurement with the dipole (omni-directional) antenna.

The transmission of the trigger signal (short current pulse) from the computer to the borehole transmitter antenna and for the transmission of data from the receiver antenna to the control unit are accomplished using fibre optic cables. The advantages of using fibre optic cables are that:

- the fibre optic cables have no electrical conductivity
- they will not support waves propagating along the borehole
- they will not pick up electrical noise and
- as the signal is digitised down hole there will be no deterioration of the signal along the cable.

The consequence of the above advantages is that the quality of the received signal is independent of cable length.

There is no direct connection between the transmitter and the receiver and both antenna are connected directly to the control unit. The system also provides absolute timing of the transmitted pulses and a calibrated gain in the receiver makes is possible to measure travel times and amplitudes. The absolute time measurement is, however, dependent upon the length of the fibre optic cable and therefore is a quantity which has to be obtained through direct measurement for a given set of fibre optic cables.

General	
Frequency range	20-80 MHz
Performance factor	150 dB
Sampling time accuracy	0.2 ns
Operating pressure, max.	150 Bar
Operating temperature, max.	45°C
Minimum borehole diameter	56 mm
Transmitter	
Antenna type	Dipole (22 or 60 MHz)
Pulse repetition frequency	43 kHz
Peak power	500 W
Antenna length (22/60 MHz antenna)	2.30/0.91 m
Operating time	30 hr
Probe diameter	48 mm
Probe length 22 MHz with 2.6 m battery	5.3 m
Probe length 60 MHz with 1.3 m battery	2.6 m
Weight 22/60 MHz (net)	16/11 kg
Power	Rechargeable NiCd pack
Omni-directional receiver	
Antenna type	Dipole (22 or 60 MHz)
Bandwidth	10-200 MHz
A/D converter	16 bit
Least significant bit at antenna terminals	1 μV
Data transmission rate	1.2 MBit/sec
Antenna length (22/60 MHz antenna)	2.30/0.91 m
Operating time	10 hr
Probe diameter	48 mm
Probe length 22 MHz with 2.6 m battery	5.3 m
Probe length 60 MHz with 1.3 m battery	2.6 m
Weight 22/60 MHz (net)	18/21 kg
Weight	18 kg
Power	Rechargeable NiCd pack

Table 3-1 Technical specifications of the RAMAC borehole radar system.

Directional receiver	
Antenna type	4-element directional array
Bandwidth	10-200 MHz
A/D converter	16 bit
Least significant bit at antenna terminals	1 μV
Data transmission rate	1.2 MBit/sec
Antenna rotation sensors	
- gravity sensor, accuracy	3°
- fluxgate magnetometer, accuracy	3°
Antenna length	1.00 m
Operating time (with 3.0 m battery)	8 hr
Probe length (with 3.0 m battery)	6.0 m
Probe diameter	48 mm
Probe weight (net)	18 kg
Power	Rechargeable NiCd pack
Control Unit	
Microprocessor	RCA 1806
Clock frequency	5 MHz
Sampling frequency	30-3000 MHz
No of samples	256-4096
No of stacks	1-32767
Time window	0-11μs
Weight	14 kg
Computer unit	
IBM/AT compatible with math co-processor	
Operating system	MS-DOS 3.3
Display	Monochrome EGA
Data storage	1.44 MB floppy
	40 MB Hard disk
Power supply	110/220 V AC
Weight	23 kg

Table 3-1 cont. Technical specifications of the RAMAC borehole radar system.

3.2 Principles of Operation

The RAMAC system can be used both in cross-hole and in single hole modes. In the survey conducted at Sellafield only single hole measurements were performed.

In single hole reflection measurements the transmitter and receiver are moved along the borehole with measurements being made with fixed increments. The distance between transmitter and receiver is kept constant during the measurements by the use of glass fibre spacer rods. The result of this type of measurement is displayed in the form of a diagram where the position of the probes is shown along one axis and the propagation distance along the other axis. The amplitude of the received signal is shown in a grey scale where black corresponds to large positive signals, white to large negative signals, and grey to small signals. The distance to a reflecting object is determined by measuring the difference in arrival time between the direct and the reflected pulse. For a planar reflector (for example a fracture plane) the reflection point will follow the line on the plane representing the projection of the borehole onto the plane (Figure 3-1) as the radar system is moved along the borehole. The change in distance to the reflector as a function of borehole length can be used to determine the angle of intersection (θ in Figure 3-1) between the borehole and the plane.

The directional antenna is used to determine the azimuth (ϕ) to the reflecting plane (or any other reflector).

The directional antenna array produces four composite signals, one from each loop antenna. These signals can be decomposed into one omni-directional signal (commonly referred to as the dipole signal), two directional signals (representing two orthogonal magnetic field components), and a checksum. The checksum provides a measure of the quality of the recorded signals and is always small if the antenna is functioning correctly. The directional signals are used to derive the direction of the incoming radiation (i.e. the azimuth to a reflector).

The rotation of the antenna array in the borehole cannot be controlled from surface and the orientation of the antenna array therefore has to be measured downhole in order to determine the absolute location of a reflector. The directional receiver has two directional sensors to determine the rotation of the antenna array around the axis of the borehole relative to a reference direction. The sensors are:

- a gravity sensor which senses the rotation of the directional antenna array in relation to the vertical. This sensor does not give reliable data in a vertical or near vertical borehole.

- a three component flux gate magnetometer which measures the three components of the magnetic field. The two components in the plane perpendicular to the axis of the borehole are used to determine the rotation of the antenna array relative to the total magnetic field vector. This sensor does not give reliable data in a borehole nearly parallel to the magnetic field vector.

3.3 Modifications to the RAMAC System for the Sellafield Survey

The diameter of the borehole probes (48 mm) is considerably smaller than the diameter of Borehole 7A (6¼", 159 mm). It was therefore recognized that due to the large difference in probe and borehole diameters, the borehole probes would be surrounded by a relatively large annulus of borehole fluid and this was expected to adversely affect the radar results as the boreholes at Sellafield contain saline groundwater at depth. To reduce the amount of borehole fluid between the antennas and the borehole wall, the probes were modified by attaching plastic covers which covered both the transmitter and receiver antennas. The covers also had the effect of centralizing the probes in the borehole. The plastic covers were constructed from a plastic which had a relative dielectric permittivity of approximately 4 and their use increased the diameter of the antennas to 125 mm.

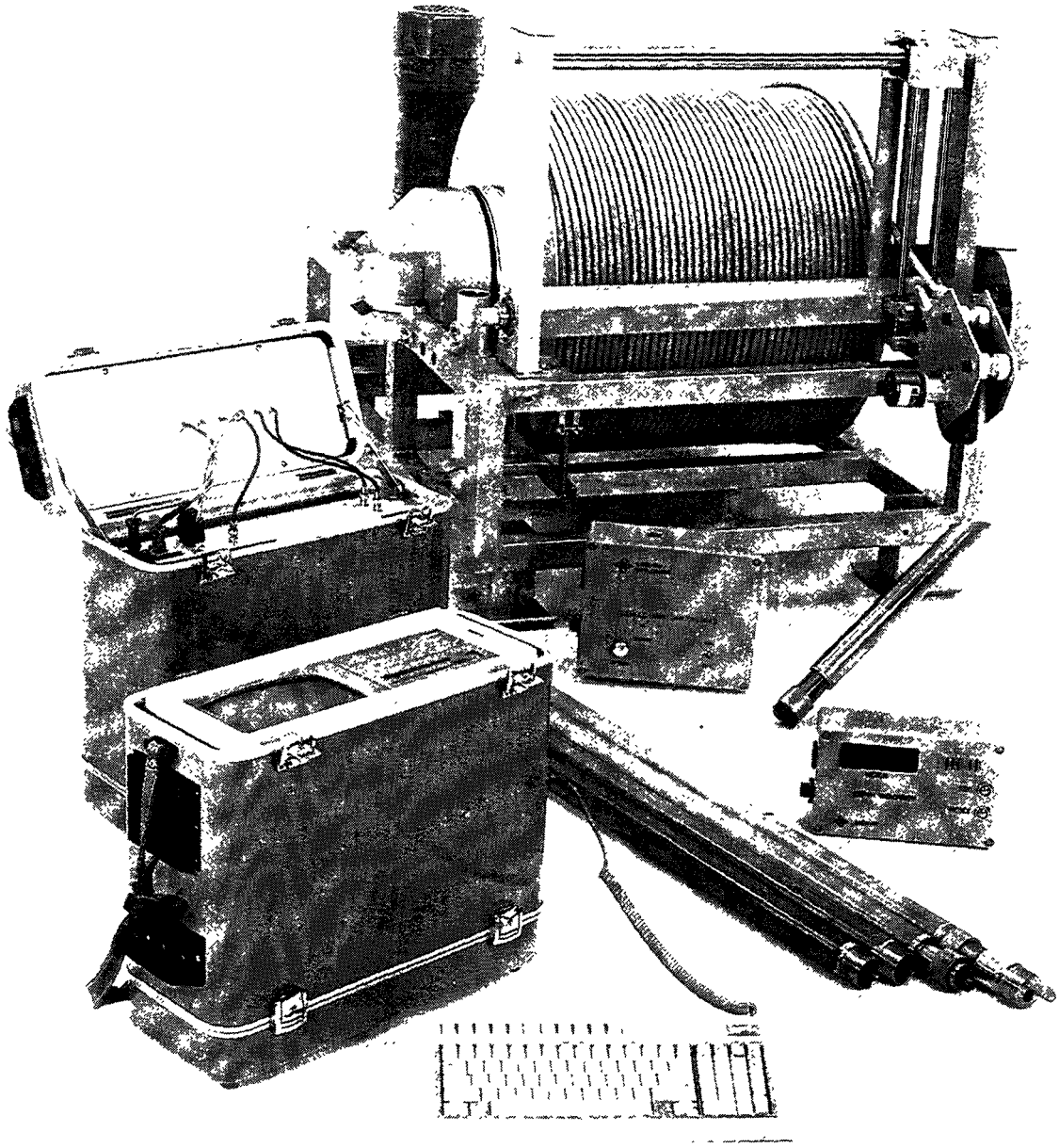

Plate 1 Components of the RAMAC borehole radar survey equipment

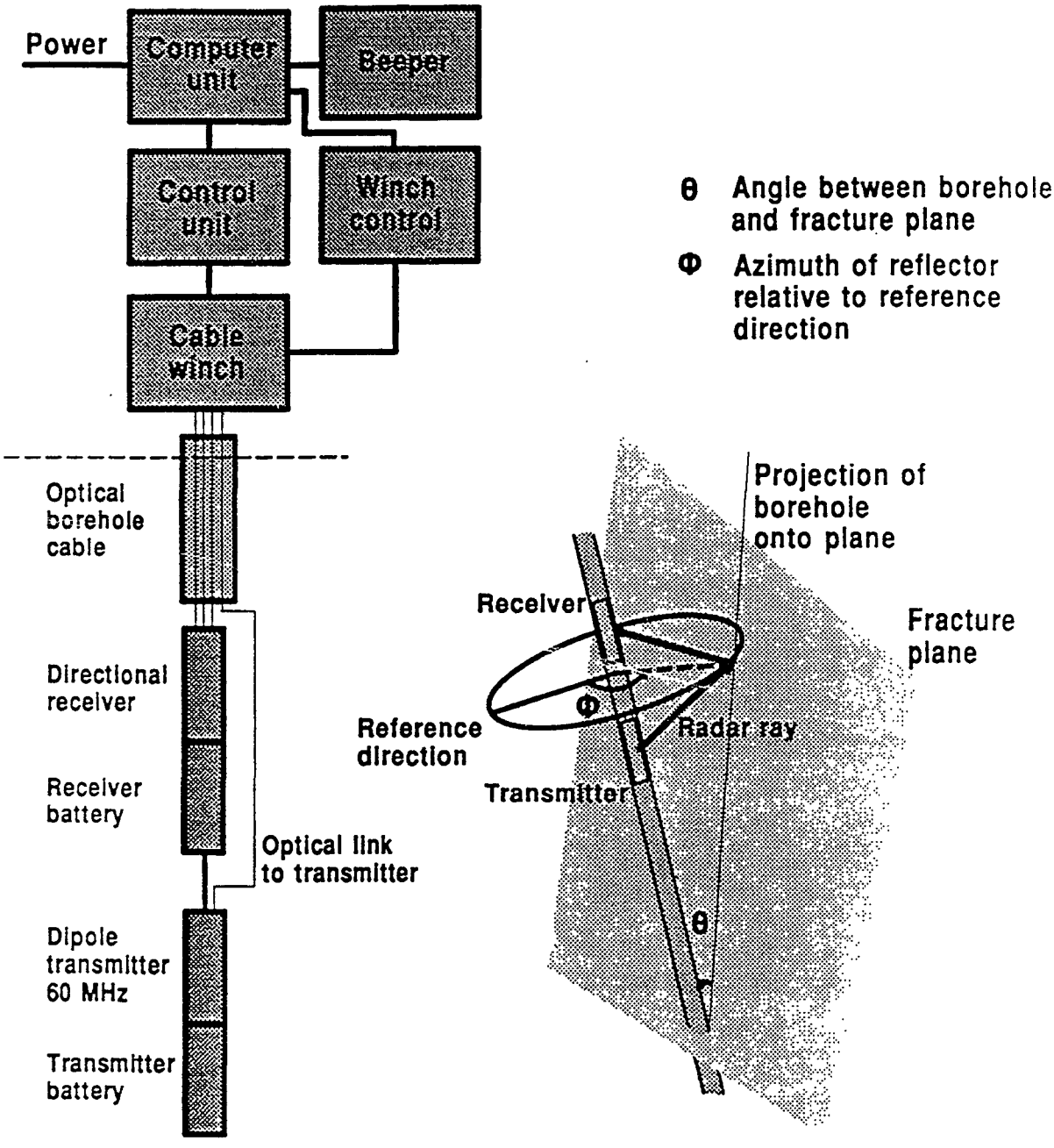

Figure 3-1 Schematic diagram of the components of the RAMAC directional borehole radar system and principles of operation.

4. SURVEY DESIGN

The borehole radar survey was designed to be a trial of the equipment, methodologies and processing techniques to determine the applicability of such surveys to the detection and delineation of fractures and fracture systems at distance from the borehole. Furthermore, the survey was designed to determine the range and resolution of the system and to assess the systems applicability for further single hole radar reflection surveys and cross-hole surveys. The objectives of the borehole radar trial are presented fully in Section 2.

The survey was designed as a trial as there was uncertainty over the likely success of a borehole radar survey due to the high salinity of the groundwaters within the BVG at Sellafield.

During the survey design phase it was established that the survey would be conducted using two methodologies:

- an omni-directional survey using a 22 MHz transmitter frequency and
- an additional directional survey using a 60 MHz transmitter frequency.

the surveys would be undertaken over the section of the borehole which was within the Borrowdale Volcanic Group (BVG) 576.5 - 1010 metres below Rotary Table (mbRT).

The 22 MHz omni-directional survey data would strongly support the data from the directional survey, allowing for any weak reflections at maximum ranges to be interpreted with greater confidence.

The spacing, or increment, between survey measurement points is a compromise between structural resolution and cost efficiency but in general a close spacing between measurement points is required with higher transmitted frequencies. Consequently measurement intervals were designed to be 1.0 metre for the 22 MHz omni-directional survey and 0.5 metre for the 60 MHz directional survey as it was anticipated that a higher resolution would be obtained with the 60 MHz systems than the 22 MHz systems. Additional spacings were evaluated but it was considered that greater spacings could lead to angle aliasing of reflectors and in extreme cases reflectors may not be resolved due to a lack of continuity, whilst smaller increments which might lead to an enhancement of reflector continuity would increase the survey time and it was considered that the spacings selected represented the optimum intervals.

Other acquisition parameters including the spacing between the transmitter and receiver antennas, sampling frequency, signal position, number of samples and the number of stacks required would be determined on site.

The acquisition of an additional omni-directional survey using a 60 MHz frequency was considered, during the design phase, to be an optional survey element. The decision whether to run this element of the survey would be a site based operational decision made on the basis of the quality of the data acquired by the 22 MHz survey.

4.1 Borehole Radar Survey

The borehole radar survey was conducted in Borehole 7A at Sellafield and consisted of four main acquisition elements, which were:

- velocity determination runs
- 22 MHz Omni-directional Survey
- 60 MHz Omni-directional Survey
- 60 MHz Directional Survey.

The acquisition elements were essentially as designed with the inclusion of the optional 60 MHz omni-directional survey and velocity determination runs which form an integral part of the survey.

The quality of the data acquired with the 22 MHz omni-directional survey was such that it made it necessary to acquire data using the 60 MHz omni-directional transmitter, this will be discussed in Section 5.

Each acquisition element of the survey was preceded by surface testing and function checks to ensure that the radar equipment was functioning correctly.

The survey were designed such that all data acquisition would be confined to the section of the borehole which was entirely within the Borrowdale Volcanic Group. However, an on site decision was made to include, within the survey interval, the Carboniferous Limestone and a section of the Brockram which would allow a comparison to be made of the range and resolution within different lithostratigraphic units.

5. DATA ACQUISITION

5.1 Introduction to the Data Acquisition Runs

The survey was undertaken between 16 January 1993 and the 19 January 1993 by personnel from ABEM GeoScience, Målå, Sweden and Conterra AB, Uppsala, Sweden.

The on-site survey work undertaken in Borehole 7A was sub-divided into four distinct elements as listed below:

1. Velocity Determination Runs
2. 22 MHz Omni-directional Survey
3. 60 MHz Omni-directional Survey
4. 60 MHz Directional Survey

Before any of the survey elements were undertaken the time base constant of the system was determined and a functional test of the 60 MHz omni-directional system was undertaken, both of which were performed on surface.

Preceding each survey element surface testing and function checks were conducted to ensure that the radar equipment was functioning correctly and these are briefly discussed in the following sections. Surface testing and downhole checks were also conducted at times during some of the survey elements as a consequence of the antenna encountering 'obstructions' and due to equipment malfunctions.

A summary of the acquisition runs forming the radar survey is presented in the following table and each survey element is discussed in the following sub-sections. All depths quoted have been corrected to rotary table and are given in terms of mbRT (metres below Rotary Table), unless otherwise stated. The survey intervals relative

to the top of the casing, used as a datum during the survey, at a height of 1.61 metres above ground level and 4.54 mbRT, the depth correction and survey intervals relative to rotary table are presented as a table in Appendix A. The relevant trace numbers for each run, antenna array length, antenna separation and the distance to the measurement point from the top of array are also presented in the table in Appendix A.

Run No.	Date	Description	Survey Interval mbRT
1	16 Jan 93	Time base determination	surface
2	16 Jan 93	System Function Test 60 MHz omni-directional system	surface
3	16 Jan 93	i) Determine depth accuracy of winch and control system ii) Preliminary assessment of radar range iii) 1st Velocity Determination run 2nd Velocity Determination run 3rd Velocity Determination run	443.14 - 452.14 508.14 - 608.14 708.14 - 733.14 711.14 - 735.14 709.14 - 733.64
4	17 Jan 93	System Function Test, 22 MHz omni-directional system	surface
5	17 Jan 93	22 MHz omni-directional survey	519.78 - 958.78
6	17 Jan 93	60 MHz omni-directional survey. (equipment malfunction)	517.64 - 753.64
7	17 Jan 93	60 MHz omni-directional survey (equipment malfunction)	742.64 - 863.14
8	18 Jan 93	60 MHz omni-directional survey (equipment malfunction)	742.64 - 749.64
9	18 Jan 93	60 MHz omni-directional survey	743.08 - 956.08
10	18 Jan 93	System Function Check, 60 MHz directional system	surface
11	18 Jan 93	60 MHz directional survey	518.80 - 598.80
12	19 Jan 93	System Function Check, 60 MHz directional system	surface
13	19 Jan 93	60 MHz directional survey	i) 648.80 - 768.80 ii) 840.80 - 875.80 iii) 890.80 - 918.80 iv) 943.80 - 954.80

5.2 Preliminary Function Test Runs

5.2.1 Time Base Determination - Run 1

Prior to conducting any of the acquisition runs it was necessary to determine the time base of the system.

The time base determination formed Run 1 of the survey and the specification for this run is given in Table 5-1.

Site	Sellafield	Date	16 January 1993
Borehole	7A	Hole diameter	159 mm
Purpose	Time base determination		
Sampling frequency Signal position	1034.14 MHz 0.6847 μs	Number of samples Number of stacks	512 128
Trace 1-5 6-11	Distance between Transmitter and Receiver Short fibre Optical fibre added with length of 29.10 m		10m

Table 5-1. Specifications for borehole radar Run 1.

The time base was determined by measuring the time it takes for light to propagate a known distance in an optical fibre. The speed of light in the optical fibre used was 201 m/μs (this is a quantity determined and provided by the supplier of the optical fibre). The measurements were performed by placing both the transmitter and receiver vertically on the ground 10 metres apart and recording the arrival of the direct wave using, in the first instance a short optical fibre and then by adding an optical fibre 29.10 metres in length. The delay in arrival time resulting from the propagation of the direct wave in the additional length of optical fibre is used to calculate the time base of the system. The time base was determined to be 9.188 μsec.

A plot of the recorded traces is given in Figure 5-1

5.2.2 System Function Test 60 MHz Omni-directional System - Run 2

A system function test of the 60 MHz omni-directional system was undertaken before any data was acquired for the velocity determination runs and these tests comprised Run 2 of the survey. The system function test was performed by placing the borehole probes vertically on the ground surface and measuring the received signal for three different distances, 10, 20 and 30 metres, between the transmitter and receiver.

The specifications for this system test are given in Table 5-2 below.

Site	Sellafield	Date	16 January 1993
Borehole	7A	Hole diameter	159 mm
Purpose	Functional check of 60 MHz omni-directional system		
Sampling frequency Signal position	1034.14 MHz 0.8000 μs	Number of samples Number of stacks	512 128
Trace 1-5 6-10 11-15	Distance between Transmitter-Receiver 10 m 20 m 30 m		

Table 5-2. Specifications for borehole radar Run 2.

5.3 Velocity Determination Runs

The velocity determination runs (Run 3) were undertaken on the 16 January 1993 using the 60 MHz omni-directional radar system. In total Run 3 was composed of five sub-runs which were undertaken principally to determine the velocity of propagation of electro-magnetic pulses generated by the radar system within the Borrowdale Volcanic Group (BVG).

Run 3 was, however, also used to determine the depth accuracy of the control system and winch and to assess the radar range within the various litho-stratigraphic units represented within the borehole. The specifications for these runs are presented in Table 5-3.

Site	Sellafield	Date	16 January 1993
Borehole	7A	Hole diameter	159 mm
Purpose	Determination of radar velocity in the BVG. Check of radar performance in different litho-stratigraphic units. Control of depth recording system.		
System	60 MHz omni-directional		
Sampling frequency Signal position Depth increment	1034.14 MHz 0.6847 μs 0.5 m	Number of samples Number of stacks	512 128 256(*)
Trace 1-19 21-223 250-300 301-350(*) 351-400	Depth interval (mbRT) 443.14-452.14 508.14-608.14 708.14-733.14 711.14-735.14(*) 709.14-733.64	Antenna Separation (metres) 5.9 5.9 5.9 11.9(*) 7.9	

Table 5-3. Specifications for borehole radar Run 3.

A summary of the five component runs of Run 3 is presented below.

Run No.	Description	Survey Interval mbRT
3	i) Determine depth accuracy of winch and controlsystem	443.14 - 452.14
	ii) Preliminary assessment of radar range	508.14 - 608.14
	iii) 1st Velocity determination run	708.14 - 733.14
	iv) 2nd Velocity determination run	711.14 - 735.14
	v) 3rd Velocity determination run	709.14 - 733.64

The first run was undertaken over the depth range 443.14 - 452.14 mbRT, covering the bottom of the casing, in order to determine the depth accuracy of the depth control system and the winch. A 2 metre spacer rod was used between the receiver and transmitter, equivalent to an antenna separation of 5.9 metres. Measurements were made with an increment of 0.5 metre and were recorded as traces 1-19.

As the metallic casing effectively attenuates all radar signals it would be expected that a radar signal should only be received when both antenna are below the casing. Figure 5-2 shows the amplitude of the direct wave as a function of borehole depth (mbRT) for the interval at the casing shoe and the corresponding radar map is shown as Figure 5-3.

From Figure 5-2 it is clear that the amplitude of the direct wave begins to increase at a depth of 445.2 mbRT and reached a maximum amplitude at a depth of 446.7 mbRT which represents the position of the mid point between the antennas. Therefore, the centre of the receiver antenna, which is at the top of the down hole array, was at 443.8 mbRT. The casing was known to have been set to a depth of 444.7 mbRT and therefore the depth reading of the system is under reading by 0.9+/- 0.5m at a depth of approximately 445 mbRT. The range in the error estimate is a consequence of the finite length of the receiver antenna (0.91m) and the 0.5m interval between measurement points.

The second run, covering the depth interval 508.14 - 608.14 mbRT, was undertaken to assess the radar range within the different litho-stratigraphic units represented within the borehole. The surveyed interval encompassed a section of the Brockram, the Carboniferous Limestone and a section of the Borrowdale Volcanic Group (BVG). A 2 metre spacer rod was used between the receiver and transmitter, equivalent to an antenna separation of 5.9 metres. Measurements were made with an increment of 0.5 metre and were recorded as traces 21-223.

The radar map from this part of the survey is shown in Figure 5-4. A large amplitude direct wave and several reflections from discontinuities were observed within the Carboniferous Limestone (523.5 to 576.5 mbRT). Within the top of the BVG no signal was recorded, and it was assumed that this was a consequence of the low resistivity of the formation. In the Brockram a small amplitude direct wave was observed within a 7 metre interval above the limestone but no signal was recorded over the interval 508 to 516 mbRT.

The final three components of Run 3 were run to determine the radar velocity within the BVG. The propagation velocity is normally determined from cross-hole or borehole to surface measurements. However, measurements of these types could not be performed as no other borehole, which was deep enough, was located close to Borehole 7A and this prevented a cross-hole determination and a borehole to surface determination was not possible as a consequence of the depth of the BVG below surface and the overlying cover sequences.

For this survey the velocity was determined by undertaking three runs over essentially the same, approximately 25 metre section of the borehole, within the BVG, with different transmitter (TX) - receiver (RX) separations for each run, as detailed below:

i) TX - RX separation 5.9 metres (2 metre spacer rod)
ii) TX - RX separation 11.9 metres (8 metre spacer rods)
iii) TX - RX separation 7.9 metres (4 metre spacer rods)

The selected test interval was located between 710 to 735 mbRT, this interval was selected on the basis of the available wireline resistivity logs. The radar maps from the three runs are presented in Figures 5-5 to 5-7.

The first run covered the interval 708.14 - 733.14 mbRT, the second covered the interval 711.14 - 735.14 mbRT and the third covered the interval 709.14 - 733.64

mbRT. All measurements were made with an increment of 0.5 metres.

Problems were encountered during these runs when 'obstructions' were encountered at approximately 573, 637 and 643 metres below top of casing. The radar antenna passed these points after several attempts and it was considered that these 'obstructions' possibly resulted from a change in the diameter of the borehole or a slight deviation of the borehole.

5.4 22 MHz Omni-directional Survey

Prior to undertaking the 22 MHz omni-directional survey (Run 5) a system function test was conducted (Run 4).

5.4.1 System Function Test 22 MHz Omni-directional System - Run 4

A system function test of the 22 MHz omni-directional system was undertaken prior to the acquisition of any downhole data. The system function test was performed by placing the borehole probes vertically on the ground surface and measuring the received signal for three different distances of 20, 30 and 40 metres between the transmitter and receiver.

The specifications for this system test are given in Table 5-4 below.

Site	Sellafield	Date	17 January 1993
Borehole	7A	Hole diameter	159 mm
Purpose	Functional check of 22 MHz omni-directional system		
Sampling frequency Signal position	499.29 MHz 1.4416 μs	Number of samples Number of stacks	512 64
Trace 1-5 6-10 11-15	Distance between Transmitter-Receiver 20 m 30 m 40 m		

Table 5-4. Specifications for borehole radar Run 4.

5.4.2 22 MHz Omni-directional Survey - Run 5

The 22 MHz omni-directional survey (Run 5) was undertaken on 17 January 1993 and covered the depth range 519.78 - 958.78 mbRT. This survey was undertaken in an attempt to obtain maximum range within the BVG. Based on the good results within the Carboniferous Limestone obtained during Run 3 this stratigraphical unit was included in Run 5. The specifications for this run are given in Table 5-5 below.

Site	Sellafield	Date	17 January 1993
Borehole	7A	Hole diameter	159 mm
Purpose	Data acquisition, 22 MHz omni-directional system		
Sampling frequency Signal position Depth increment Correction to mbRT Antenna separation	356.67 MHz 1.5136 μs 1.0 m 9.78 m 7.39 m	Number of samples Number of stacks Measurement point from top of system	512 128 5.24 m
Trace 1-440	Depth interval (mbRT) 519.76-958.76		

Table 5-5. Specifications for borehole radar Run 5.

An obstruction was encountered at 958.78 mbRT, equivalent to 965.79 mbRT (to base of the radar tool) and the survey terminated at this depth. Measurements were made at 1 metre intervals and a 2 metre spacer rod was used between the transmitter and receiver, which is equivalent to an antenna separation of 7.39, the data was recorded as traces 1 - 440. The radar maps from this phase of the survey are shown as Figures 5-8 to 5-12.

The results showed that where a signal was recorded it appeared to be dominated by a guided wave propagating within the borehole reflected from discontinuities within the radar antenna. These were represented by oscillations (ringing) in the radar maps in all sections of the borehole. The reflected wave arrived with opposite phase, approximately 0.37 μs after the first arrival which corresponds to a propagation distance of the order of 12.3 metres if the velocity of propagation in water (33 m/μs) is assumed. This propagation distance is approximately twice the transmitter-receiver antenna separation which implies that the wave is most probably a guided wave which is reflected at the antennas due to the impedence contrast resulting from the plastic covers over the antennas.

Within the radar maps presented (Figures 5-8 to 5-12) reflectors are not observed.

5.5 60 MHz Omni-directional Survey - Runs 6 to 9

The 60 MHz omni-directional survey conducted in Borehole 7A was performed to obtain data with a better resolution than that anticipated from the 22 MHz omni-directional survey.

The 60 MHz omni-directional survey commenced on 17 January 1993 (Run 6) and was completed on 18 January 1993 (Run 9) following equipment malfunctions. The designed survey interval was identical to that for the 22 MHz omni-directional survey. Prior to the survey being conducted function checks and surface tests were carried out

which showed the equipment to be functioning correctly.

The specifications for Run 6 are given in Table 5-6 below.

Site	Sellafield	Date	17 January 1993
Borehole	7A	Hole diameter	159 mm
Purpose	Data acquisition, 60 MHz omni-directional system		
Sampling frequency Signal position Depth increment Correction to mbRT Antenna separation	820.2 MHz 0.6847 μs 0.5 m 7.64 m 4.89 m	Number of samples Number of stacks Measurement point from top of system	512 128 3.10 m
Trace 11-474	Depth interval (mbRT) 517.64-749.14		

Table 5-6. Specifications for borehole radar Run 6.

The radar antenna array was assembled using a 0.5 metre spacer rod, equivalent to an antenna separation of 4.89 metres. The survey started at a depth of 517.64 mbRT (Run 6) with measurements being made at 0.5 metre intervals. At a depth of 749.14 mbRT it was apparent that a direct radar pulse was not being recorded and that a malfunction had occurred. Therefore the radar antenna array was pulled out of the hole. Inspection suggested that the malfunction could have resulted from an obstruction in the optical fibre, and it was suggested that this may have been caused by damage to an 'O' ring. This was repaired and the radar antenna array was reassembled using a 0.5 metre spacer rod to continue the survey.

Following satisfactory surface system function checks the survey re-started (Run 7) at a depth of 742.64 mbRT with measurements being made at 0.5 metre intervals. At a depth of 863.14 mbRT it was noted that a direct radar pulse was not being recorded, suggesting that the radar transmitter was not functioning. The radar

antenna array was, therefore, pulled out of the hole and the survey was suspended.

Inspection of the optical fibre on the 18 January 1993 showed slight damaged which could have rendered the optical fibre pressure sensitive and this was replaced. The 60 MHz omni-directional radar antenna array was reassembled using a 0.5 metre spacer rod and tested at the surface, with all checks being satisfactory, prior to running in hole, to continue the survey from 742.64 mbRT (Run 8). At a depth of 749.64 mbRT it again appeared that the transmitter was not working, as a direct radar pulse was not being recorded, so the radar antenna array was pulled out of the hole.

The transmitter was replaced and the system was re-tested before running in hole. The replacement transmitter increased the antenna separation to 5.78 metres. The specifications for Run 9 are given in Table 5-7 below.

Site	Sellafield	Date	18 January 1993
Borehole	7A	Hole diameter	159 mm
Purpose	Data acquisition, 60 MHz omni-directional system		
Sampling frequency Signal position Depth increment Correction to mbRT Antenna separation	820.2 MHz 0.5766 μs 0.5 m 8.08 m 5.78 m	Number of samples Number of stacks Measurement point from top of system	512 128 3.54 m
Trace 11-438	Depth interval (mbRT) 743.08-956.08		

Table 5-7. Specifications for borehole radar Run 9.

The survey recommenced at 743.08 mbRT (Run 9) with measurements being made at 0.5 metre intervals and continued to a depth of 956.08 mbRT where an obstruction was encountered at an equivalent depth of 963.29 mbRT (to base of radar). The radar was then pulled out of the hole.

The data acquired for these runs after correction of the DC-level shift are shown in Figures 5-13 to 5-18. In these figures reflections are evident only within the Carboniferous Limestone section of the borehole. In the parts of the BVG where a measurable direct wave is detected no clear reflections are observed.

As the 60 MHz omni-directional survey of Borehole 7A was performed in two runs using two different transmitters a small difference in the amplitude can be observed between the results from the two surveys. The somewhat smaller amplitude in the second run was a consequence of the change of transmitter, which resulted in a larger transmitter-receiver spacing for Run 9.

It is evident from the raw data plots that detectable radar signals are observed only in certain intervals of the borehole. A simple measure of the quality of the radar signal is the amplitude of the direct wave which propagates along the borehole. Figure 5-19 shows the peak-to-peak amplitude of the direct wave as a function of borehole depth for the 60 MHz omni-directional antenna. Borehole intervals with relatively large radar amplitudes are found in the interval 523.5-576.5 mbRT which corresponds to the Carboniferous Limestone. Within the BVG relatively large radar amplitudes were obtained between 688 and 768 mbRT. There are also a number of shorter intervals with measurable radar amplitudes between 844 mbRT and 956 mbRT.

5.6 60 MHz Directional Survey - Runs 11 and 13

The 60 MHz directional survey commenced on 18 January 1993 and was completed on 19 January 1993.

Before undertaking the 60 MHz directional survey the transmitter and receiver equipment were set up for surface system function checks and directional sensor checks. The system function test of the 60 MHz directional system was performed

by placing both borehole probes vertically on the ground surface and measuring the received signal. The surface testing (Run 10) revealed a problem with the optical connections in the directional receiver. This was repaired and re-tested before undertaking additional directional sensor checks. The directional sensor checks were performed to ensure that the directional sensor correctly measured the orientation of the incoming radiation, this was accomplished by placing the transmitter in four different directions relative to the receiver. The transmitter was placed 15 metres to the north, east, south and west of the receiver, with both held vertically on the ground. The specifications for Run 10 are given in Table 5-8 below.

Site	Sellafield	Date	18 January 1993
Borehole	7A	Hole diameter	159 mm
Purpose	Functional check of 60 MHz directional system		
Sampling frequency Signal position	820.20 MHz 0.7208 μs	Number of samples Number of stacks	512 8
Distance between Transmitter-Receiver		15 m	
Trace 1-3 4-6 7-9 10-13	Transmitter location North East South West		

Table 5-8. Specifications for borehole radar Run 10.

During these tests strong winds prevailed making it impossible to keep the antennas in a fixed position. This compromised the quality of the results and although the directional sensors were found to be operating correctly the results could not be used further. Therefore the test was repeated on the following day, 19 January 1993. The antenna separation for this test was 10 metres and the results, which confirmed the correct function of the directional antenna system, formed Run 12. The specifications for Run 12 are presented in Table 5-9 below.

Site	Sellafield	Date	19-1-93
Borehole	7A	Hole diameter	159 mm
Purpose	Functional check of 60 MHz directional system		
Sampling frequency Signal position	820.20 MHz 0.5766 μs	Number of samples Number of stacks	512 32
Distance between Transmitter-Receiver		10 m	
Trace 1-10 11-20 21-30 31-40	Transmitter location North East South West		

Table 5-9. Specifications for borehole radar Run 12.

Based on the results of the 60 MHz omni-directional survey, discussed in Section 5.5, several zones were selected for surveying, as it was considered that in other intervals no information would be recorded due to the generally smaller signal amplitudes obtained with the directional survey equipment. The designed survey intervals are set out below, along with the actual depth intervals surveyed which were determined interactively by monitoring the real time screen display of the radar image.

Designed Survey Intervals mbRT		**Actual Survey Intervals mbRT**		**Run No.**
From	**To**	**From**	**To**	
518.80	598.80	518.80	598.80	11
648.80	773.80	648.80	768.80	13
833.80	878.80	840.80	875.80	13
890.80	920.80	890.80	918.80	13
943.80	955.80	943.80	954.80	13

Run 11 was undertaken on 18 January 1993 and covered the depth interval 518.80 - 598.80 mbRT. The radar antenna was assembled using a 0.5 metre spacer rod, equivalent to an antenna separation of 7.32 metres. Measurements were made at 0.5 metre intervals. The specifications for Run 11 are presented in Table 5-10 below.

Site	Sellafield	Date	18 January 1993
Borehole	7A	Hole diameter	159 mm
Purpose	Data acquisition, 60 MHz directional system		
Sampling frequency Signal position Depth increment Correction to mbRT Antenna separation	820.2 MHz 0.5766 μs 0.5 m 8.80 m 7.32 m	Number of samples Number of stacks Measurement point from top of system	512 128 4.26 m
Trace 1-161	Depth interval (mbRT) 518.80-598.80		

Table 5-10. Specifications for borehole radar Run 11.

The 60 MHz directional survey was completed on 19 January 1993, Run 13, which included the lower four designed survey intervals. The radar antenna was assembled using a 0.5 metre spacer rod, equivalent to an antenna separation of 7.32 metres. Measurements were made of 0.5 metre intervals. The specifications for Run 13 are presented in Table 5-11 below.

Site	Sellafield	Date	19 January 1993
Borehole	7A	Hole diameter	159 mm
Purpose	Data acquisition, 60 MHz directional system		
Sampling frequency Signal position Depth increment Correction to mbRT Antenna separation	820.2 MHz 0.5766 μs 0.5 m 8.80 m 7.32 m	Number of samples Number of stacks Measurement point from top of system	512 128 4.26 m
Trace 3-243 250-320 325-381 385-406	Depth interval (mbRT) 648.80-768.80 840.80-875.80 890.80-918.80 943.80-954.80		

Table 5-11. Specifications for borehole radar Run 13.

Figure 5-20 displays the checksum signal obtained from the directional antenna array which provides a quality control of the directional antenna data. The amplitude of this checksum signal is considerably smaller than the dipole signal (Figure 5-21) obtained from the directional antenna which confirms the proper functioning of the directional antenna array.

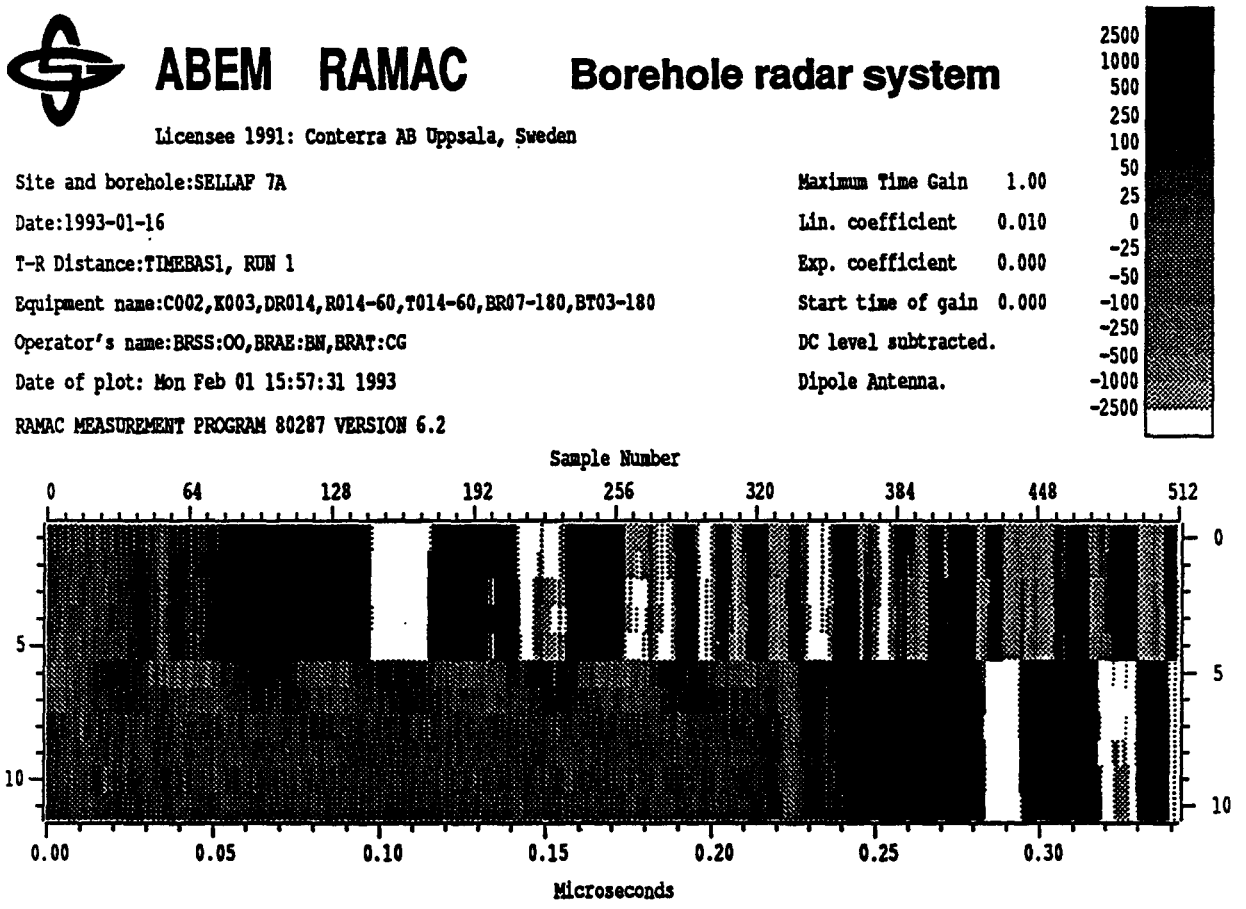

Figure 5-1 Data summary and plot of recorded traces for Run 1 - Time Base Determination

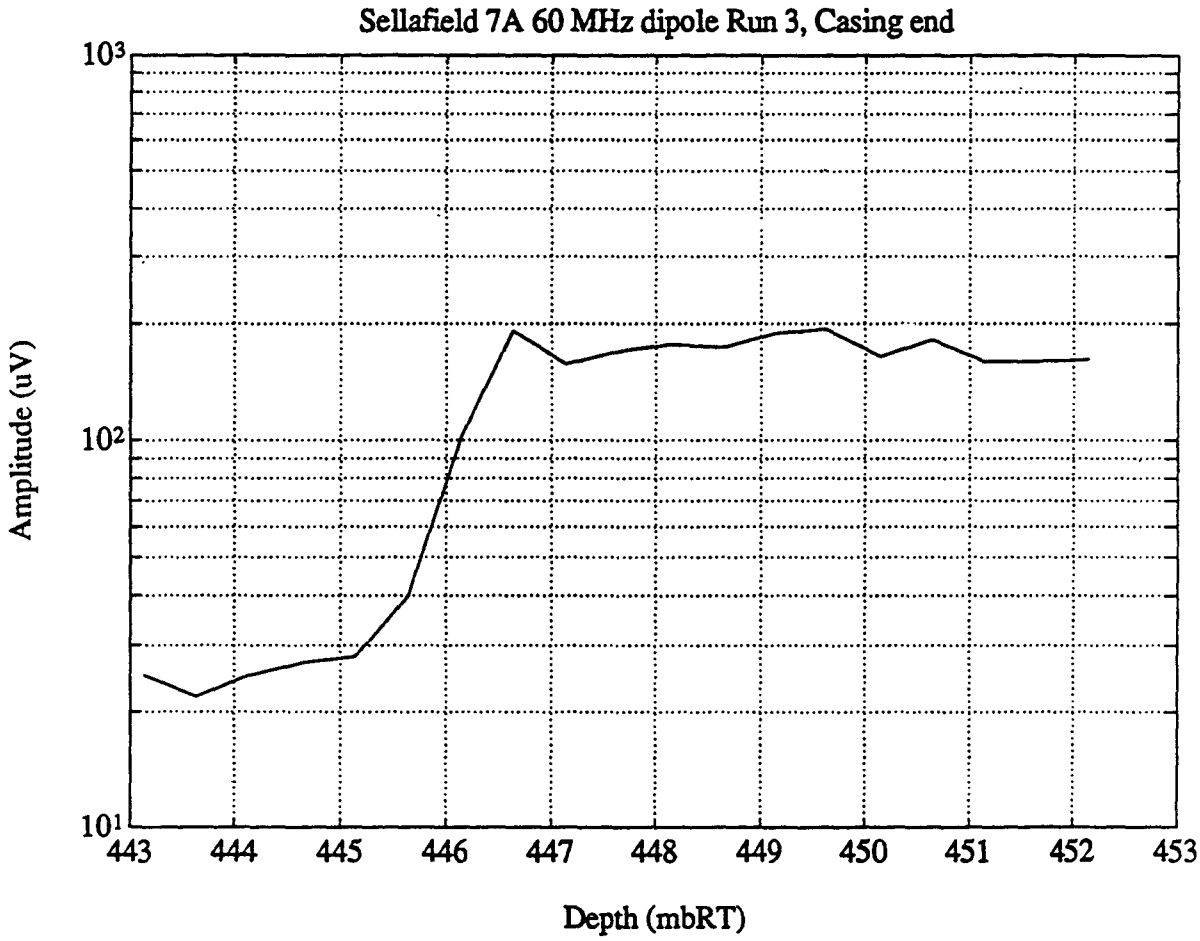

Figure 5-2 Peak to peak amplitude of the direct wave as a function of depth for an interval which includes the end of the casing (444.7 mbRT)

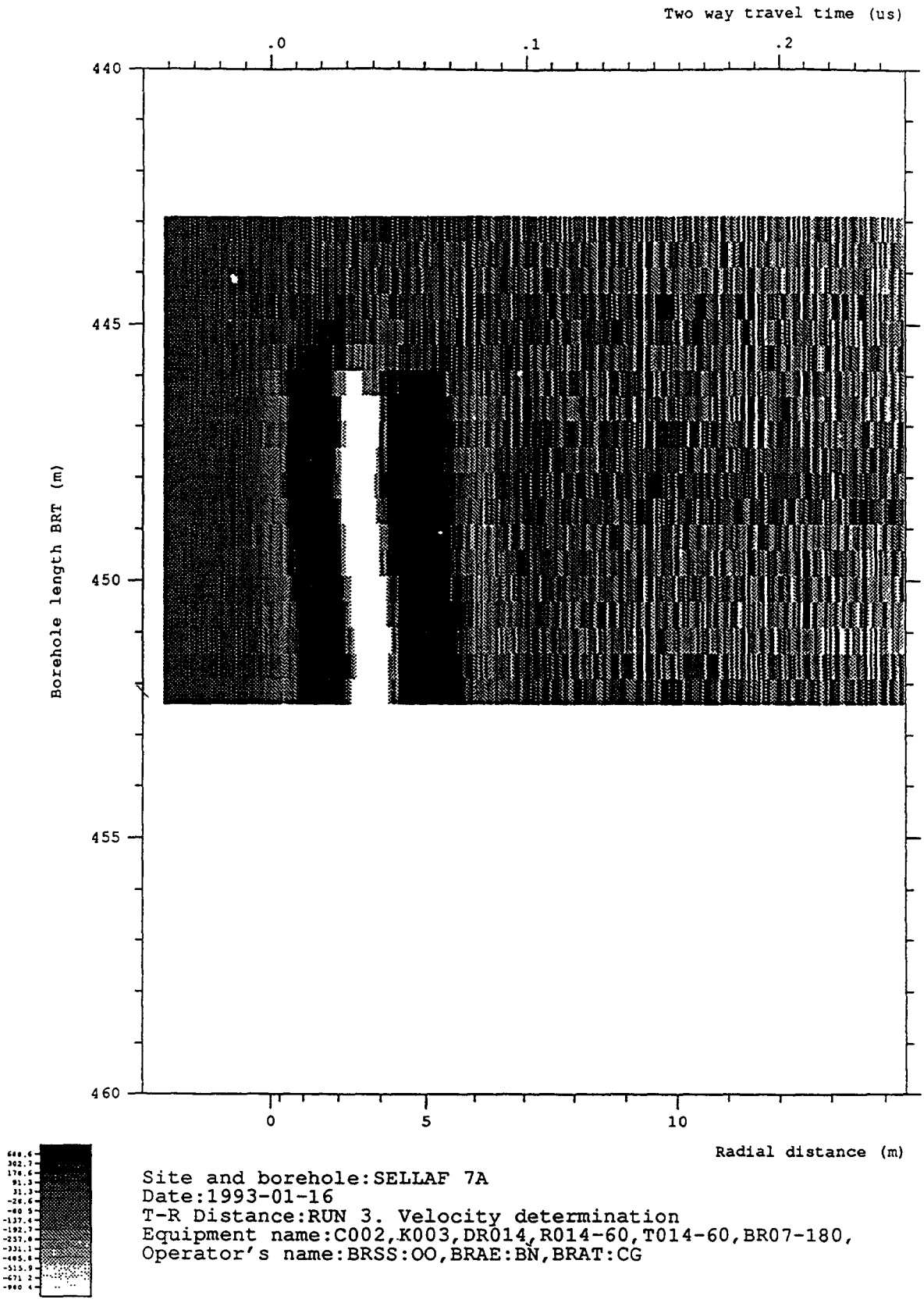

Figure 5-3 Radar map from Run 3i - Determination of depth accuracy and casing end

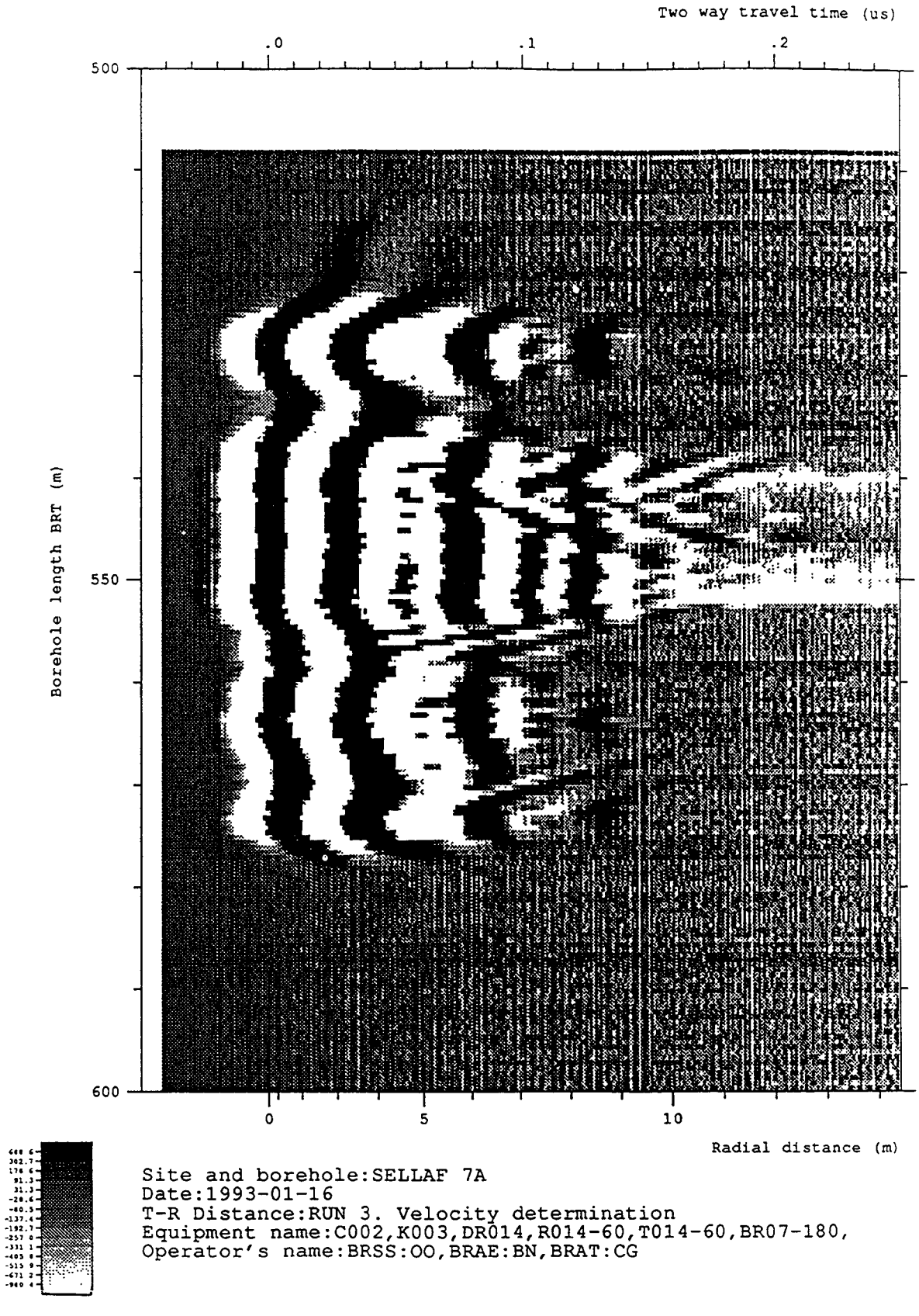

Figure 5-4 Radar map from Run 3ii - Preliminary assessment of radar range

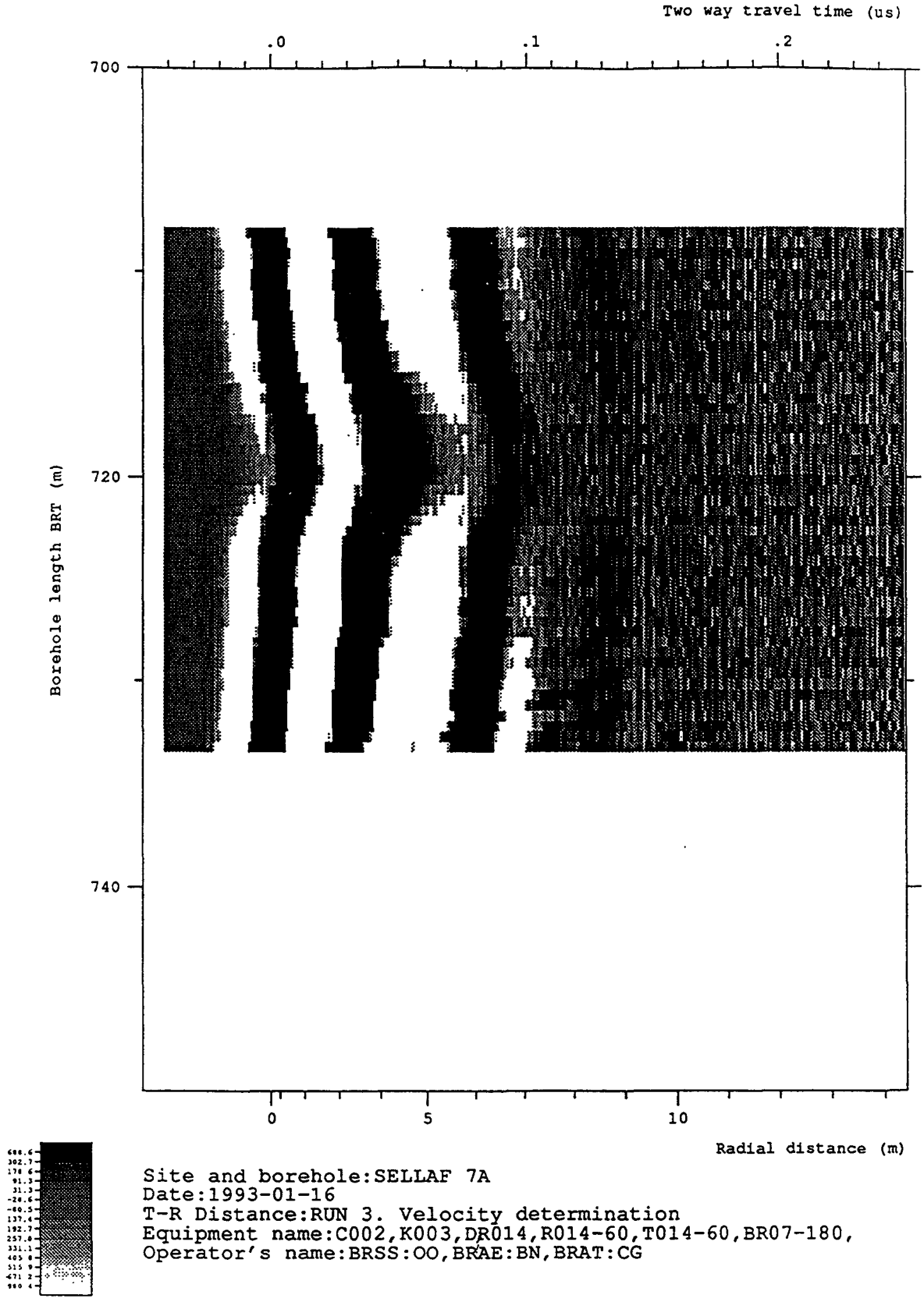

Figure 5-5 Radar map from Run 3iii first velocity determination run, transmitter to receiver separation 5.9 metres.

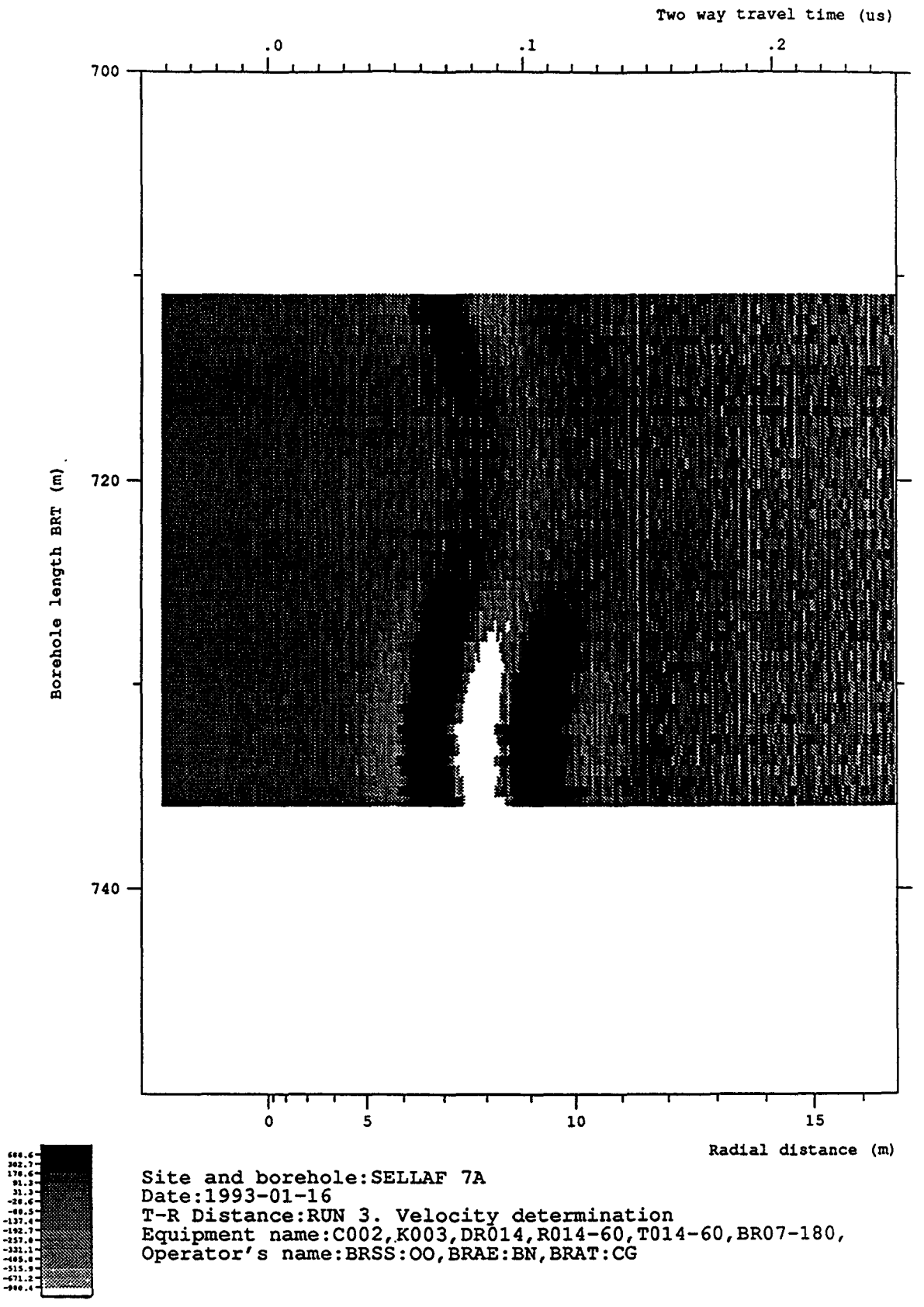

Figure 5-6 Radar map from Run 3iv second velocity determination run, transmitter to receiver separation 11.9 metres.

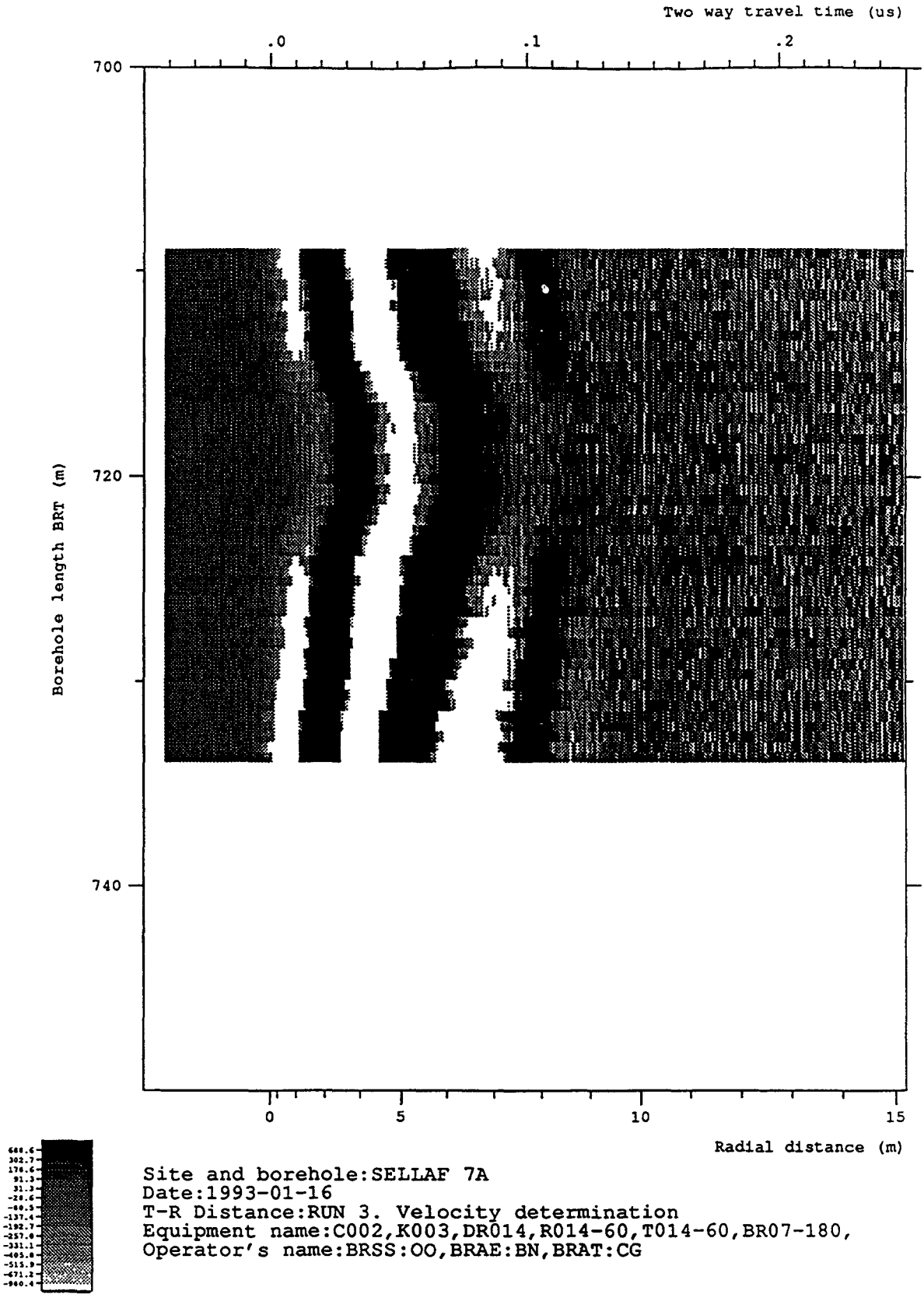

Figure 5-7 Radar map from Run 3v third velocity determination run, transmitter to receiver separation 7.9 metres.

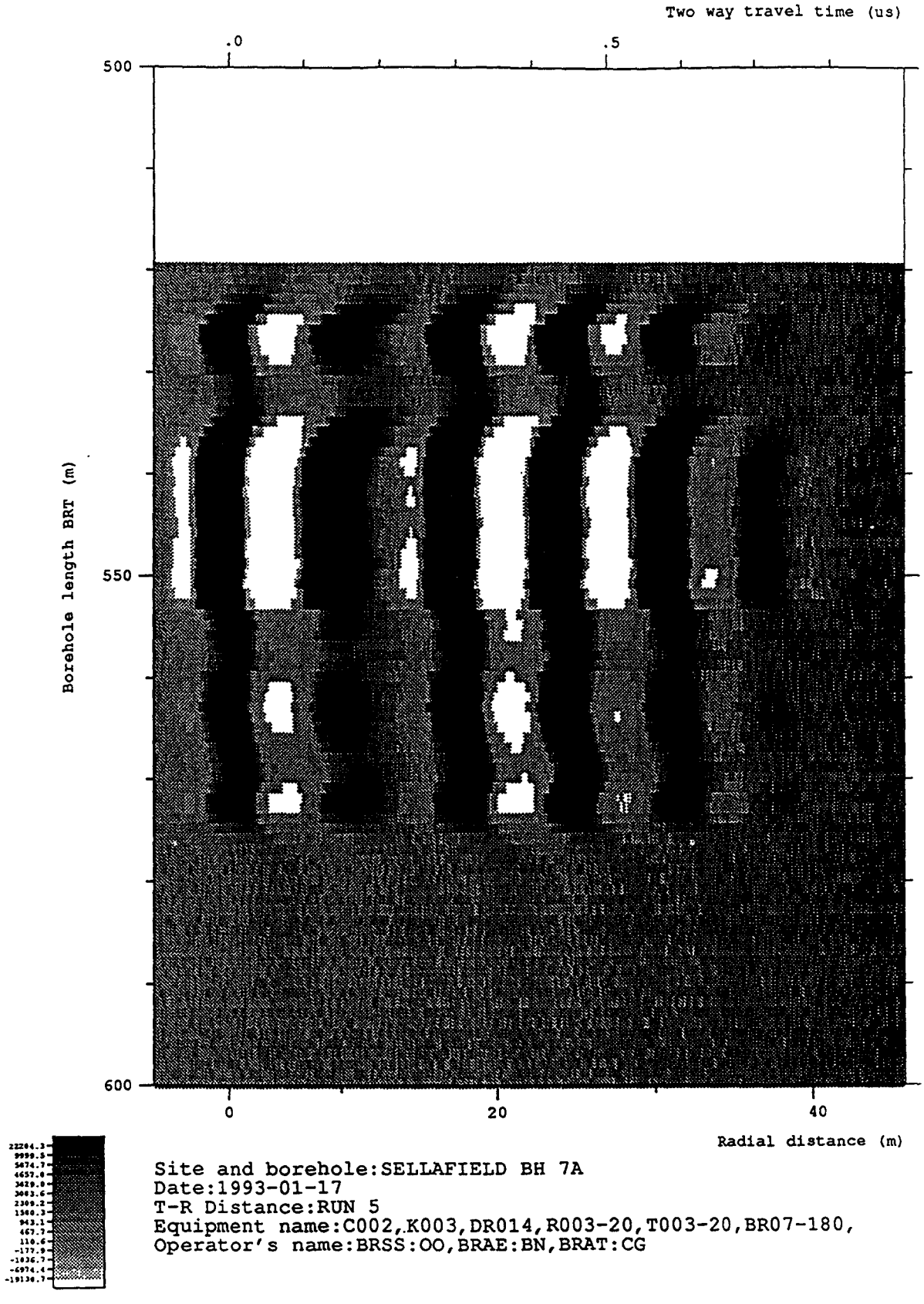

Figure 5-8 Radar map from Run 5, 22 MHz omni-directional survey (519.76 - 600.00 mbRT)

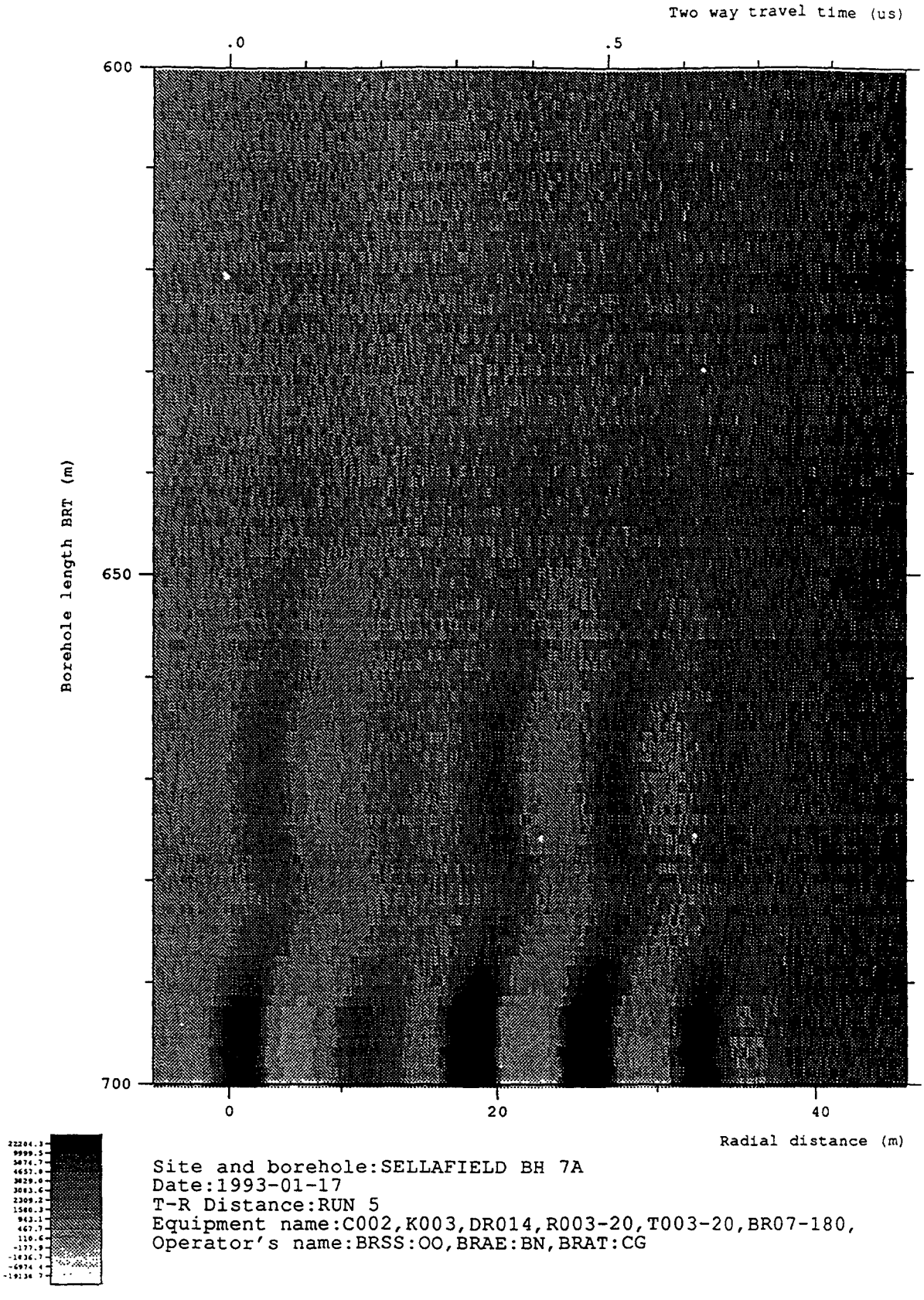

Figure 5-9 Radar map from Run 5, 22 MHz omni-directional survey (600.00 - 700.00 mbRT)

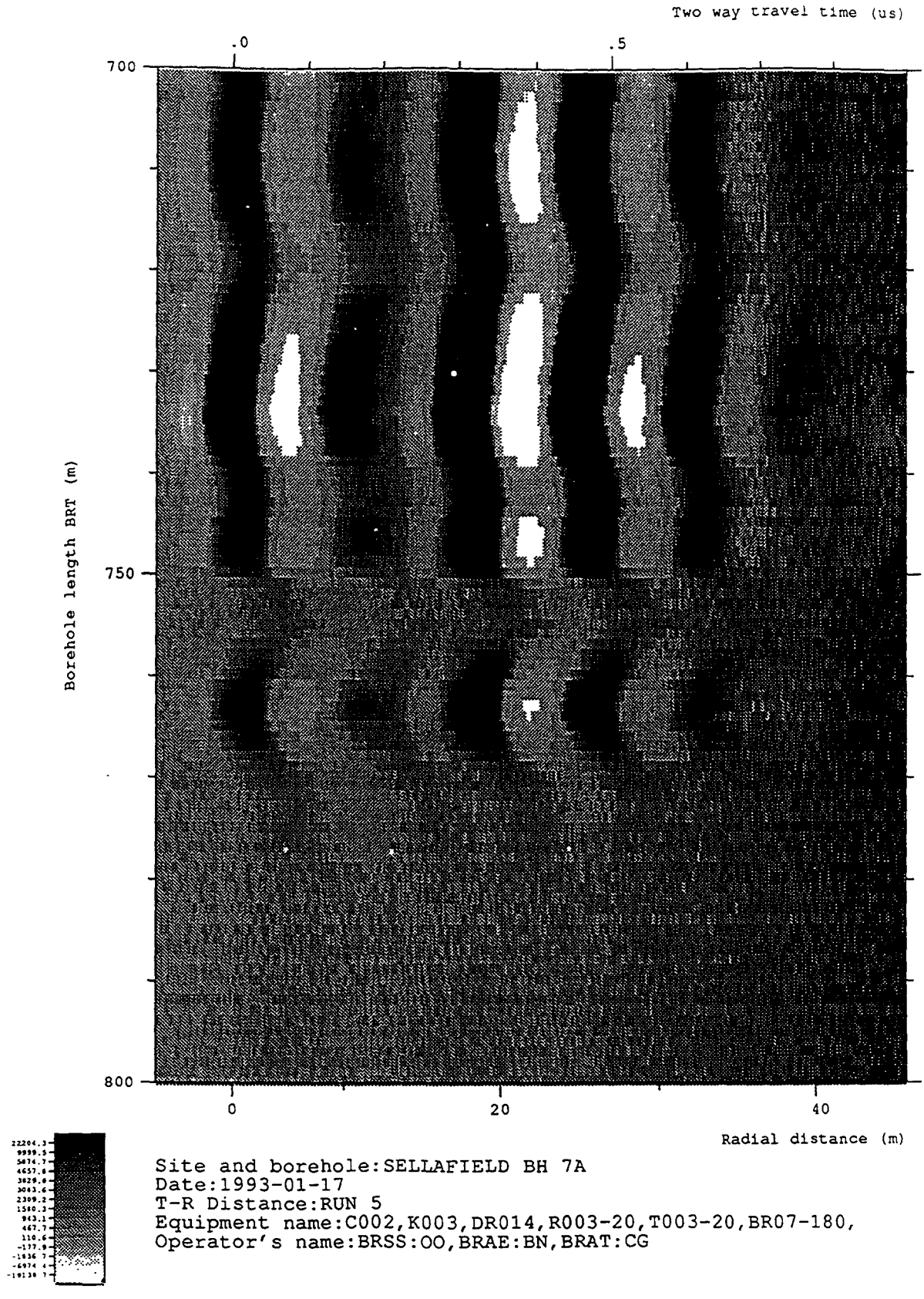

Figure 5-10 Radar map from Run 5, 22 MHz omni-directional survey (700.00 - 800.00 mbRT)

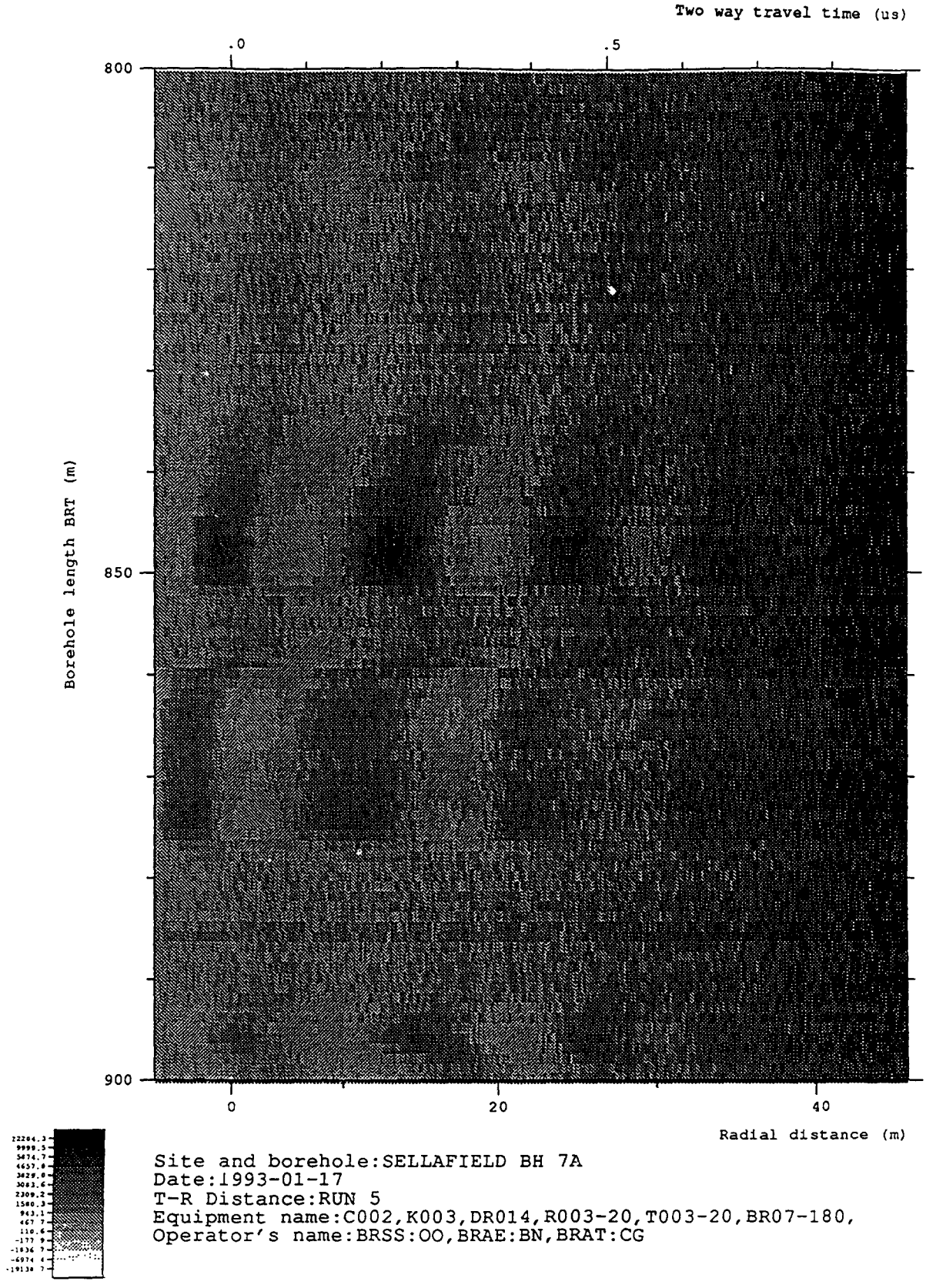

Figure 5-11 Radar map from Run 5, 22 MHz omni-directional survey (800.00 - 900.00 mbRT)

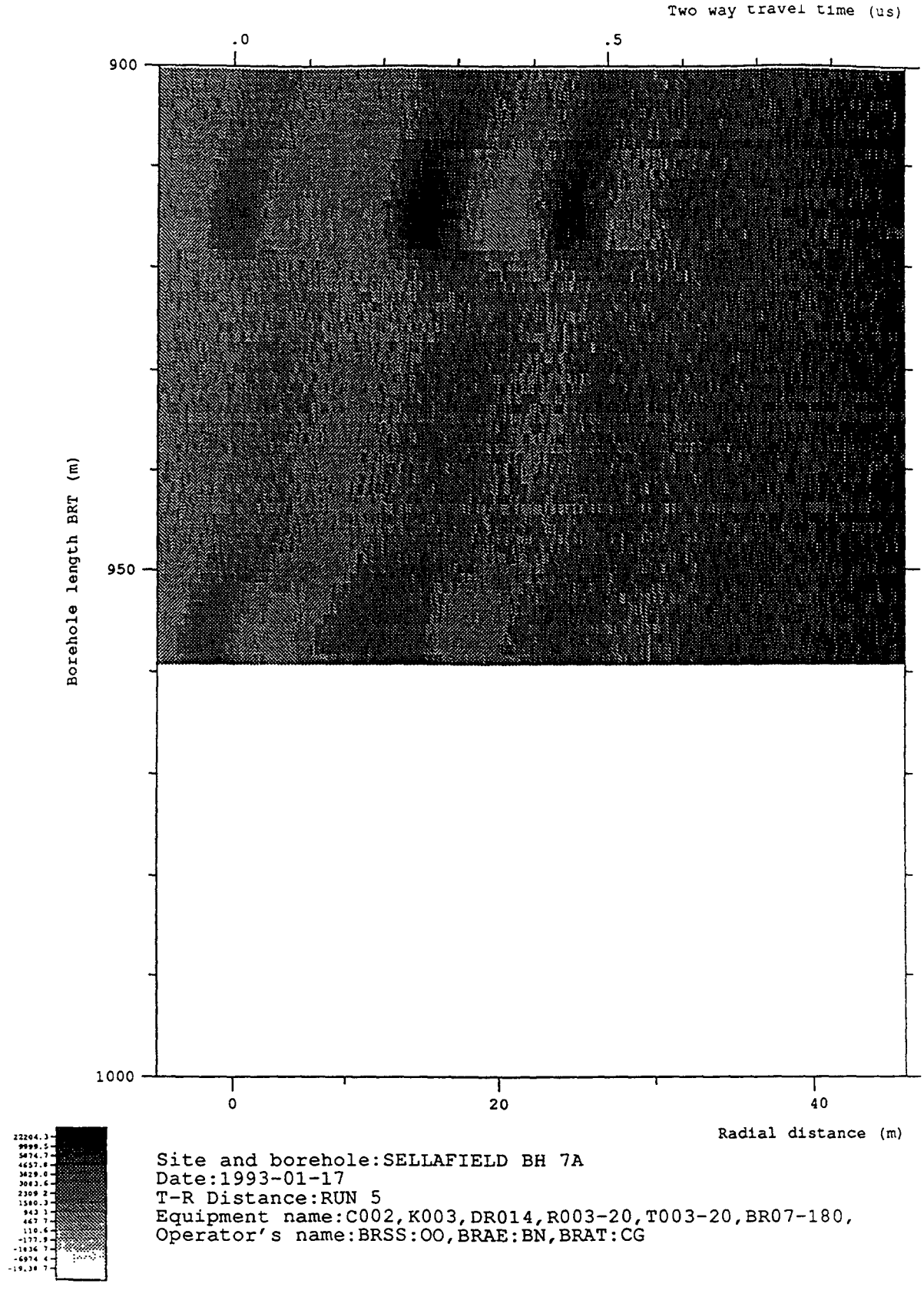

Figure 5-12 Radar map from Run 5, 22 MHz omni-directional survey (900.00 - 958.76 mbRT)

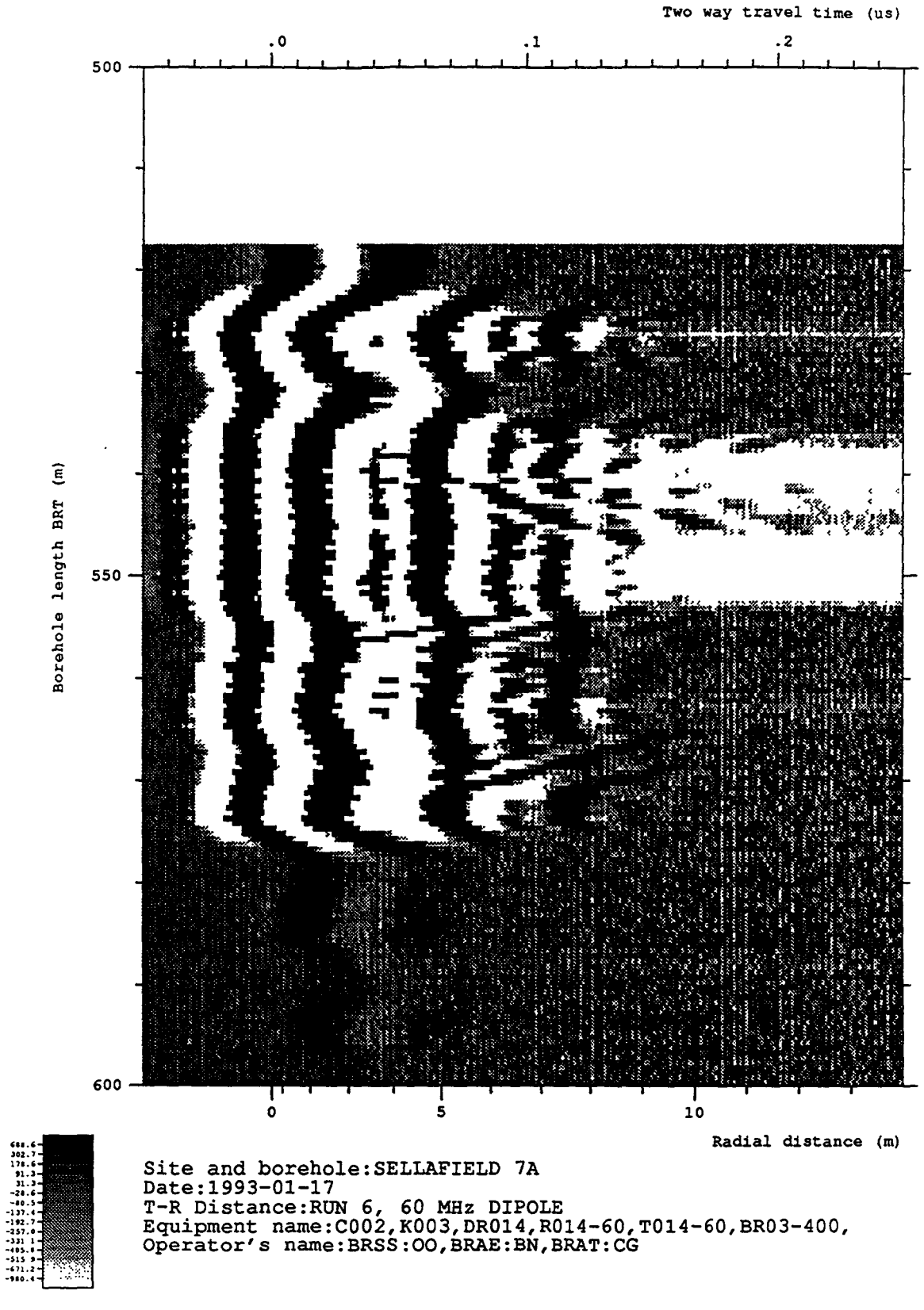

Figure 5-13 Radar map from Run 6, 60 MHz omni-directional survey (517.64 - 600.00 mbRT)

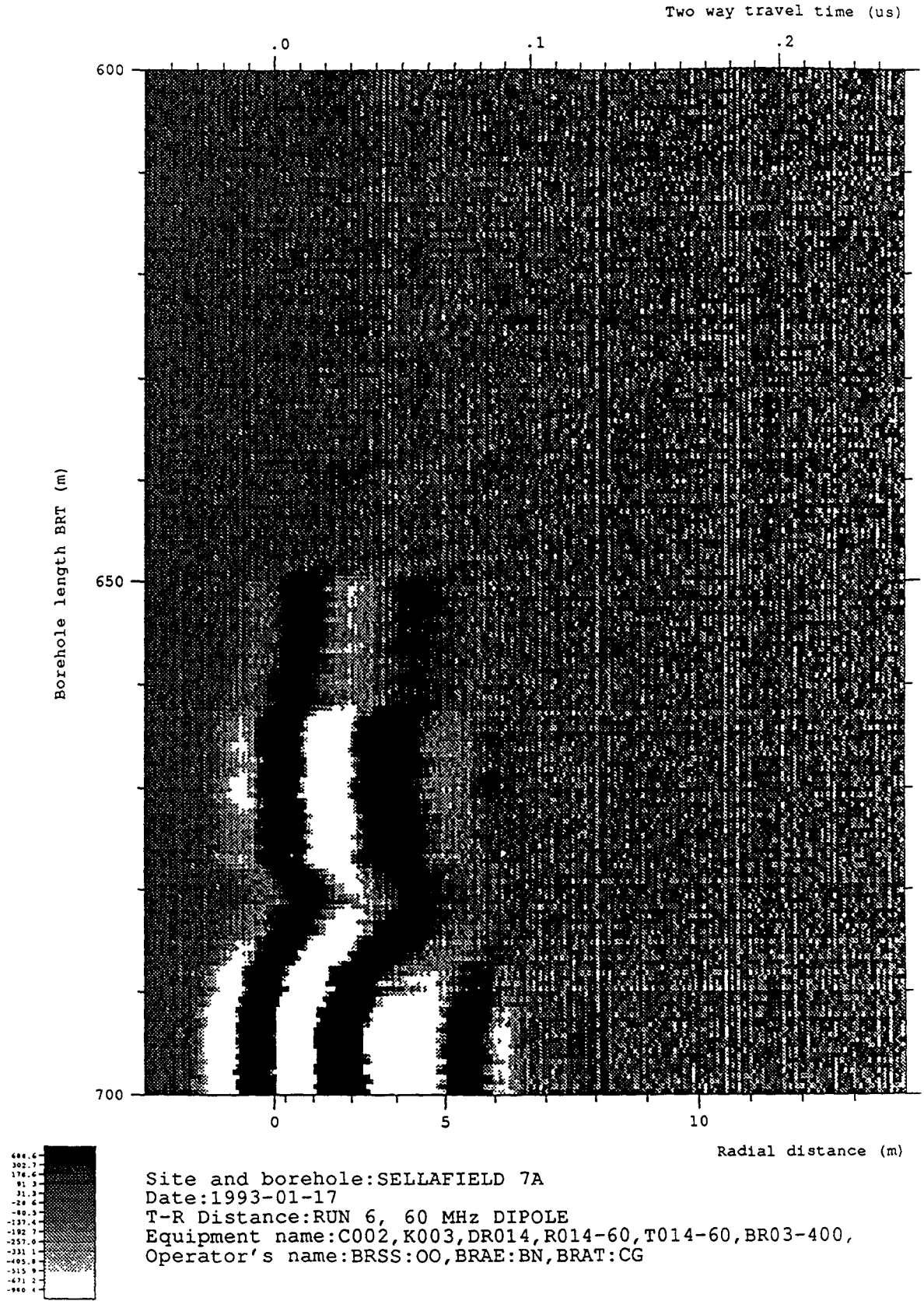

Figure 5-14 Radar map from Run 6, 60 MHz omni-directional survey (600.00 - 700.00 mbRT)

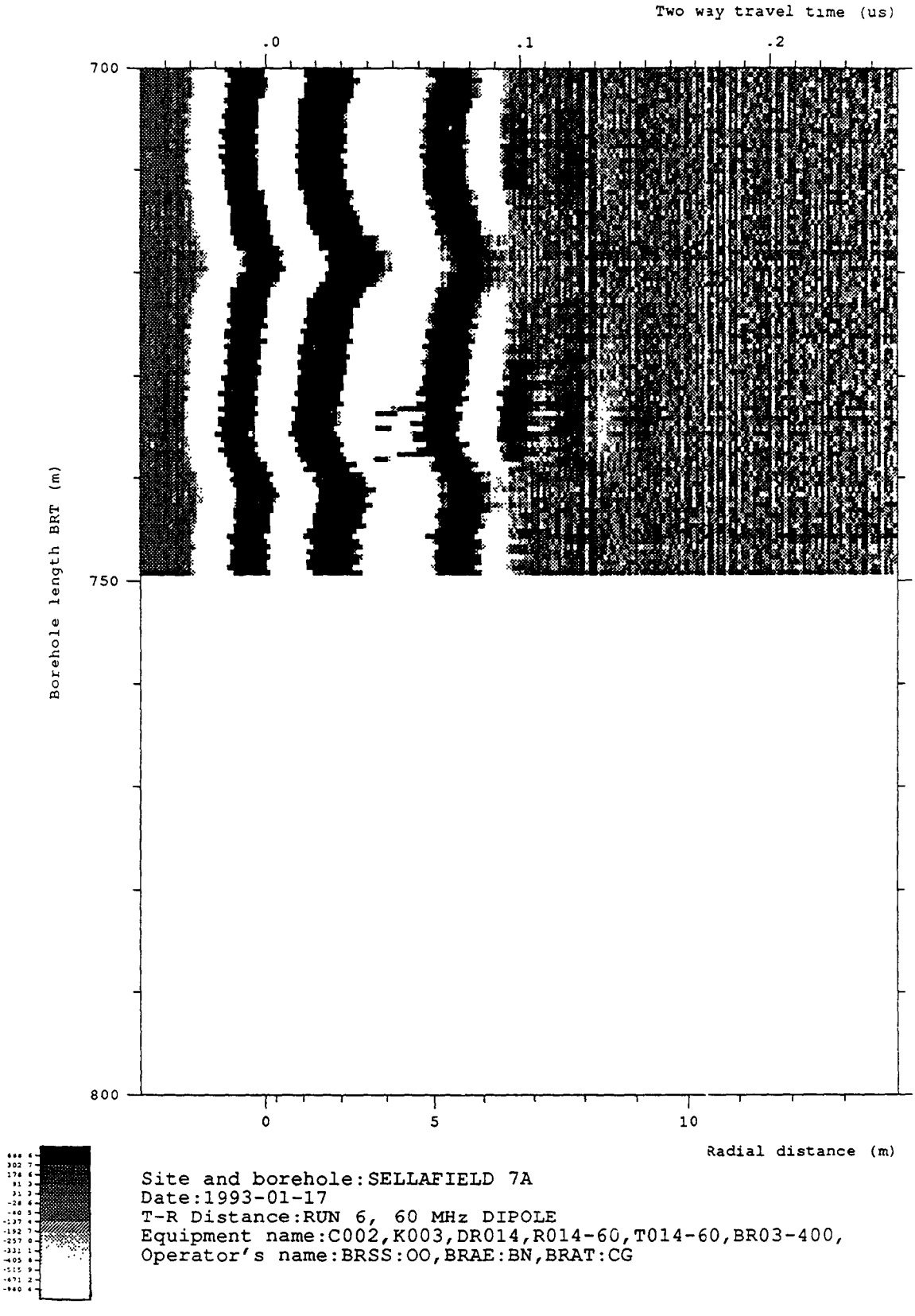

Figure 5-15 Radar map from Run 6, 60 MHz omni-directional survey (700.00 - 749.14 mbRT)

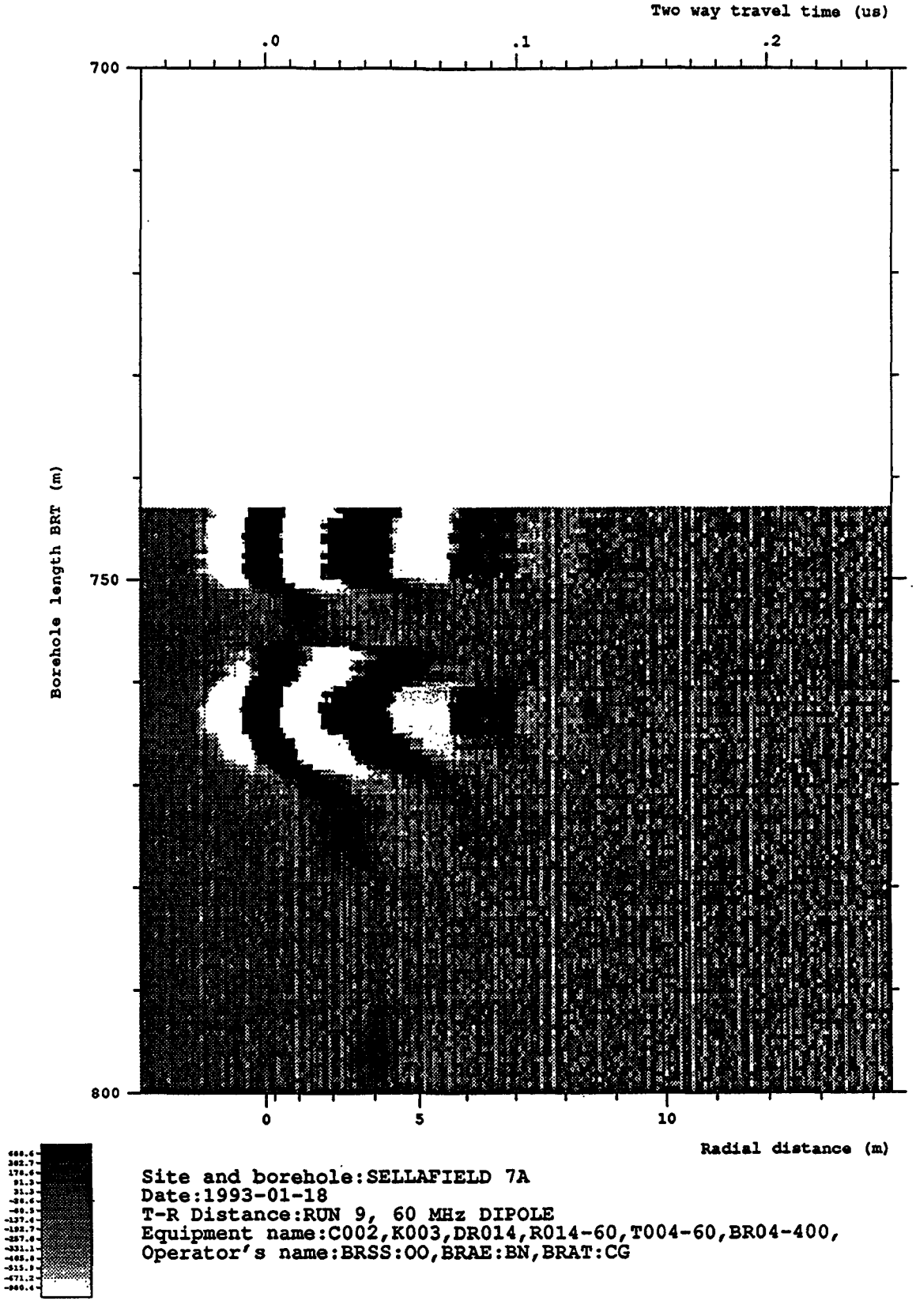

Figure 5-16 Radar map from Run 9, 60 MHz omni-directional survey (743.08 - 800.00 mbRT)

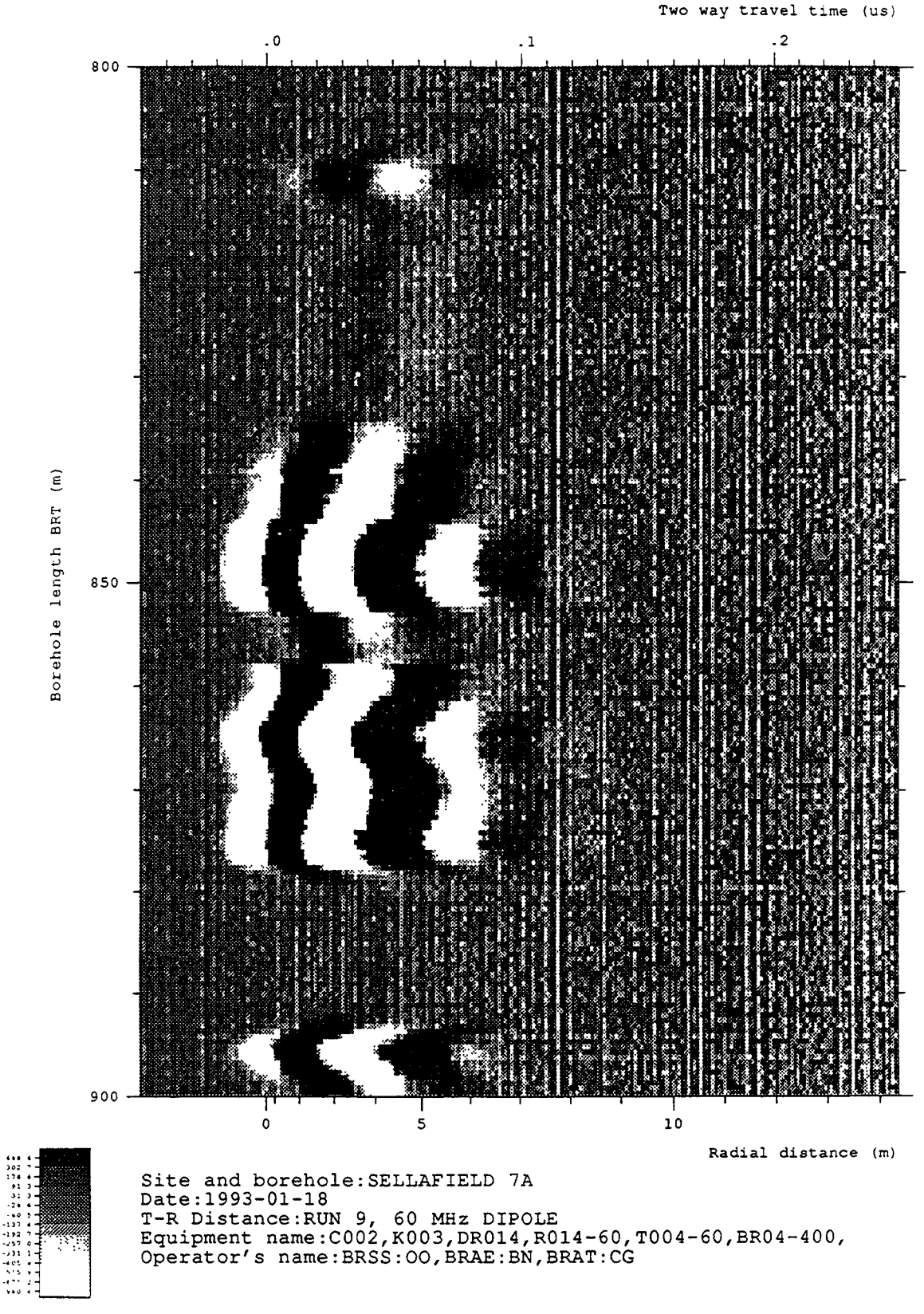

Figure 5-17 Radar map from Run 9, 60 MHz omni-directional survey (800.00 - 900.00 mbRT)

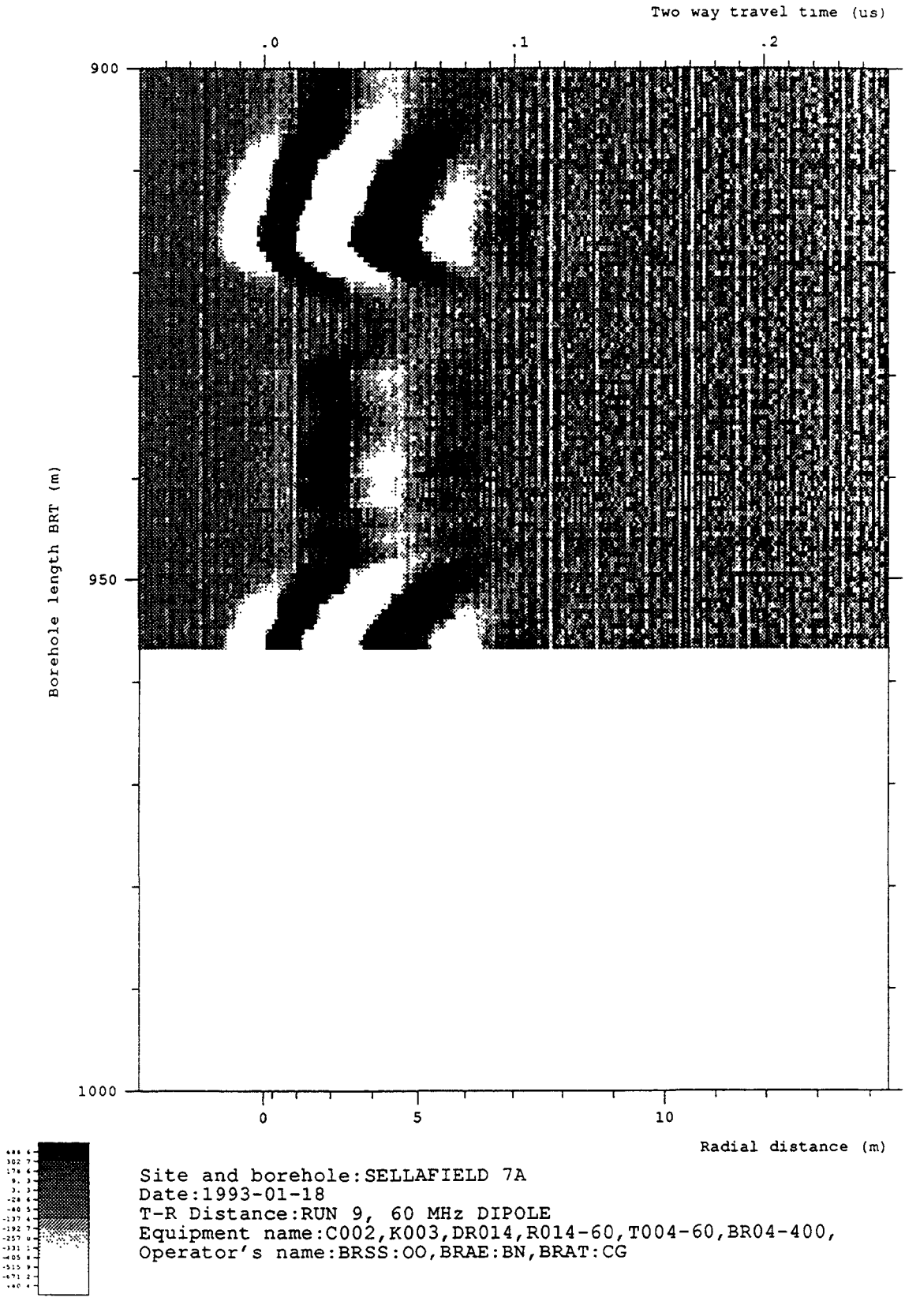

Figure 5-18 Radar map from Run 9, 60 MHz omni-directional survey (900.00 - 956.08 mbRT)

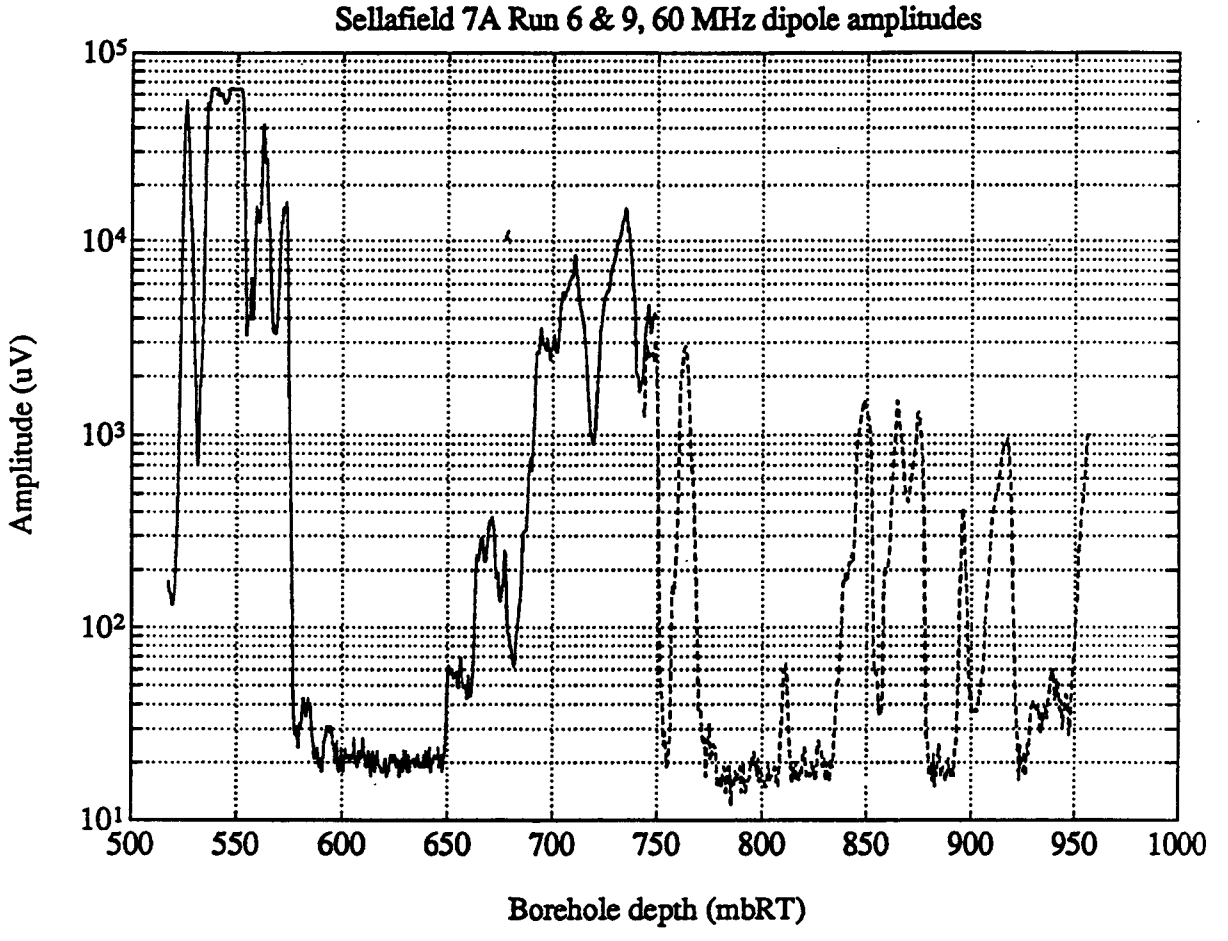

Figure 5-19 Peak to peak amplitude as a function of depth for the direct wave between transmitter and receiver for the 60 MHz omni-directional survey, Runs 6 and 9

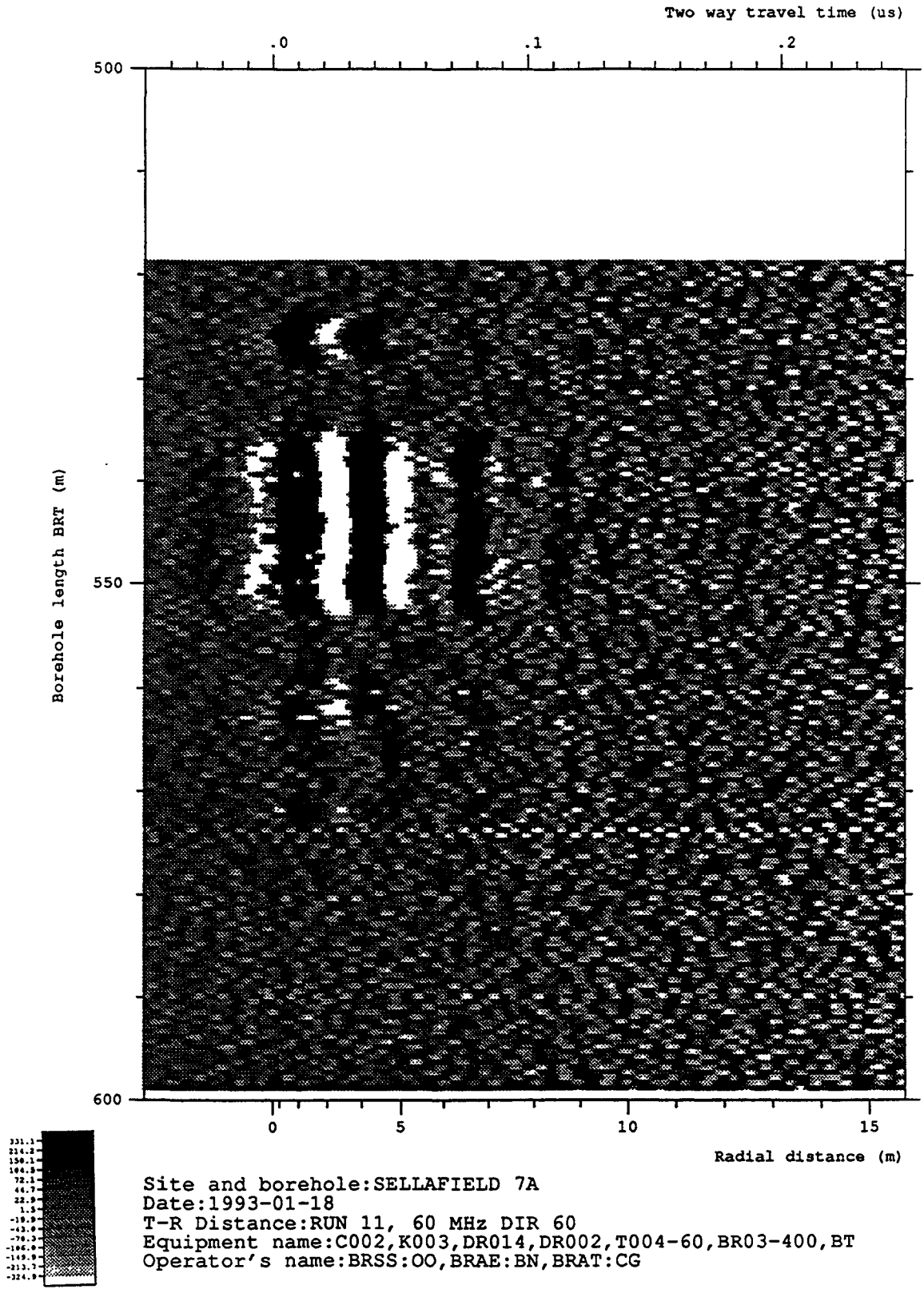

Figure 5-20 Checksum signal obtained from the 60 MHz directional antenna array

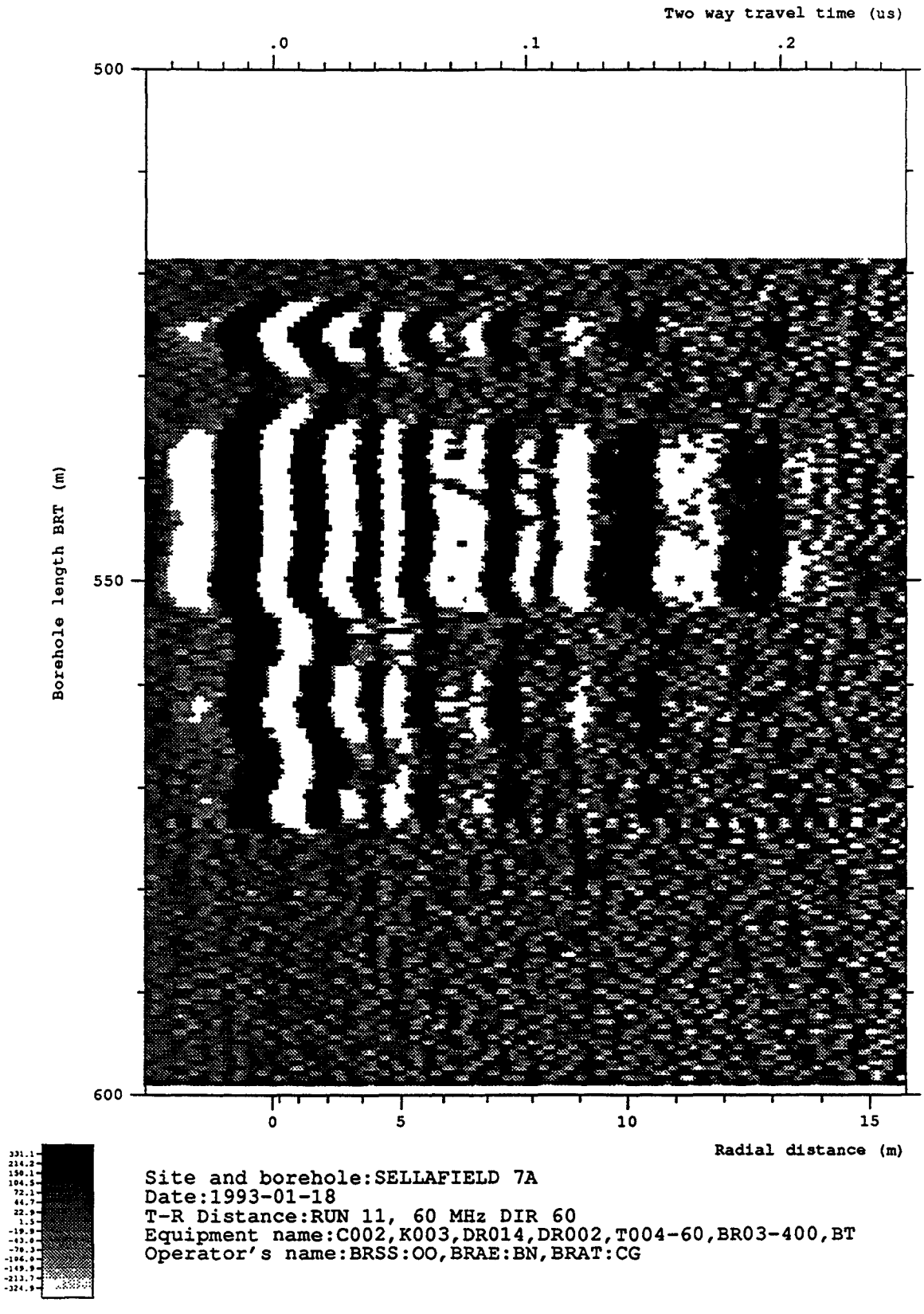

Figure 5-21 Dipole signal obtained from the 60 MHz directional antenna array

6. PROCESSING OF THE RADAR DATA

A limited amount of preliminary processing of the radar data was undertaken on site, this was accomplished both during acquisition phases and following the completion of the radar survey. This is briefly discussed below on the basis of the survey runs which include run numbers 3, 5, 6, 9, 11, and 13. Further detailed processing of the acquired data, reflector identification and the determination of the orientation of the reflectors was undertaken in the offices of the Contractor.

6.1 Initial Processing

6.1.1 Run 3 - Velocity Determination Run

Very limited data processing was required to be undertaken on the relevant data from the velocity determination run. The processing sequence used was as follows:

- DC removal
- Amplitude and arrival time picking
- Plotting

Figure 6-1 shows the arrival time of the direct wave propagating along the borehole as a function of depth for the three transmitter-receiver separations. It is evident that a larger separation results in a delay of the first arrival. The spikes on the curve are due to low signal to noise ratio for the largest transmitter-receiver separation. Figure 6-2 shows the differences in delay between the 7.9 m and 5.9 m, the 11.9 m and 7.9 m, and the 11.9 m and 5.9 m separations, i.e. the travel time for distances of 2, 4 and 6 m, respectively. It is evident that the travel time is proportional to the propagation distance. Hence, the velocity determination has not been compromised by near field or dispersion effects.

The average propagation time over the interval 725-730 mbRT is approximately 66 samples for a propagation distance of 6 m. This corresponds to a travel time of 63.8 ns, which yields a velocity of propagation of 94 m/μs. This corresponds to a relative dielectric permittivity of approximately 10.2. The relation between radar velocity (v) and relative dielectric permittivity (ϵ_r) is

$$v = \frac{c}{\sqrt{(\epsilon_r \mu_r)}}$$

where c is the speed of light in vacuum and μ_r is relative magnetic permeability. The relative magnetic permeability is 1 for most sedimentary rocks.

6.1.2 Run 5 - 22 MHz Omni-directional Survey

A very similar sequence of processing steps was used to process the data from run 5. The processing sequence was as follows:

- DC removal
- Amplitude and arrival time picking
- Depth corrected plotting

Only a limited amount of processing was undertaken as the results for this run showed that where a signal was recorded it appeared to be dominated by a guided wave propagating within the borehole, reflected from discontinuities within the radar antenna, and no reflections could be seen within the data. These were represented by oscillations (ringing) in the radar maps in all sections of the borehole.

The observed reflected wave arrives with opposite phase, approximately 0.37 μs after the first arrival. This corresponds to a propagation distance of approximately 12.3 m if the velocity of water (33 m/μs) is assumed. This distance is approximately twice

the transmitter-receiver antenna separation which implies that the reflected wave is most probably a guided wave which is reflected at the antennas due to the impedence contrast resulting from the plastic covers over the antennas.

The raw data which is presented in Figures 5-8 to 5-12 (Section 5) displayed no evident reflectors. Several attempts were made to enhance reflections through processing, for example band-pass and moving average filtering techniques were applied, but none of the attempts proved successful. It appeared that the 22 MHz antennas radiated very little energy into the formation. Most of the energy appeared to have propagated as a guided wave along the borehole, seen as oscillations or ringing. This is substantiated by the fact that the guided wave observed after the first arrival has an amplitude which is of the order of 70-75% of the direct wave.

Figure 6-3 shows the amplitude of the direct wave as a function of borehole depth. Large radar amplitudes are observed in the interval 522-575 mbRT corresponding to the location of the Carboniferous Limestone. In the BVG large radar amplitudes were observed in the interval 688-768 mbRT. In addition, a number of shorter intervals with measurable radar signals occur between 840 m and the bottom of the measured borehole interval at 957 mbRT. For the rest of the BVG no measurable radar signal was obtained.

6.1.3 Runs 6 and 9 - 60 MHz Omni-directional Survey

The same processing sequence was used to process the results from both Runs 6 and 9, which jointly formed the 60 MHz omni-directional survey and consequently they are considered together. The processing steps used for both sets were as set out below:

- DC removal
- Fast Fourier Transform (FFT)

- Band-pass filtering
- Moving average filtering
- Amplitude and arrival time picking
- Depth corrected plotting
- Reflector identification and determination of orientations

The 60 MHz omni-directional data after correction of the DC-level shift is shown in Figures 5-13 to 5-18 (Section 5). In the DC-corrected data reflections are evident only in the Carboniferous Limestone section of the borehole, 523.5 to 576.5 mbRT. In the parts of the BVG where a measurable direct wave was detected no clear reflections were observed in the DC-corrected data.

It was evident from the raw data plots that detectable radar signals were observed only in certain intervals of the borehole. A simple measure of the quality of the radar signal is the amplitude of the direct wave which propagates along the borehole. Figure 5-19 (Section 5) shows the peak-to-peak amplitude of the direct wave as a function of borehole depth for the 60 MHz omni-directional antenna. There is a very good correlation with the corresponding data from the run with the 22 MHz system shown in Figure 6-3. Borehole intervals with relatively large radar amplitudes are found in the interval 523.5-576.5 mbRT which corresponds to the Carboniferous Limestone. In the BVG relatively large radar amplitudes were observed between 688 and 768 mbRT and a number of shorter intervals with measurable radar amplitudes were observed between 844 mbRT and 956 mbRT.

As the 60 MHz omni-directional survey of Borehole 7A was performed in two runs, the interval 743-750 mbRT was measured twice and in Figure 5-19 (Section 5) a small difference in the amplitudes can be observed between the two runs. The somewhat smaller amplitude for the second run was due to a change of transmitter, which resulted in a larger transmitter-receiver spacing for Run 9.

6.1.4 Runs 11 and 13 - 60 MHz Directional Survey

The 60 MHz directional survey was similarly formed from two runs and the same preliminary on site processing sequence was used to process the results from both runs. The processing of the directional data had been identified as being a time intensive process and it had therefore been decided that the majority of processing would be undertaken in the offices of the Contractor and only preliminary processing was undertaken on site. Therefore the on site processing comprised the following steps:

- DC removal
- Reflector identification and determination of orientations

The signal amplitudes obtained in the directional survey were generally smaller than the corresponding amplitudes obtained from the 60 MHz omni-directional survey. This is exemplified in Figure 6-4 where the amplitude of the dipole signal is displayed as a function of borehole depth. The largest peak-to-peak amplitudes in the Carboniferous Limestone are approximately 3 mV compared to approximately 60 mV for the omni-directional data over the same interval (Figure 5-19, Section 5).

Figure 5-20 (Section 5) displays the checksum signal obtained from the directional antenna array. This signal provides a quality control of the directional antenna data; the amplitude of the checksum signal is considerably smaller than the dipole signal (Figure 5-21, Section 5) obtained from the directional antenna; and confirms the proper functioning of the directional antenna array.

6.2 Further Processing of the Radar Data

Further processing of the radar data acquired during the acquisition period was undertaken in the offices of the Contractor. The processing steps tested and used are briefly highlighted.

6.2.1 22 MHz Omni-directional Survey

The data from the 22 MHz omni-directional run were dominated by a borehole guided wave, as discussed above, but attempts to remove the effects of the guided wave propagating within the borehole were made using different processing techniques in order to extract information about geological features within the formations. Band-pass filtering and moving average filtering were undertaken but little or no improvement was obtained. All processing techniques applied were unsuccessful and it was concluded that the 22 MHz system provided no useful information about the geological conditions in Borehole 7A, except what could be deduced from the amplitude of the direct wave (Figure 6-3). Therefore no further processing of the data from this element of the survey was undertaken.

6.2.2 60 MHz Omni-directional Survey

The 60 MHz omni-directional survey was processed using a number of different techniques. These processing techniques were also evaluated to obtain the optimum processing sequence for processing both the 60 MHz omni-directional and directional survey data.

Several different processing techniques and steps were evaluated and tested on this data set in order to find the most appropriate algorithms to enhance and increase the resolution of radar reflectors present within the survey results and those tested are set out below:

- DC removal
- Spectral analysis
- Fast Fourier Transform (FFT)
- Band-pass filtering
- Moving average filtering
- Moving average filtering applied to band-pass filtered data
- Amplitude and arrival time picking
- Static corrections
- Mute
- Trace equalisation
- Automatic gain control (AGC)
- Deconvolution
- F - K filtering
- Cross correlation
- Adaptive filtering
- Depth corrected plotting

A summary of the algorithms tested is presented below and examples of the results obtained are also included. Following DC removal, spectral analyses of the recorded traces were undertaken and an example of a recorded trace and its spectral content is shown in Figure 6-5. The displayed trace is from a depth of 542.14 mbRT, within the Carboniferous Limestone. The recorded traces are dominated by the direct arrival, the wave which propagates along the borehole, and the following oscillations (ringing). The dominant frequency of the recorded signal is approximately 40 MHz which is significantly lower than the nominal frequency of 60 MHz for the antennas used. The reason for the difference between the dominant frequency of the recorded signal and the nominal frequency of the system is that the transmitter generates a dominant wavelength which is roughly twice the length of the antenna and the transmitted frequency is dependent upon the properties of the formation. In principle, this implies that the dominant frequency will be proportional to the velocity of the

medium. In addition, the dominant frequency in most formations is lowered due to an increase in attenuation with frequency. The major reason for the dominant frequency being lower than the nominal frequency is that the velocity of the BVG is considerably lower than the velocity in the granitic formations for which the borehole radar antenna were originally designed.

Figure 6-6 shows a recorded trace and the corresponding power spectrum from a relatively resistive part of the BVG. The magnitude of the signal is considerably smaller than the one shown in Figure 6-5 and the peak of the spectrum is at about 32 MHz.

In order to improve the signal to noise ratio, band-pass filtering was applied to the data. The band-pass filtering improved the signal to noise ratio and the reflections in the limestone could be resolved more clearly. However, band-pass filtering did not appear to improve the results in the BVG (Figures 6-7 to 6-12).

A useful filter to enhance reflections for data dominated by the direct wave between transmitter and receiver is the moving average filter. For a moving average filter an average is calculated from a number of adjacent traces (in this case 5) and the current trace (the centre trace) is subtracted from the average. In this way signals which are constant along the borehole (e.g. the direct pulse and the ringing normally associated with it) are removed. The application of the moving average filter to the band-pass filtered data increased the number of reflections observed in the data, particularly in the limestone. After filtering several reflections could also be differentiated in the BVG (Figures 6-13 to 6-18).

From the radar maps (Figures 6-13 to 6-18) it was evident that the velocity of propagation varied with depth in the borehole and the subsequent variations in arrival time caused the generation of artifacts in the moving average filtered data. To improve the radar image static corrections can be applied, i.e. the traces are time

shifted so that the direct wave appears at the same time for all traces. The time corrections applied are shown in Figures 6-19 and 6-20 for Runs 6 and 9, respectively. For the borehole intervals where the time correction is either 20 or 50 samples, no direct pulse was observed and these arbitrary values were used. Based on the time corrections, it was possible to estimate the variation in radar velocity along the borehole. The result is shown in Figure 6-21, where the straight horizontal lines represent areas where there is no data. The radar velocity in the limestone (523-578m bRT) is approximately 100 m/μs, whilst for the BVG the radar velocity is lower and variable. In the borehole interval 680-769 mbRT the radar velocity is approximately 90 m/μs, and in the interval 827-957 mbRT the radar velocity has a range of approximately 75-80 m/μs. In the intervals where the radar amplitudes are very low the radar velocity would appear to be in the range 55-70 m/μs. Figure 6-22 shows the dielectric constant as a function of borehole depth based on the velocity data.

The moving average filtered data after static corrections for the borehole interval 517-600 mbRT are shown in Figure 6-23. The artifacts seen in Figure 6-13 which were associated with variations in arrival time (e.g. at $\approx$523 mbRT and $\approx$575 mbRT) are effectively not observed following these corrections. This has had the effect of making the reflected events more distinguishable.

The radar map after trace equalization (i.e. all traces are adjusted to the same magnitude) and with static corrections are shown in Figure 6-24. The same data after moving average filtering is shown in Figure 6-25 This procedure resulted in a slight improvement to the radar image compared to the moving average filtered data without trace equalization (Figure 6-23) for borehole intervals with sufficient signal to noise ratios. In borehole intervals with no measurable radar signal the noise is amplified resulting in a very noisy image.

The result of deconvolution after static corrections and the use of Automatic Gain

Control (AGC) is shown in Figure 6-26. The ringing of the direct pulse is significantly reduced and the strongest reflectors are enhanced, however, no enhancement of reflectors was observed in the BVG where signals were weaker.

The result of FK-filtering after AGC and static corrections where spatial frequencies corresponding to the direct pulse have been suppressed by 40 dB is shown in Figure 6-27. The result of FK-filtering is similar to the result obtained from the moving average filter. The FK-filter provides significant enhancement of reflectors, particularly in the limestone.

Cross-correlations were computed with two different signals;

i) with the average of 35 traces from the limestone section of the borehole after band-pass filtering (Figure 6-28) and

ii) with a synthetic pulse similar to the transmitted pulse (Figure 6-29).

Cross-correlation enhanced the signal to noise ratio but unfortunately also enhanced the ringing of the direct pulse. Reflectors evident in the band-pass filtered data are also seen in the correlated data, but cross correlation cannot be considered to provide any significant improvement.

The result of adaptive filtering after static corrections and AGC is shown in Figure 6-30. The result is similar to that obtained after deconvolution. The ringing of the direct pulse is reduced and the strongest reflectors are enhanced compared to band-pass filtered data. The adaptive filter provides the best improvement where signal to noise ratios are low.

Following the assessment of various processing algorithms reflector identification was based on the data having being processed by a moving average filter applied to the

data after trace equalisation and static corrections. It was considered that this represented the most effective processing technique and the application of a moving average filter was the most effective filter applied. The corresponding radar maps for the entire borehole are shown in Figures 6-31 to 6-35.

6.2.3 60 MHz Directional Survey

Following the evaluation of the different processing techniques the most appropriate sequence, discussed above, was also applied to the data acquired during the 60 MHz directional survey. Therefore the data set was processed by a moving average filter after DC removal and band-pass filtering.

The band-pass filtered dipole component obtained from Run 11 is shown in Figure 5-21 (Section 5). The dipole components obtained from the directional survey were processed and these were plotted after depth correction, for every 10° of azimuth (Figures 6-36 to 6-71), for the depth interval 518.80-598.80m bRT.

In the band-pass filtered data most reflections are still obscured by the direct wave and a moving average filter was subsequently applied to the data. After moving average filtering several reflections can be observed in the directional data from the limestone. The moving average filtered data for every 10 degree azimuthal increment are shown in Figures 6-72 to 6-108 for the depth interval 518.80-598.80 mbRT.

The radar maps of the dipole component obtained from Run 13 with the directional antenna are shown in Figures 6-109 to 6-111. Signal amplitudes are generally low and no reflected events were observed in these radar maps. A moving average filter was applied to the data from Run 13 and the radar maps of the moving average filtered dipole component are shown in Figure 6-112 to 6-114. In these radar maps a few reflectors can be observed in the depth interval of 725-750 mbRT.

The moving average filtered data for every 10° azimuthal increments are shown in Figures 6-115 to 6-151. The unfiltered directional component for an azimuth of 0 degrees is shown in Figure 6-152 to facilitate comparison with the corresponding moving average filtered data shown in Figure 6-115. Azimuthal plots for the depth interval below 770 mbRT have not been produced as reflections could not be identified in the directional data below this level.

6.3 Reflector Identification

6.3.1 Principles

The data collected in single hole radar measurements are displayed in the form of a radar map, a diagram where the position of the centre point of the antenna array is indicated along one axis and the travel time (or distance from the borehole) along the other axis. The distance to a reflecting object is determined by measuring the difference in arrival time between the direct and the reflected pulses. The principle of single hole reflection measurements and the characteristic patterns generated by plane and point reflectors is shown in Figure 6-153.

Interpretation of radar data essentially requires the identification of events in the radar maps which are similar to the characteristic patterns for plane and point reflectors. In principle, the patterns are matched to a nomogram which contains calculated patterns for plane reflectors intersecting the borehole at different angles and point reflectors at different distances from the borehole (Figure 6-154). In practice, the interpretation is made with the interactive interpretation programme RADINTER. In this programme the patterns of model reflectors are interactively fitted to patterns in the radar map. Nomograms and printouts of the radar maps are then used to check the identification made with RADINTER. The angle of intersection between a reflector and the borehole is determined in the same way both for the omni-directional and directional data.

For data obtained with the directional antenna, the azimuthal direction to a reflector is determined from the two directional signals extracted from the directional antenna array. The two directional signals are combined to produce a radar map for an arbitrary azimuth. In practice, a radar map is produced for every 10° increment of azimuth (Figures 6-72 to 6-108 and 6-115 to 6-151). To find the azimuth to a reflector the azimuthal radar maps are searched to identify where the reflection pattern disappears or is minimally visible, this occurs for two angles 180° apart. Once the minima have been found the maximum signal which is in-phase with the dipole signal is then located, this occurs at either +90° or -90° from the minimum. The azimuth to the reflector is then -90° from the direction where the dipole and the directional signals are in phase. For example in Figure 6-91 the directional signal is at a maximum for the reflected event seen between a depth of 535 to 545 mbRT, whilst in Figure 6-100, which is in the minimum direction (90° from the maximum), the reflected event has vanished. This direction therefore defines the azimuth of the reflector.

6.3.2 Reflectors Identified

The identification of reflectors was made on the basis of the moving average filtered data after static correction and trace equalisation. Reflectors were in the first instance identified in the omni-directional data and corroborated by the identification of reflectors in the F-K filtered data. The azimuth and dip direction of the reflectors were determined, where possible, from the directional data. The reflectors identified in the data are listed in Table 6-1 and the corresponding events in the radar maps are shown in Figure 6-155 to 6-159 with the events identified by the ID numbers listed in Table 6-1. The azimuth and dip direction were calculated and given relative to magnetic North, this required the orientation and magnitude of the magnetic field vector at the borehole. At Borehole 7A the orientation and magnitude of the megnetic field vector are:

Declination	6°24 West
Inclination	68.7°
Total intensity	48980 nT

The deviation of the borehole would also affect the accuracy of the orientation information, however, the deviation data showed that the deviation of the borehole from vertical was only 2.5° at the bottom of the borehole. As this was smaller than the uncertainties in the determination of the azimuth, which were approximately 10°, the deviation of the borehole was ignored when calculating the dip and dip direction of reflectors.

The determination of the intersection angle between the reflector and the borehole is dependent on the propagation velocity. As shown in Figure 6-21 this varied significantly within the borehole, and the following velocities were used for different sections of the borehole.

Borehole interval	Velocity
520 - 580 mbRT	100m/μs
680 - 770 mbRT	92m/μs
830 - 960 mbRT	80m/μs

The reflectors were divided into four classes based on a qualitative estimate of the magnitude of the reflections. The classes are:

U	Uncertain
1	Weak
2	Meduim
3	Strong

The results of the classification are included in Table 6-1. A strong reflector is generally associated with a linear black and white pattern in the radar maps which has a significant extent. Weaker reflectors generally appear as shades of grey and have a limited extent in the radar maps.

In total, 26 reflectors were identified in the omni-directional data from Borehole 7A. Of these reflectors, 10 were located in the Carboniferous Limestone and 16 in the BVG. It was possible to determine the azimuth for 4 of the reflectors in the Carboniferous Limestone and 1 in the BVG. The magnitude of the reflectors is generally weaker in the BVG than in the limestone. It should also be noted that no radar signal at all was obtained for about half the borehole length within the BVG.

The accuracy in the depths of the intersections is estimated to be within +/- 2m. Approximately one metre of this inaccuracy can be attributed to the wavelength of the transmitted radar waves which limits both resolution and depth determination. The remainder of the inaccuracy can be attributed to the depth recording system. The accuracy in the depth of the intersections also depends upon the angle of intersection between the borehole and the reflecting plane. The accuracy is better for a reflector which intersects the hole with a large angle than for a reflector which intersects the hole obliquely.

6.3.3 Radar Range

The radar range, the distance to which reflection events can be observed in the radar maps, shows significant variations within the borehole. The average range obtained for the 60 MHz omni-directional and directional antennas in different intervals is set out below:

Borehole interval (mbRT)	Range	
	omni-directional	directional
520-580 (limestone)	10-15 m	5-10 m
680-770 (BVG)	5-8 m	5 m
830-960 (BVG)	≈5 m	0 m

In the remaining parts of the BVG the radar provided no information.

Table 6-1 List of radar reflectors identified from the 60 MHz omni-directional and 60 MHz directional surveys in Borehole 7A.

ID no.	Type	Depth of intersection apex	BH interval observed		Magnitude	Azimuth	Linear reflector			Point	Comments
		(mbRT)	from (mbRT)	to (mbRT)	U=uncertain 1=weak 2=medium 3=strong	(deg)	Angle (deg)	Dip (deg)	Dipdir (deg)	Distance (m)	
13	Plane	492.3	518	533	U		18.9	71			Undulating and discontinuous
6	Plane	525.7	518	547	2		34.7	55			
1	Plane	531.7	522	550	3	280	32.7	57	100		
5	Plane	538.5	524	546	2	255	38.5	52	75		
10	Plane	547.9	533	545	2		48.1	42			
17	Plane	550.4	554	570	1		33.7	56			
X	Point	551.1			U					3.2	Seen only in FK-filtered data
4	Plane	557.5	534	570	3	60	33.4	57	240		Upper limb used for phase determination
2	Plane	561.5	548	558	2	-	90	0			

ID no.	Type	Depth of intersection apex	BH interval observed		Magnitude	Azimuth	Linear reflector			Point	Comments
		(mbRT)	from (mbRT)	to (mbRT)	U=uncertain 1=weak 2=medium 3=strong	(deg)	Angle (deg)	Dip (deg)	Dipdir (deg)	Distance (m)	
3	Plane	578.6	563	574	3	60-90	42.2	48	240-270		Limestone-BVG boundary, faint in directional data
9	Plane	692.2	695	702	1		82.7	7			
15	Plane	710.1	712	727	2		35.4	55			
16	Plane	733.2	728	732	1		90.0	0			
7	Plane	739.7	734	738	1	50	68.2	22	230		
8	Plane	743.8	737	742	1		90.0	0			
9/4	Plane	745.8	745	758	U		23.9	66			
11	Plane	747.6	740	746	1		55.2	35			
9/2	Plane	758.0	750	756	1		68.3	22			
18	Plane	765.6	767	772	1		57.6	32			
9/6	Plane	839.9	841	848	1		90	0			

ID no.	Type	Depth of intersection apex	BH interval observed		Magnitude	Azimuth	Linear reflector			Point	Comments
		(mbRT)	from (mbRT)	to (mbRT)	U=uncertain 1=weak 2=medium 3=strong	(deg)	Angle (deg)	Dip (deg)	Dipdir (deg)	Distance (m)	
9/1	Plane	854.5	847	851	1		46.6	43			
9/8	Plane	857.5	860 878	865 886	U		18.1	72			
9/7	Plane	858.3	850	855	1		61.8	28			
9/10	Plane	908.8	910	917	1		44.0	46			
9/9	Plane	933.6	920	955	1		24	66			
9/11	Plane	956.6	951	955	1		90	0			

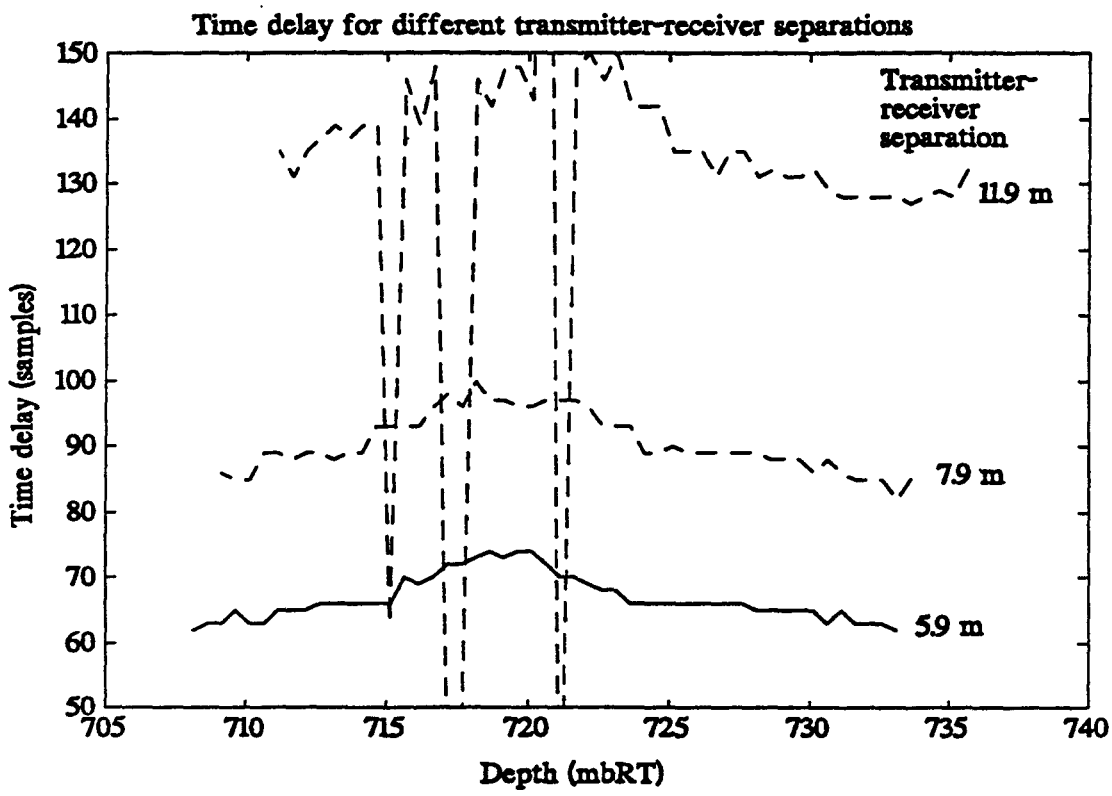

Figure 6-1 Arrival time of the direct wave propagating along the borehole as a function of depth for the three transmitter-receiver separations

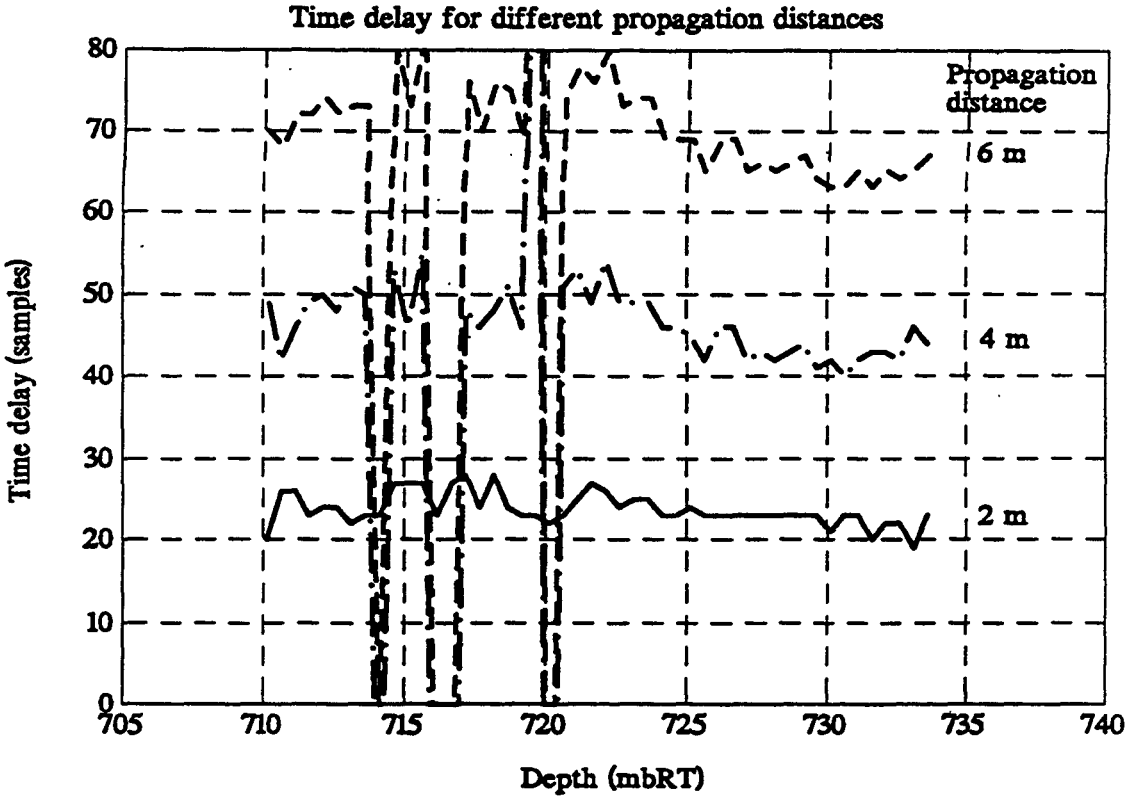

Figure 6-2 Travel time differences for propagation distances of 2, 4 and 6 m

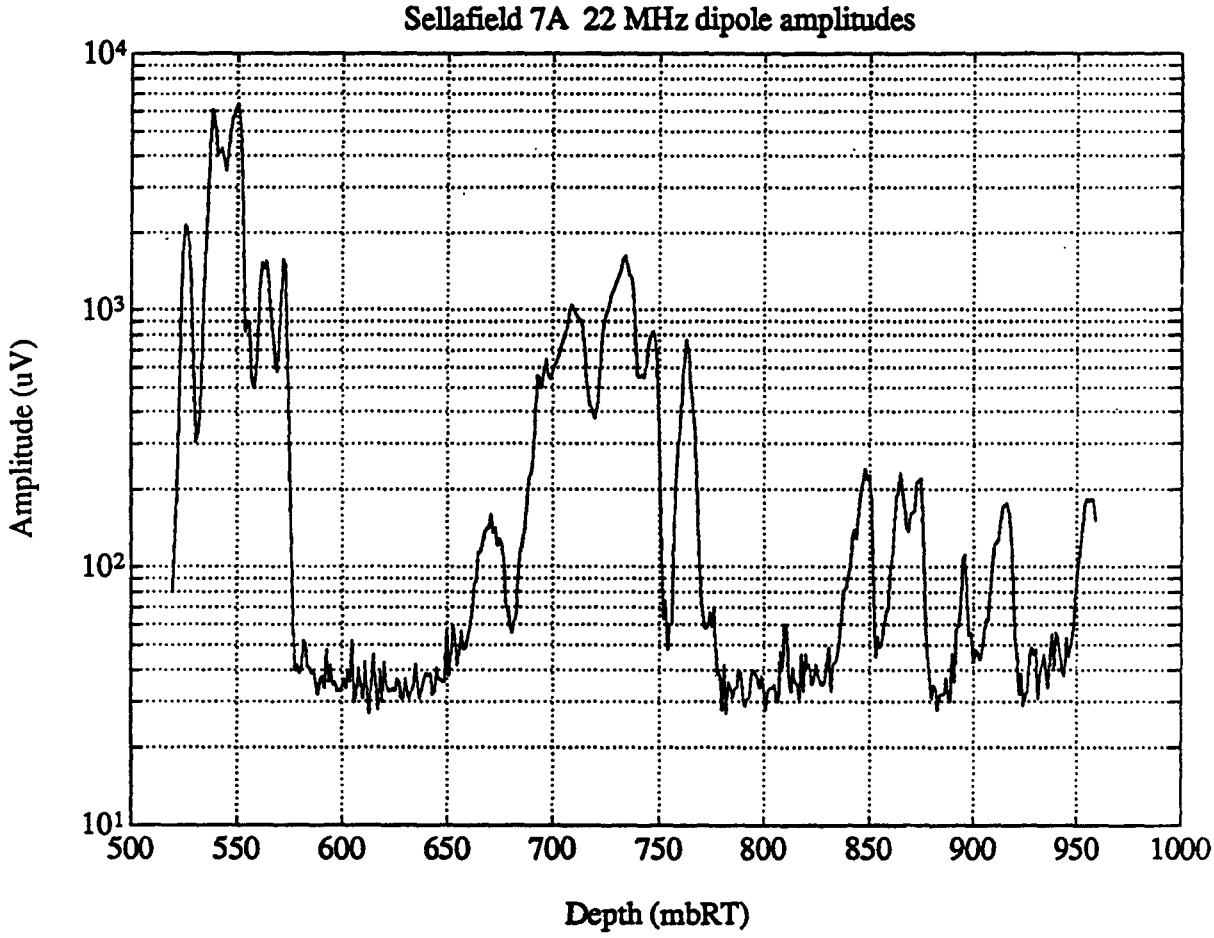

Figure 6-3 Peak to peak amplitude as a function of depth for the direct wave between the transmitter and receiver for the 22 MHz omni-directional survey

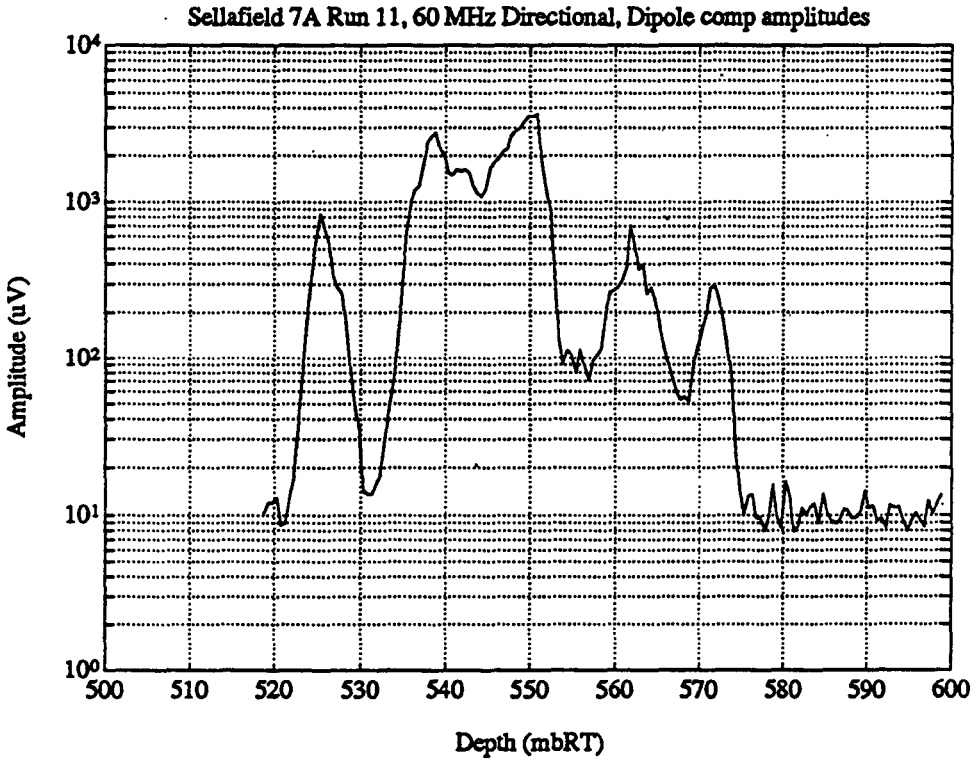

Figure 6-4 Peak to peak amplitude as a function of depth for the direct wave between the transmitter and receiver for the 60 MHz directional survey, dipole component

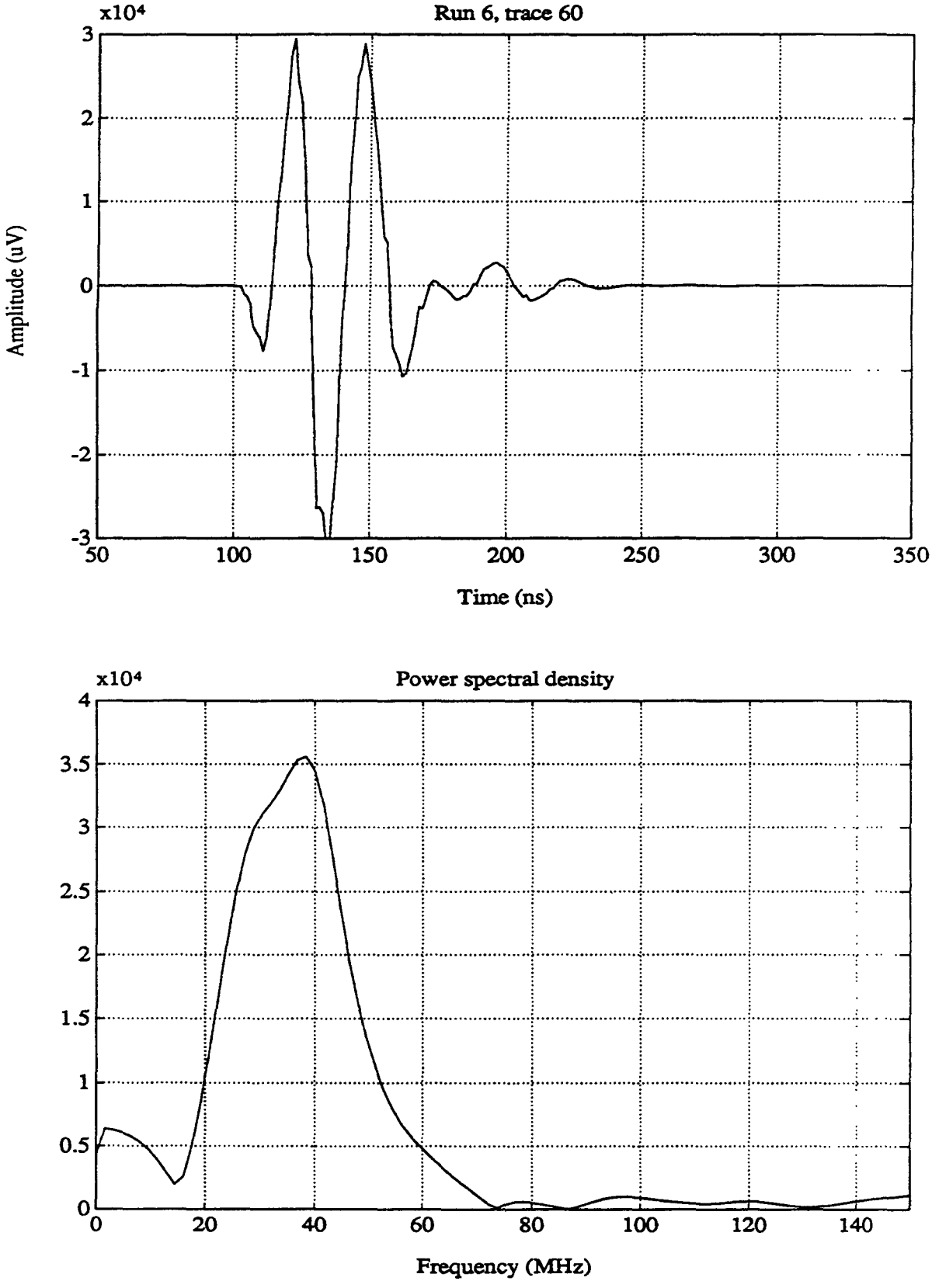

Figure 6-5 Radar signal (upper) recorded by the 60 MHz omni-directional system at a depth of 542.12 mbRT and the spectral content of the siganl (lower)

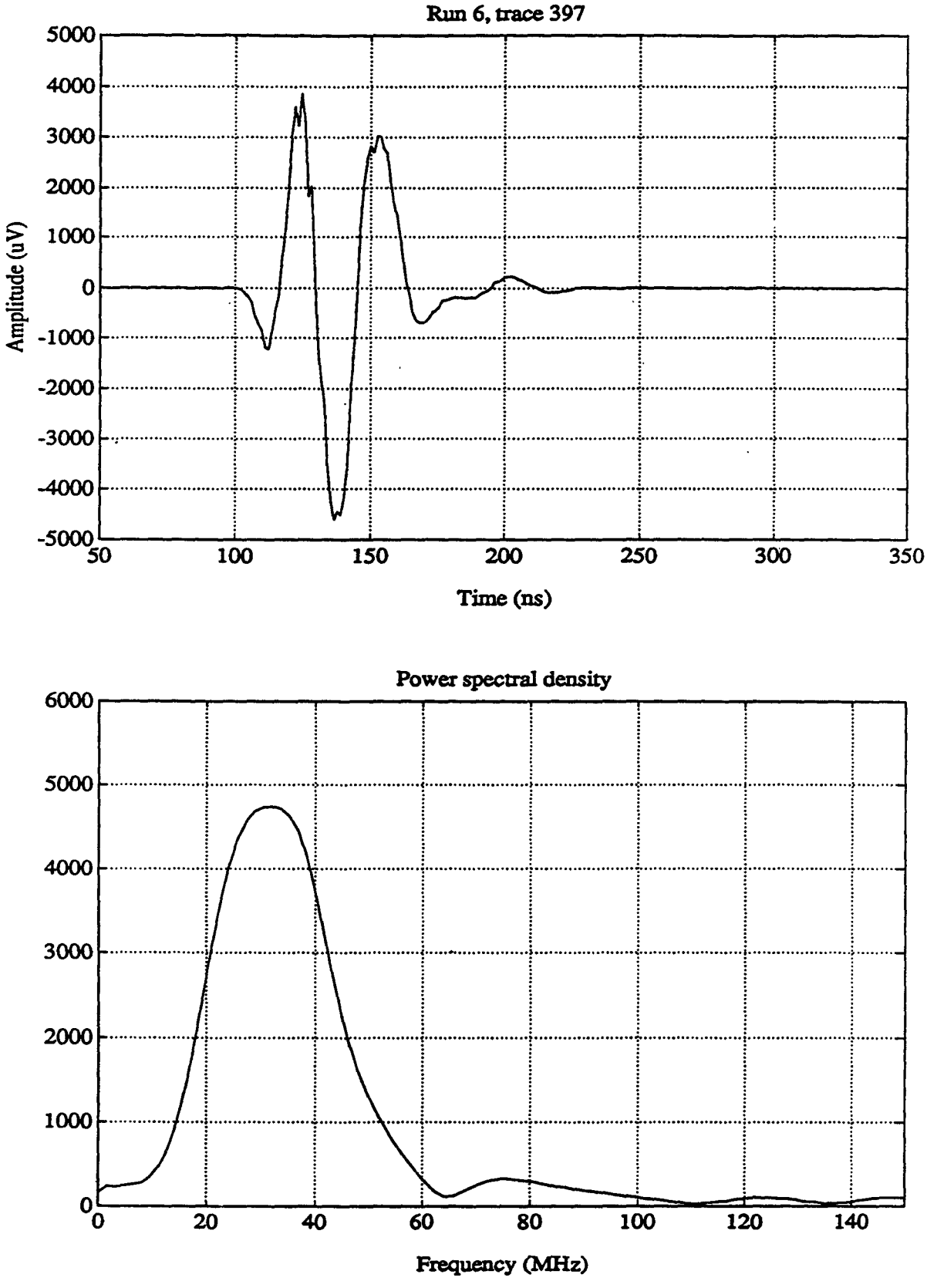

Figure 6-6 Radar signal (upper) recorded by the 60 MHz omni-directional system at a depth of 710.64 mbRT and the spectral content of the siganl (lower)

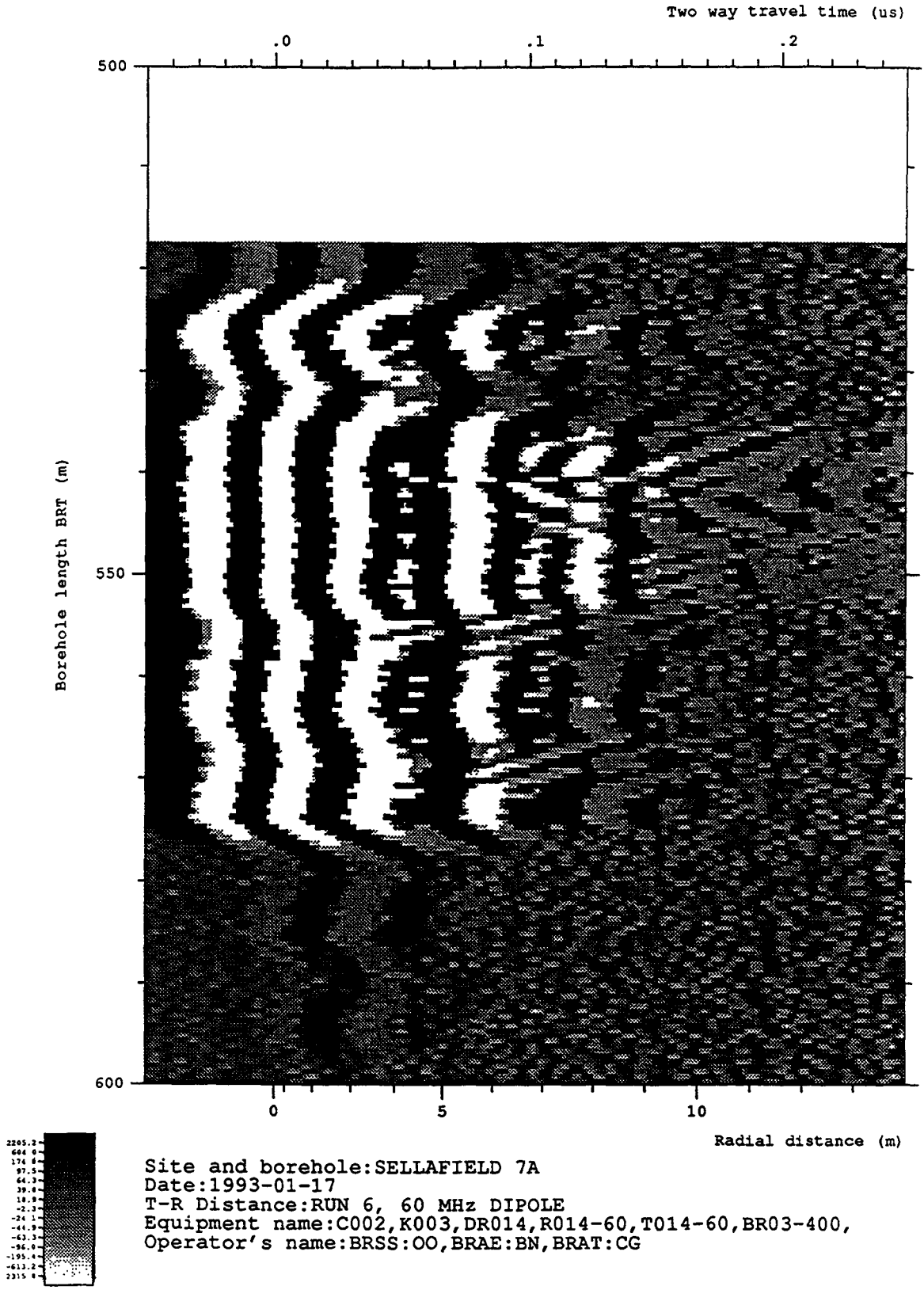

Figure 6-7 Radar map from Run 6, 60 MHz omni-directional survey (517.64 - 600.00 mbRT) after band pass filtering

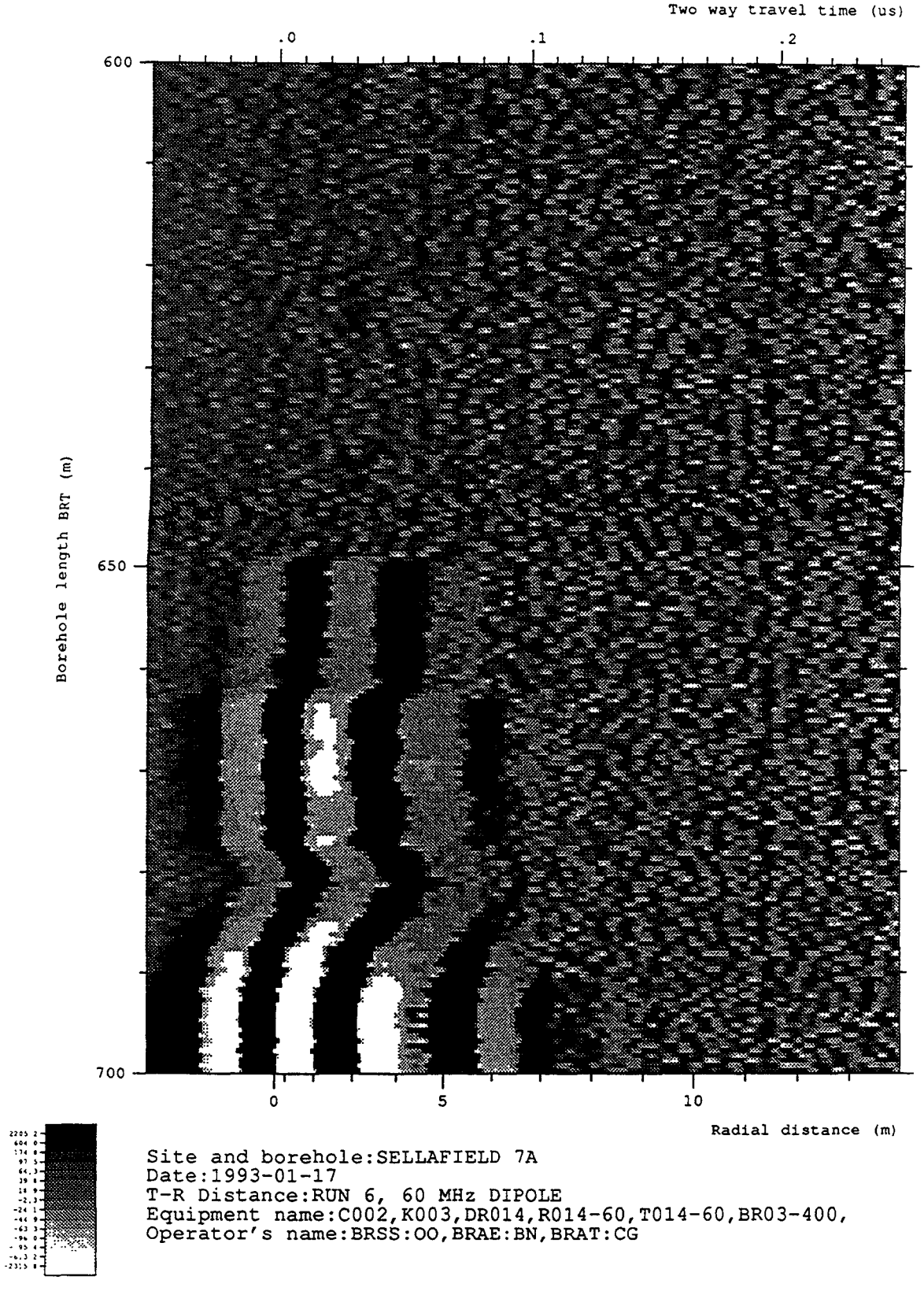

Figure 6-8 Radar map from Run 6, 60 MHz omni-directional survey (600.00 - 700.00 mbRT) after band pass filtering

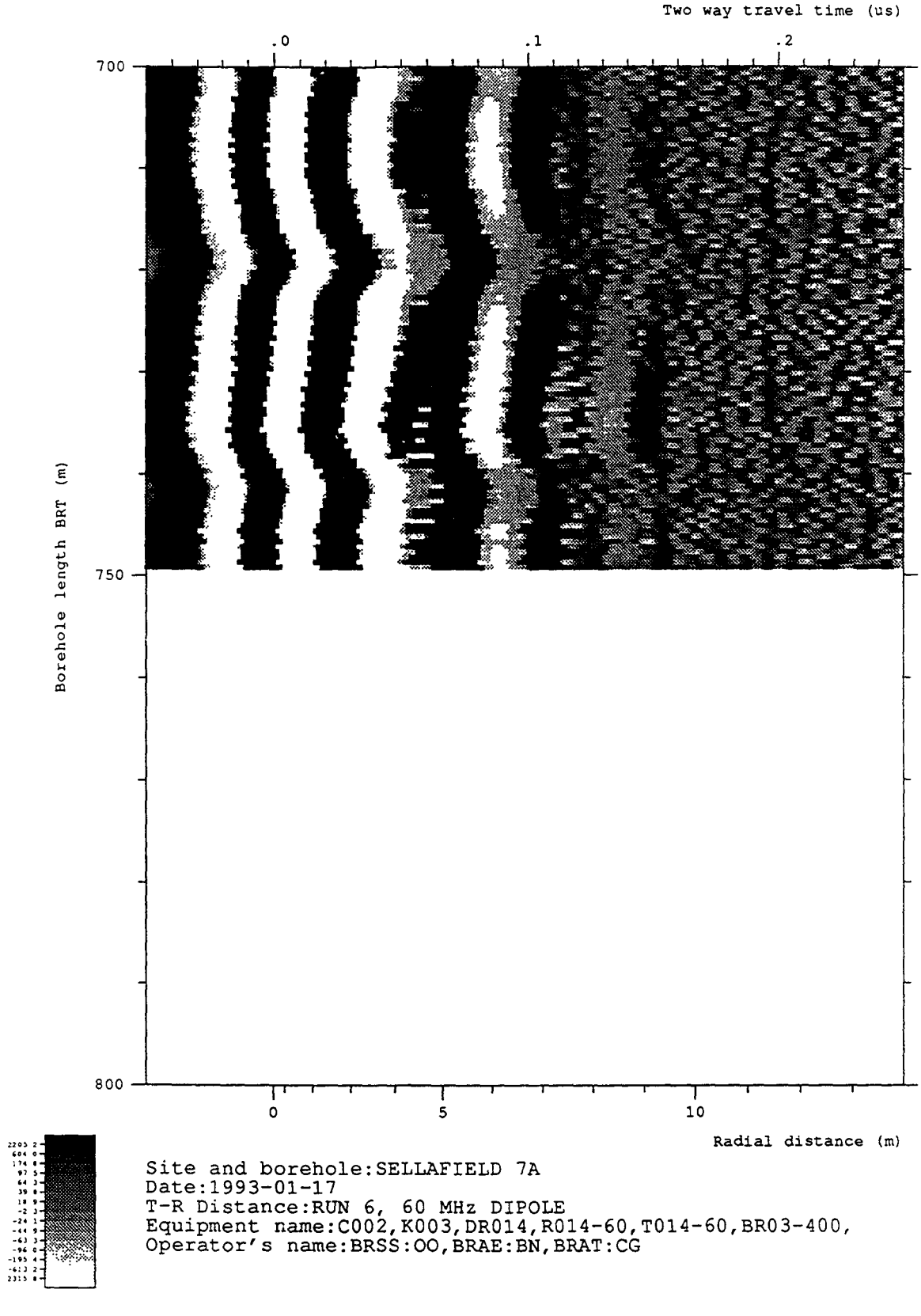

Figure 6-9 Radar map from Run 6, 60 MHz omni-directional survey (700.00 - 749.14 mbRT) after band pass filtering

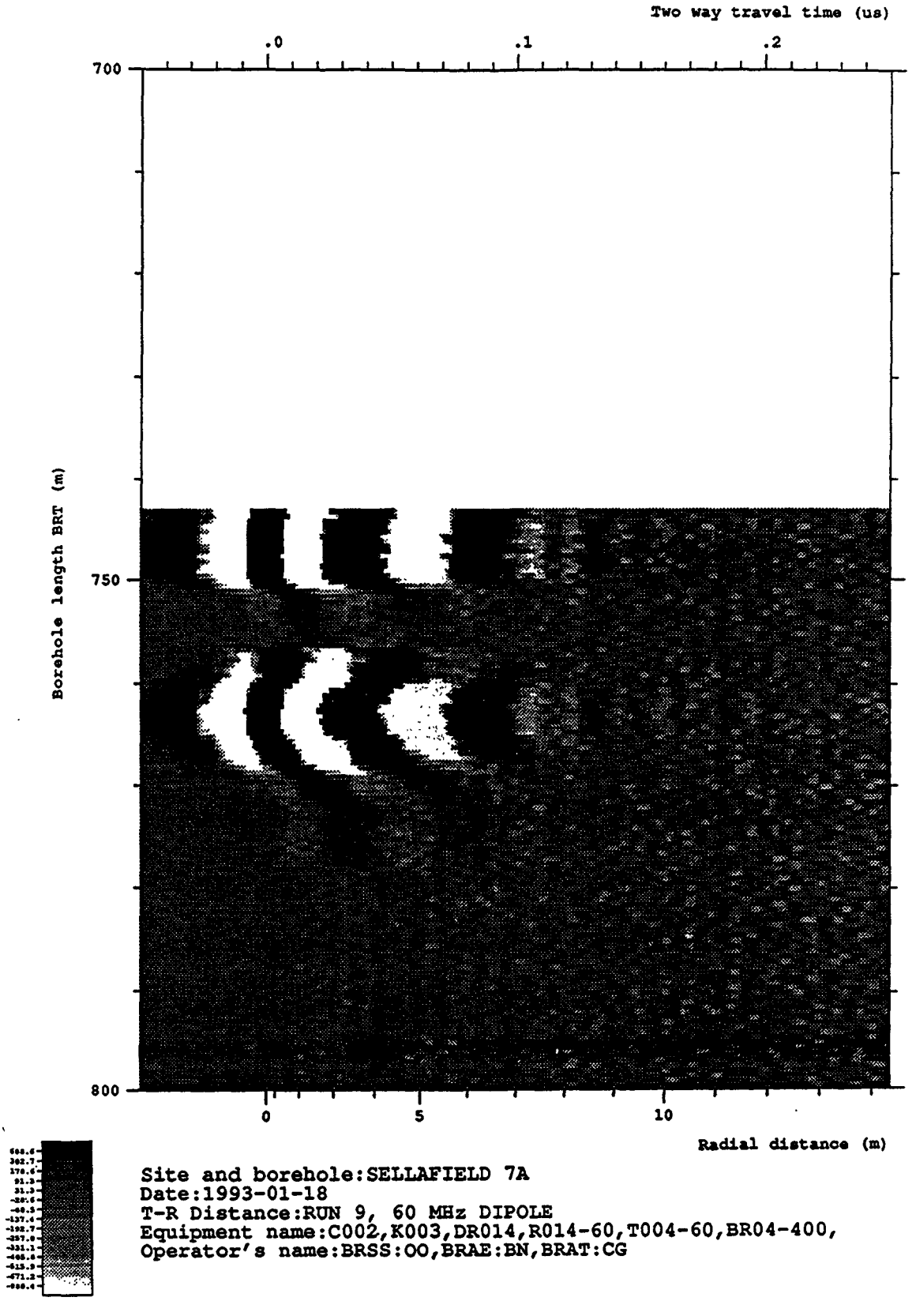

Figure 6-10 Radar map from Run 9, 60 MHz omni-directional survey (743.08 - 800.00 mbRT) after band pass filtering

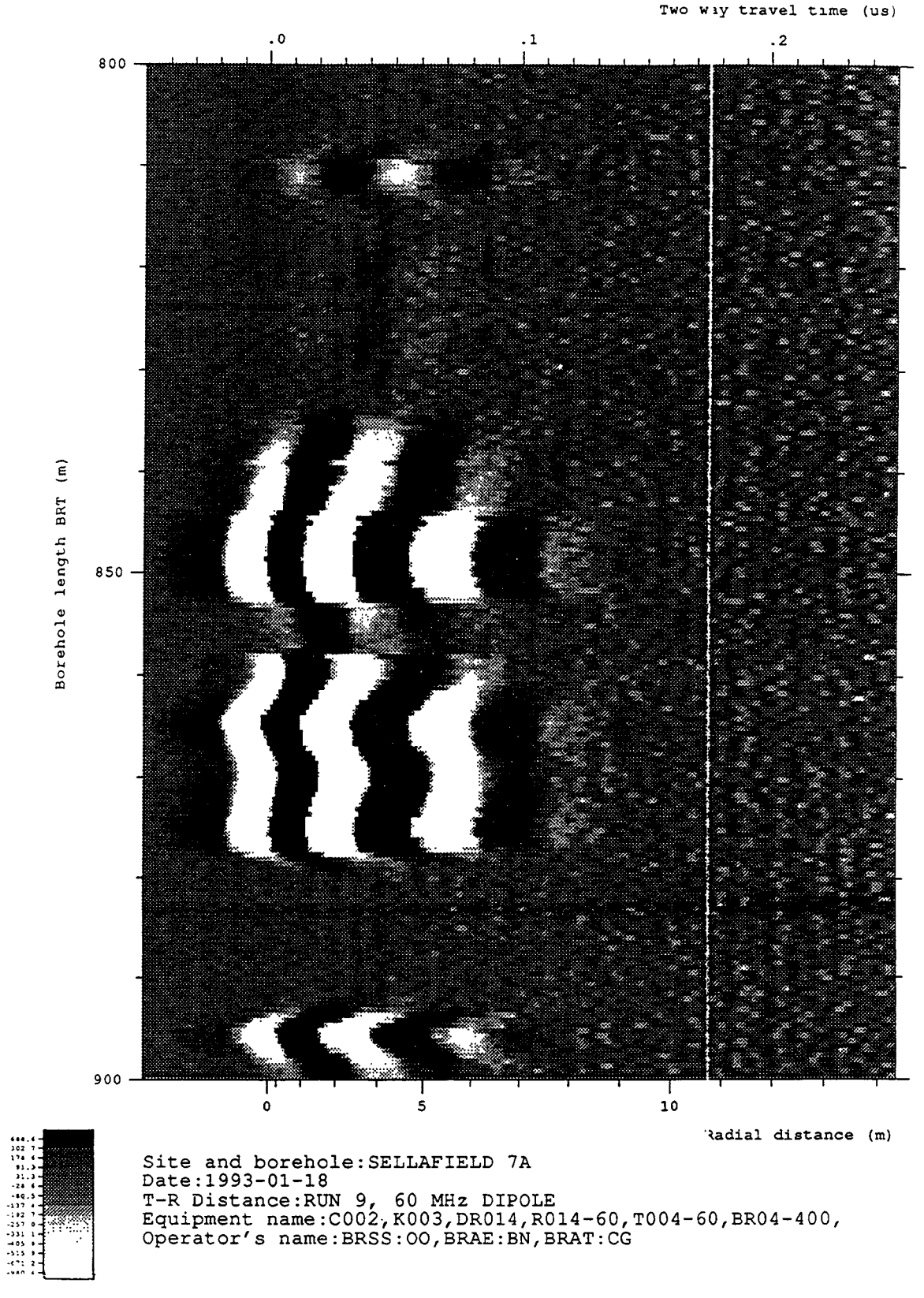

Figure 6-11 Radar map from Run 9, 60 MHz omni-directional survey (800.00 - 900.00 mbRT) after band pass filtering

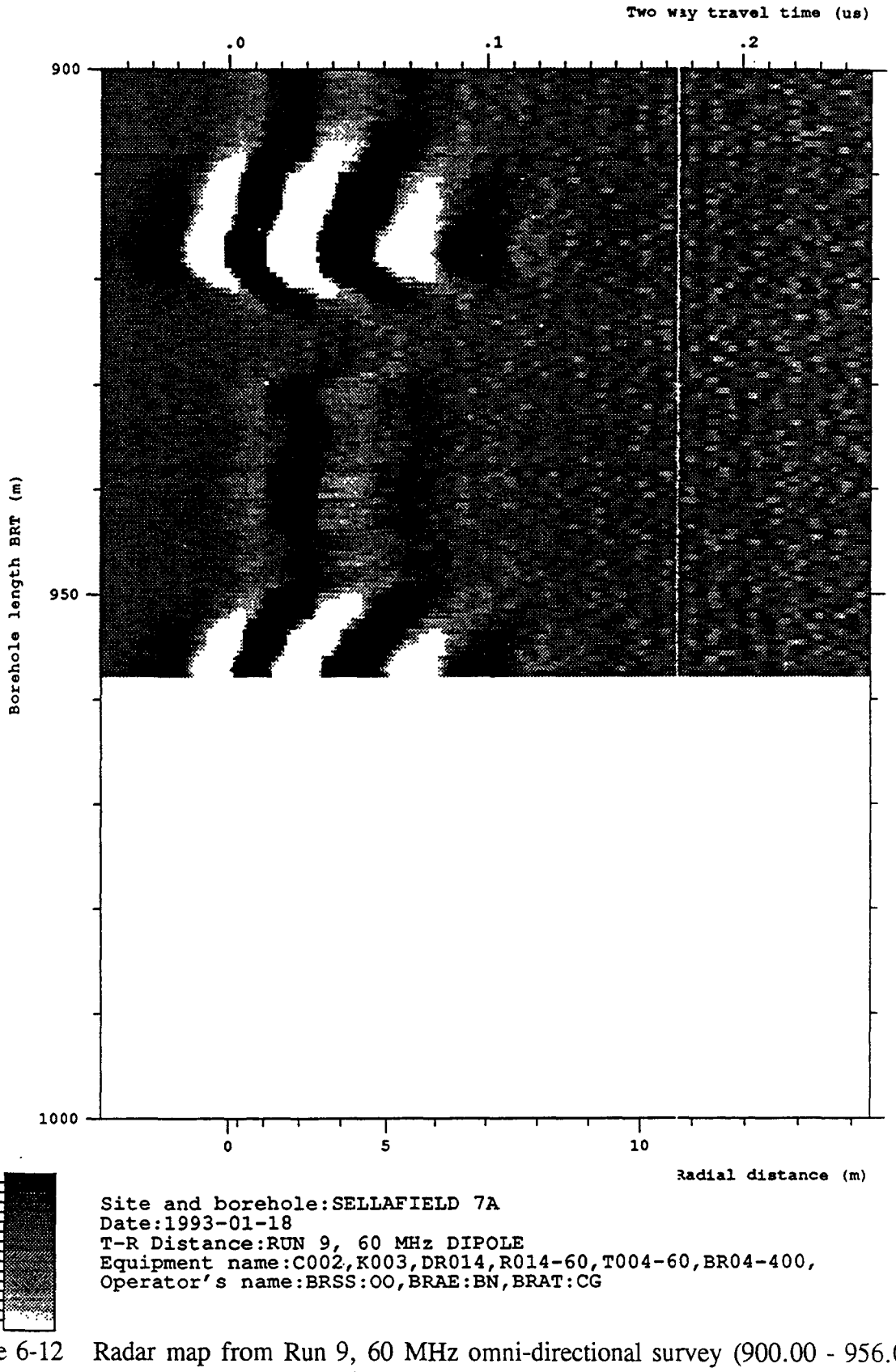

Figure 6-12 Radar map from Run 9, 60 MHz omni-directional survey (900.00 - 956.08 mbRT) after band pass filtering

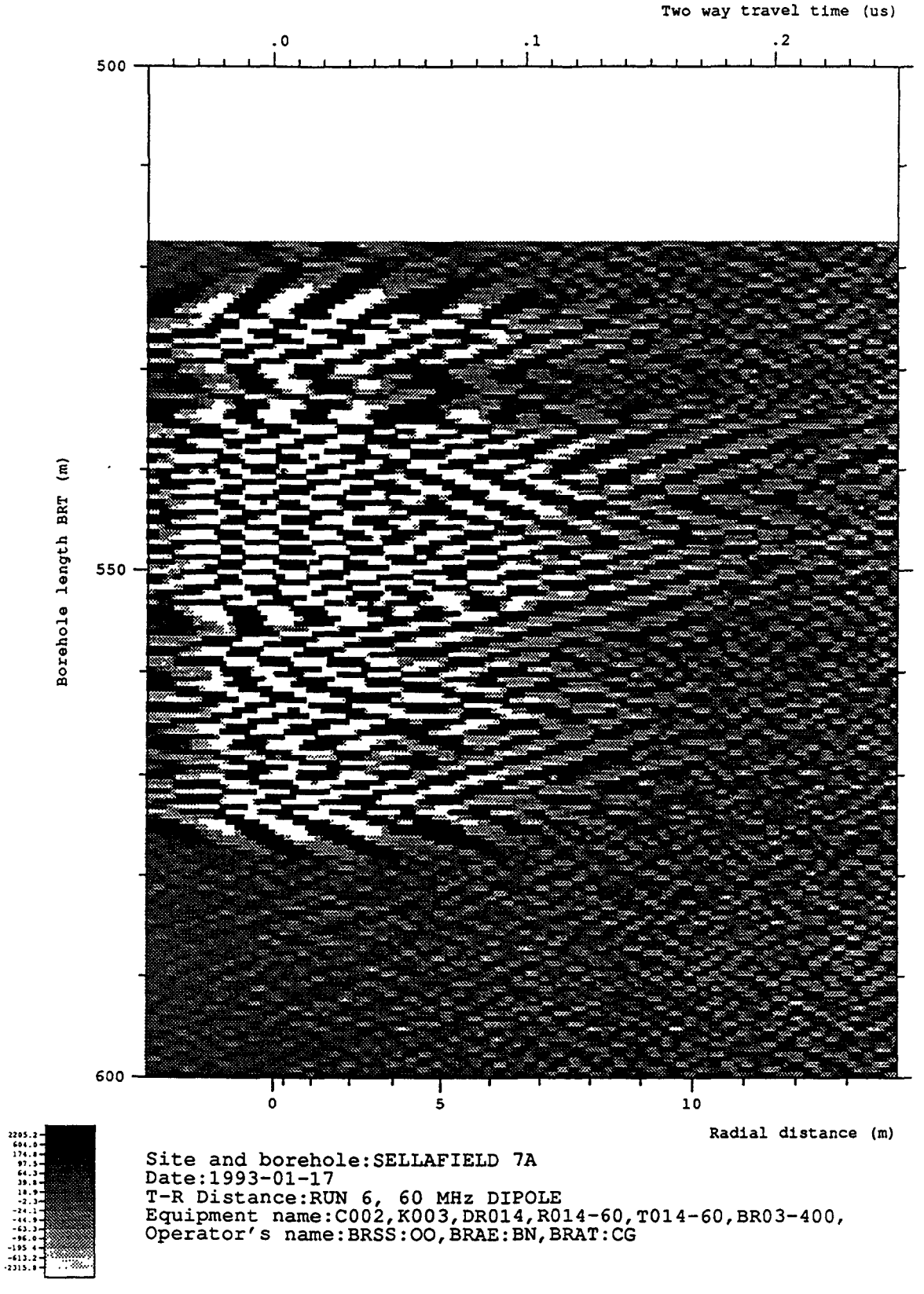

Figure 6-13 Radar map from Run 6, 60 MHz omni-directional survey (517.64 - 600.00 mbRT) after the application of a moving average filter to the band pass filtered data

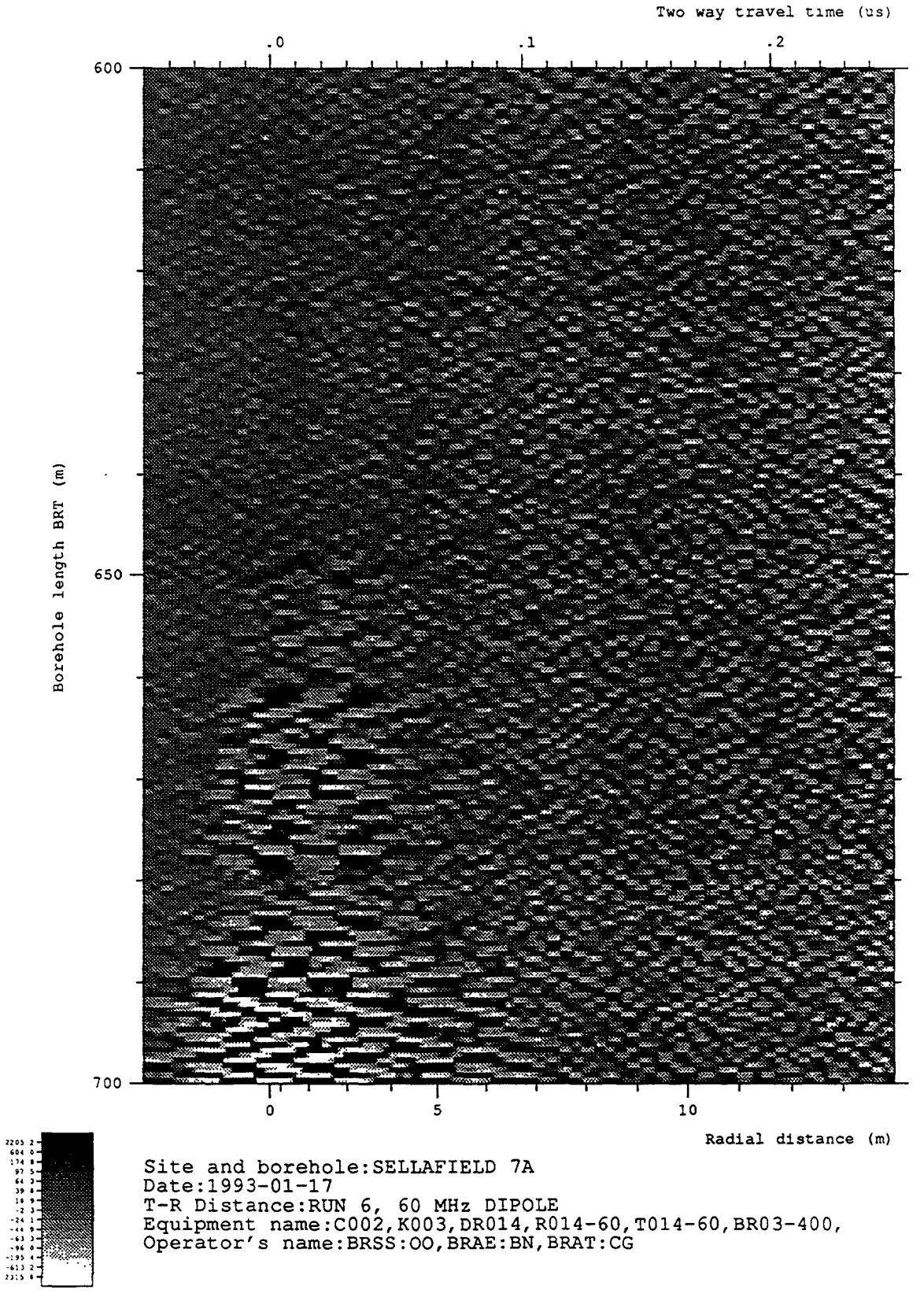

Figure 6-14 Radar map from Run 6, 60 MHz omni-directional survey (600.00 - 700.00 mbRT) after the application of a moving average filter to the band pass filtered data

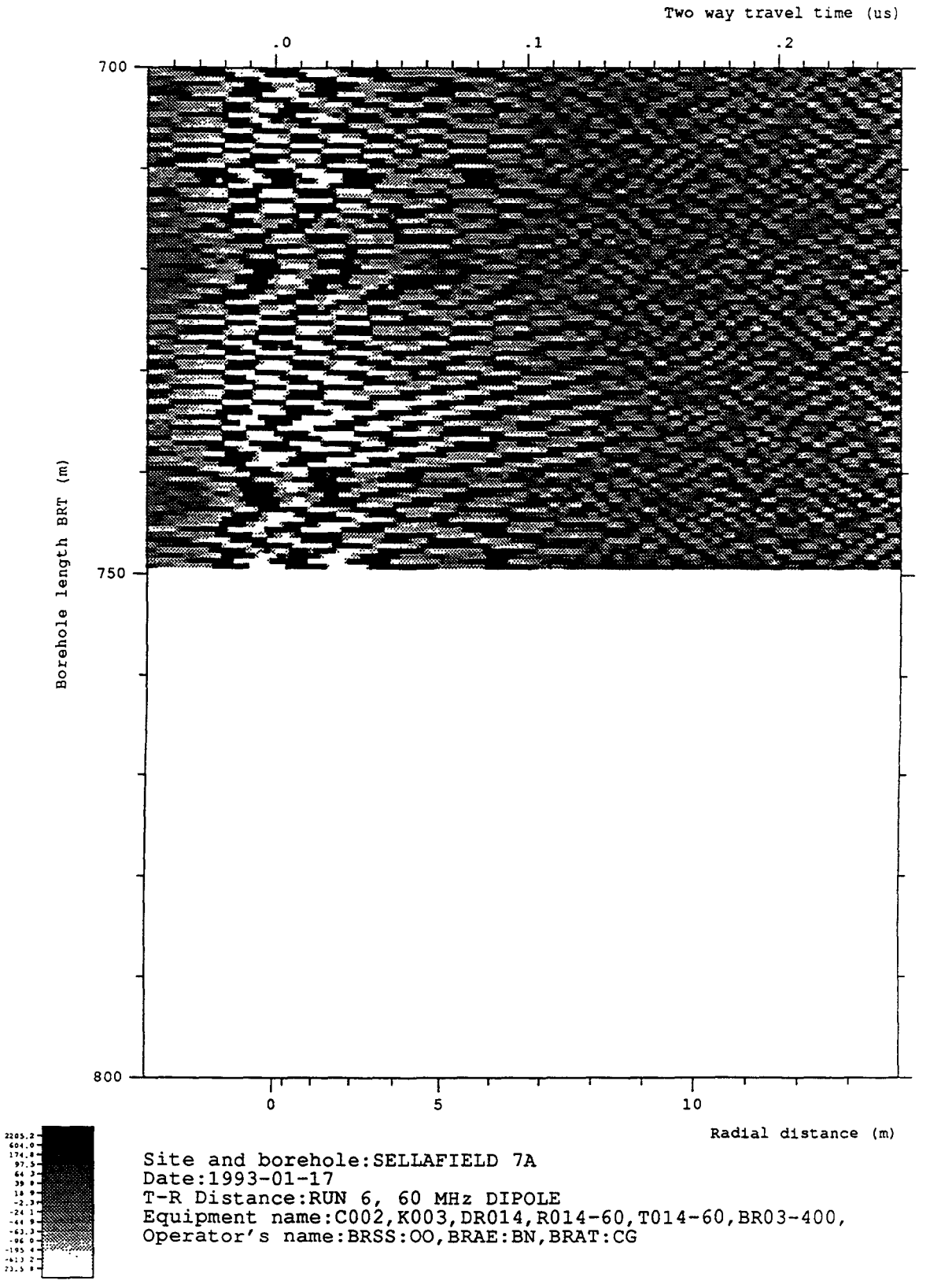

Figure 6-15 Radar map from Run 6, 60 MHz omni-directional survey (700.00 - 749.14 mbRT) after the application of a moving average filter to the band pass filtered data

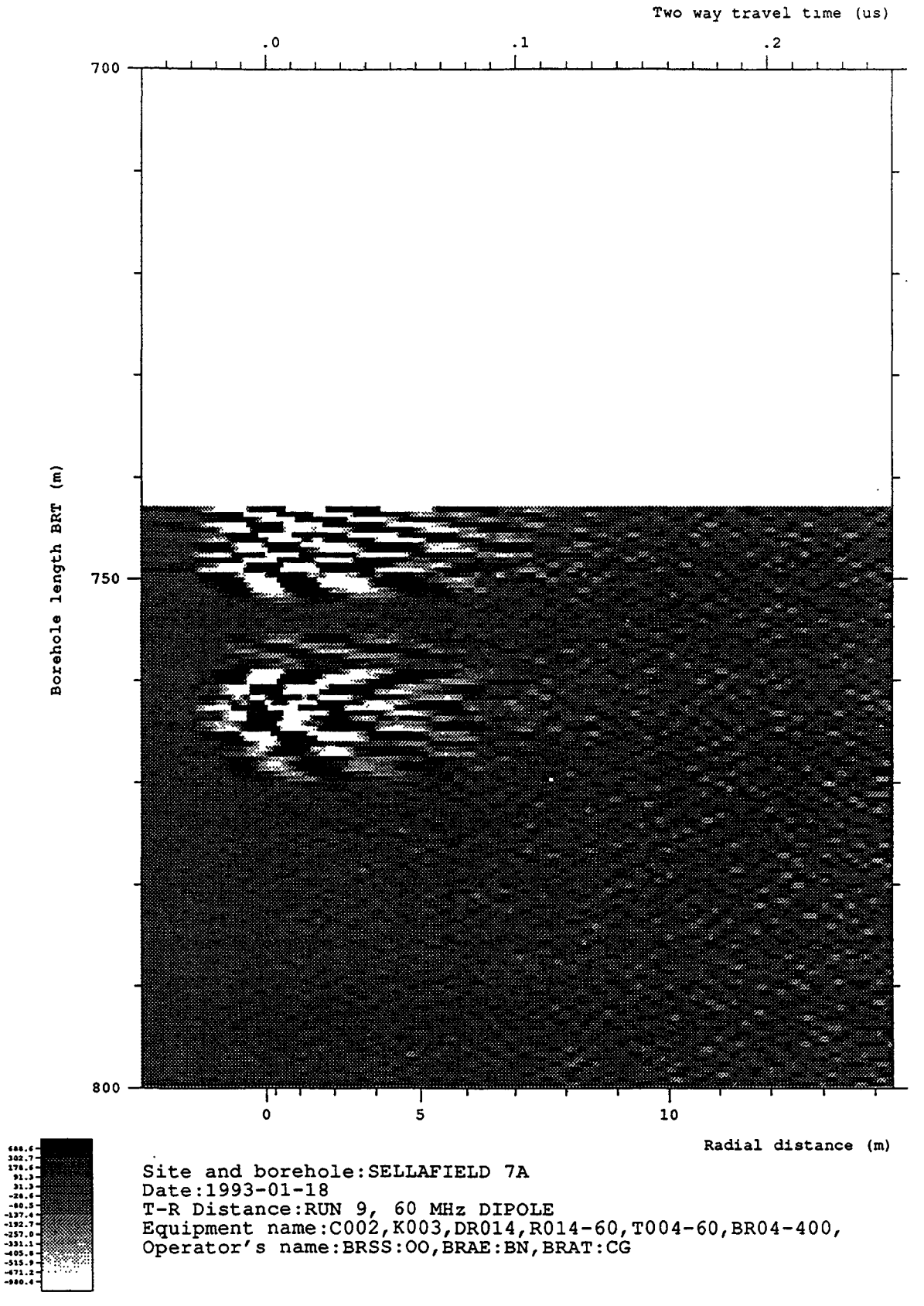

Figure 6-16 Radar map from Run 9, 60 MHz omni-directional survey (743.08 - 800.00 mbRT) after the application of a moving average filter to the band pass filtered data

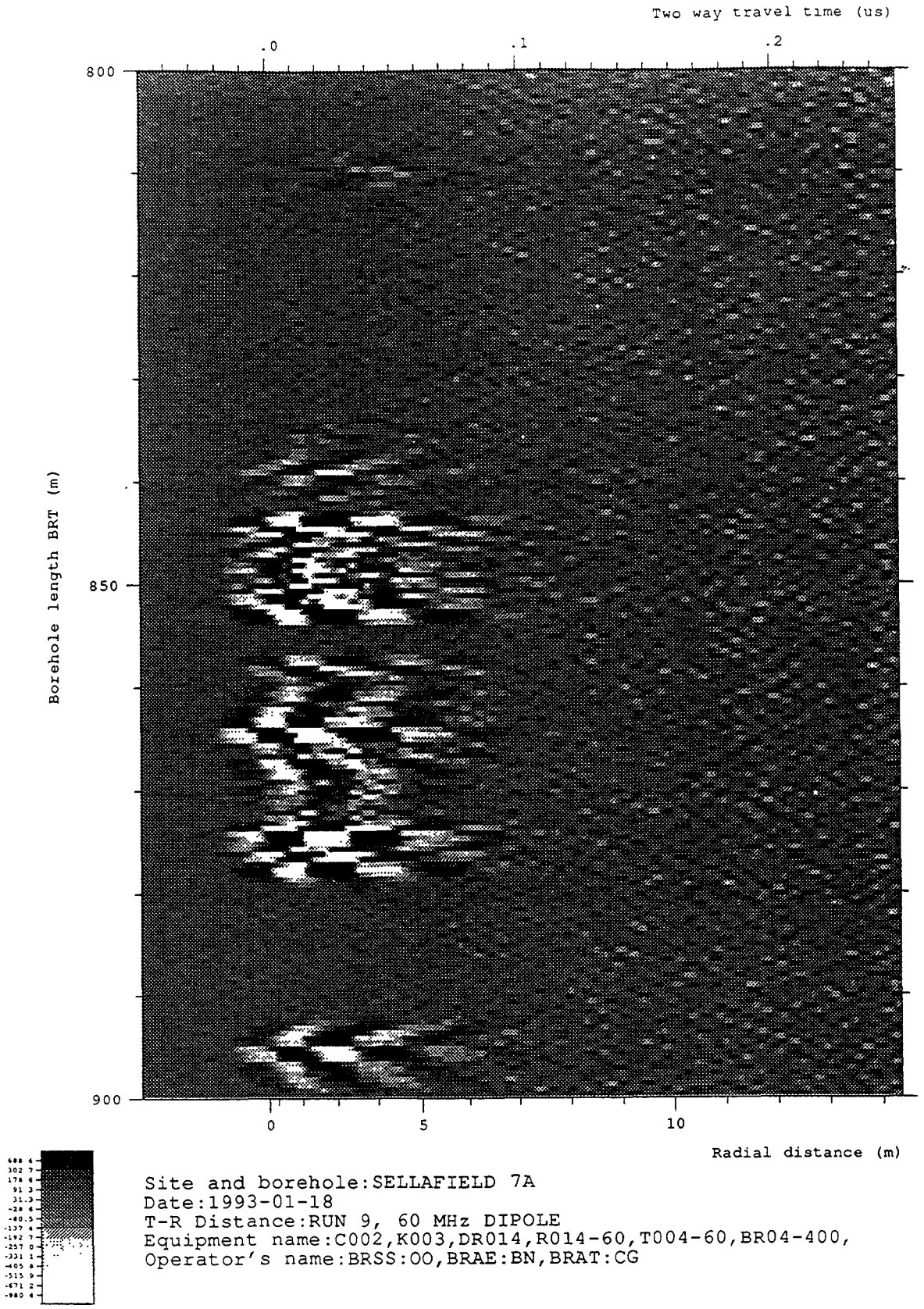

Figure 6-17 Radar map from Run 9, 60 MHz omni-directional survey (800.00 - 900.00 mbRT) after the application of a moving average filter to the band pass filtered data

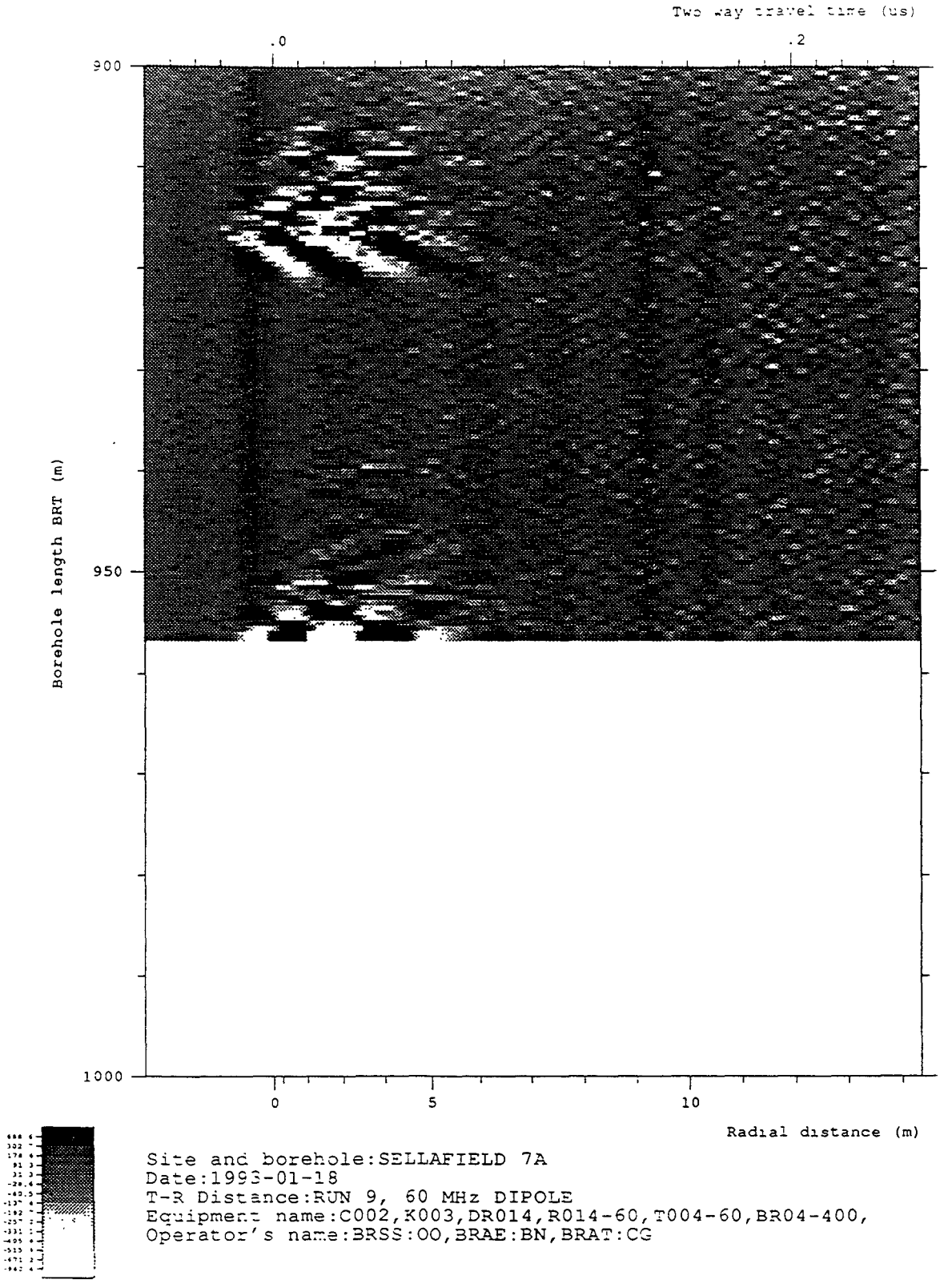

Figure 6-18 Radar map from Run 9, 60 MHz omni-directional survey (900.00 - 956.08 mbRT) after the application of a moving average filter to the band pass filtered data

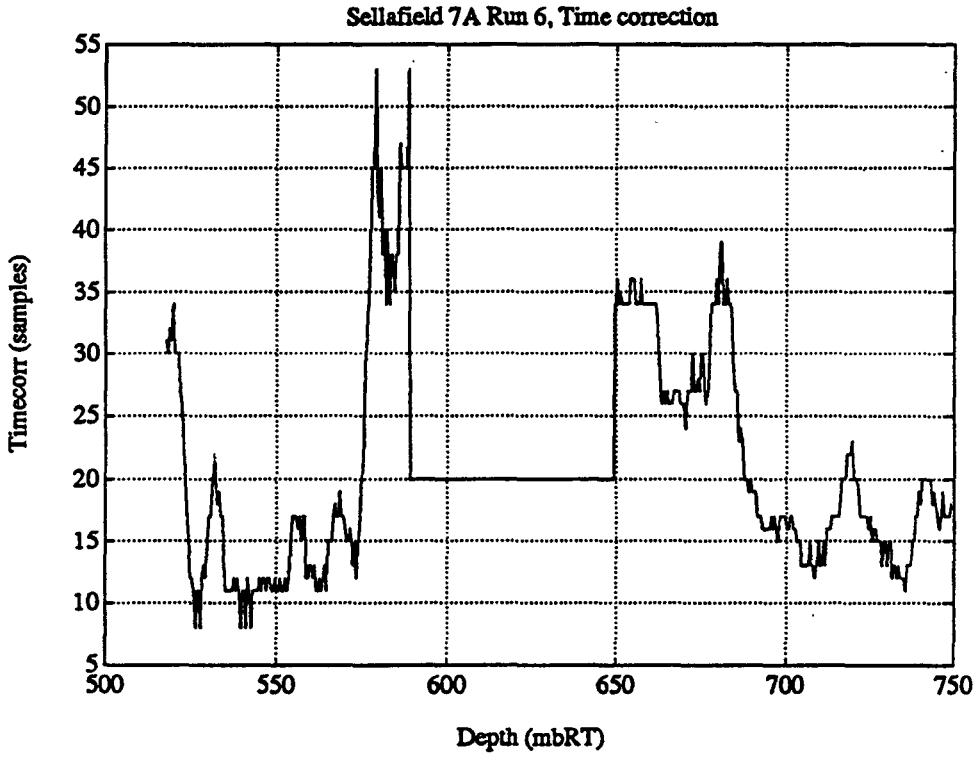

Figure 6-19 Static corrections applied to the Run 6 data

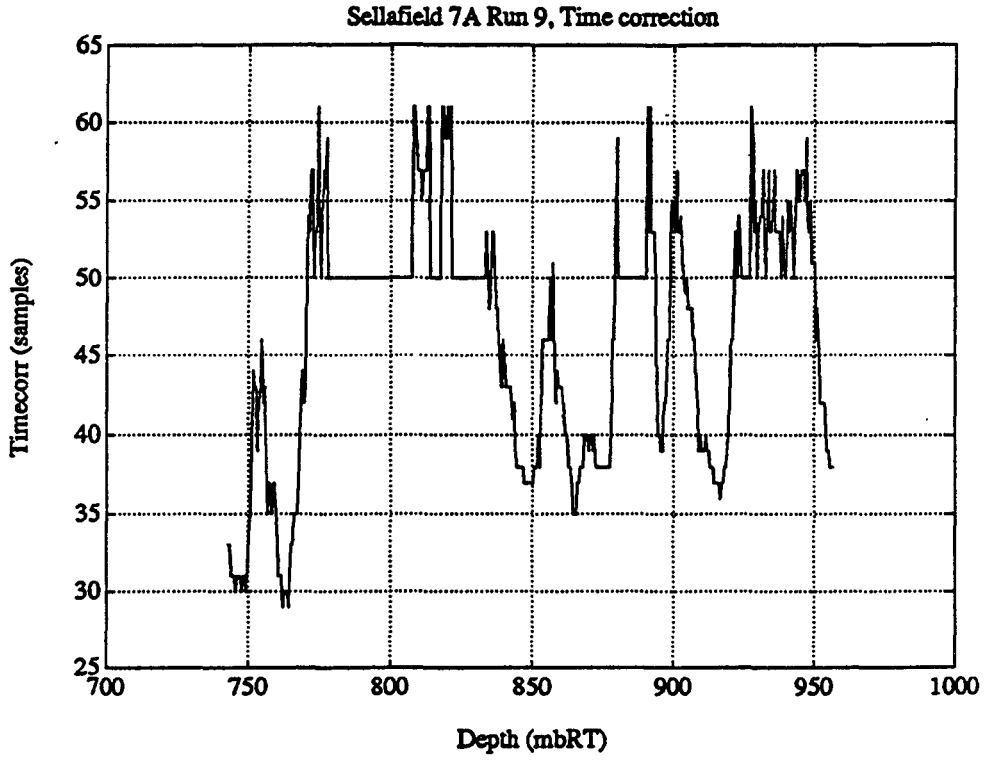

Figure 6-20 Static corrections applied to the Run 9 data

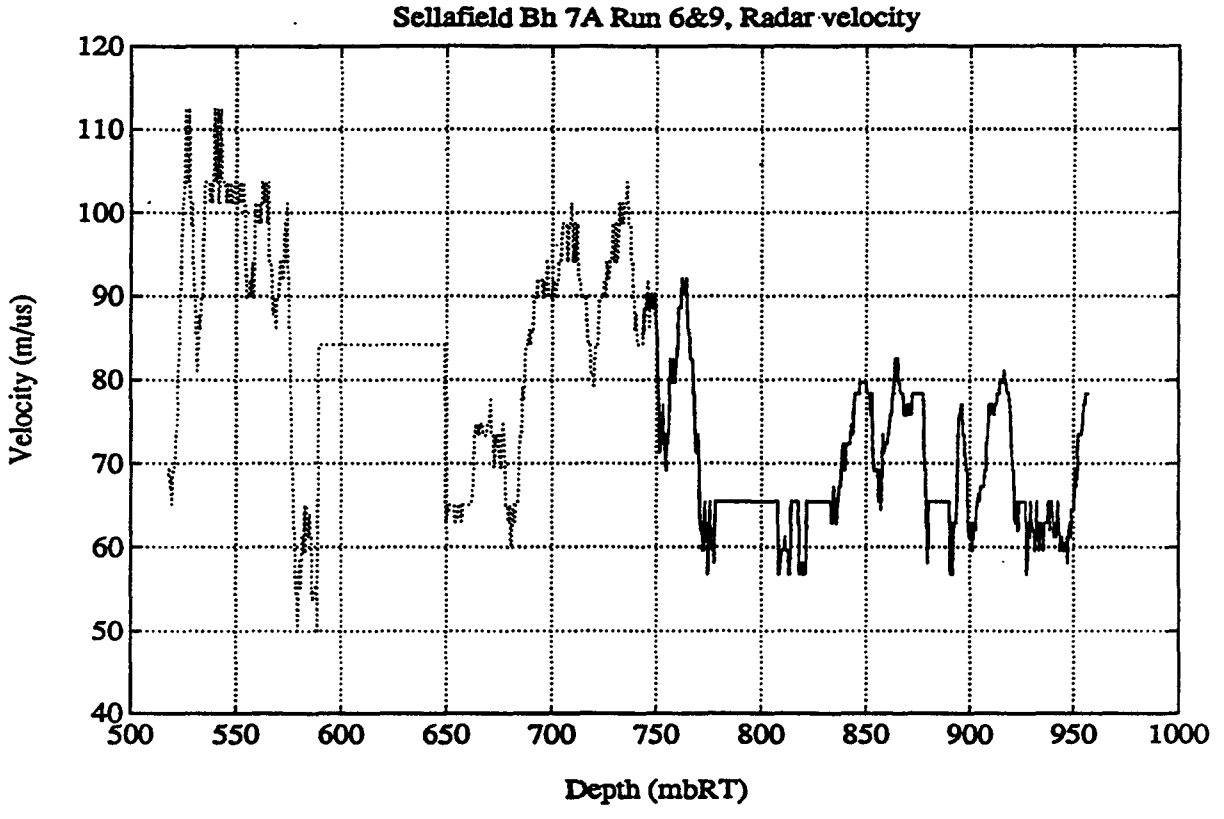

Figure 6-21 Radar velocity as a function of borehole depth for Runs 6 and 9

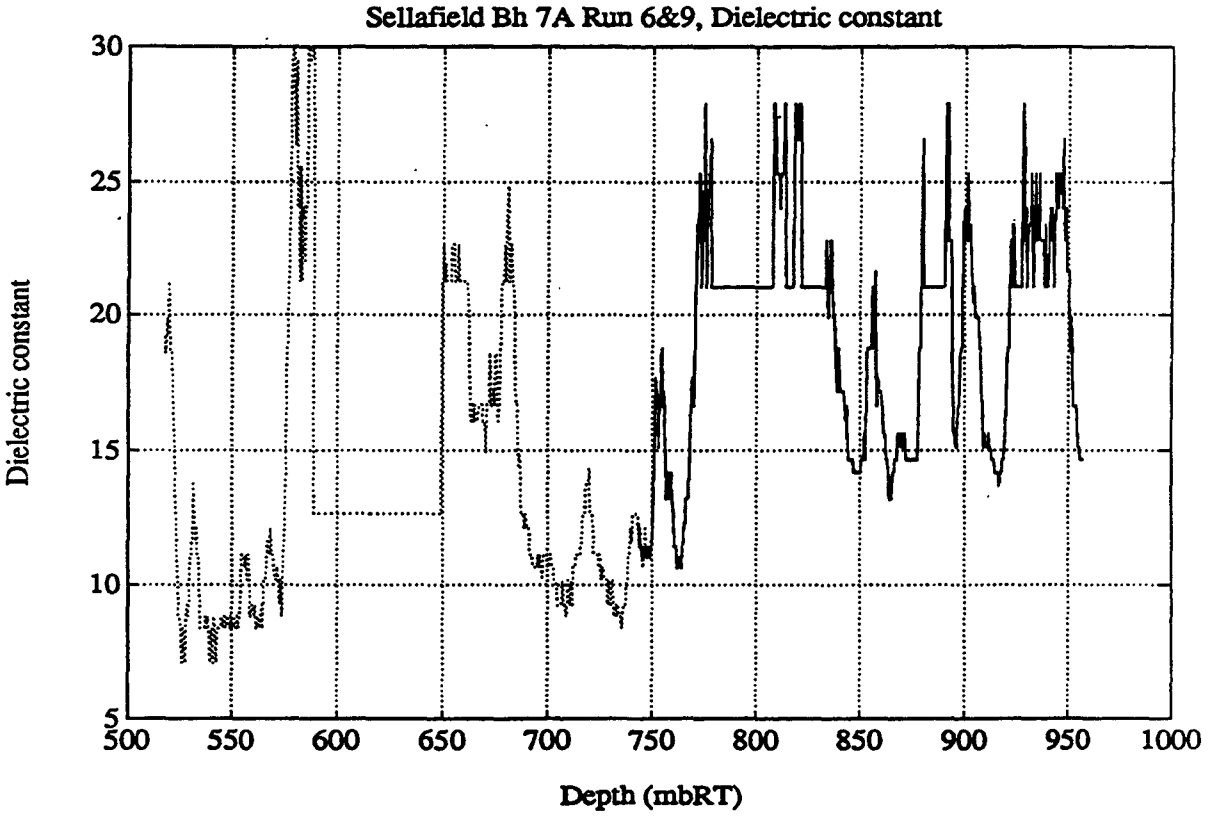

Figure 6-22 Dielectric constant as a function of borehole depth for Runs 6 and 9

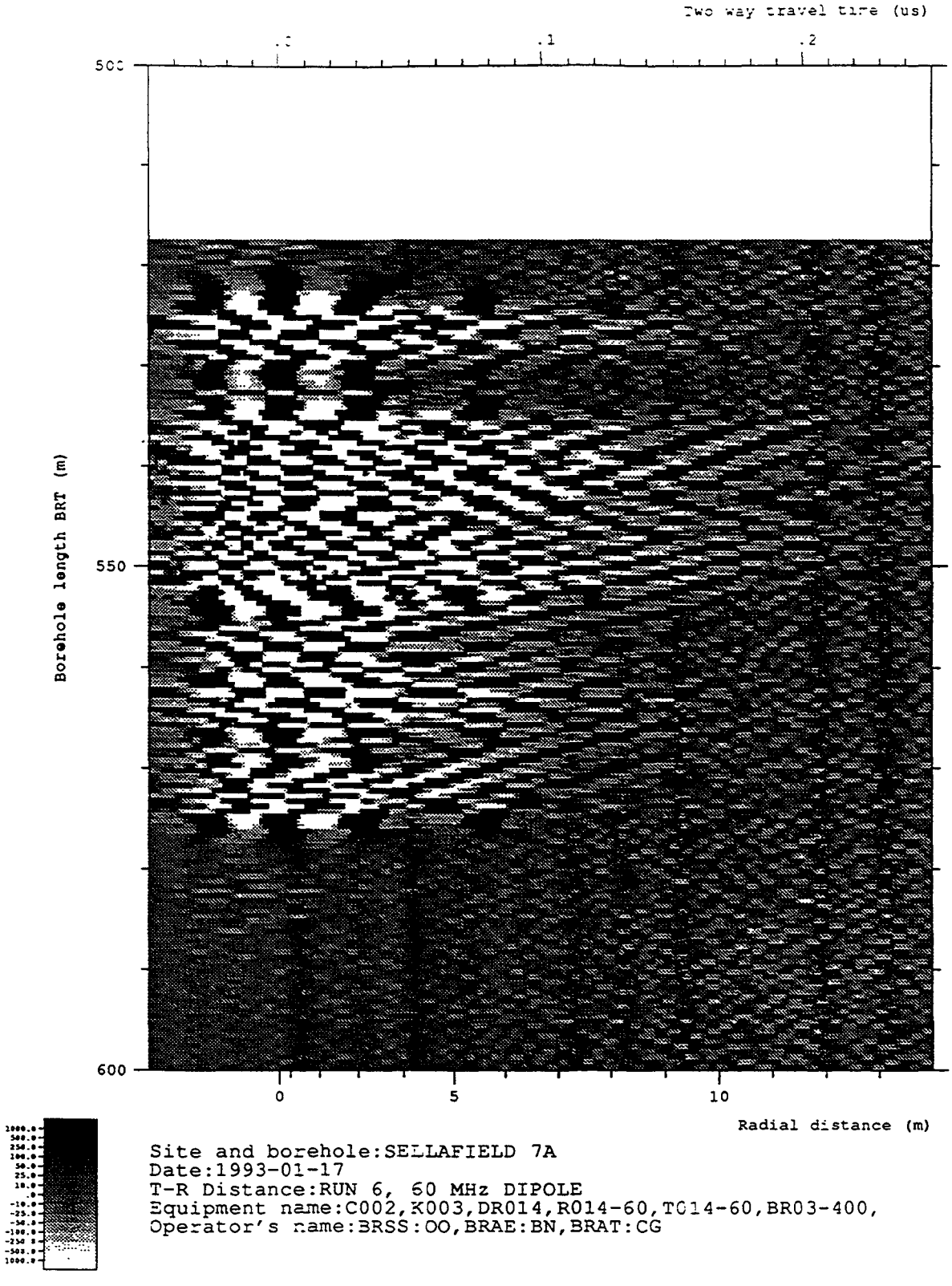

Figure 6-23 Moving average filtered data after static corrections for the interval 517.64 - 600.00 mbRT from Run 6, 60 MHz omni-directional survey

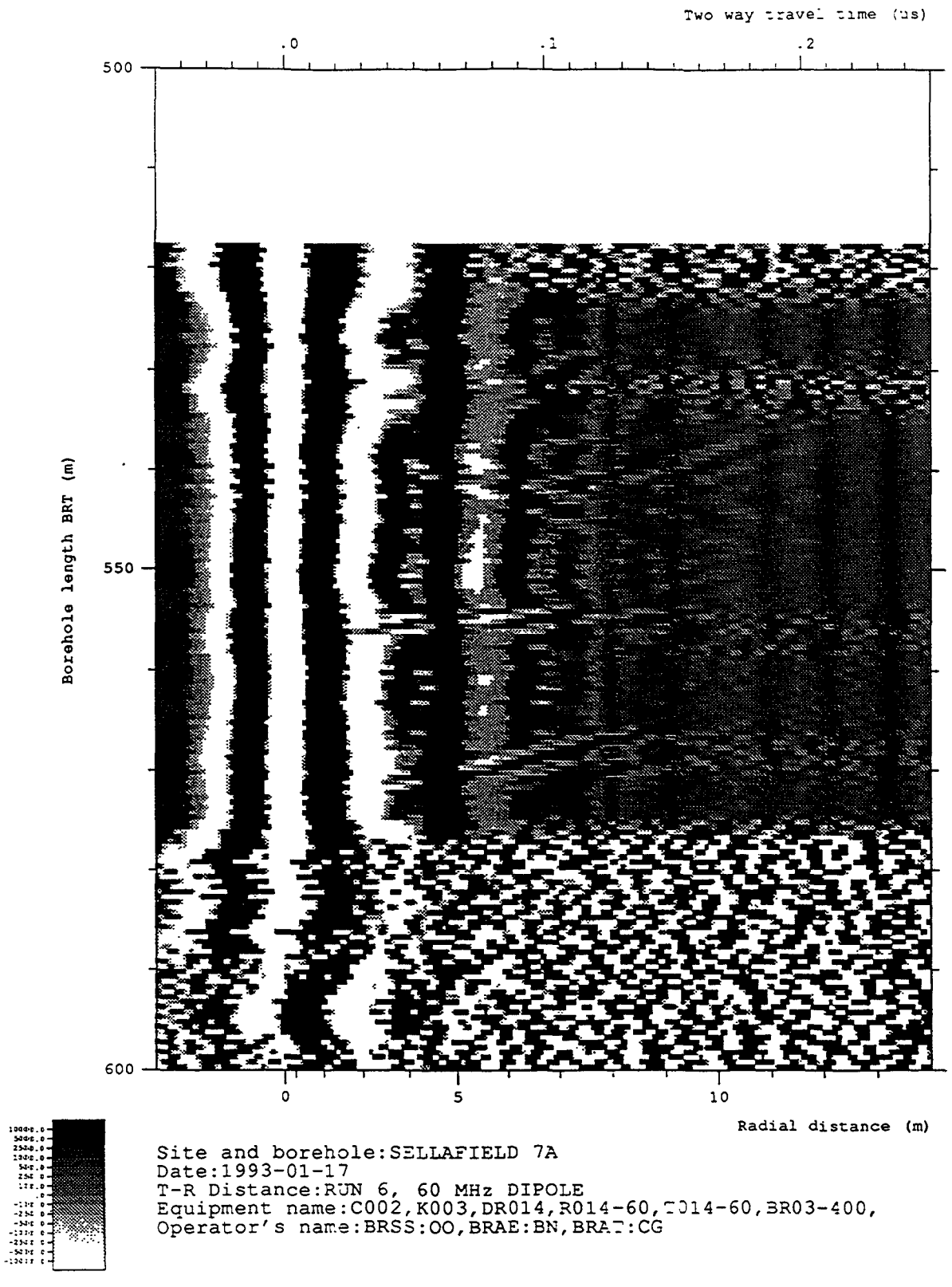

Figure 6-24 Radar map after trace equalisation and static corrections for the interval 517.64 - 600.00 mbRT from Run 6, 60 MHz omni-directional survey

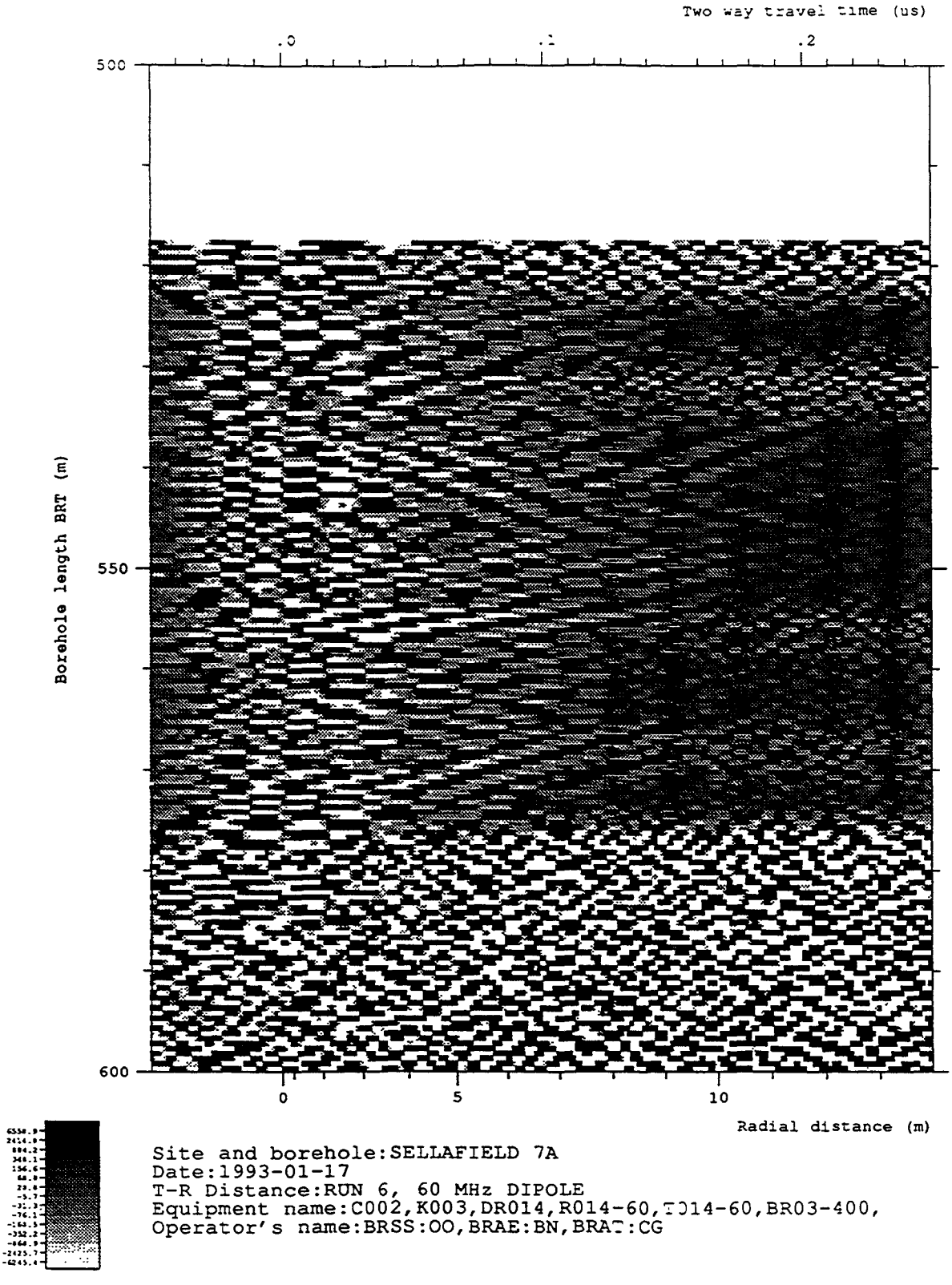

Figure 6-25 Radar map of the data (processing sequence) shown in Figure 6-24 after moving average filtering

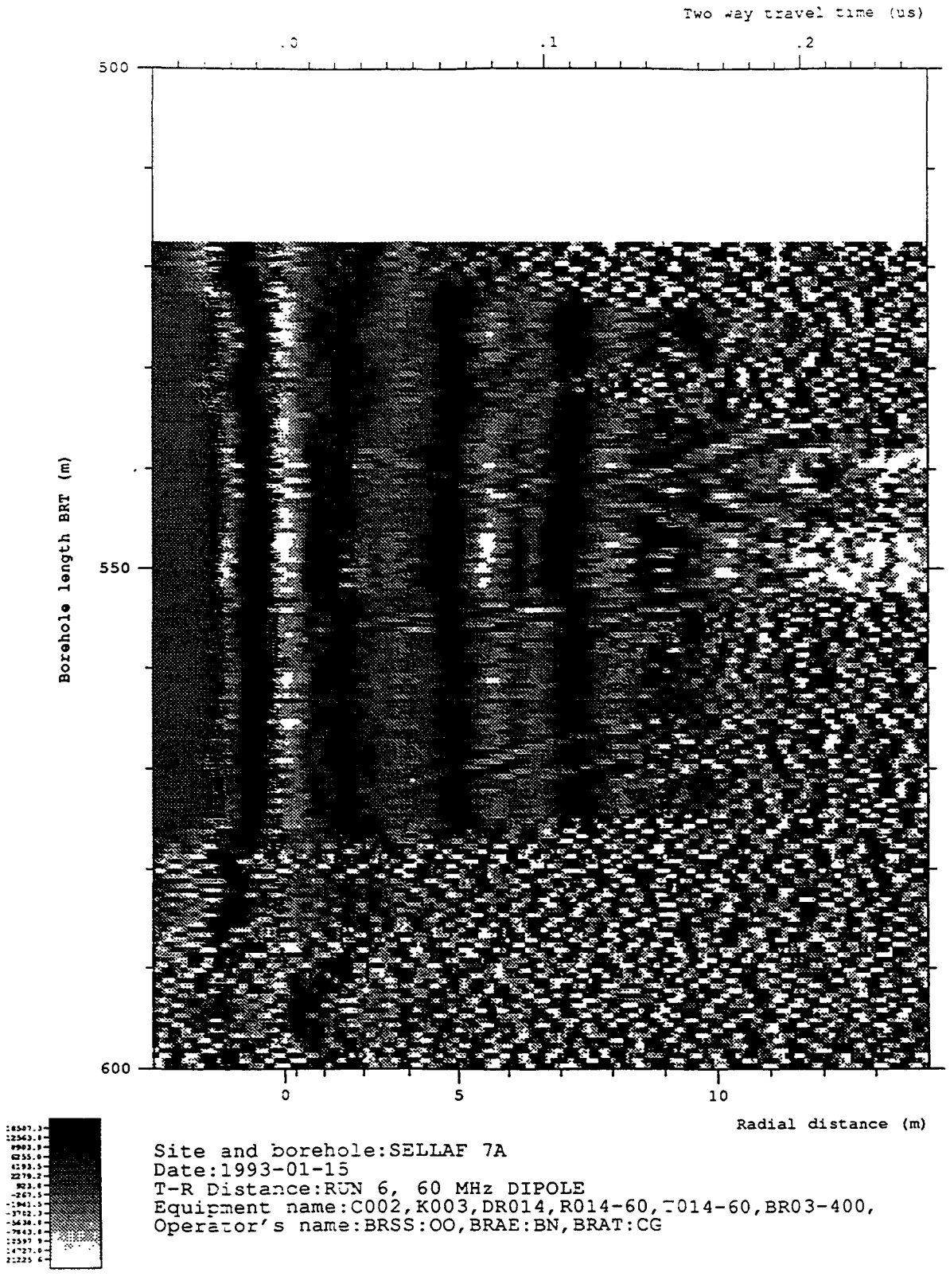

Figure 6-26 Radar map for the interval 517.64 - 600.00 mbRT from Run 6, 60 MHz omni-directional survey showing the result of deconvolution after static corrections and Automatic Gain Control (AGC)

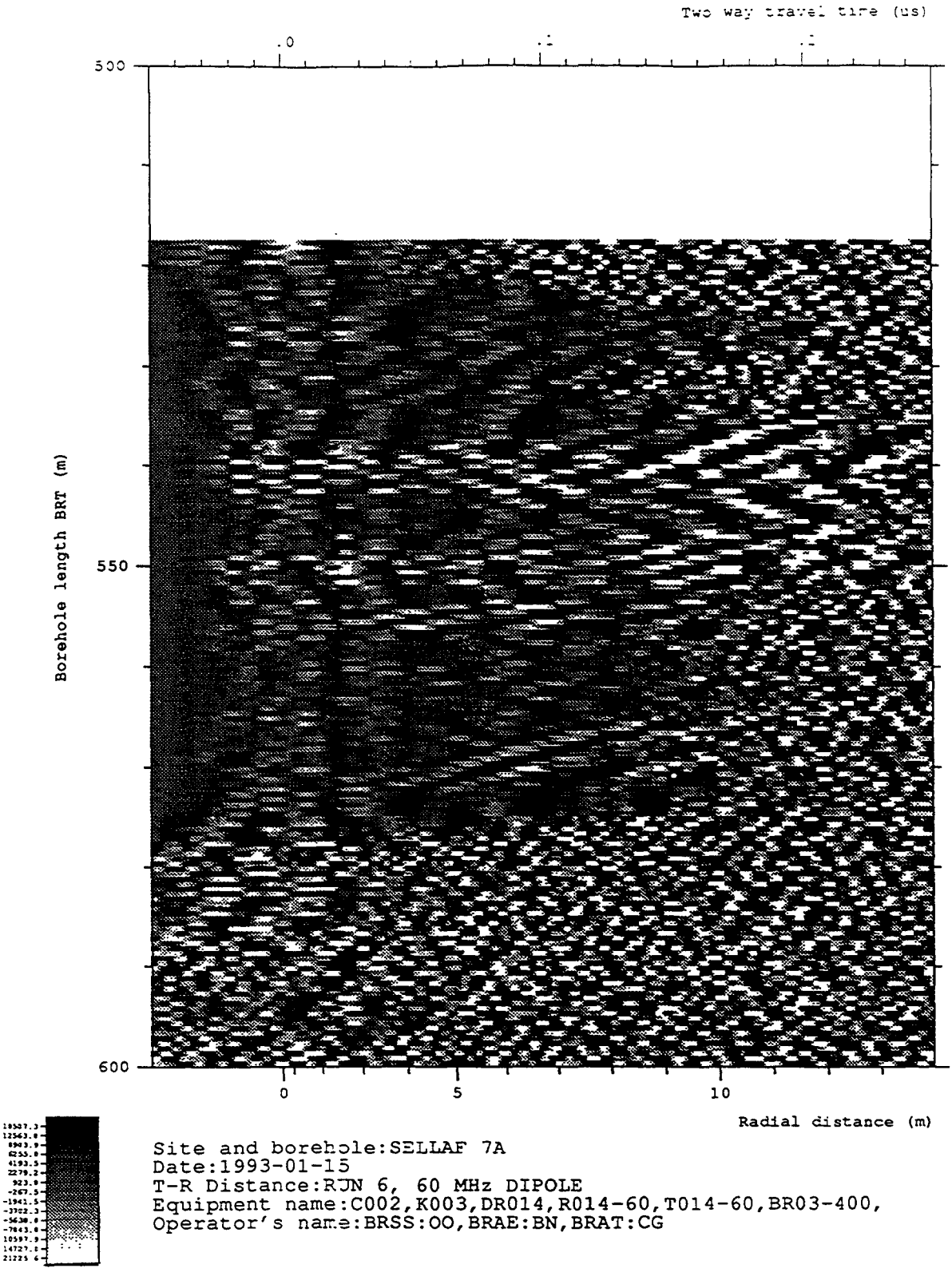

Figure 6-27 The result of FK-filtering after AGC and static corrections where spatial frequencies corresponding to the direct pulse have been suppressed by 40 dB for the interval 517.64 - 600.00 mbRT from Run 6, 60 MHz omni-directional survey

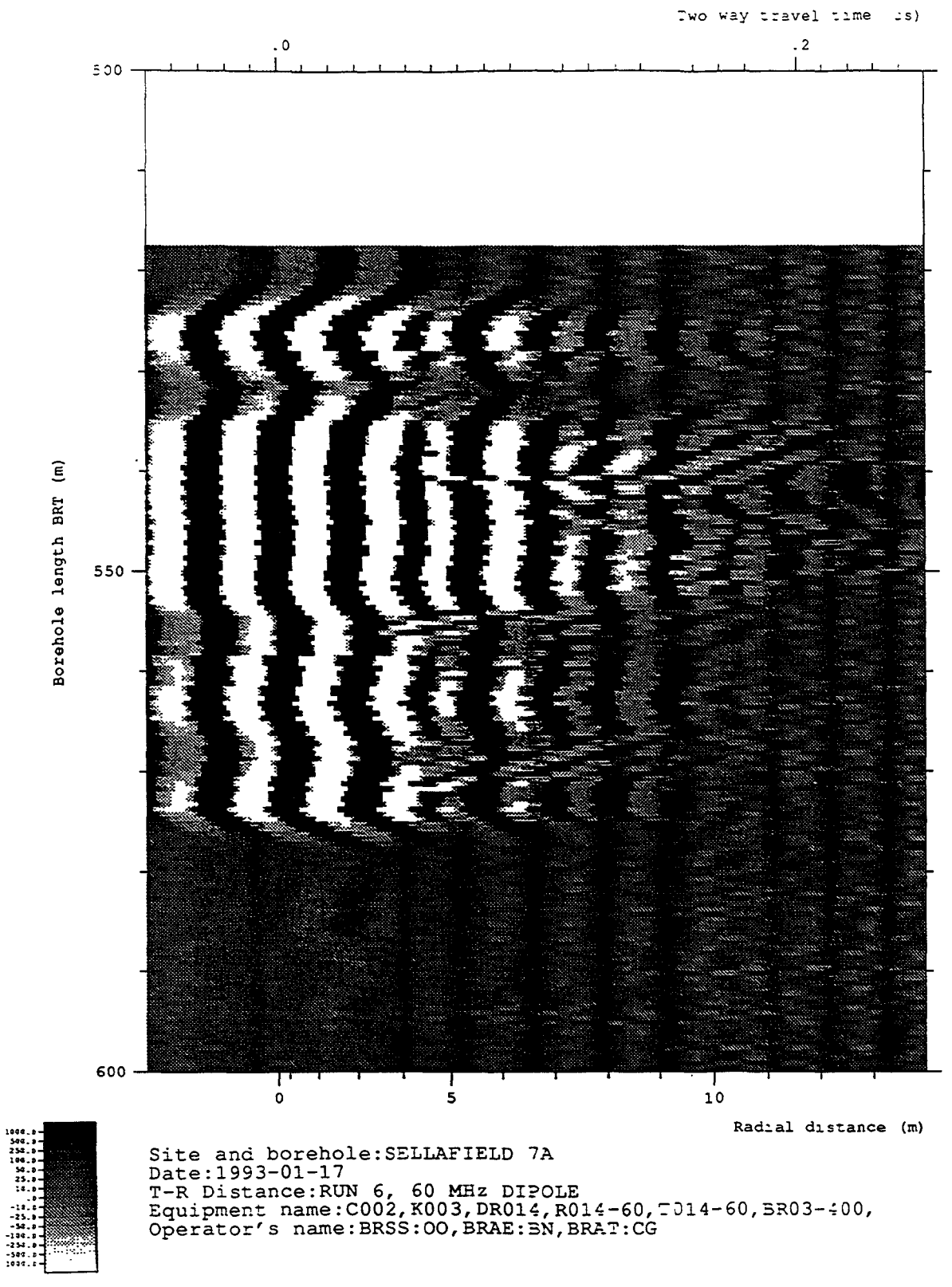

Figure 6-28 Shows the radar map for the interval 517.64 - 600.00 mbRT from Run 6, 60 MHz omni-directional survey after cross-correlation with the average of 35 traces from the limestone section of the borehole after band-pass filtering

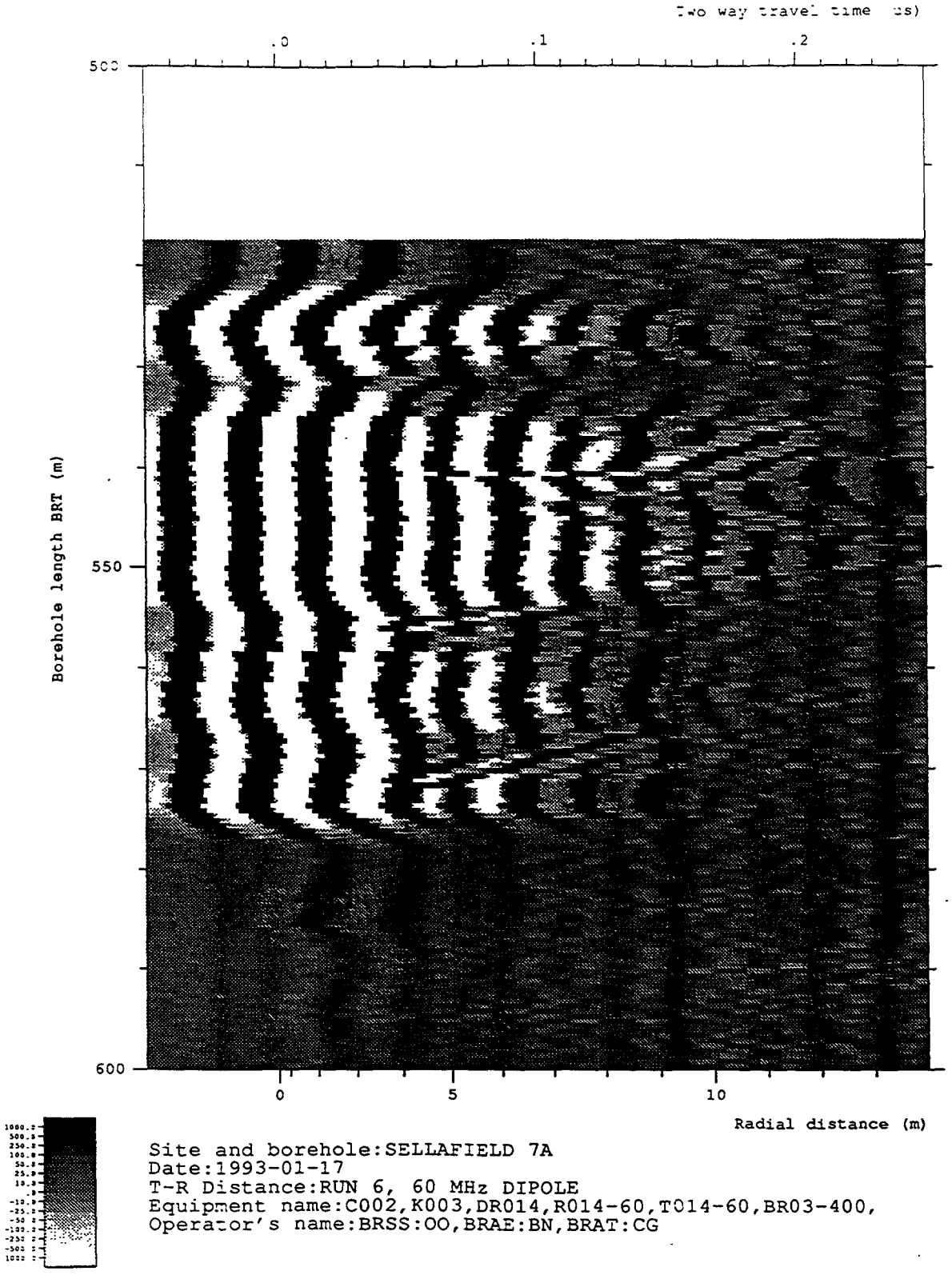

Figure 6-29 Shows the radar map for the interval 517.64 - 600.00 mbRT from Run 6, 60 MHz omni-directional survey after cross-correlation with a synthetic pulse similar to the transmitted pulse

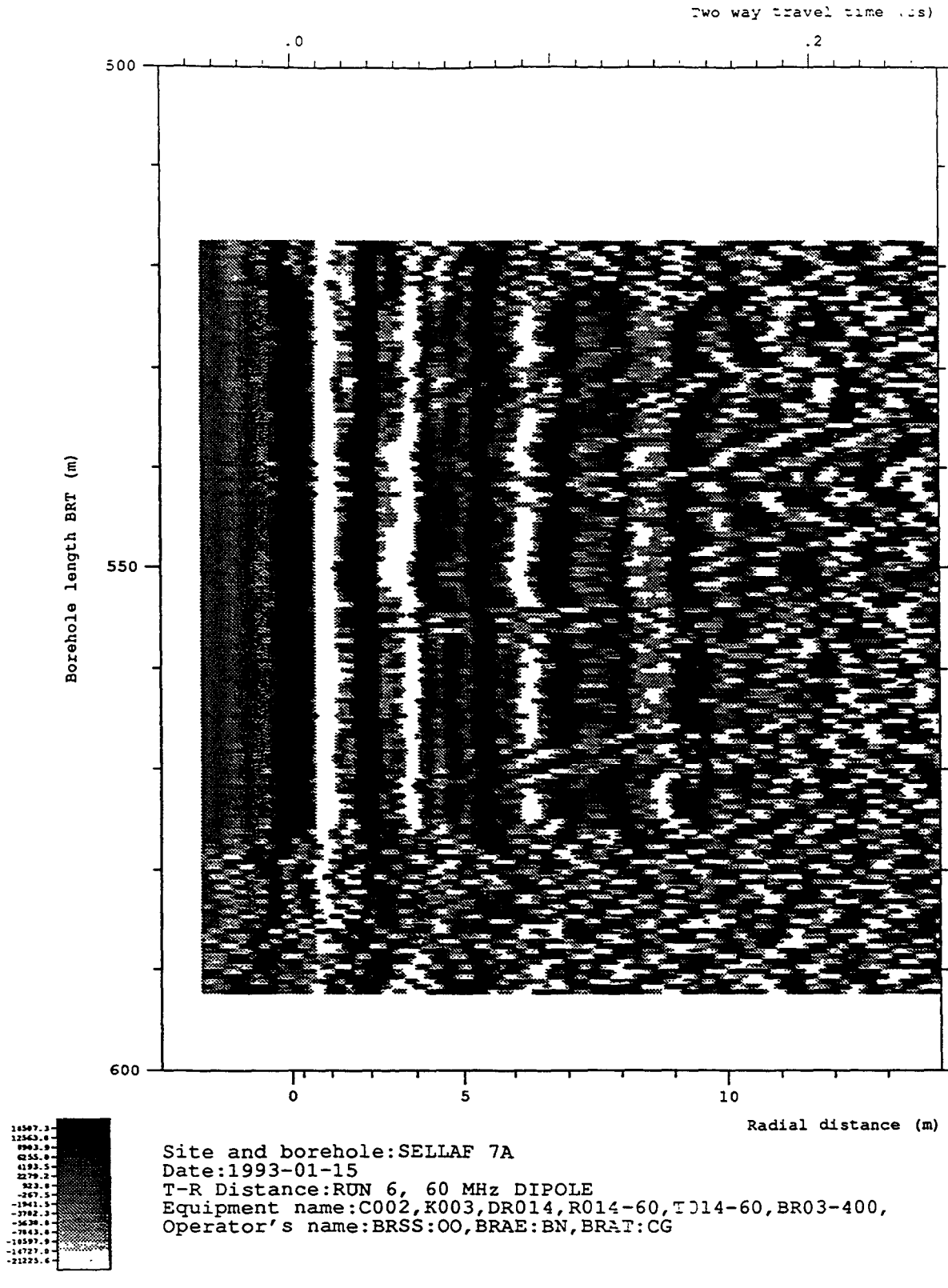

Figure 6-30 The result of adaptive filtering after static corrections and AGC for the interval 517.64 - 600.00 mbRT from Run 6, 60 MHz omni-directional survey

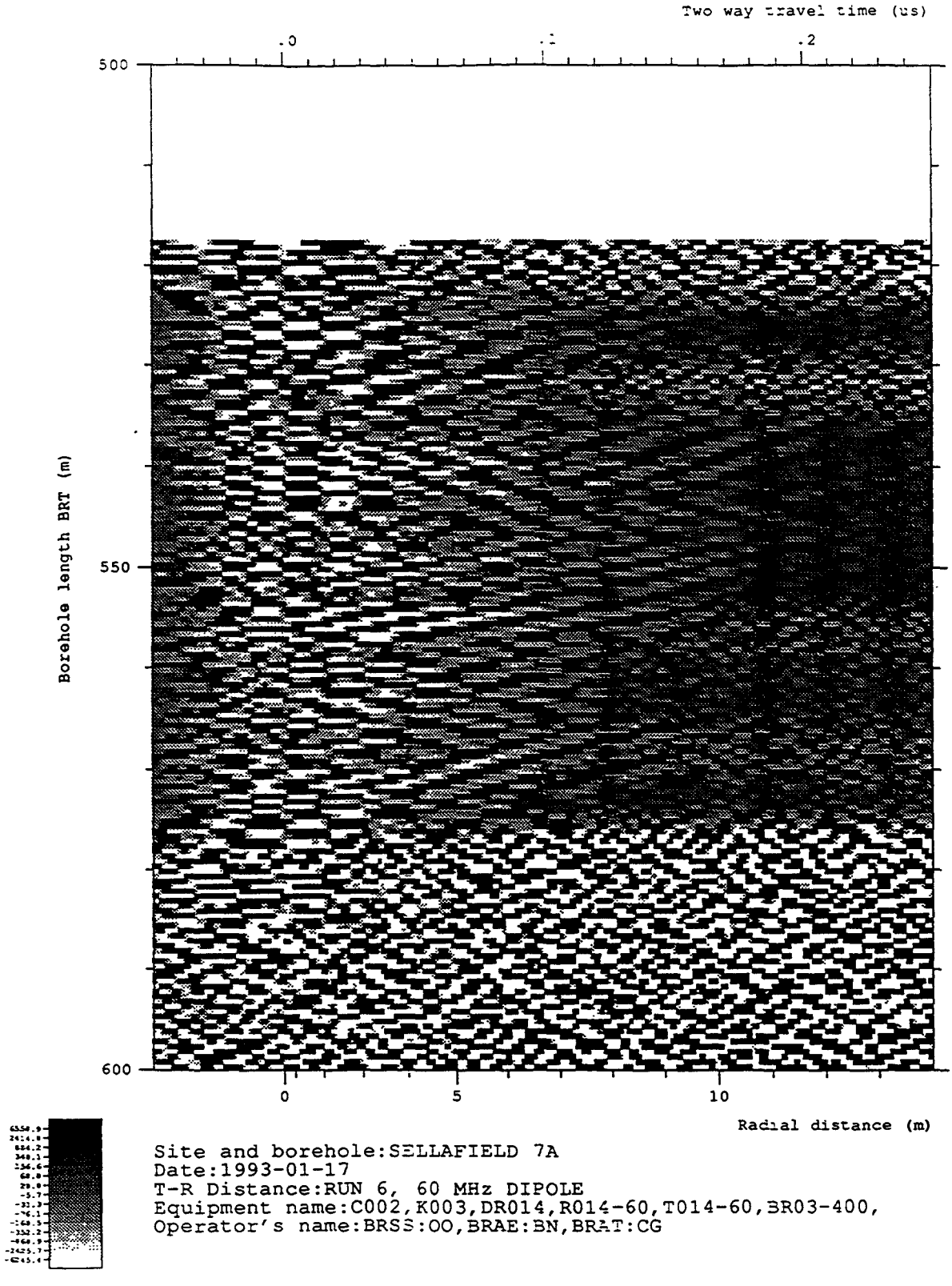

Figure 6-31 Radar map from Run 6, 60 MHz omni-directional survey (517.64 - 600.00 mbRT) after the application of a moving average filter to the data after trace equalisation and static corrections

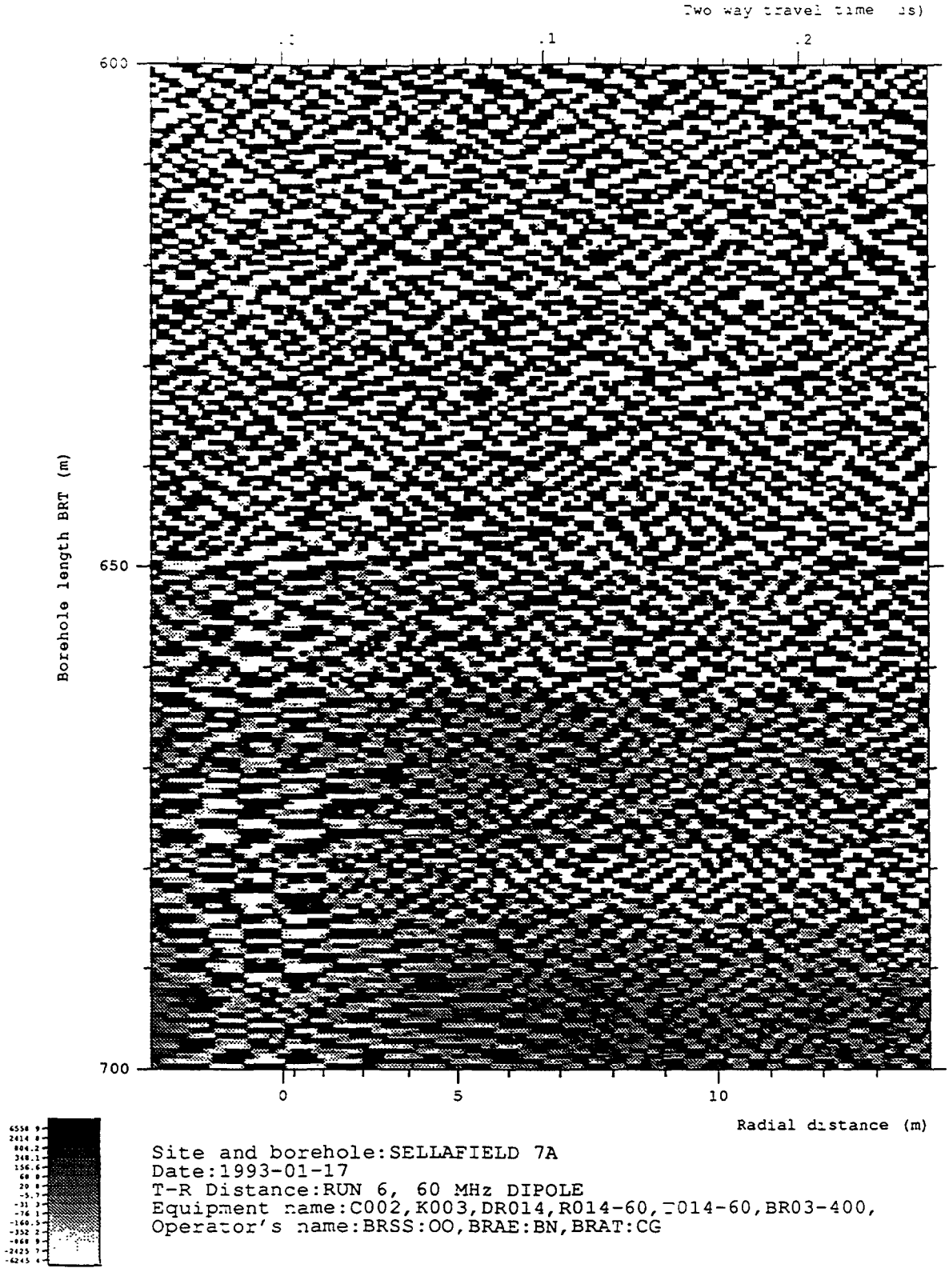

Figure 6-32 Radar map from Run 6, 60 MHz omni-directional survey (600.00 - 700.00 mbRT) after the application of a moving average filter to the data after trace equalisation and static corrections

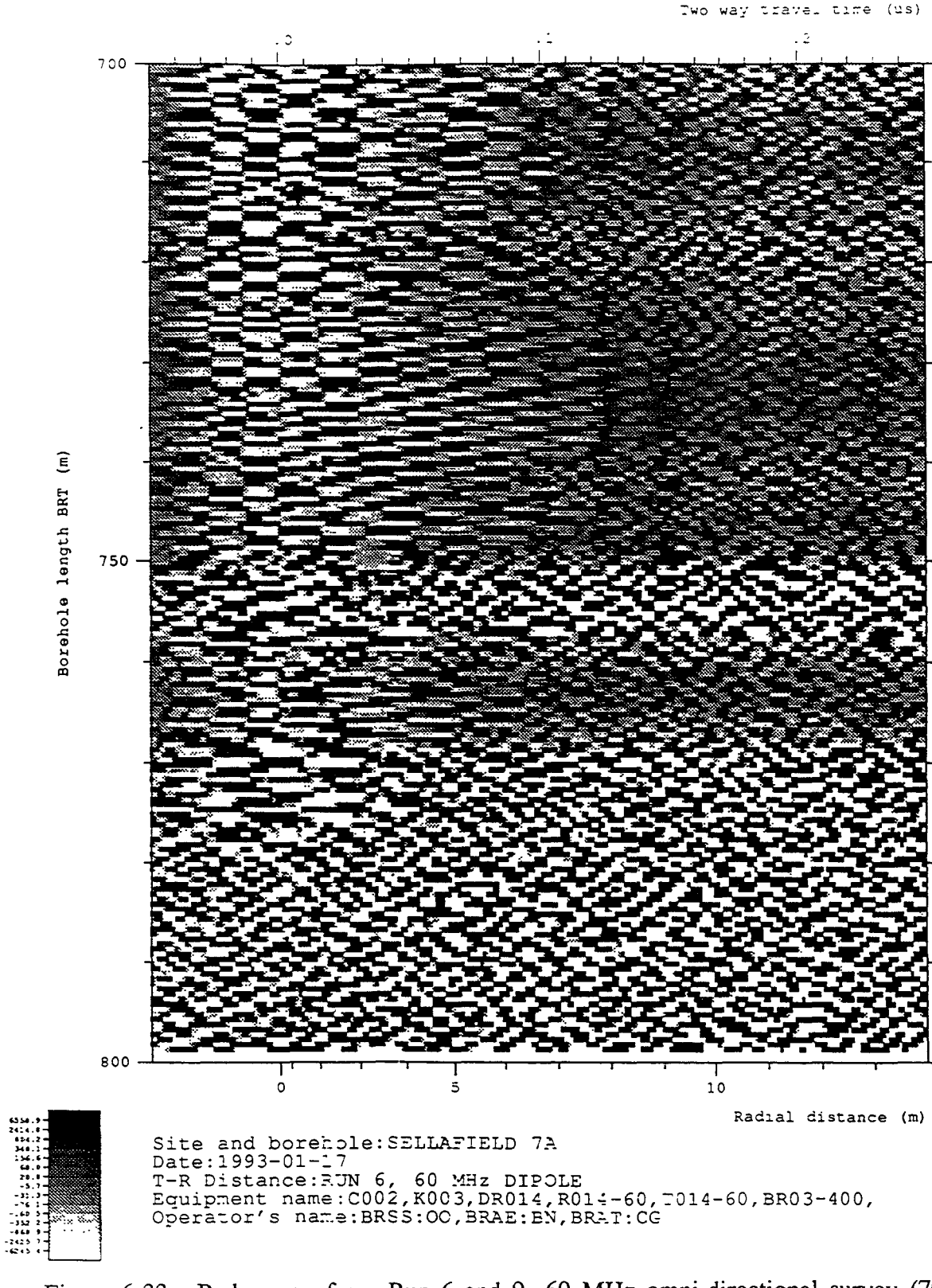

Figure 6-33 Radar map from Run 6 and 9, 60 MHz omni-directional survey (700.00 - 800.00 mbRT) after the application of a moving average filter to the data after trace equalisation and static corrections

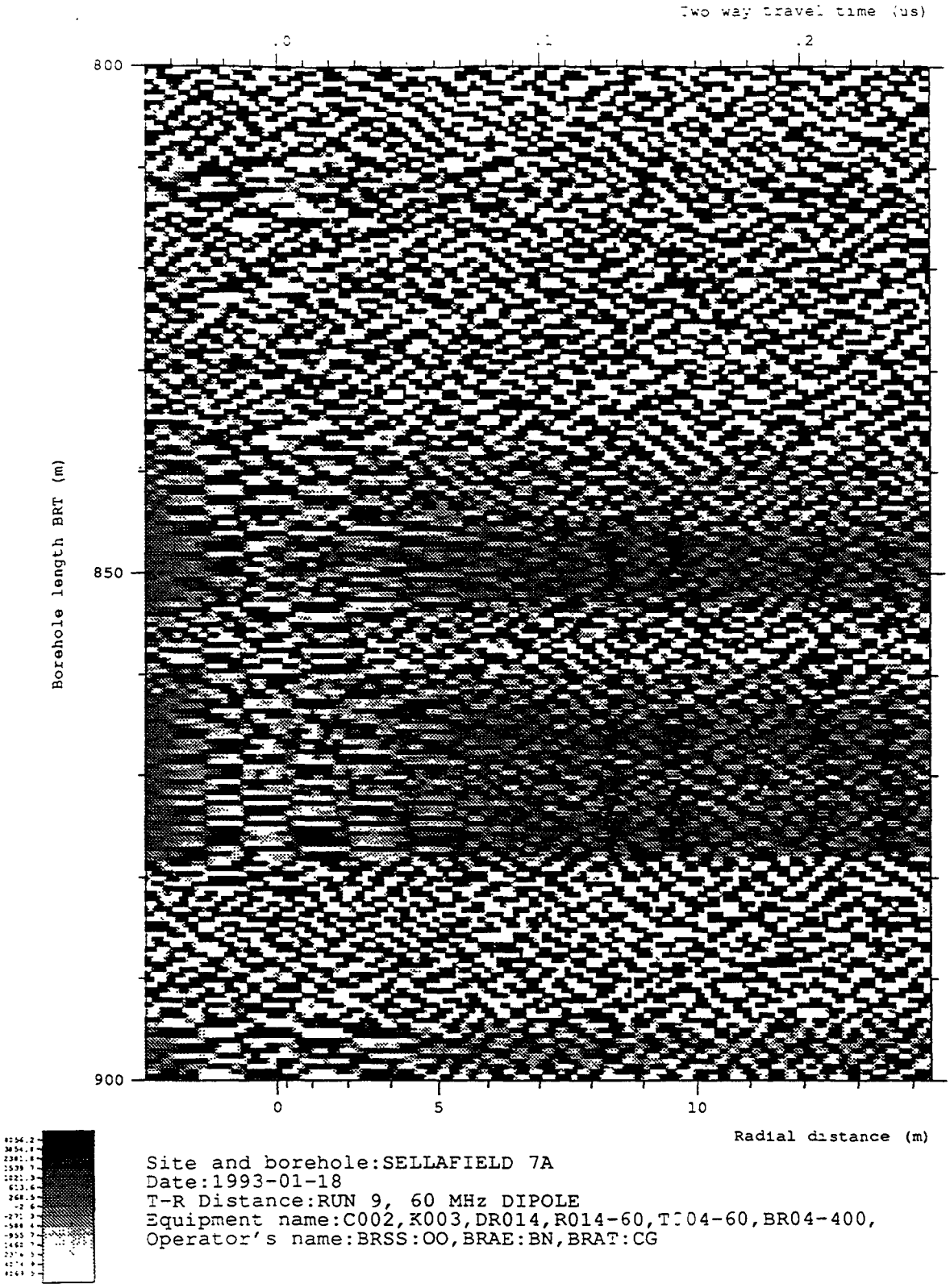

Figure 6-34 Radar map from Run 9, 60 MHz omni-directional survey (800.00 - 900.00 mbRT) after the application of a moving average filter to the data after trace equalisation and static corrections

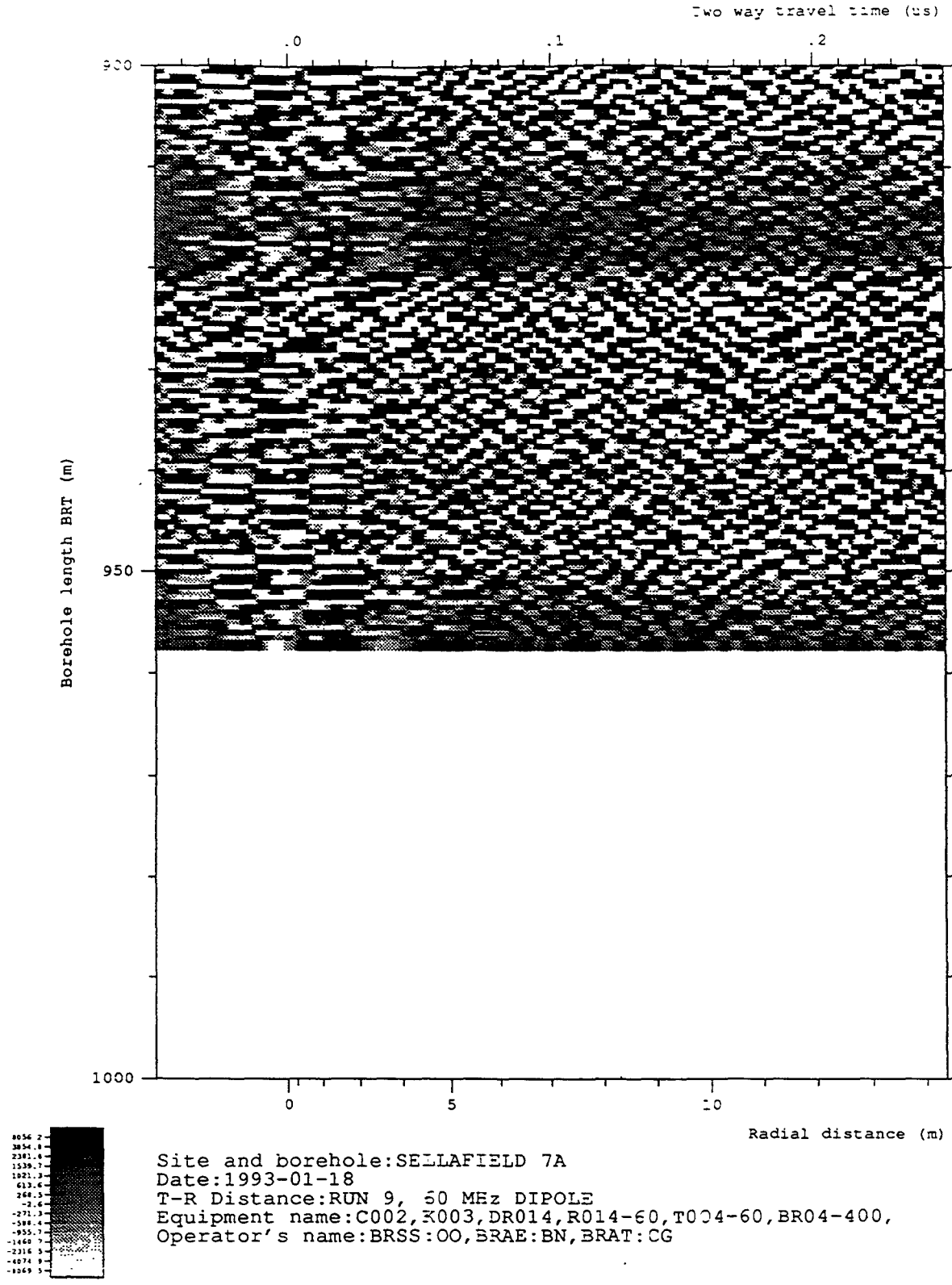

Figure 6-35 Radar map from Run 9, 60 MHz omni-directional survey (900.00 - 956.08 mbRT) after the application of a moving average filter to the data after trace equalisation and static corrections

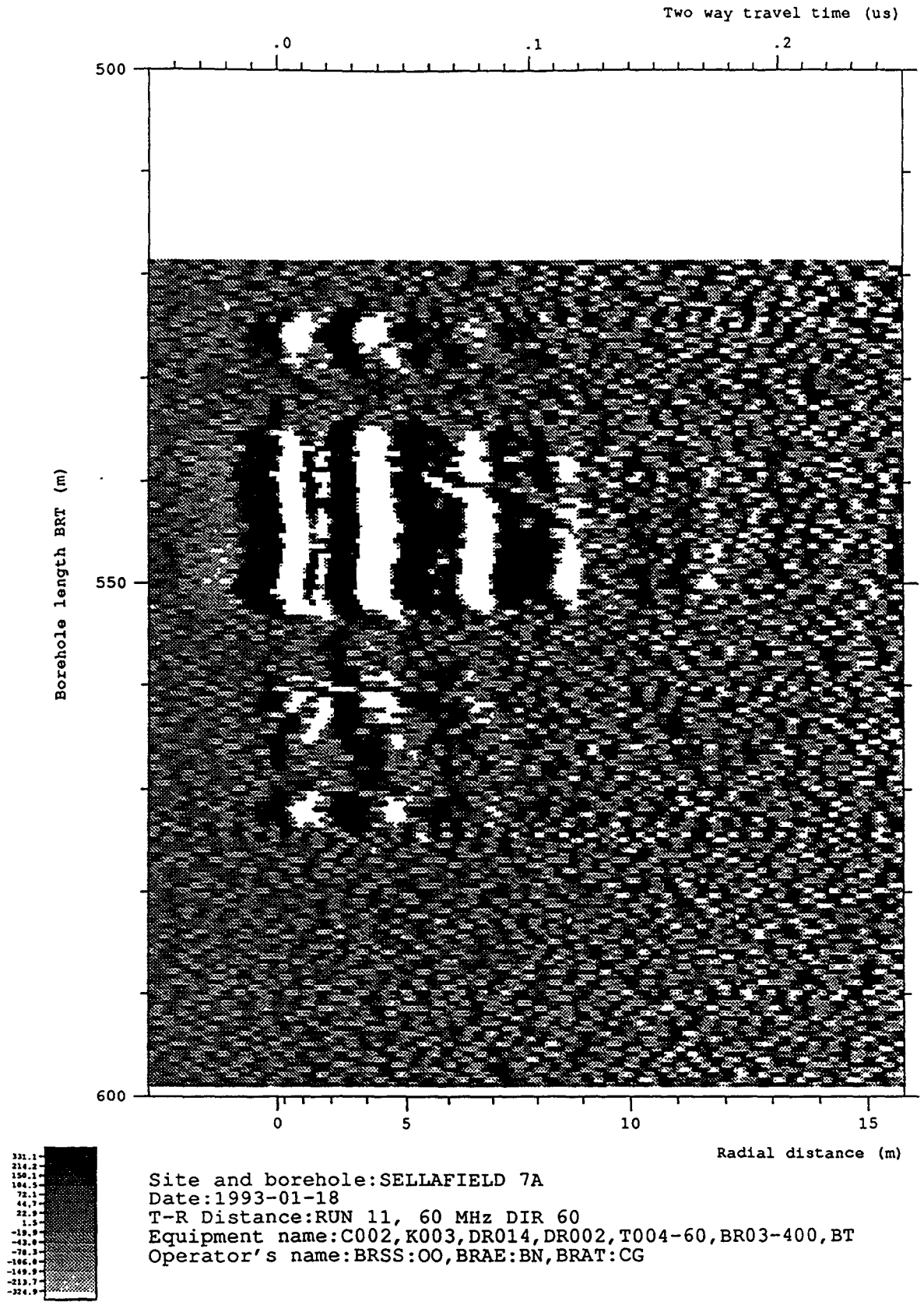

Figure 6-36 Radar map of the dipole component from the 60 MHz directional survey Run 11 after depth correction and band pass filtering for the depth interval 518.80 to 598.80 mbRT at an azimuth of 0°

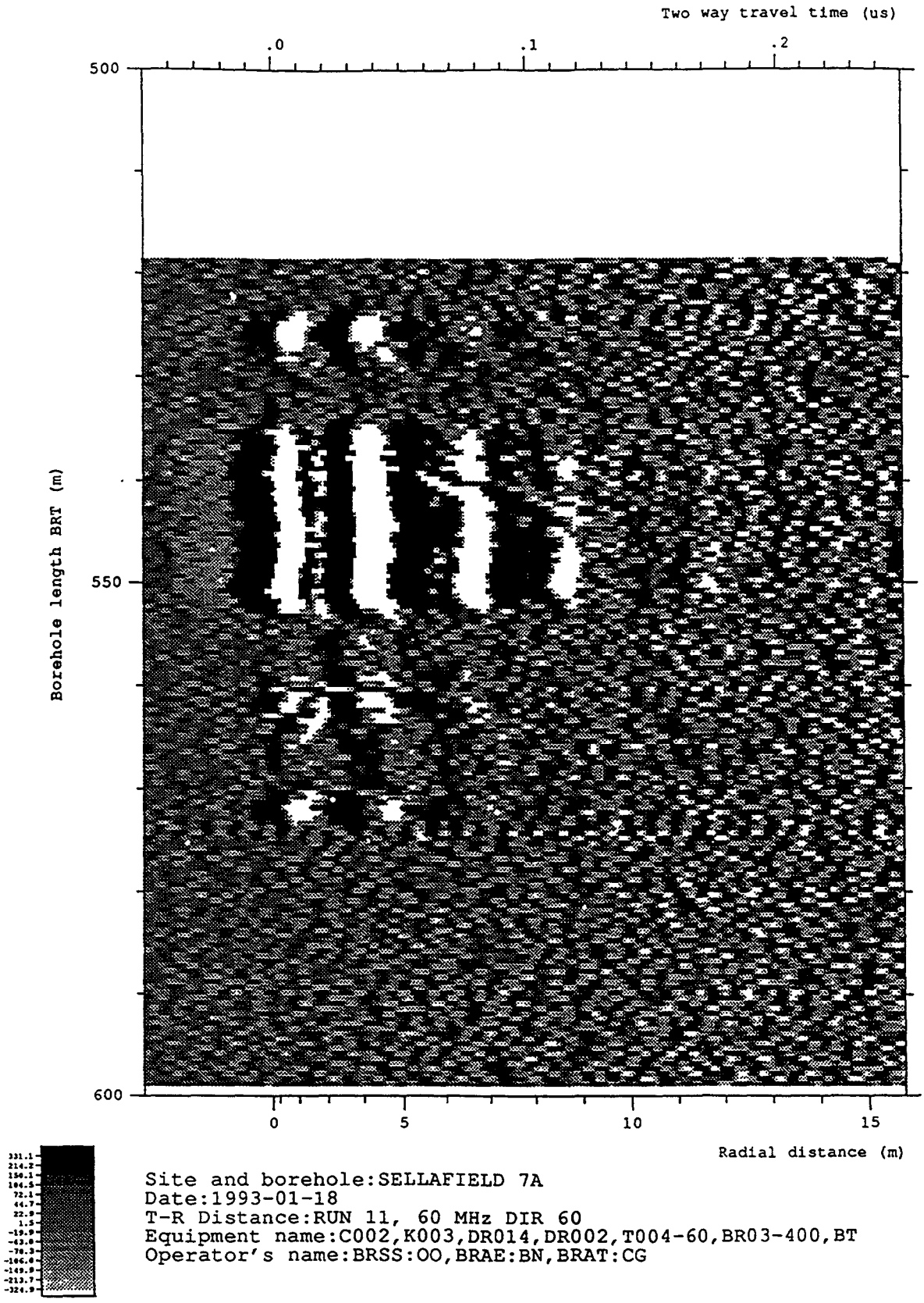

Figure 6-37 Radar map of the dipole component from the 60 MHz directional survey Run 11 after depth correction and band pass filtering for the depth interval 518.80 to 598.80 mbRT at an azimuth of 10°

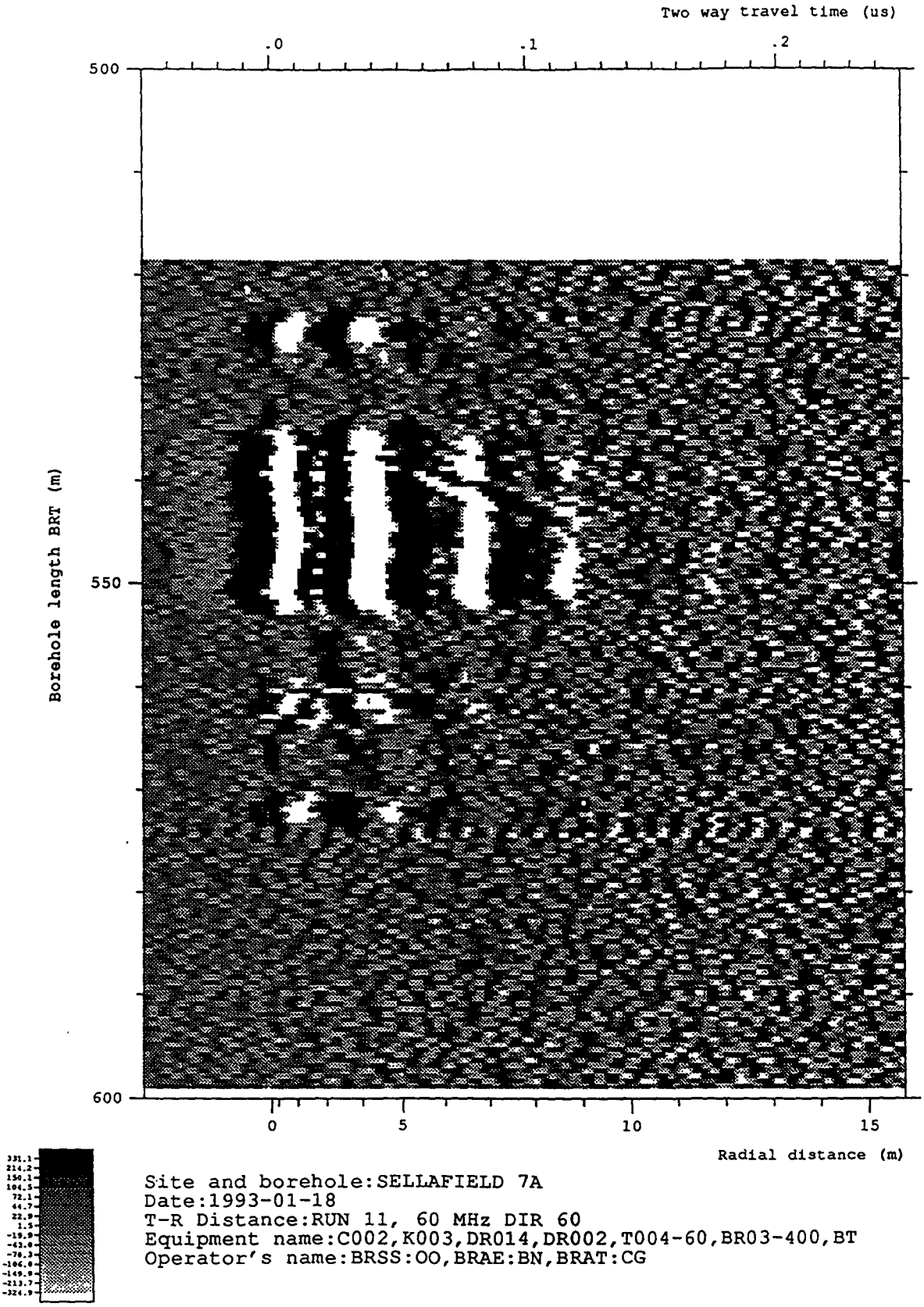

Figure 6-38 Radar map of the dipole component from the 60 MHz directional survey Run 11 after depth correction and band pass filtering for the depth interval 518.80 to 598.80 mbRT at an azimuth of 20°

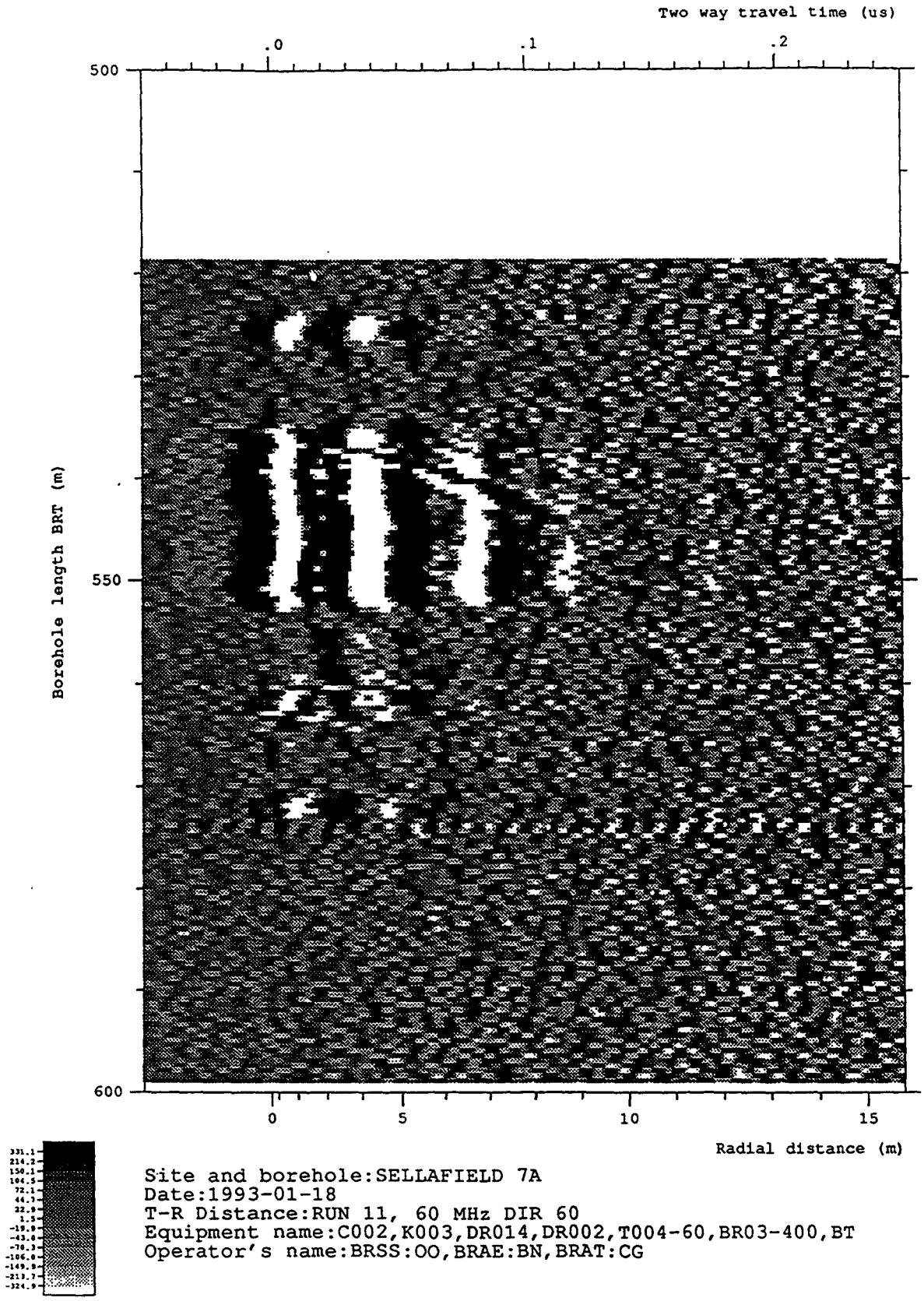

Figure 6-39 Radar map of the dipole component from the 60 MHz directional survey Run 11 after depth correction and band pass filtering for the depth interval 518.80 to 598.80 mbRT at an azimuth of 30°

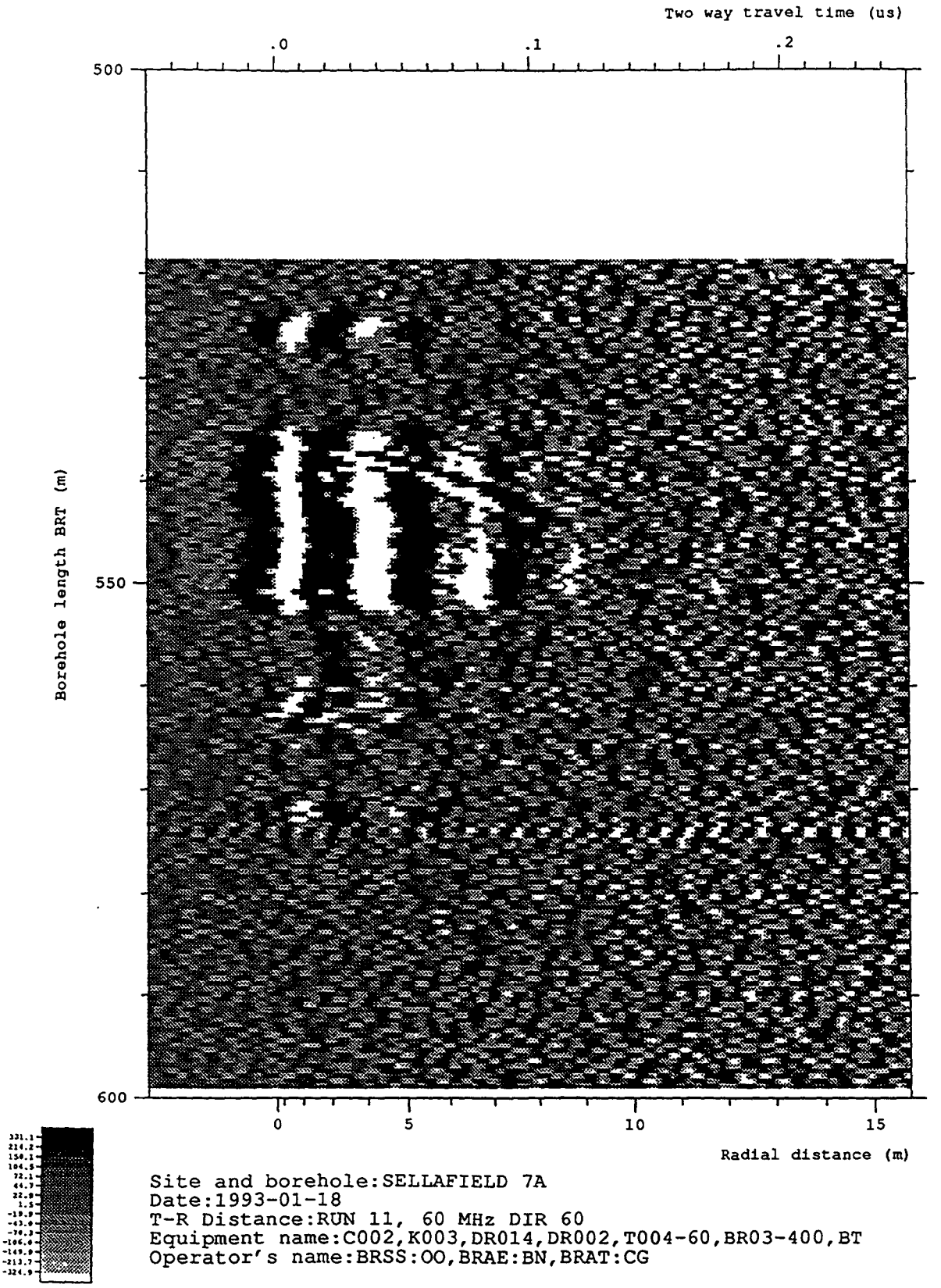

Figure 6-40 Radar map of the dipole component from the 60 MHz directional survey Run 11 after depth correction and band pass filtering for the depth interval 518.80 to 598.80 mbRT at an azimuth of 40°

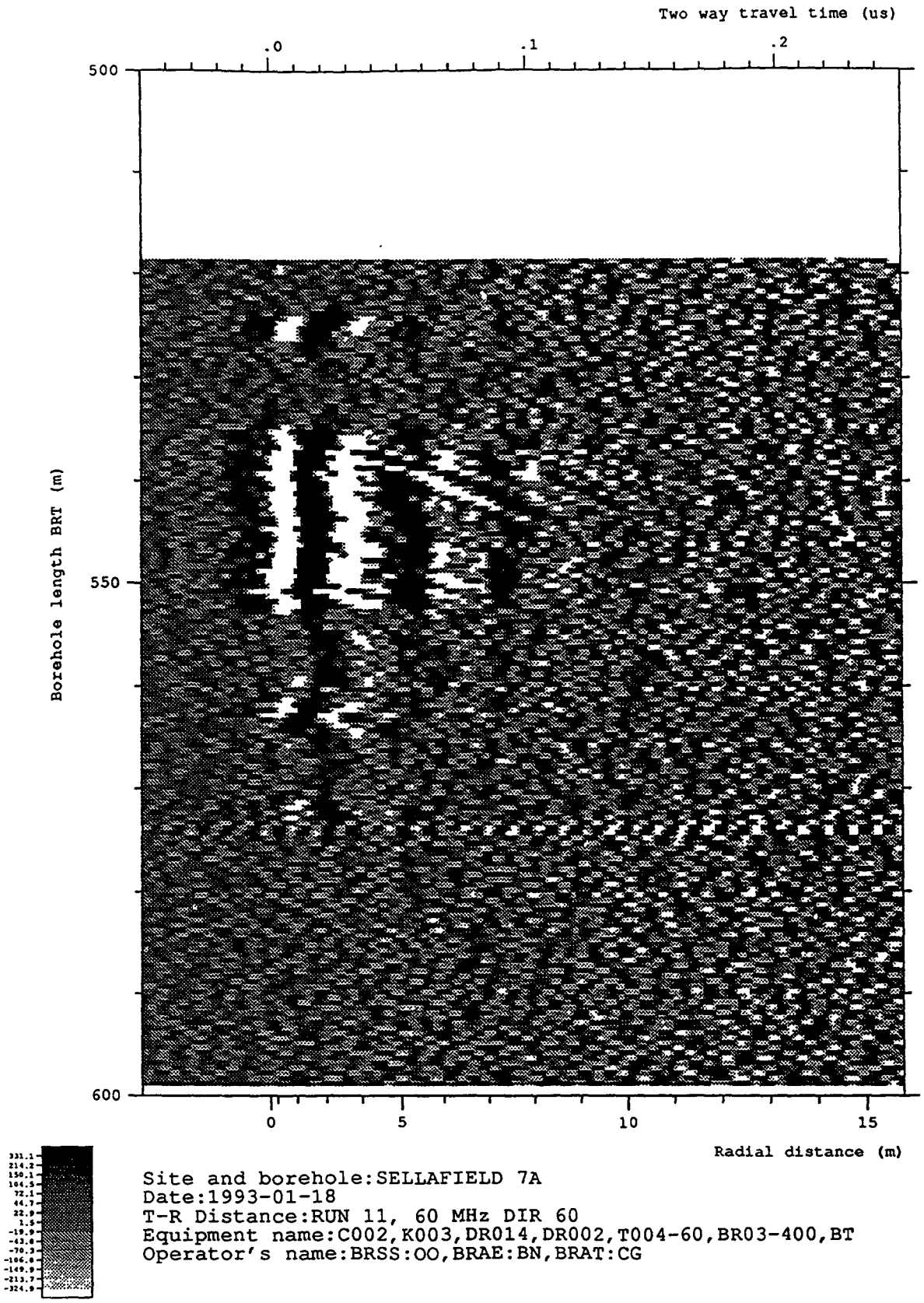

Figure 6-41 Radar map of the dipole component from the 60 MHz directional survey Run 11 after depth correction and band pass filtering for the depth interval 518.80 to 598.80 mbRT at an azimuth of 50°

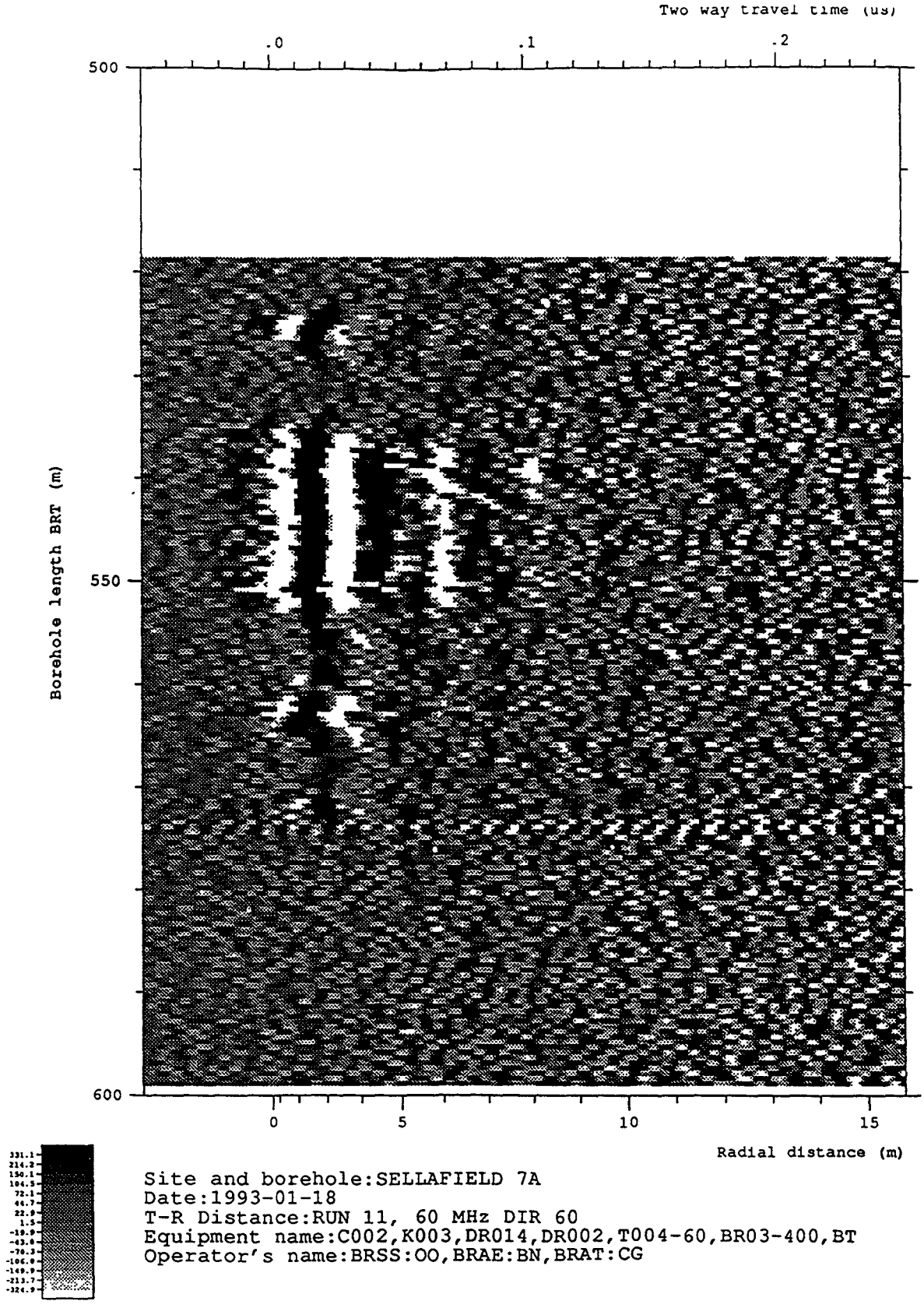

Figure 6-42 Radar map of the dipole component from the 60 MHz directional survey Run 11 after depth correction and band pass filtering for the depth interval 518.80 to 598.80 mbRT at an azimuth of 60°

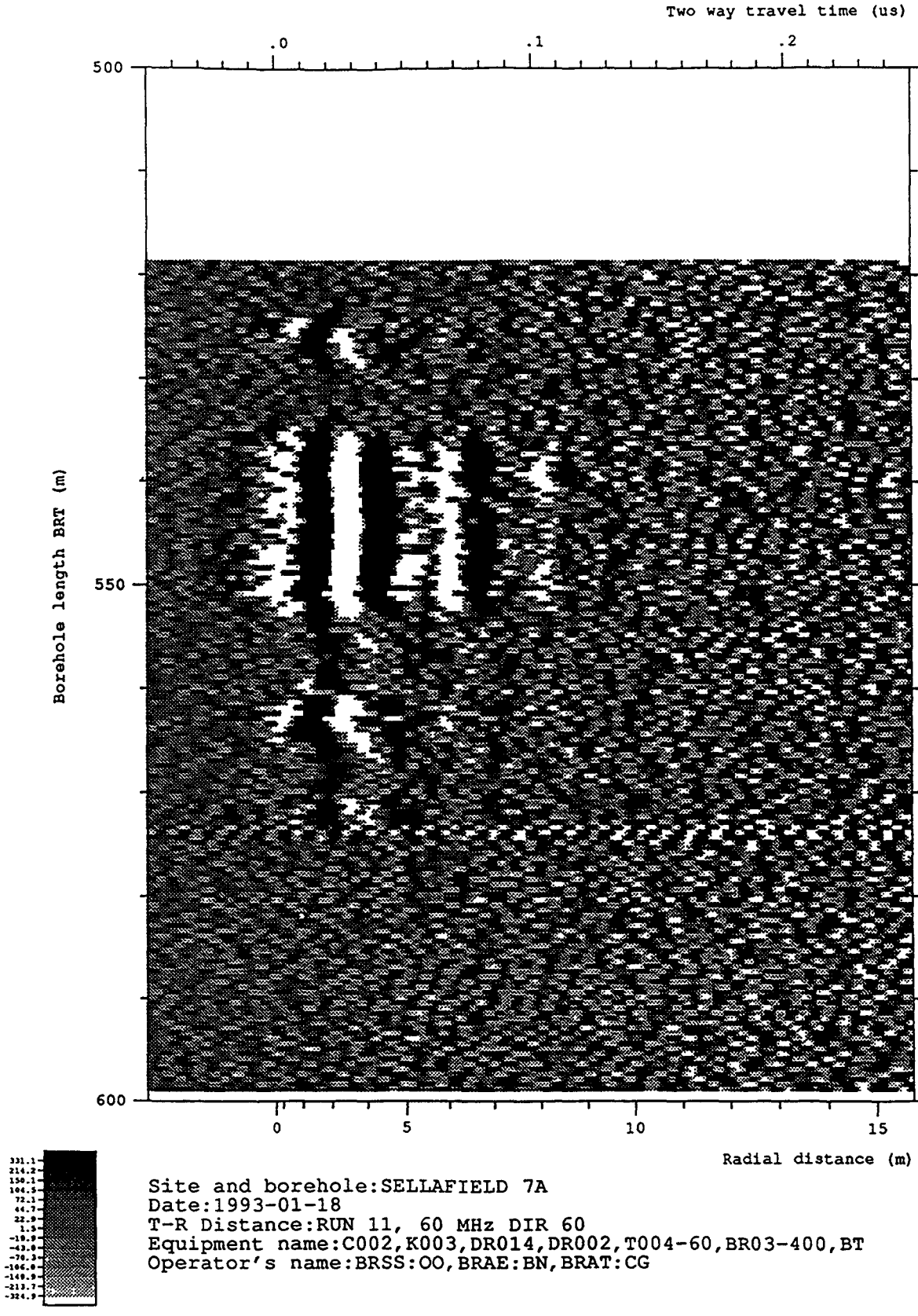

Figure 6-43 Radar map of the dipole component from the 60 MHz directional survey Run 11 after depth correction and band pass filtering for the depth interval 518.80 to 598.80 mbRT at an azimuth of 70°

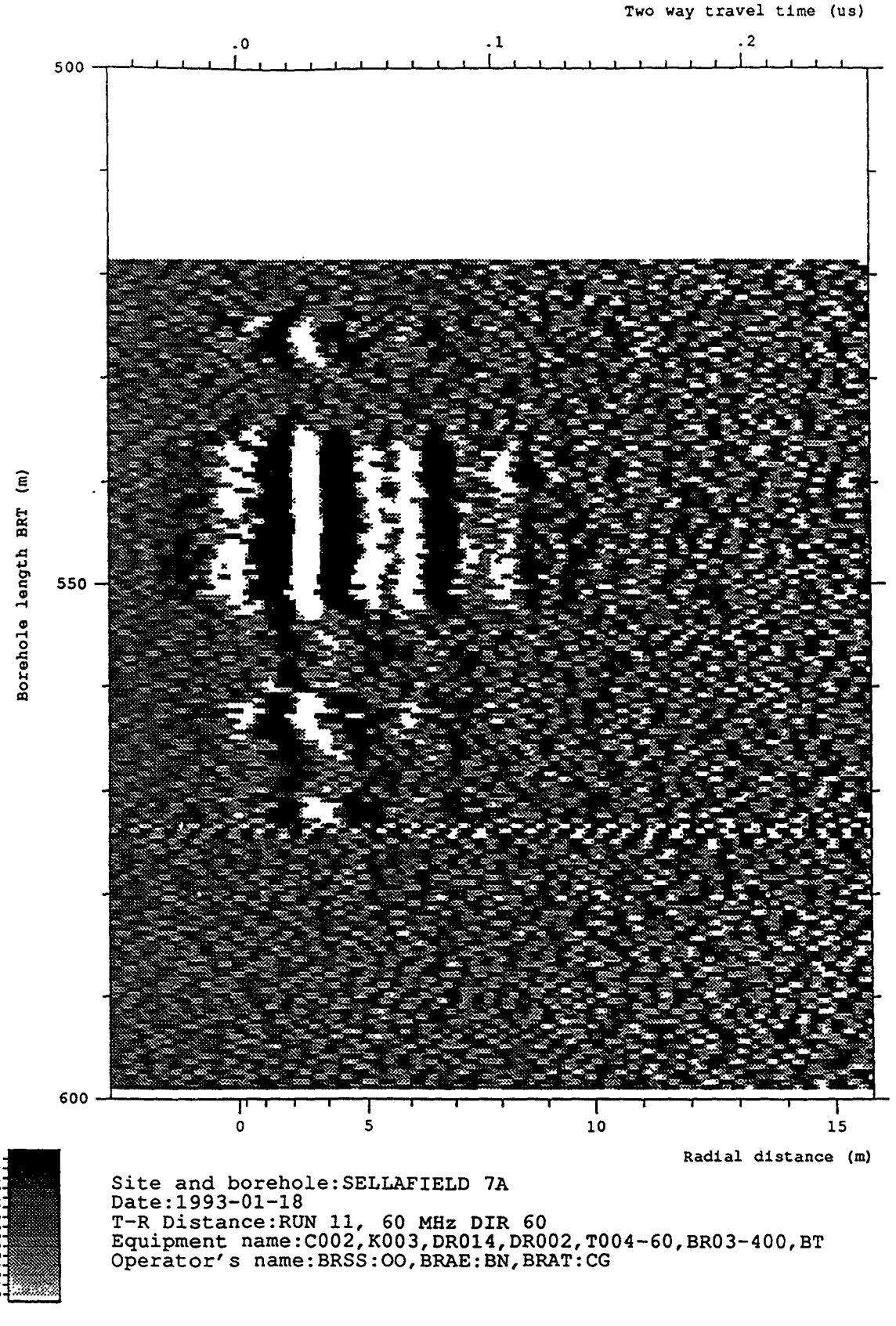

Figure 6-44 Radar map of the dipole component from the 60 MHz directional survey Run 11 after depth correction and band pass filtering for the depth interval 518.80 to 598.80 mbRT at an azimuth of 80°

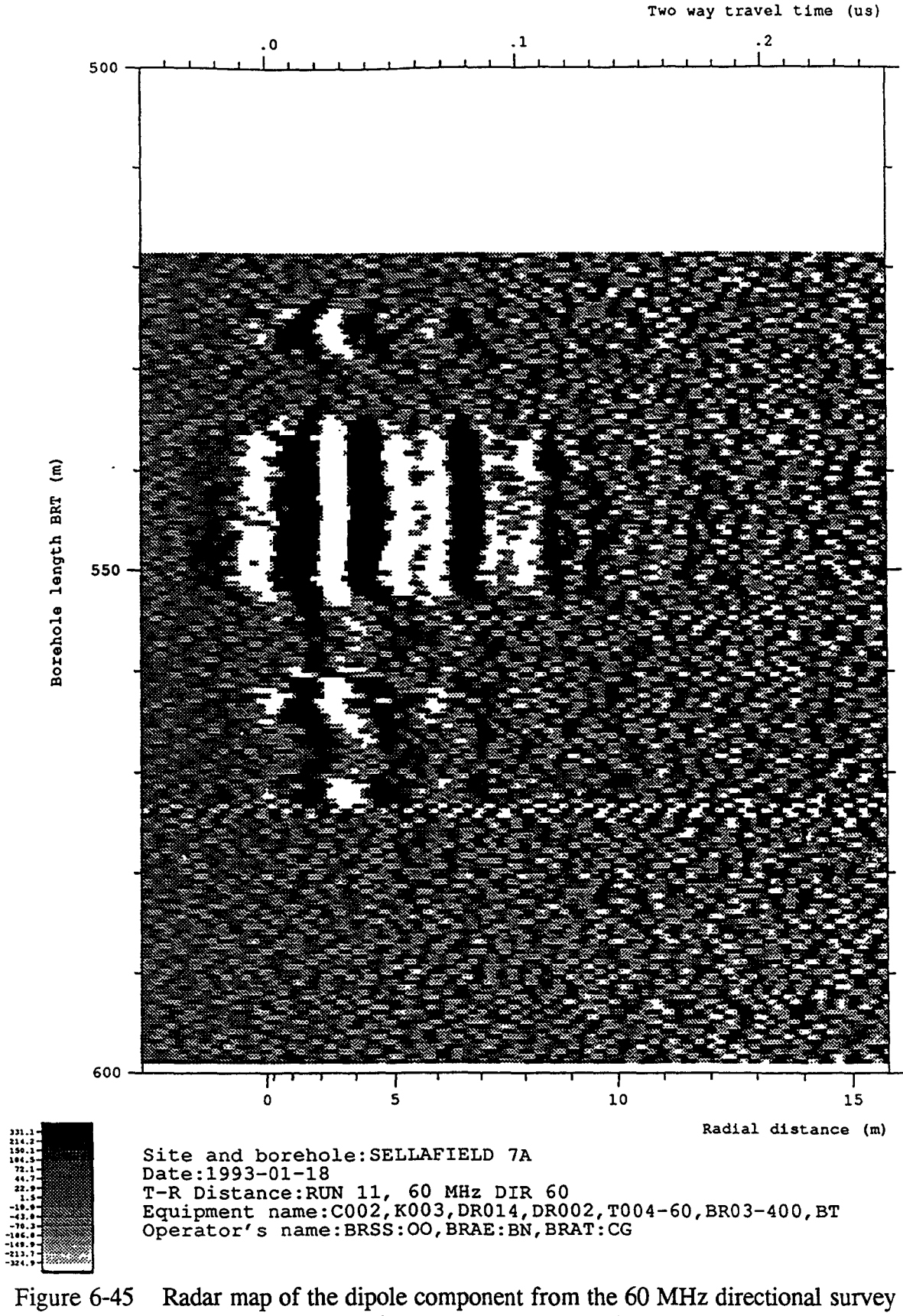

Figure 6-45 Radar map of the dipole component from the 60 MHz directional survey Run 11 after depth correction and band pass filtering for the depth interval 518.80 to 598.80 mbRT at an azimuth of 90°

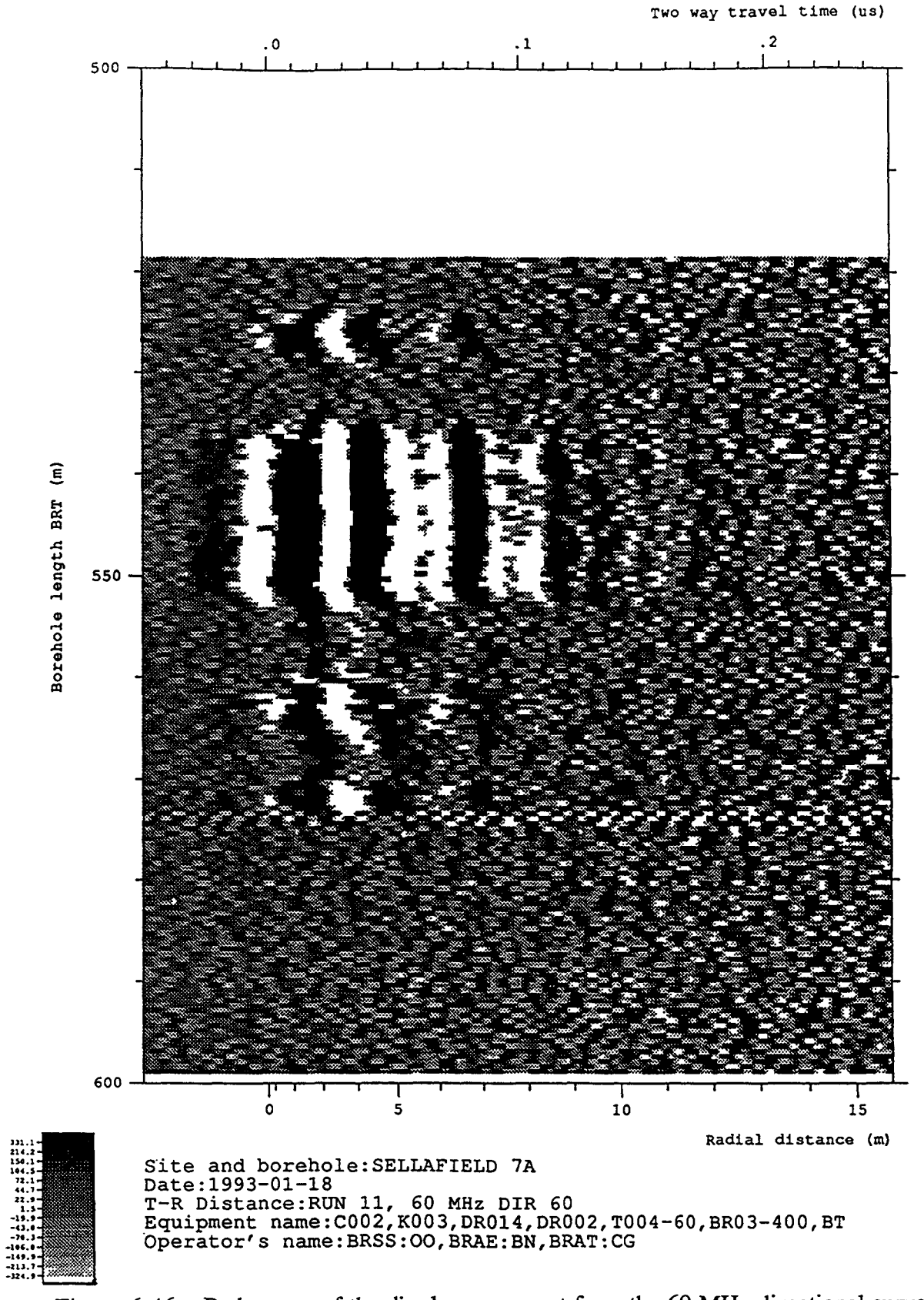

Figure 6-46 Radar map of the dipole component from the 60 MHz directional survey Run 11 after depth correction and band pass filtering for the depth interval 518.80 to 598.80 mbRT at an azimuth of 100°

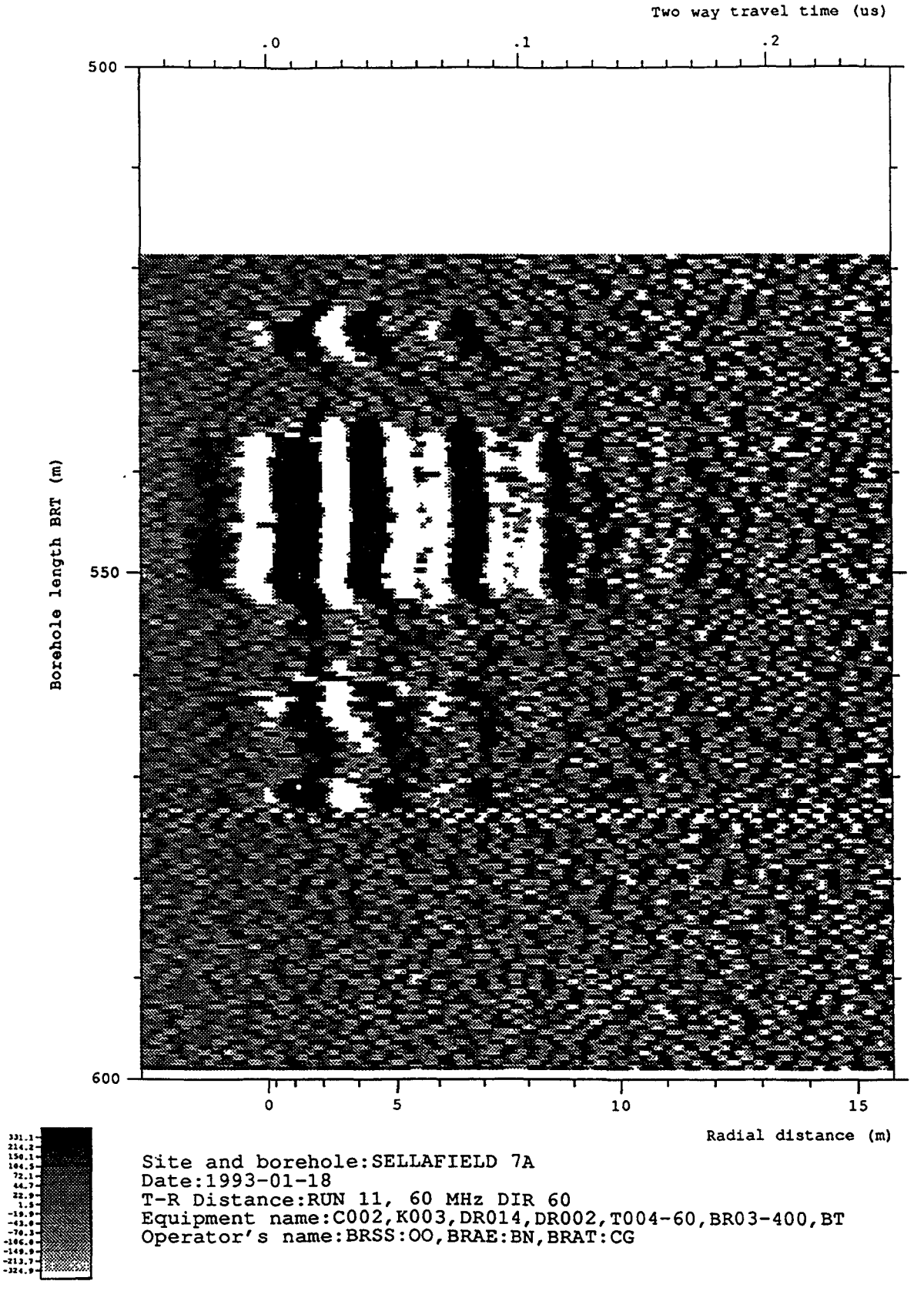

Figure 6-47 Radar map of the dipole component from the 60 MHz directional survey Run 11 after depth correction and band pass filtering for the depth interval 518.80 to 598.80 mbRT at an azimuth of 110°

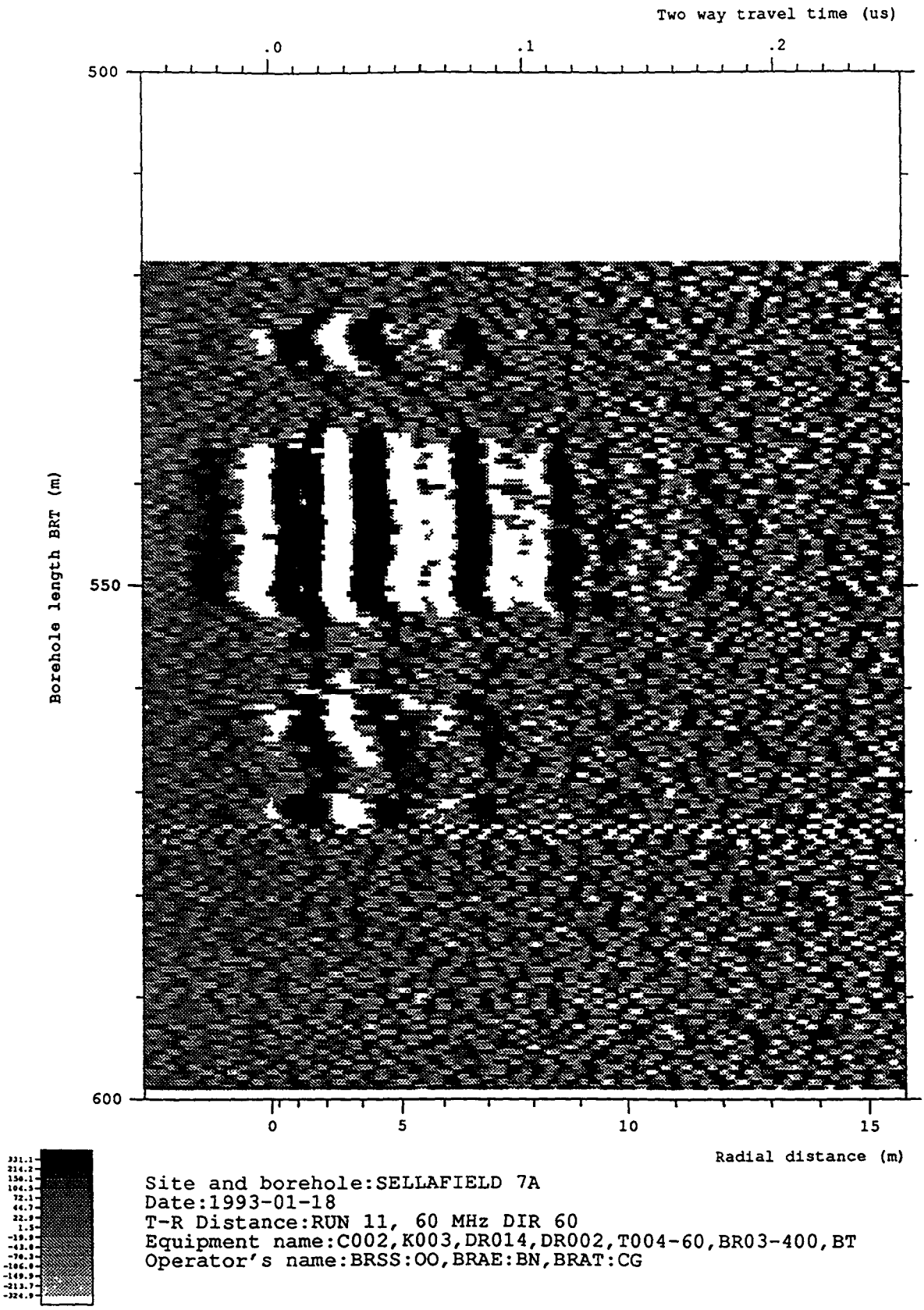

Figure 6-48 Radar map of the dipole component from the 60 MHz directional survey Run 11 after depth correction and band pass filtering for the depth interval 518.80 to 598.80 mbRT at an azimuth of 120°

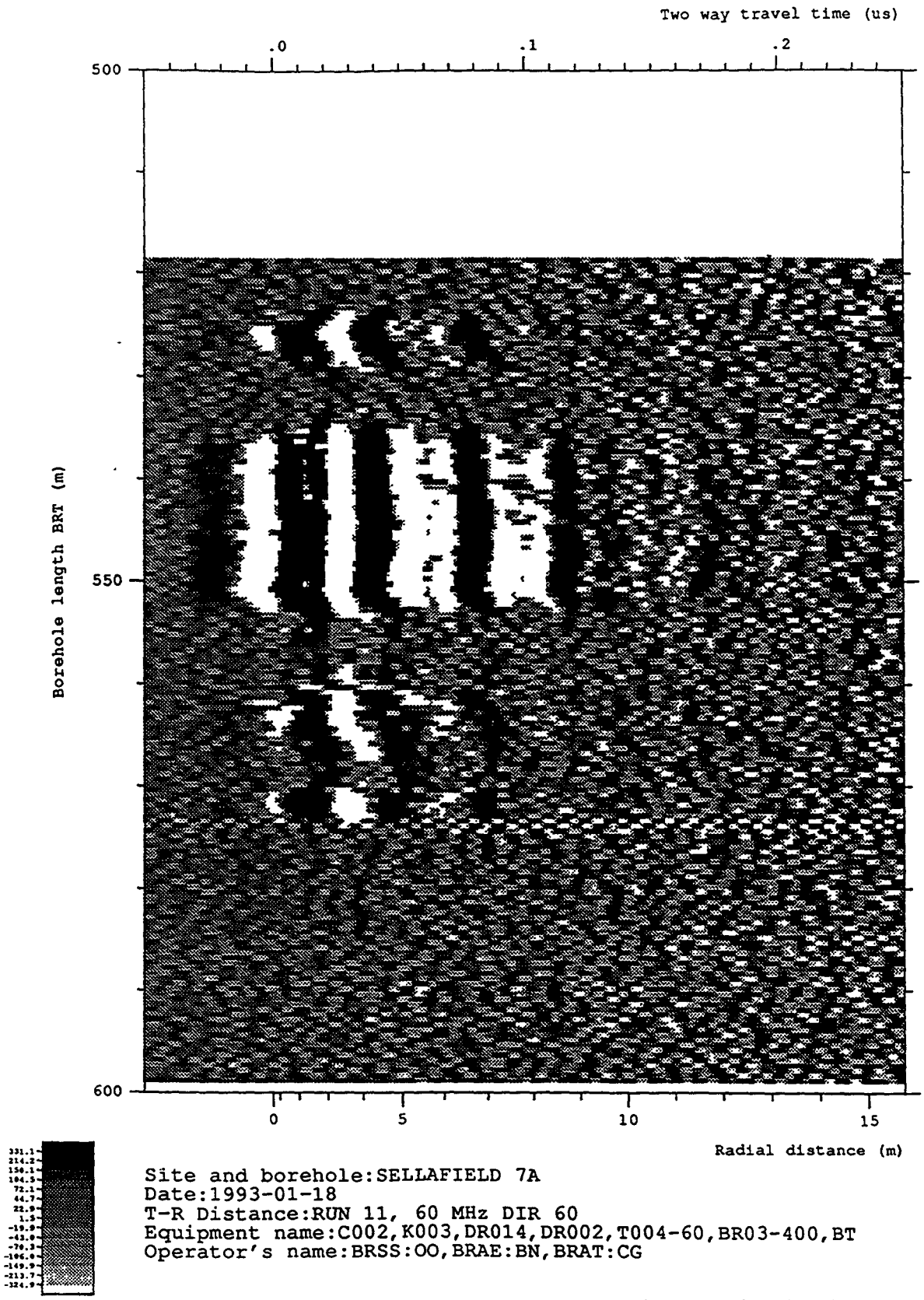

Figure 6-49 Radar map of the dipole component from the 60 MHz directional survey Run 11 after depth correction and band pass filtering for the depth interval 518.80 to 598.80 mbRT at an azimuth of 130°

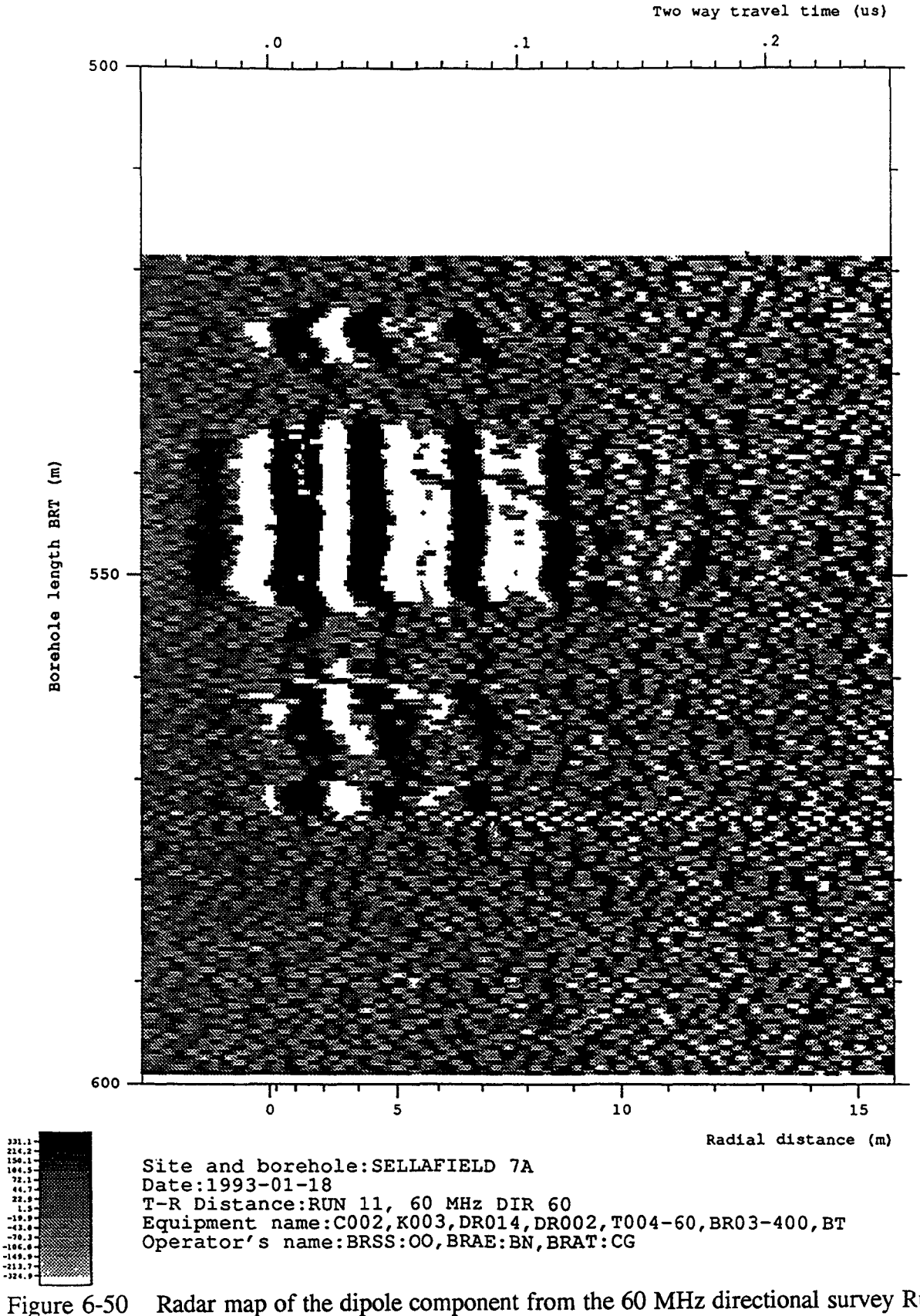

Figure 6-50 Radar map of the dipole component from the 60 MHz directional survey Run 11 after depth correction and band pass filtering for the depth interval 518.80 to 598.80 mbRT at an azimuth of 140°

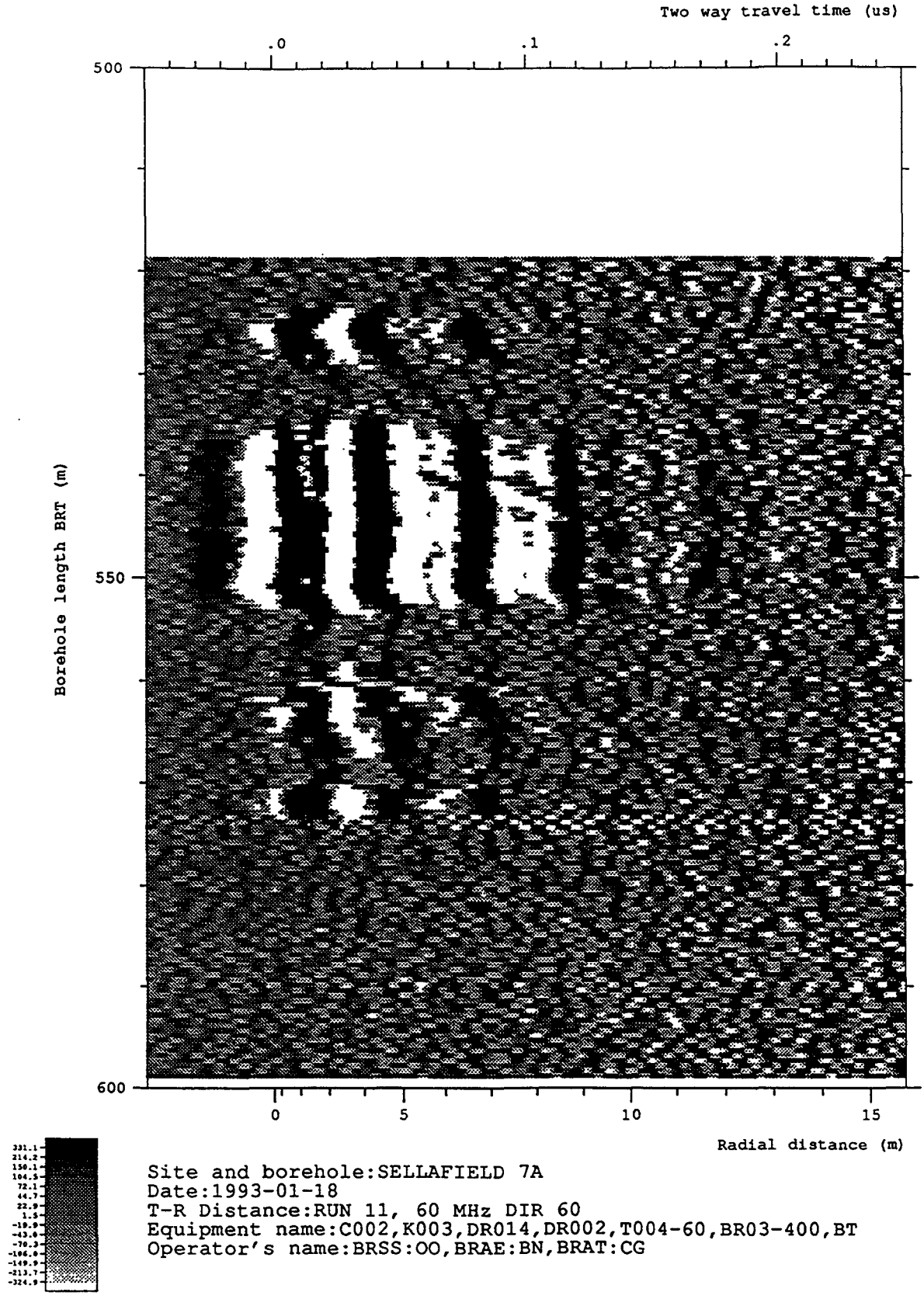

Figure 6-51 Radar map of the dipole component from the 60 MHz directional survey Run 11 after depth correction and band pass filtering for the depth interval 518.80 to 598.80 mbRT at an azimuth of 150°

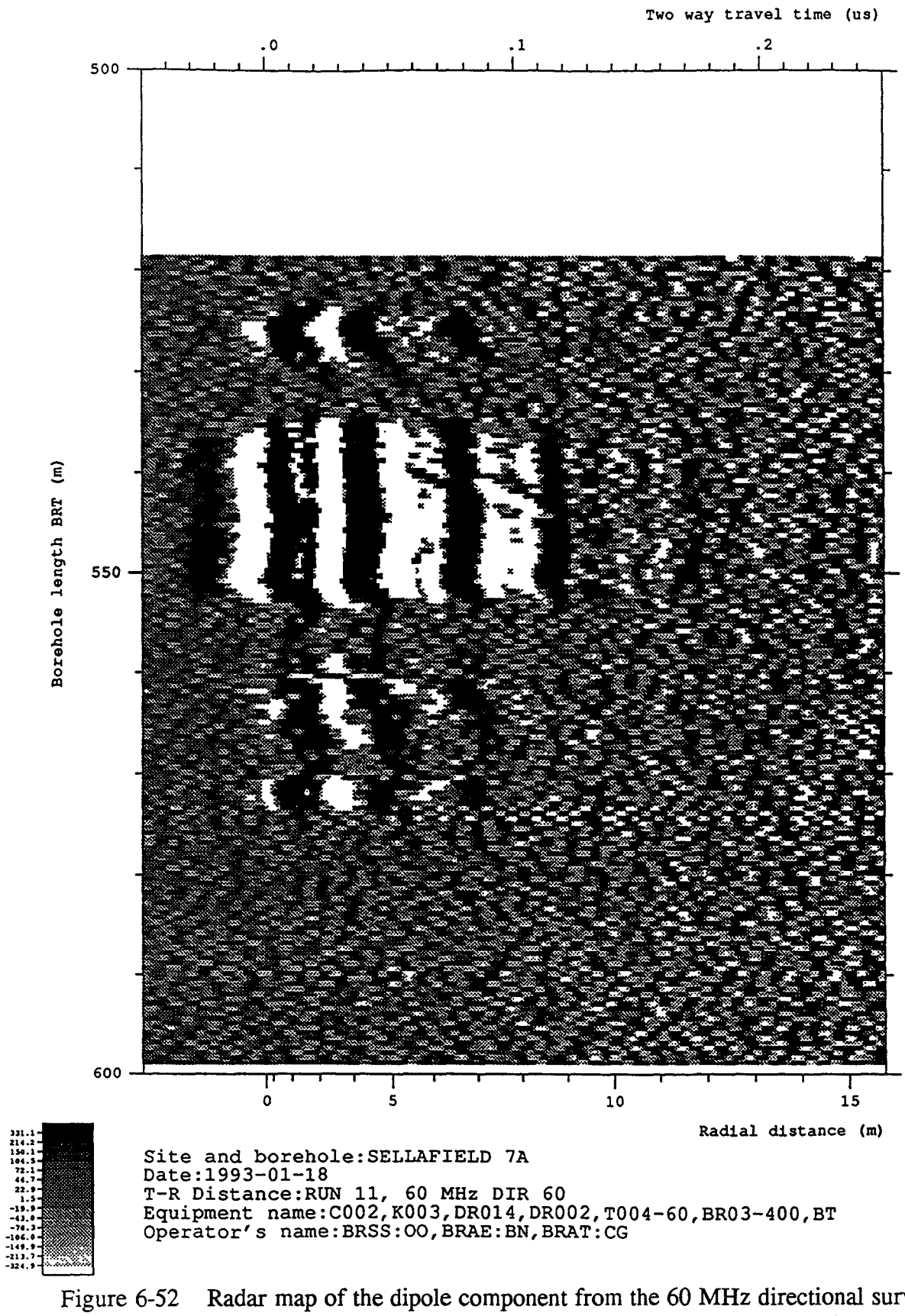

Figure 6-52 Radar map of the dipole component from the 60 MHz directional survey Run 11 after depth correction and band pass filtering for the depth interval 518.80 to 598.80 mbRT at an azimuth of 160°

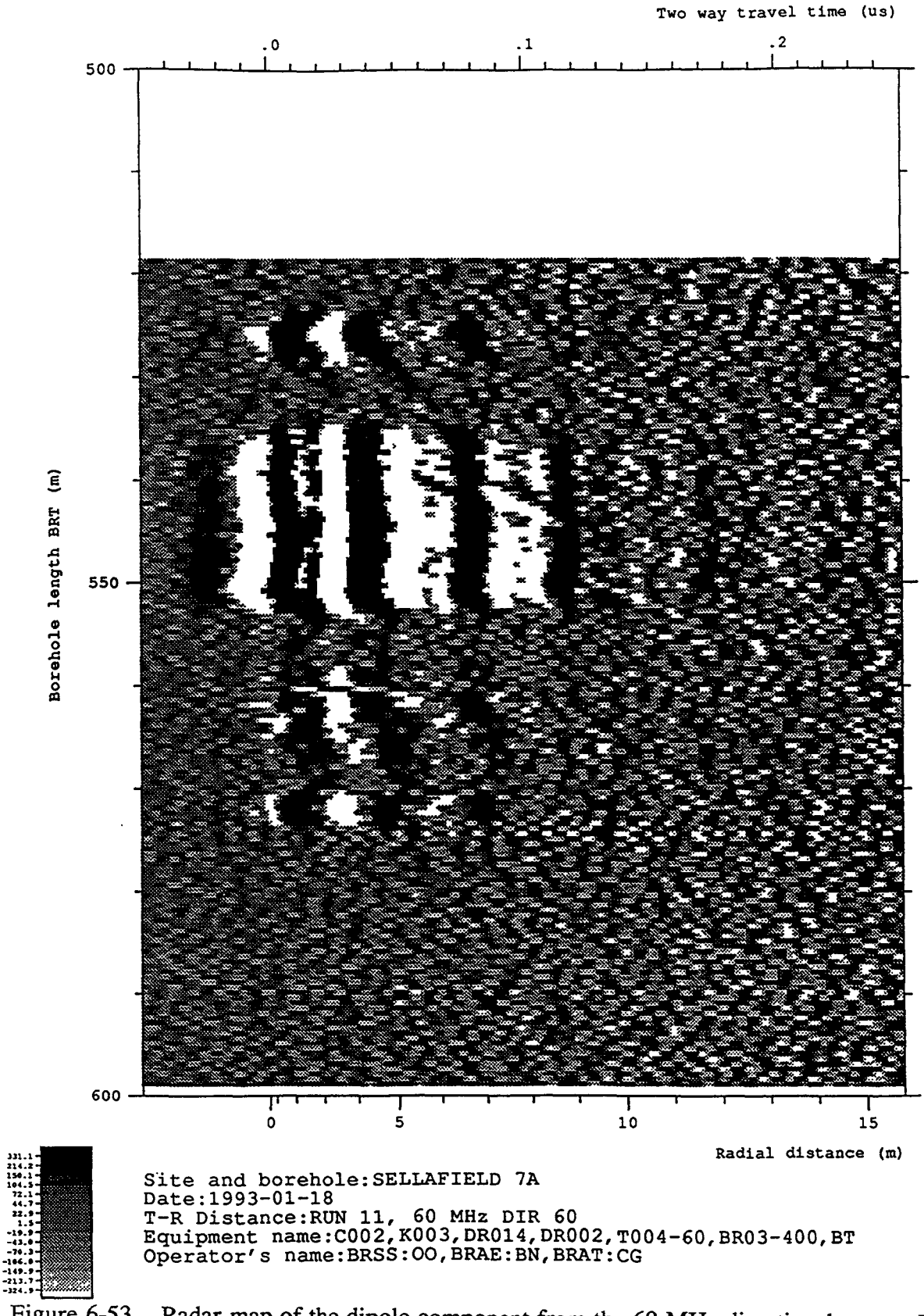

Figure 6-53 Radar map of the dipole component from the 60 MHz directional survey Run 11 after depth correction and band pass filtering for the depth interval 518.80 to 598.80 mbRT at an azimuth of 170°

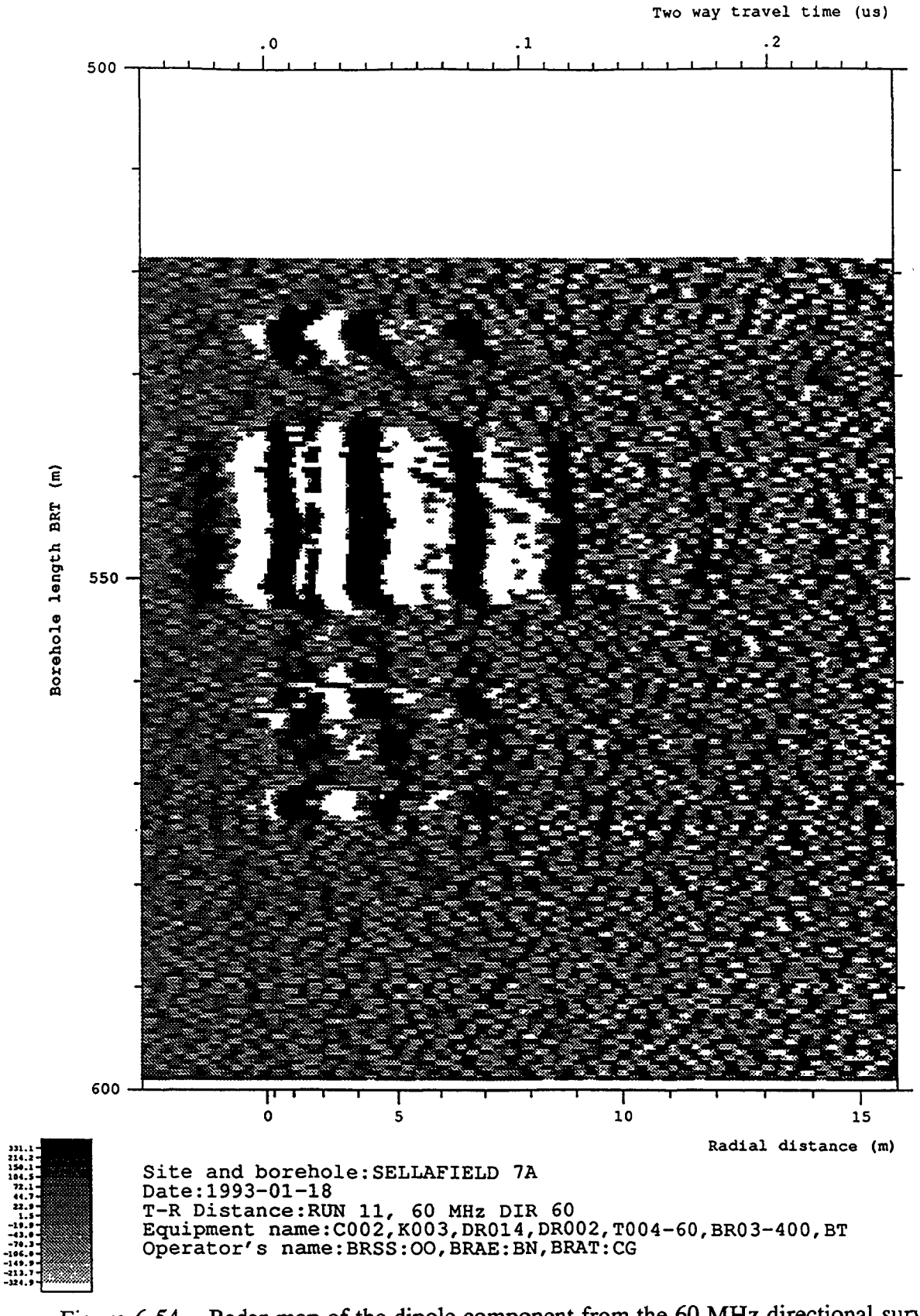

Figure 6-54 Radar map of the dipole component from the 60 MHz directional survey Run 11 after depth correction and band pass filtering for the depth interval 518.80 to 598.80 mbRT at an azimuth of 180°

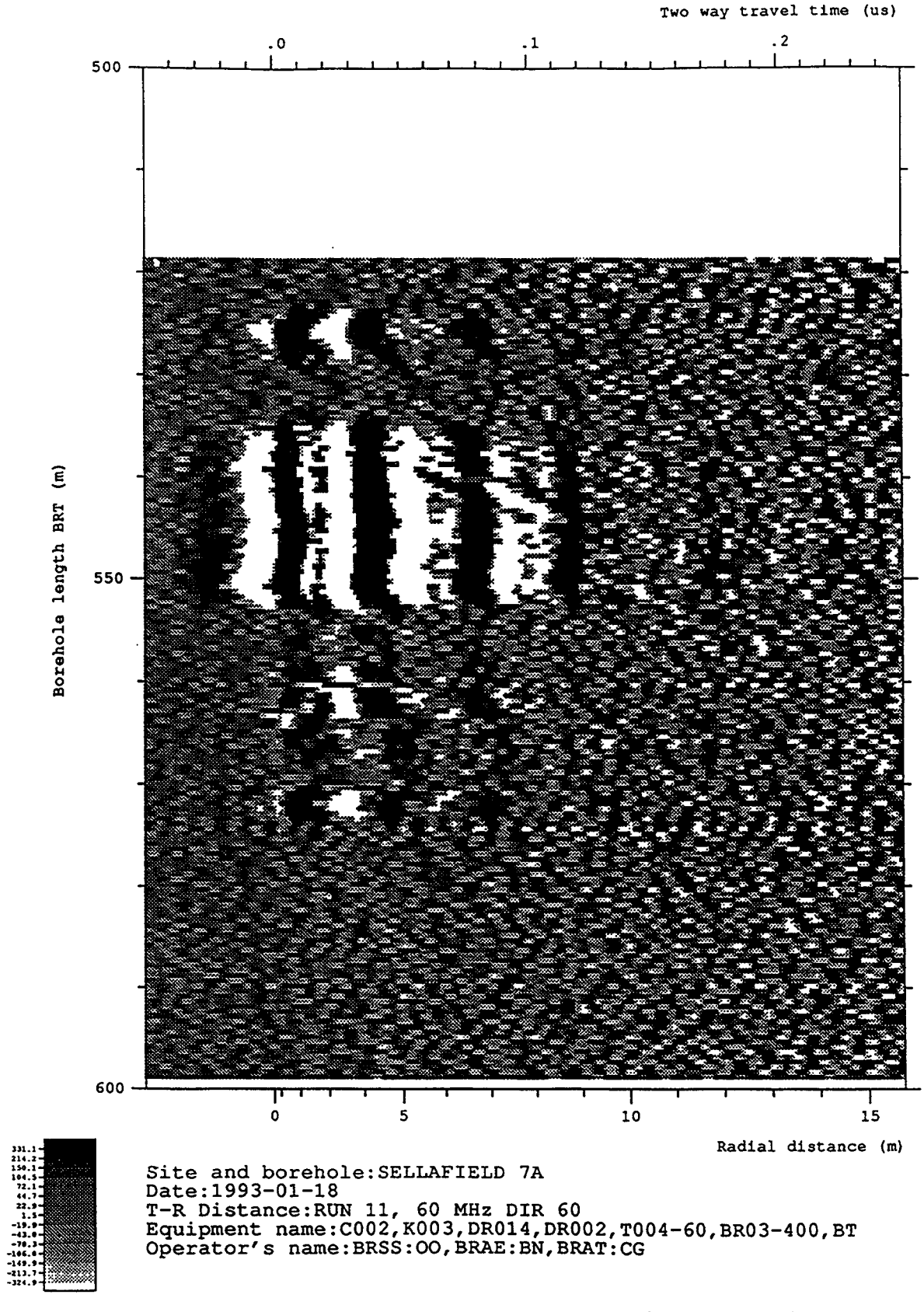

Figure 6-55 Radar map of the dipole component from the 60 MHz directional survey Run 11 after depth correction and band pass filtering for the depth interval 518.80 to 598.80 mbRT at an azimuth of 190°

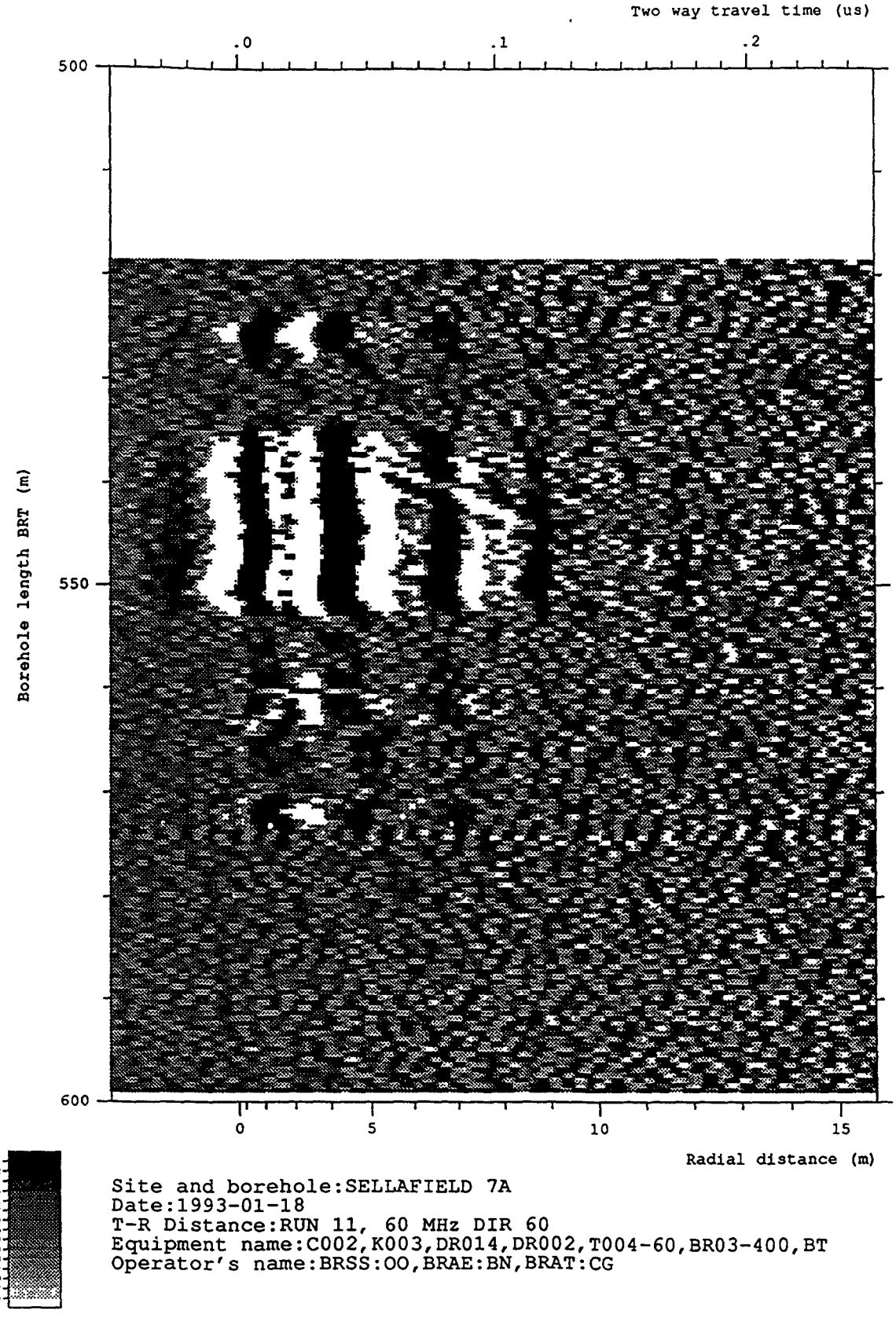

Figure 6-56 Radar map of the dipole component from the 60 MHz directional survey Run 11 after depth correction and band pass filtering for the depth interval 518.80 to 598.80 mbRT at an azimuth of 200°

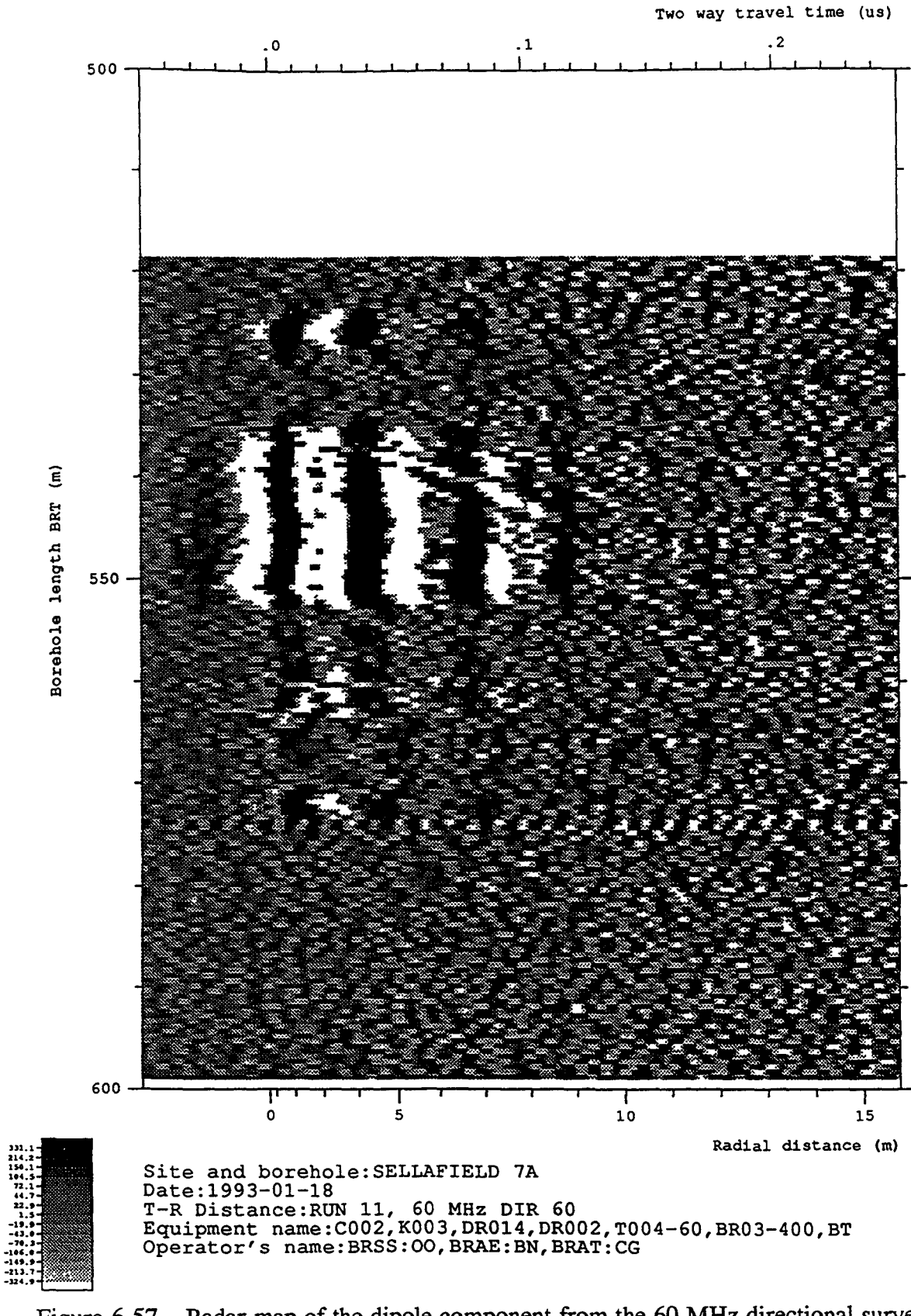

Figure 6-57 Radar map of the dipole component from the 60 MHz directional survey Run 11 after depth correction and band pass filtering for the depth interval 518.80 to 598.80 mbRT at an azimuth of 210°

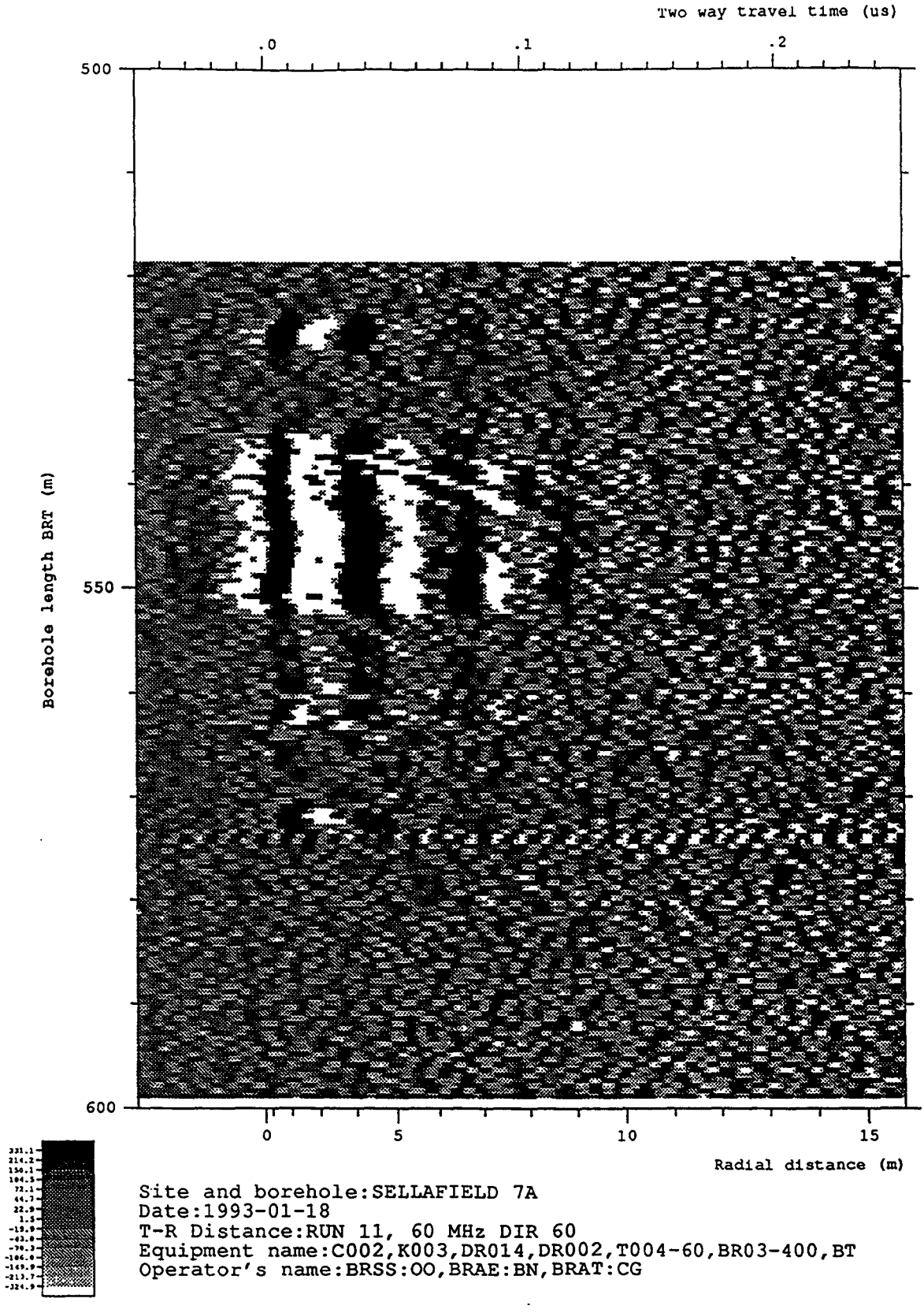

Figure 6-58 Radar map of the dipole component from the 60 MHz directional survey Run 11 after depth correction and band pass filtering for the depth interval 518.80 to 598.80 mbRT at an azimuth of 220°

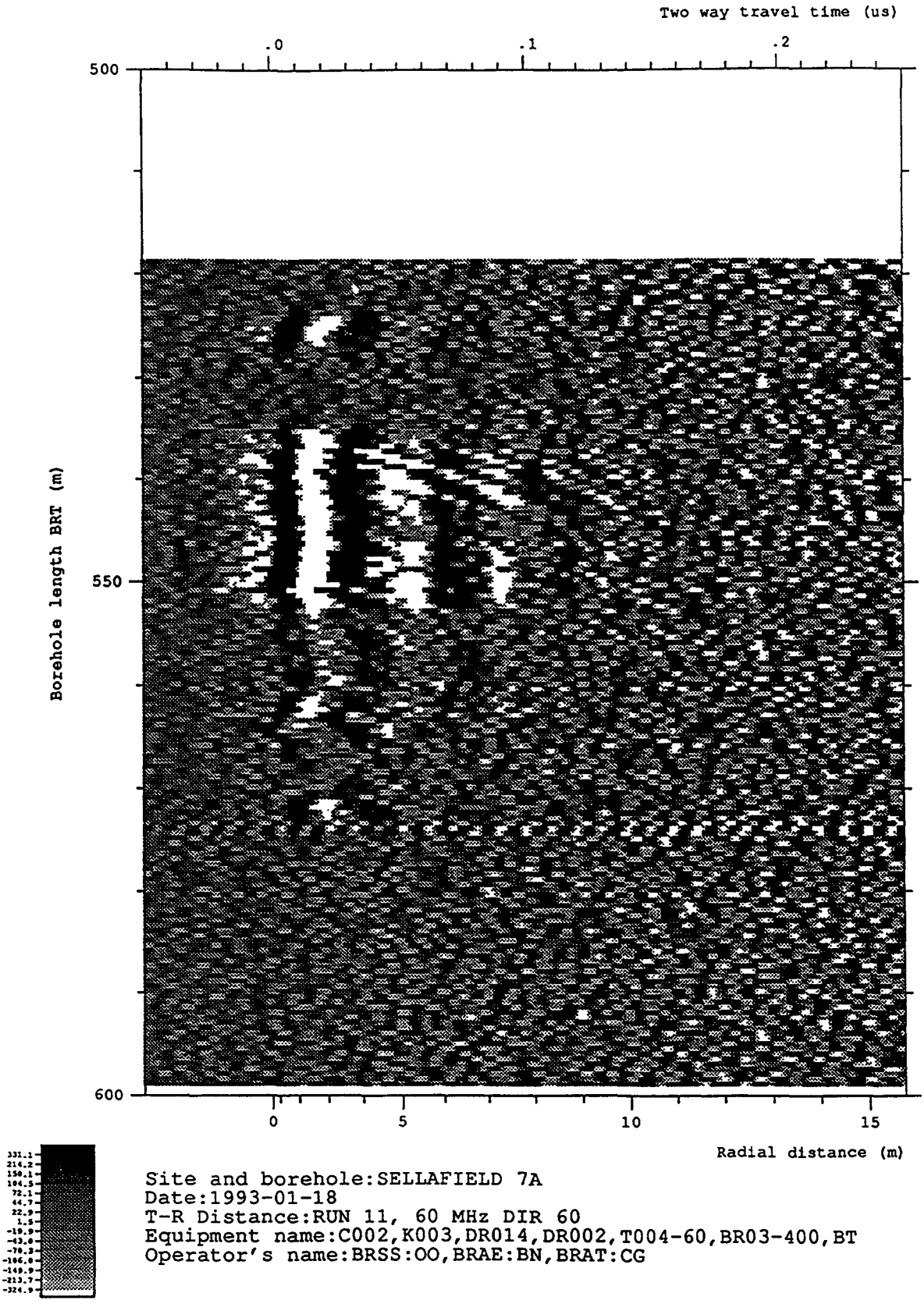

Figure 6-59 Radar map of the dipole component from the 60 MHz directional survey Run 11 after depth correction and band pass filtering for the depth interval 518.80 to 598.80 mbRT at an azimuth of 230°

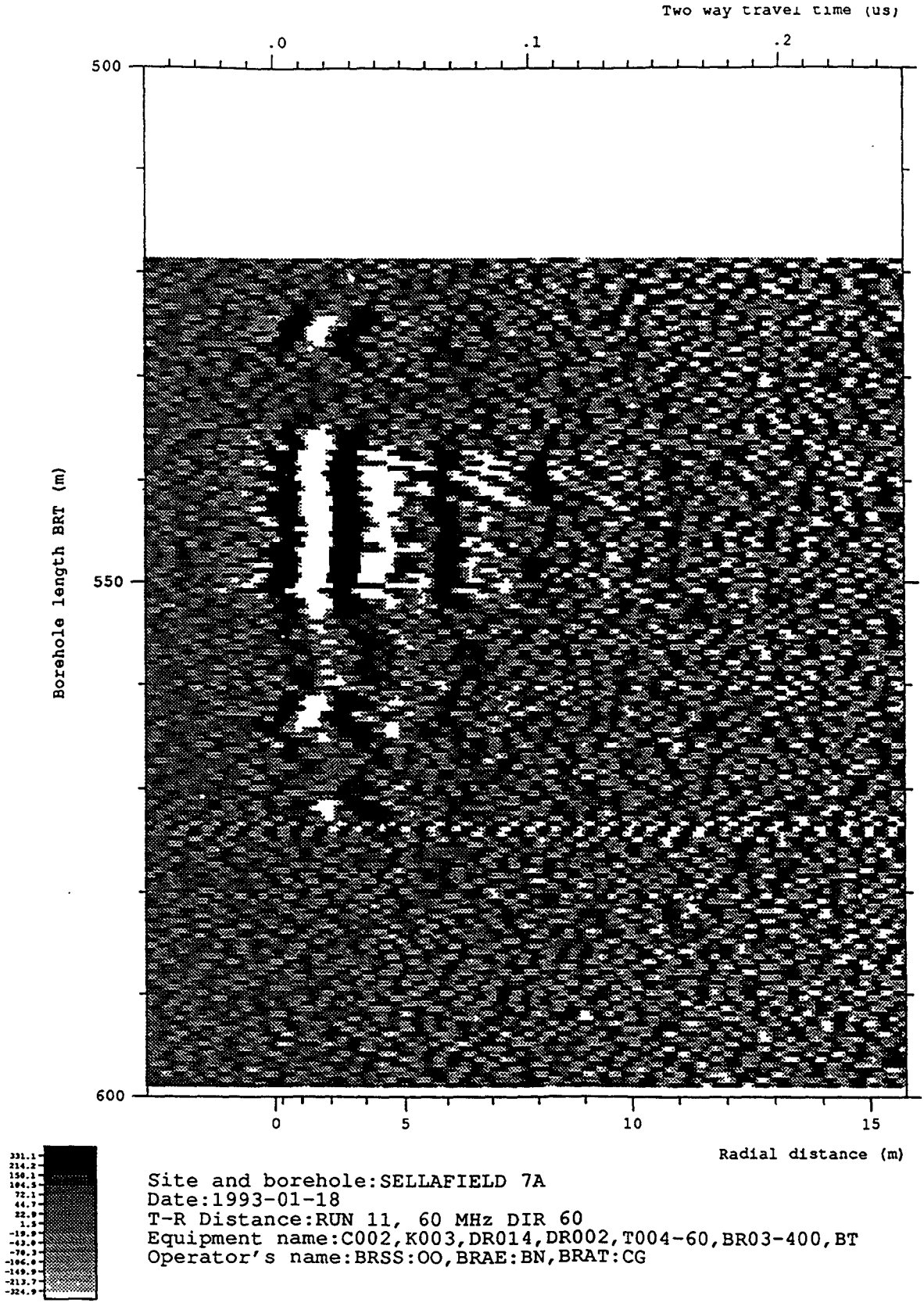

Figure 6-60 Radar map of the dipole component from the 60 MHz directional survey Run 11 after depth correction and band pass filtering for the depth interval 518.80 to 598.80 mbRT at an azimuth of 240°

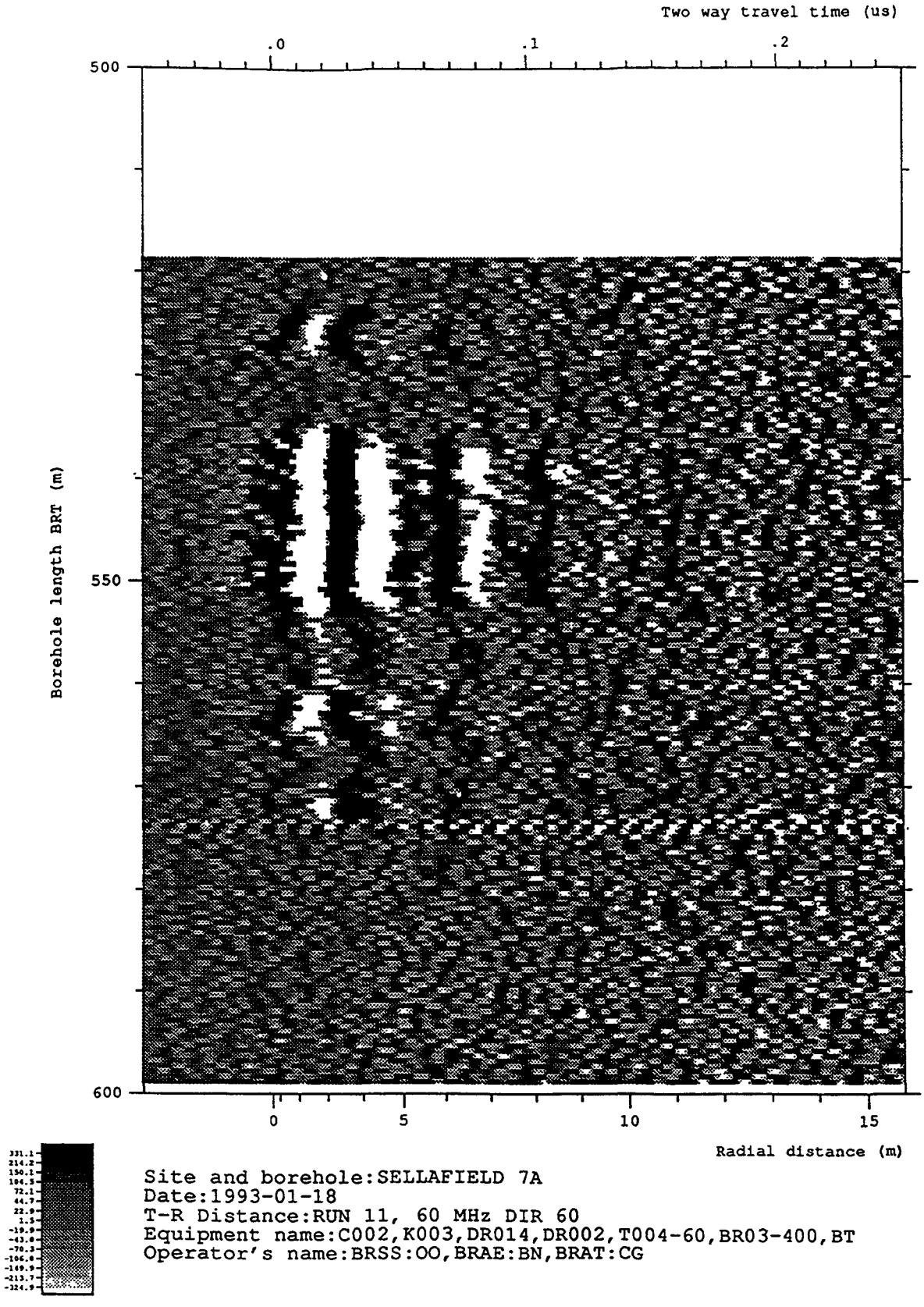

Figure 6-61 Radar map of the dipole component from the 60 MHz directional survey Run 11 after depth correction and band pass filtering for the depth interval 518.80 to 598.80 mbRT at an azimuth of 250°

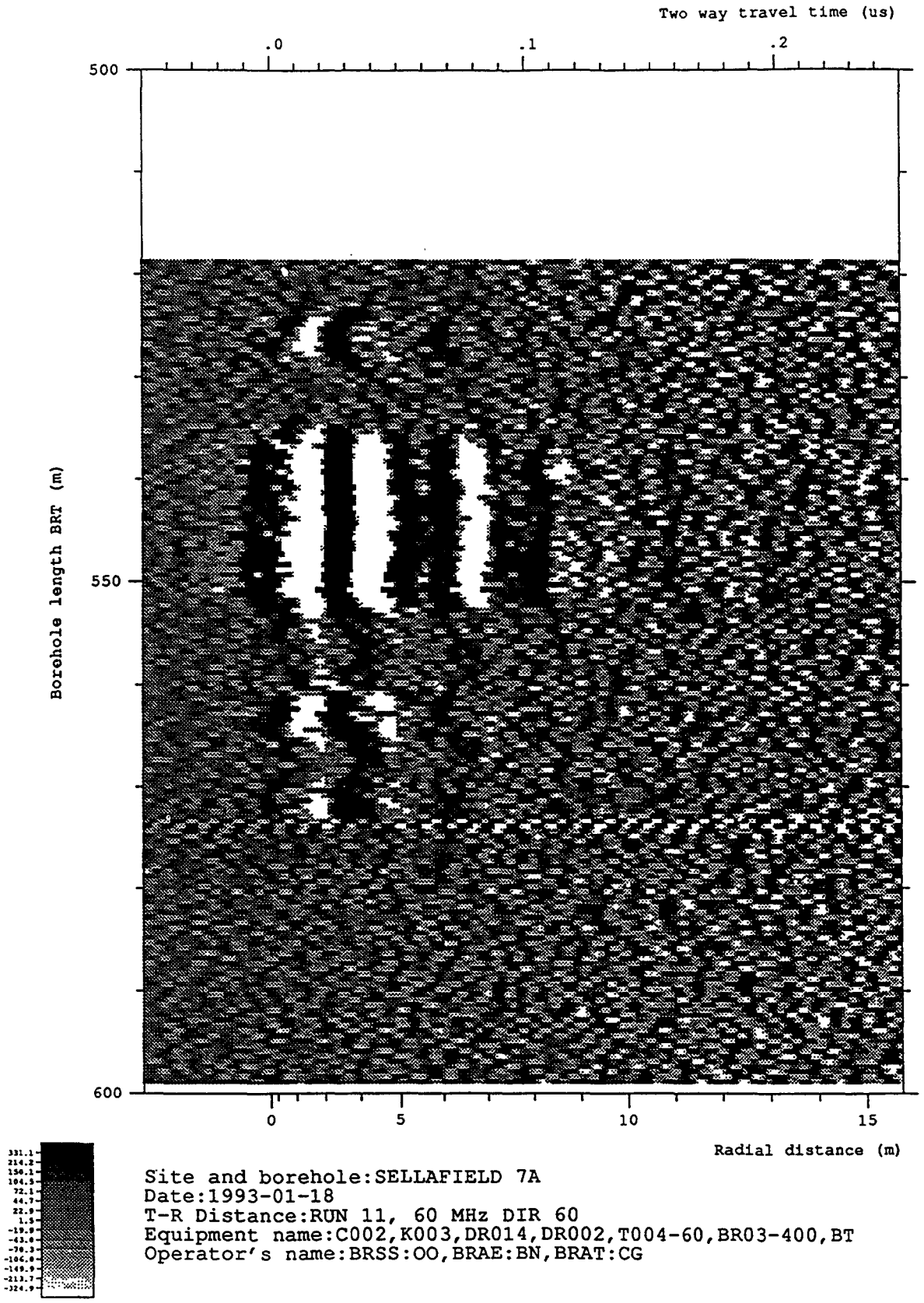

Figure 6-62 Radar map of the dipole component from the 60 MHz directional survey Run 11 after depth correction and band pass filtering for the depth interval 518.80 to 598.80 mbRT at an azimuth of 260°

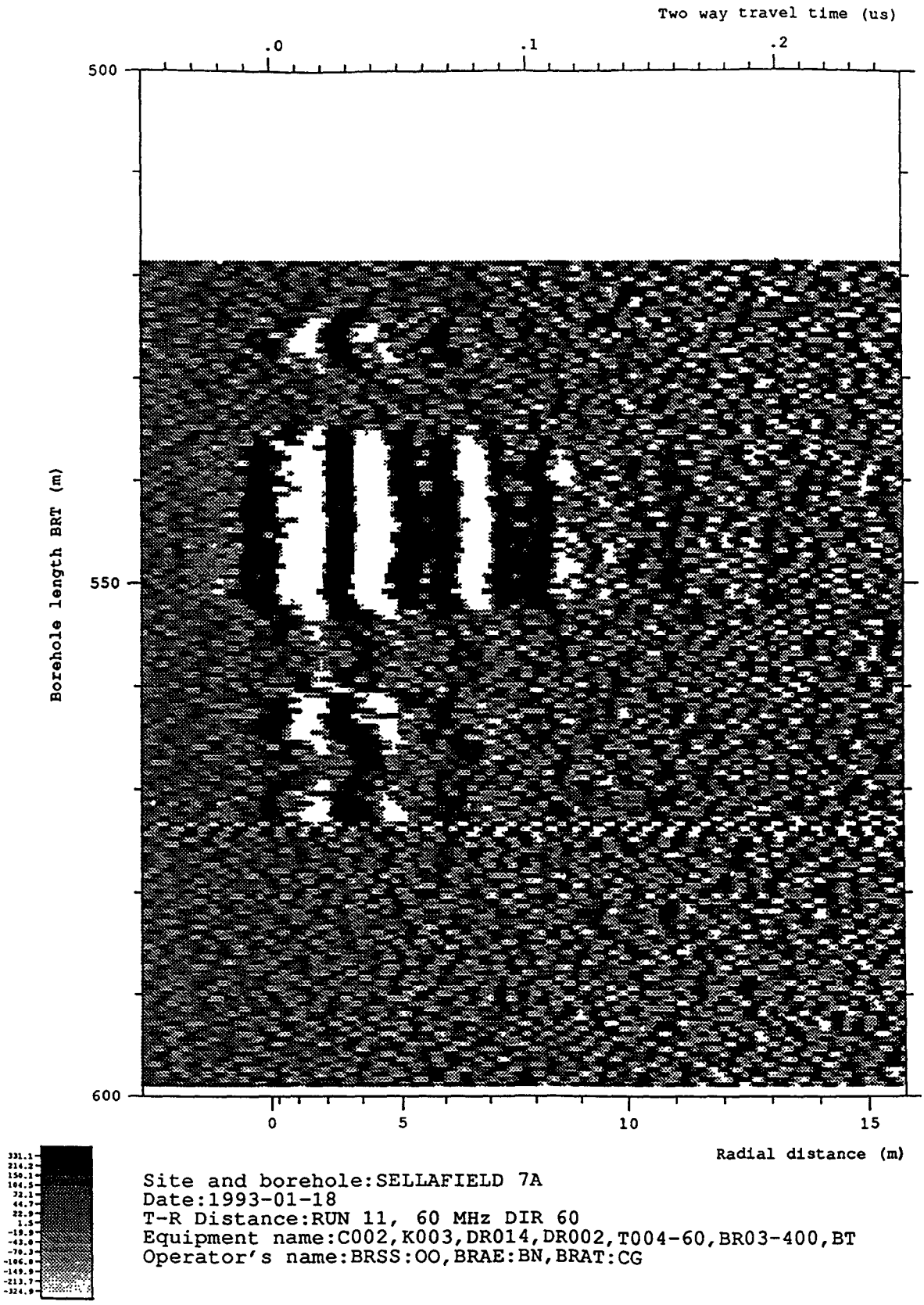

Figure 6-63 Radar map of the dipole component from the 60 MHz directional survey Run 11 after depth correction and band pass filtering for the depth interval 518.80 to 598.80 mbRT at an azimuth of 270°

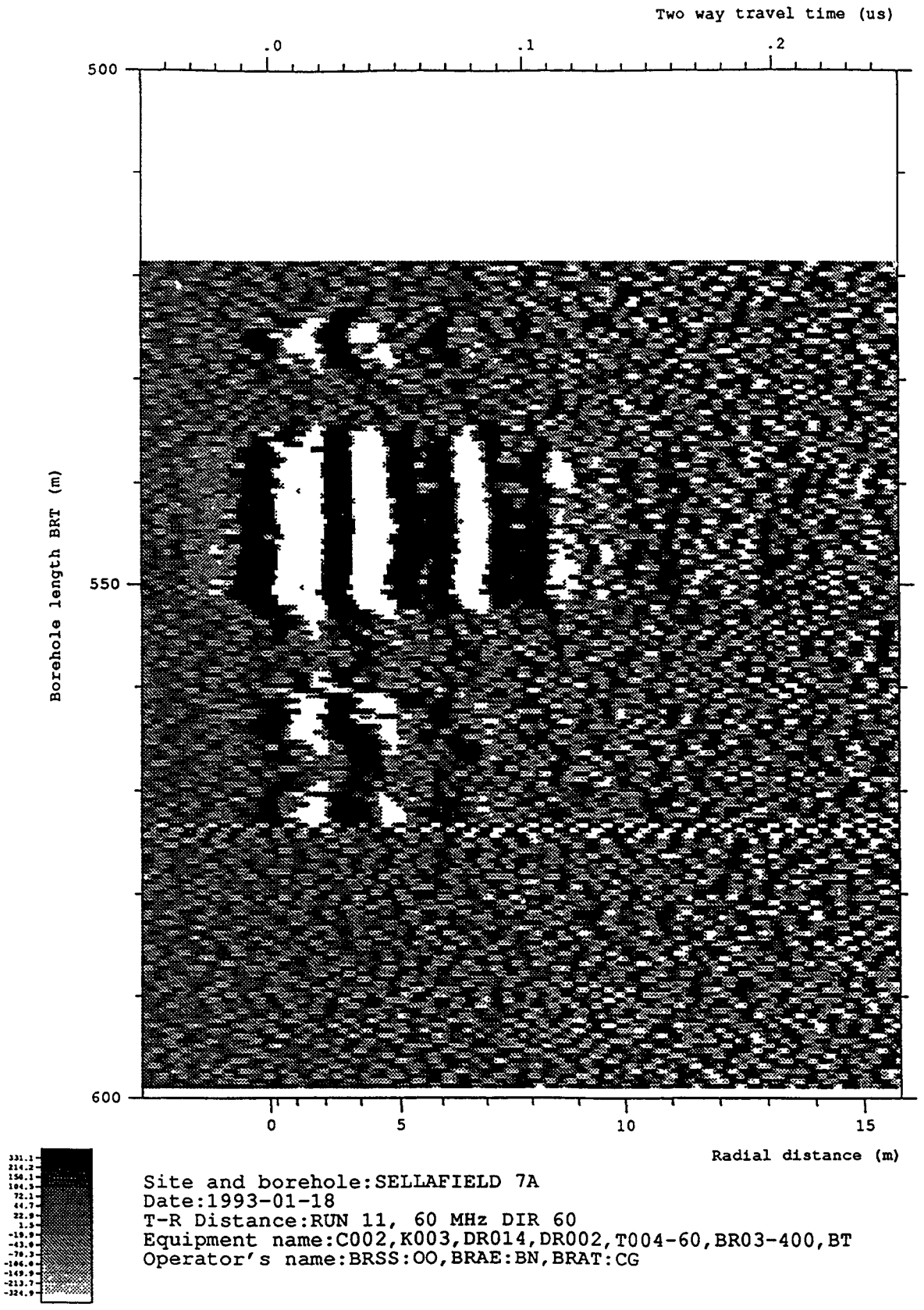

Figure 6-64 Radar map of the dipole component from the 60 MHz directional survey Run 11 after depth correction and band pass filtering for the depth interval 518.80 to 598.80 mbRT at an azimuth of 280°

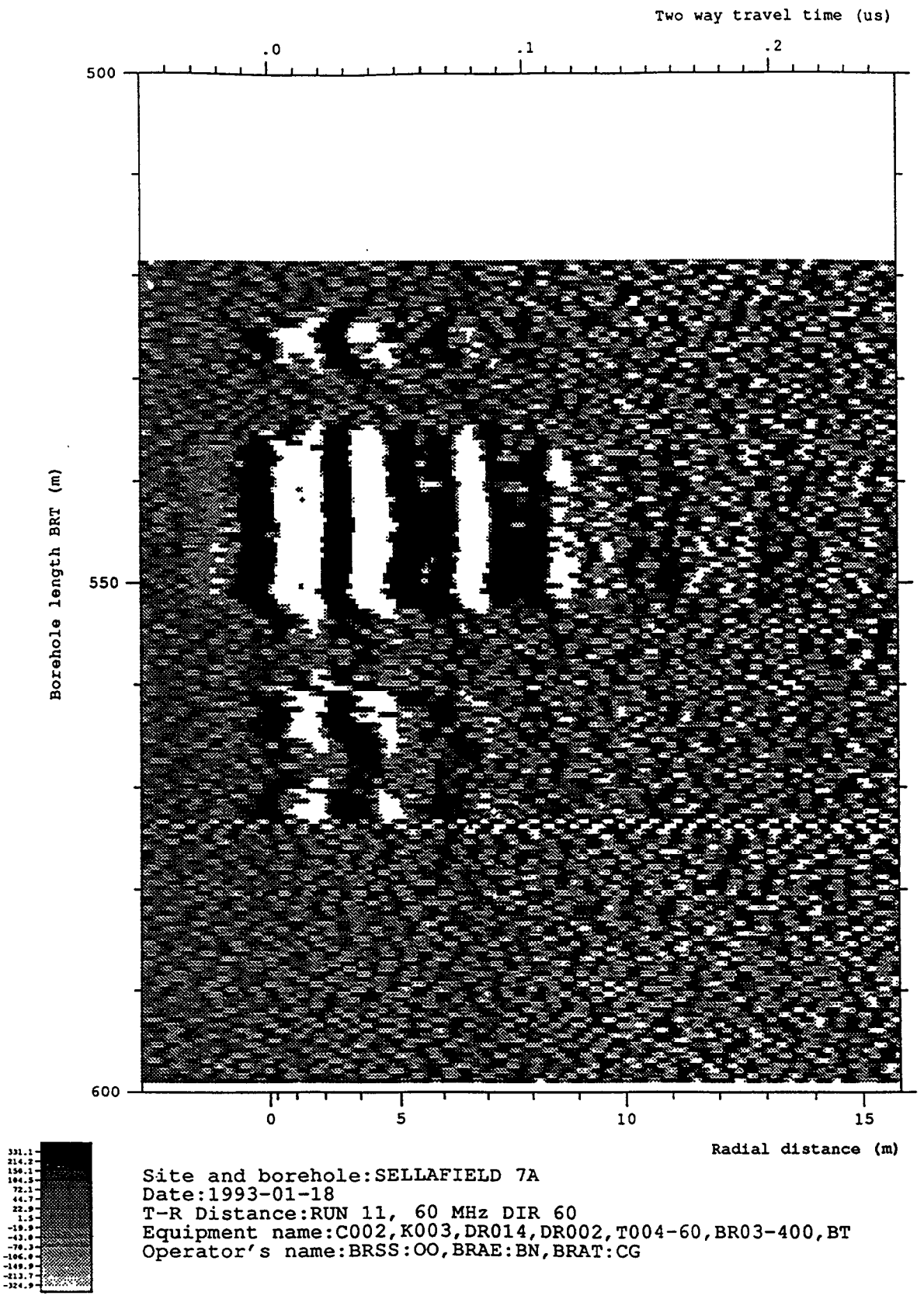

Figure 6-65 Radar map of the dipole component from the 60 MHz directional survey Run 11 after depth correction and band pass filtering for the depth interval 518.80 to 598.80 mbRT at an azimuth of 290°

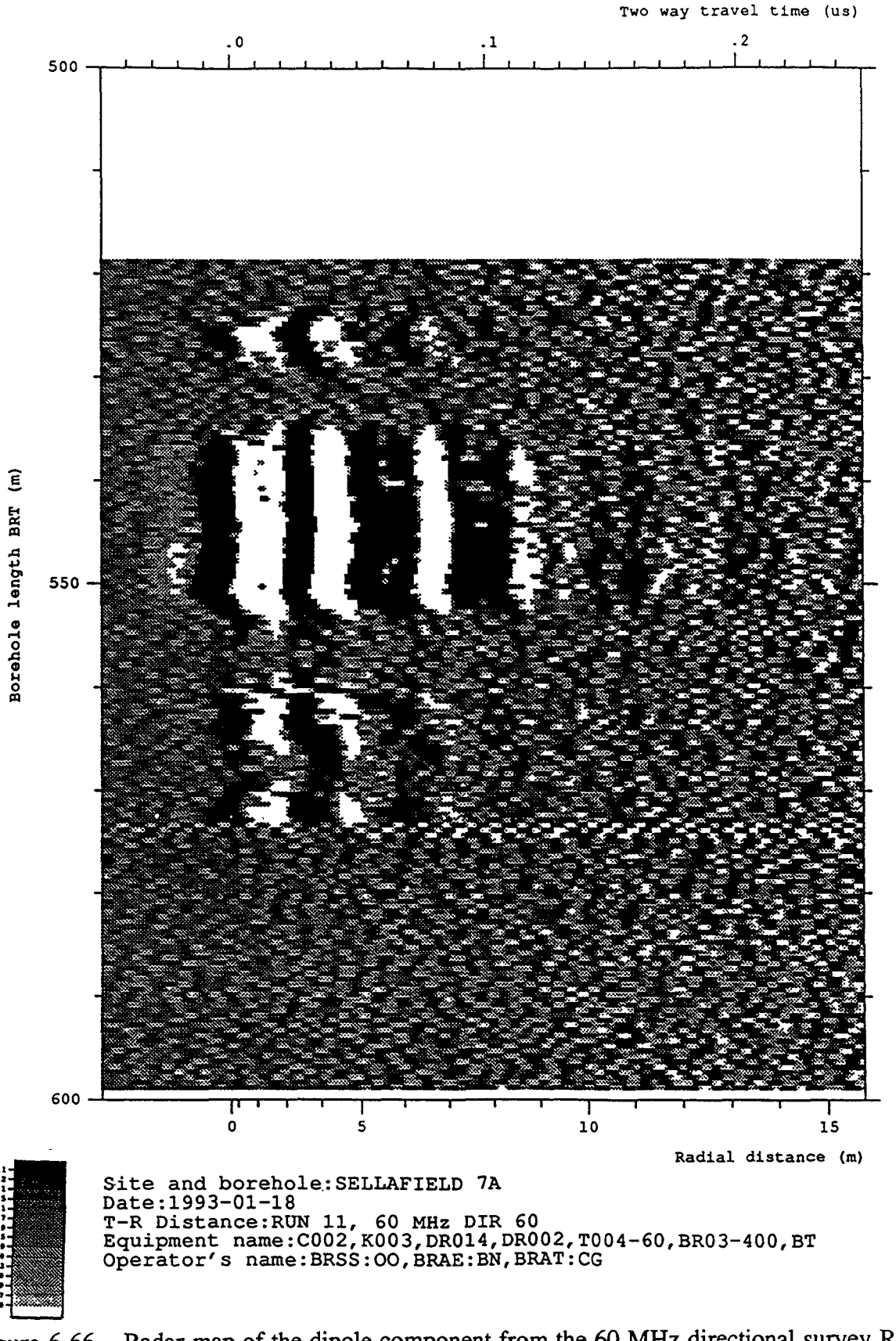

Figure 6-66 Radar map of the dipole component from the 60 MHz directional survey Run 11 after depth correction and band pass filtering for the depth interval 518.80 to 598.80 mbRT at an azimuth of 300°

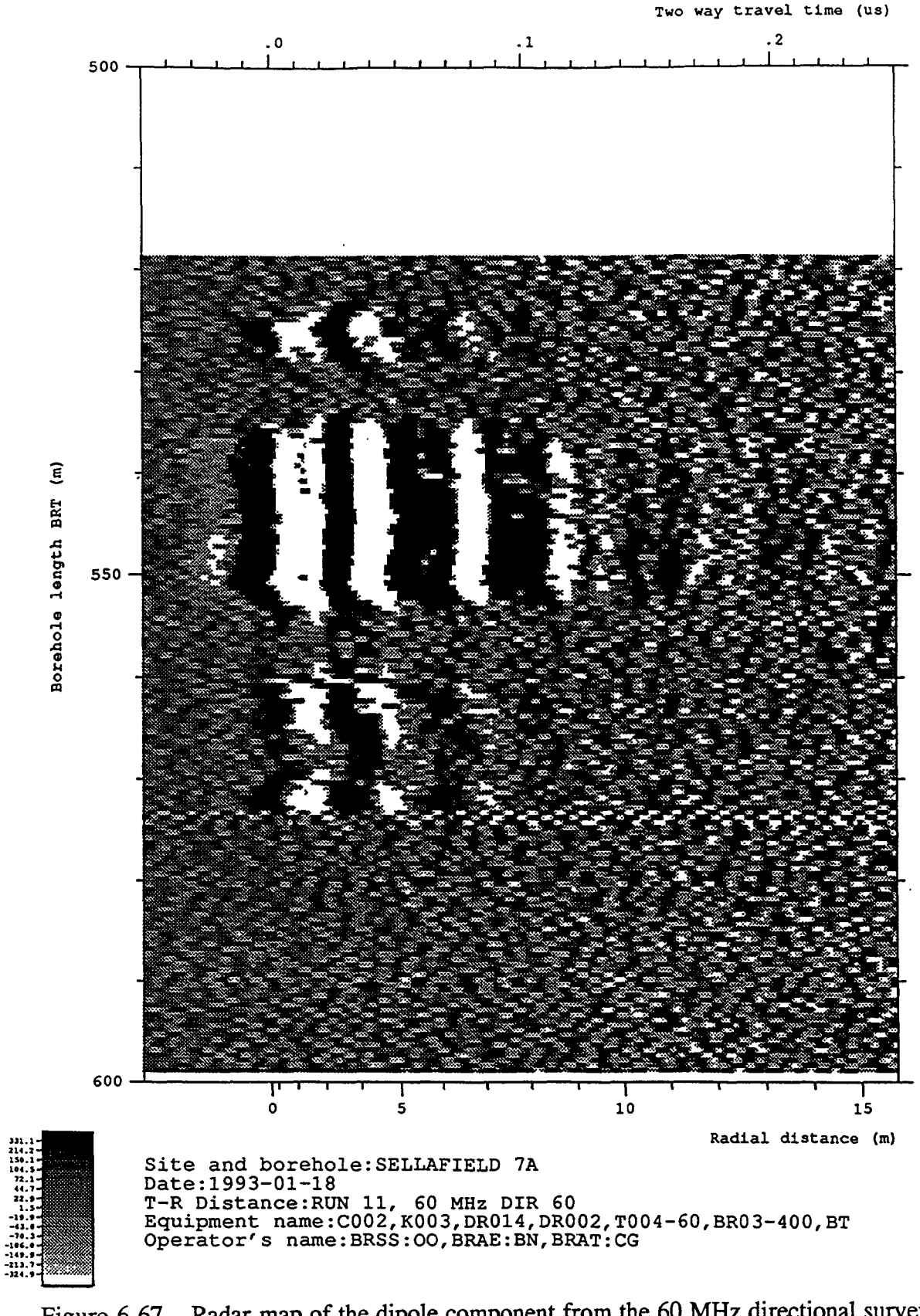

Figure 6-67 Radar map of the dipole component from the 60 MHz directional survey Run 11 after depth correction and band pass filtering for the depth interval 518.80 to 598.80 mbRT at an azimuth of 310°

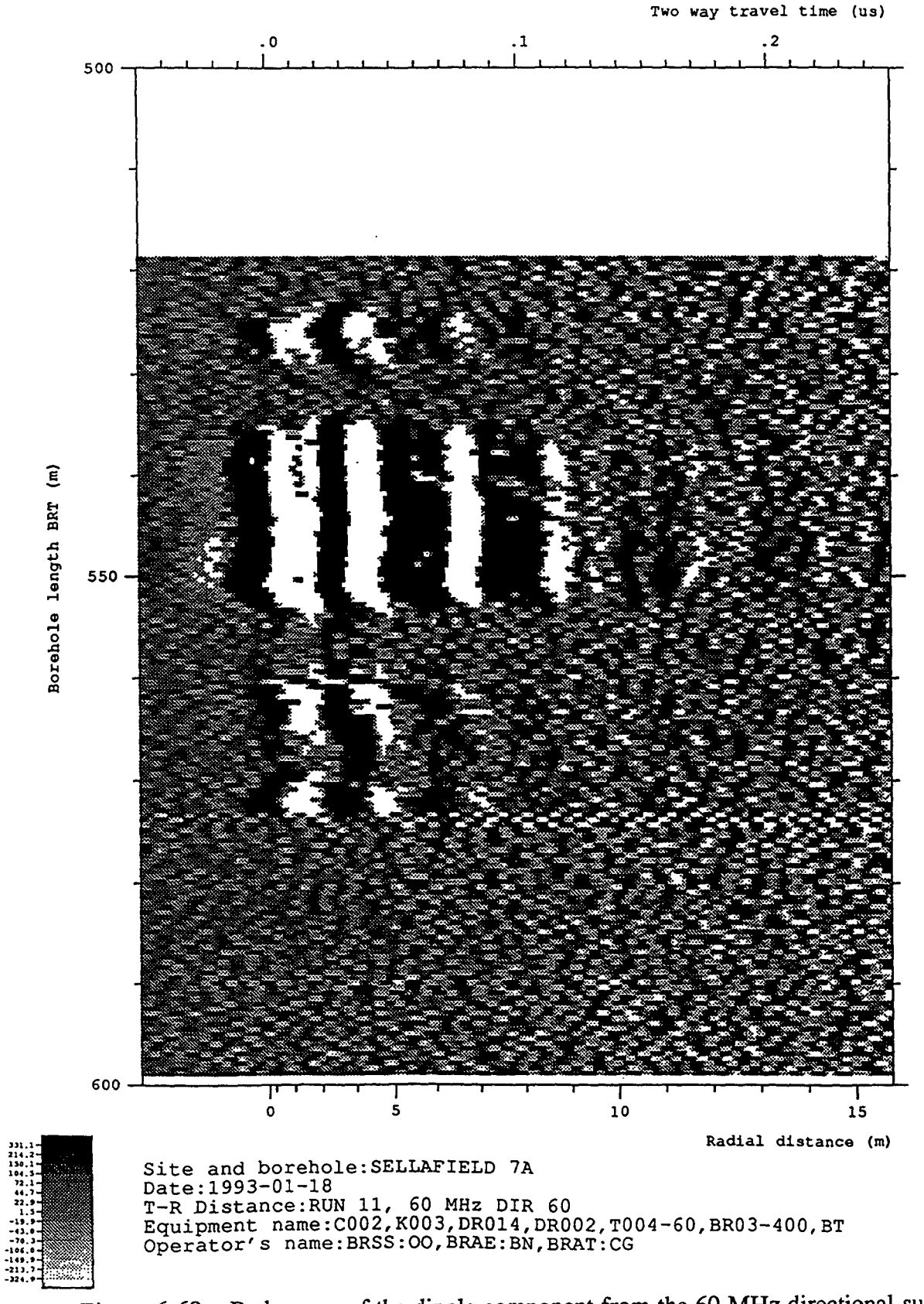

Figure 6-68 Radar map of the dipole component from the 60 MHz directional survey Run 11 after depth correction and band pass filtering for the depth interval 518.80 to 598.80 mbRT at an azimuth of 320°

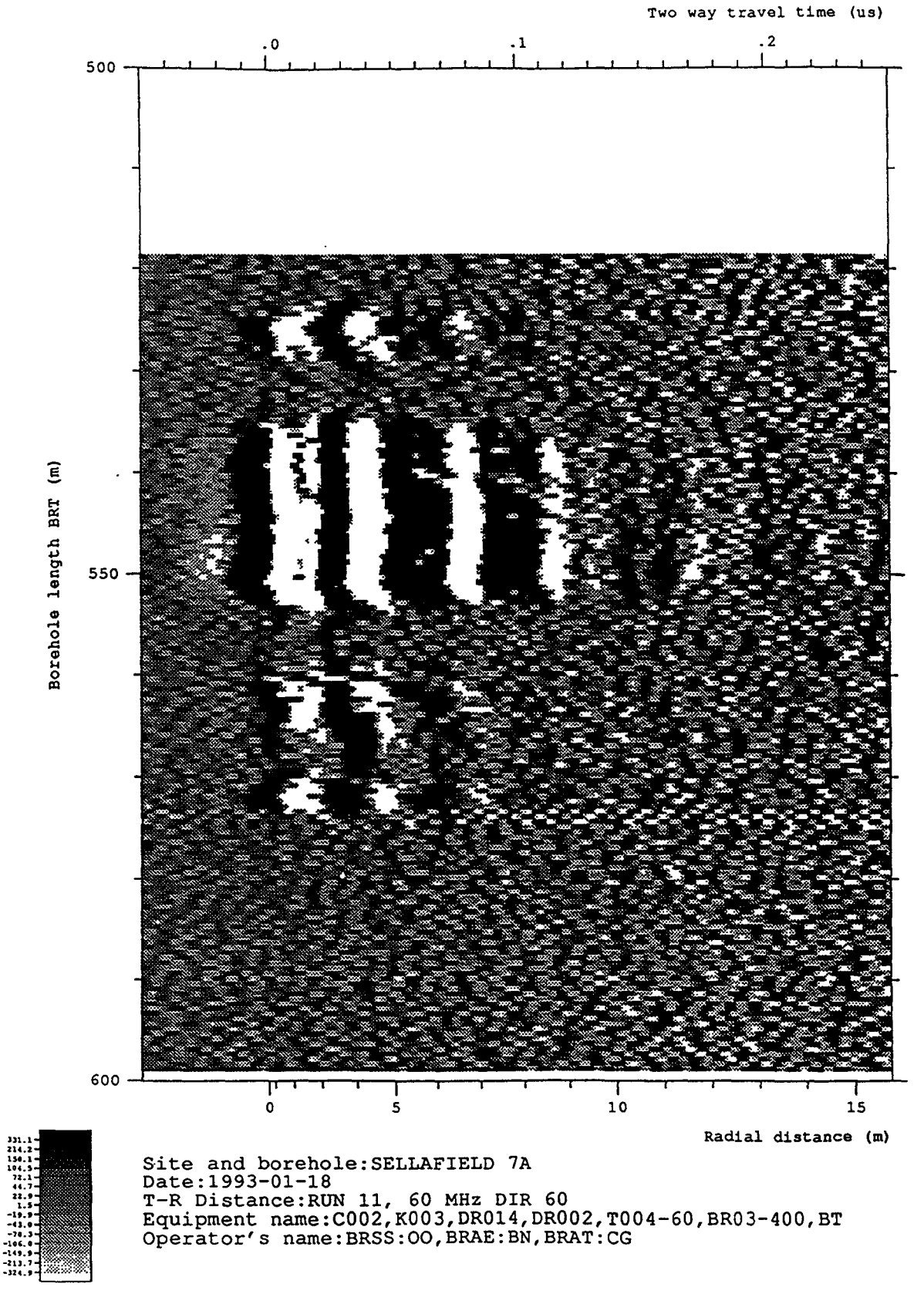

Figure 6-69 Radar map of the dipole component from the 60 MHz directional survey Run 11 after depth correction and band pass filtering for the depth interval 518.80 to 598.80 mbRT at an azimuth of 330°

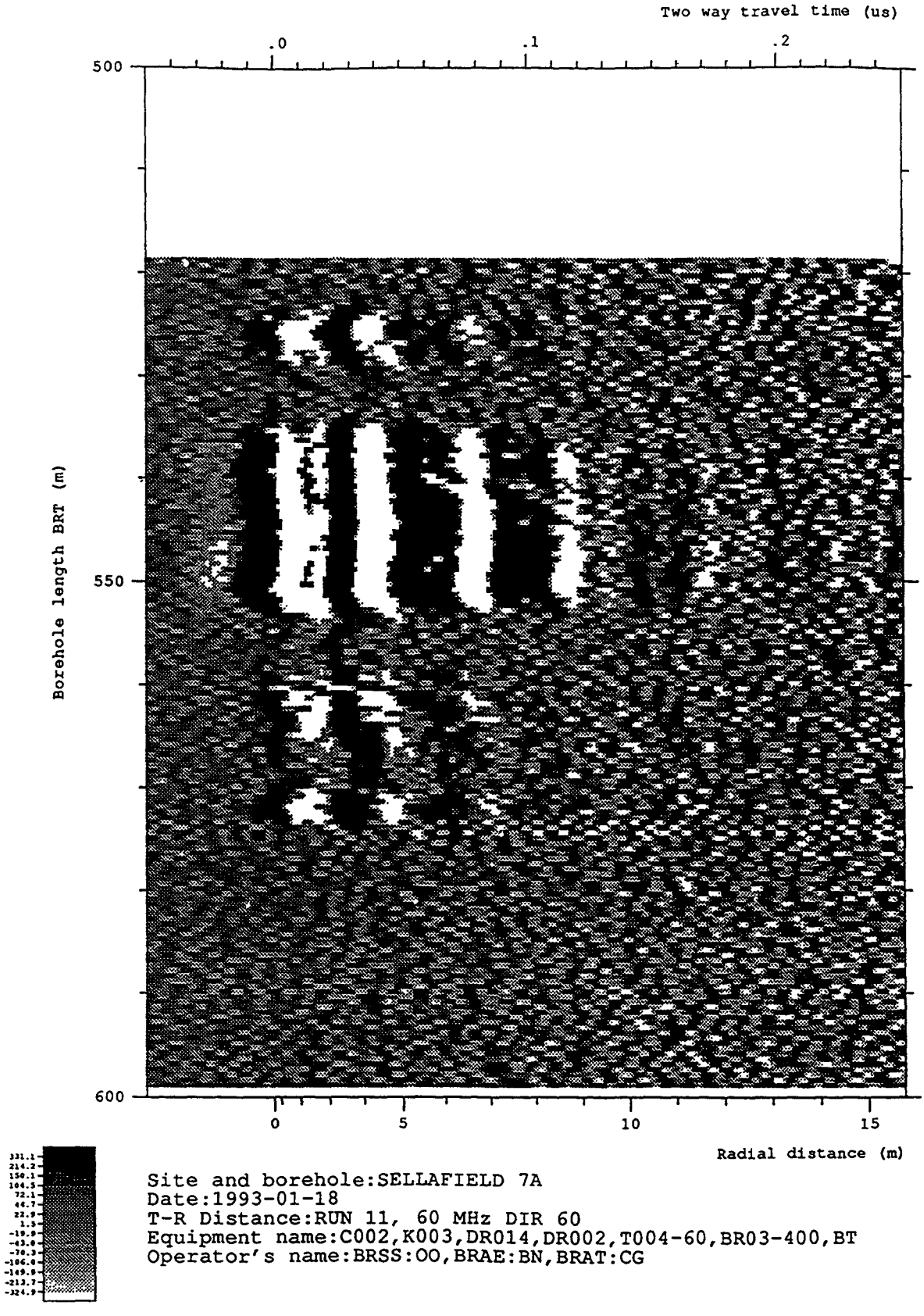

Figure 6-70 Radar map of the dipole component from the 60 MHz directional survey Run 11 after depth correction and band pass filtering for the depth interval 518.80 to 598.80 mbRT at an azimuth of 340°

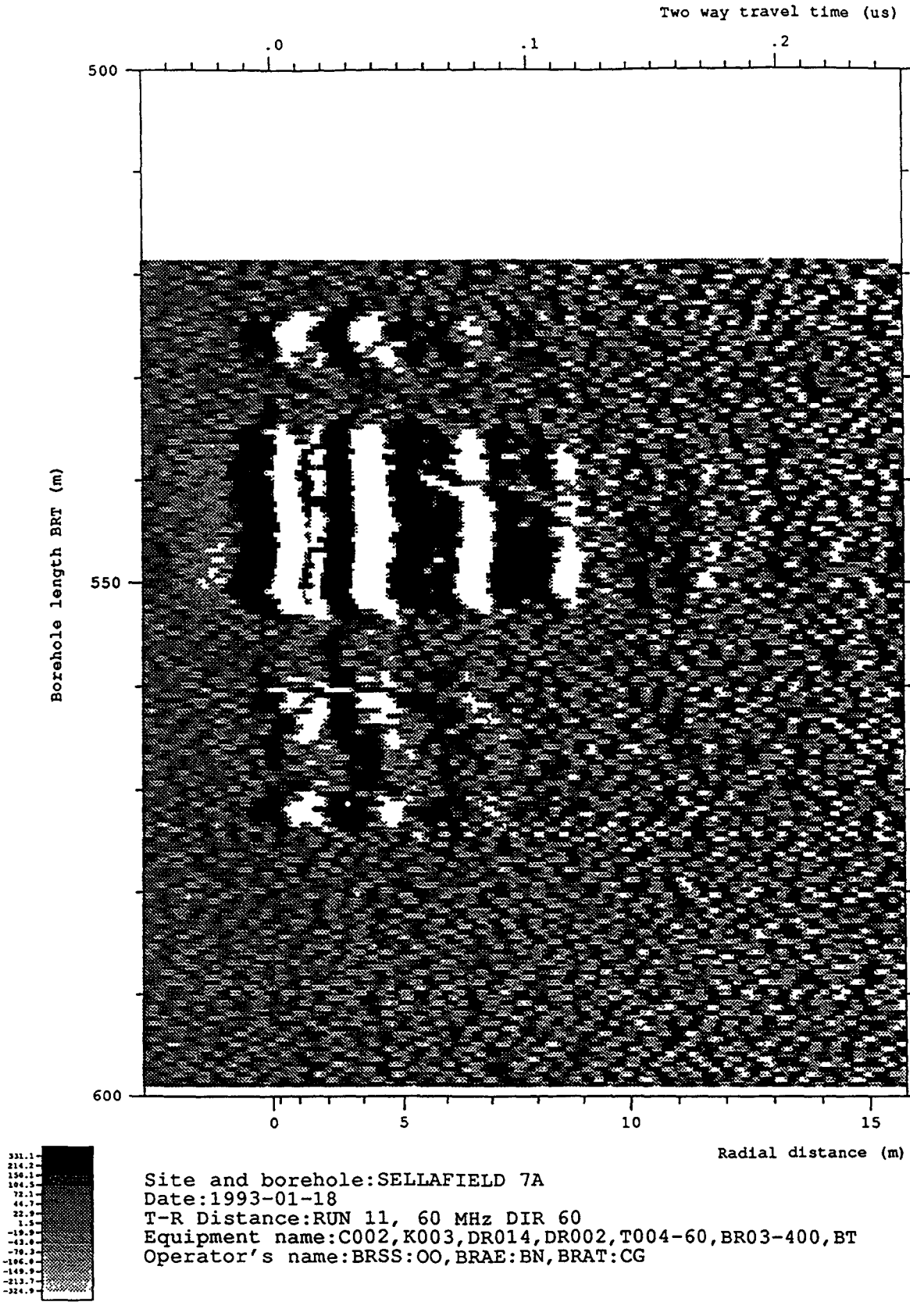

Figure 6-71 Radar map of the dipole component from the 60 MHz directional survey Run 11 after depth correction and band pass filtering for the depth interval 518.80 to 598.80 mbRT at an azimuth of 350°

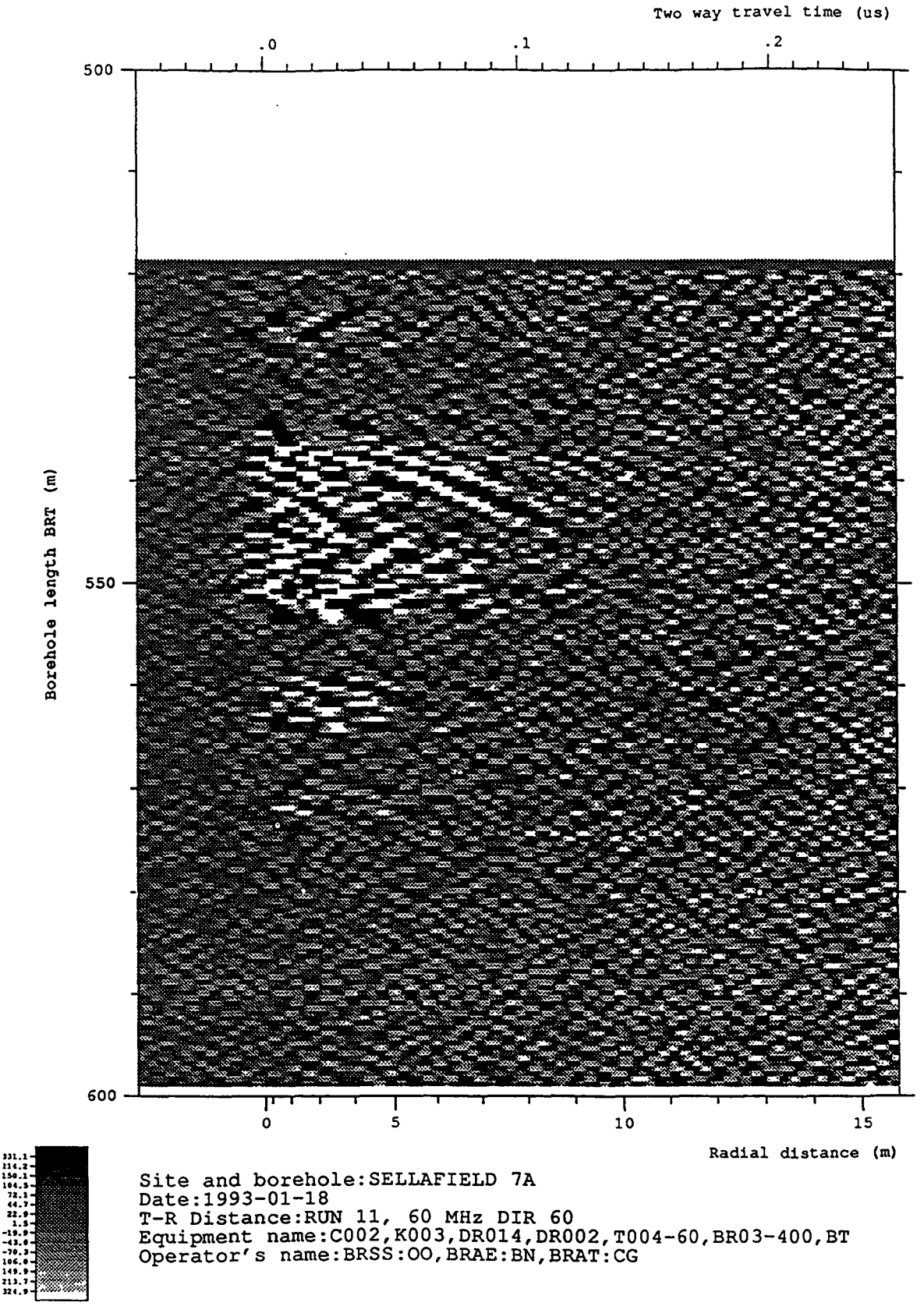

Figure 6-72 Radar map of the dipole component from the 60 MHz directional survey Run 11 after depth correction and the application of a moving average filter for the depth interval 518.80 to 598.80 mbRT at an azimuth of 0°

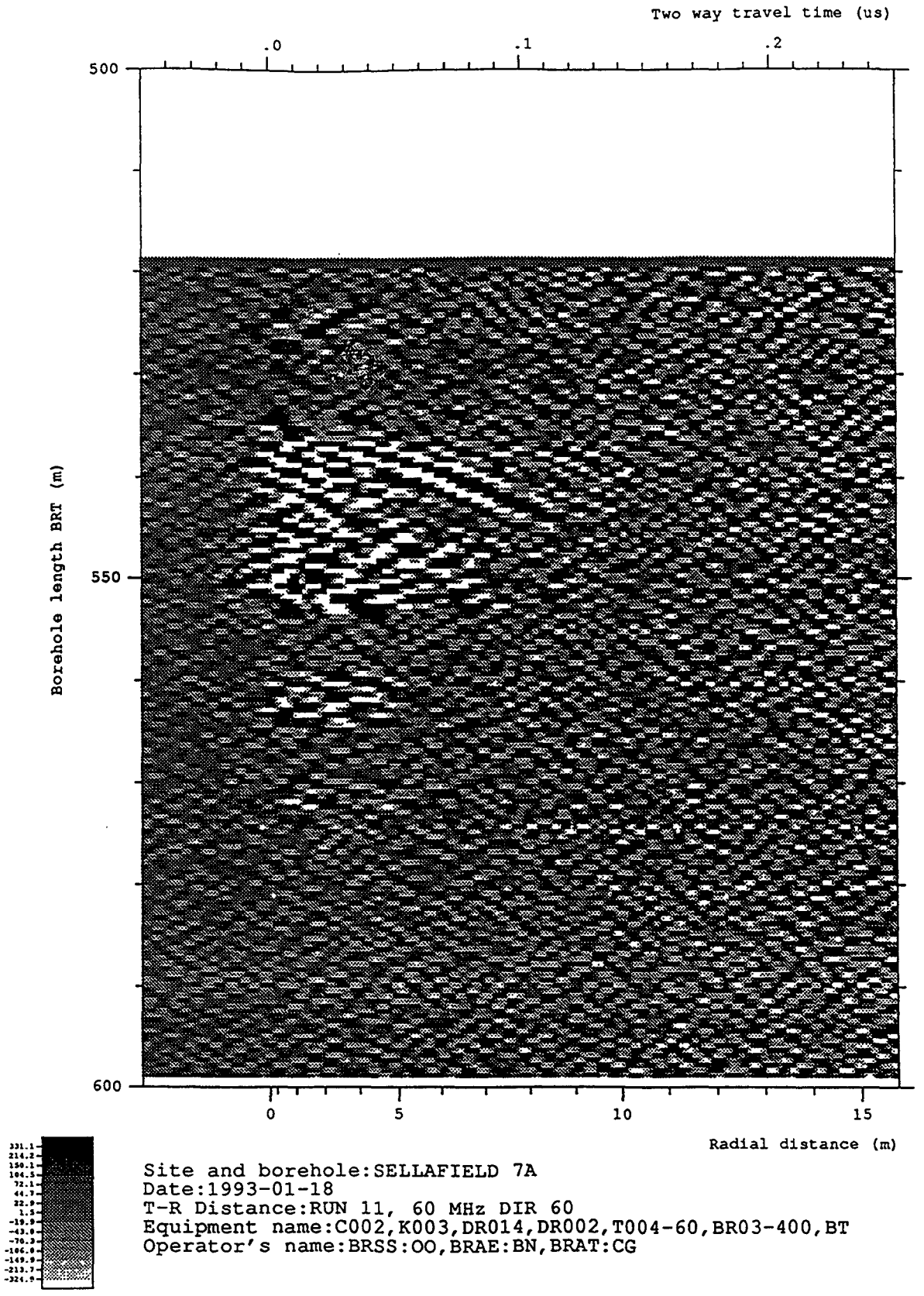

Figure 6-73 Radar map of the dipole component from the 60 MHz directional survey Run 11 after depth correction and the application of a moving average filter for the depth interval 518.80 to 598.80 mbRT at an azimuth of 10°

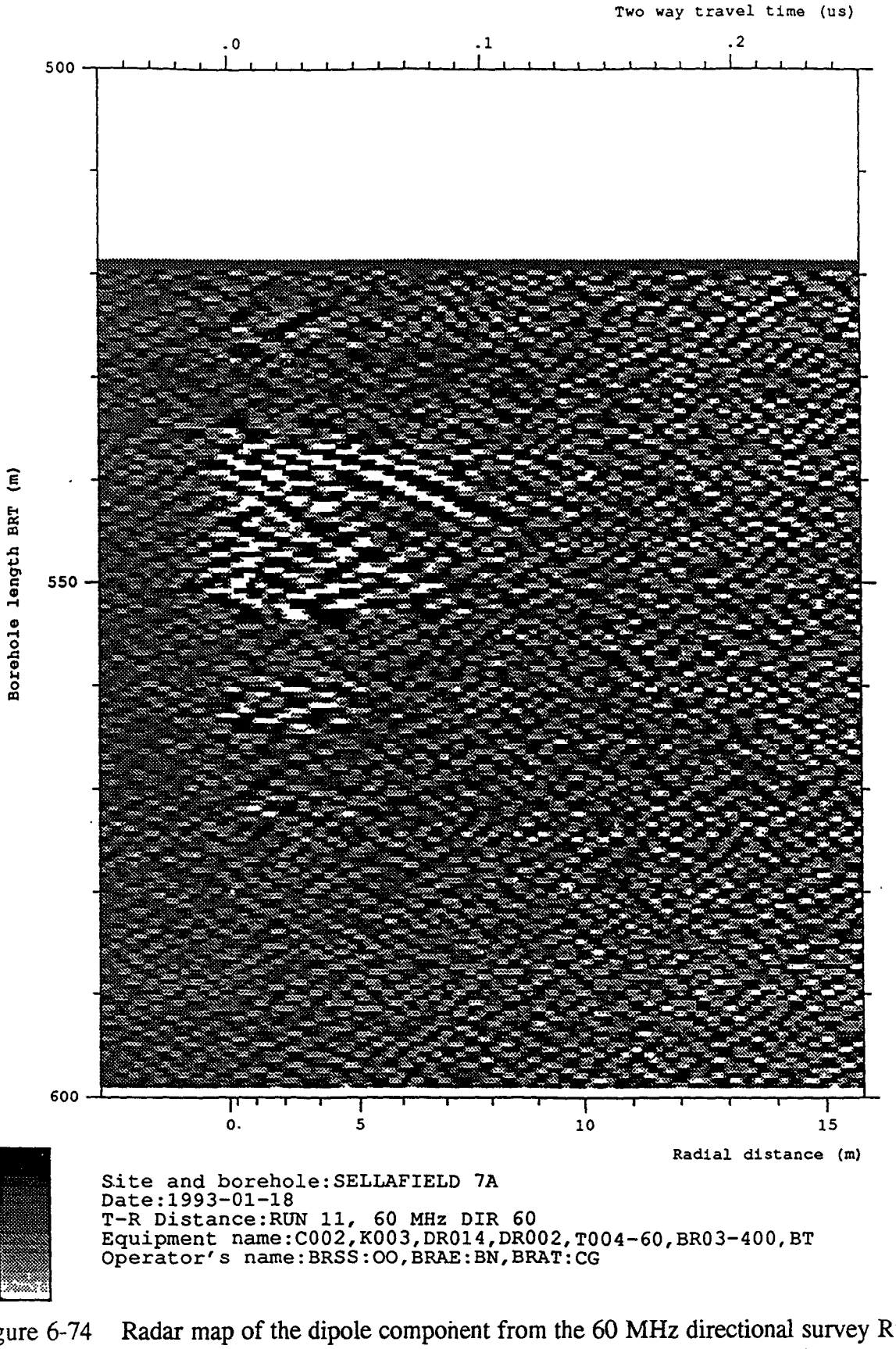

Figure 6-74 Radar map of the dipole component from the 60 MHz directional survey Run 11 after depth correction and the application of a moving average filter for the depth interval 518.80 to 598.80 mbRT at an azimuth of 20°

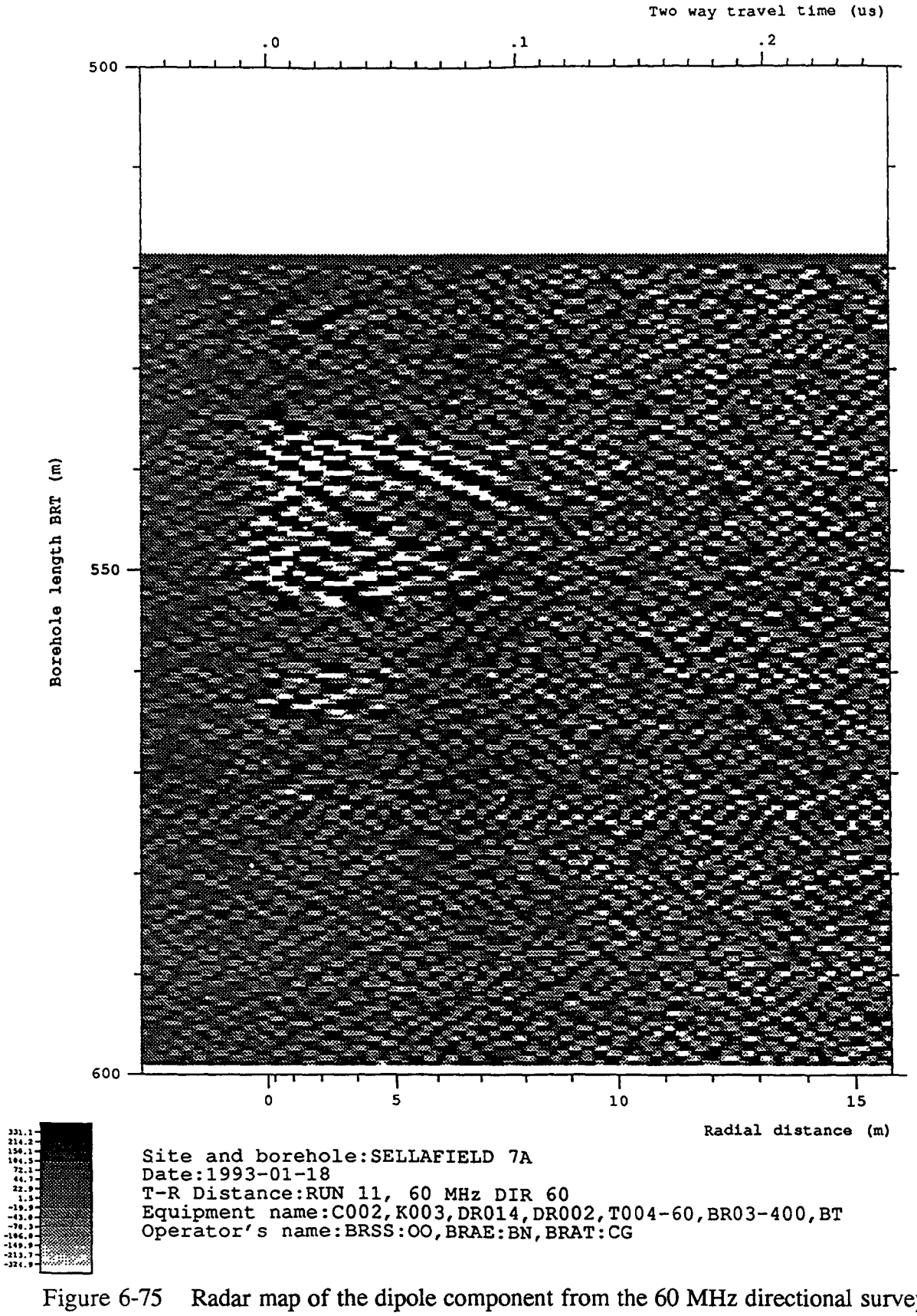

Figure 6-75 Radar map of the dipole component from the 60 MHz directional survey Run 11 after depth correction and the application of a moving average filter for the depth interval 518.80 to 598.80 mbRT at an azimuth of 30°

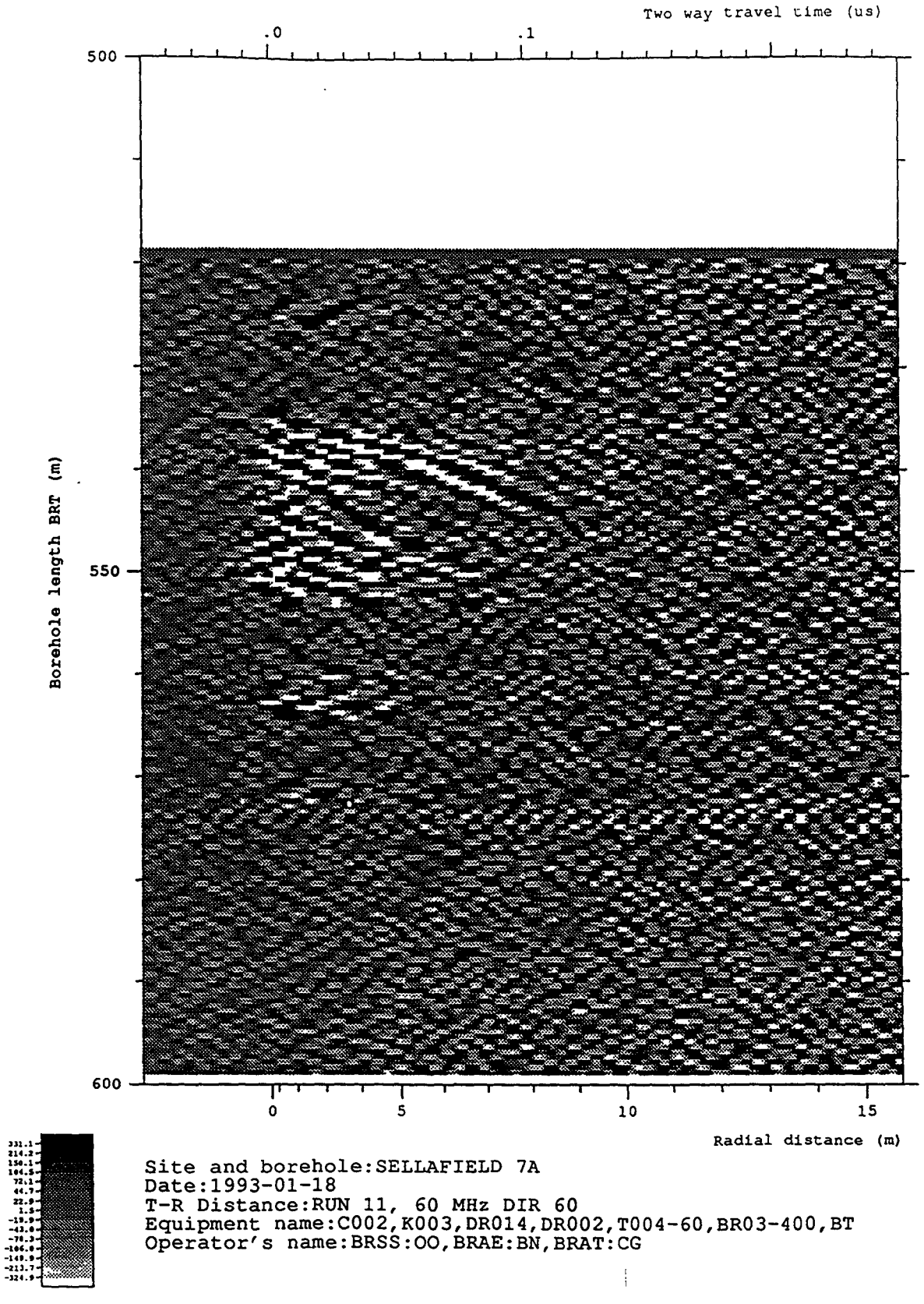

Figure 6-76 Radar map of the dipole component from the 60 MHz directional survey Run 11 after depth correction and the application of a moving average filter for the depth interval 518.80 to 598.80 mbRT at an azimuth of 40°

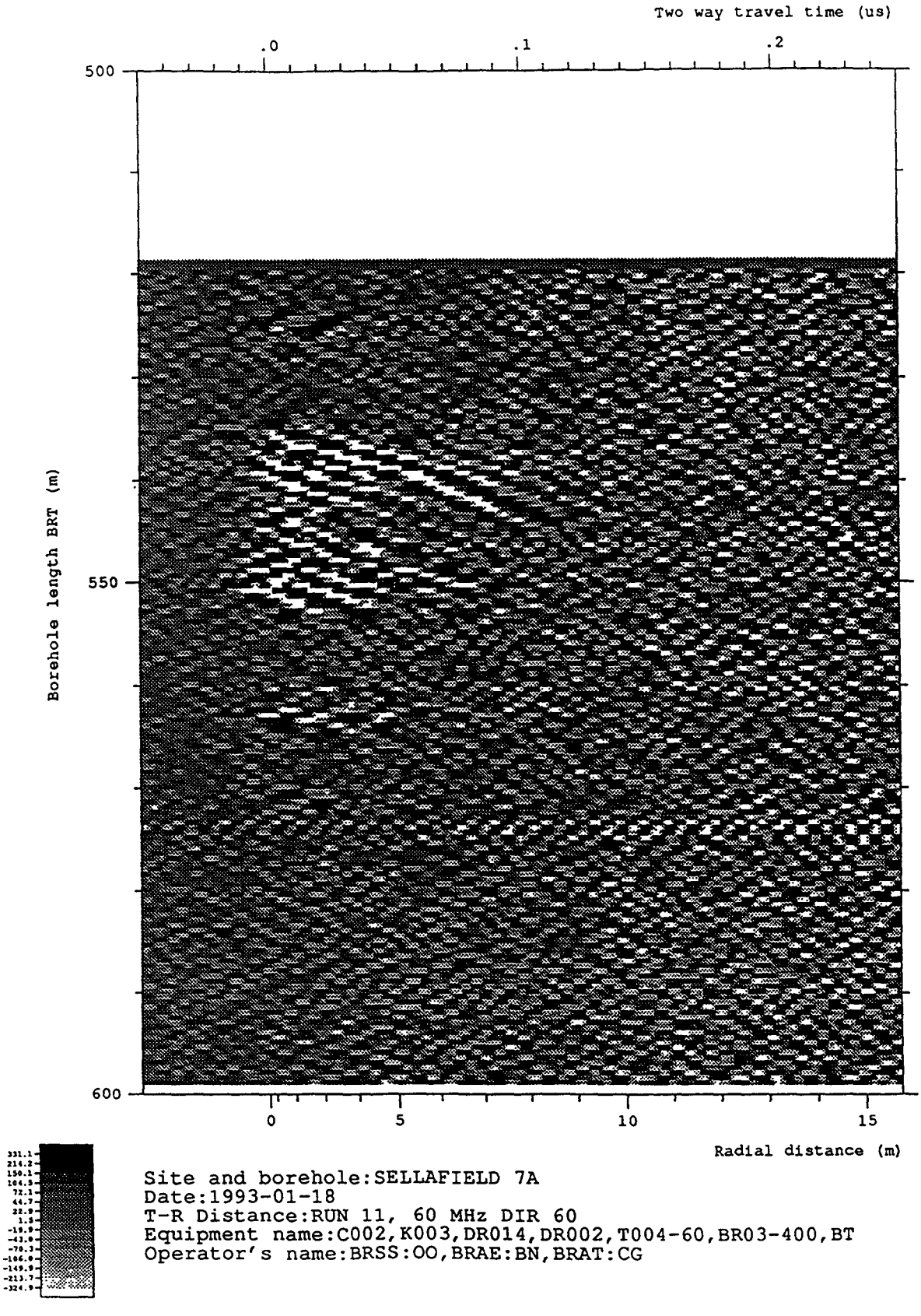

Figure 6-77 Radar map of the dipole component from the 60 MHz directional survey Run 11 after depth correction and the application of a moving average filter for the depth interval 518.80 to 598.80 mbRT at an azimuth of 50°

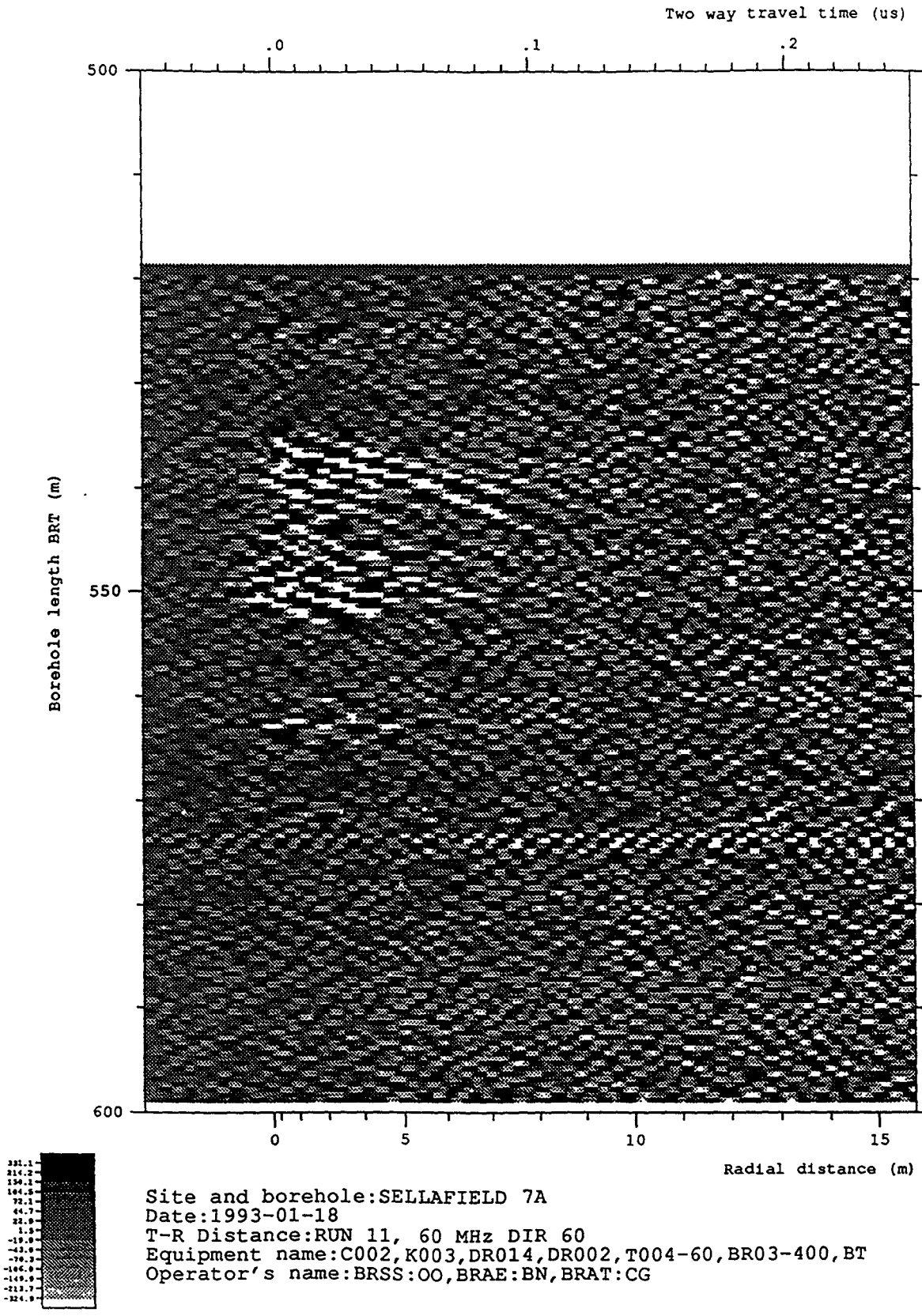

Figure 6-78 Radar map of the dipole component from the 60 MHz directional survey Run 11 after depth correction and the application of a moving average filter for the depth interval 518.80 to 598.80 mbRT at an azimuth of 60°

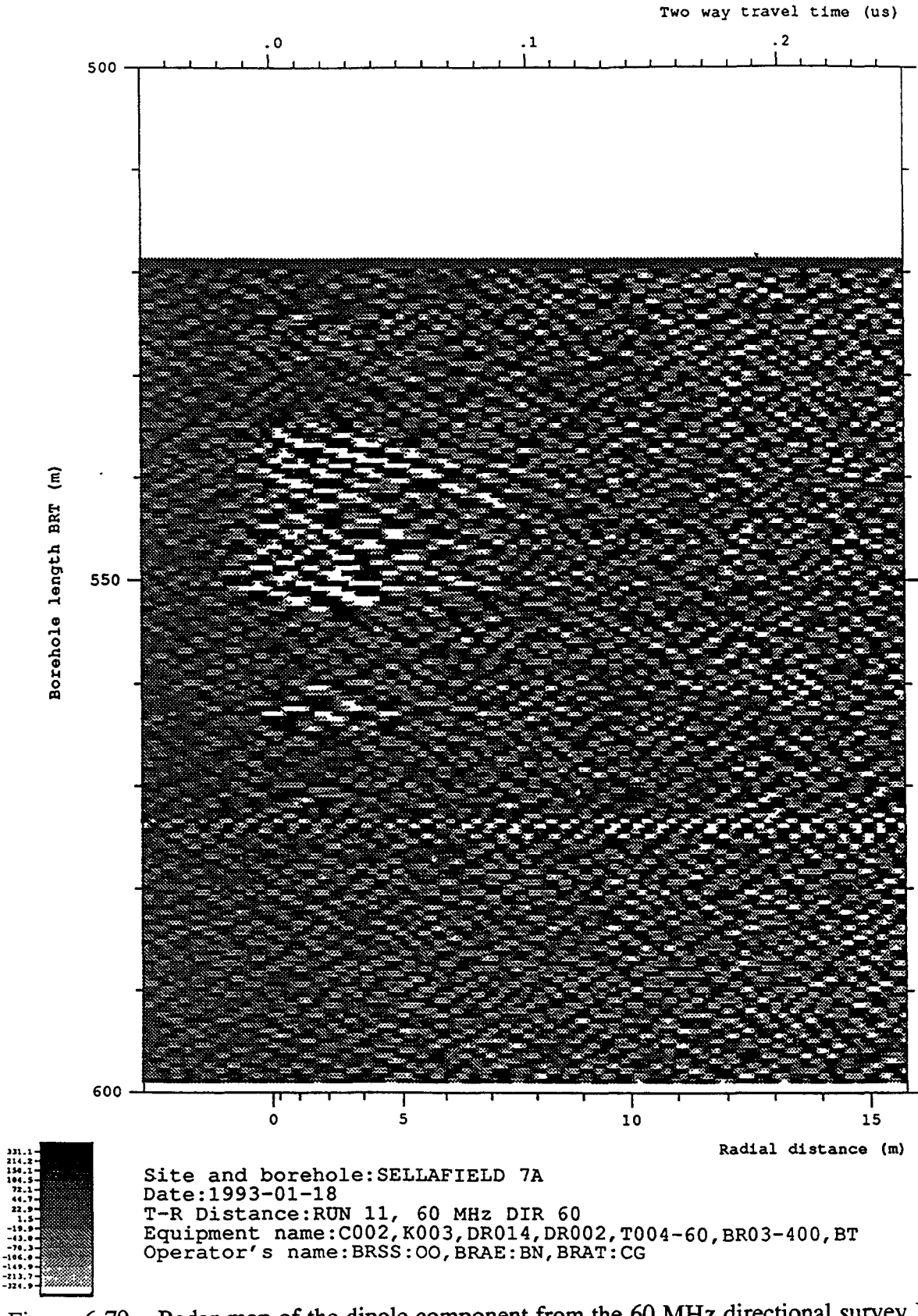

Figure 6-79 Radar map of the dipole component from the 60 MHz directional survey Run 11 after depth correction and the application of a moving average filter for the depth interval 518.80 to 598.80 mbRT at an azimuth of 70°

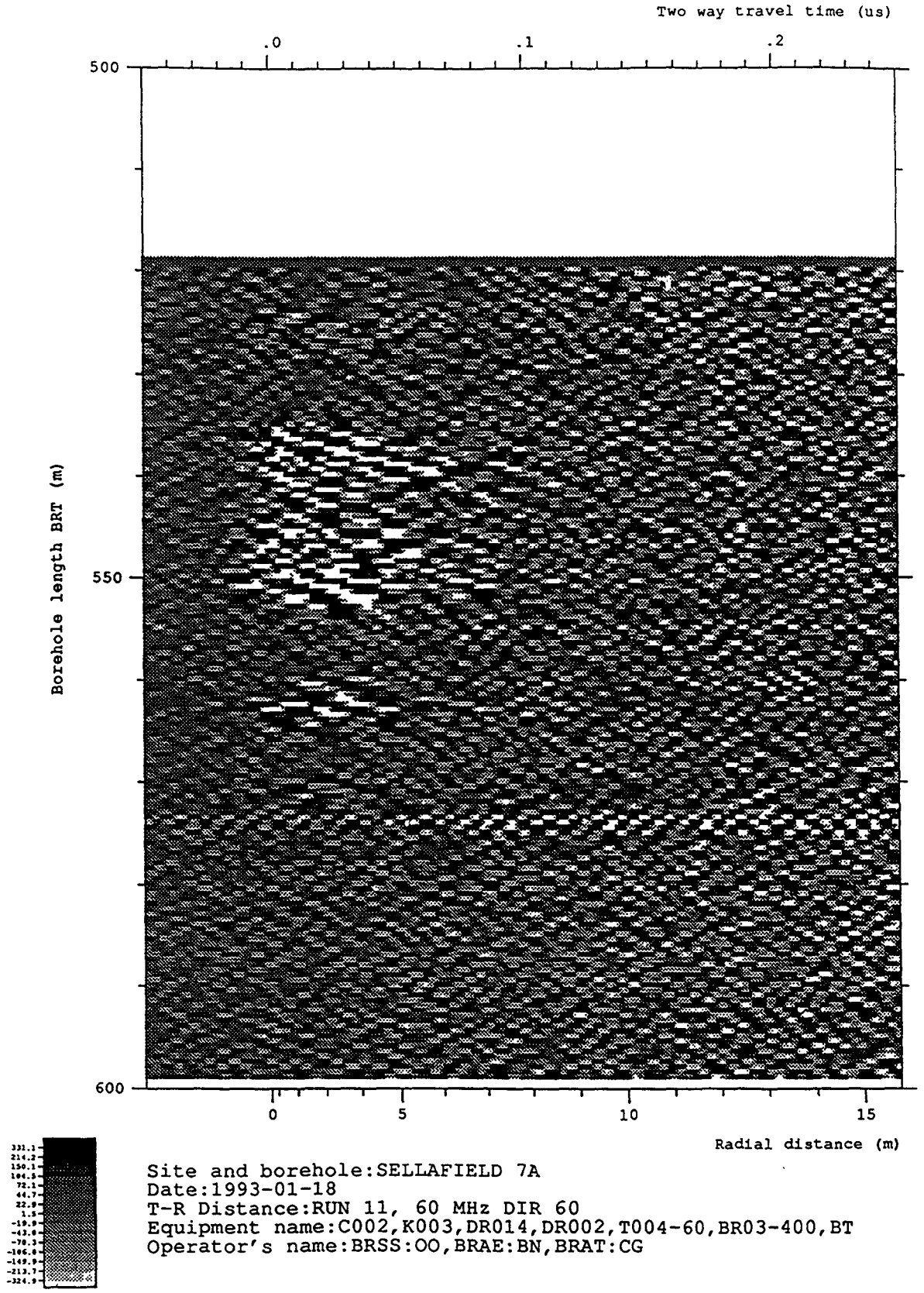

Figure 6-80 Radar map of the dipole component from the 60 MHz directional survey Run 11 after depth correction and the application of a moving average filter for the depth interval 518.80 to 598.80 mbRT at an azimuth of 80°

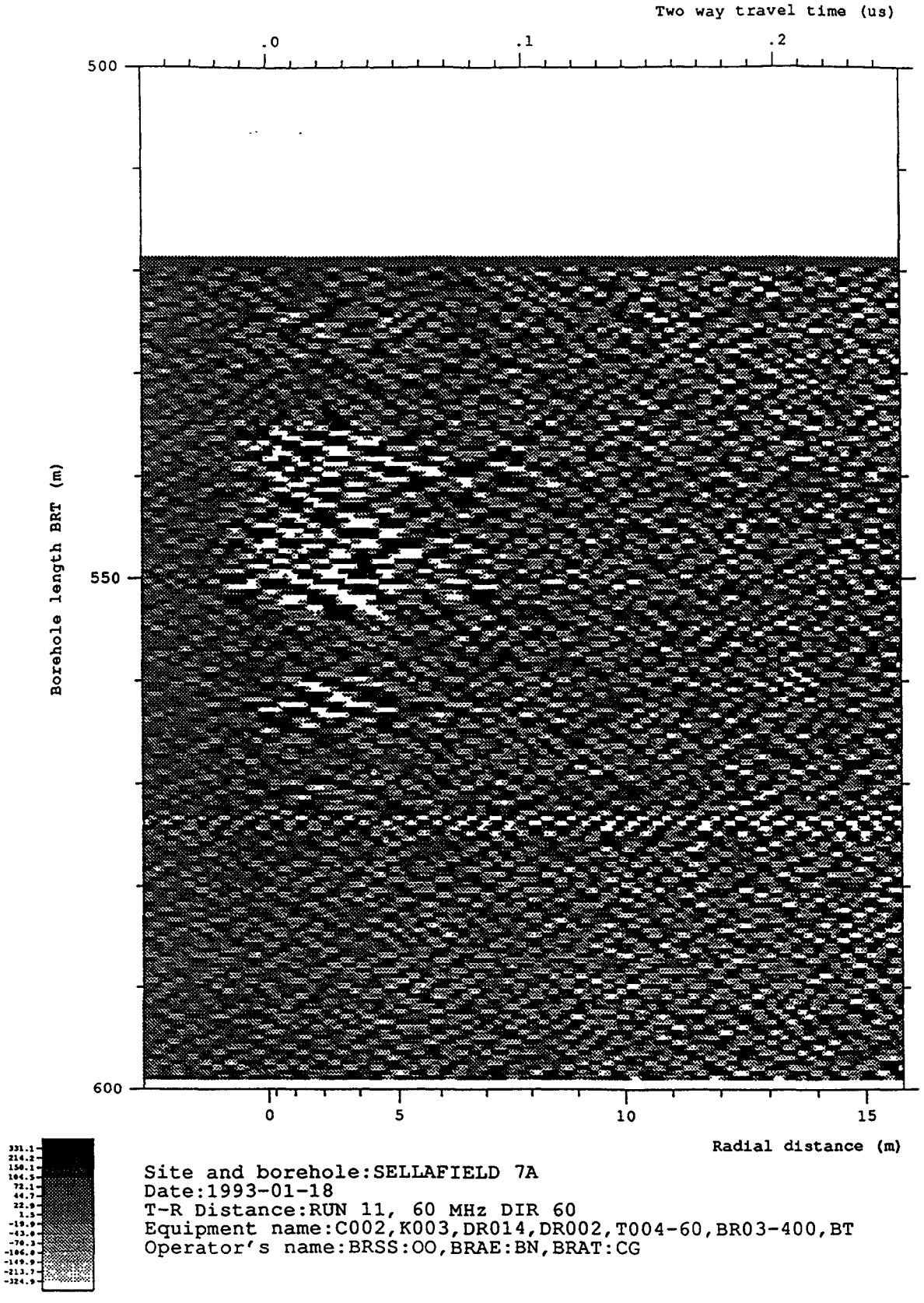

Figure 6-81 Radar map of the dipole component from the 60 MHz directional survey Run 11 after depth correction and the application of a moving average filter for the depth interval 518.80 to 598.80 mbRT at an azimuth of 90°

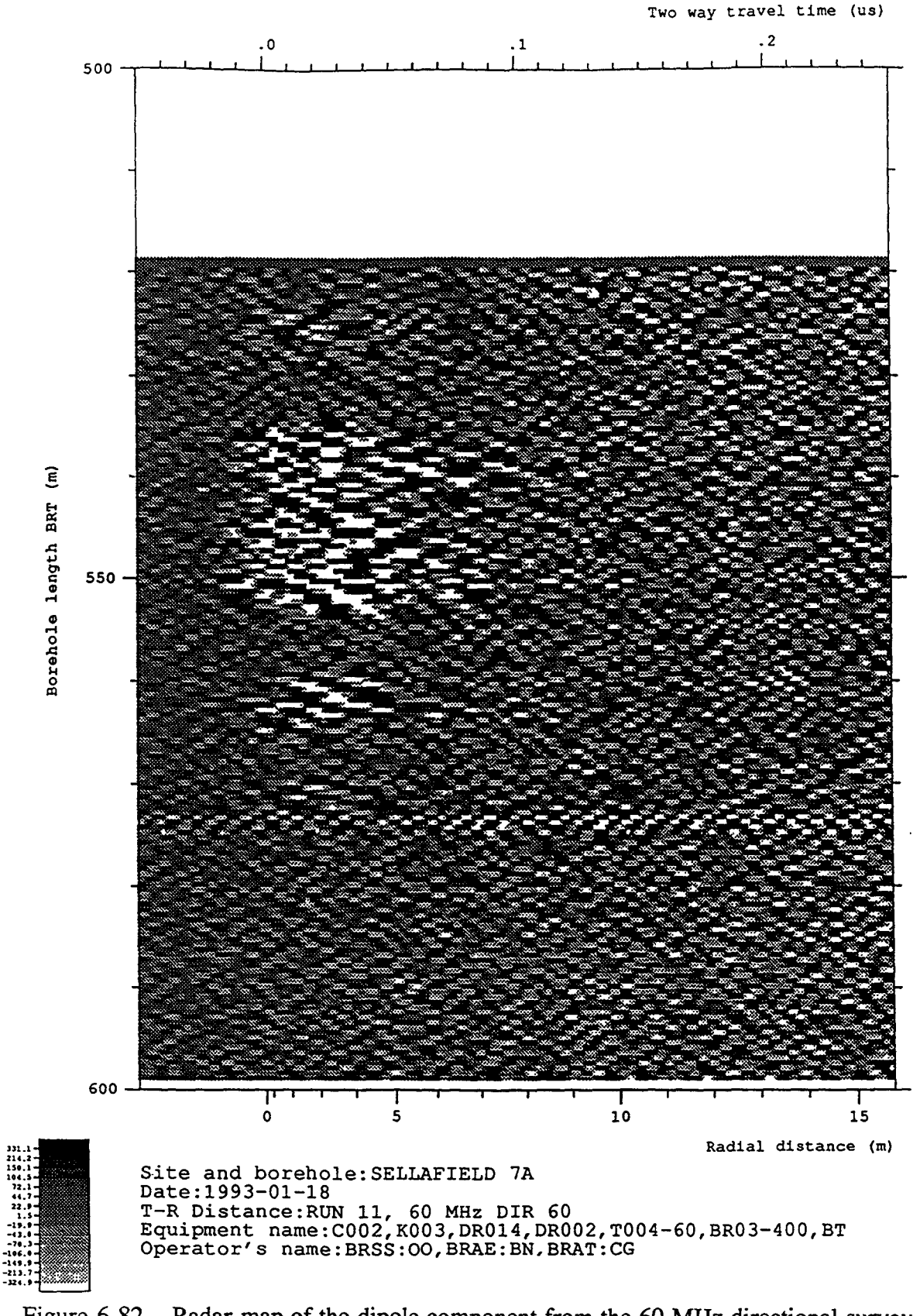

Figure 6-82 Radar map of the dipole component from the 60 MHz directional survey Run 11 after depth correction and the application of a moving average filter for the depth interval 518.80 to 598.80 mbRT at an azimuth of 100°

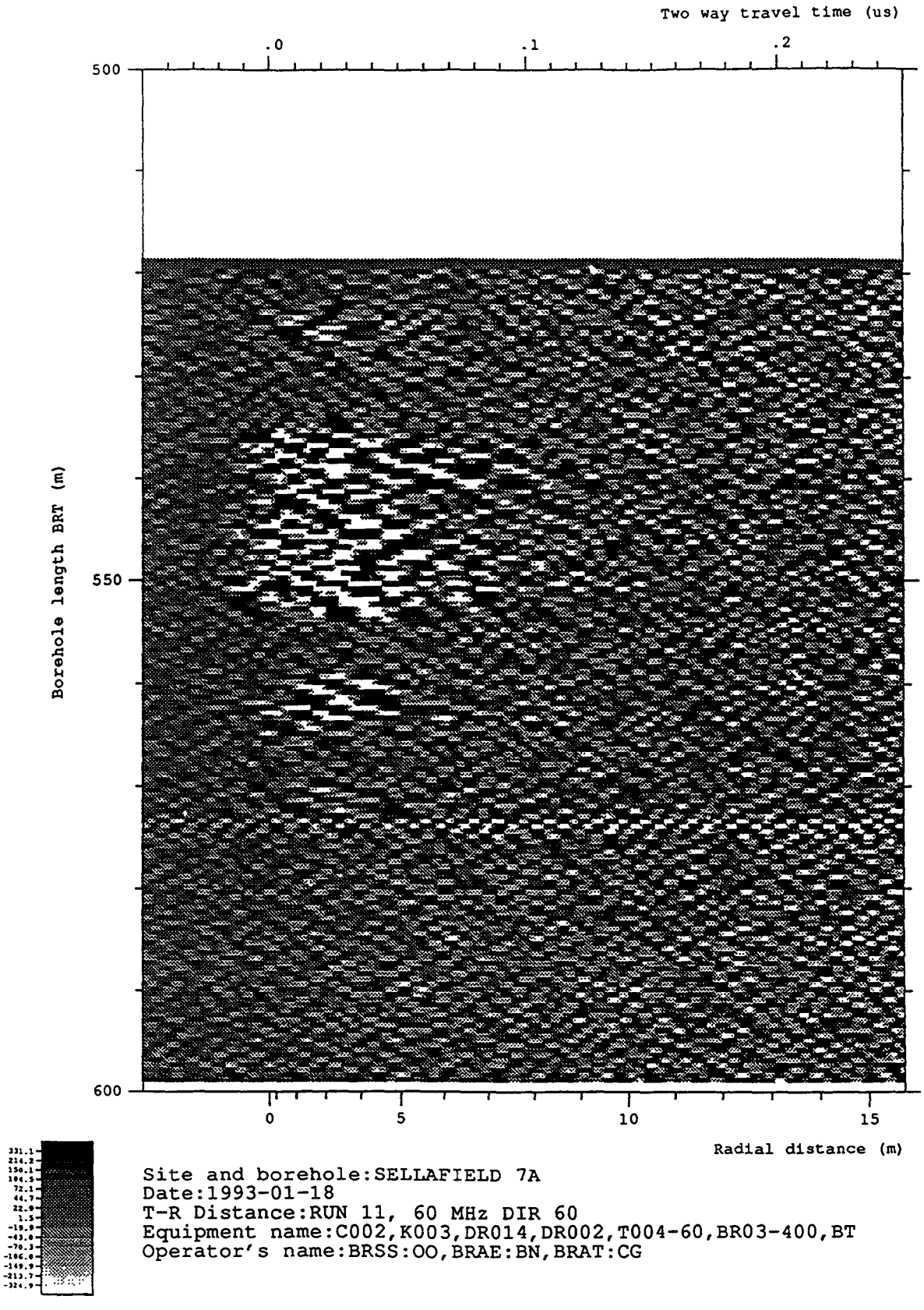

Figure 6-83 Radar map of the dipole component from the 60 MHz directional survey Run 11 after depth correction and the application of a moving average filter for the depth interval 518.80 to 598.80 mbRT at an azimuth of 110°

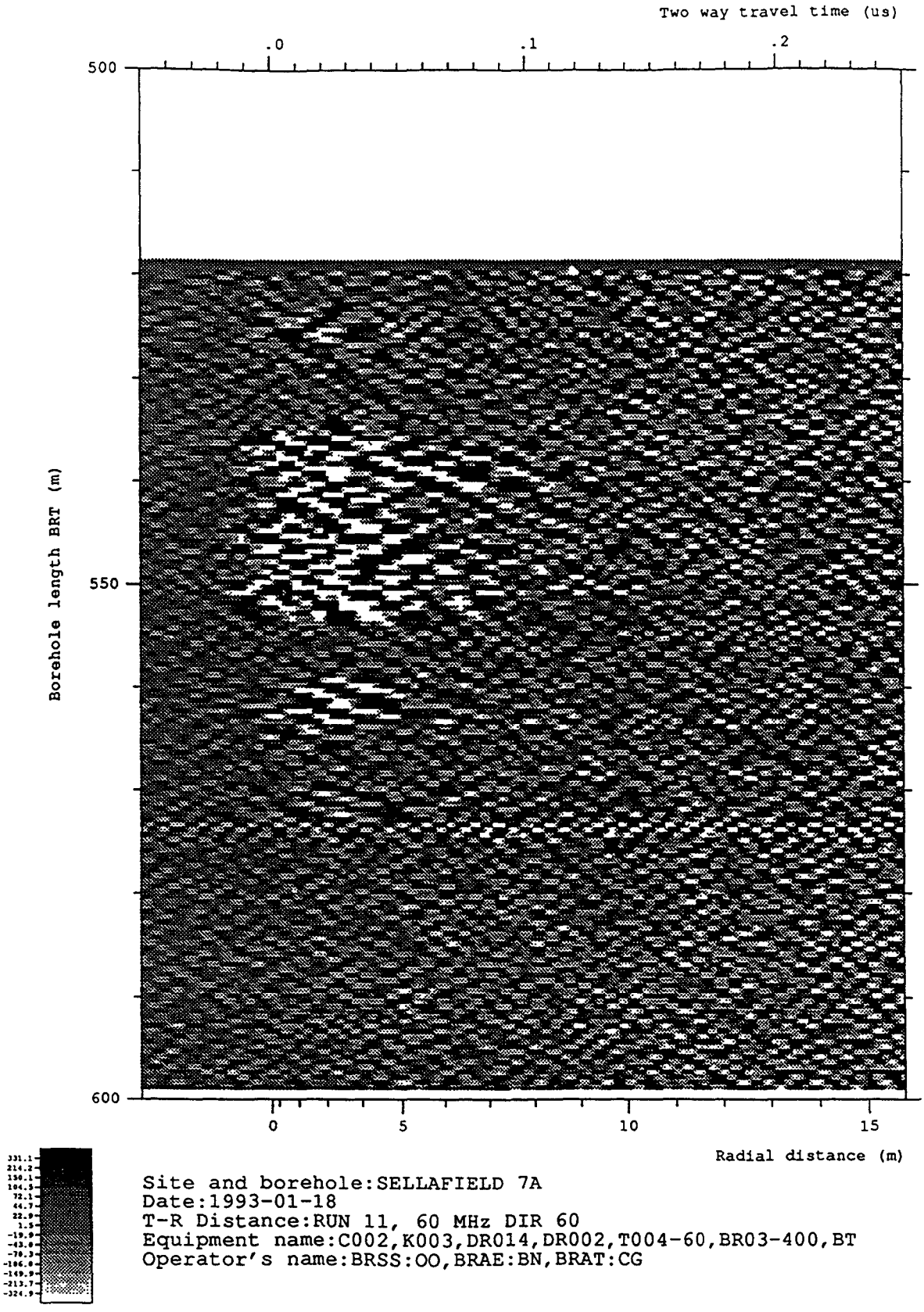

Figure 6-84 Radar map of the dipole component from the 60 MHz directional survey Run 11 after depth correction and the application of a moving average filter for the depth interval 518.80 to 598.80 mbRT at an azimuth of 120°

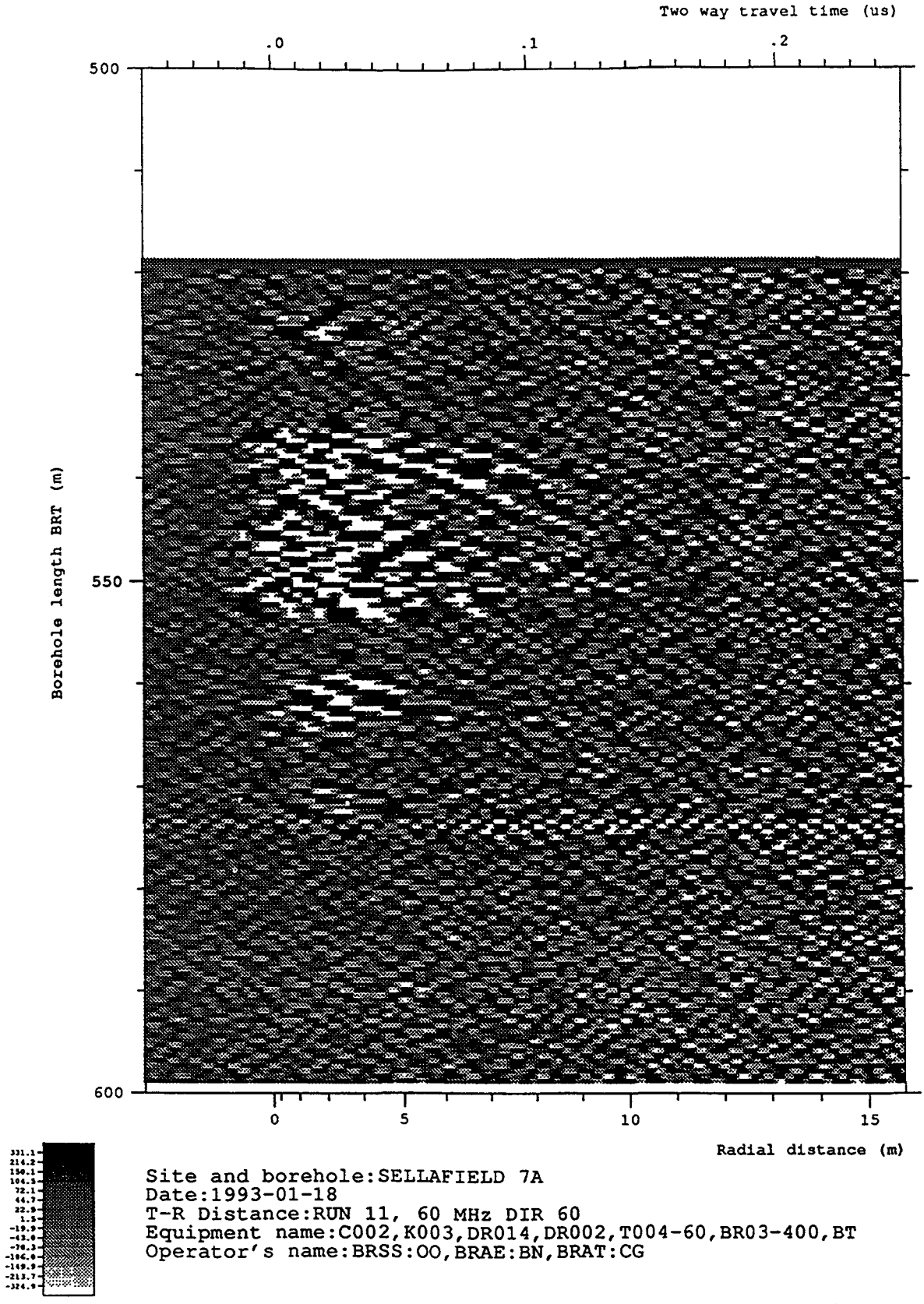

Figure 6-85 Radar map of the dipole component from the 60 MHz directional survey Run 11 after depth correction and the application of a moving average filter for the depth interval 518.80 to 598.80 mbRT at an azimuth of 130°

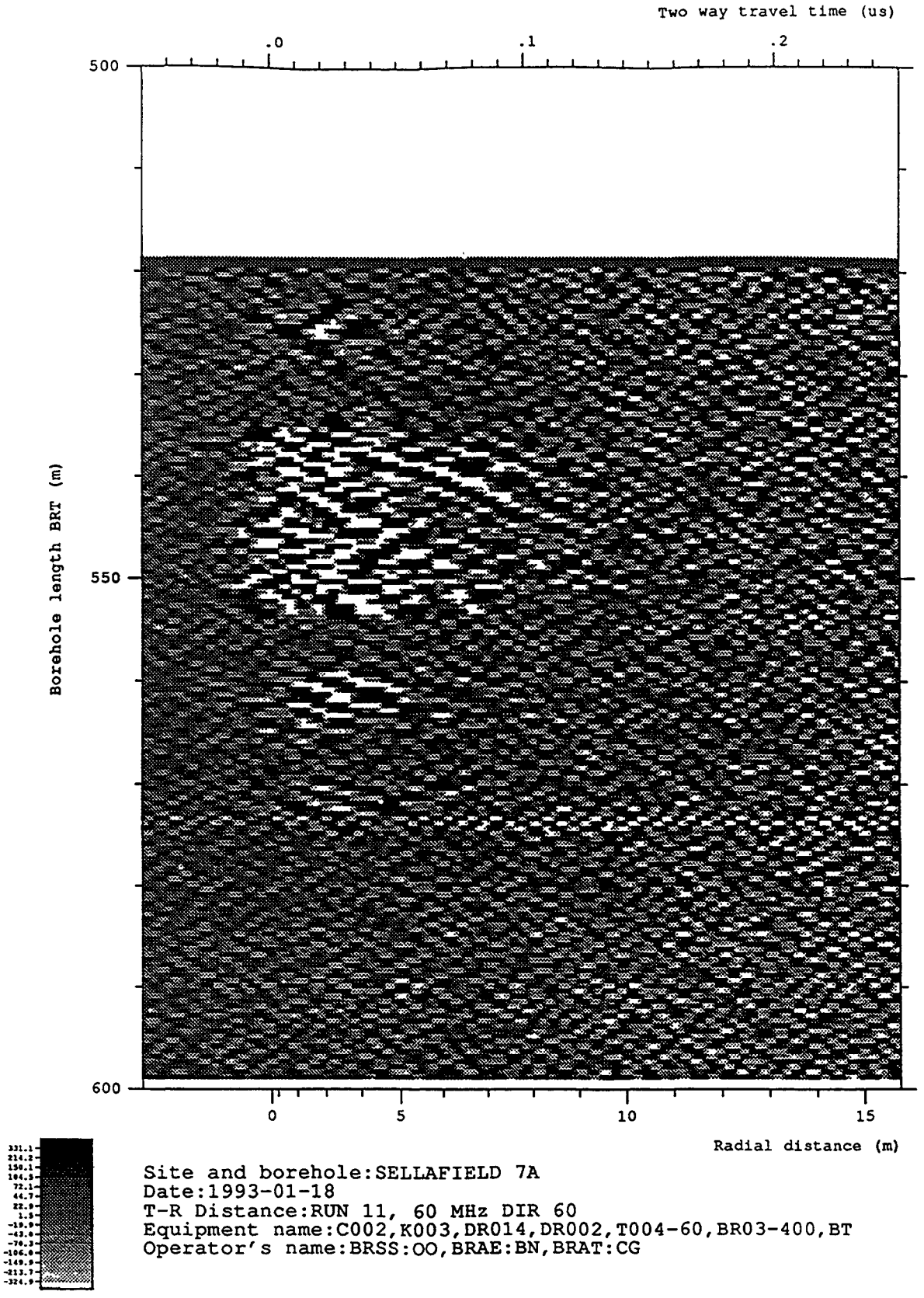

Figure 6-86 Radar map of the dipole component from the 60 MHz directional survey Run 11 after depth correction and the application of a moving average filter for the depth interval 518.80 to 598.80 mbRT at an azimuth of 140°

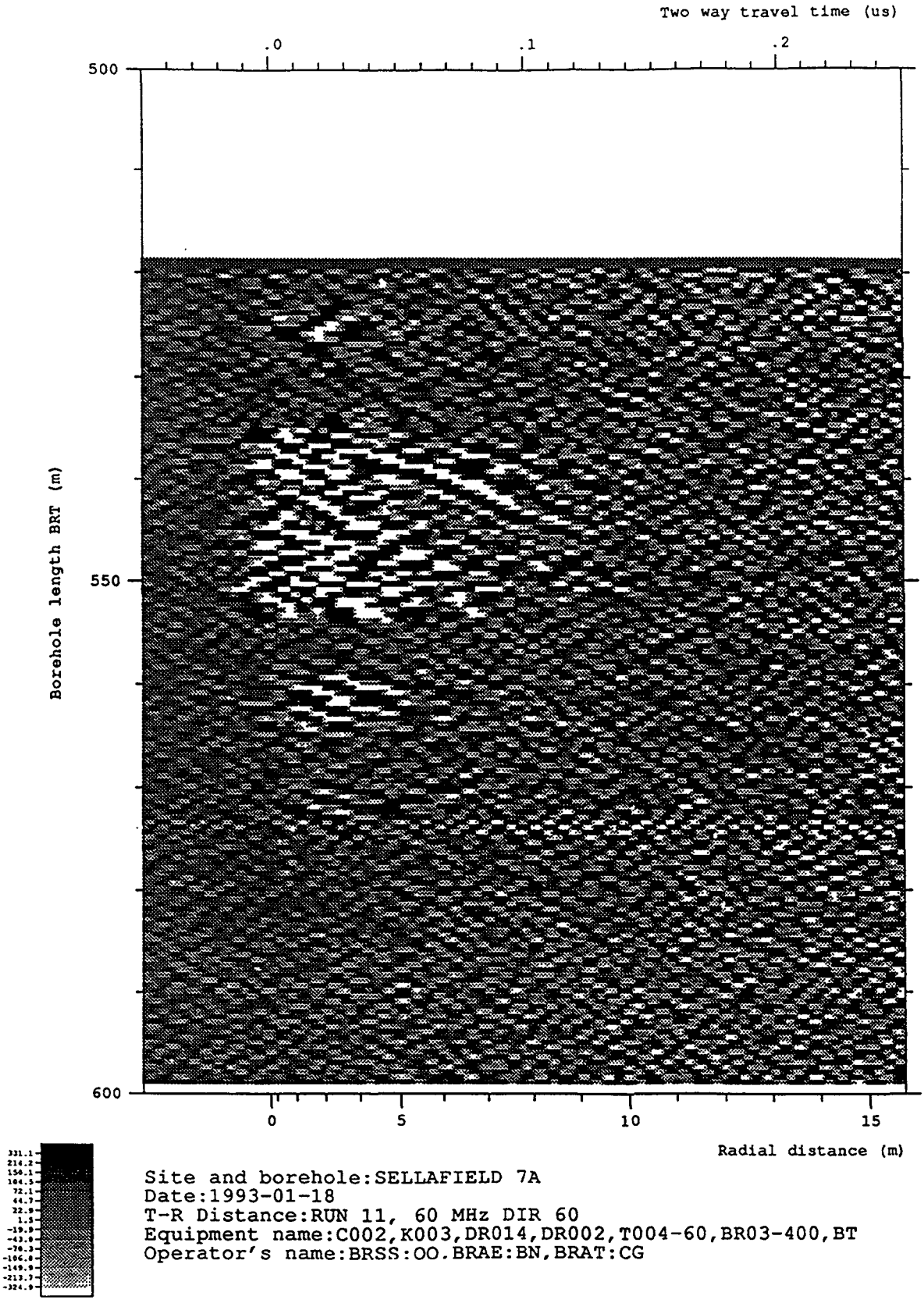

Figure 6-87 Radar map of the dipole component from the 60 MHz directional survey Run 11 after depth correction and the application of a moving average filter for the depth interval 518.80 to 598.80 mbRT at an azimuth of 150°

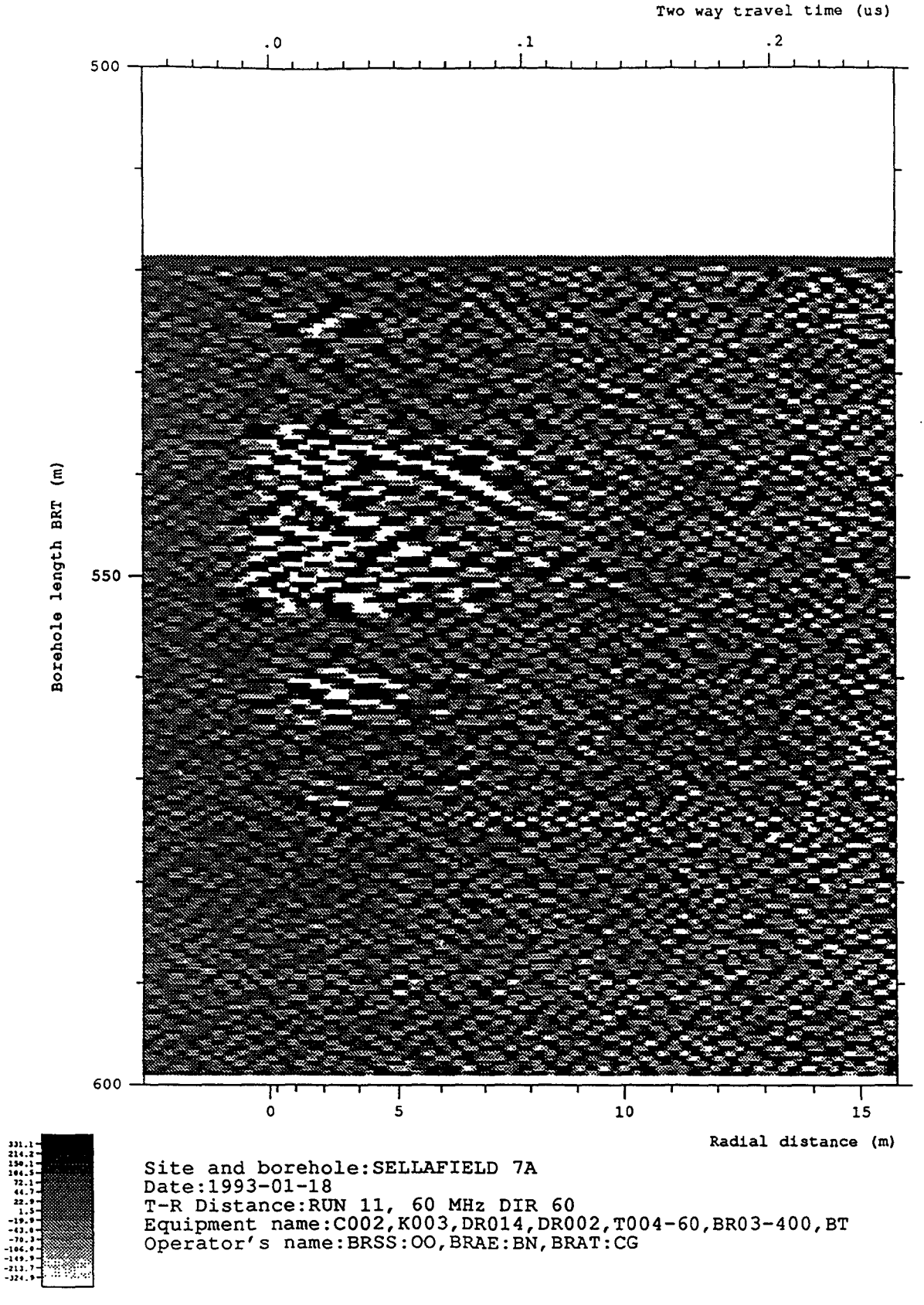

Figure 6-88 Radar map of the dipole component from the 60 MHz directional survey Run 11 after depth correction and the application of a moving average filter for the depth interval 518.80 to 598.80 mbRT at an azimuth of 160°

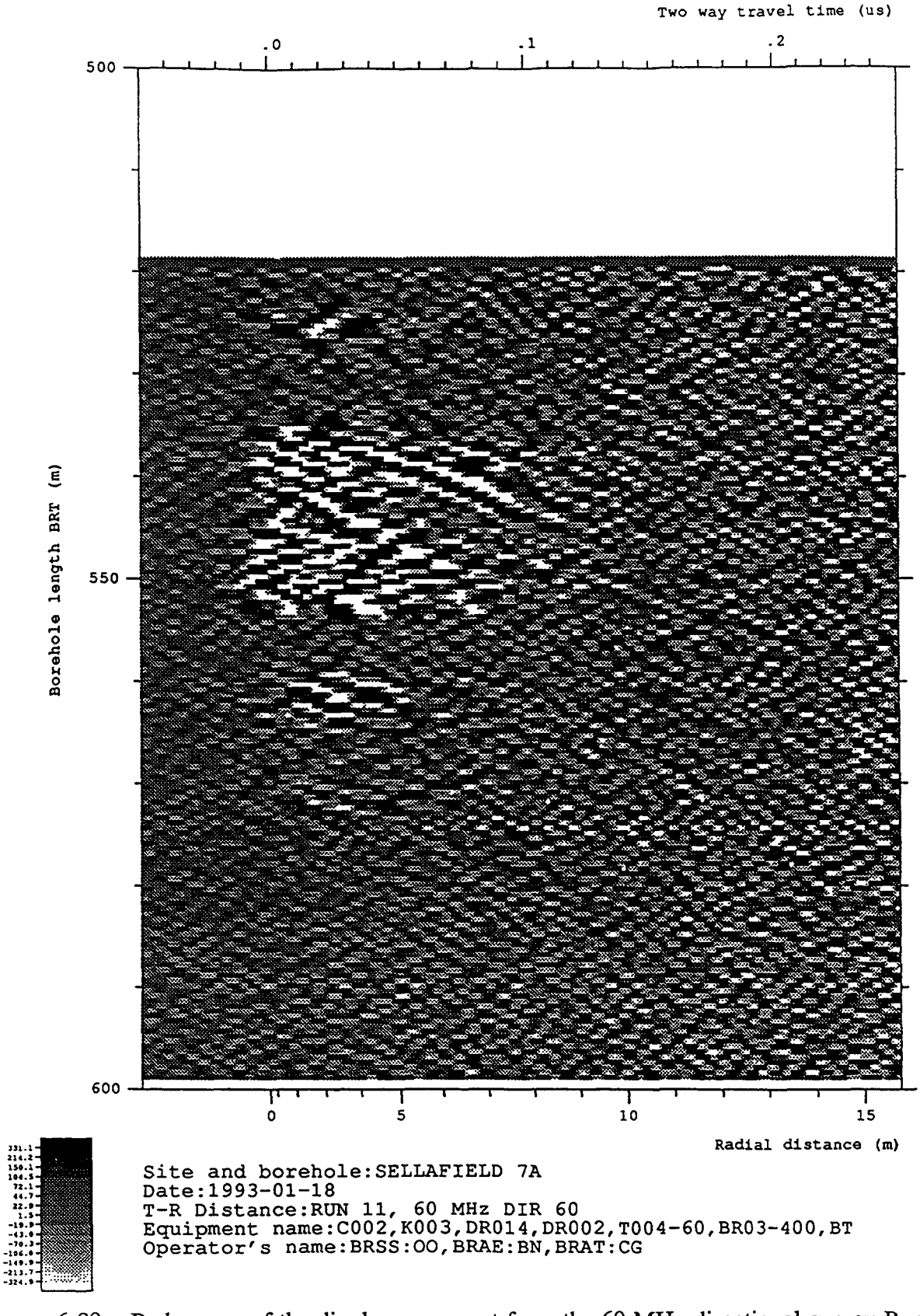

Figure 6-89 Radar map of the dipole component from the 60 MHz directional survey Run 11 after depth correction and the application of a moving average filter for the depth interval 518.80 to 598.80 mbRT at an azimuth of 170°

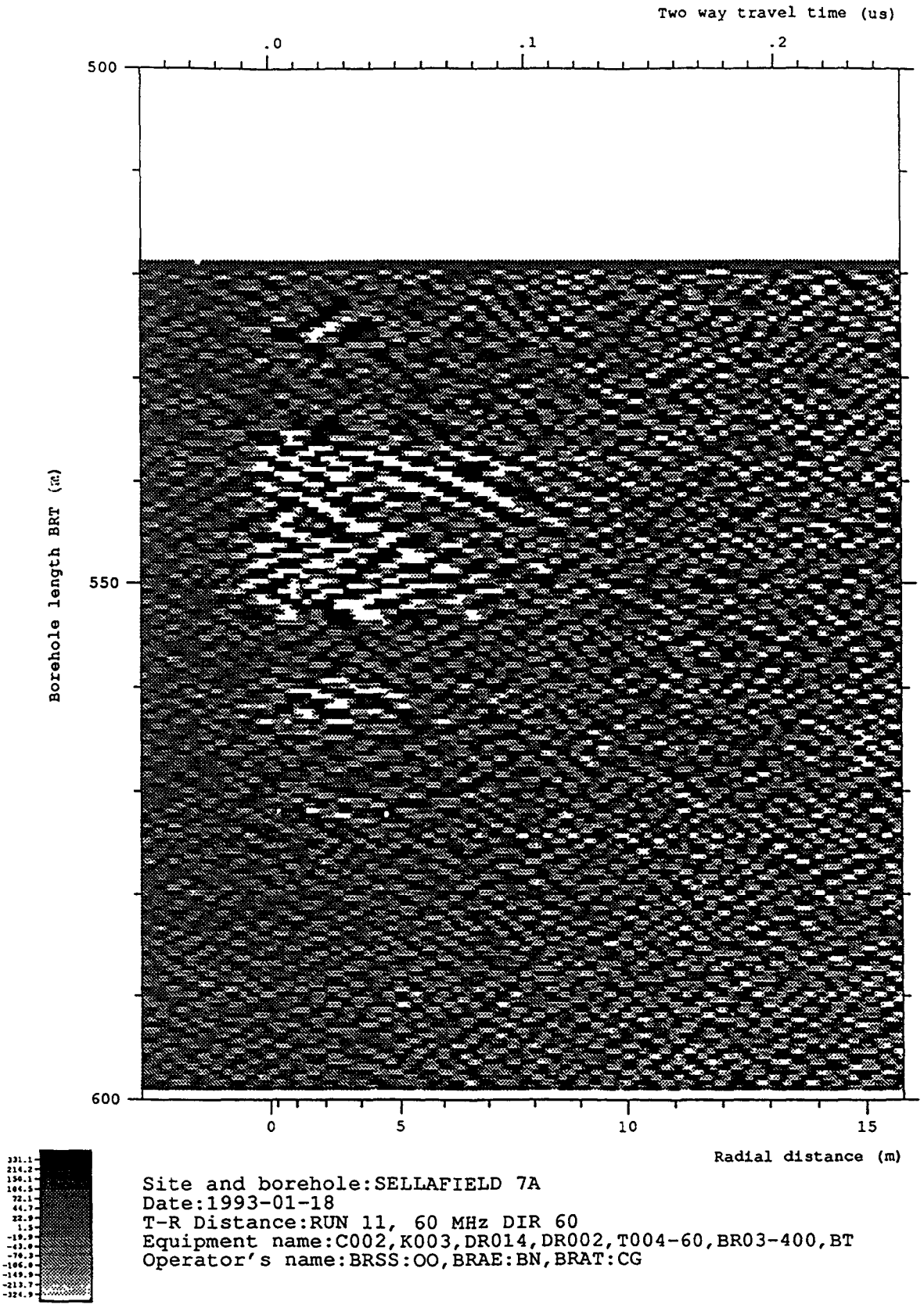

Figure 6-90 Radar map of the dipole component from the 60 MHz directional survey Run 11 after depth correction and the application of a moving average filter for the depth interval 518.80 to 598.80 mbRT at an azimuth of 180°

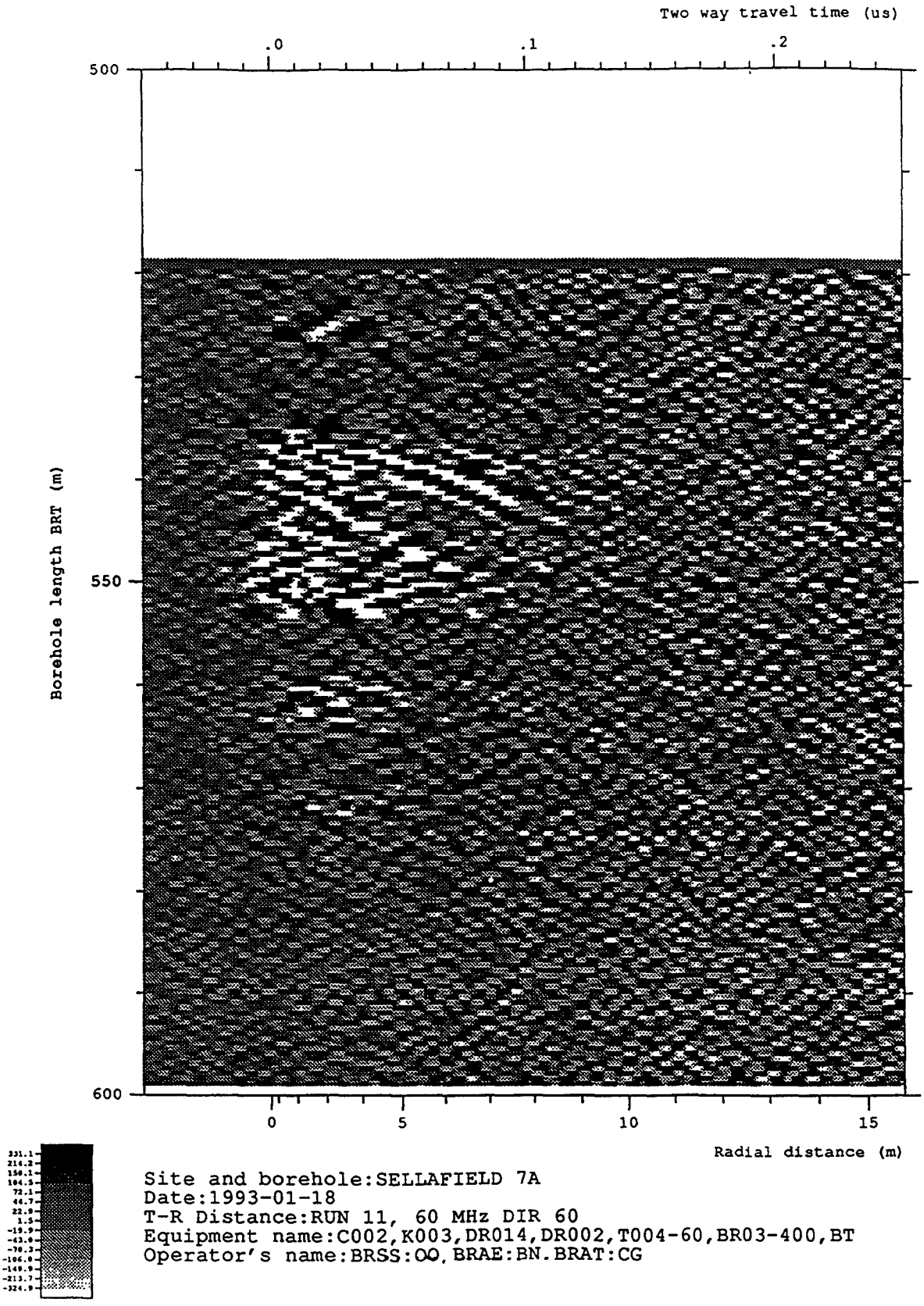

Figure 6-91 Radar map of the dipole component from the 60 MHz directional survey Run 11 after depth correction and the application of a moving average filter for the depth interval 518.80 to 598.80 mbRT at an azimuth of 190°

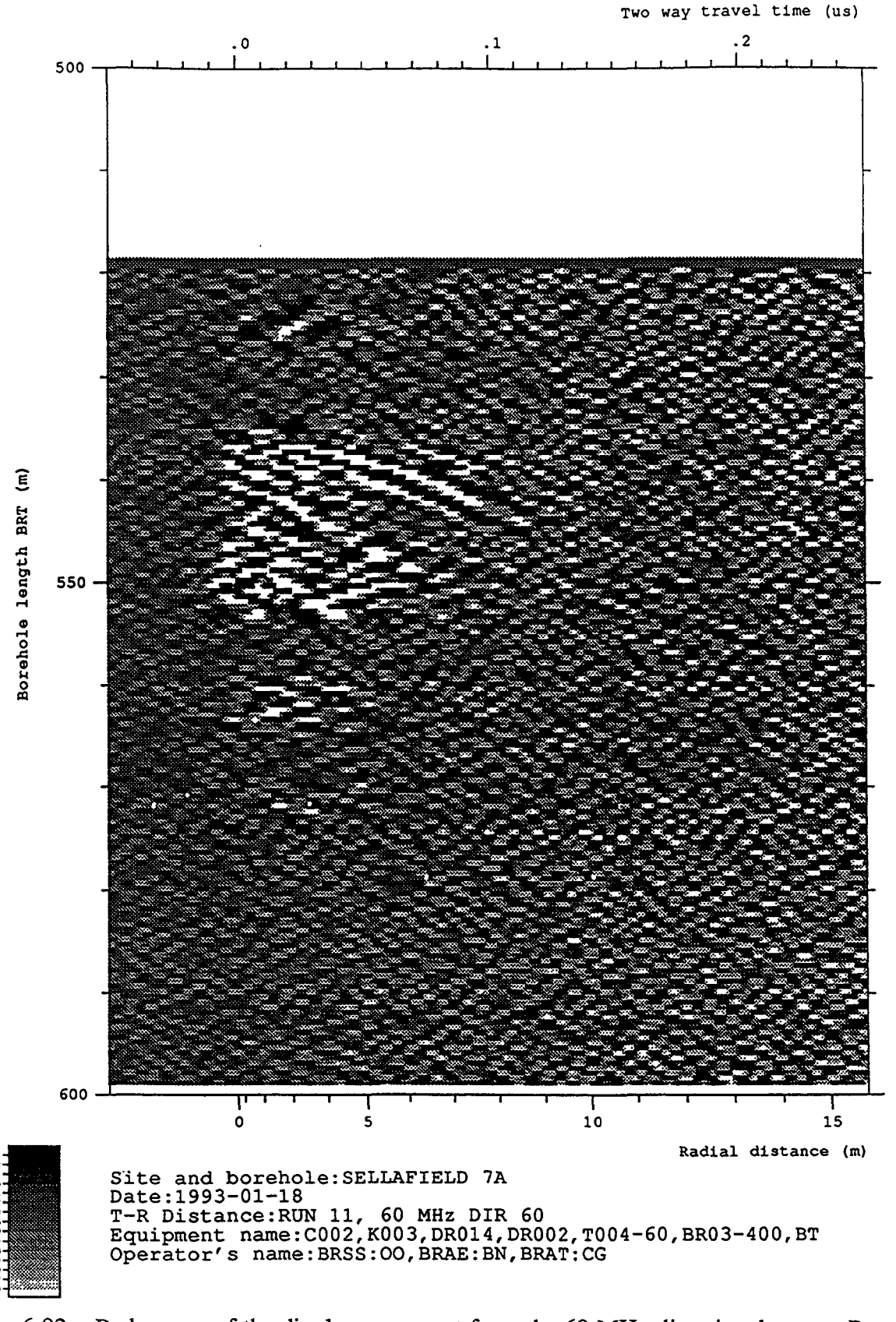

Figure 6-92 Radar map of the dipole component from the 60 MHz directional survey Run 11 after depth correction and the application of a moving average filter for the depth interval 518.80 to 598.80 mbRT at an azimuth of 200°

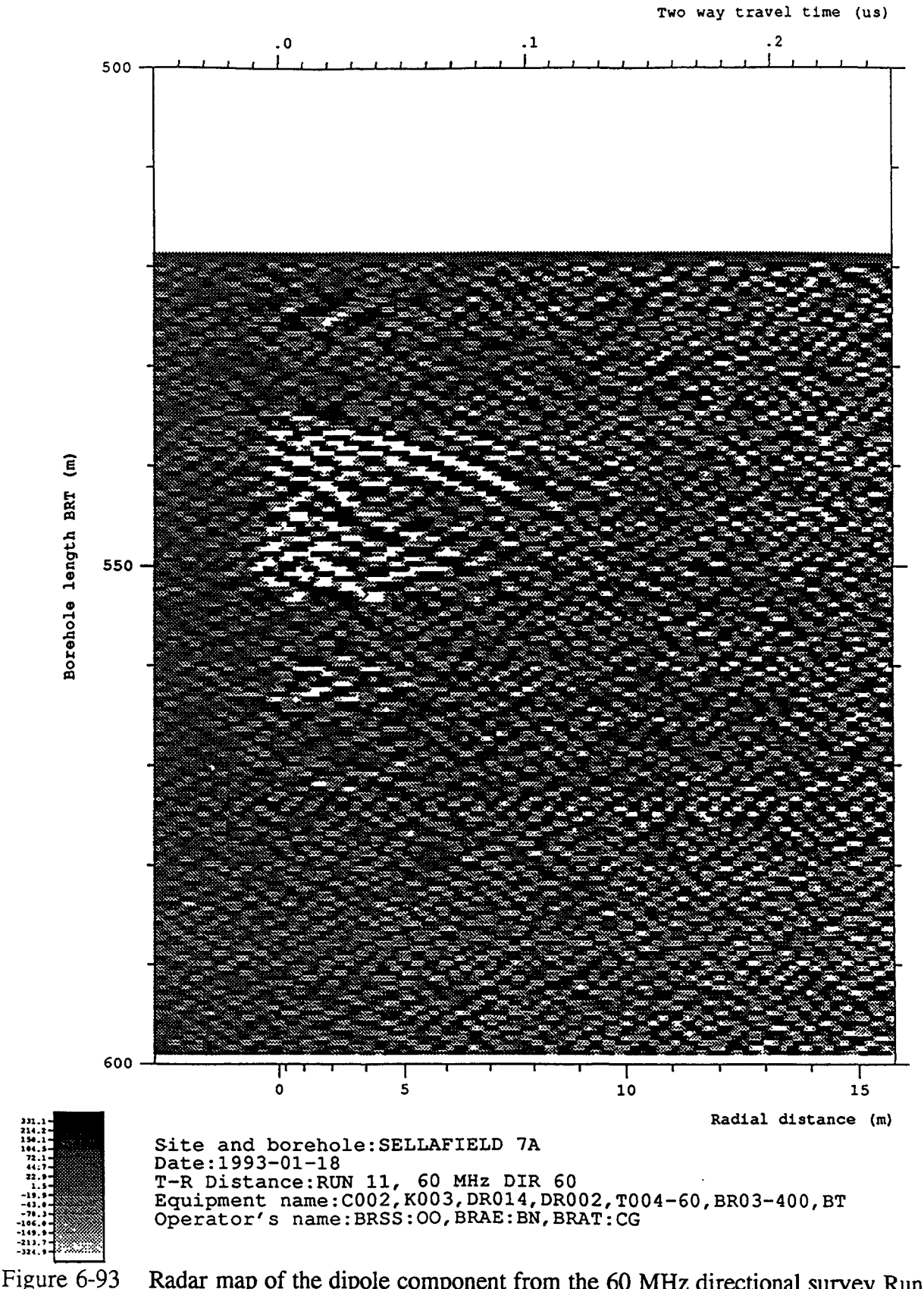

Figure 6-93 Radar map of the dipole component from the 60 MHz directional survey Run 11 after depth correction and the application of a moving average filter for the depth interval 518.80 to 598.80 mbRT at an azimuth of 210°

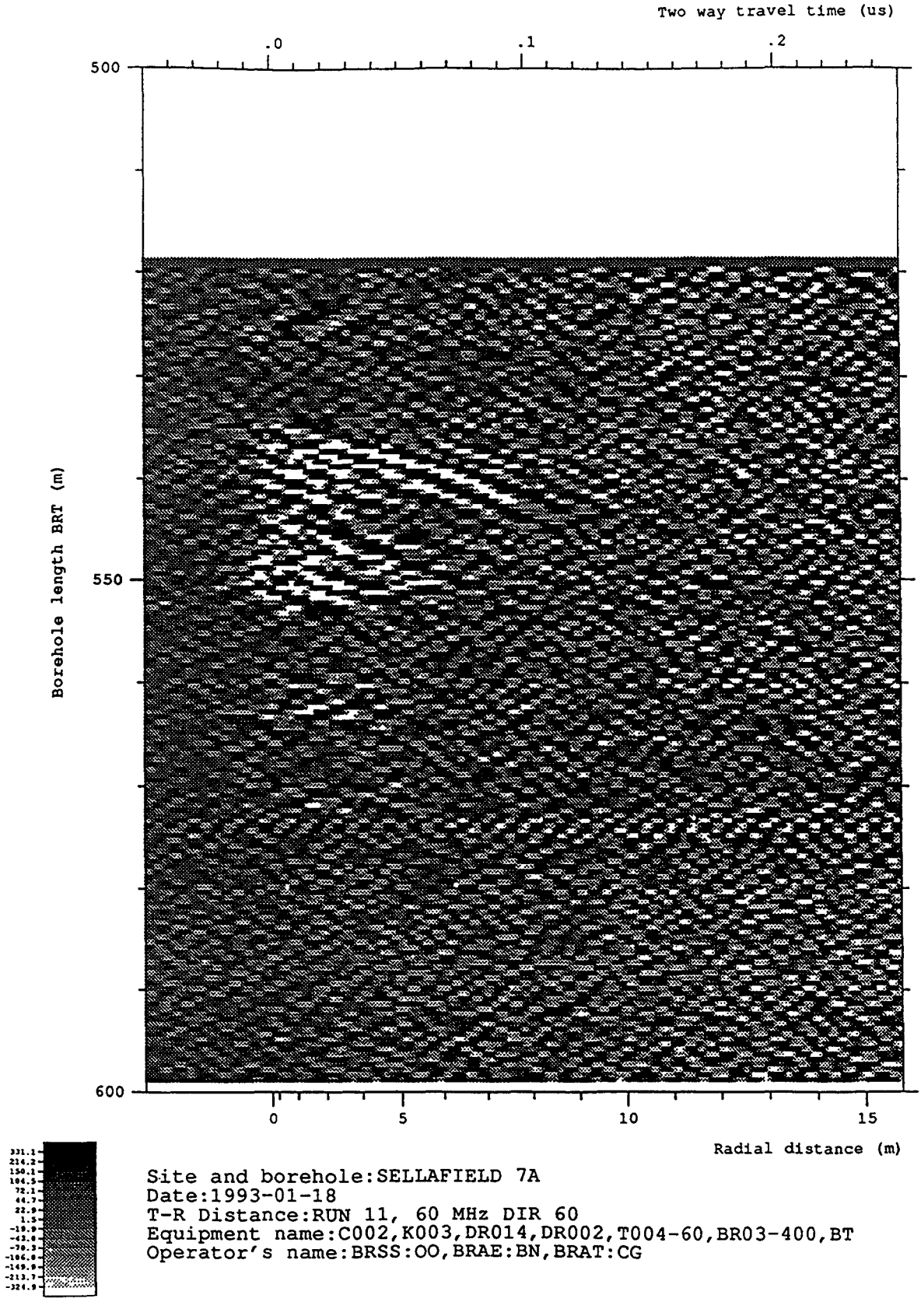

Figure 6-94 Radar map of the dipole component from the 60 MHz directional survey Run 11 after depth correction and the application of a moving average filter for the depth interval 518.80 to 598.80 mbRT at an azimuth of 220°

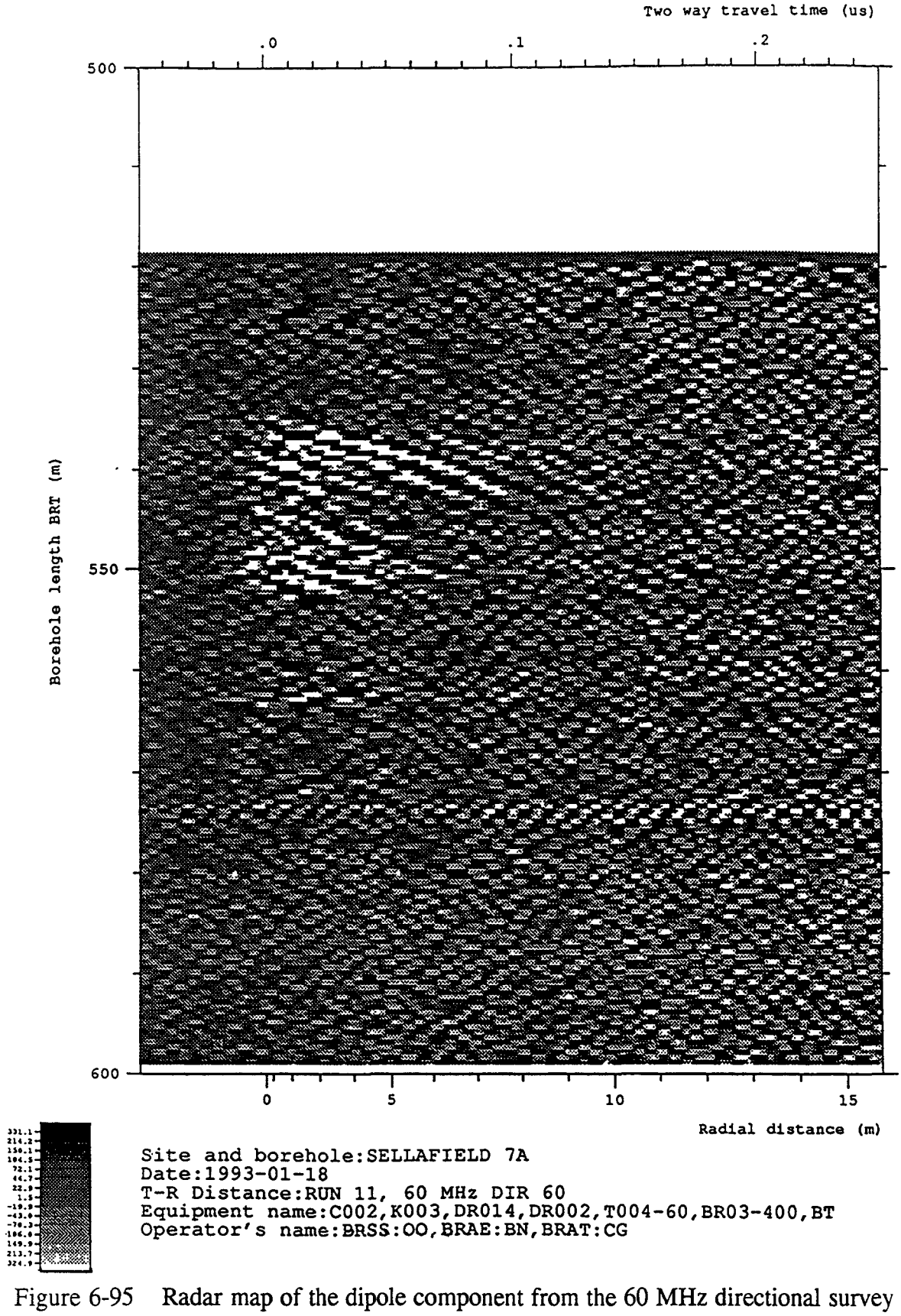

Figure 6-95 Radar map of the dipole component from the 60 MHz directional survey Run 11 after depth correction and the application of a moving average filter for the depth interval 518.80 to 598.80 mbRT at an azimuth of 230°

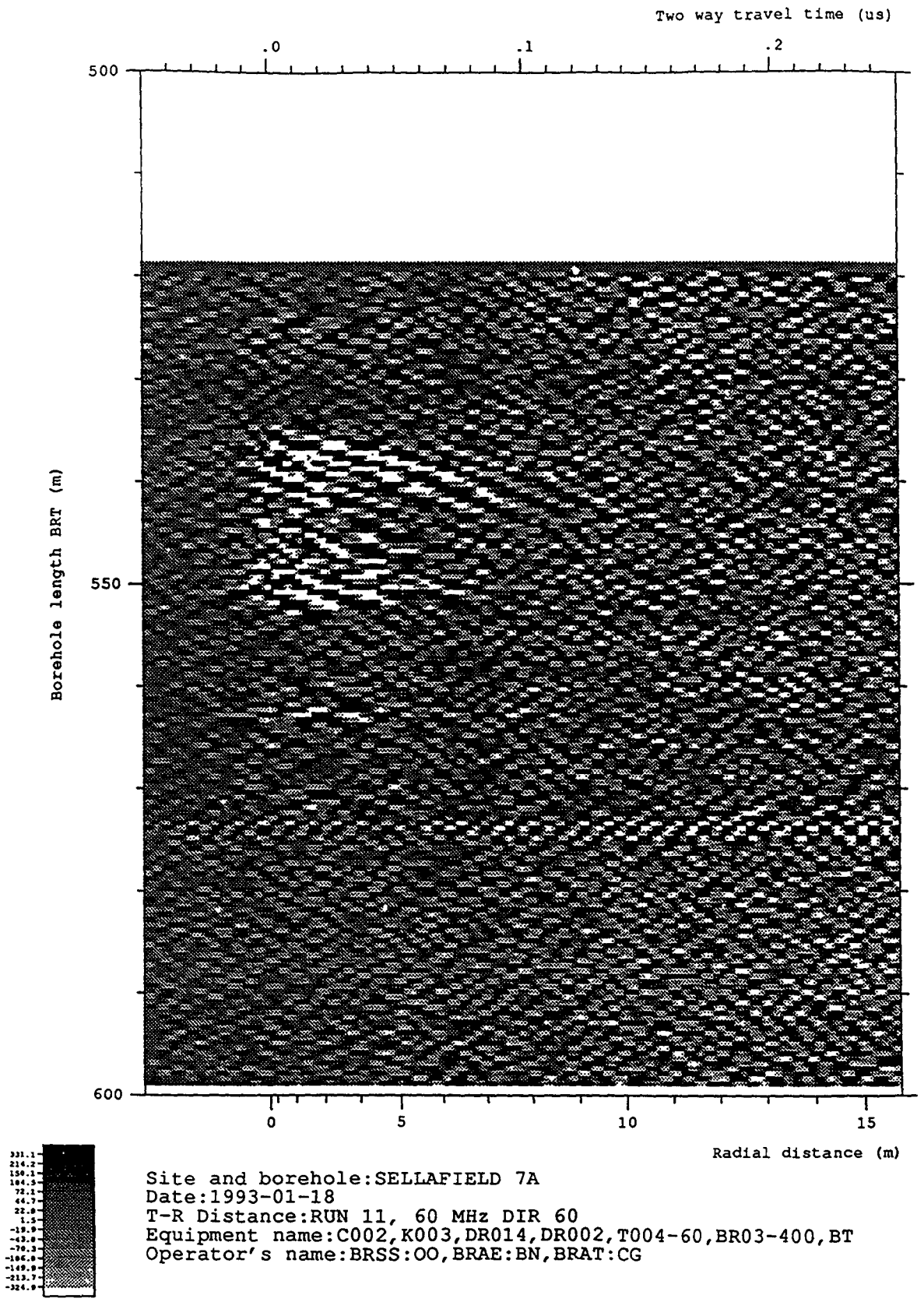

Figure 6-96 Radar map of the dipole component from the 60 MHz directional survey Run 11 after depth correction and the application of a moving average filter for the depth interval 518.80 to 598.80 mbRT at an azimuth of 240°

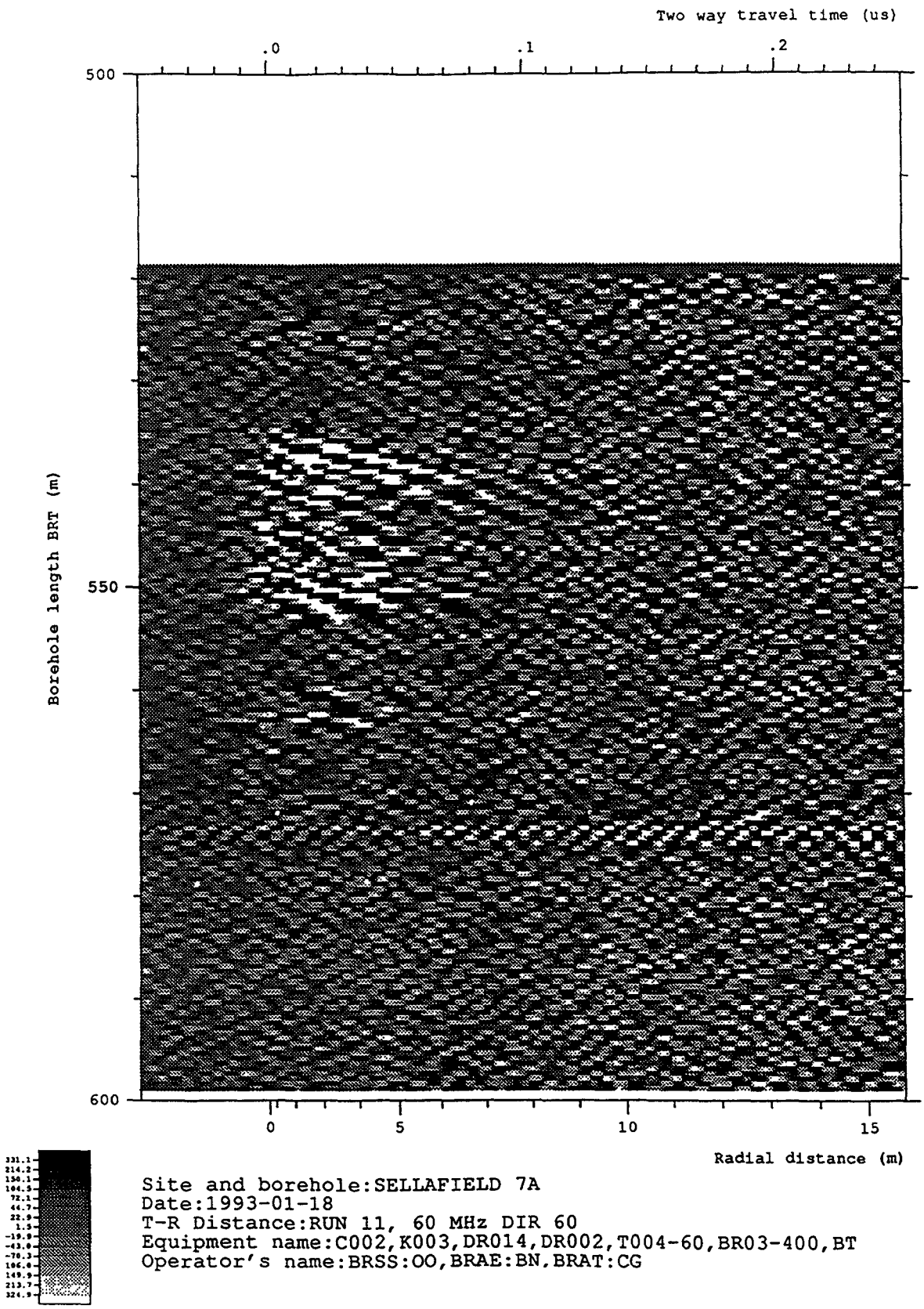

Figure 6-97 Radar map of the dipole component from the 60 MHz directional survey Run 11 after depth correction and the application of a moving average filter for the depth interval 518.80 to 598.80 mbRT at an azimuth of 250°

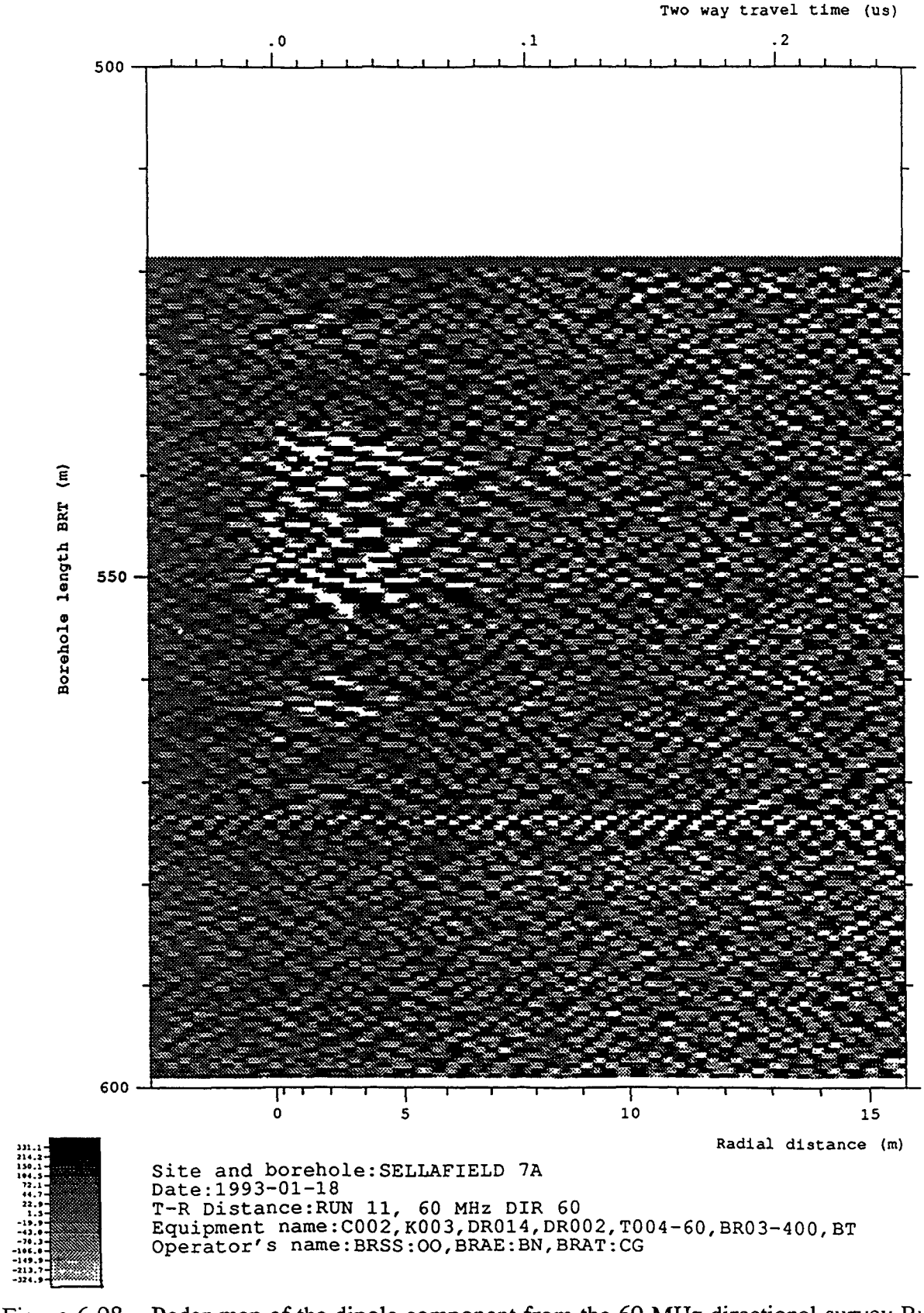

Figure 6-98 Radar map of the dipole component from the 60 MHz directional survey Run 11 after depth correction and the application of a moving average filter for the depth interval 518.80 to 598.80 mbRT at an azimuth of 260°

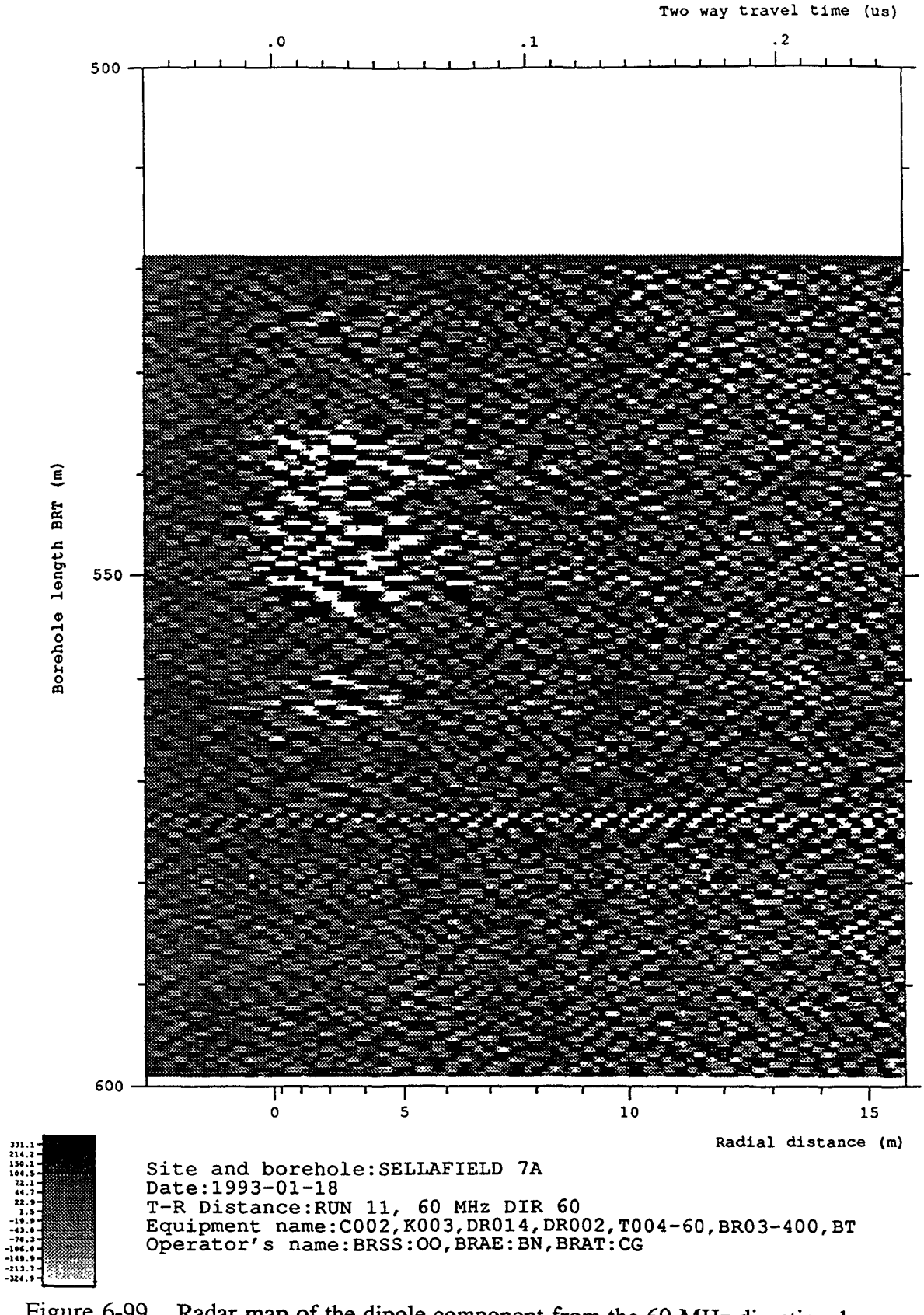

Figure 6-99 Radar map of the dipole component from the 60 MHz directional survey Run 11 after depth correction and the application of a moving average filter for the depth interval 518.80 to 598.80 mbRT at an azimuth of 270°

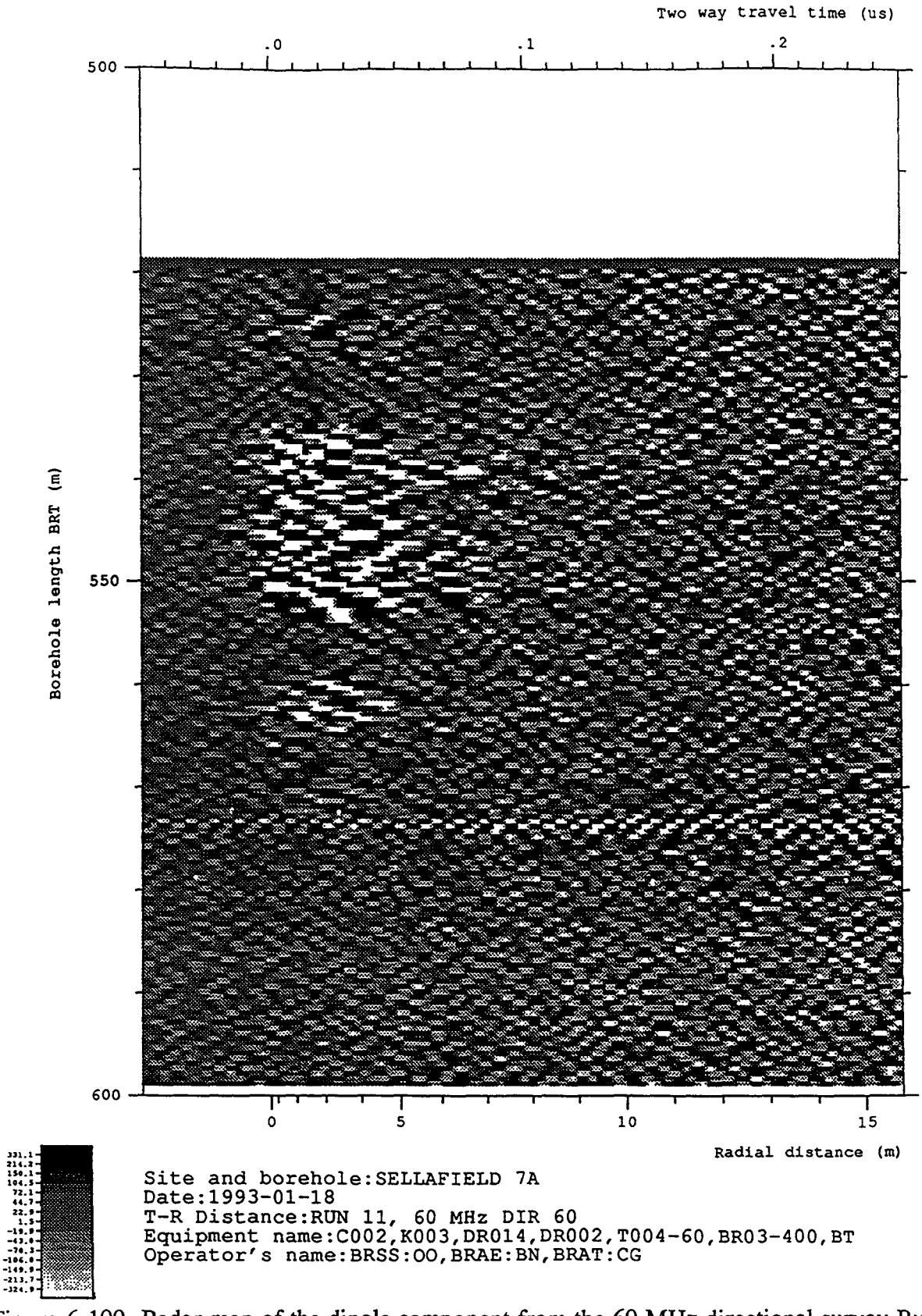

Figure 6-100 Radar map of the dipole component from the 60 MHz directional survey Run 11 after depth correction and the application of a moving average filter for the depth interval 518.80 to 598.80 mbRT at an azimuth of 280°

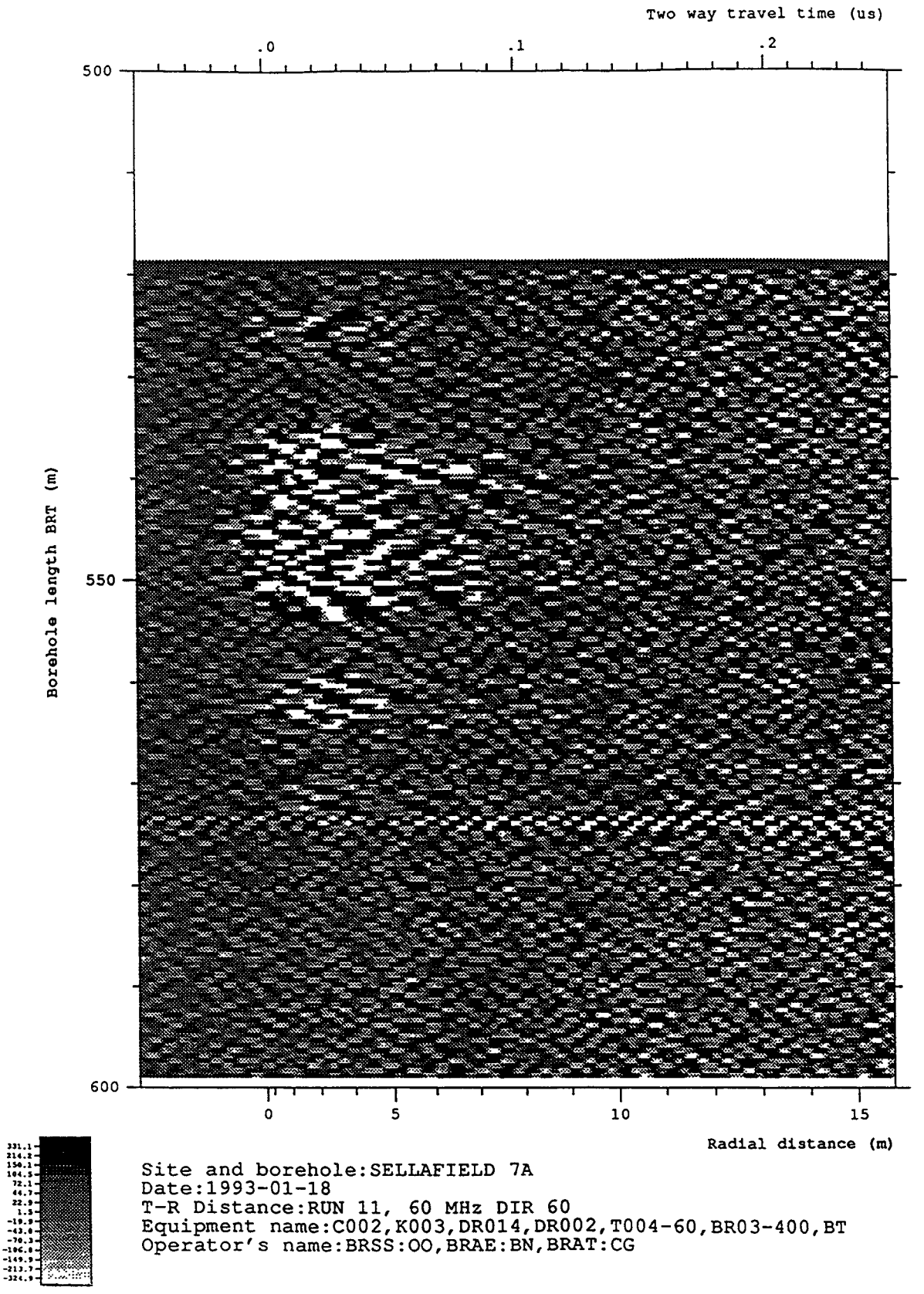

Figure 6-101 Radar map of the dipole component from the 60 MHz directional survey Run 11 after depth correction and the application of a moving average filter for the depth interval 518.80 to 598.80 mbRT at an azimuth of 290°

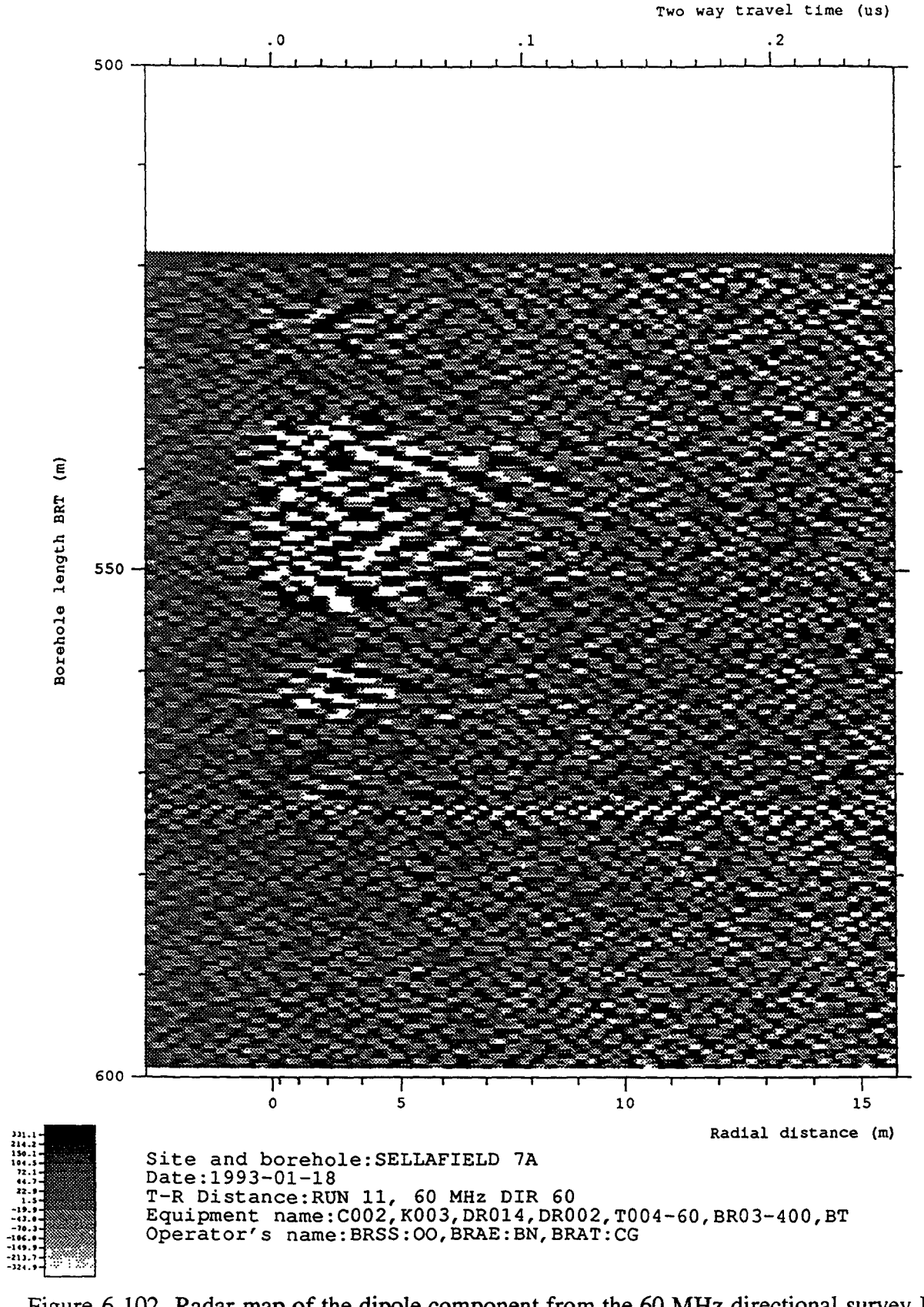

Figure 6-102 Radar map of the dipole component from the 60 MHz directional survey Run 11 after depth correction and the application of a moving average filter for the depth interval 518.80 to 598.80 mbRT at an azimuth of 300°

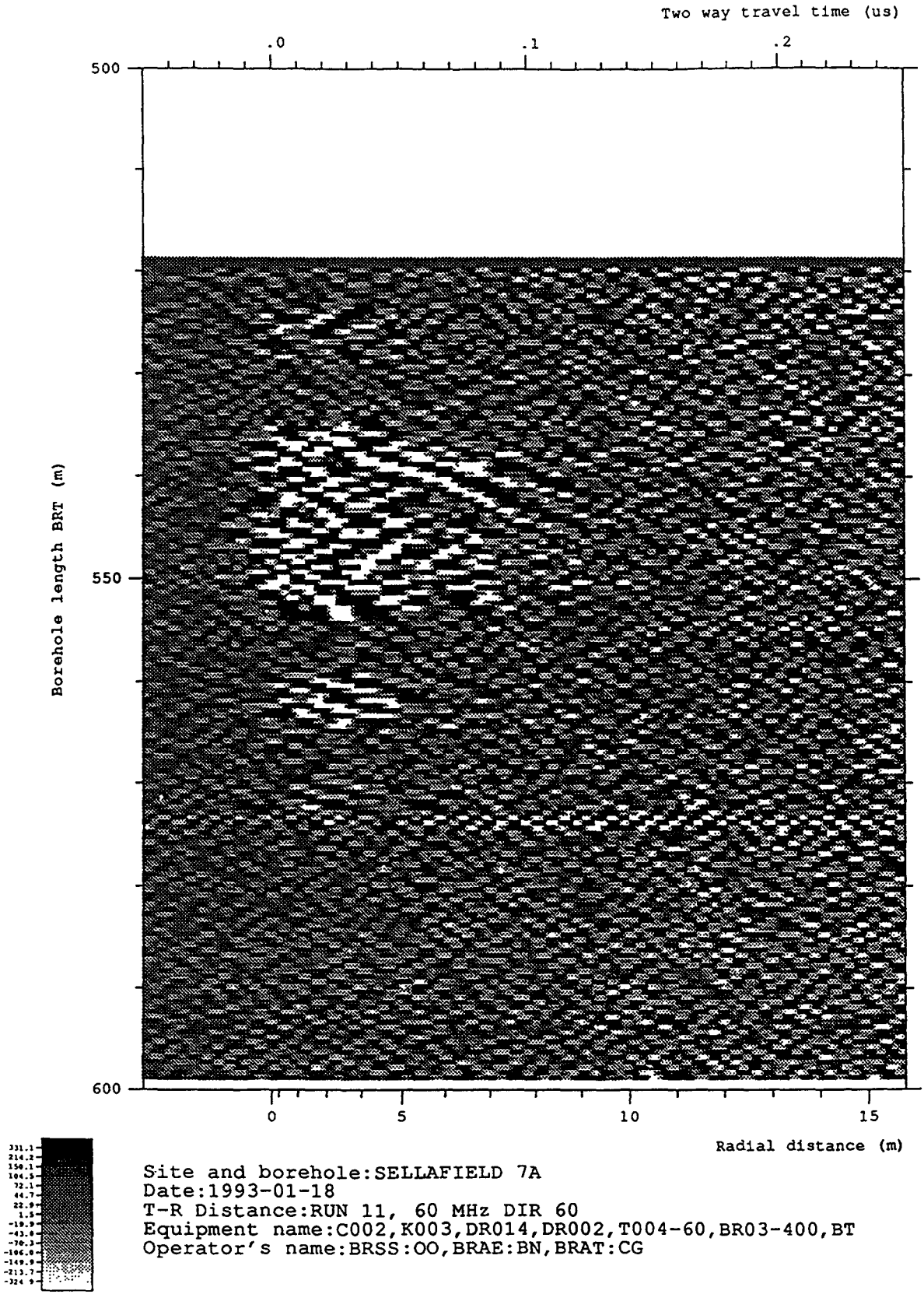

Figure 6-103 Radar map of the dipole component from the 60 MHz directional survey Run 11 after depth correction and the application of a moving average filter for the depth interval 518.80 to 598.80 mbRT at an azimuth of 310°

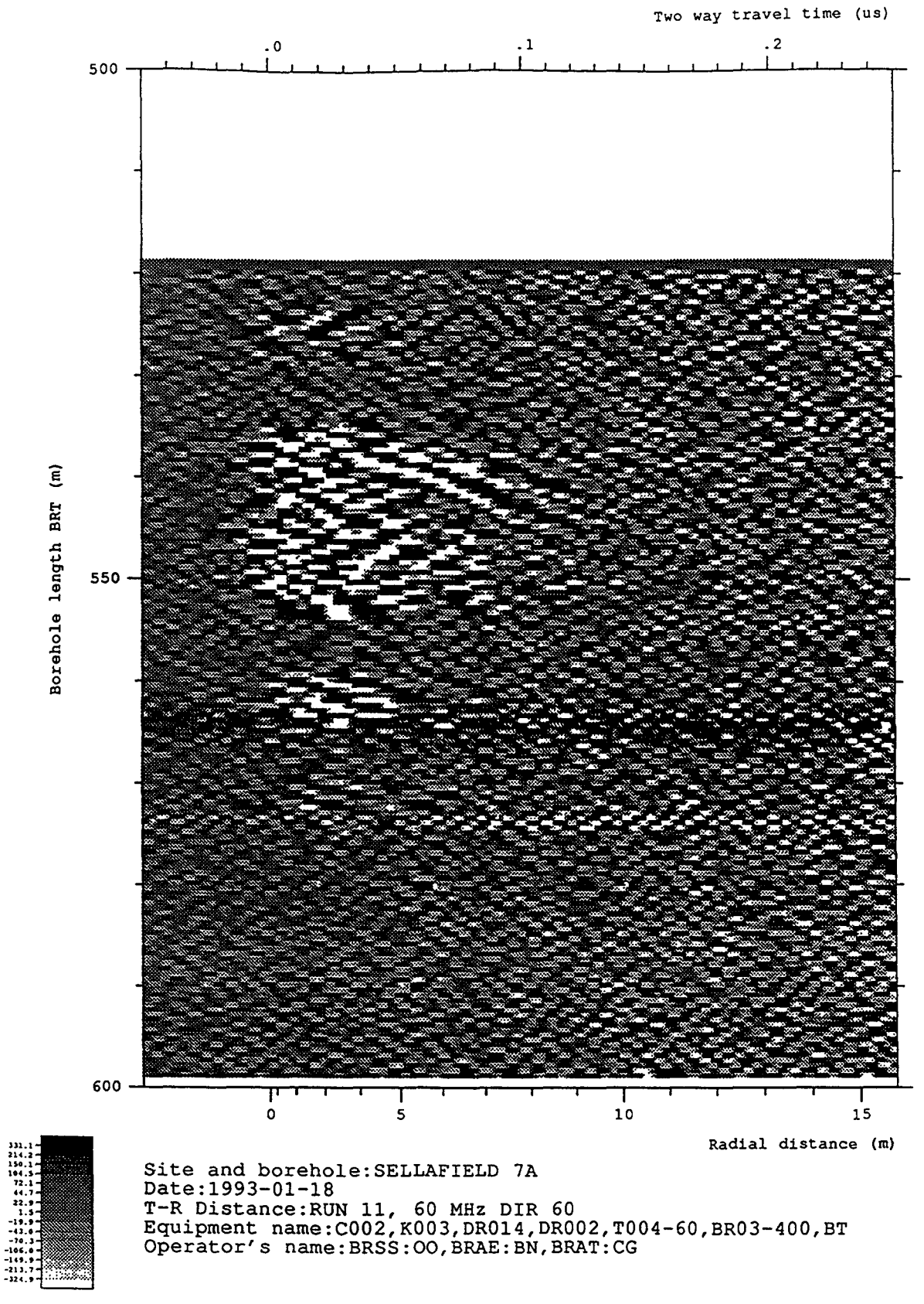

Figure 6-104 Radar map of the dipole component from the 60 MHz directional survey Run 11 after depth correction and the application of a moving average filter for the depth interval 518.80 to 598.80 mbRT at an azimuth of 320°

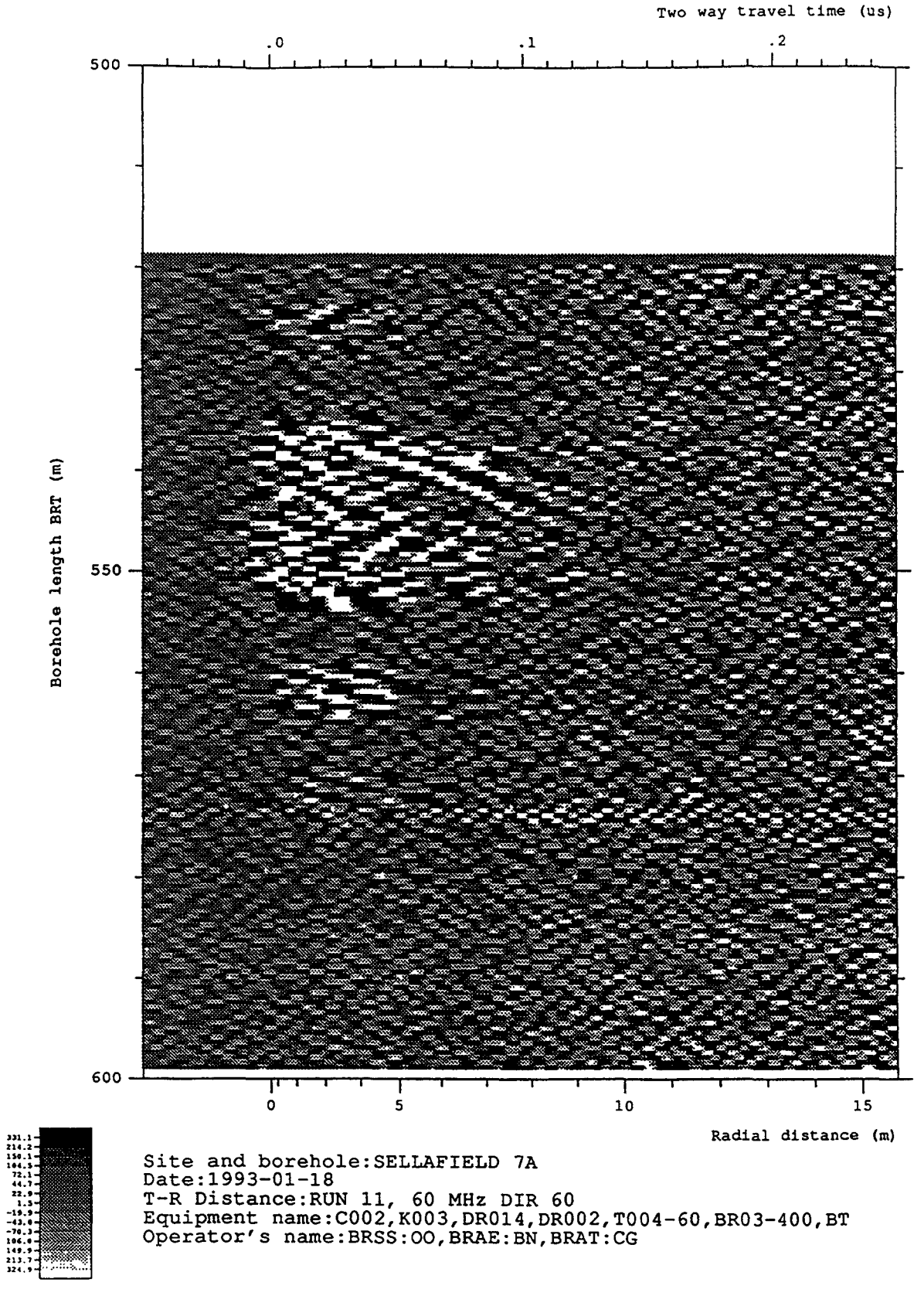

Figure 6-105 Radar map of the dipole component from the 60 MHz directional survey Run 11 after depth correction and the application of a moving average filter for the depth interval 518.80 to 598.80 mbRT at an azimuth of 330°

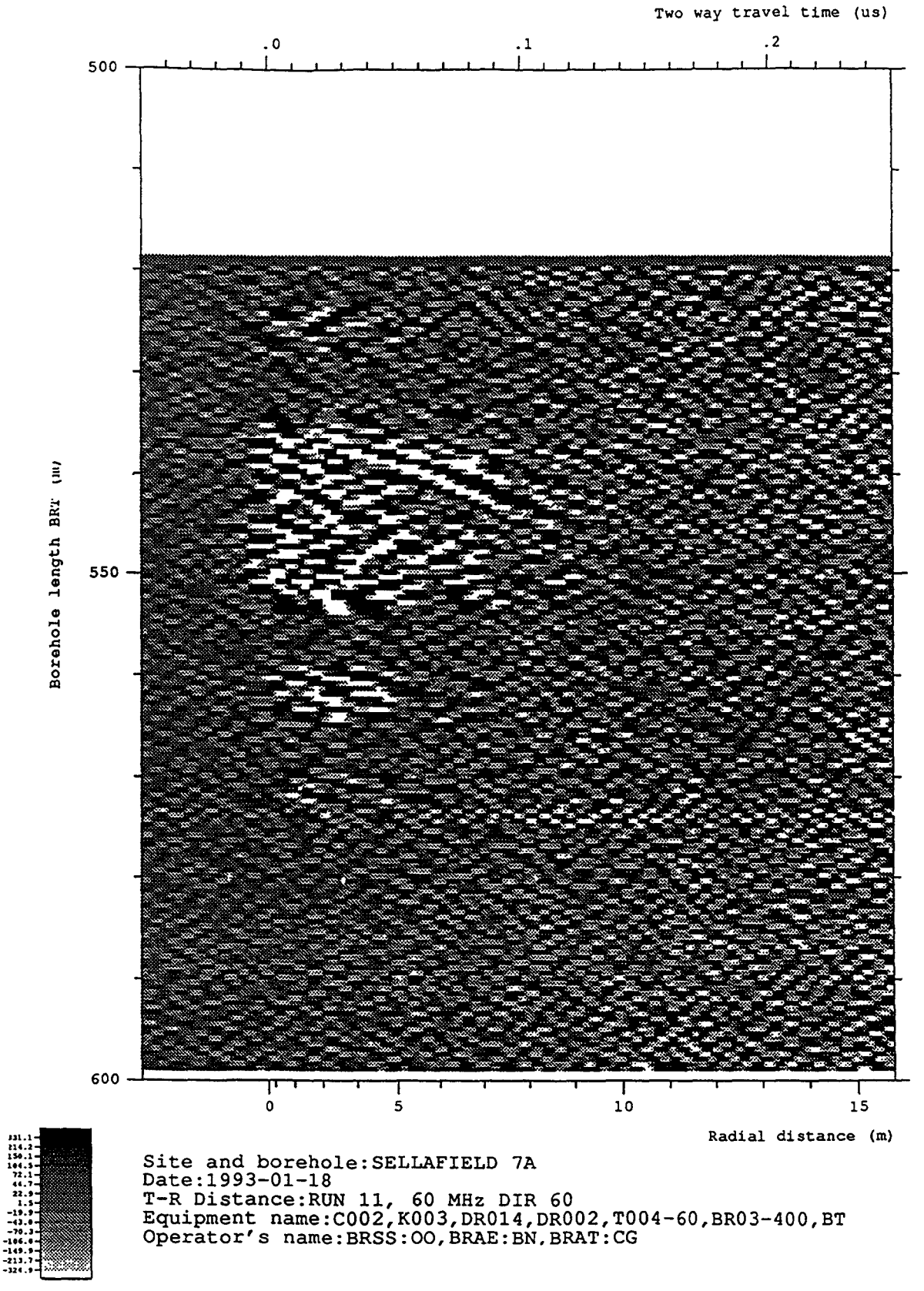

Figure 6-106 Radar map of the dipole component from the 60 MHz directional survey Run 11 after depth correction and the application of a moving average filter for the depth interval 518.80 to 598.80 mbRT at an azimuth of 340°

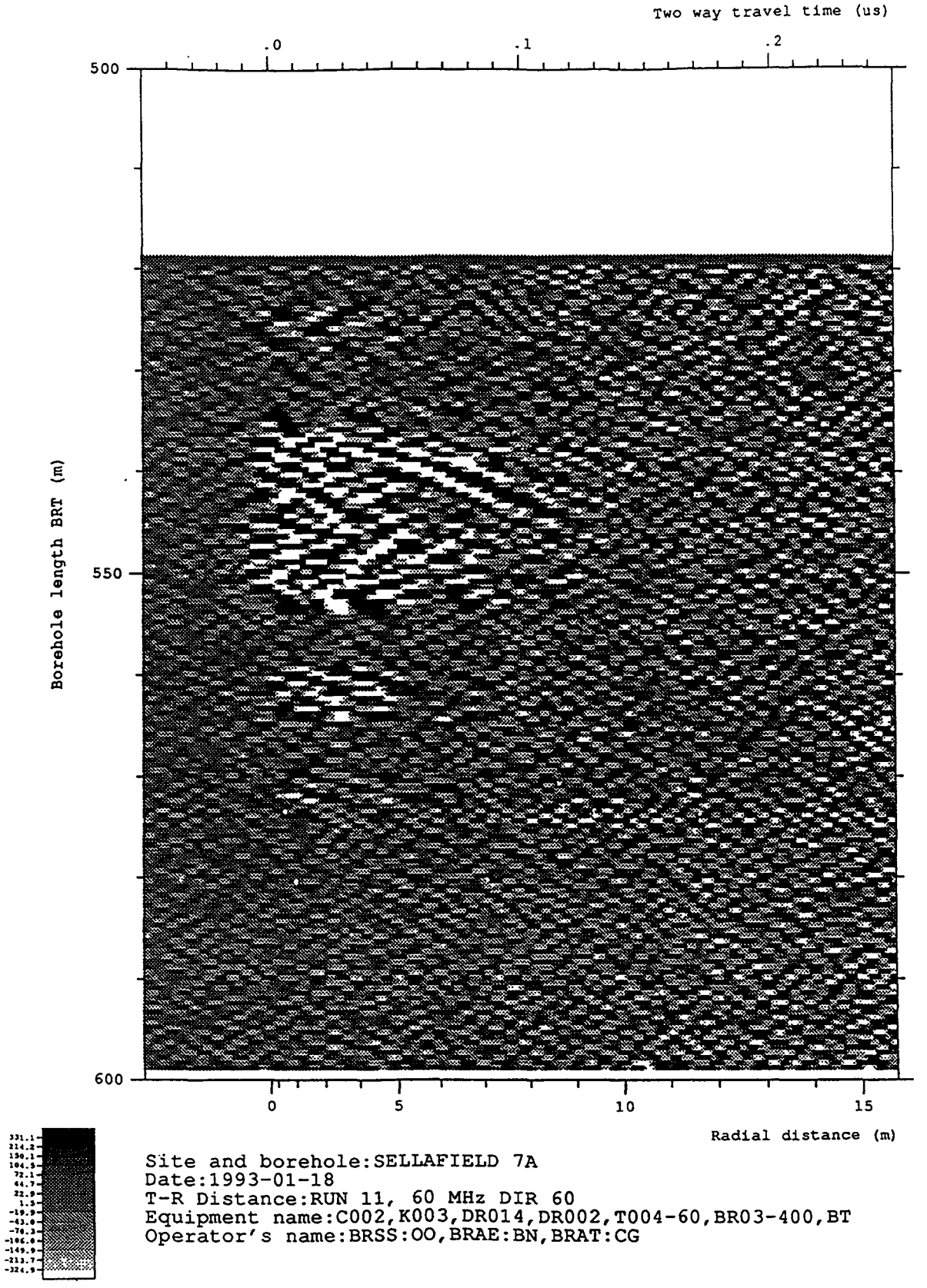

Figure 6-107 Radar map of the dipole component from the 60 MHz directional survey Run 11 after depth correction and the application of a moving average filter for the depth interval 518.80 to 598.80 mbRT at an azimuth of 350°

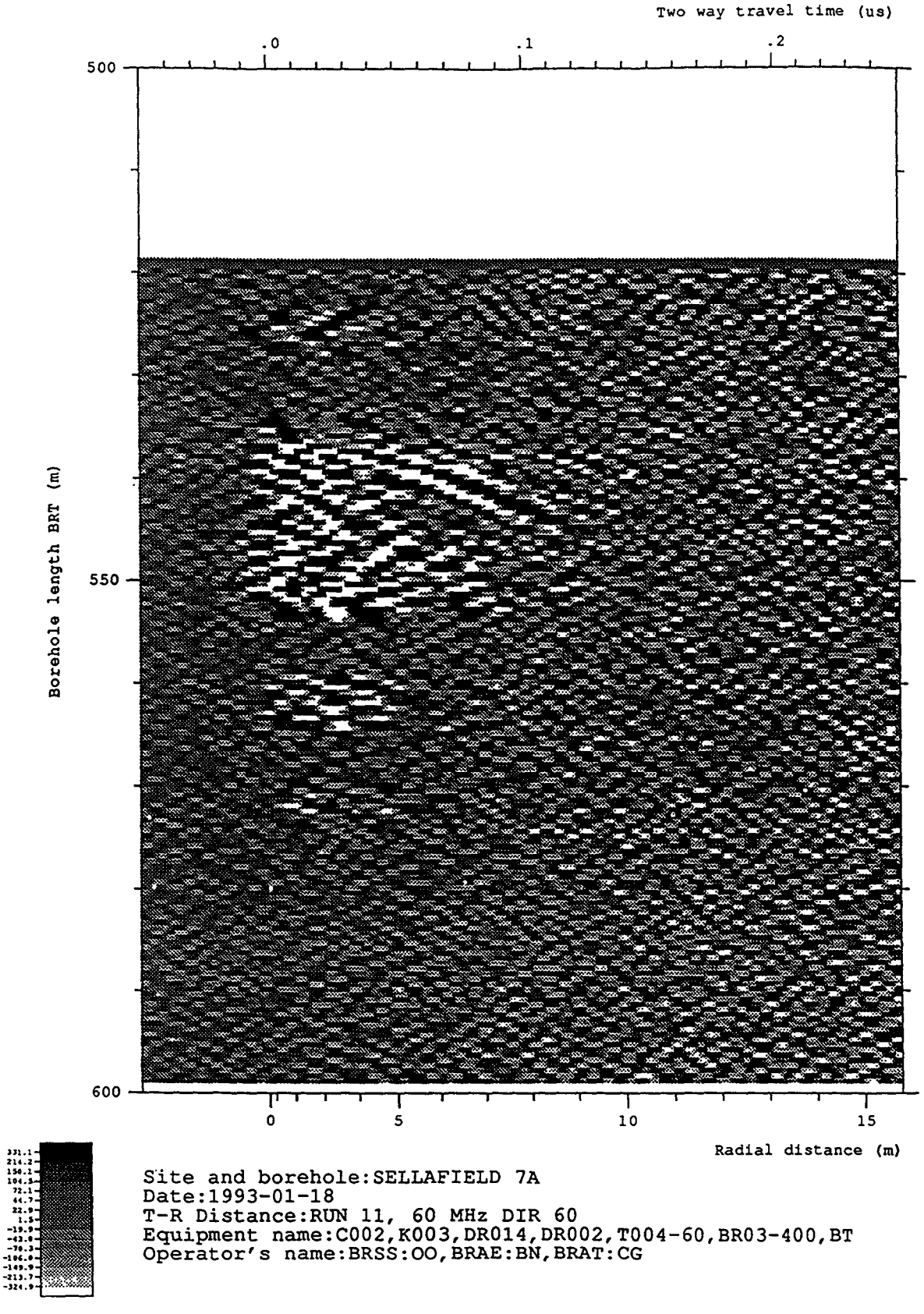

Figure 6-108 Radar map of the dipole component from the 60 MHz directional survey Run 11 after depth correction and the application of a moving average filter for the depth interval 518.80 to 598.80 mbRT at an azimuth of 360°

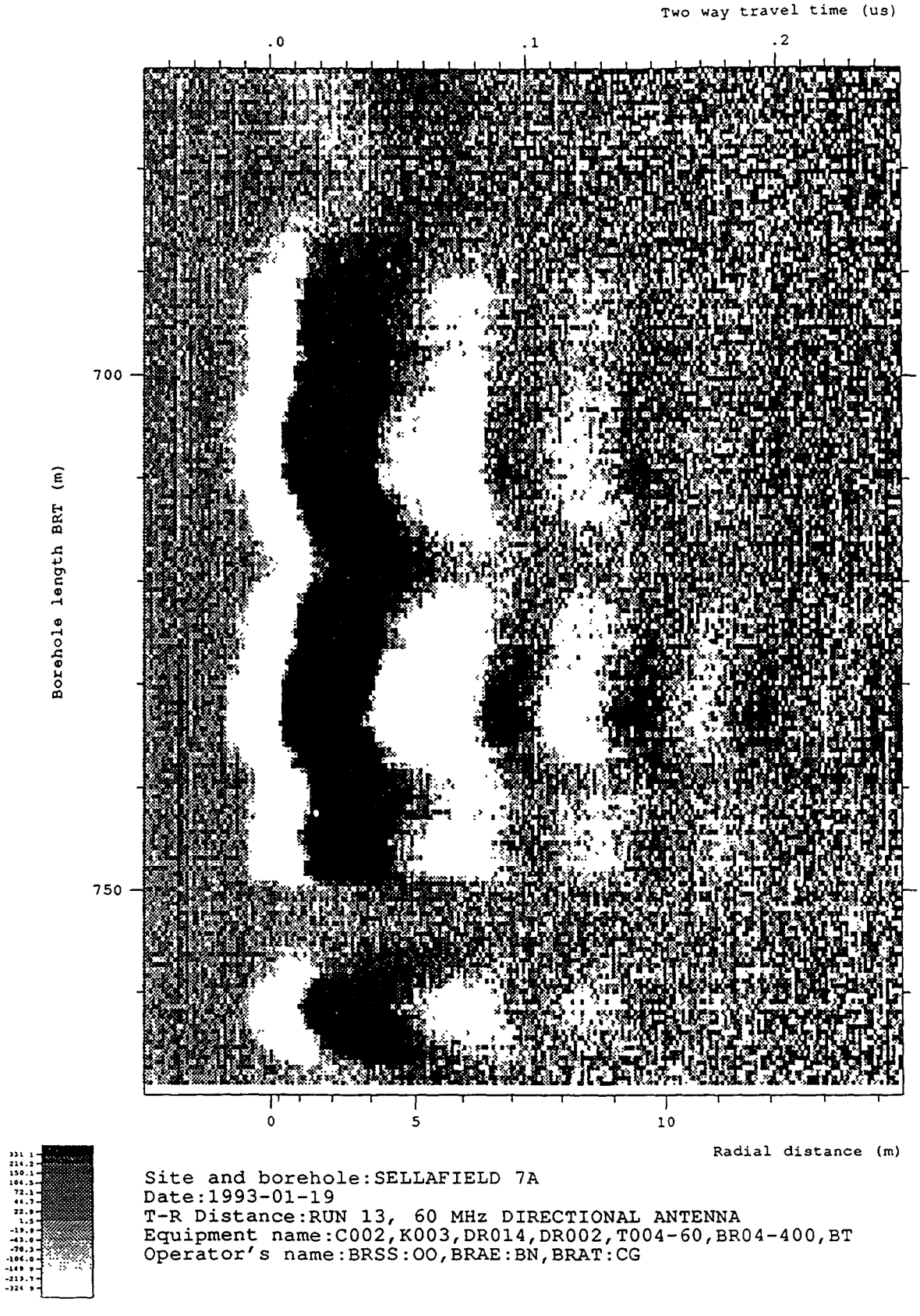

Figure 6-109 Radar map of the dipole component from the 60 MHz directional survey Run 13 (648.80 to 768.80 mbRT)

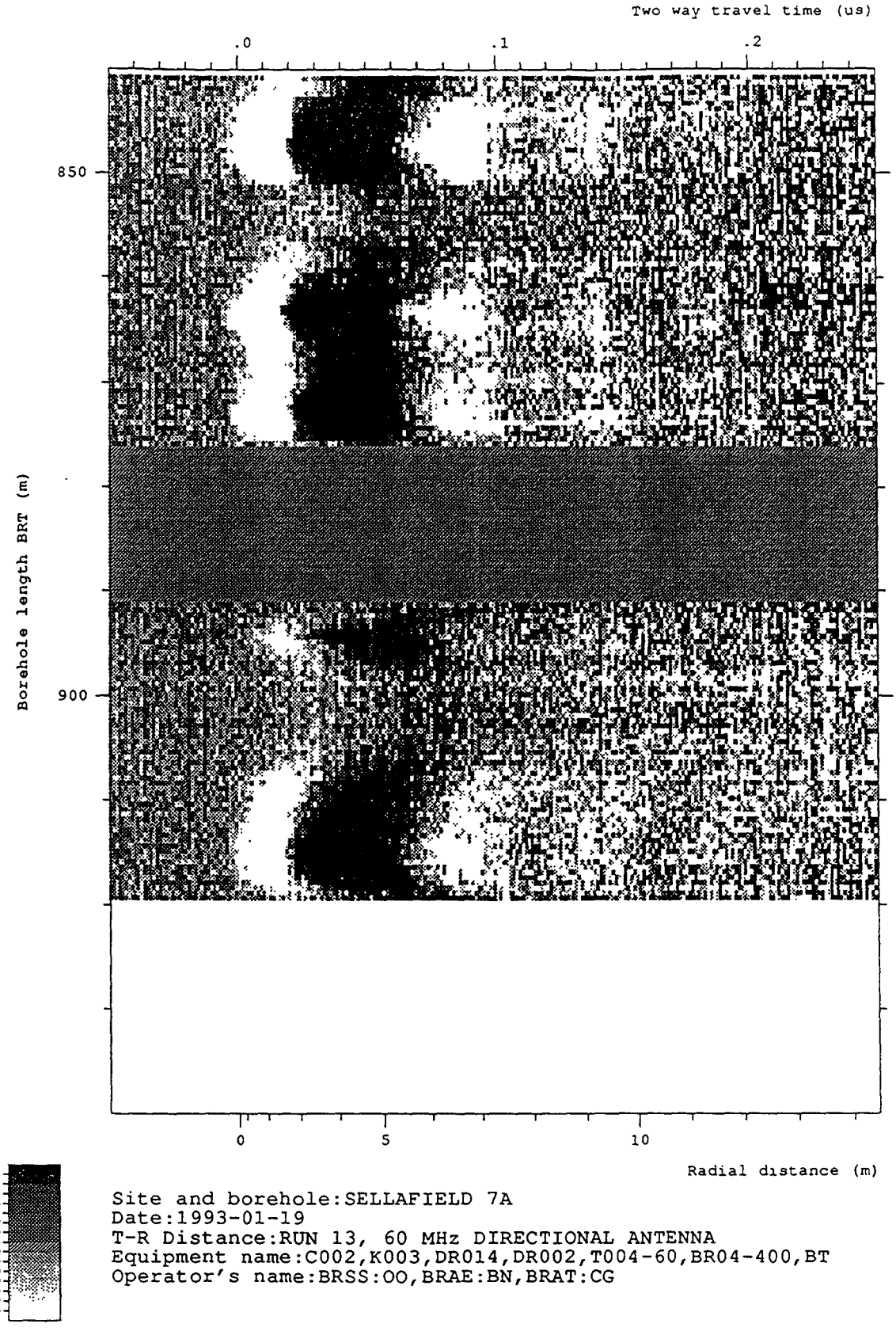

Figure 6-110 Radar map of the dipole component from the 60 MHz directional survey Run 13 (840.80 to 875.80 mbRT and 890.80 to 918.90 mbRT)

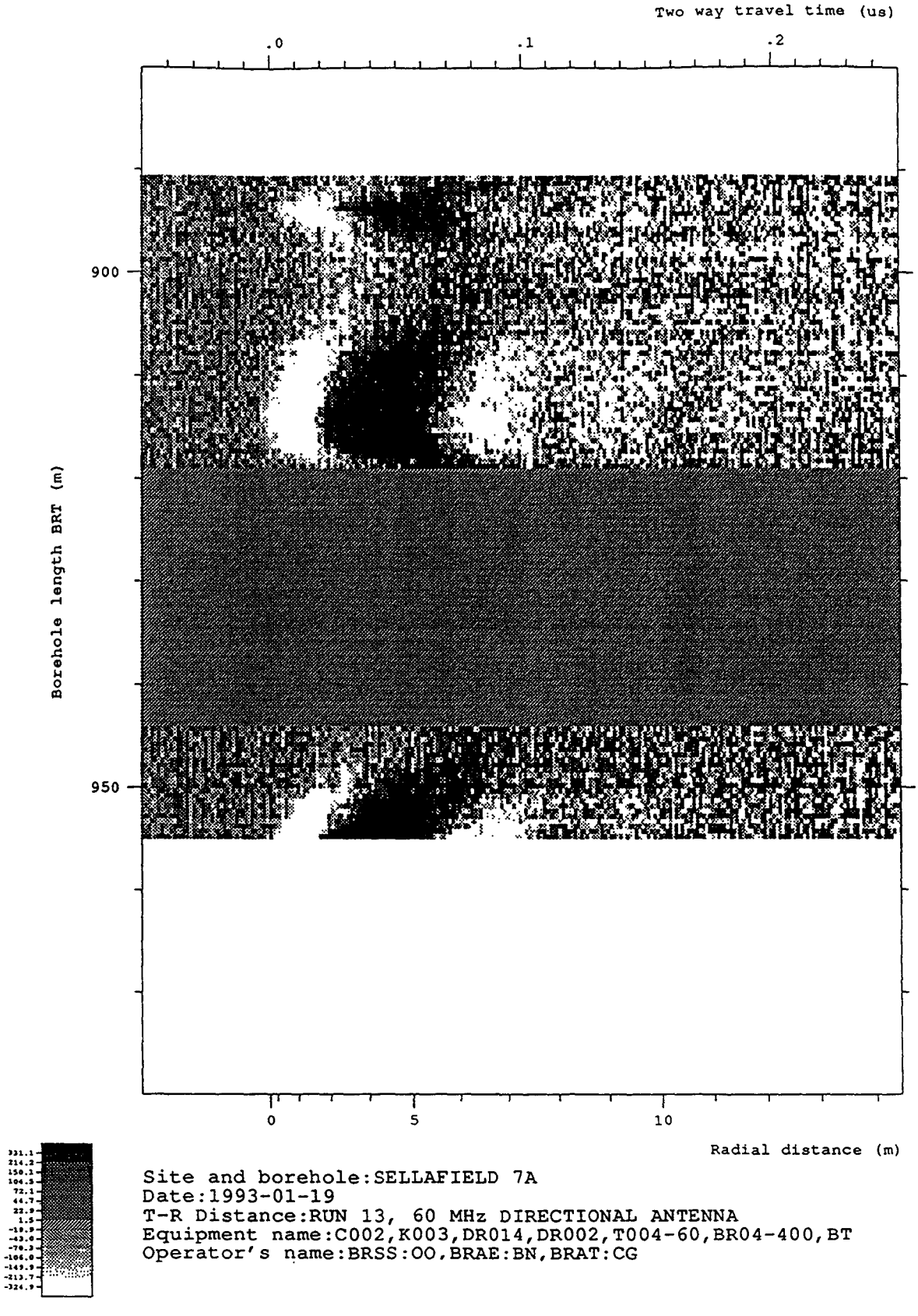

Figure 6-111 Radar map of the dipole component from the 60 MHz directional survey Run 13 (890.80 to 918.80 mbRT and 943.80 to 954.80 mbRT)

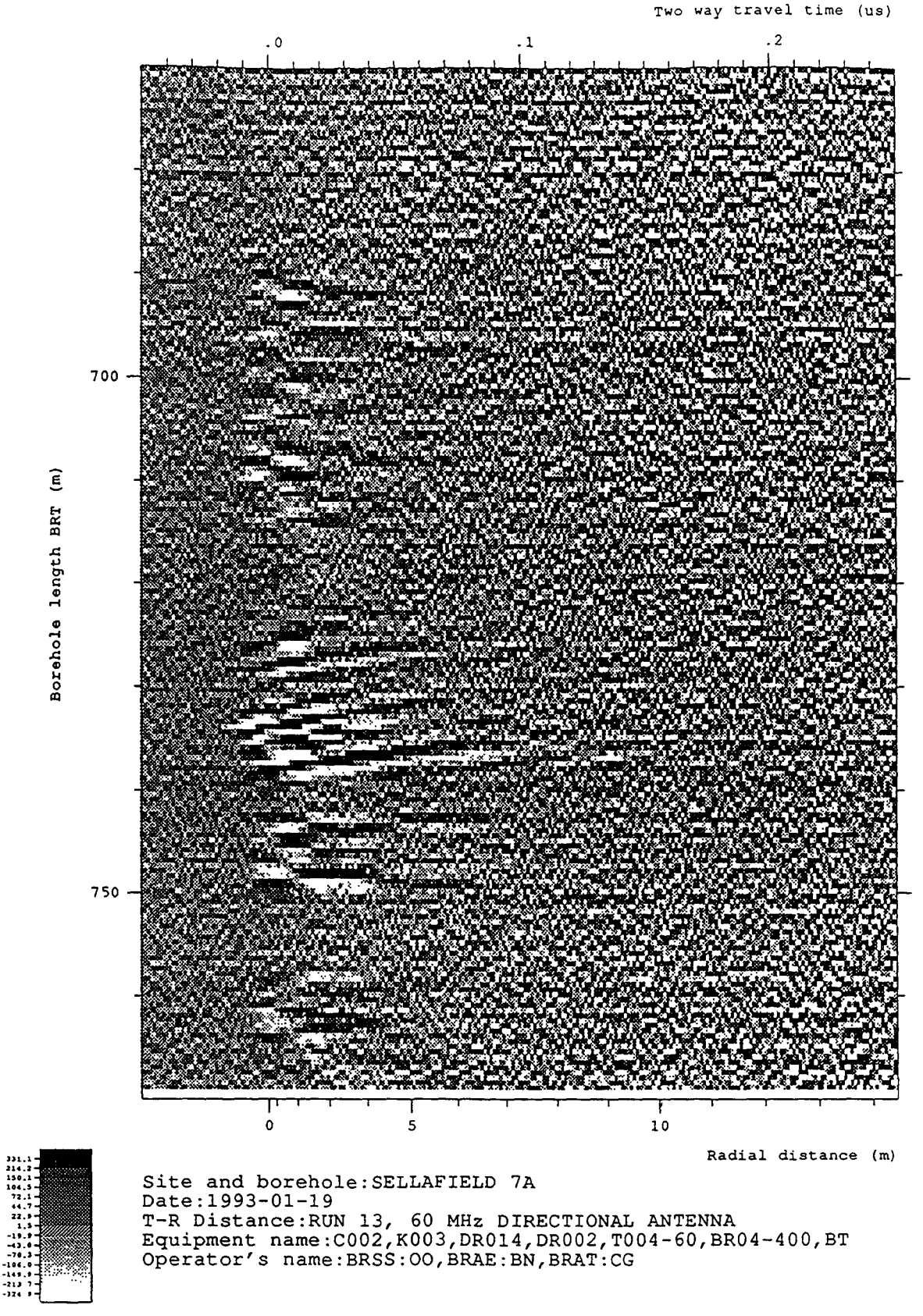

Figure 6-112 Radar map of the moving average filtered dipole component from the 60 MHz directional survey Run 13 (648.80 to 768.80 mbRT)

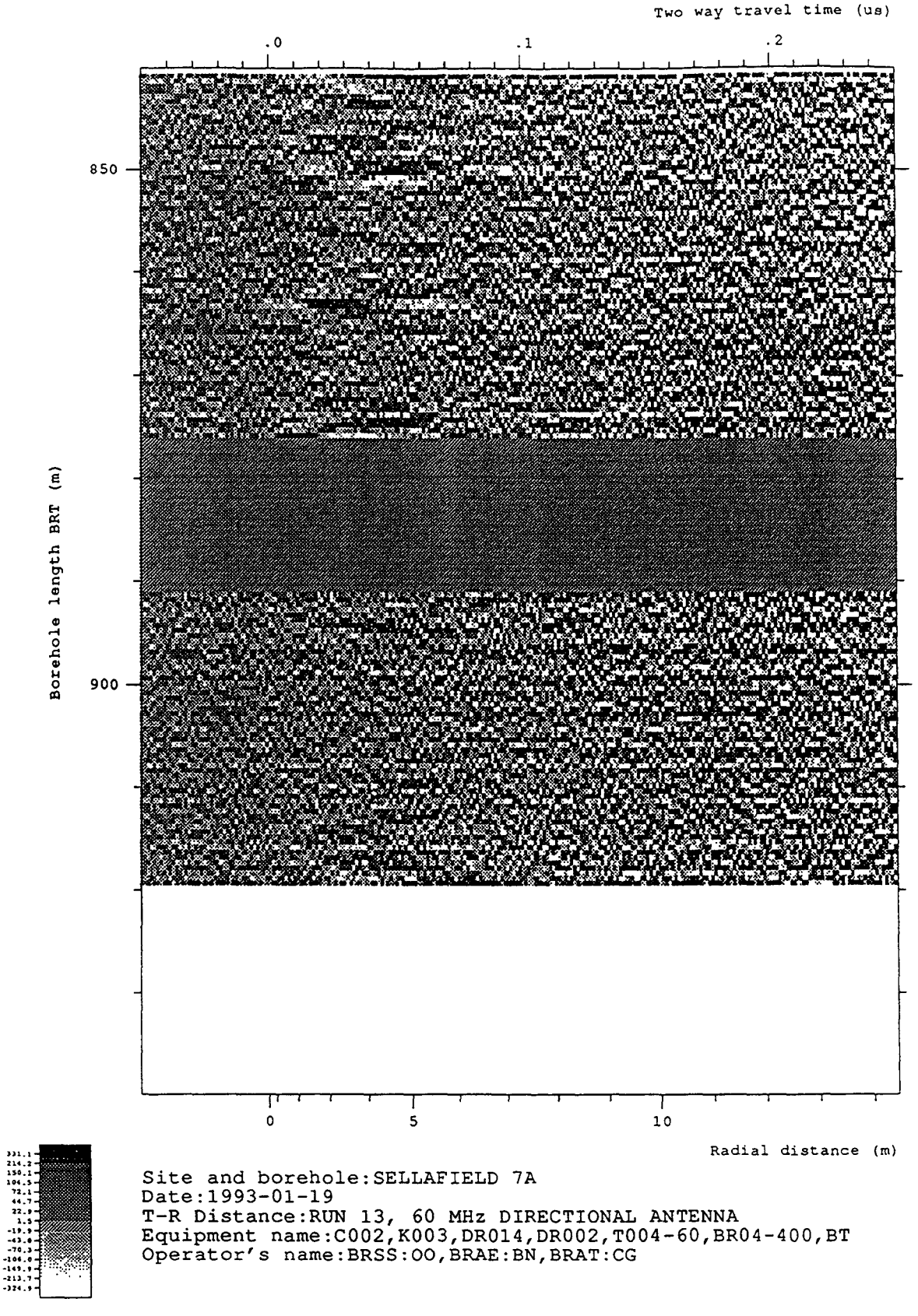

Figure 6-113 Radar map of the moving average filtered dipole component from the 60 MHz directional survey Run 13 (840.80 to 875.80 mbRT and 890.80 to 918.90 mbRT)

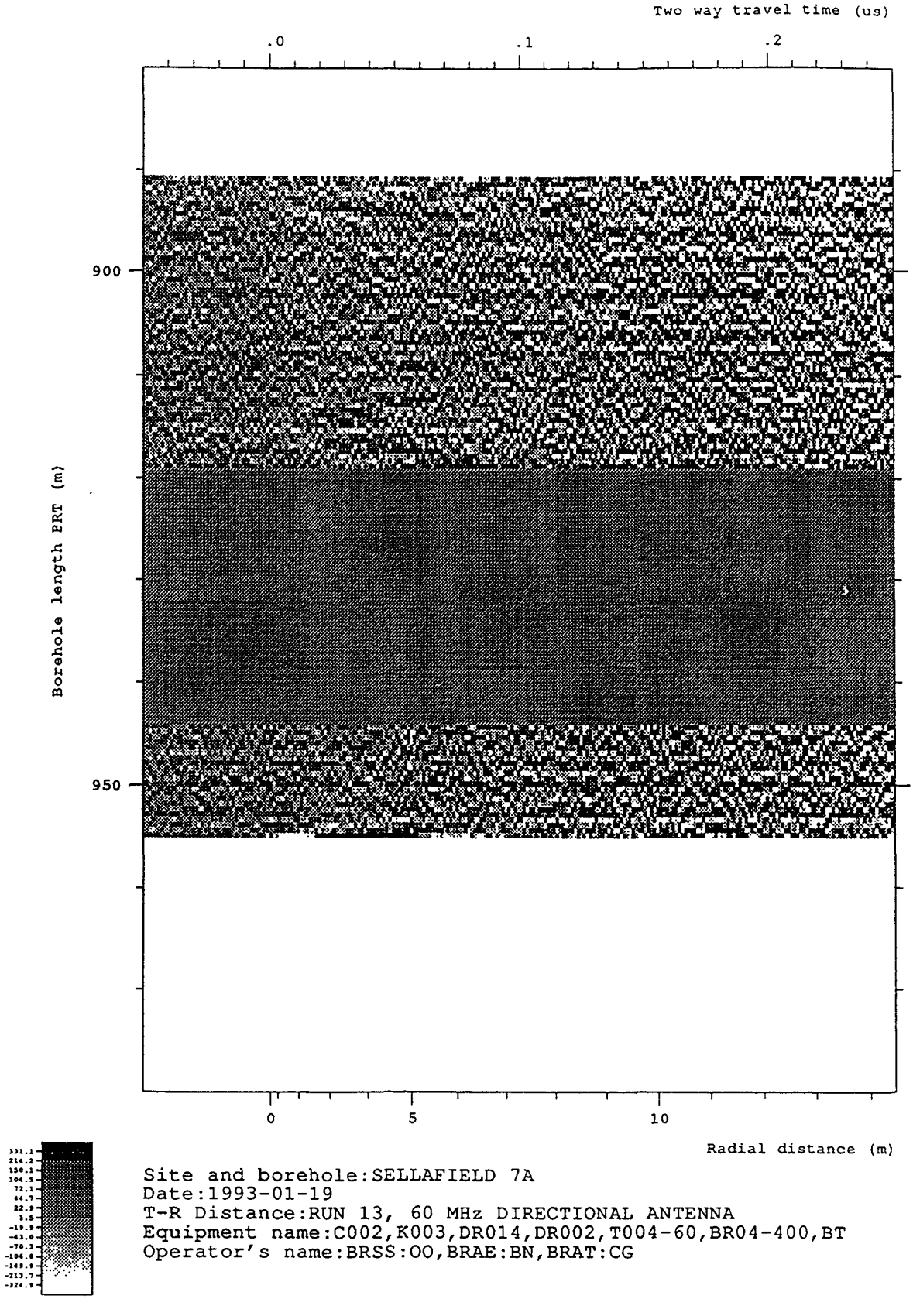

Figure 6-114 Radar map of the moving average filtered dipole component from the 60 MHz directional survey Run 13 (890.80 to 918.80 mbRT and 943.80 to 954.80 mbRT)

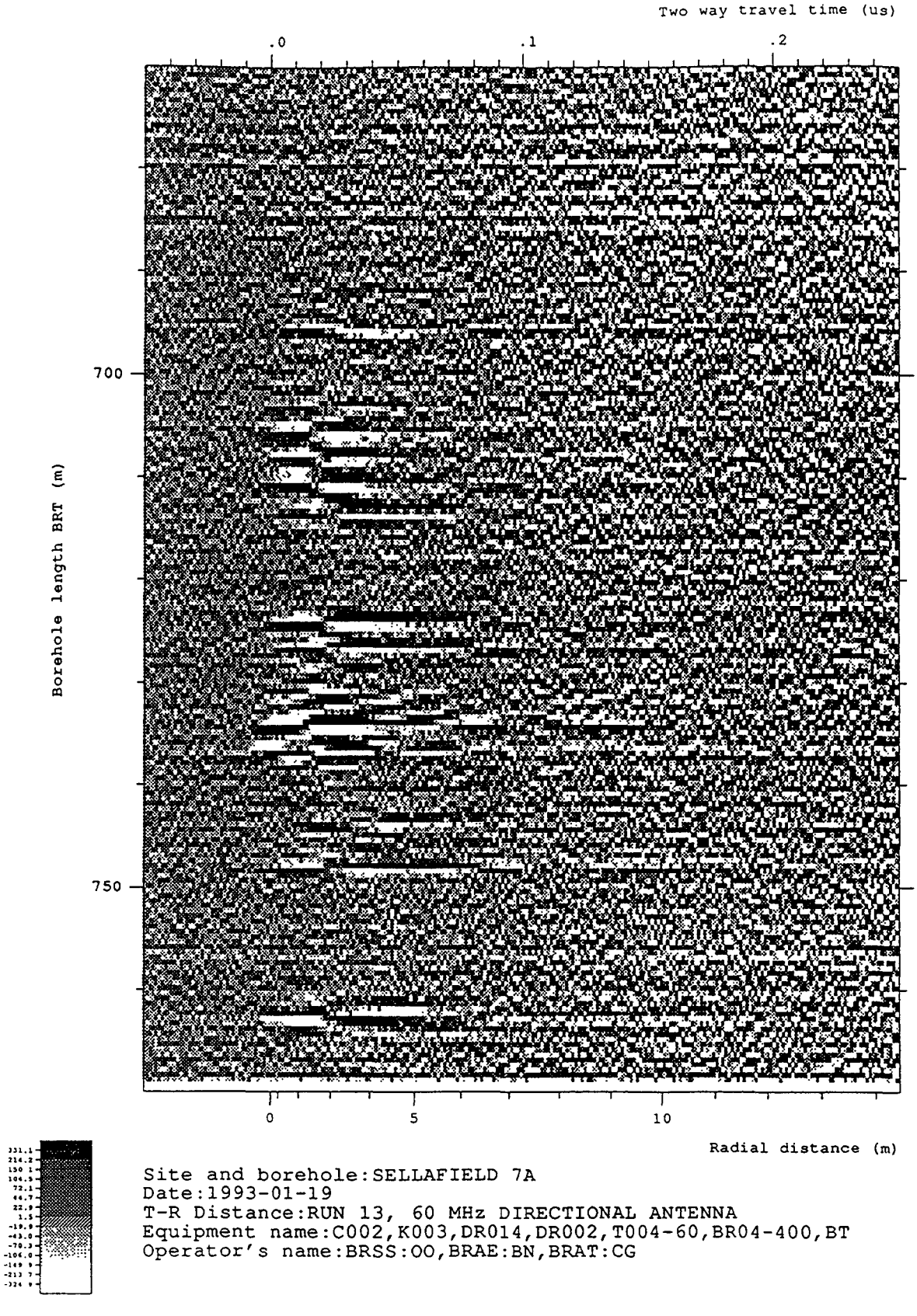

Figure 6-115 Radar map of the moving average filtered dipole component from the 60 MHz directional survey Run 13 (648.80 to 768.80 mbRT) at an azimuth of 0°

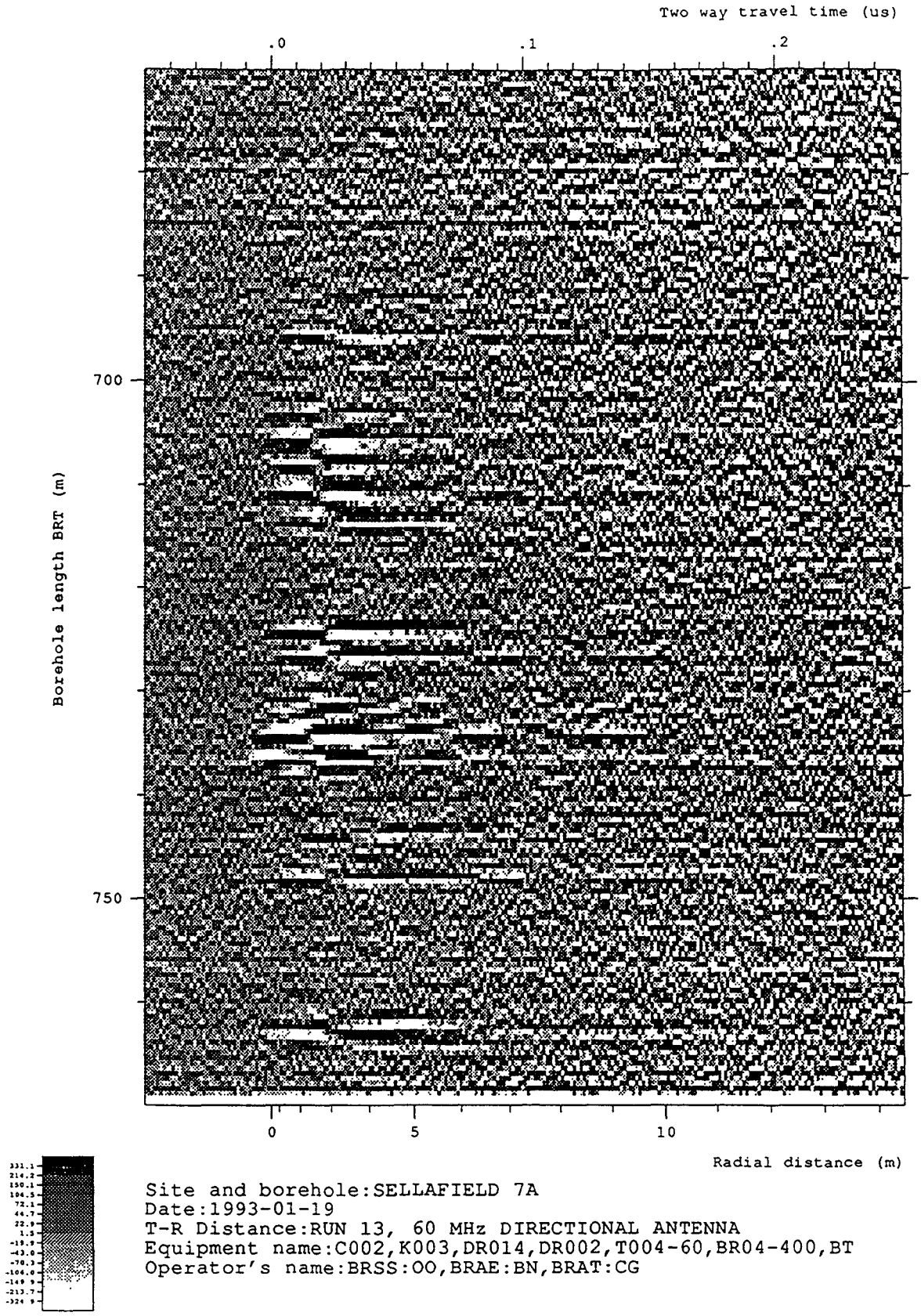

Figure 6-116 Radar map of the moving average filtered dipole component from the 60 MHz directional survey Run 13 (648.80 to 768.80 mbRT) at an azimuth of 10°

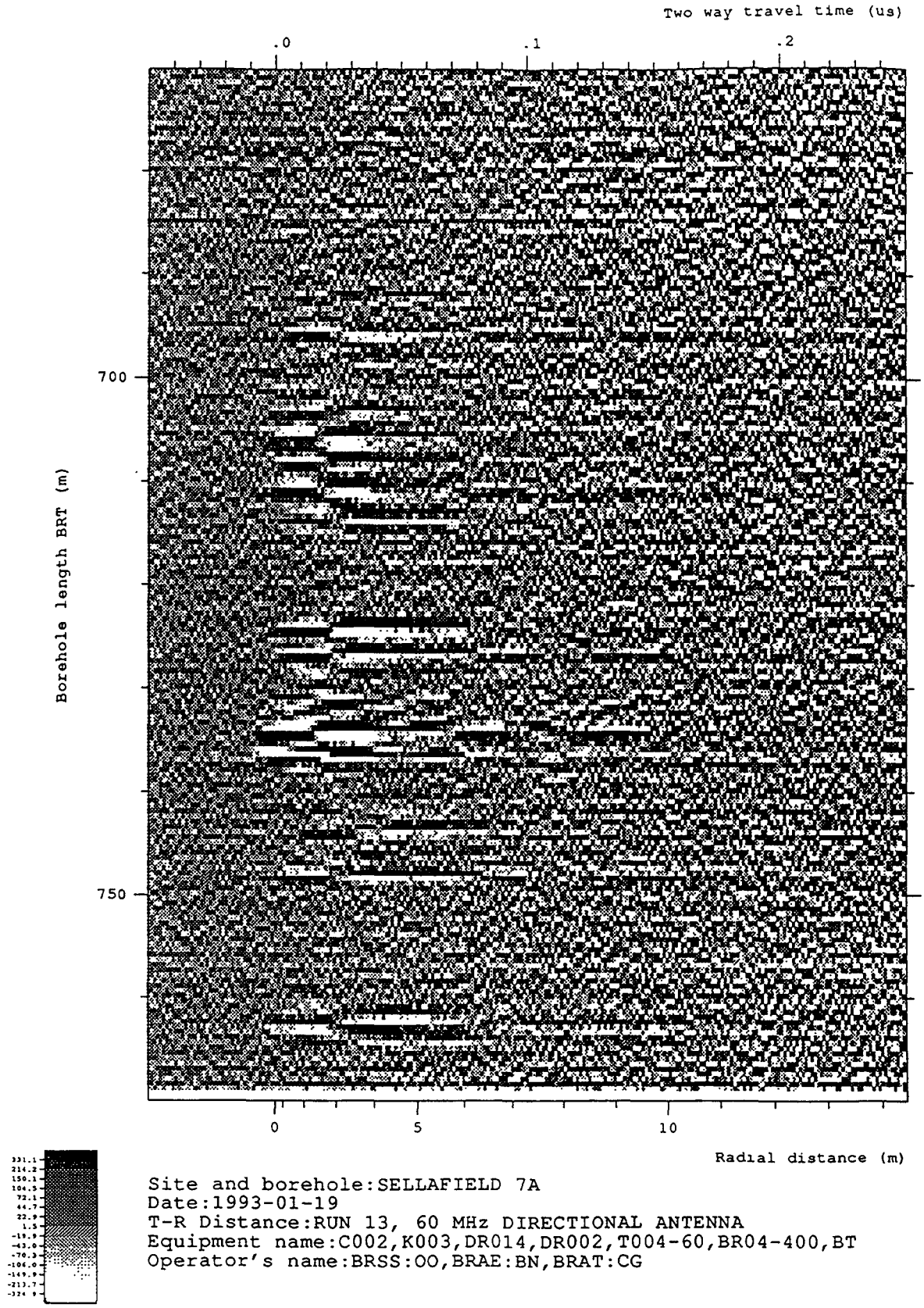

Figure 6-117 Radar map of the moving average filtered dipole component from the 60 MHz directional survey Run 13 (648.80 to 768.80 mbRT) at an azimuth of 20°

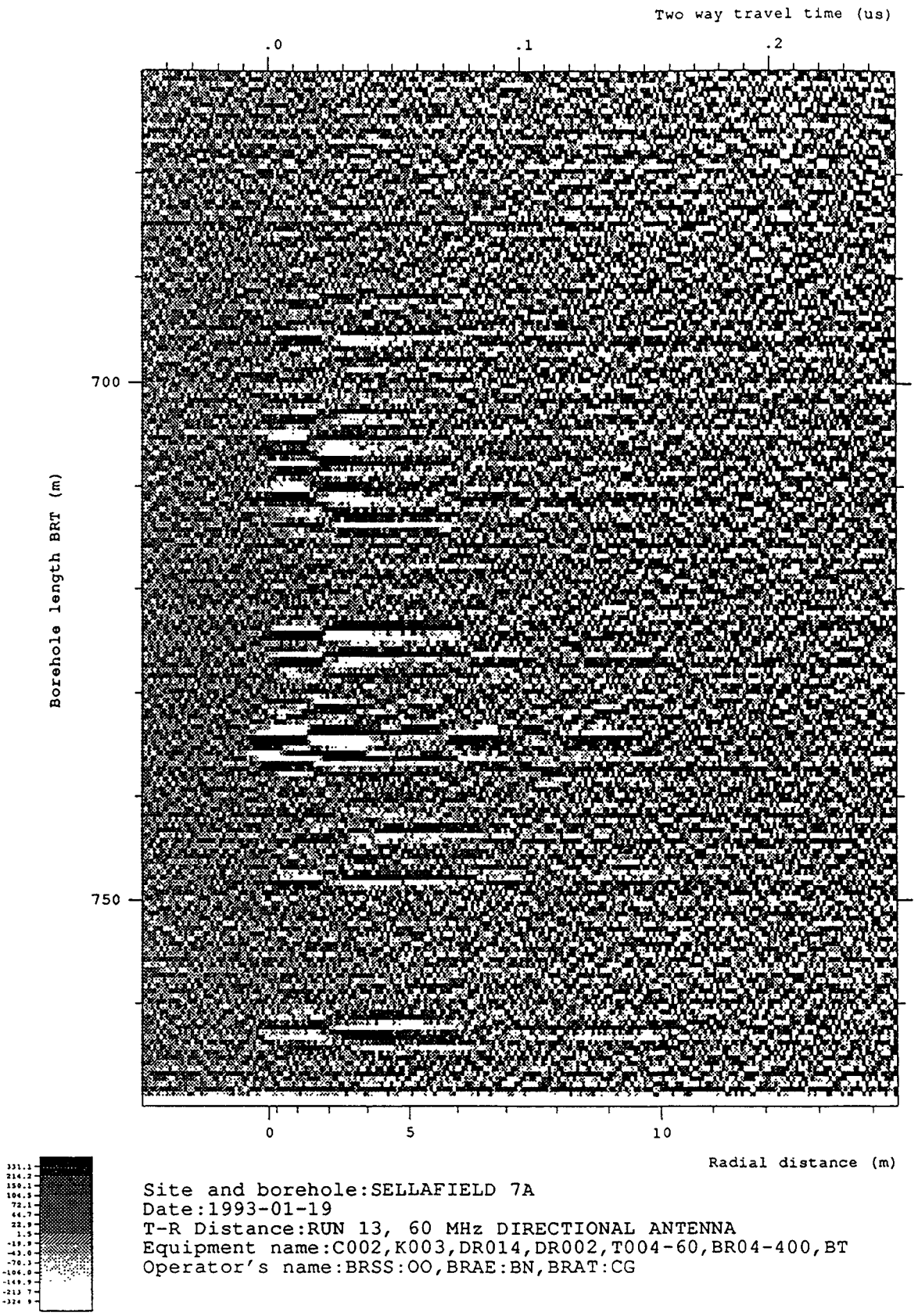

Figure 6-118 Radar map of the moving average filtered dipole component from the 60 MHz directional survey Run 13 (648.80 to 768.80 mbRT) at an azimuth of 30°

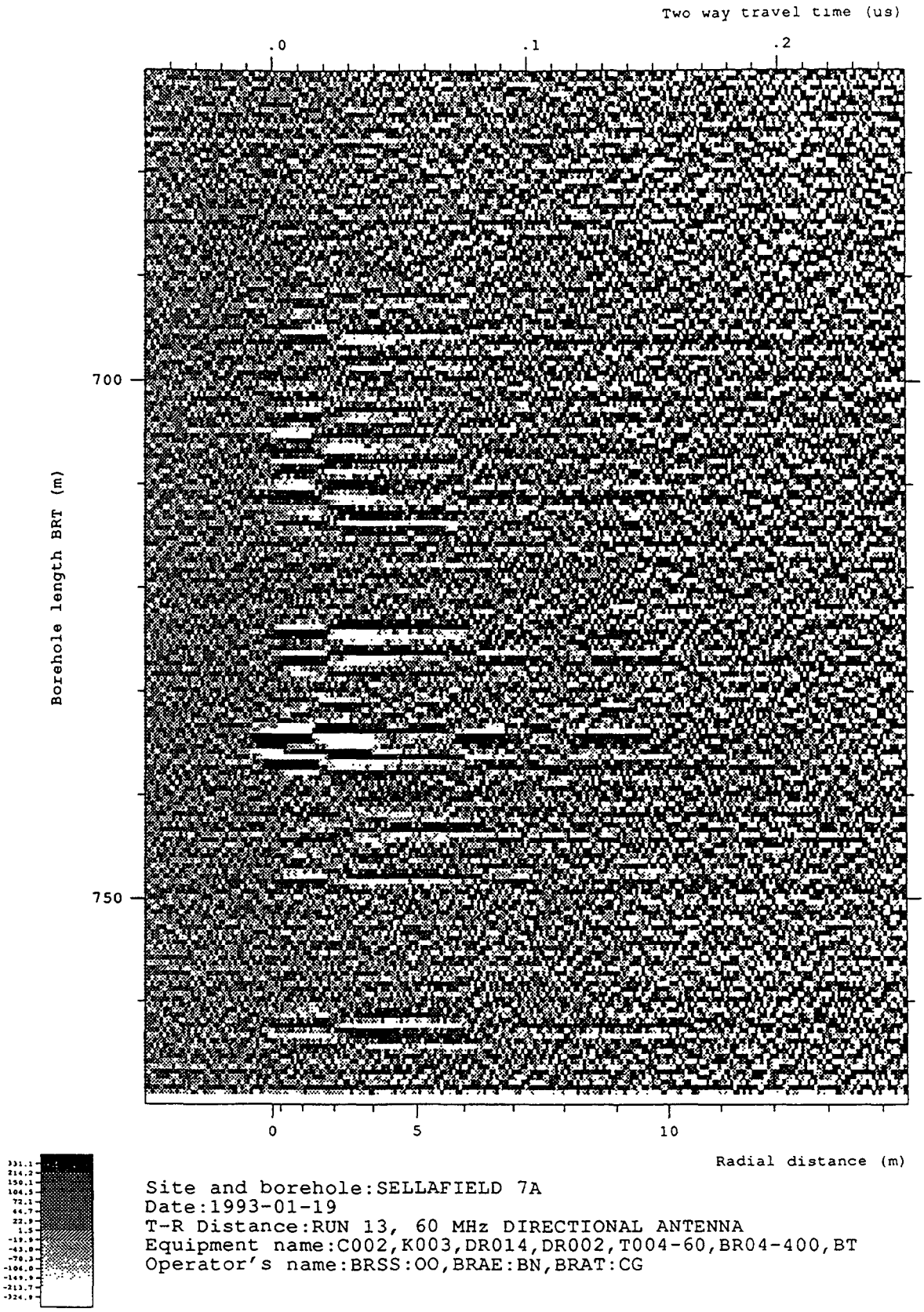

Figure 6-119 Radar map of the moving average filtered dipole component from the 60 MHz directional survey Run 13 (648.80 to 768.80 mbRT) at an azimuth of 40°

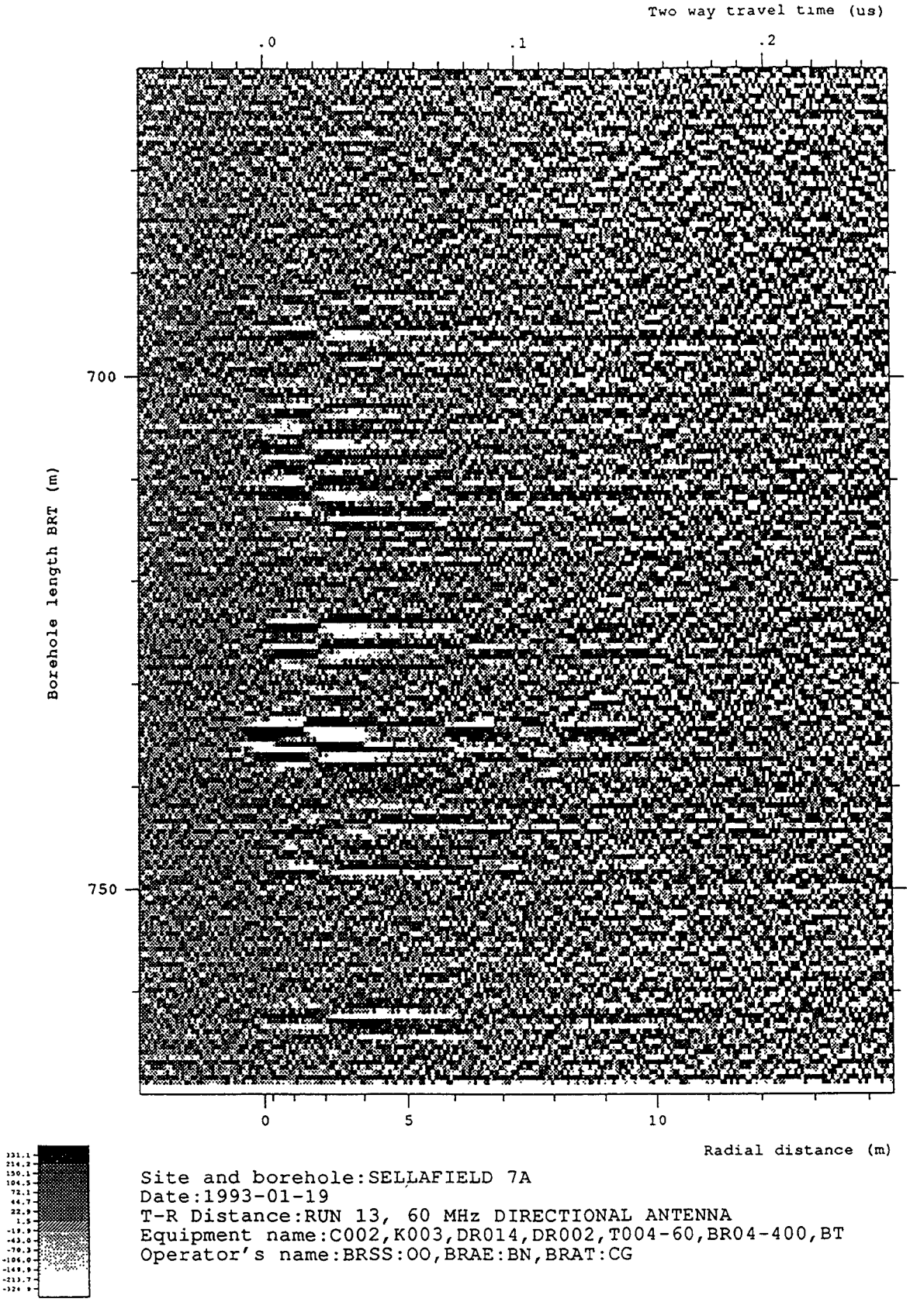

Figure 6-120 Radar map of the moving average filtered dipole component from the 60 MHz directional survey Run 13 (648.80 to 768.80 mbRT) at an azimuth of 50°

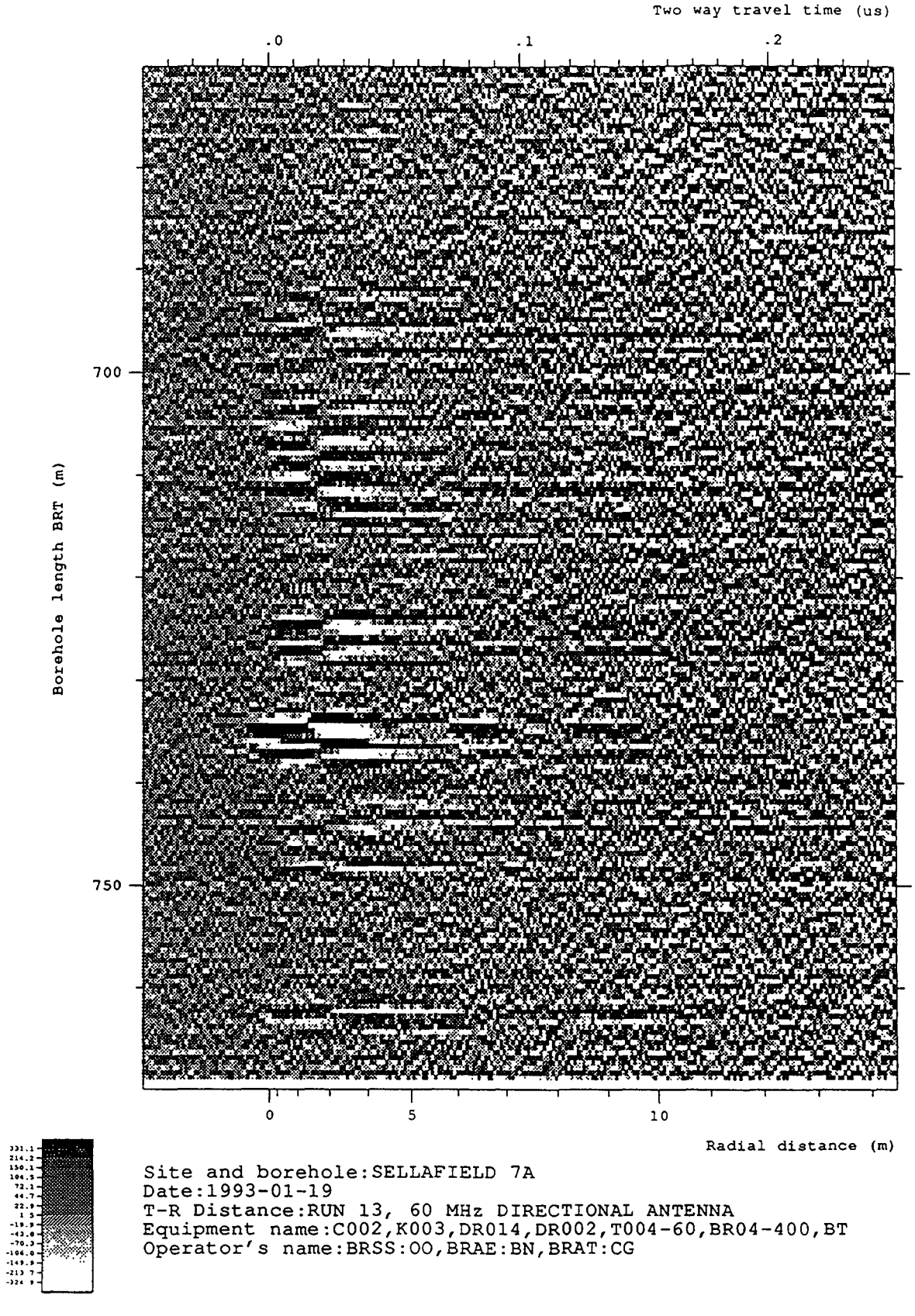

Figure 6-121 Radar map of the moving average filtered dipole component from the 60 MHz directional survey Run 13 (648.80 to 768.80 mbRT) at an azimuth of 60°

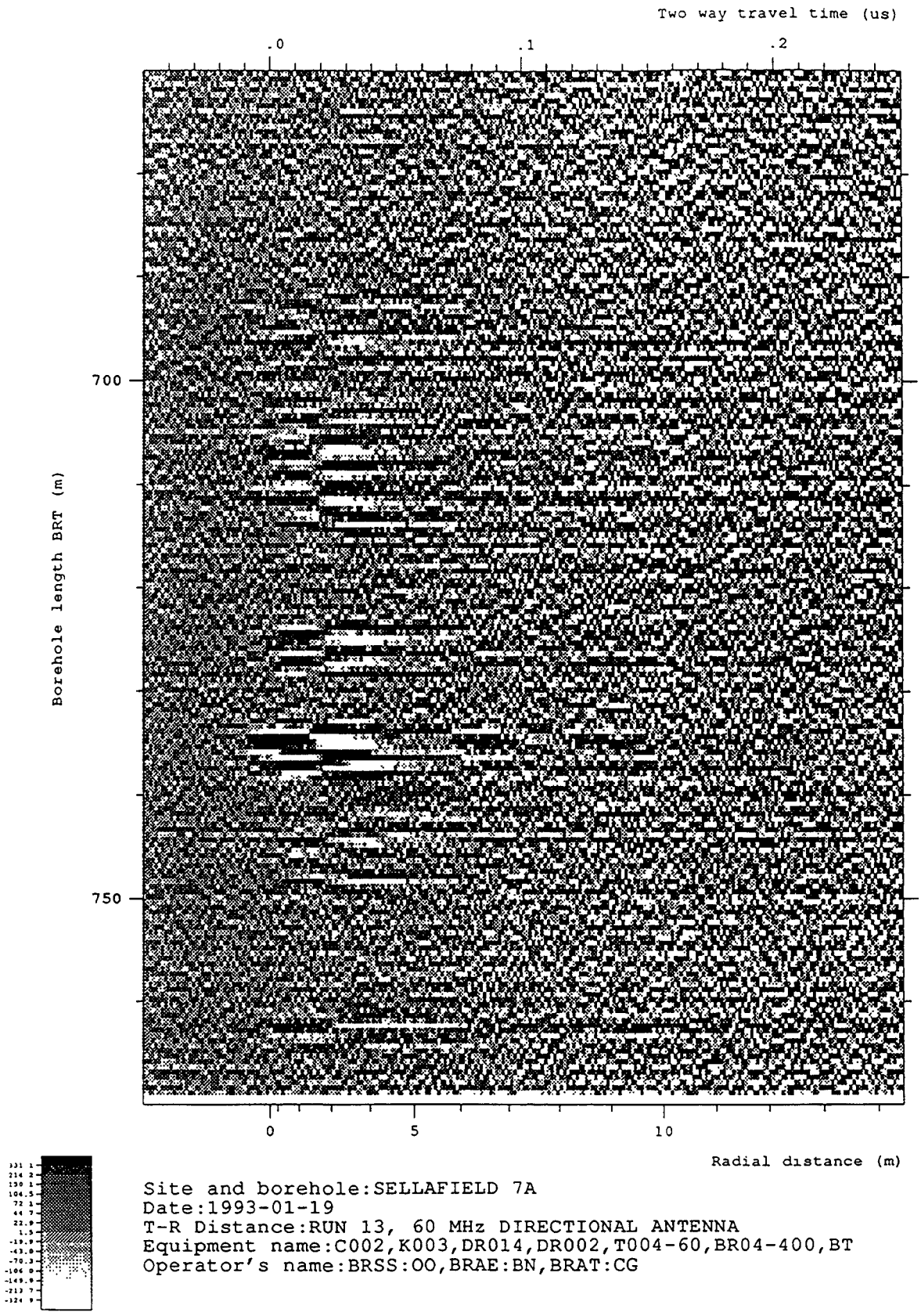

Figure 6-122 Radar map of the moving average filtered dipole component from the 60 MHz directional survey Run 13 (648.80 to 768.80 mbRT) at an azimuth of 70°

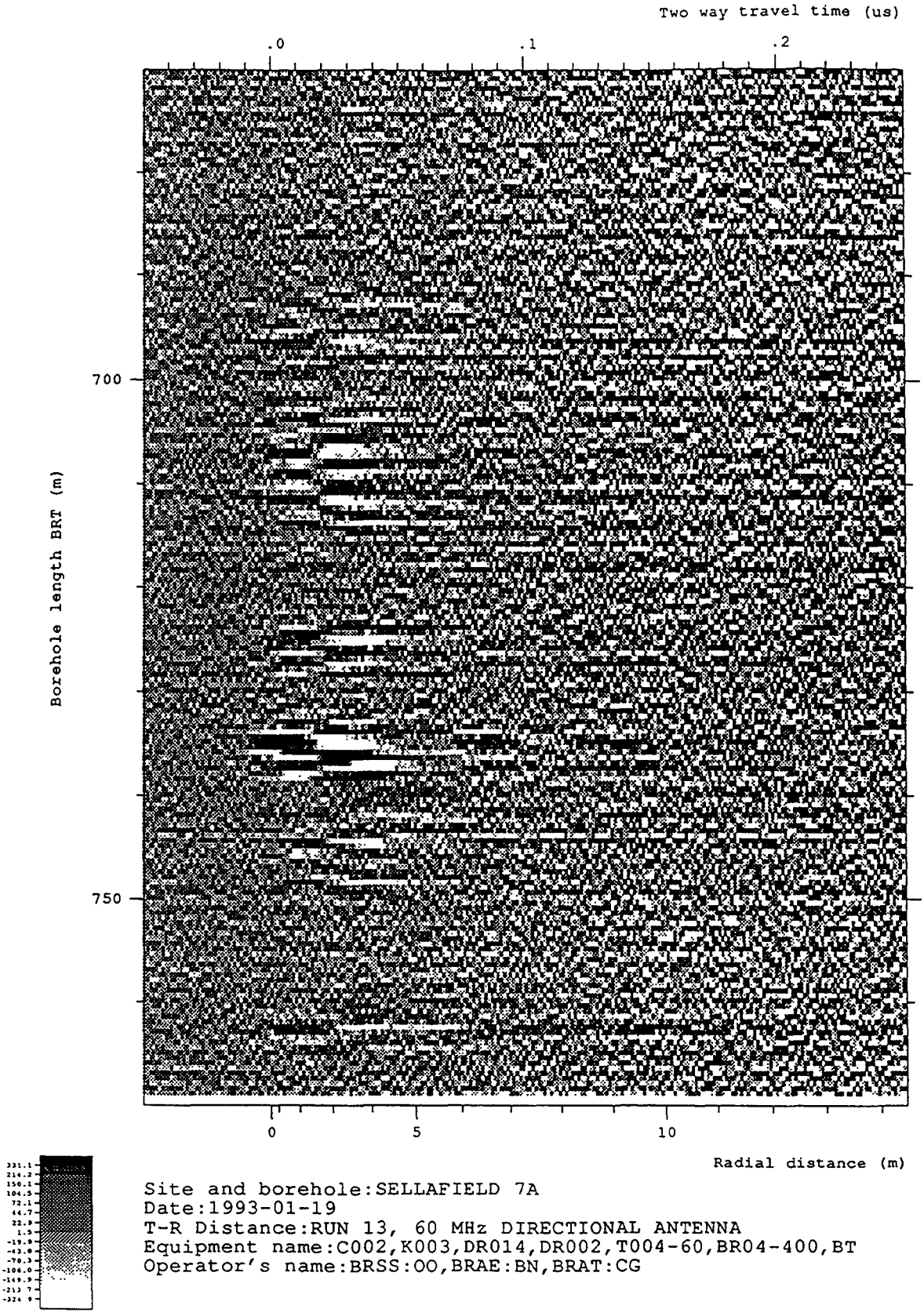

Figure 6-123 Radar map of the moving average filtered dipole component from the 60 MHz directional survey Run 13 (648.80 to 768.80 mbRT) at an azimuth of 80°

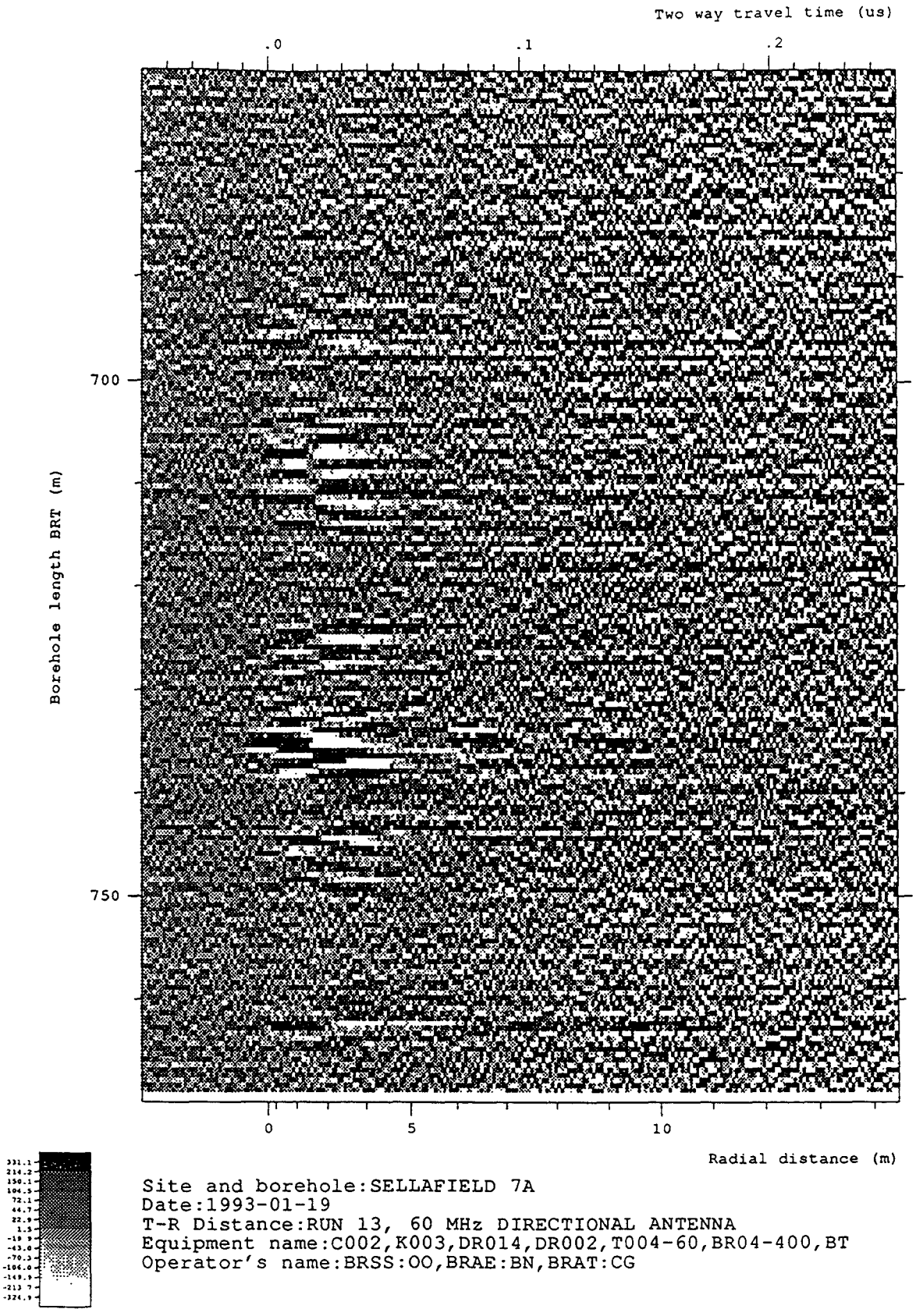

Figure 6-124 Radar map of the moving average filtered dipole component from the 60 MHz directional survey Run 13 (648.80 to 768.80 mbRT) at an azimuth of 90°

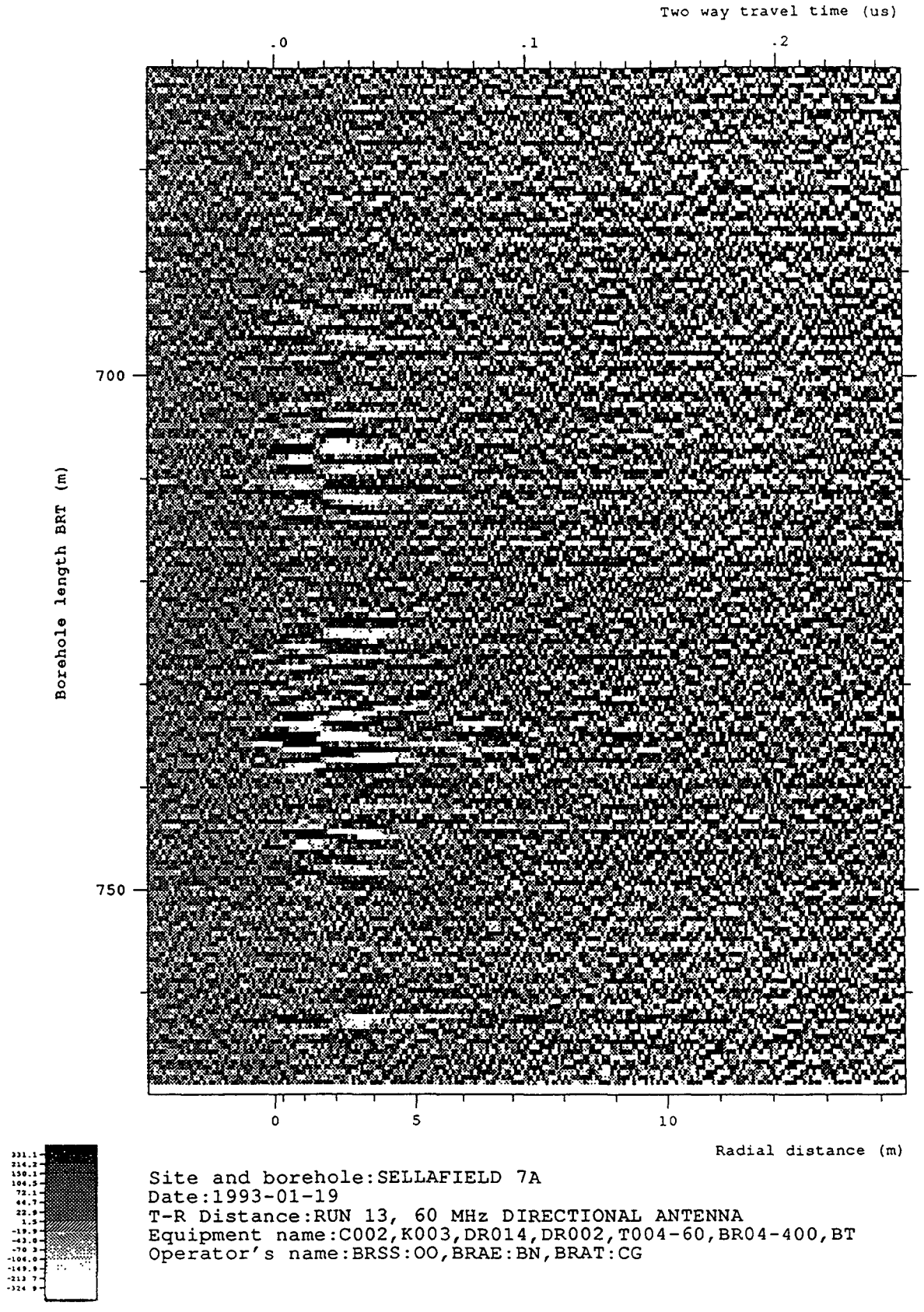

Figure 6-125 Radar map of the moving average filtered dipole component from the 60 MHz directional survey Run 13 (648.80 to 768.80 mbRT) at an azimuth of 100°

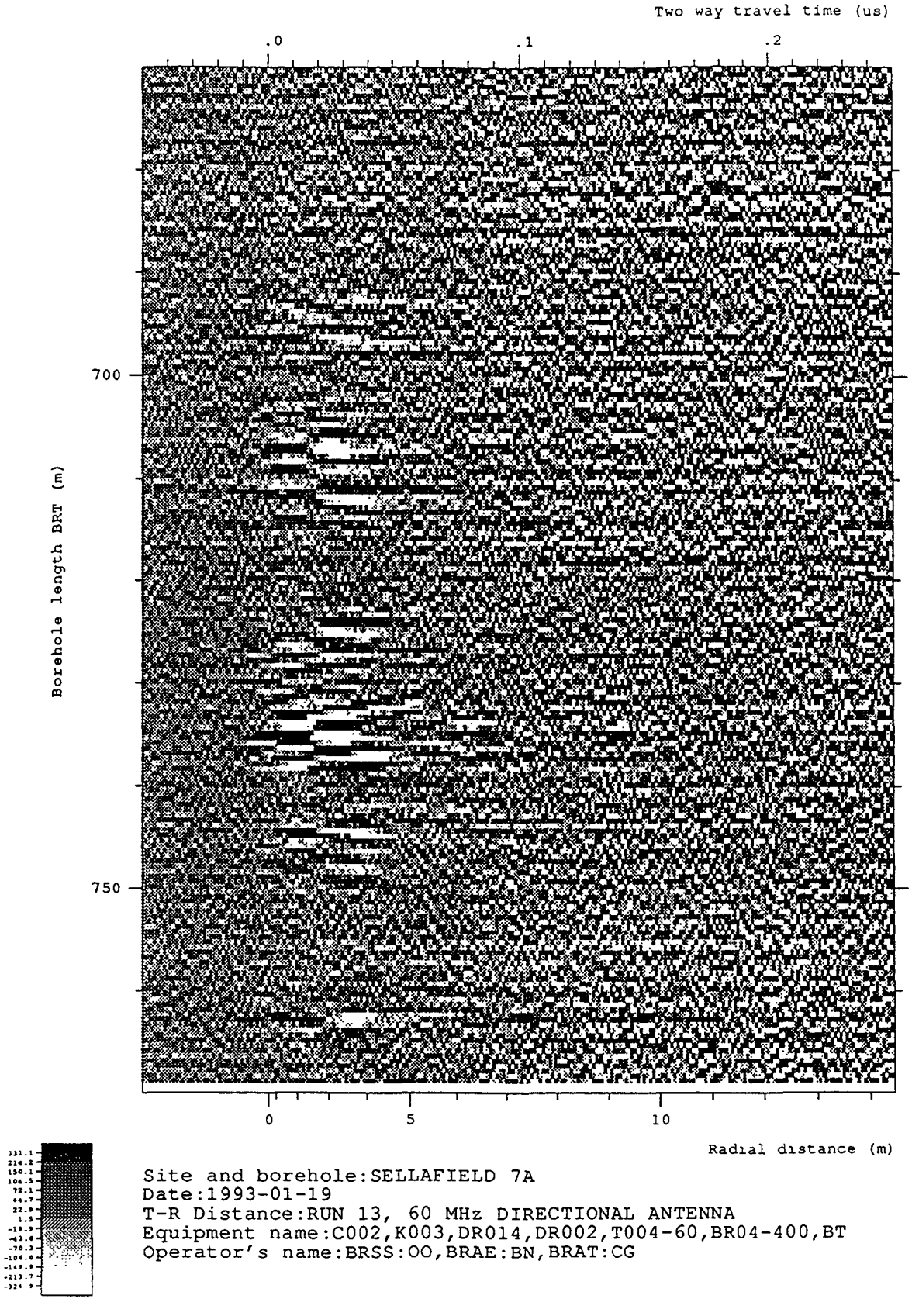

Figure 6-126 Radar map of the moving average filtered dipole component from the 60 MHz directional survey Run 13 (648.80 to 768.80 mbRT) at an azimuth of 110°

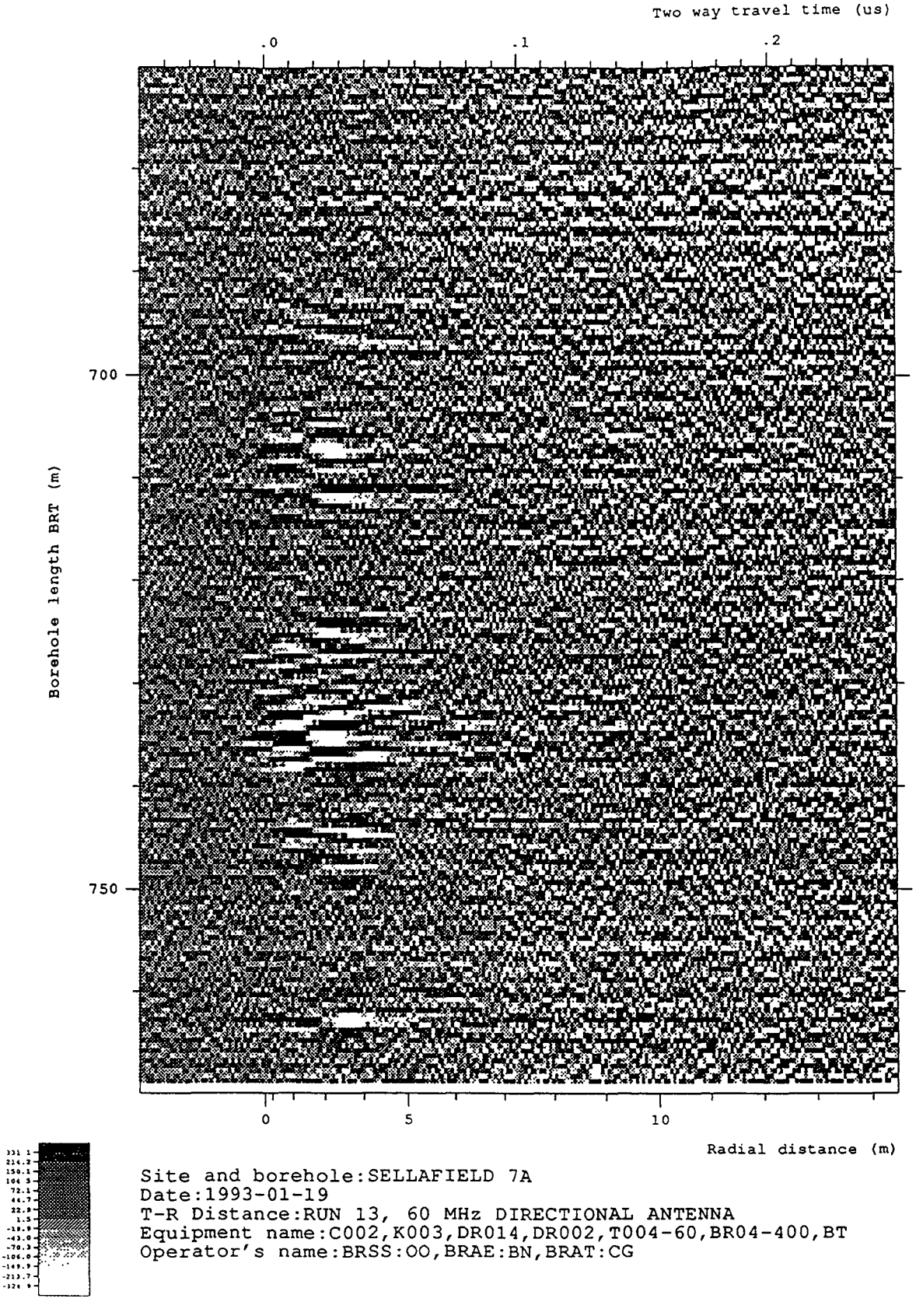

Figure 6-127 Radar map of the moving average filtered dipole component from the 60 MHz directional survey Run 13 (648.80 to 768.80 mbRT) at an azimuth of 120°

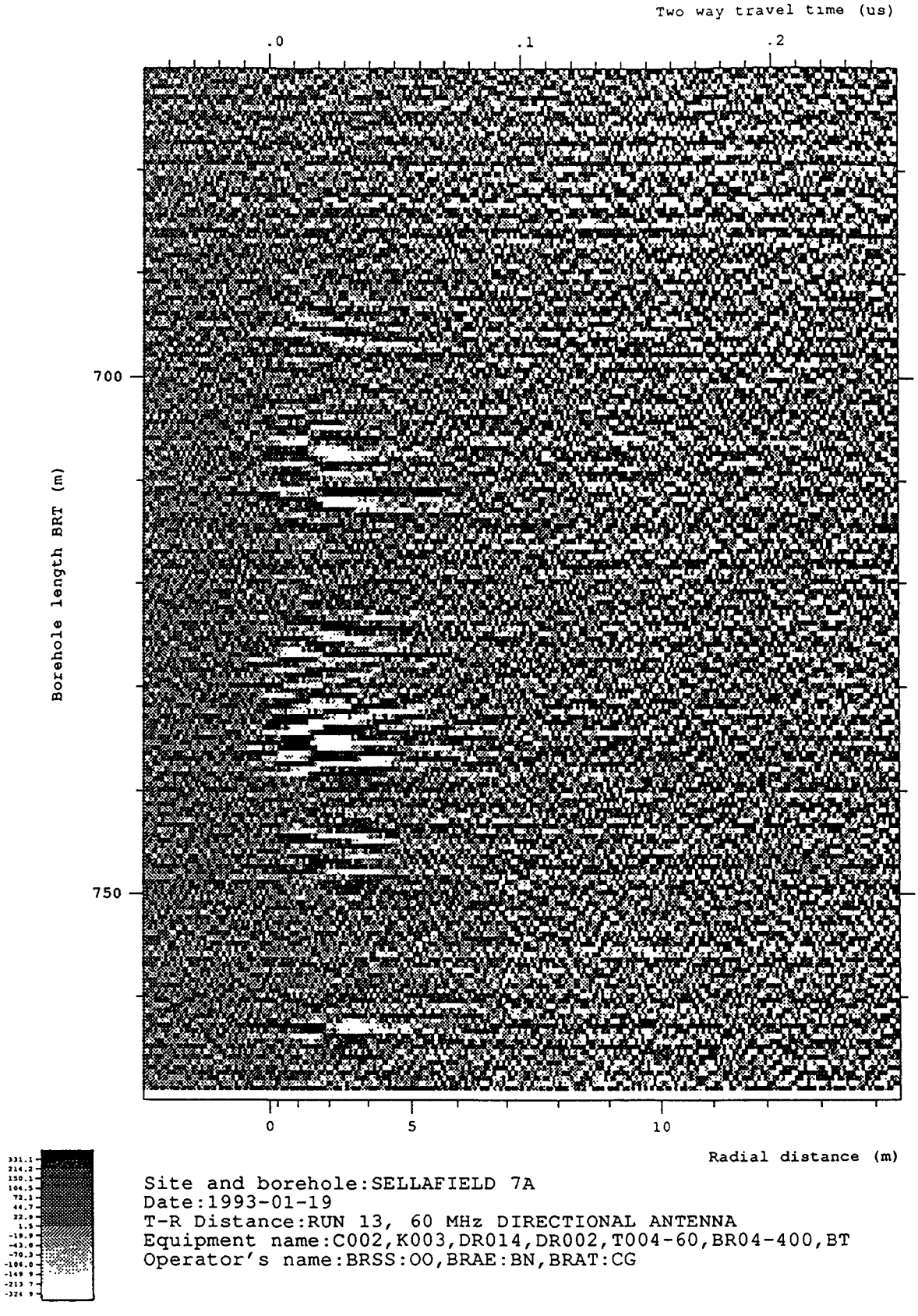

Figure 6-128 Radar map of the moving average filtered dipole component from the 60 MHz directional survey Run 13 (648.80 to 768.80 mbRT) at an azimuth of 130°

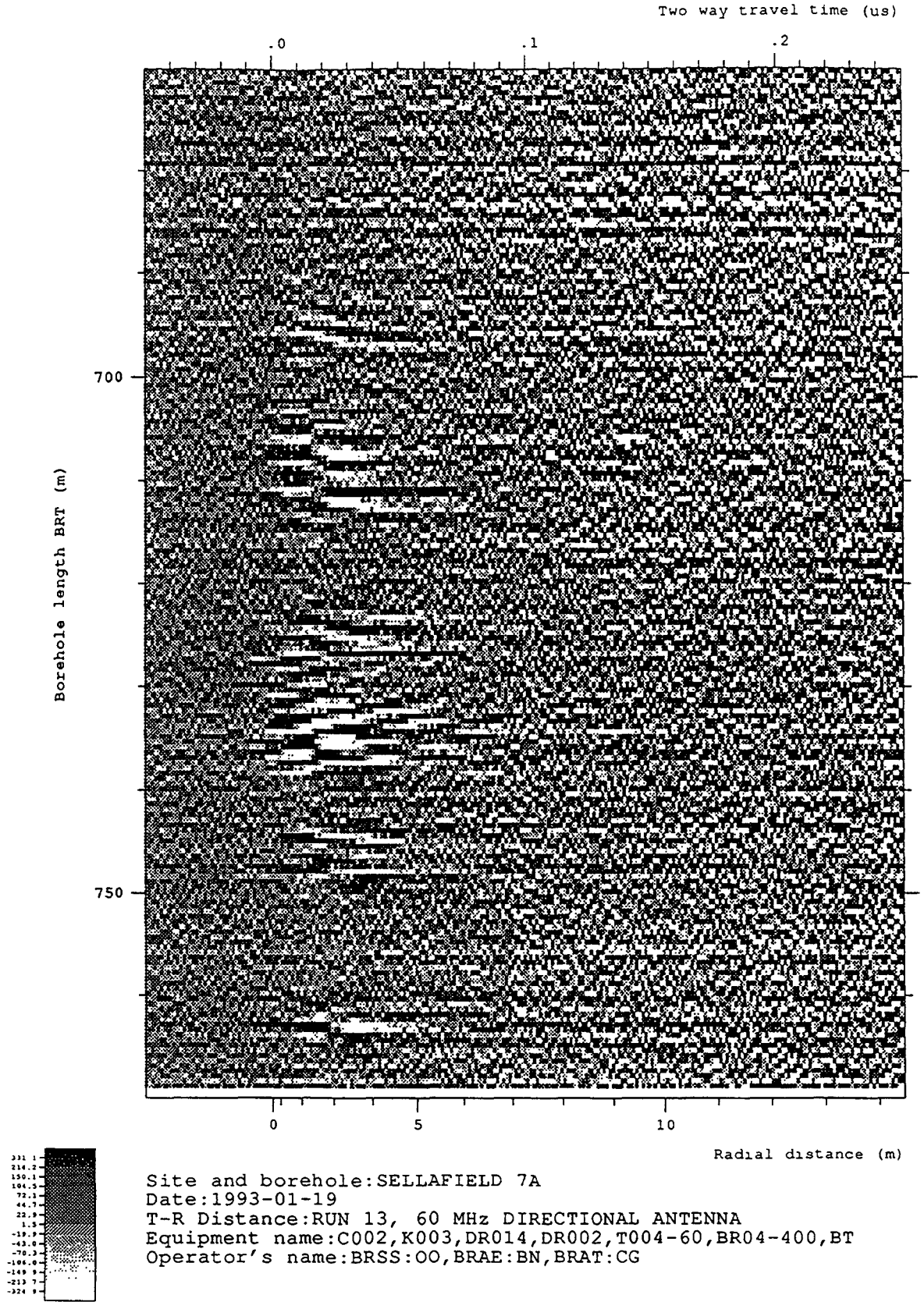

Figure 6-129 Radar map of the moving average filtered dipole component from the 60 MHz directional survey Run 13 (648.80 to 768.80 mbRT) at an azimuth of 140°

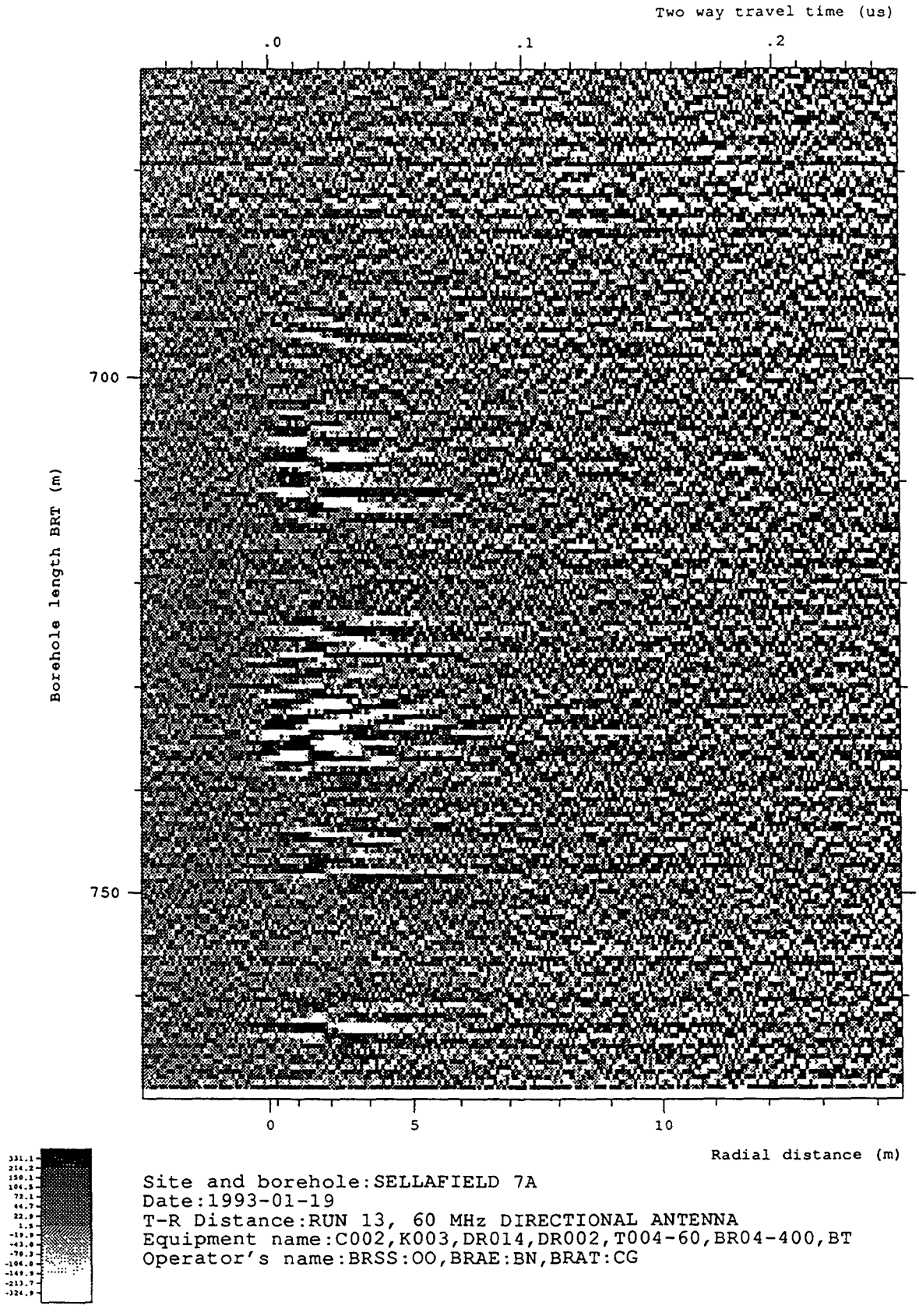

Figure 6-130 Radar map of the moving average filtered dipole component from the 60 MHz directional survey Run 13 (648.80 to 768.80 mbRT) at an azimuth of 150°

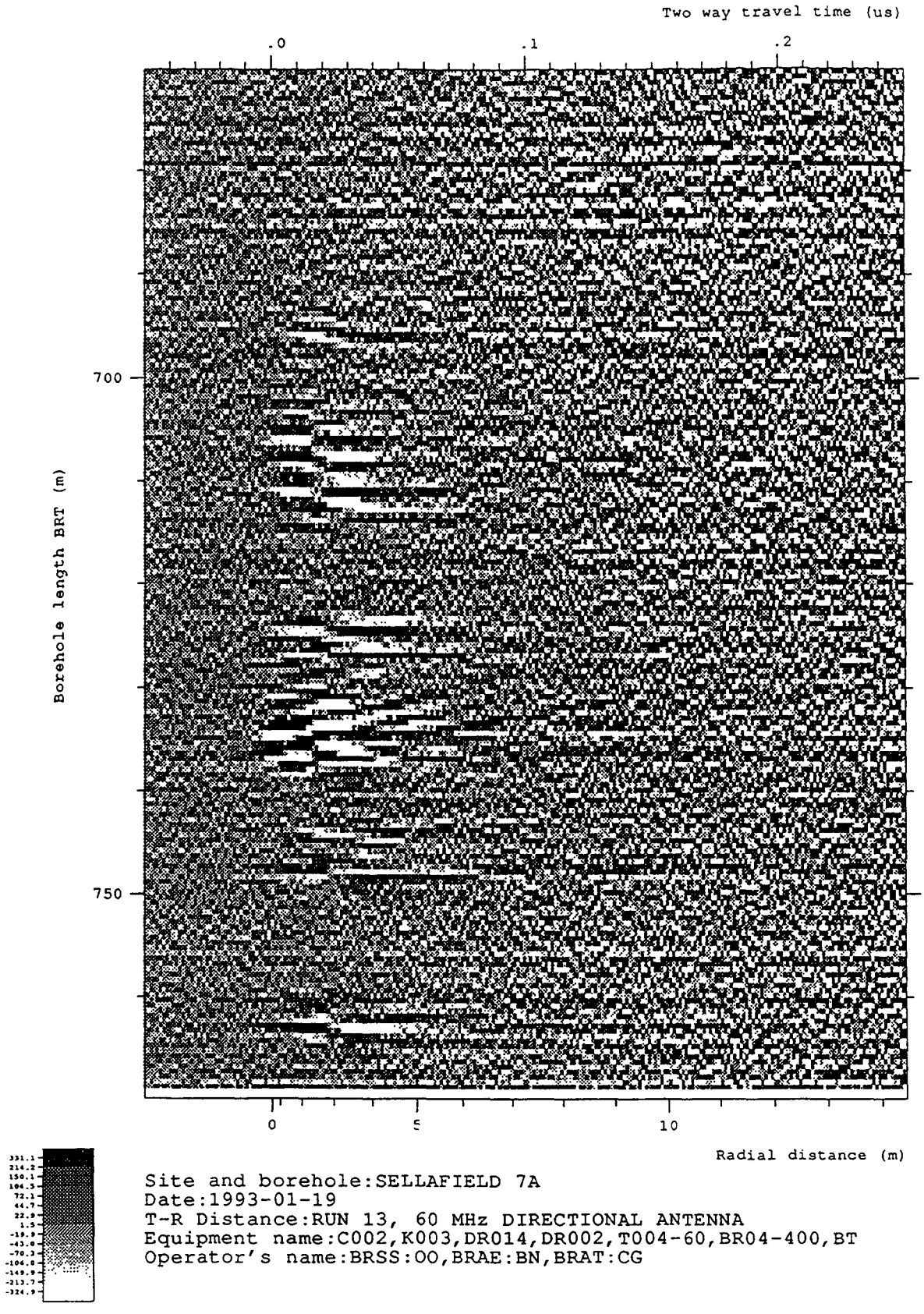

Figure 6-131 Radar map of the moving average filtered dipole component from the 60 MHz directional survey Run 13 (648.80 to 768.80 mbRT) at an azimuth of 160°

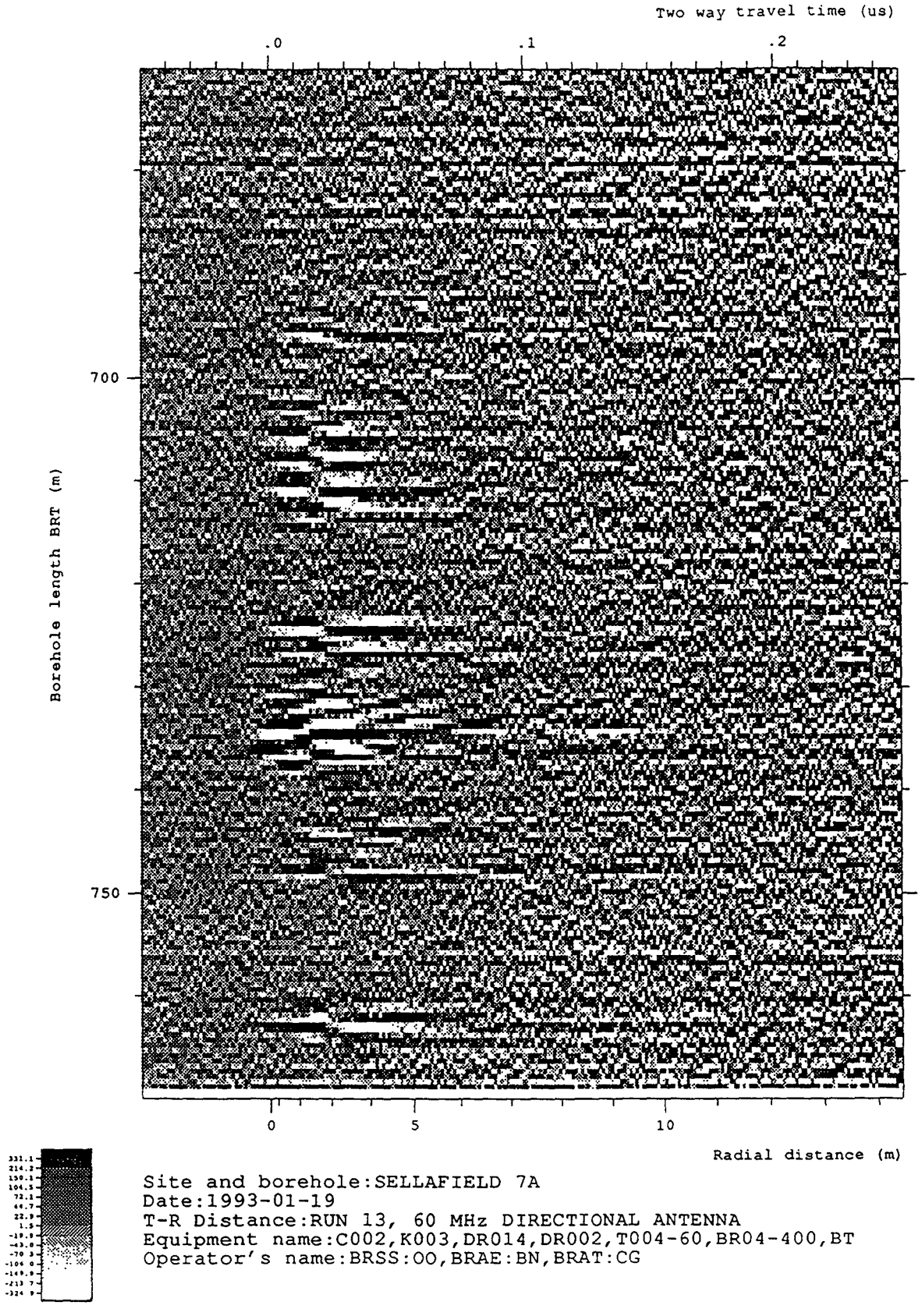

Figure 6-132 Radar map of the moving average filtered dipole component from the 60 MHz directional survey Run 13 (648.80 to 768.80 mbRT) at an azimuth of 170°

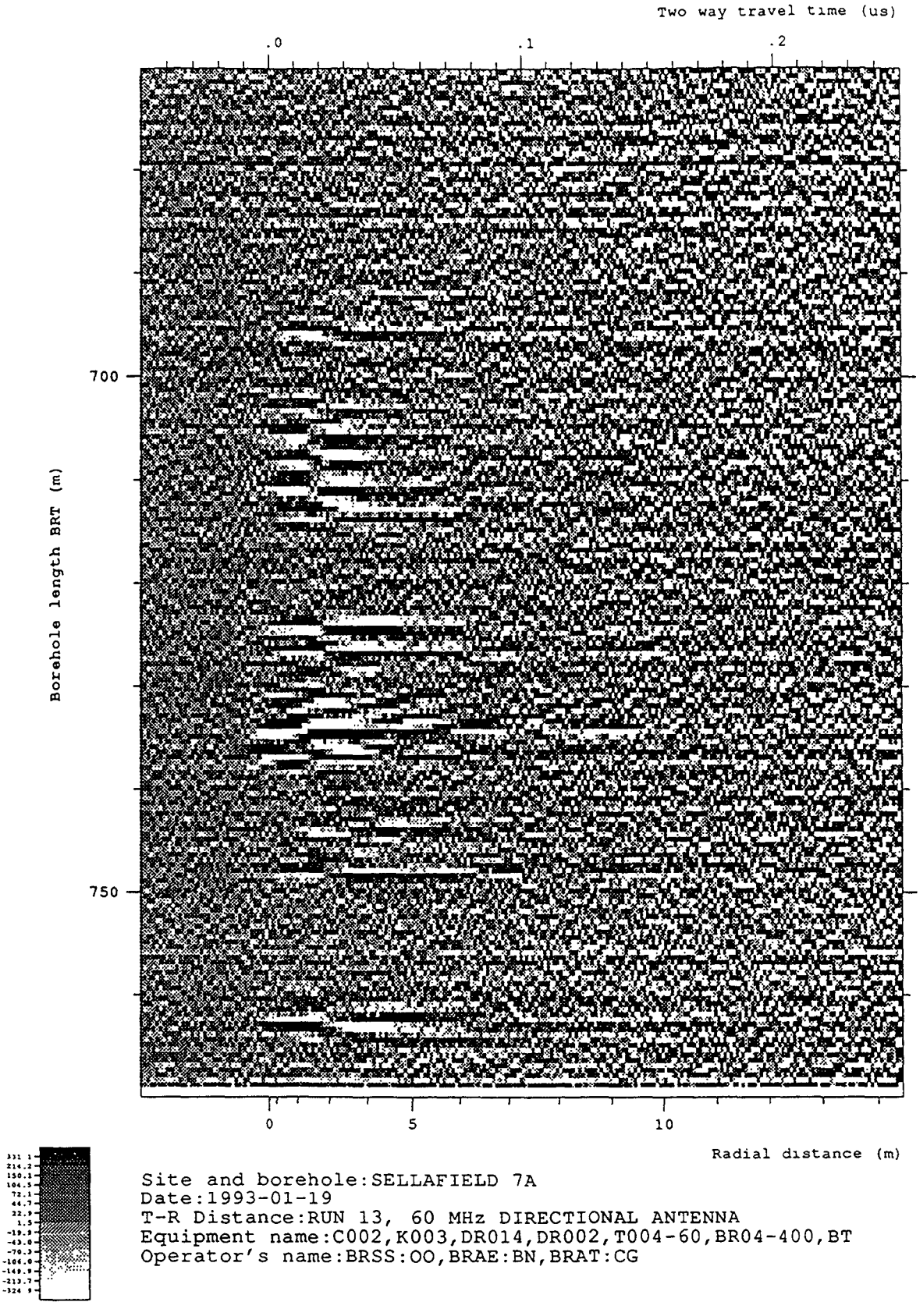

Figure 6-133 Radar map of the moving average filtered dipole component from the 60 MHz directional survey Run 13 (648.80 to 768.80 mbRT) at an azimuth of 180°

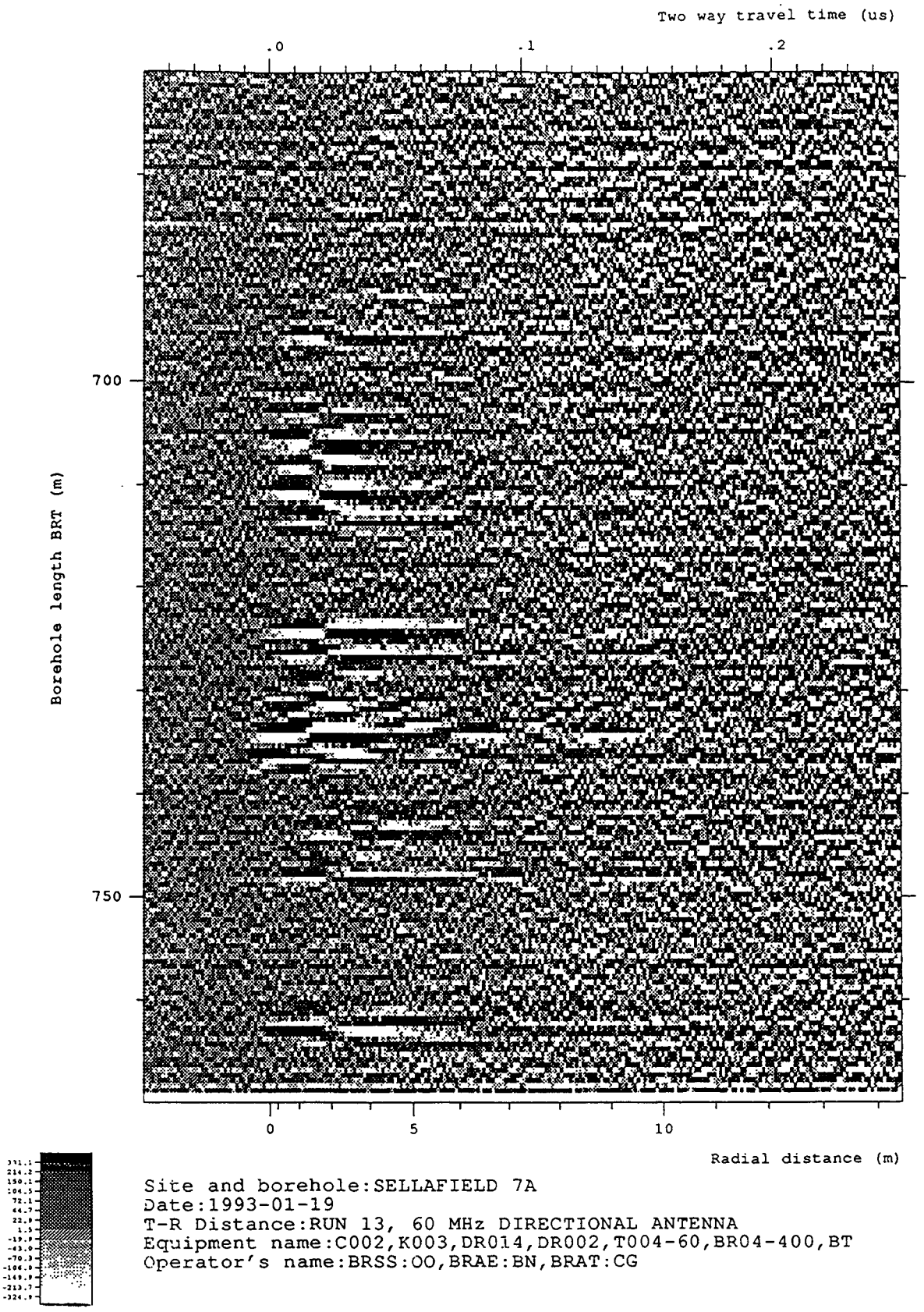

Figure 6-134 Radar map of the moving average filtered dipole component from the 60 MHz directional survey Run 13 (648.80 to 768.80 mbRT) at an azimuth of 190°

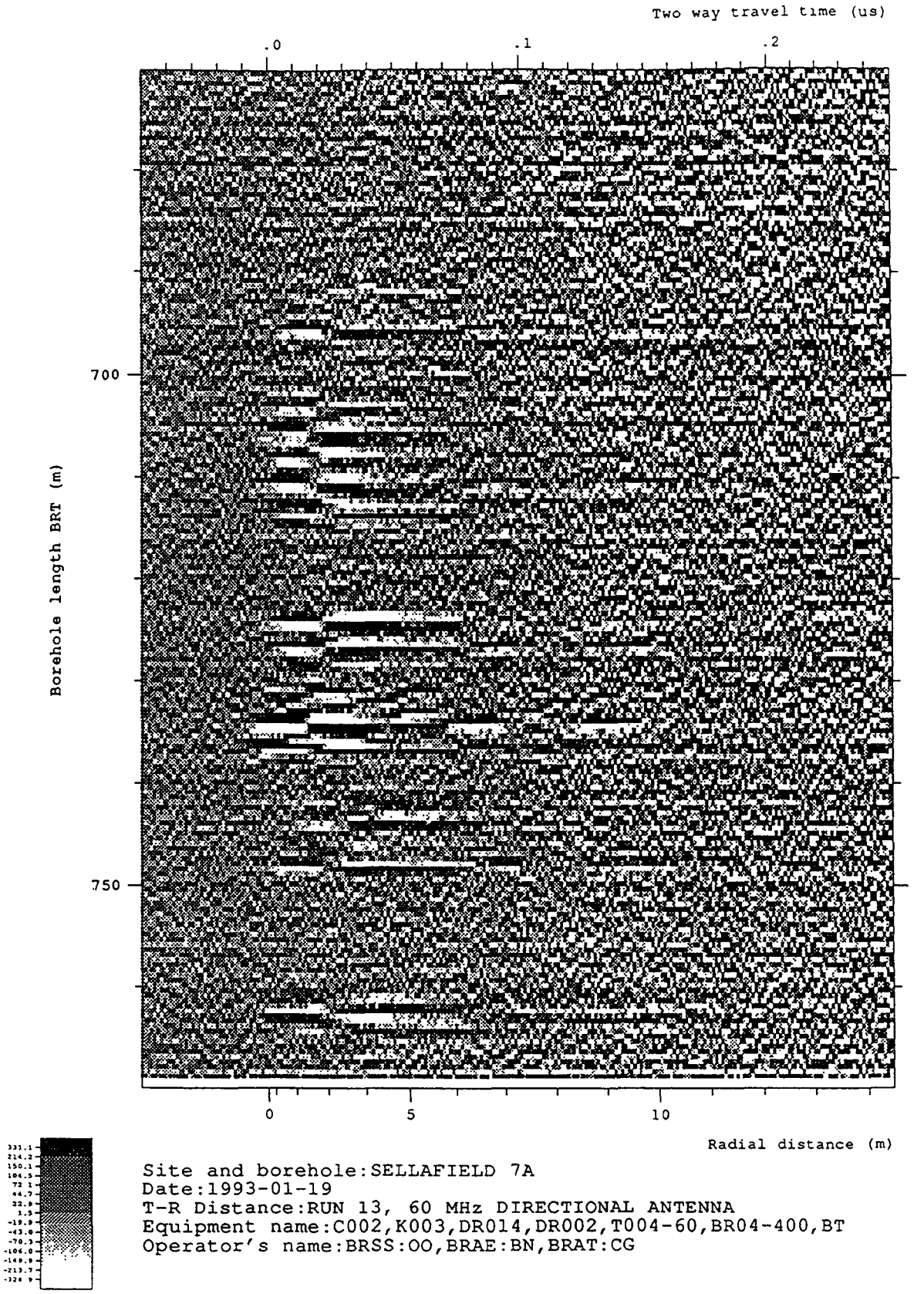

Figure 6-135 Radar map of the moving average filtered dipole component from the 60 MHz directional survey Run 13 (648.80 to 768.80 mbRT) at an azimuth of 200°

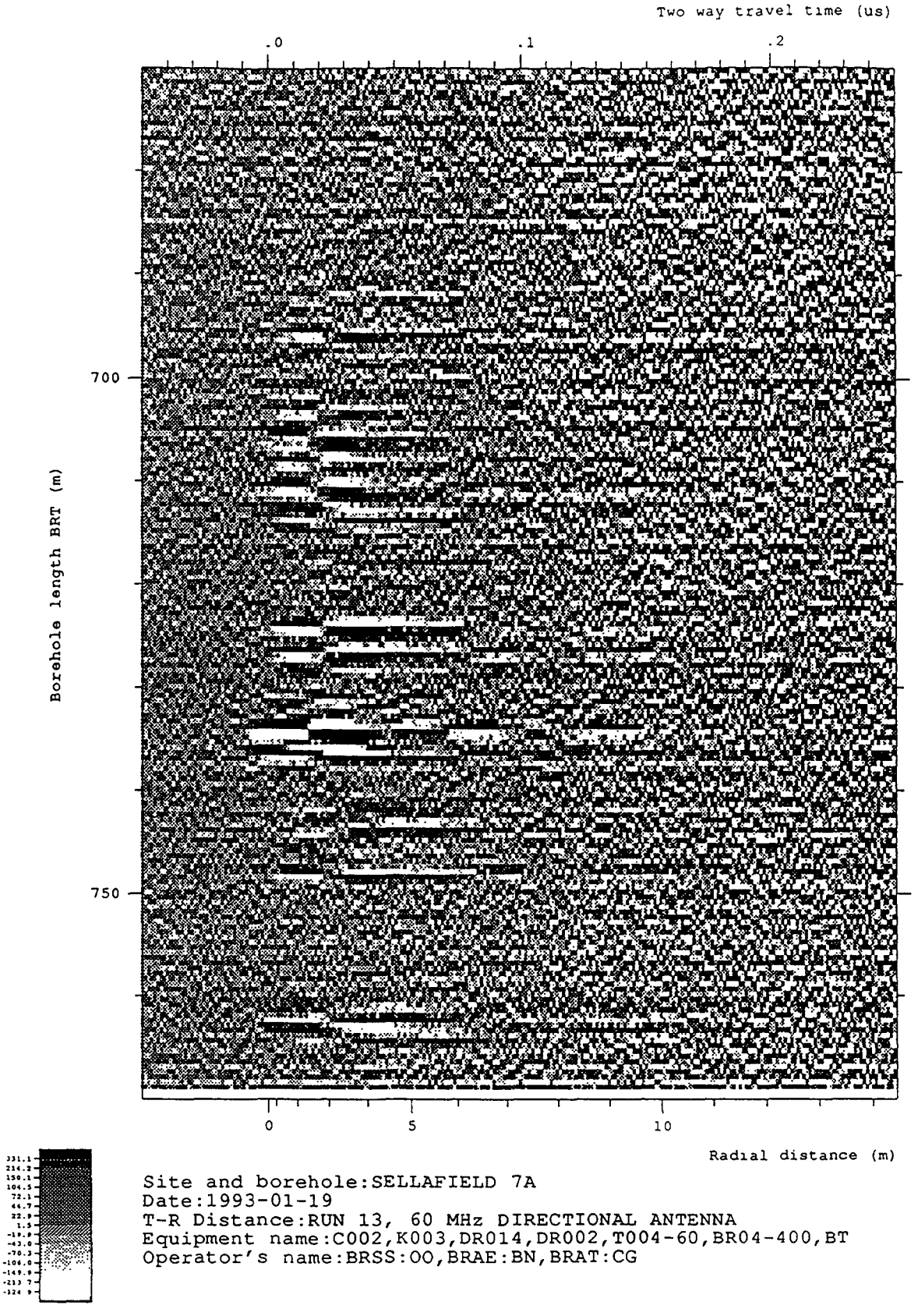

Figure 6-136 Radar map of the moving average filtered dipole component from the 60 MHz directional survey Run 13 (648.80 to 768.80 mbRT) at an azimuth of 210°

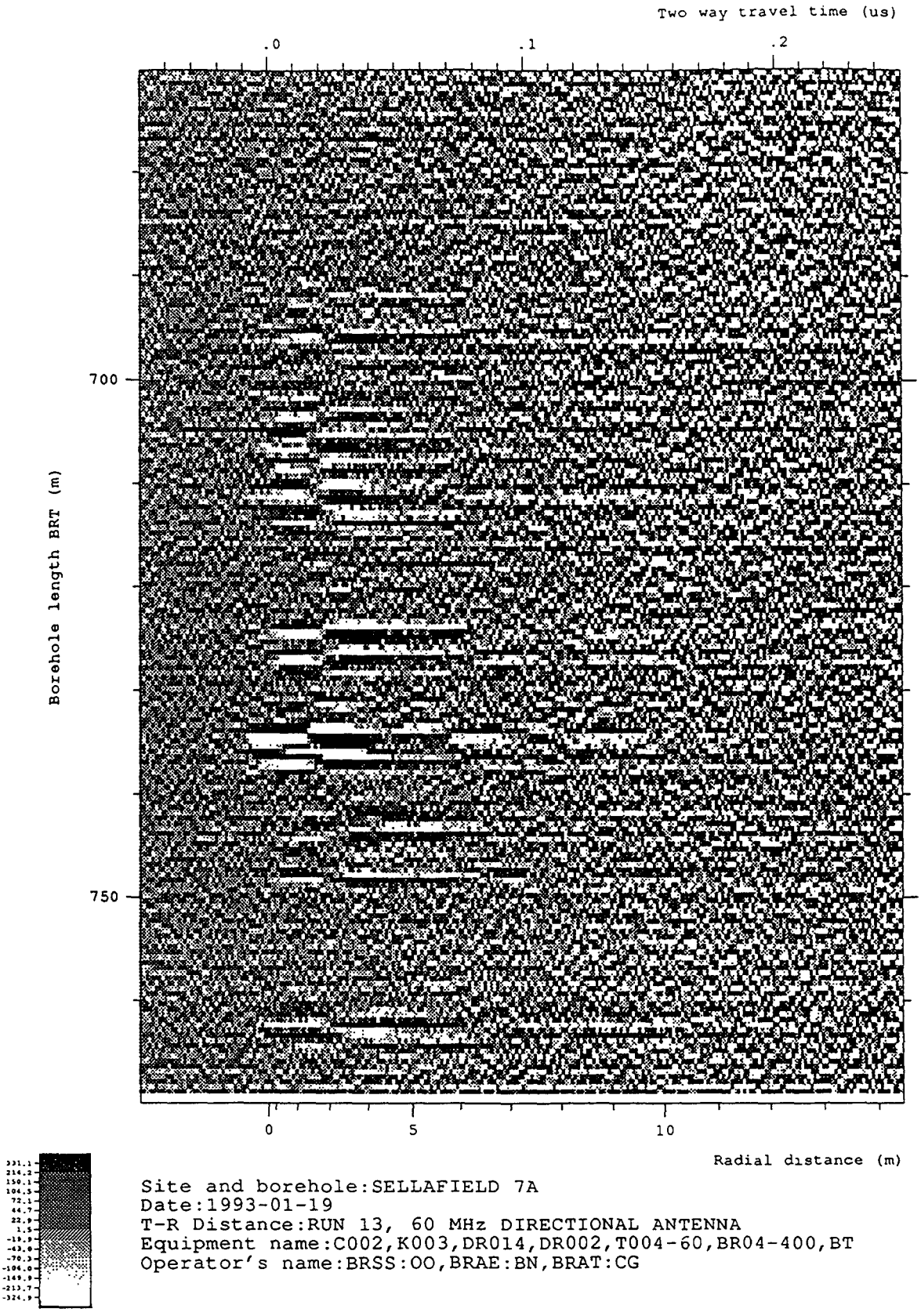

Figure 6-137 Radar map of the moving average filtered dipole component from the 60 MHz directional survey Run 13 (648.80 to 768.80 mbRT) at an azimuth of 220°

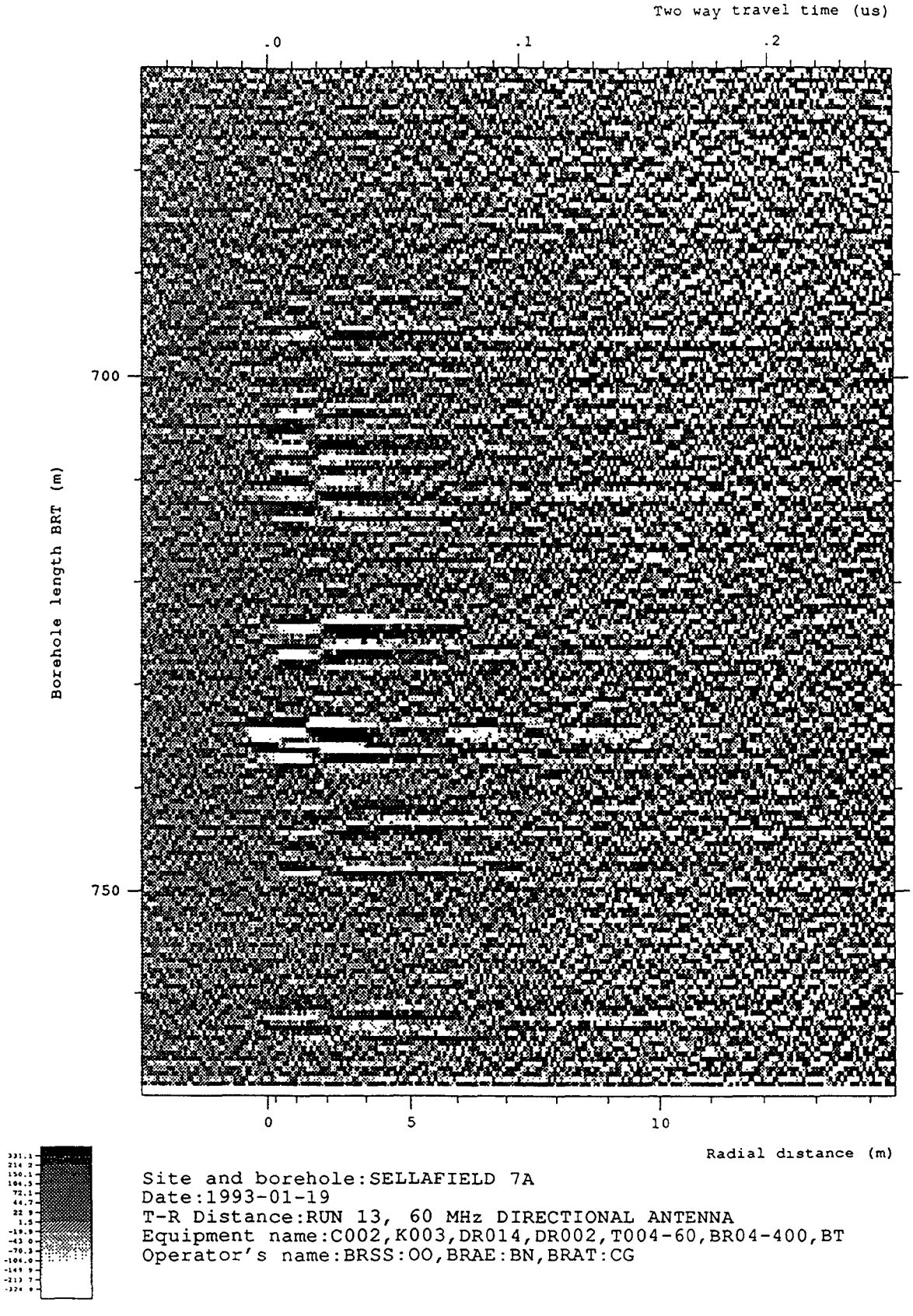

Figure 6-138 Radar map of the moving average filtered dipole component from the 60 MHz directional survey Run 13 (648.80 to 768.80 mbRT) at an azimuth of 230°

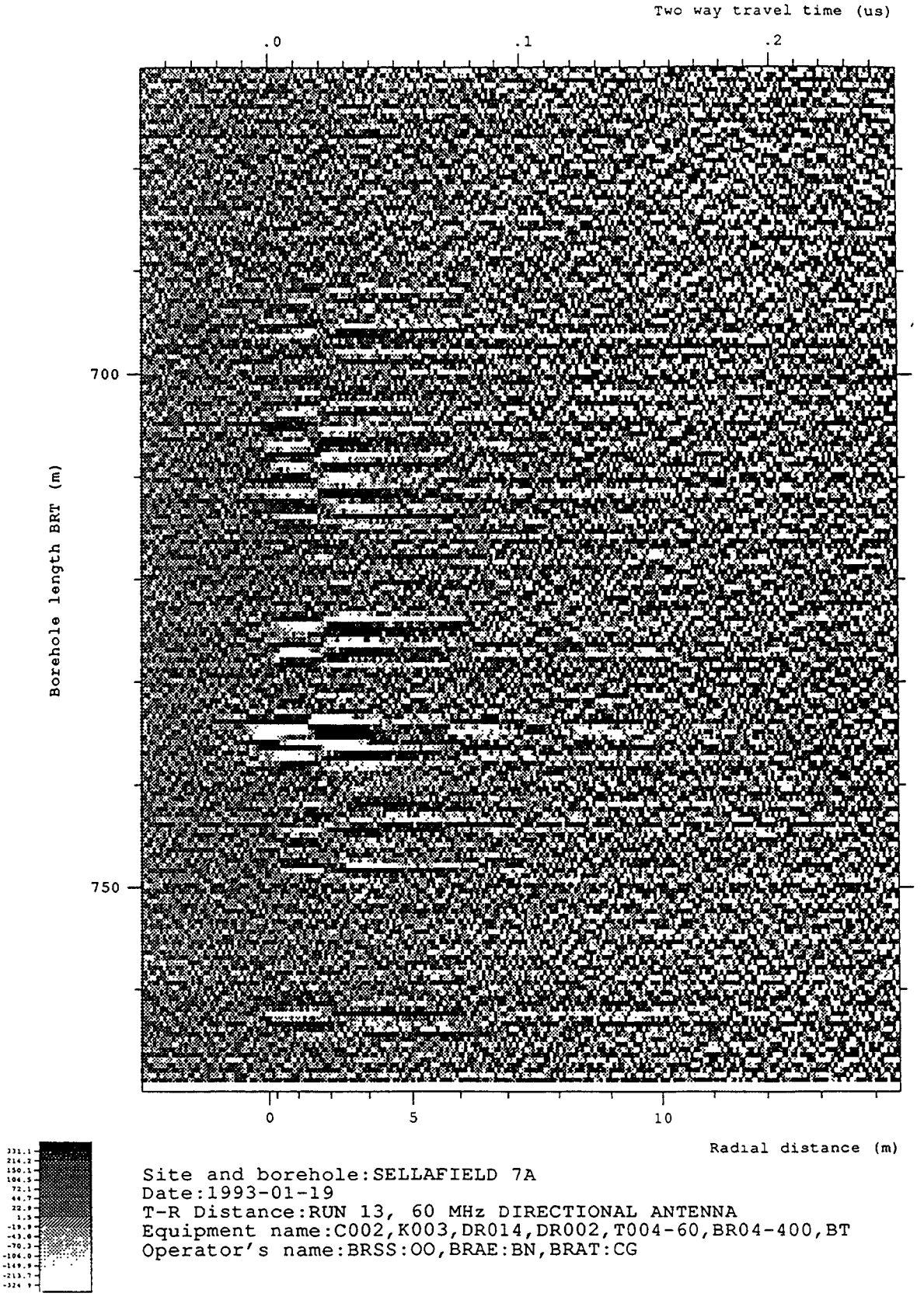

Figure 6-139 Radar map of the moving average filtered dipole component from the 60 MHz directional survey Run 13 (648.80 to 768.80 mbRT) at an azimuth of 240°

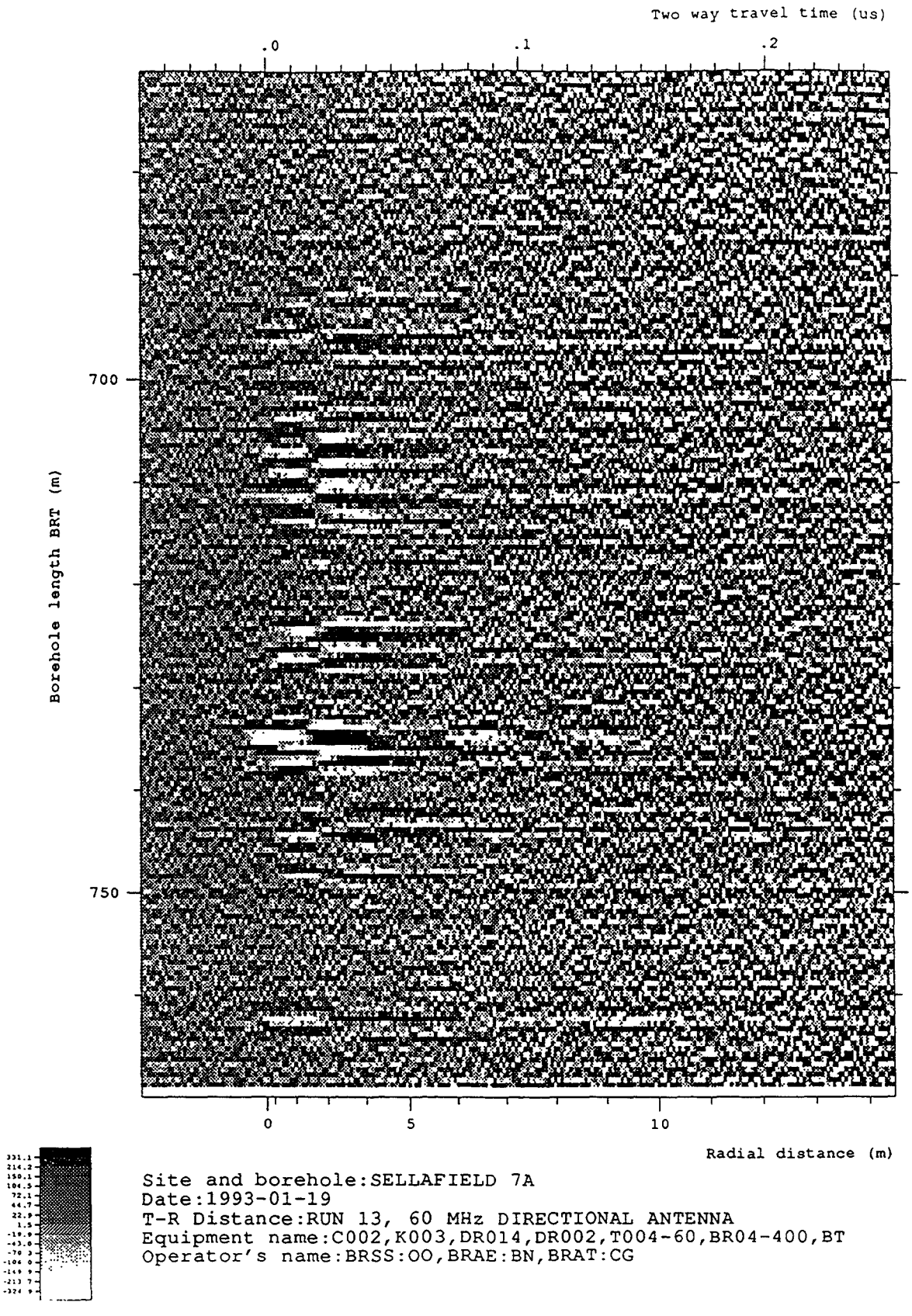

Figure 6-140 Radar map of the moving average filtered dipole component from the 60 MHz directional survey Run 13 (648.80 to 768.80 mbRT) at an azimuth of 250°

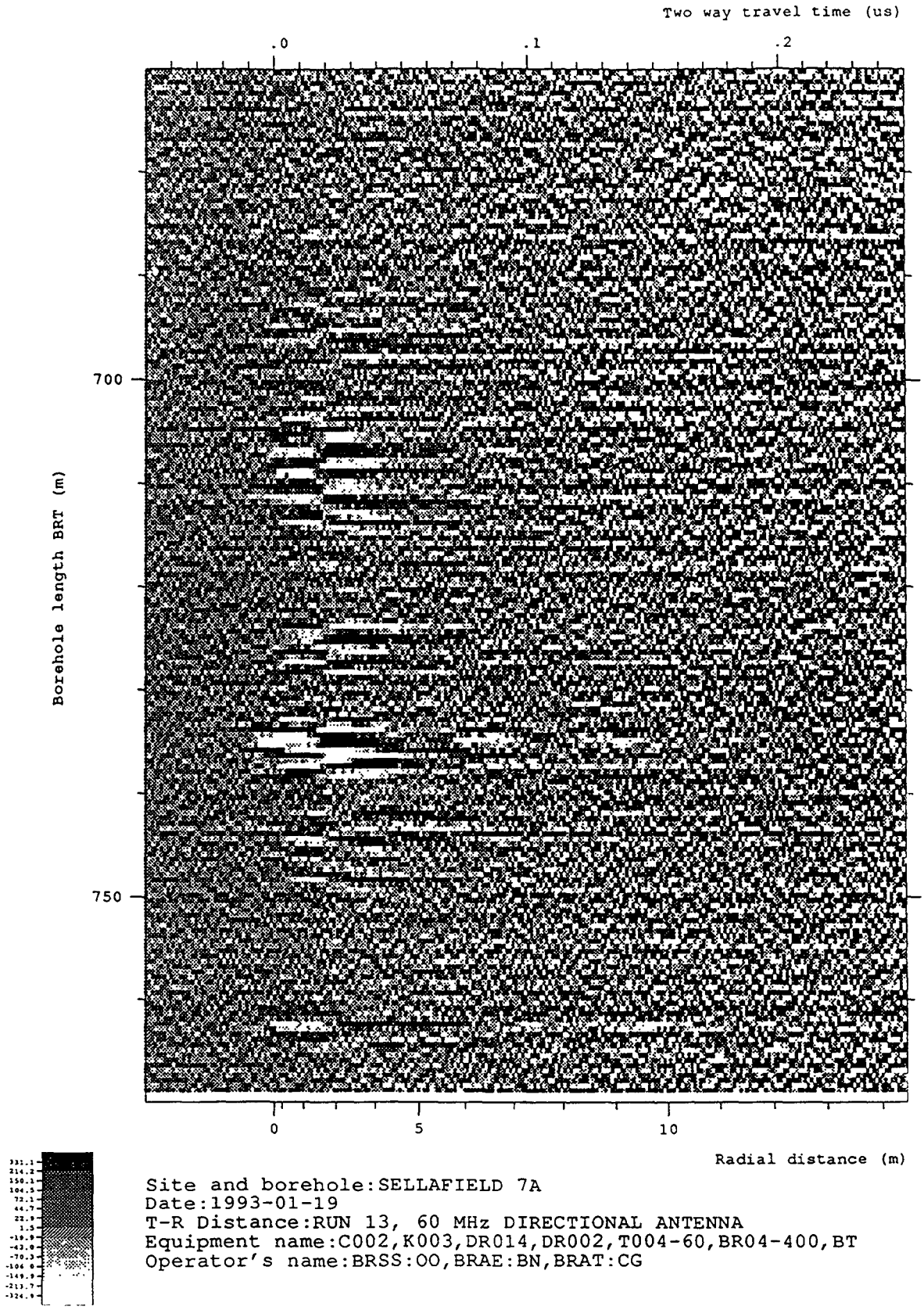

Figure 6-141 Radar map of the moving average filtered dipole component from the 60 MHz directional survey Run 13 (648.80 to 768.80 mbRT) at an azimuth of 260°

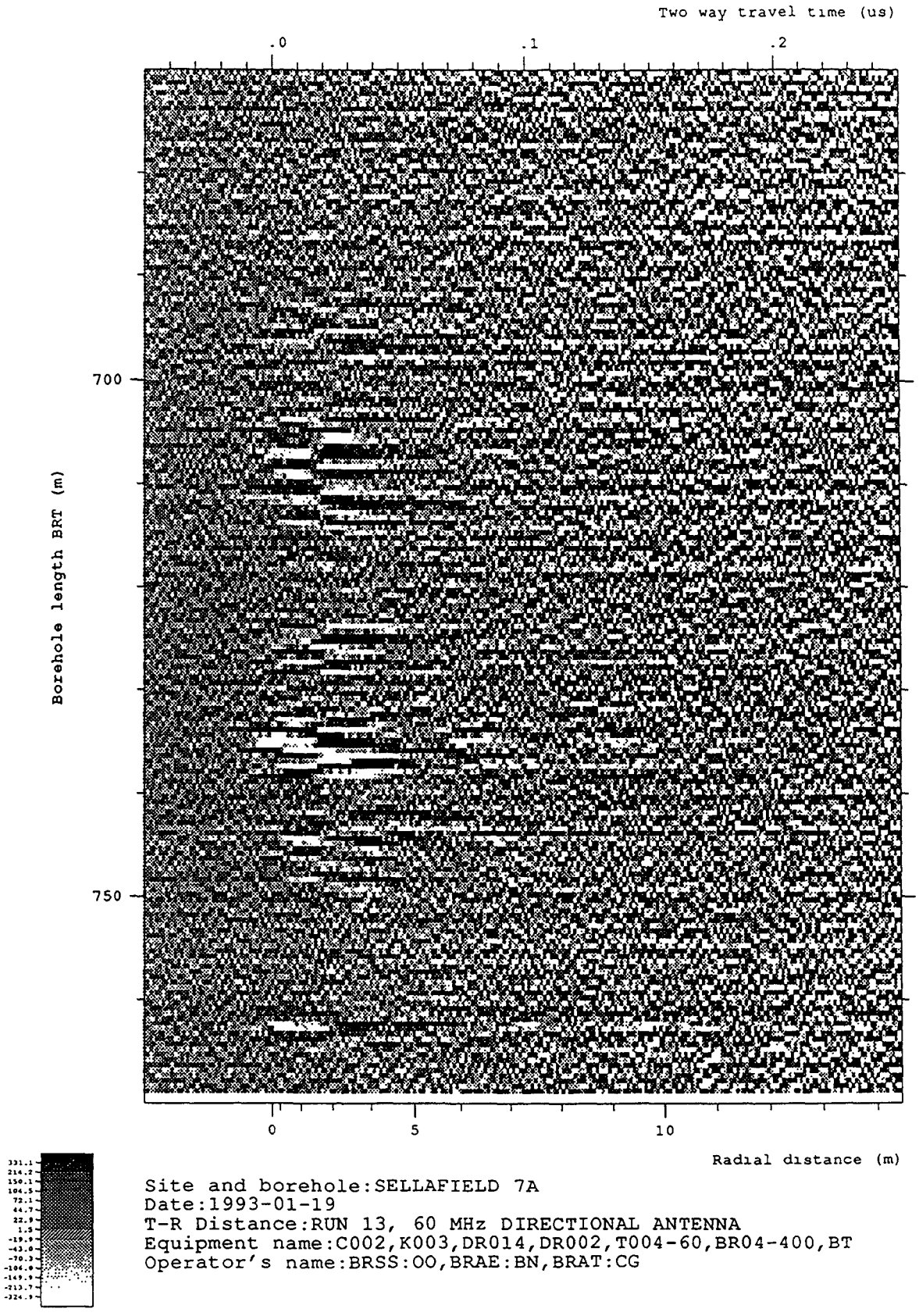

Figure 6-142 Radar map of the moving average filtered dipole component from the 60 MHz directional survey Run 13 (648.80 to 768.80 mbRT) at an azimuth of 270°

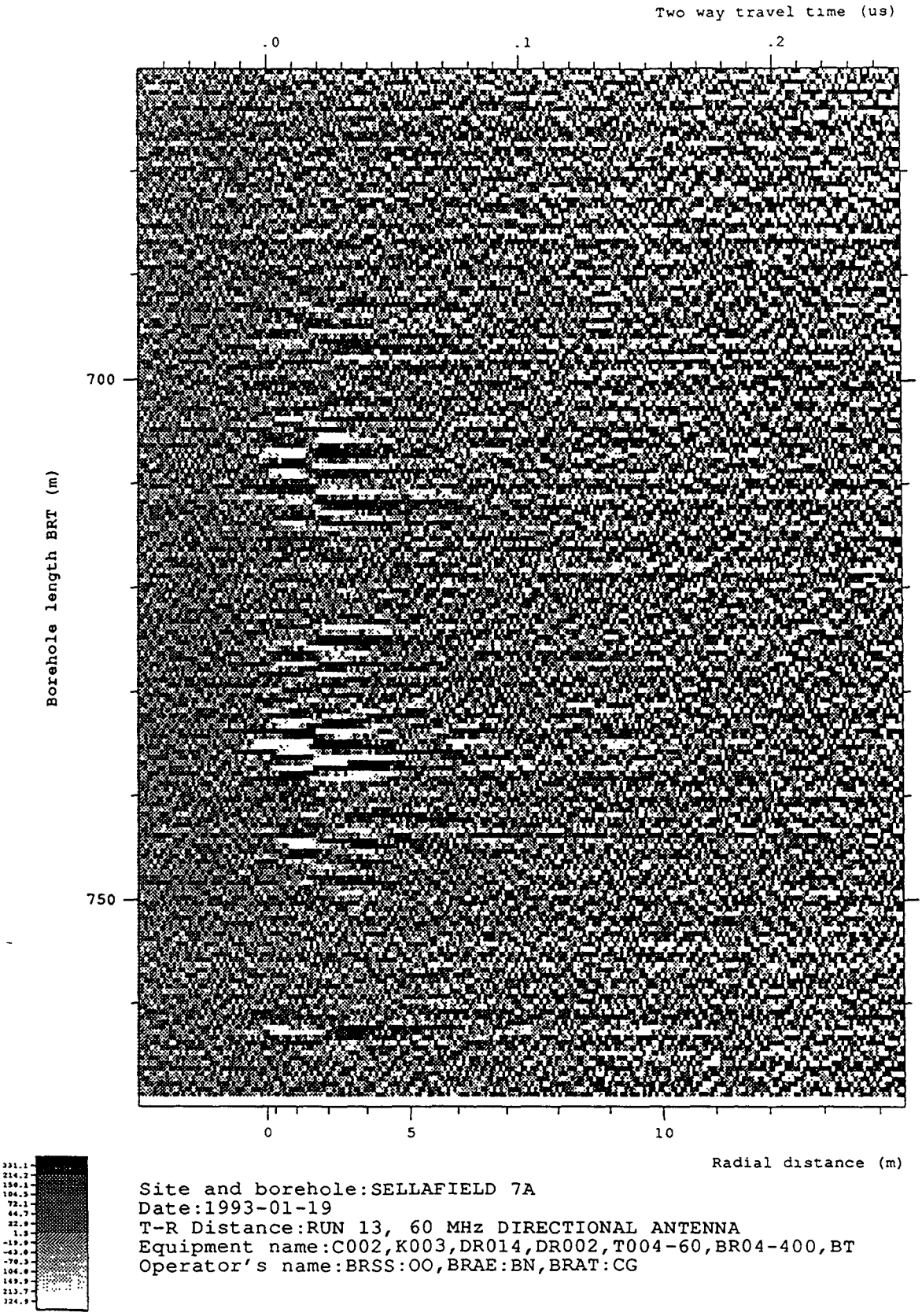

Figure 6-143 Radar map of the moving average filtered dipole component from the 60 MHz directional survey Run 13 (648.80 to 768.80 mbRT) at an azimuth of 280°

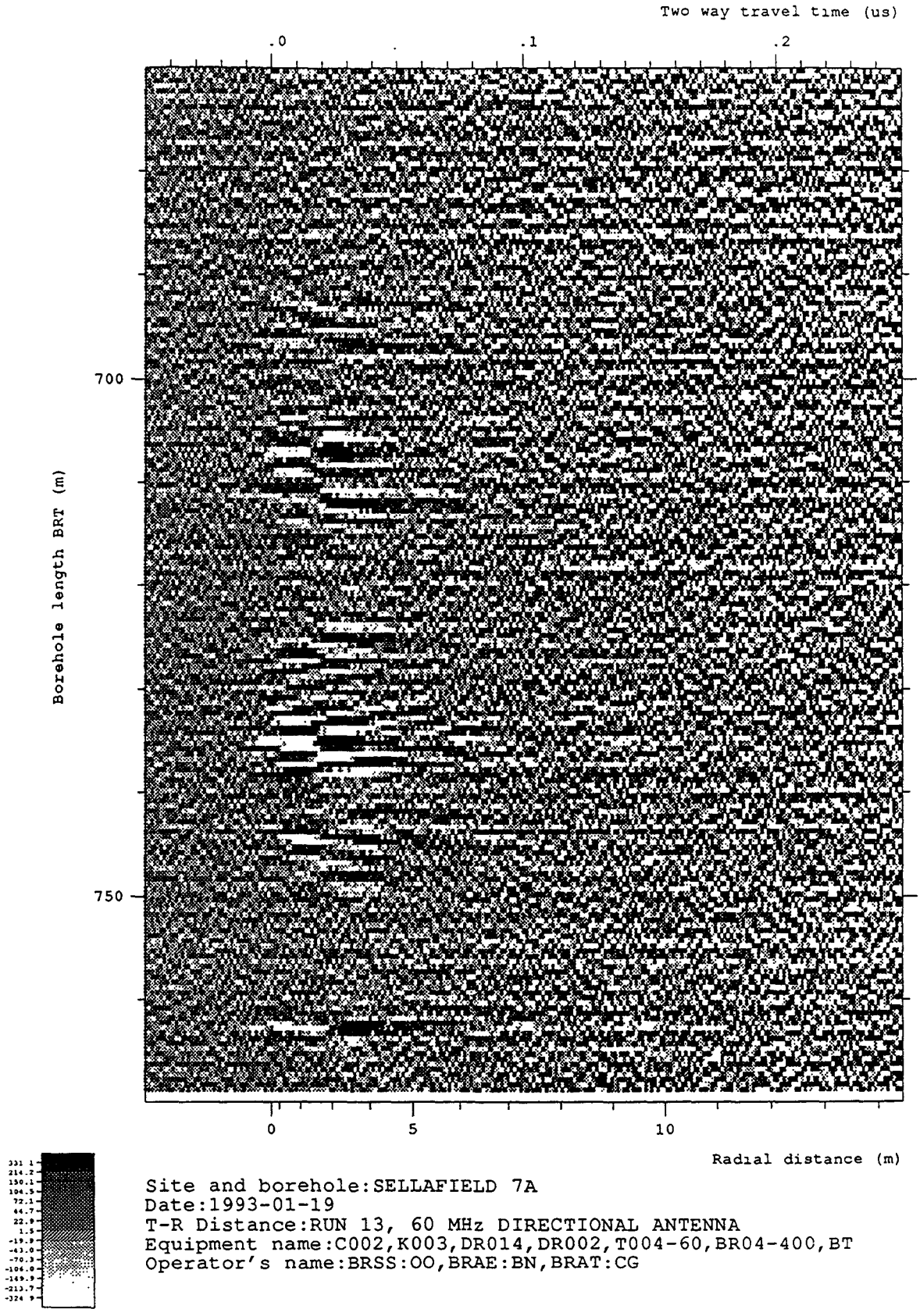

Figure 6-144 Radar map of the moving average filtered dipole component from the 60 MHz directional survey Run 13 (648.80 to 768.80 mbRT) at an azimuth of 290°

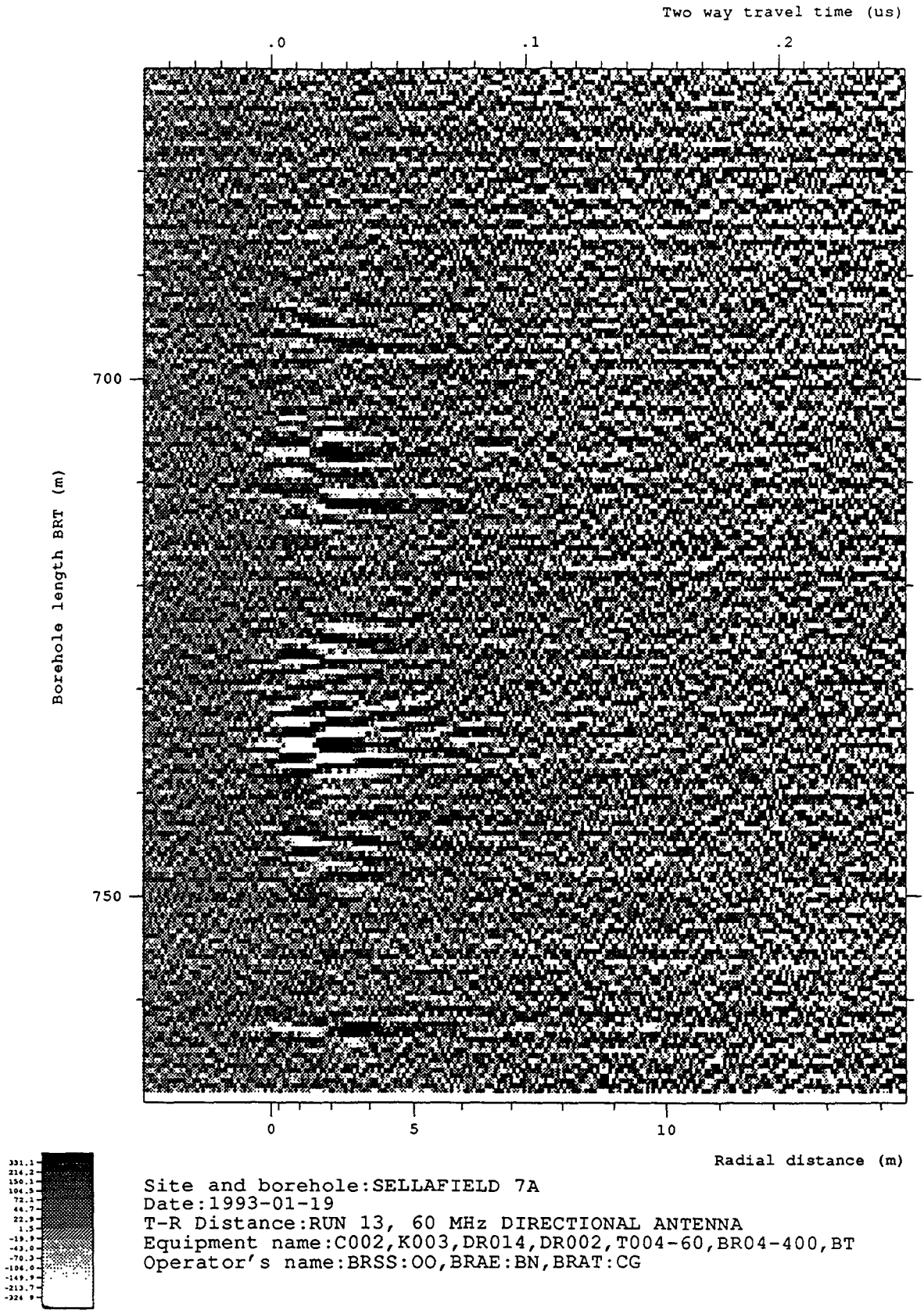

Figure 6-145 Radar map of the moving average filtered dipole component from the 60 MHz directional survey Run 13 (648.80 to 768.80 mbRT) at an azimuth of 300°

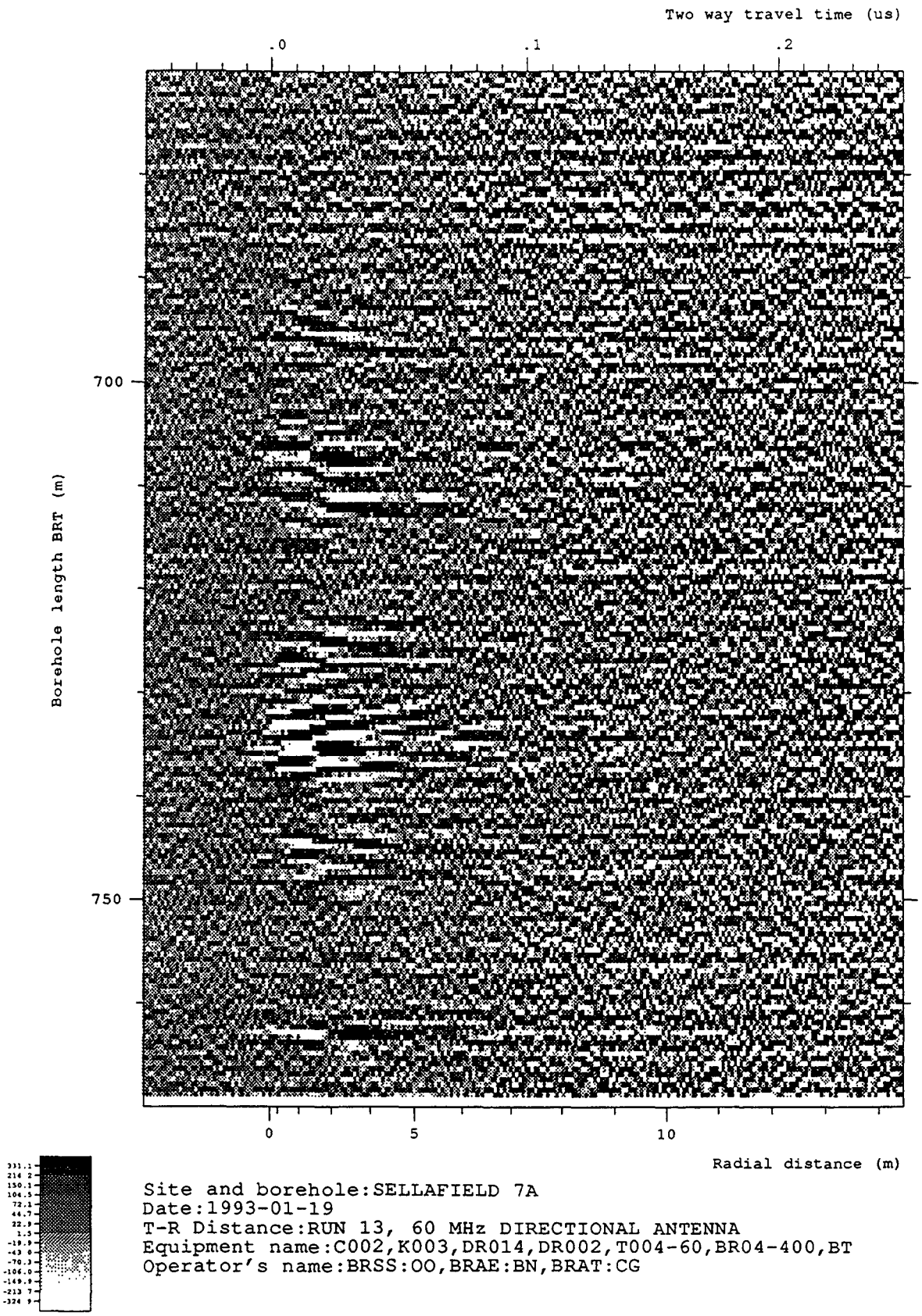

Figure 6-146 Radar map of the moving average filtered dipole component from the 60 MHz directional survey Run 13 (648.80 to 768.80 mbRT) at an azimuth of 310°

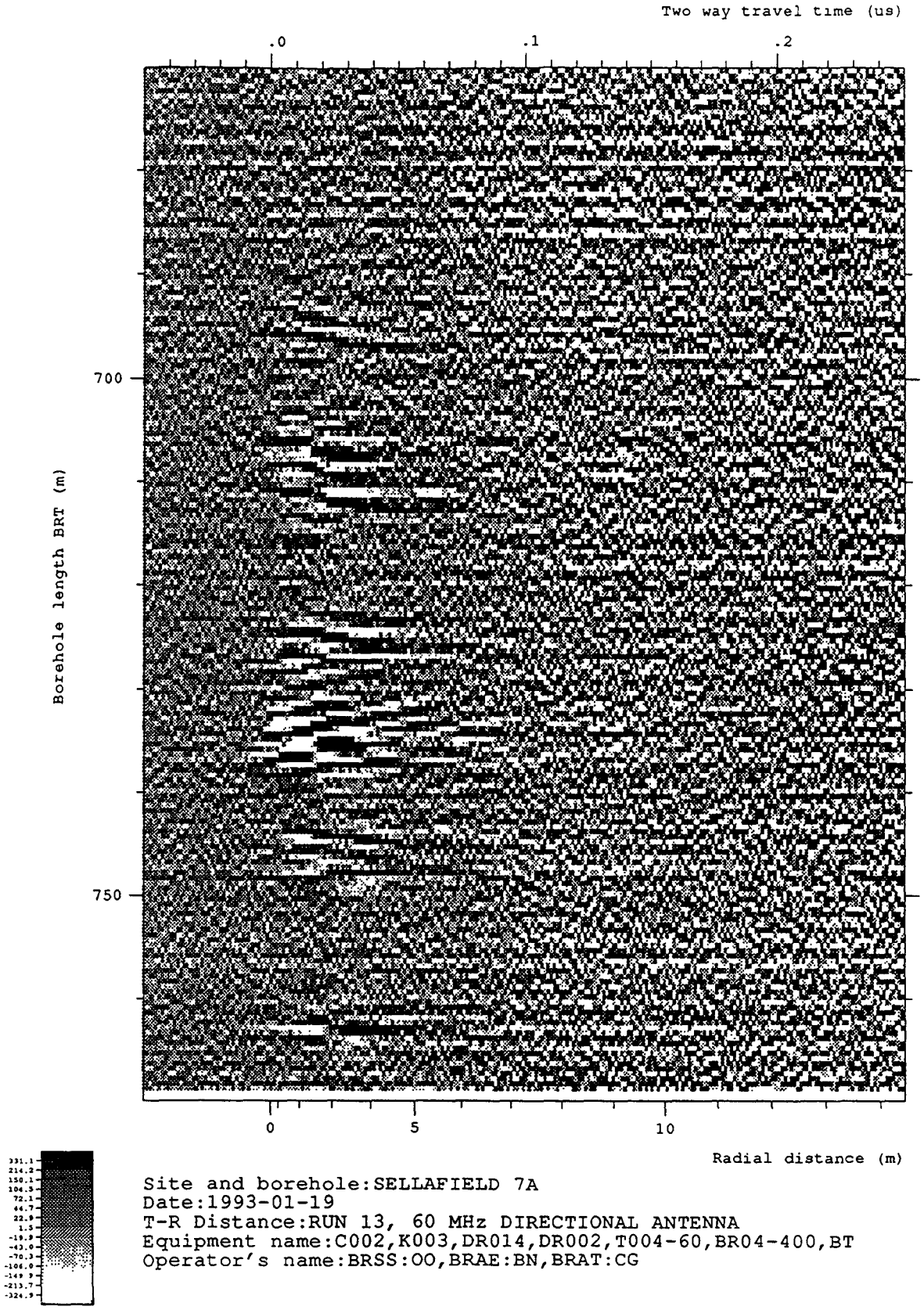

Figure 6-147 Radar map of the moving average filtered dipole component from the 60 MHz directional survey Run 13 (648.80 to 768.80 mbRT) at an azimuth of 320°

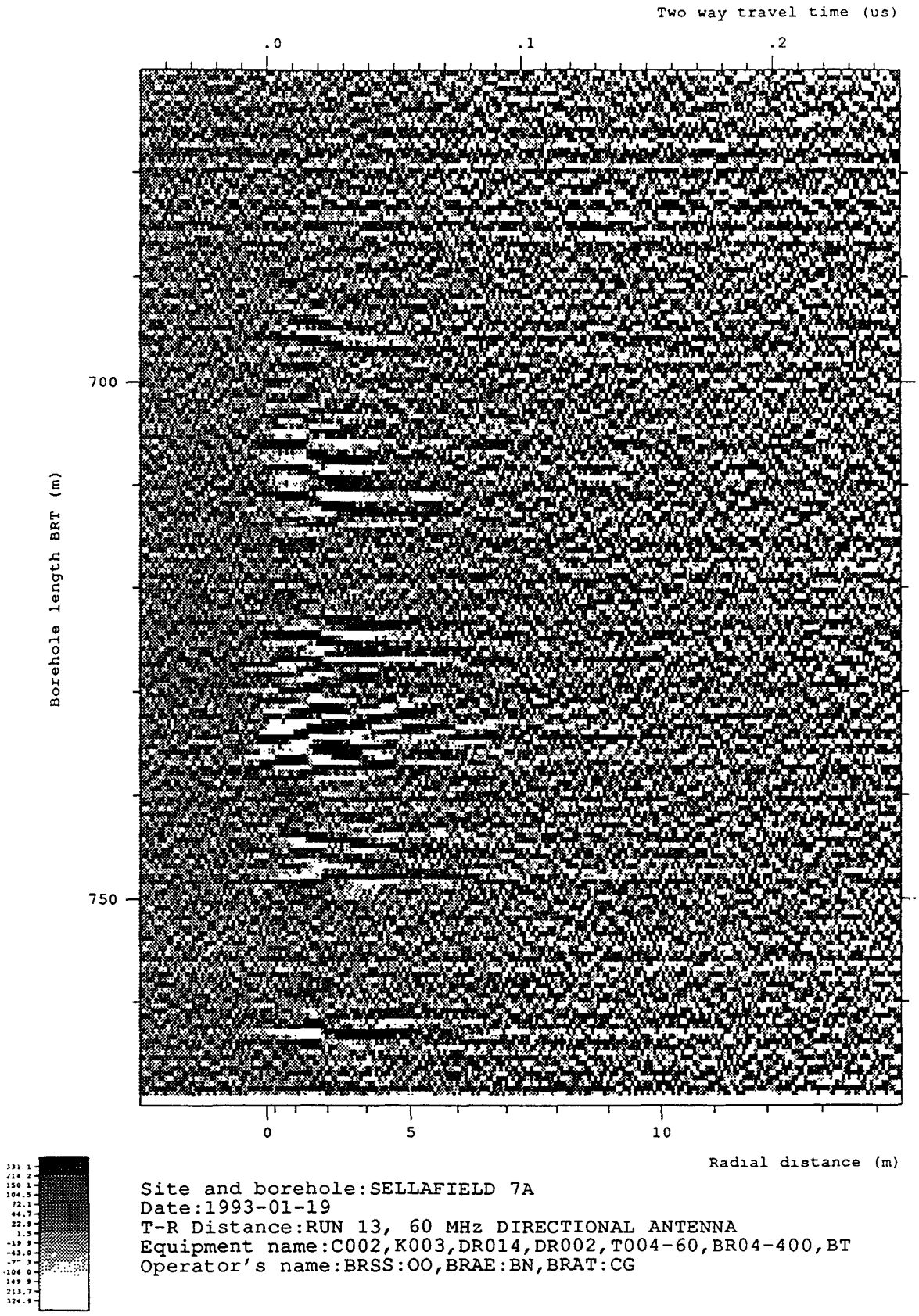

Figure 6-148 Radar map of the moving average filtered dipole component from the 60 MHz directional survey Run 13 (648.80 to 768.80 mbRT) at an azimuth of 330°

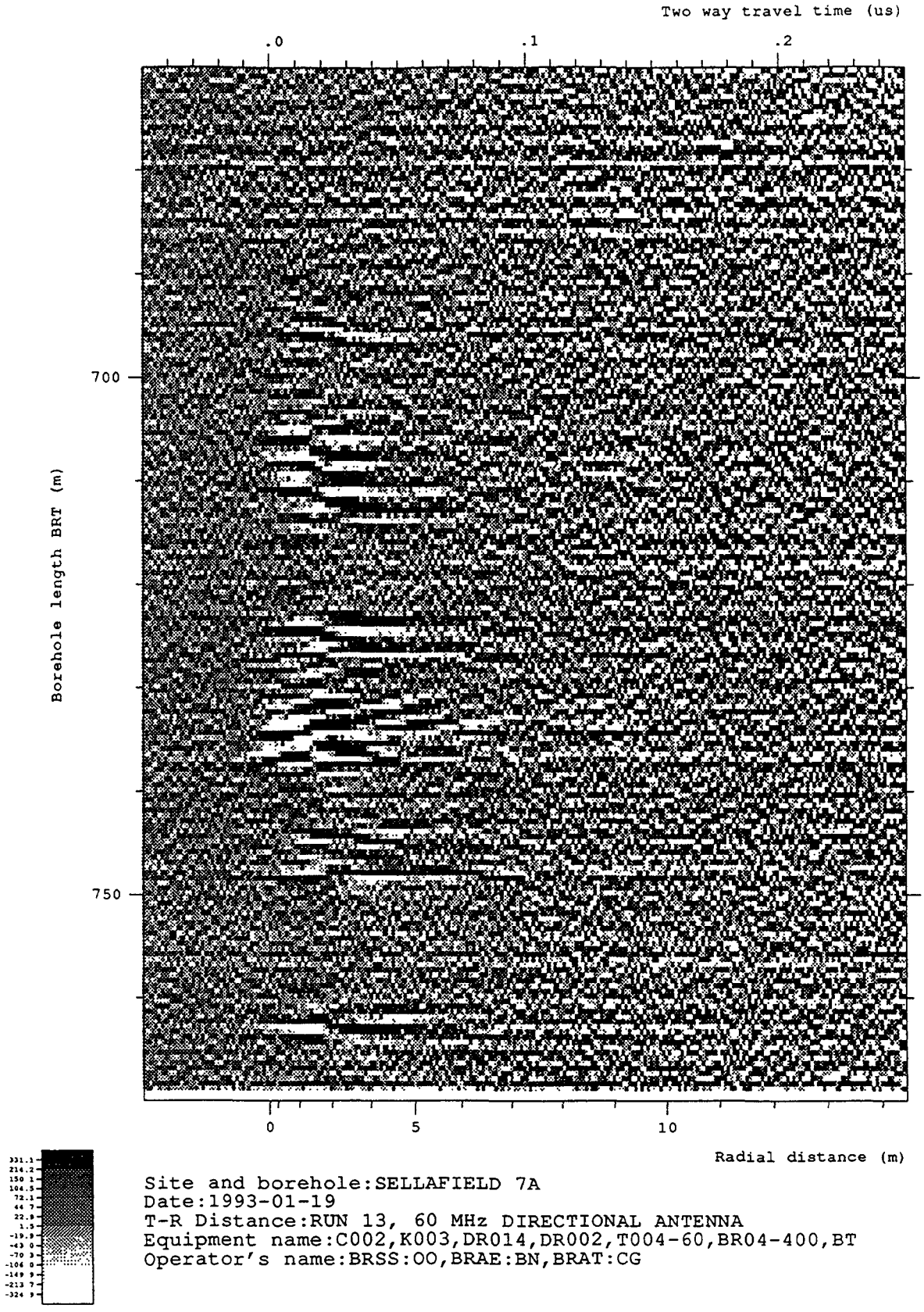

Figure 6-149 Radar map of the moving average filtered dipole component from the 60 MHz directional survey Run 13 (648.80 to 768.80 mbRT) at an azimuth of 340°

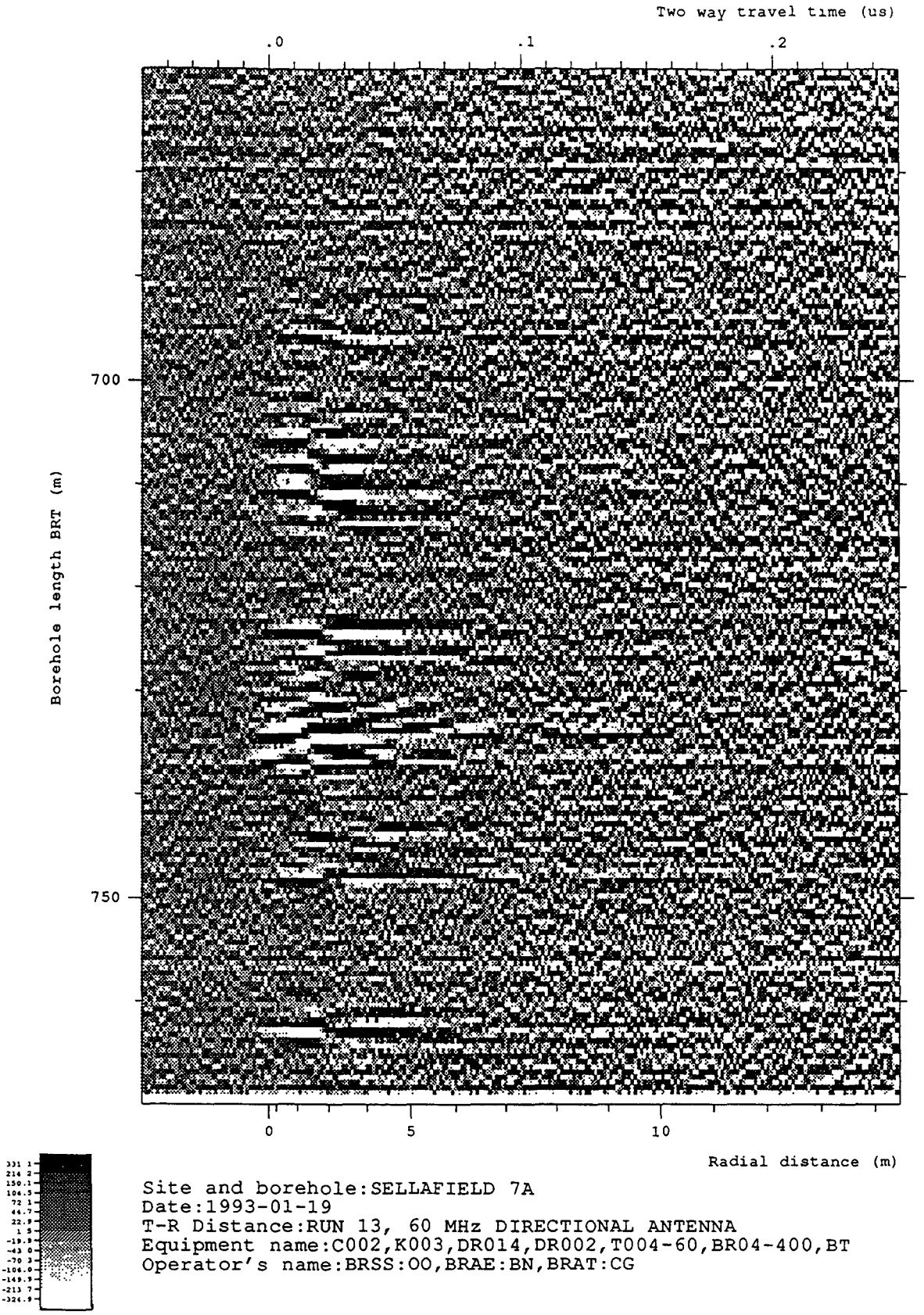

Figure 6-150 Radar map of the moving average filtered dipole component from the 60 MHz directional survey Run 13 (648.80 to 768.80 mbRT) at an azimuth of 350°

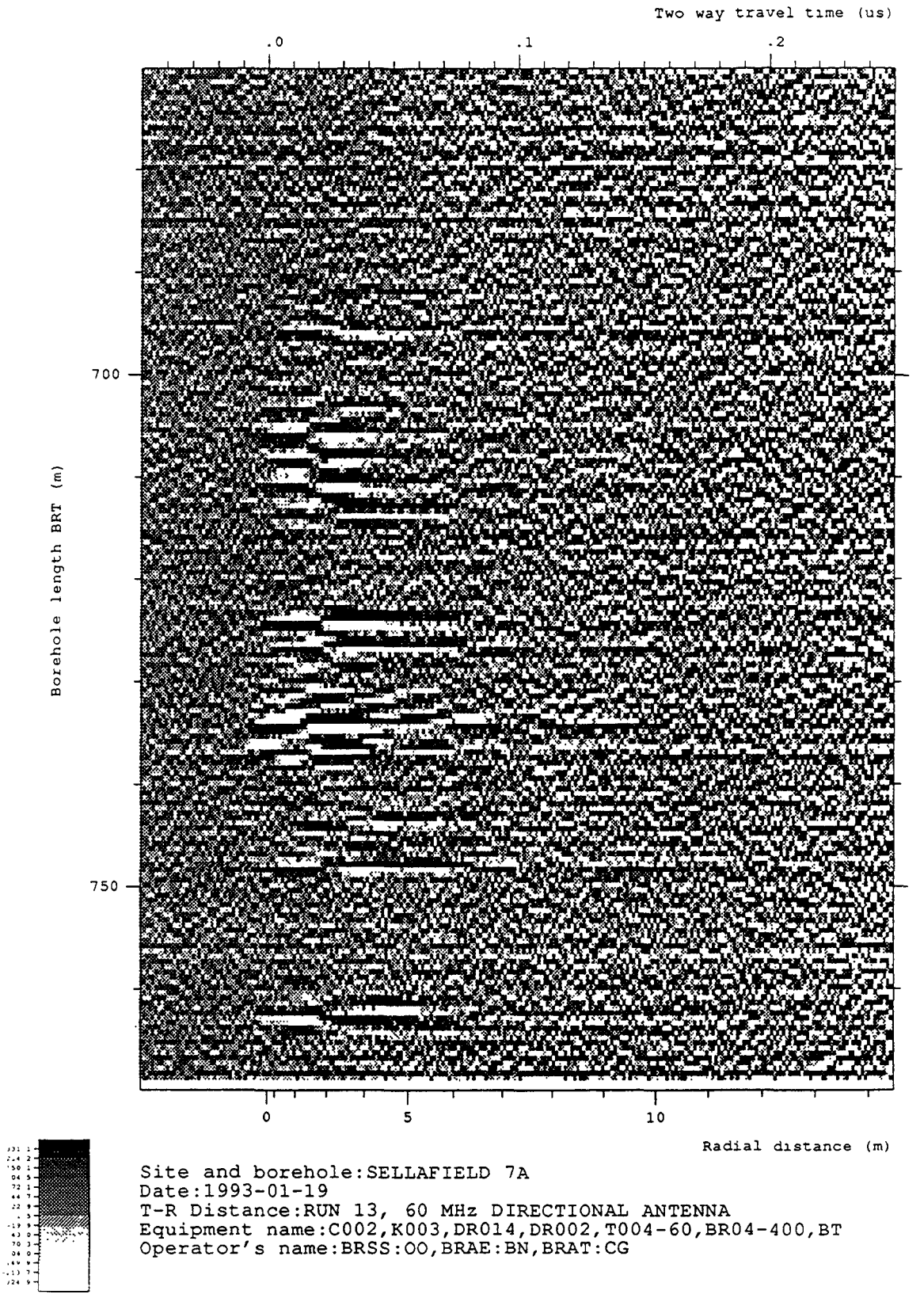

Figure 6-151 Radar map of the moving average filtered dipole component from the 60 MHz directional survey Run 13 (648.80 to 768.80 mbRT) at an azimuth of 360°

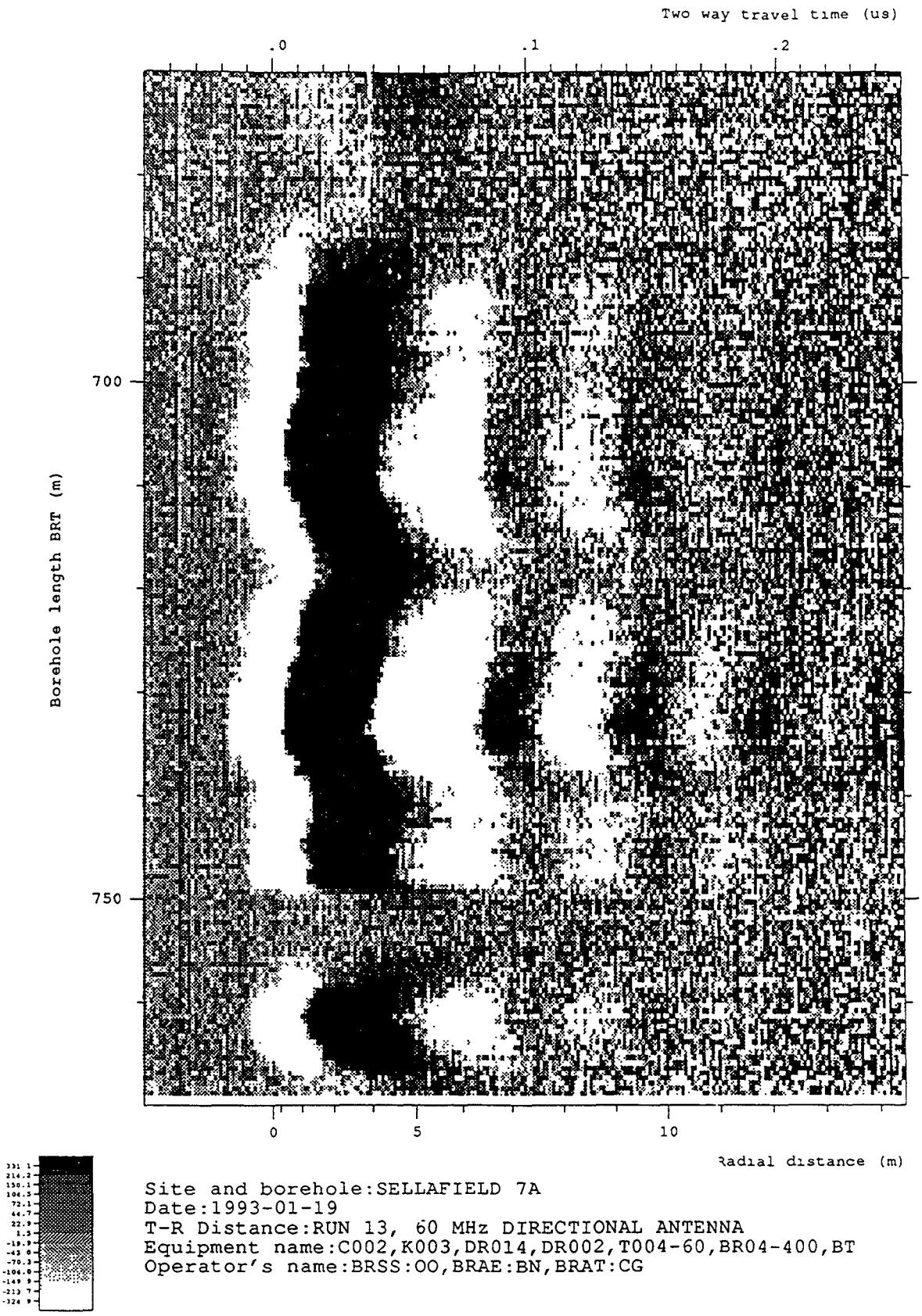

Figure 6-152 Radar map of the unfiltered dipole component from the 60 MHz directional survey Run 13 (648.80 to 768.80 mbRT) at an azimuth of 0°

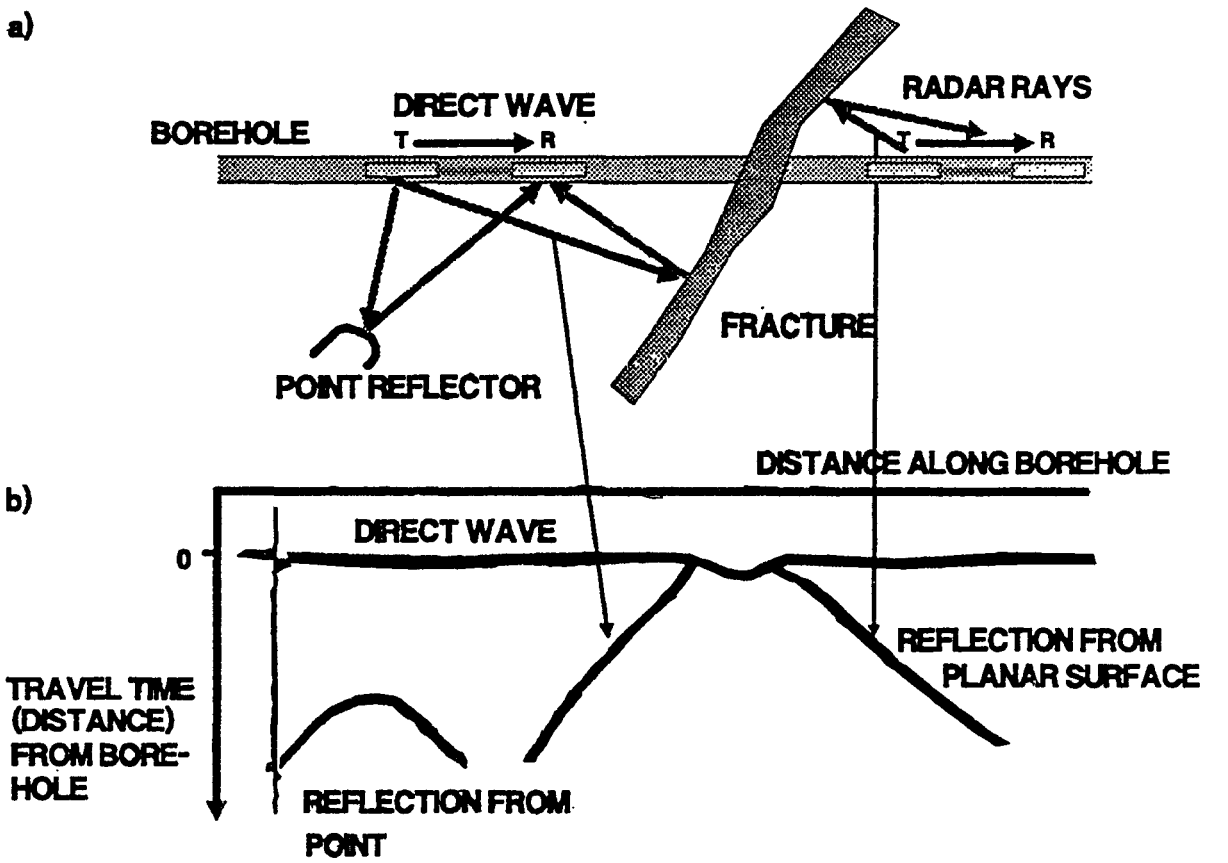

Figure 6-153 (a) Principle of single hole reflection radar measurements and (b) the characteristic patterns generated by plane and point reflectors

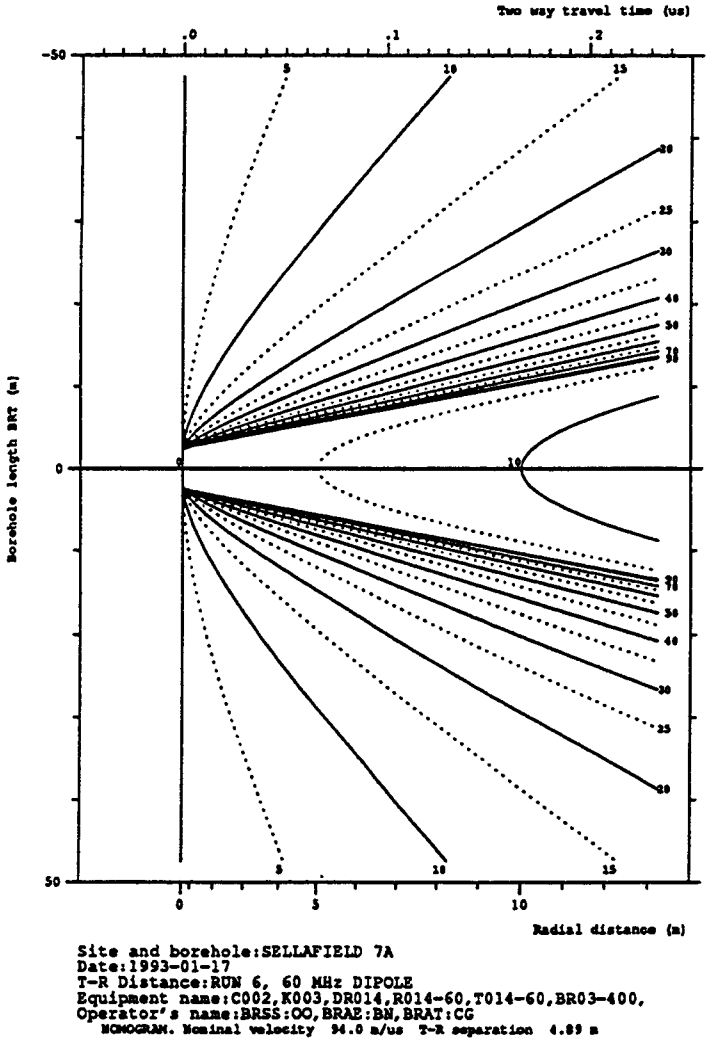

Figure 6-154 Nomogram for planar and point reflectors used to determine angle of intersection and distance to point reflectors

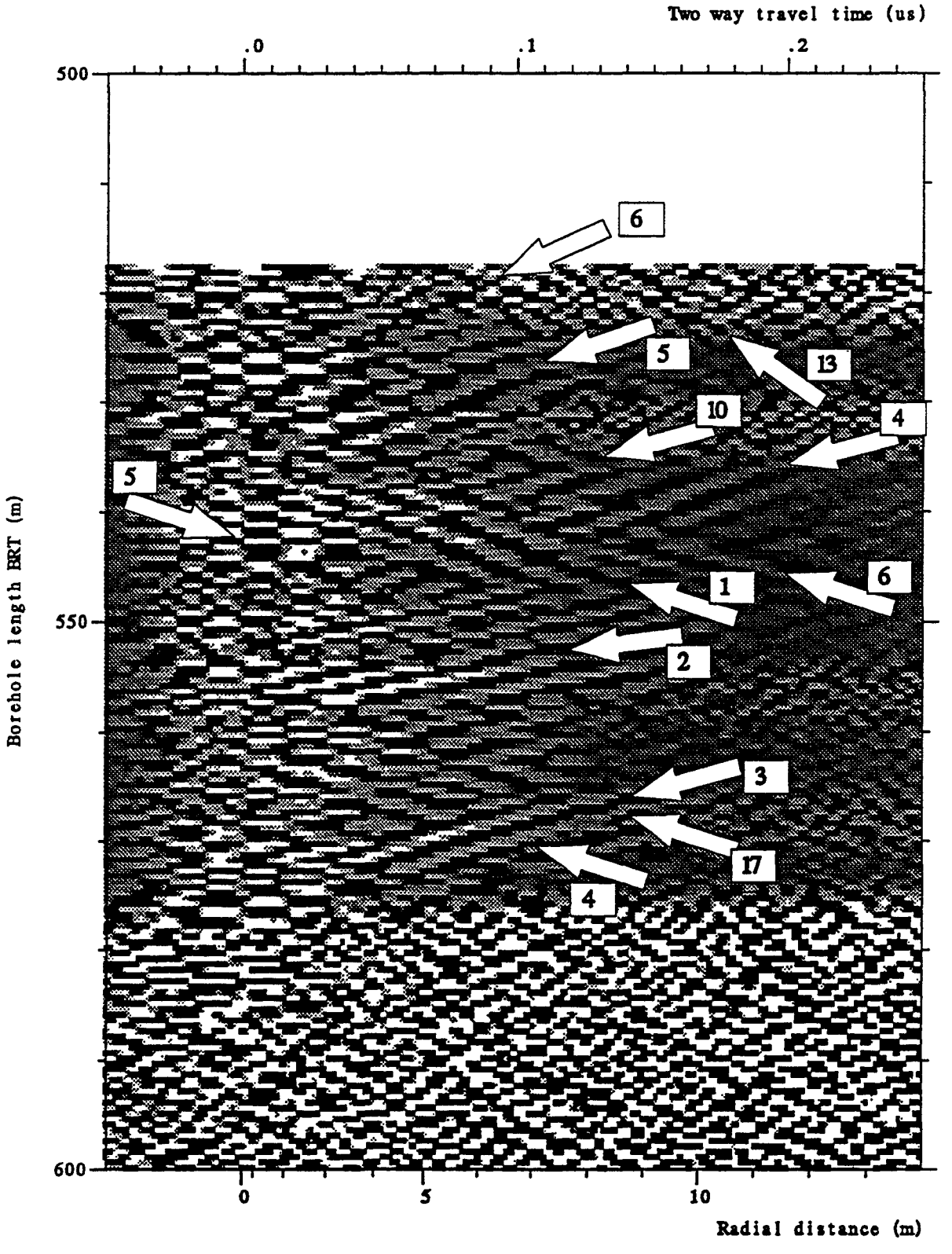

Figure 6-155 Radar reflectors identified in the interval 518.80 to 600.00 mbRT

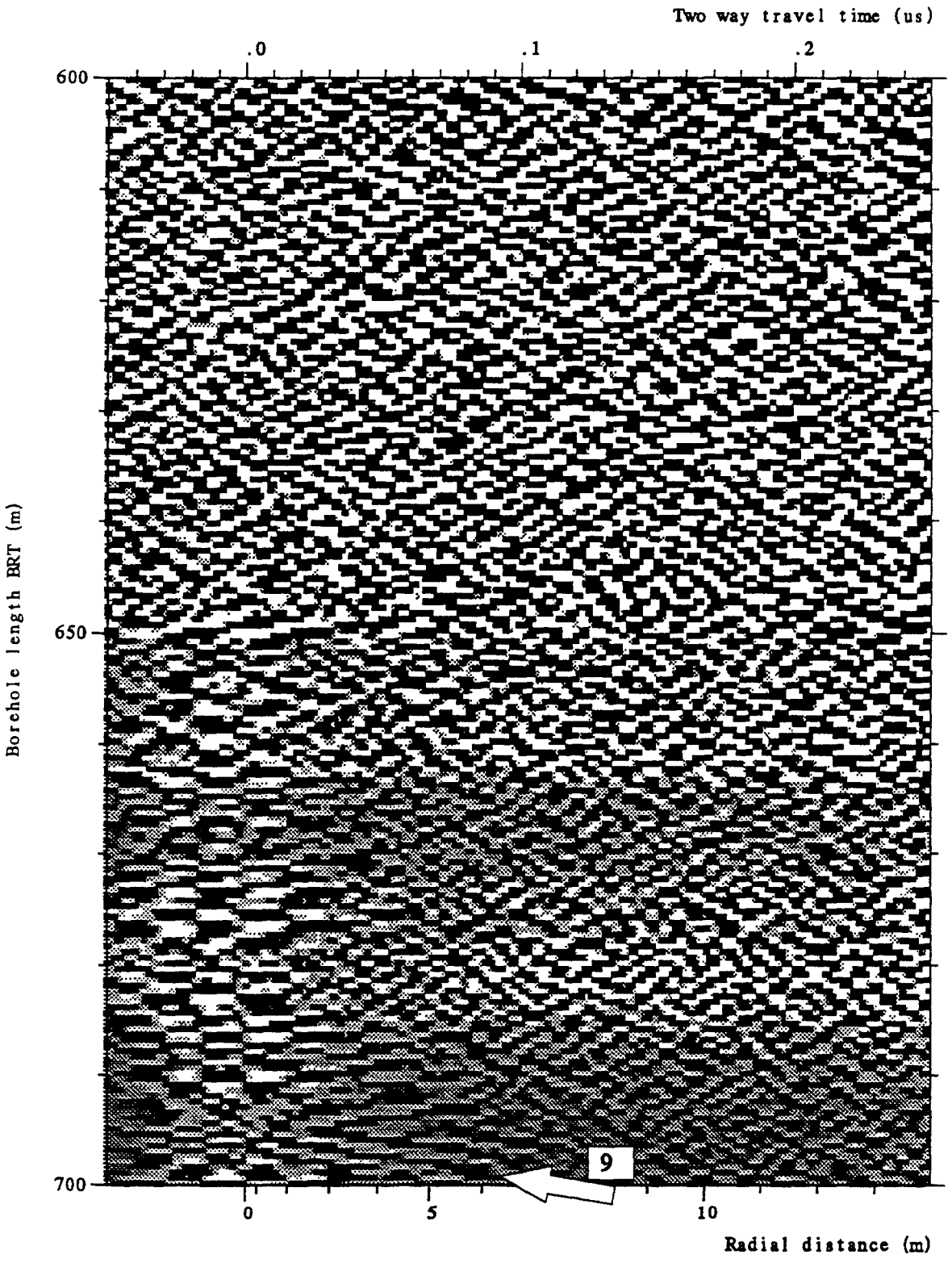

Figure 6-156 Radar reflectors identified in the interval 600.00 to 700.00 mbRT

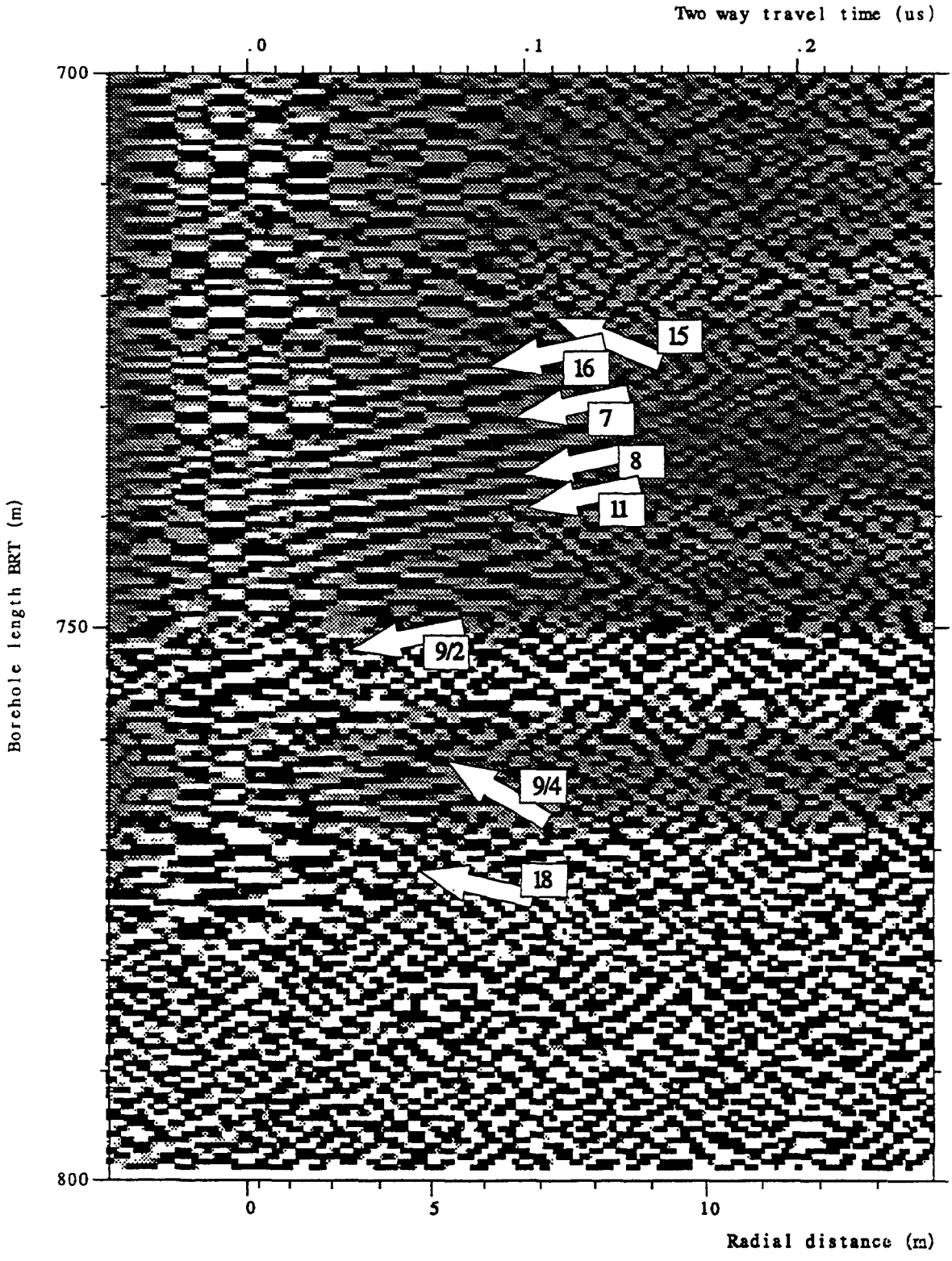

Figure 6-157 Radar reflectors identified in the interval 700.00 to 800.00 mbRT

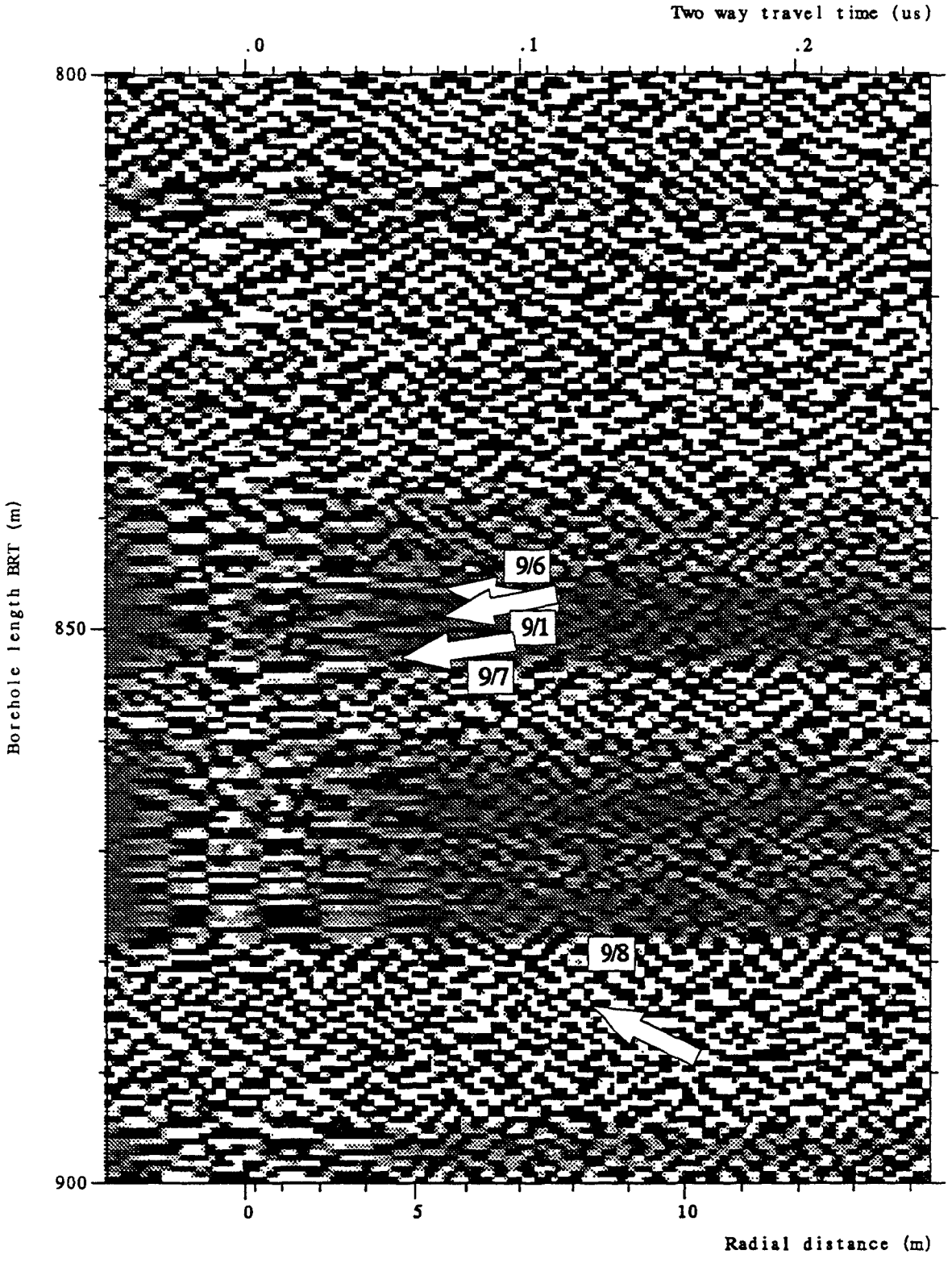

Figure 6-158 Radar reflectors identified in the interval 800.00 to 900.00 mbRT

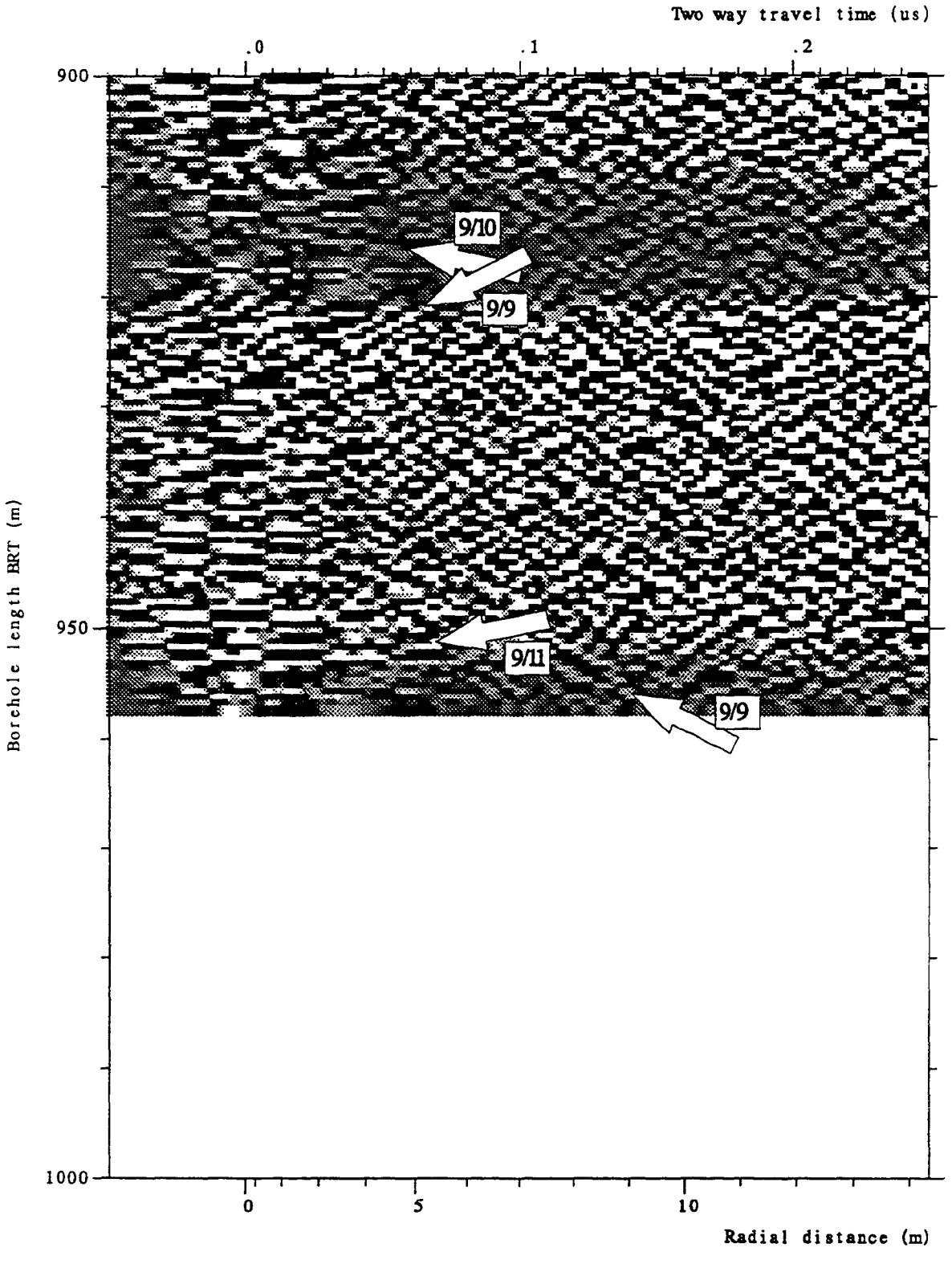

Figure 6-159 Radar reflectors identified in the interval 900.00 to 954.80 mbRT

7. CORRELATION OF THE RADAR DATA WITH GEOPHYSICAL WIRELINE LOGS

7.1 Introduction

To address the sixth and seventh objectives of the survey outlined in Section 2, a comparison of the radar results with other geophysical wireline logs was performed. The radar data have been compared with the wireline logs listed below:

LLS	Laterolog Shallow
LLD	Laterolog Deep
LLG	Laterolog Groeningen
MSFL	Microspherically focused
NPHI	Neutron Porosity
ACON	Fluid conductivity

In order to correlate the radar data with other geophysical wireline logs it must be appreciated that the different data sources have different resolutions and different information contents. The wireline logs provide information about the properties of the rock mass in the immediate vicinity of the borehole wall. The dimensions of the volume of investigation varies from a few centimetres for the MSFL to metres for the LLD. The radar, however, is used to provide information about rock properties, normally in terms of location, extent, and orientation of geological features at a distance from the borehole. The direct radar wave which propagates along the borehole from transmitter to receiver provides information which is similar to that of the wireline logs. The amplitude and velocity of the direct wave represents an average of the electrical properties of the rock mass in a cylinder centred on the borehole with a length of about 5-7 m and a radius of 1-2 m. Therefore for a comparison to be meaningful, data of similar information content and comparable resolution needs to be compared.

Based on the above it is evident that radar amplitude and velocity are the quantities that are comparable to the data provided by the geophysical wireline logs with the exception of the fluid conductivity log, ACON, which provides information about the properties of the borehole fluid which are not directly related to the properties of the rock at the location of the measurements. The fluid conductivity is, however, expected to have an indirect influence on radar results in that a high fluid conductivity will increase attenuation of the radar waves. Based on the above discussion it would be expected that the LLD log would be most readily comparable to the radar amplitude and velocity. However, a meaningful comparison requires data to be of comparable resolution and all data therefore have to be averaged or filtered to a common resolution before correlations are made.

The information provided by the radar on the location and orientation of reflectors cannot be compared directly or quantitatively with the wireline logs. In this case, the predicted intersection of a reflector with the borehole has to be compared to the shape of the wireline logs in the same borehole section. If an anomaly is observed in the wireline logs at the location predicted from the radar results it can be inferred that the radar has detected a feature that intersects the borehole.

To enable a successful correlation of the wireline logs with the radar results it is a requirement that the data have the same depth readings. It has been assumed that the depth readings of the resistivity and neutron logs are correct and that a correction should be applied to the radar data. As a basis for estimating the depth error in the radar data a visual comparison was made of the radar peak-to-peak amplitude from the 60 MHz omni-directional survey with the LLD log.

The LLD log and radar amplitude are both sensitive to the electrical properties of the rock mass and should qualitatively yield similar information. This can be verified by an inspection of a plot of the data (Figures 7-1 and 7-2). The plots for 100 m long intervals of these logs were compared visually in order to determine an average depth

correction for each 100 m interval. The depth of the radar amplitude data were then adjusted in order to obtain agreement with the LLD log on the location of well defined anomalies. The results of this comparison are present below. The depth interval 600-700 mbRT contained no significant radar amplitude anomalies so the number given for this interval is uncertain and is shown in brackets.

Depth interval (mbRT)	Radar depth error (m)
500-600	-1.0 m
600-700	(-1.0 m)
700-800	-2.0 m (Run 6)/ -1.5 m (Run 9)
800-900	-1.7 m
900-1000	-2.6 m

Based on the assumption of a constant offset at the beginning of each run and an error proportional to the surveyed depth the following depth corrections were applied to the radar data from Runs 6 and 9 of the 60MHz omni-directional survey:

$$xc_6 = x_6 + 1.0\ m + (x_6 - 517.46\ m) * 0.005$$
$$xc_9 = x_9 + 1.5\ m + (x_9 - 743.08\ m) * 0.005$$

where x_i are the original depth readings and xc_i are the corrected depths. A depth offset of approximately 1 m at a depth of 520 m is in agreement with the results of the test of the depth accuracy of the RAMAC system which was conducted as part of Run 3. This test showed that at the bottom of the casing (at 444.7 mbRT) the radar depth reading was short by 0.9+/-0.5 m.

7.2 Correlation of Radar Amplitudes with Resistivity Logs

The resistivity logs LLD, LLG, LLS, and MSFL for the depth interval 500-1000 mbRT are shown in Figure 7-1. This figure shows general agreement in location of

anomalies for all resistivity logs. The higher resolution of the MSFL compared to the LLD is also evident. Figure 7-2 shows the neutron porosity (NPHI), the fluid conductivity (ACON), and the depth corrected 60 MHz omni-directional radar amplitude and velocity logs. A visual inspection of Figures 7-1 and 7-2 shows a general agreement in location of major anomalies for all logs except the fluid conductivity log.

Figure 7-3 shows the radar amplitude and LLD log at a larger scale to facilitate a more detailed comparison of anomalies. It can be seen that the general trends are similar but the radar amplitude shows variations of greater magnitude than the LLD log. The Carboniferous Limestone located, in the interval 523.5-576.5 mbRT, is apparent as a borehole interval of high resistivity. In the BVG (below 576.5 mbRT) there are four intervals of relatively high resistivity: 664-772, 835-882, 895-924, and 953 mbRT to the bottom of the borehole. In these intervals the radar amplitude is clearly above the noise level, which is at approximately 20 μV.

Figure 7-4 shows the radar velocity and neutron porosity at a larger scale. These logs also show qualitative agreement internally and with the logs shown in Figure 7-3. Figures 7-3 and 7-4 have been included because a correlation between the pair of logs shown in these two figures can be expected on physical grounds. Radar amplitude is a function of radar attenuation which in turn is a function of formation conductivity. Similarly, radar velocity is a function of the dielectric constant which in turn is a function of the water content (porosity) of the formation (Olsson et al., 1992).

As mentioned above, a meaningful correlation requires data to be of comparable resolution. For example, if a direct correlation of radar amplitude and the MSFL log was to be made, the MSFL data would show a large scatter due to its large variation within small depth intervals while the radar amplitude would be more constant within the same interval and this would lead to inconclusive results. Hence, the resistivity

logs and the neutron log have to be either band-pass filtered or averaged to obtain a resolution similar to that of the radar amplitude and velocity logs. In addition, cross-correlation of data must be made on a point by point basis which implies that the data must be resampled to the same measurement points.

Two alternative procedures for converting the data to a common resolution were tested.

(1) The first procedure was based on low-pass filtering the resistivity logs and resampling the data. The data processing steps were:

- low-pass filtering (zero phase) of the resistivity logs with a 6th order Butterworth filter with a cut-off frequency of 0.66 m^{-1}.

- resampling the radar data and resistivity logs for the interval 520-950 mbRT to a 0.5 metre interval by linear interpolation.

(2) The second procedure was based on averaging the data at 1 m intervals for the resistivity, neutron and radar data. This resulted in a data set with a sampling interval of 1 m for the depth interval 520-950 mbRT.

Figure 7-5 shows a comparison of the cross-plots obtained for low-pass filtered data and data averaged to 1 m intervals. From the cross-plots it is evident that the 1 m averaging produces a smaller scatter than the low-pass filtering for the LLD and porosity logs. For the radar amplitude and velocity logs there is little difference between the averaged and the low-pass filtered data. This would be expected since the radar data have little energy at the high spatial frequencies which would be affected by the differences between the two smoothing procedures applied. Based on these results it was decided to use the data averaged to 1 m intervals for the correlation studies.

A correlation matrix of the logs was computed in order to quantify the correlation. The base 10 logarithm was taken for all logs, with the exception of the radar velocity log, before computation of the correlation matrix. Then all measurement points where the radar amplitude was less than 40 μV were excluded from the data set in order to avoid biasing the results by radar data containing only noise. The number of data points excluded from the data set was 173 out of a total of 430. The resultant correlation matrix is presented below.

	Radar amplitude	Radar velocity	LLD	LLG	LLS	MSFL	NPHI
Radar amplitude	1.0000	0.9753	0.7397	0.7591	0.8375	0.8428	-0.7188
Radar velocity	0.9753	1.0000	0.7367	0.7569	0.8311	0.8578	-0.7650
LLD	0.7397	0.7367	1.0000	0.9988	0.9670	0.8015	-0.5124
LLG	0.7591	0.7569	0.9988	1.0000	0.9751	0.8160	-0.5297
LLS	0.8375	0.8311	0.9670	0.9751	1.0000	0.8747	-0.6034
MSFL	0.8428	0.8578	0.8015	0.8160	0.8747	1.0000	-0.8080
NPHI	-0.7188	-0.7650	-0.5124	-0.5297	-0.6034	-0.8080	1.0000

The absolute values of the correlation coefficients vary from 0.51 to 0.98. The correlation is therefore good between all logs, which could be determined by inspection of Figures 7-1 and 7-2.

The best correlation is between the radar amplitude and the radar velocity (correlation coefficient 0.98) whilst the correlation coefficients between radar amplitude and the resistivity logs fall in the range 0.74 to 0.84 with the highest values for the LLS and MSFL logs. This is unexpected since the best correlation would be expected between logs with similar depths of investigation. However, the averaged data for the LLS and MSFL logs are apparently better correlated to radar amplitude (and velocity) than

the LLD and LLG logs. There is a good correlation between radar velocity and neutron porosity (correlation coefficient 0.76). The lowest correlation coefficients are obtained for neutron porosity versus the LLD and LLG logs.

Various cross-plots of the logs are shown in Figures 7-6 to 7-8. These figures show all data in the interval 520-950 m including those which were excluded in the computation of the correlation matrix. The noisy radar amplitude data can be seen clustered at approximately 20 μV and as horizontal lines in the cross-plots including radar velocity (Figure 7-7). The cross-plots also include the linear regression line for the data shown in each cross-plot.

The regression line for the cross-plot between the radar amplitude and LLD, LLG and LLS resistivities all have a slope of approximately 2.3. This implies that the radar amplitude is proportional to resistivity raised to a power of 2.3. The corresponding value for the cross-plot of radar amplitudes and MSFL data is 2.1. The slopes and intercepts for the linear regression lines shown in Figures 7-6 to 7-8 are tabulated below.

	Slope	Intercept
Radar amplitude vs LLD	2.25	-2.12
Radar amplitude vs LLG	2.26	-2.14
Radar amplitude vs LLS	2.28	-2.41
Radar amplitude vs MSFL	2.08	-2.40
Radar velocity vs radar amplitude	13.5	41.8
Radar velocity vs porosity	-21.3	96.2
Radar velocity vs LLD	30.1	11.8
Radar amplitude vs porosity	-1.45	3.94
MSFL vs LLD	0.99	0.35
LLD vs porosity	-0.34	2.49

Note: These are regression coefficients for $\log_{10}$ of all data except radar velocity.

The porosity data seems to form two clusters at approximately 12% and 20% for which radar amplitude and resistivity vary considerably. These data points originate from depths below 830 mbRT where the neutron porosity data are relatively constant while most other logs exhibit large variations (Figure 7-2). These data clusters evidently bias the regression and cause the discrepancy between the regression lines and the data points for low porosity values (Figure 7-7 and 7-8).

The main objective of the correlation studies was to evaluate whether the radar reflection range could have been predicted based on the resistivity logs. The radar range and resistivity data obtained from wireline logs are not directly comparable. The radar range is estimated for a section of a borehole based on the appearance of radar reflectors in the radar maps. A radar range estimate can only be given as an average for relatively long sections of the borehole. Based on the results from the directional and omni-directional surveys of Borehole 7A radar ranges were estimated for three sections of the borehole with lengths of the order of 100 m. In order to obtain suitable data for a comparison with the estimated radar ranges the average of the LLD resistivities were computed for the corresponding sections in the borehole. The values obtained are presented below and shown graphically in Figure 7-9.

Borehole interval (mbRT)	Range onmi-directional	Average resistivity (LLD) (ohmm)	Averaging interval for resistivity (mbRT)
520-580 (limestone)	10-15 m	580	524-575
680-770 (BVG)	5-8 m	221	684-765
830-960 (BVG)	≈5 m	127	899-920

The figure also shows the regression line obtained under the assumption that radar range is a linear function of, or proportional to, the logarithm of the averaged LLD resistivity. These lines can be used to obtain estimates of radar range and are expected to provide reasonable estimates of radar range for average resistivities less

than 1000 ohmm. Extrapolation of radar ranges for higher values of resistivity should be treated with caution as there is no established relationship between radar range and DC resistivity. Anticipated ranges at higher resistivities can be obtained from radar survey data conducted at other sites. For example, at the Äspö site in Sweden radar ranges obtained are 40-50 m for resistivities of the order of 10000 ohmm (Almén and Zellman, 1991), and at Stripa (Sweden) ranges of about 70 m were obtained for resistivities of about 100000 ohmm (Olsson et al., 1992).

7.3 Correlation of Radar Reflectors with Resistivity Logs

The correlation of radar reflectors with resistivity logs was based on a comparison of predicted intersections of reflectors with the borehole and the presence of anomalies in the resistivity logs near the predicted intersection. The identified radar reflectors are presented in Table 7.1. The table also includes a column of corrected depths according to the formulas given in Section 7.1. Figures 7-10 to 7-13 show the location of radar reflectors in the borehole as double horizontal lines plotted on the LLD and MSFL resistivity logs. Each figure displays a 100 m long interval of the borehole to facilitate detailed comparison of reflector intersections with the resistivity logs. Figures 6-155 to 6-159 (Section 6) show the appearance of the identified reflectors in the radar maps for successive 100 m intervals of the borehole.

An evaluation of the correlation with the resistivity logs for each radar reflector is given in the comments column of Table 7.1. From the table it is evident that an acceptable correlation with resistivity (mainly the MSFL log) was found for 17 of the 25 reflectors. For some of the correlations there is a depth discrepancy of the order of 1 m which is considered to be acceptable as this is of the same order of magnitude as the radar resolution.

In the borehole interval 733-755 mbRT there are many resistivity anomalies and several radar reflectors, in this case the distance between the resistivity anomalies is

in some cases probably too small for radar reflectors to be generated. The large resistivity anomaly at 755 mbRT does not cause a radar reflection, but is associated with a significant reduction in radar amplitude (Figure 7-3) and range (Figure 6-157, Section 6). The absence of a reflection event at this location may be due to the low resistivity feature being nearly perpendicular to the borehole. This is a case where a radar reflection would be very weak. The weak reflectors at 859.6, 860.4, and 936.1 mbRT which appear where there are no distinct resistivity anomalies occur in a section of the BVG where the radar attenuation is high and these reflectors may therefore, be processing artifacts.

In the Carboniferous Limestone there are several strong reflectors but also many resistivity anomalies. In the limestone most of the identified reflectors are oblique to the boreholes (intersection angles of 30-45°) and this is expected to increase the errors in the estimated intersection depths. For example the radar reflector at 558.7 mbRT is classified as strong and apparently correlates with an MSFL anomaly. However, there are two large MSFL anomalies at 556.4 mbRT and 560.1 mbRT and considering the strength of the radar reflector it probably results from one of the two large MSFL anomalies, indicating an error in the intersection depth of 1.4 or 2.3 m. A depth error of this magnitude probably accounts for the apparently poor correlation with significant resistivity anomalies for the reflector at 526.7 mbRT.

The 3m discrepancy in the depth of the Carboniferous Limestone-BVG boundary indicated by the resistivity logs and the radar is unexpected as this is one of the strongest radar reflectors. The radar amplitude and the LLD resistivity (Figure 7-3) show good correlations at this depth and both indicate the depth of the boundary to be at 576.6 mbRT. Considering that the reflector is actually observed at a distance from the borehole a possible explanation for the difference in predicted and actual depth may be due to a fault displacing the reflector close to the borehole. This is supported by the fact that the reflector is actually only observed to a depth of 575 mbRT which is 5 m from the predicted intersection depth.

Table 7.1 List of radar reflectors identified from the 60 MHz omni-directional and 60 MHz directional surveys in Borehole 7A.

ID no.	Type	Depth of intersection/apex		Magnitude U=uncertain 1=weak 2=medium 3=strong	Azimuth	Linear reflector			Point	Comments
		uncorrected (mbRT)	corrected (mbRT)		(deg)	Angle (deg)	Dip (deg)	Dipdir (deg)	Distance (m)	
13	Plane	492.3	493.2	U		18.9	71			No clear resistivity anomaly at this depth
6	Plane	525.7	526.7	2		34.7	55			Located in middle of high resistivity anomaly. Reflector observed to both sides of predicted intersection. Could be reflections from upper and lower boundary of resistive interval. However, reflector oblique to borehole could make intersection depth inaccurate.
1	Plane	531.7	532.8	3	280	32.7	57	100		Correlates with large MSFL anomaly
5	Plane	538.5	539.6	2	255	38.5	52	75		Correlates with large MSFL anomaly. Reflector depth error +1 m
10	Plane	547.9	549.1	2		48.1	42			Reflector depth coincides with bottom of section with low LLD resistivity and several MSFL anomalies

ID no.	Type	Depth of intersection/apex		Magnitude U=uncertain 1=weak 2=medium 3=strong	Azimuth	Linear reflector			Point	Comments
		uncorrected (mbRT)	corrected (mbRT)		(deg)	Angle (deg)	Dip (deg)	Dipdir (deg)	Distance (m)	
17	Plane	550.4	551.6	1		33.7	56			Correlates with medium MSFL anomaly. Reflector depth error -1 m
X	Point	551.1	552.2	U					3.2	Seen only in FK-filtered data (no borehole intersection)
4	Plane	557.5	558.7	3	60	33.4	57	240		Correlates with medium MSFL anomaly (possibly a depth error of -1.4 m which would yield correlation with a large MSFL anomaly)
2	Plane	561.5	562.7	2	-	90	0			Correlates with large MSFL anomaly
3	Plane	578.6	579.9	3	60-90	42.2	48	240-270		Probably reflection off Limestone-BVG boundary. Reflector depth error +3 m.
9	Plane	692.2	694.0	1		82.7	7			Correlates with medium MSFL anomaly (one of many)
15	Plane	710.1	712.1	2		35.4	55			No distinct resistivity anomaly at this depth

ID no.	Type	Depth of intersection/apex		Magnitude U=uncertain 1=weak 2=medium 3=strong	Azimuth	Linear reflector			Point	Comments
		uncorrected (mbRT)	corrected (mbRT)		(deg)	Angle (deg)	Dip (deg)	Dipdir (deg)	Distance (m)	
16	Plane	733.2	735.3	1		90.0	0			Correlates with medium MSFL anomaly
7	Plane	739.7	741.8	1	50	68.2	22	230		Correlates with medium MSFL anomaly (one of many)
8	Plane	743.8	745.9	1		90.0	0			Correlates with medium MSFL anomaly (one of many)
9/4	Plane	745.8	747.9	U		23.9	66			Correlates with medium MSFL anomaly (one of many)
11	Plane	747.6	749.7	1		55.2	35			Correlates with medium MSFL anomaly (one of many)
9/2	Plane	758.0	759.6	1		68.3	22			Correlates with large MSFL anomaly
18	Plane	765.6	767.2	1		57.6	32			Correlates with medium MSFL anomaly
9/6	Plane	839.9	841.9	1		90	0			Correlates with large MSFL anomaly. Radar depth error -1.5m

ID no.	Type	Depth of intersection/apex		Magnitude U=uncertain 1=weak 2=medium 3=strong	Azimuth	Linear reflector			Point	Comments
		uncorrected (mbRT)	corrected (mbRT)		(deg)	Angle (deg)	Dip (deg)	Dipdir (deg)	Distance (m)	
9/1	Plane	854.5	856.6	1		46.6	43			Correlates with large MSFL anomaly. Radar depth error -0.7m
9/8	Plane	857.5	859.6	U		18.1	72			No distinct resistivity anomaly at this depth
9/7	Plane	858.3	860.4	1		61.8	28			No distinct resistivity anomaly at this depth
9/10	Plane	908.8	911.1	1		44.0	46			Correlates with lower boundary of low resistive section
9/9	Plane	933.6	936.1	1		24	66			No distinct resistivity anomaly at this depth
9/11	Plane	956.6	959.2	1		90	0			Correlates with upper boundary of resistive section. Radar depth error + 1 m

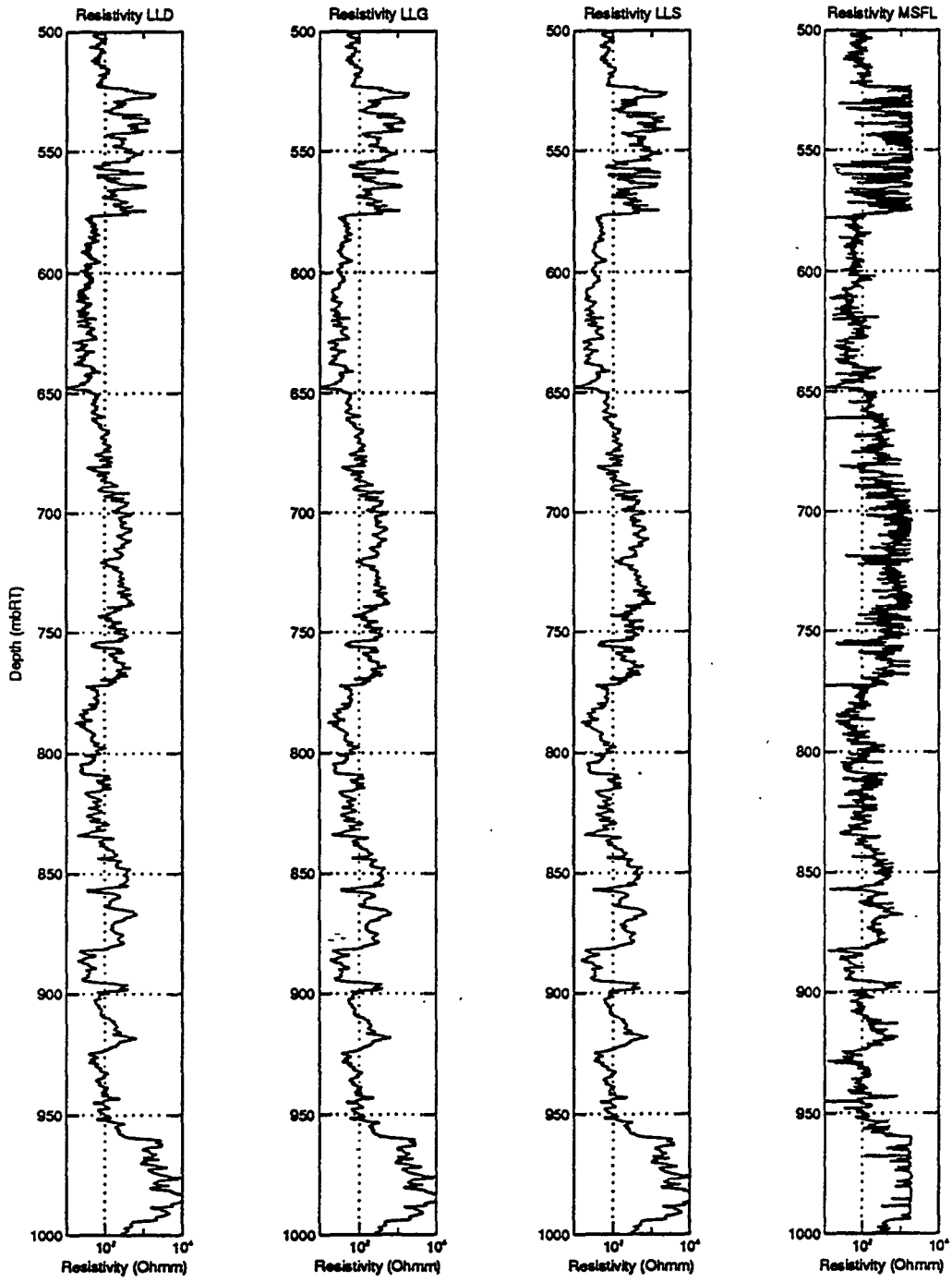

Figure 7-1 Resistivity logs (LLD, LLG, LLS, MSFL) from Borehole 7A

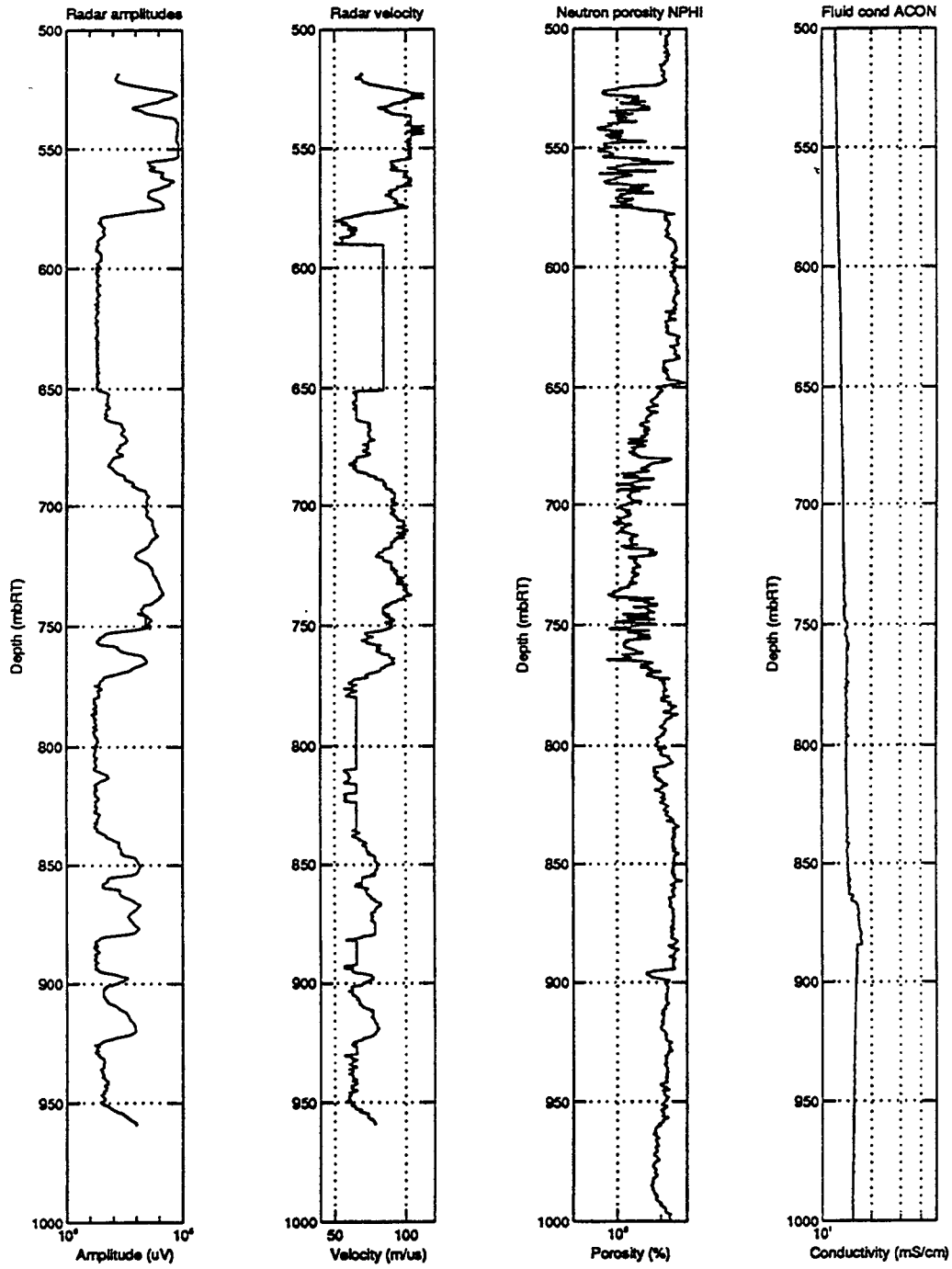

Figure 7-2 Radar amplitude and velocity (60 MHz survey data), neutron porosity (NPHI) and fluid conductivity (ACON) from Borehole 7A

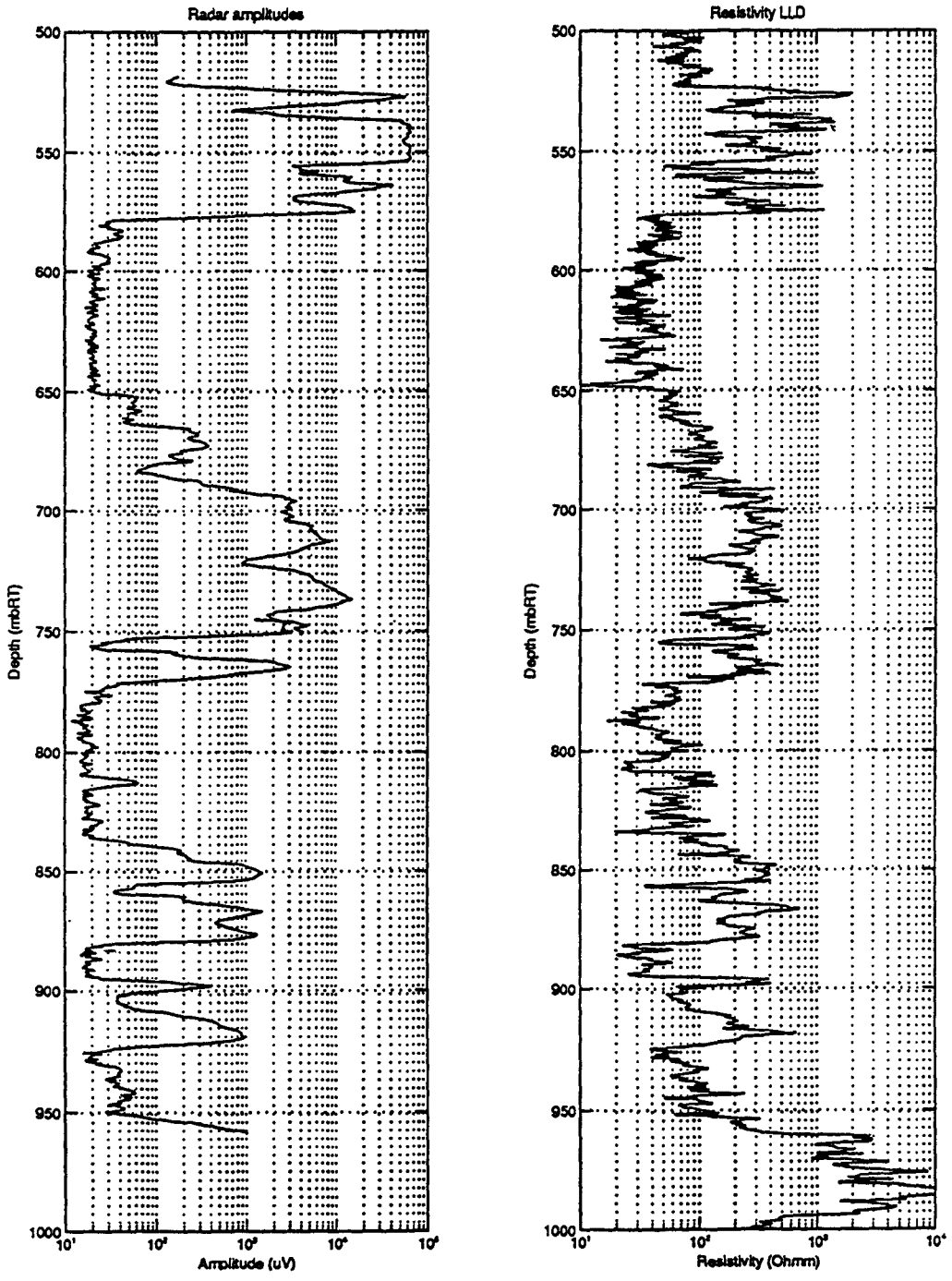

Figure 7-3 Radar peak to peak amplitude and LLD resistivity

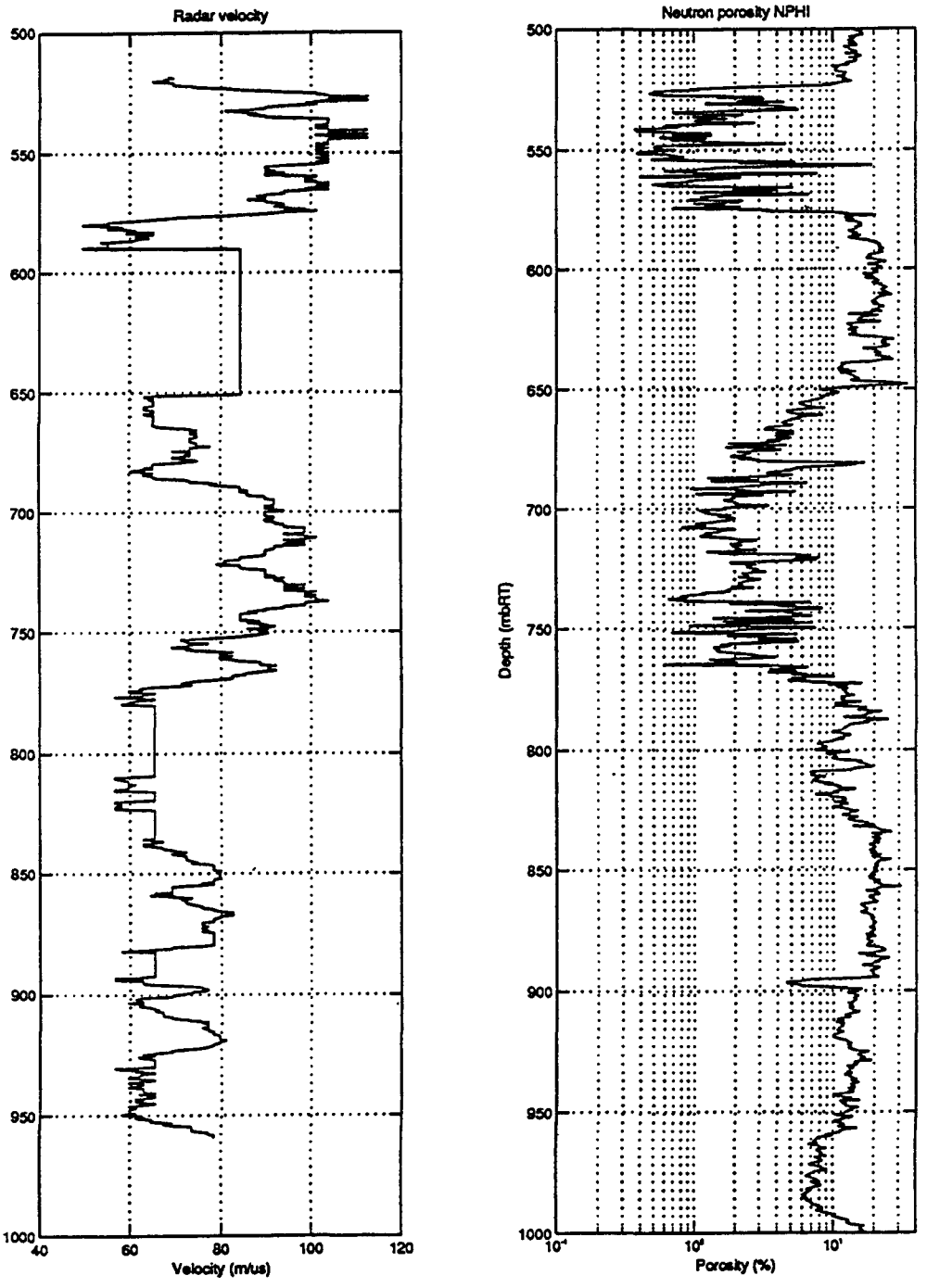

Figure 7-4 Radar velocity and neutron porosity (NPHI), (the straight line segments in the radar velocity plot represent borehole sections where no data was acquired)

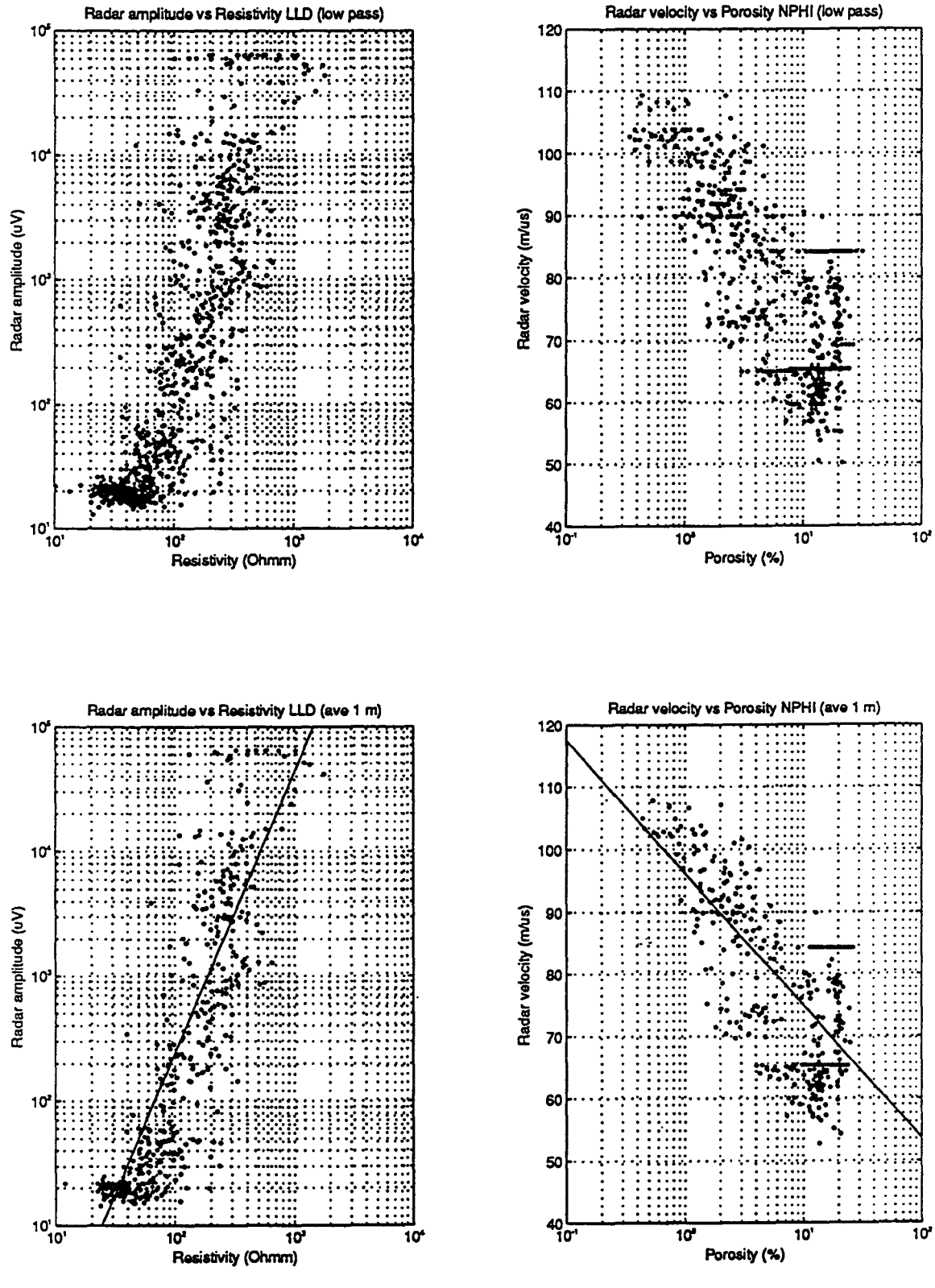

Figure 7-5 Cross plots of radar amplitude against LLD resistivity and radar velocity against porosity; the cross plots are shown for band pass filtered data (upper) and data averaged at 1m intervals (lower)

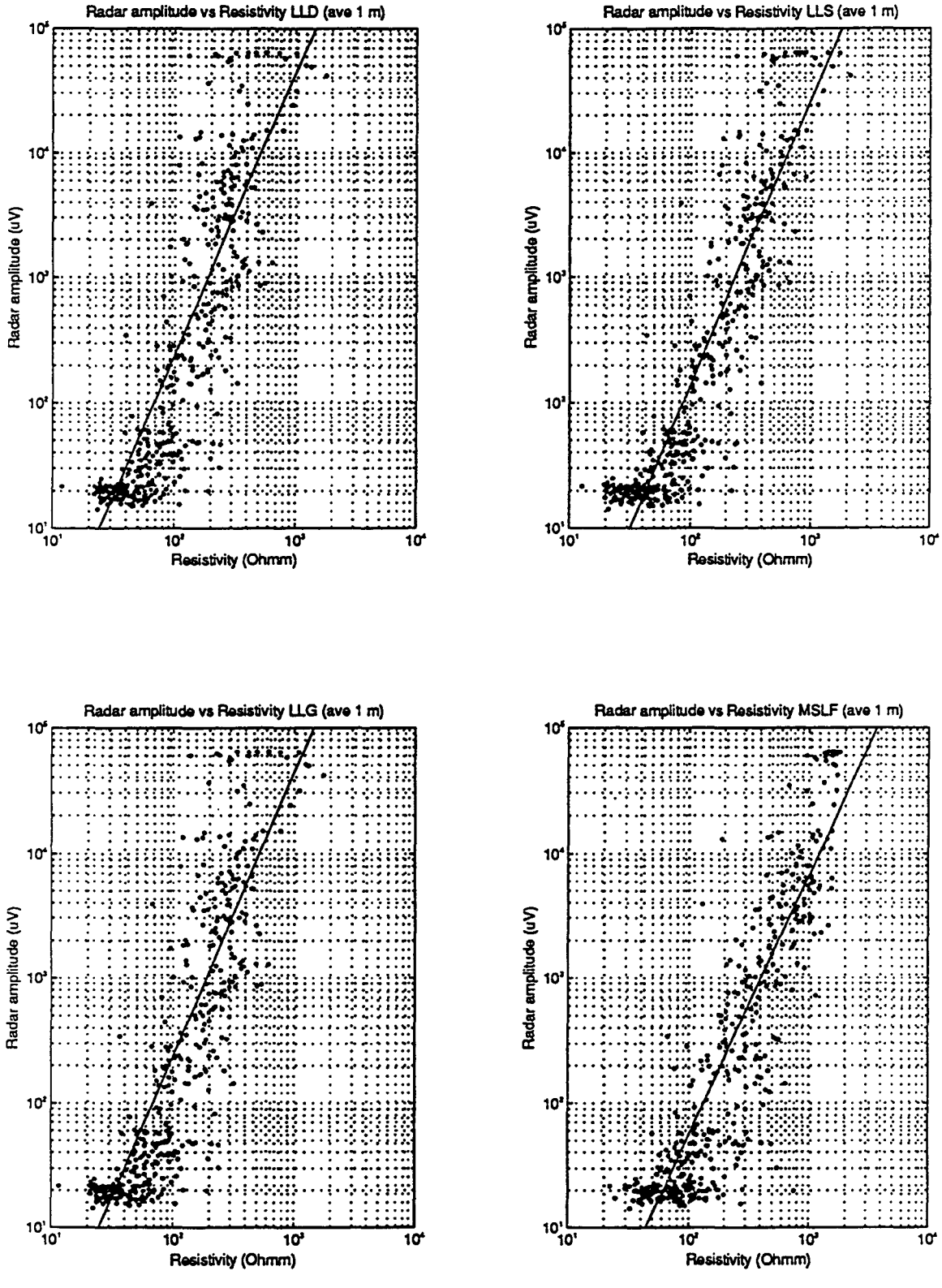

Figure 7-6 Cross plots of radar amplitude against LLD, LLS, LLG and MSFL resistivity data averaged at 1m intervals

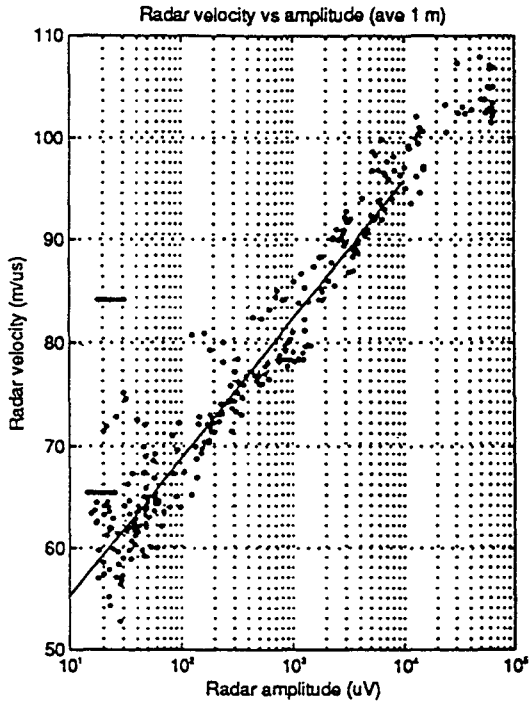

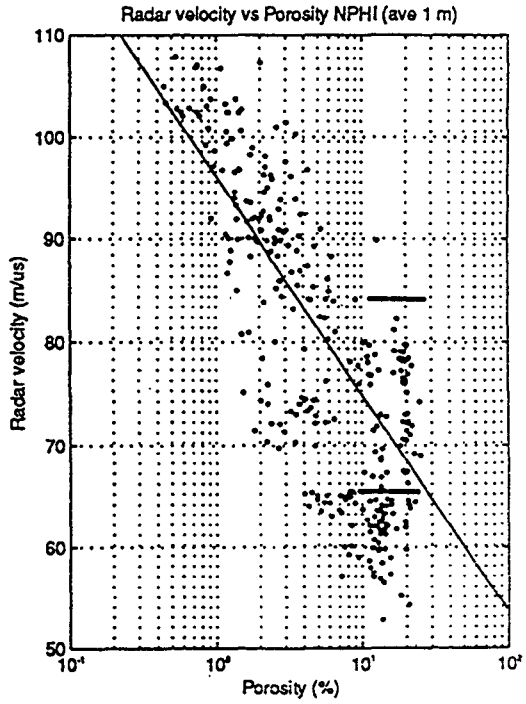

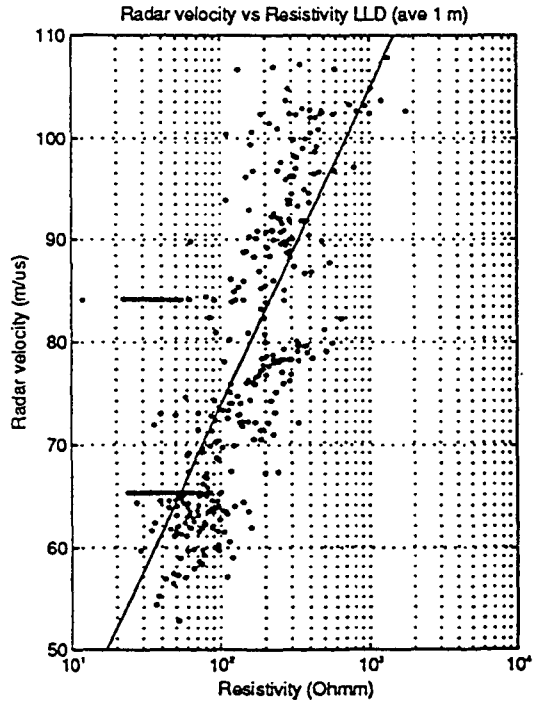

Figure 7-7 Cross plots of radar velocity against radar amplitude, porosity and LLD resistivity

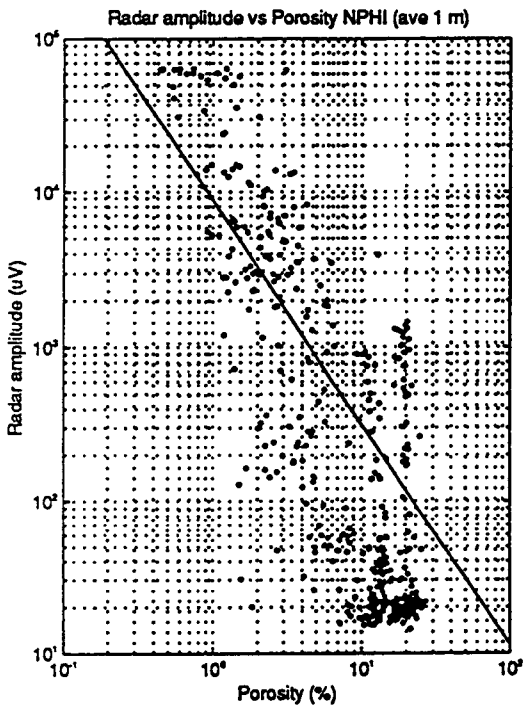

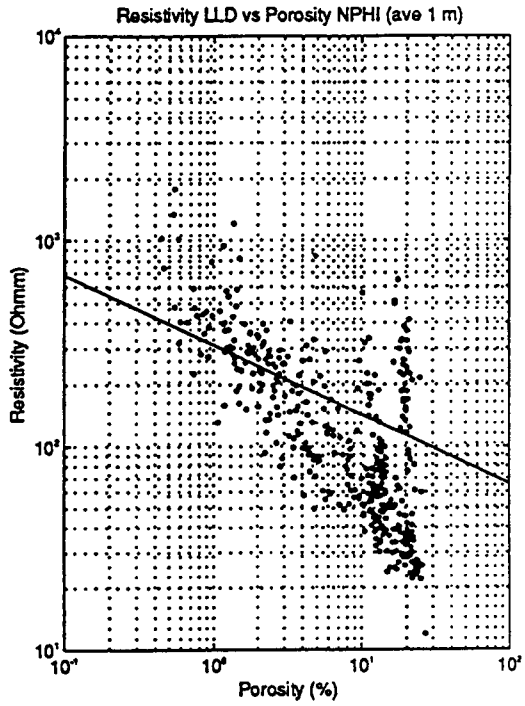

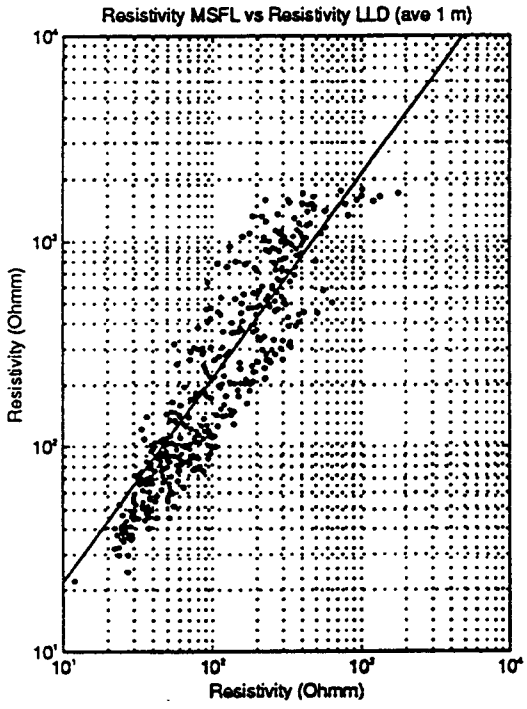

Figure 7-8 Cross plots of radar amplitude against porosity, MSFL against LLD resistivity and LLD resistivity against porosity

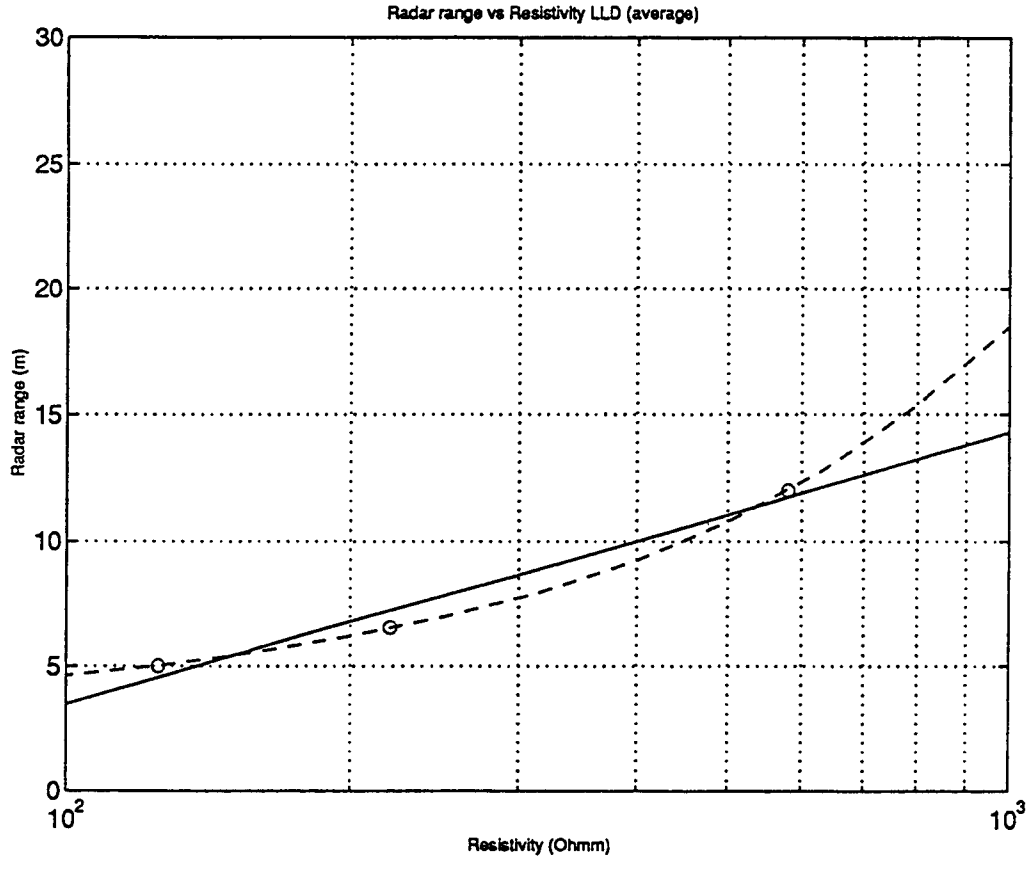

Figure 7-9 Cross plot of radar range against average resistivity (LLD) and regression line based on the three data points in the table on Page 7-8, the figure also shows the regression line obtained under the assumption that radar range is a linear function (solid line) of, or proportional to, the logarithm (dashed line) of the averaged LLD resistivity

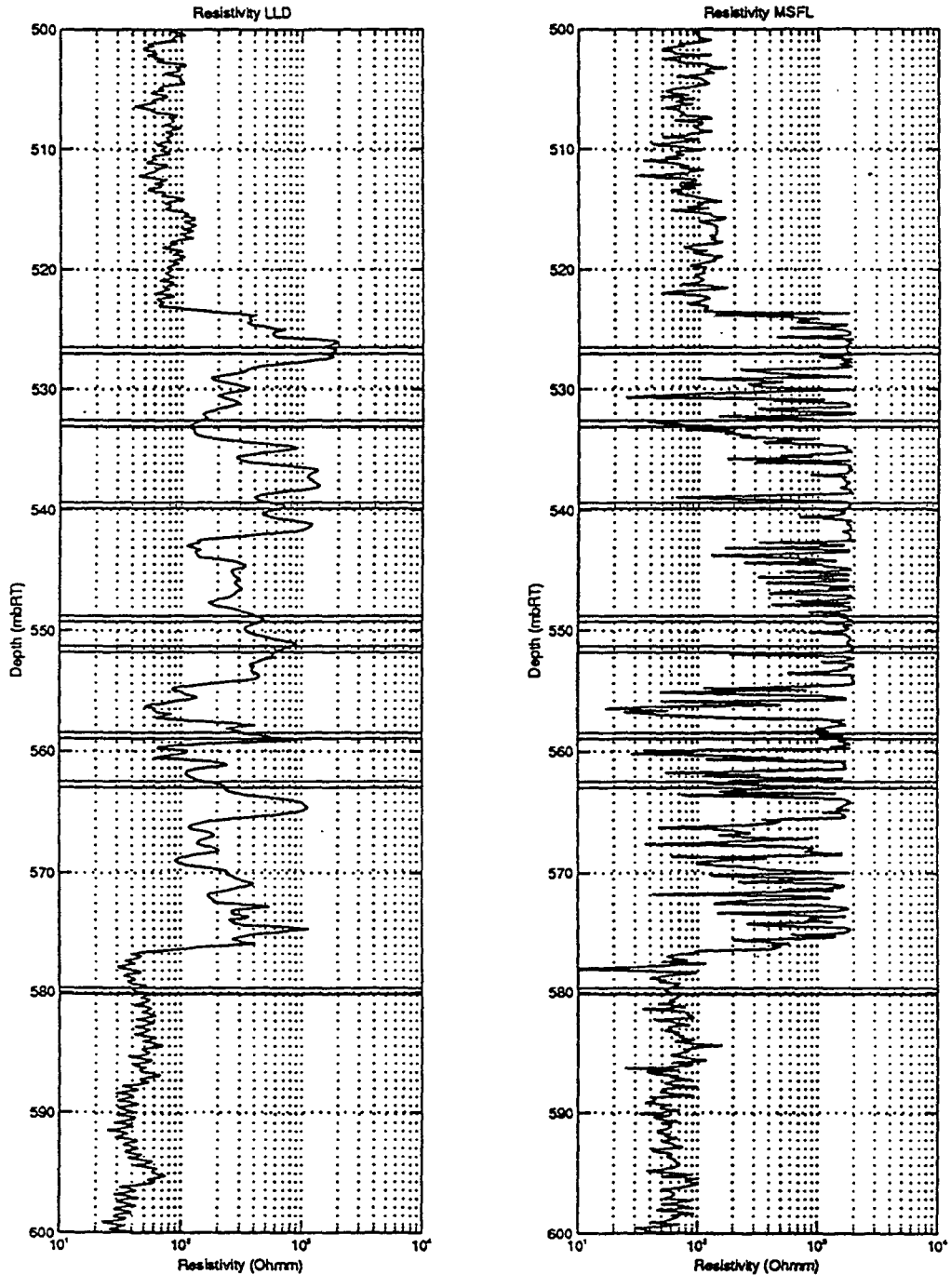

Figure 7-10 Plot of the indentified radar reflectors, LLD and MSFL resistivity logs for the interval 500 to 600 mbRT, predicted intersections of the radar reflectors with the borehole are indicated by two horizontal lines.

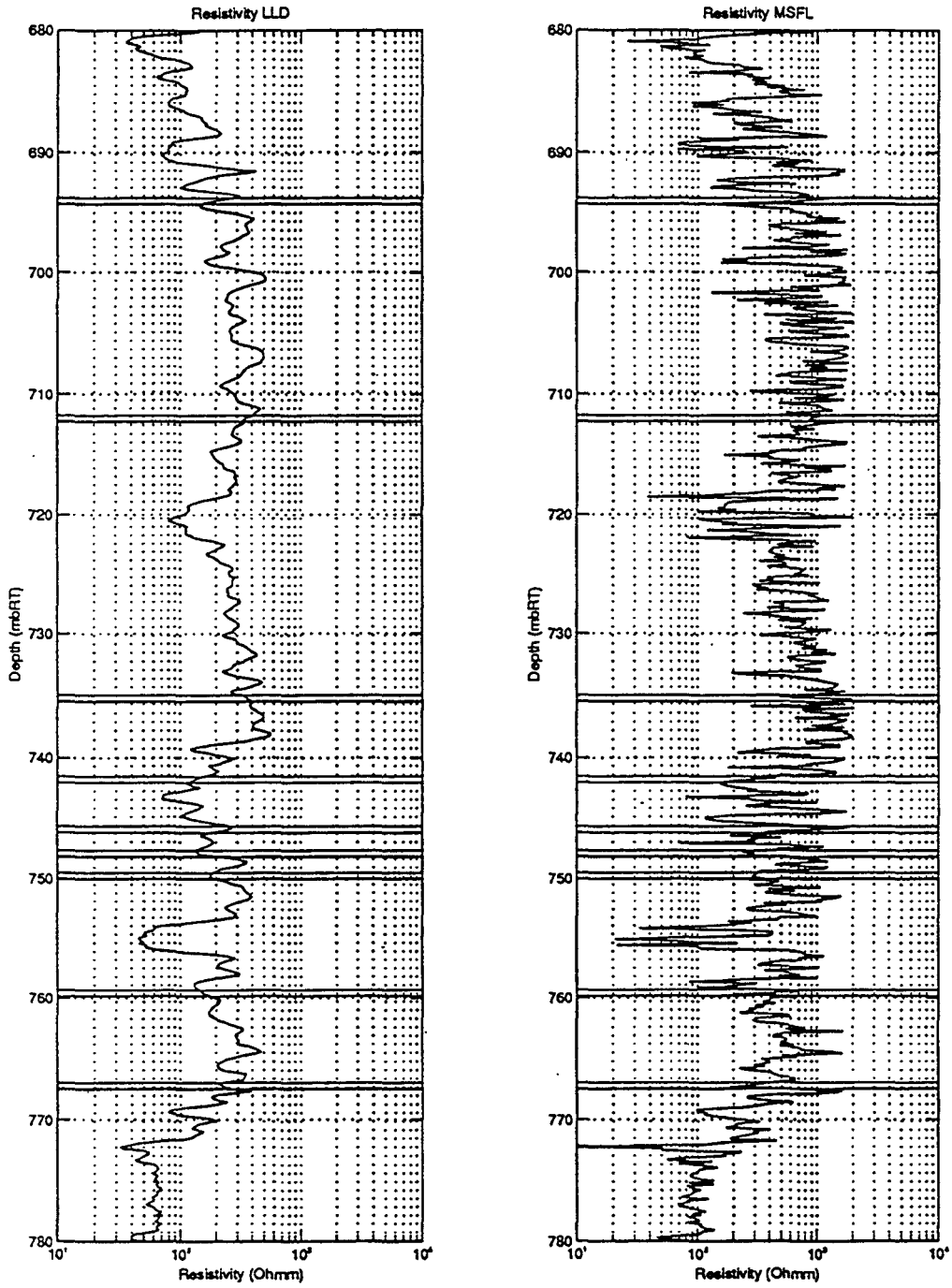

Figure 7-11 Plot of the indentified radar reflectors, LLD and MSFL resistivity logs for the interval 680 to 780 mbRT, predicted intersections of the radar reflectors with the borehole are indicated by two horizontal lines.

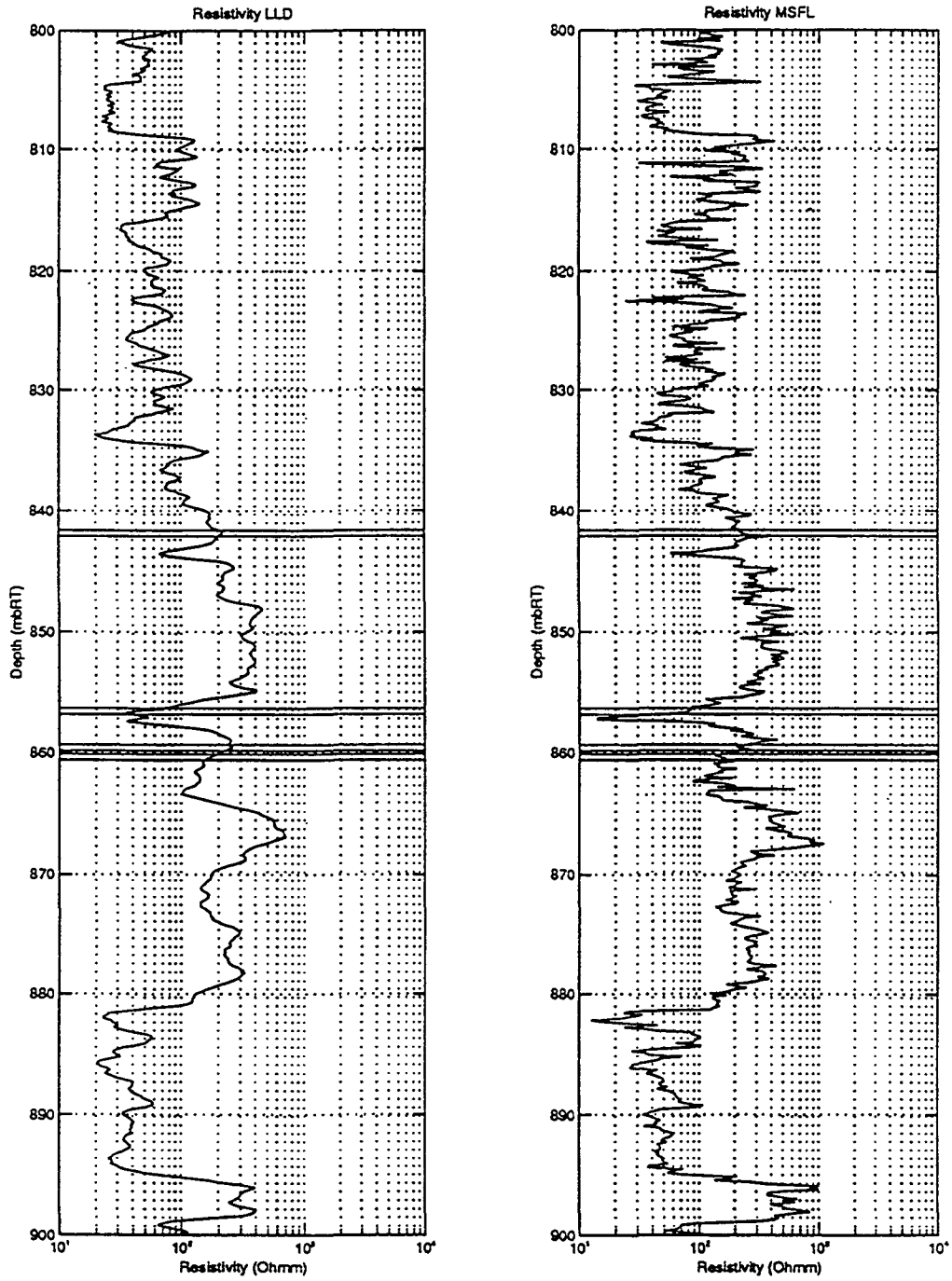

Figure 7-12 Plot of the indentified radar reflectors, LLD and MSFL resistivity logs for the interval 800 to 900 mbRT, predicted intersections of the radar reflectors with the borehole are indicated by two horizontal lines.

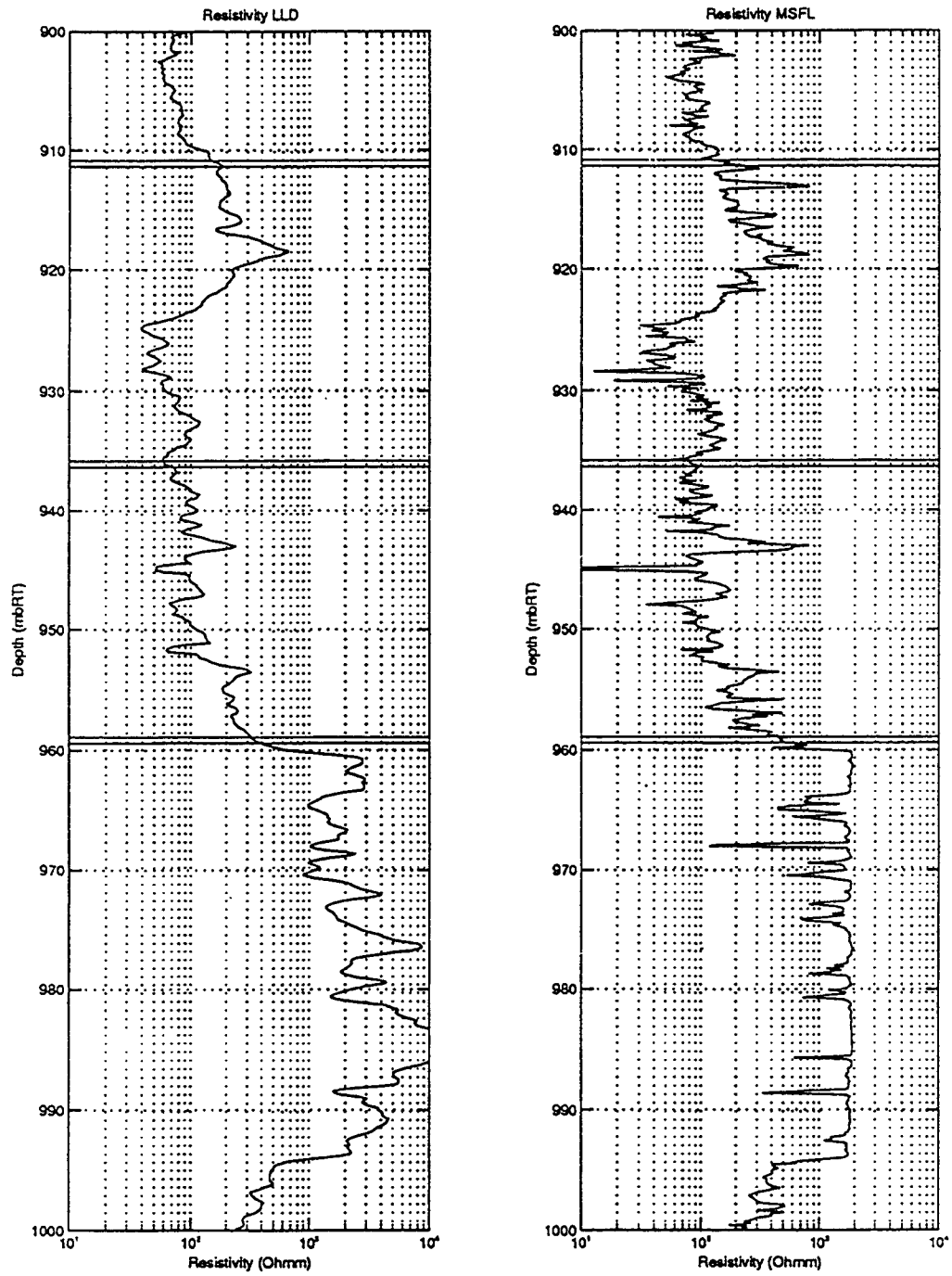

Figure 7-13 Plot of the indentified radar reflectors, LLD and MSFL resistivity logs for the interval 900 to 1000 mbRT, predicted intersections of the radar reflectors with the borehole are indicated by two horizontal lines.

8. PROGNOSIS FOR THE USE OF RADAR IN OTHER BOREHOLES AT SELLAFIELD

8.1 Introduction

The correlation of the radar data, from the borehole radar trial conducted in Borehole 7A, with the geophysical wireline logs, specifically the resistivity and neutron porosity logs, discussed in Section 7 provides a basis for the prediction of radar range in other boreholes at Sellafield. The correlations suggested that reasonable estimates of radar range would be expected to be produced, based on the geophysical wireline logs, where average resistivities are less than 1000 ohmm. Therefore based on the results from Borehole 7A and their correlation with geophysical wireline logs, the available logs and laboratory derived data from Boreholes 2, 4 and 5 have been used to derive estimates of radar range for single borehole radar reflection surveys for the respective boreholes.

8.2 Prediction of Radar Range for Other Boreholes

Radar range is a function of radar wave attenuation which is influenced by the frequency of the radar, the relative dielectric permittivity and the resistivity of the rock mass. The simplest radar theory suggests that the radar range is frequency independent. However, the radar range is dependent on resistivity and dielectric permittivity which cause dispersion and are frequency dependent. The dispersion effects of resistivity and dielectric permittivity tend to decrease and increase respectively with increasing frequency. The theoretical implication of this is that as frequency increases the range radar decreases. The use of resistivity values should be treated with caution as there are no established relationships between radar range and DC resistivity (low frequency) and therefore values at radar frequencies or AC values should be used.

Estimates of the AC resistivity values can be made from the wireline resistivity logs and the radar reflection results from Borehole 7A. Dielectric permittivity data was not, however, available for Borehole 7A and consequently values for saturated intermediate volcanic rock having low porosity were assumed. Values of dielectric permittivity, ϵ_r, in the range 8 - 12 were used in the estimation of radar ranges for Boreholes 2, 4 and 5. The values of dielectric permittivity used in the estimation of radar range are in general agreement with the measured values from Borehole 2. However, any increase in the value of permittivity or a decrease in resistivity will lead to a significant reduction in radar range.

The resistivity and dielectric permittivity are affected by a number of parameters which include:

- the total porosity of the rock
- the resistivity and dielectric permittivity of the rock matrix
- resistivity and permittivity of the borehole fluid.

To obtain the total effect of the individual components, different mixing formulas can be used.

- The effect of total porosity, including pore porosity and fracture porosity, is important as an increase in porosity leads to a lower resistivity and hence a lower radar range. This is a consequence of formation water being generally more conductive than the rock matrix. Also the higher the volumetric component of saturated porosity results in a higher value of dielectric permittivity which causes a slight reduction in radar range. This is, however, usually small in igneous and metamorphic rocks.

- Lithology affects radar range by attenuating radar waves, which results from electrically conductive minerals present within the rock matrix.

- The dielectric permittivity of the borehole fluid is relatively constant, however, the resistivity of the borehole fluid may vary considerably due to variations in the composition, generally salinity, of borehole fluids and the inflow of different formation waters into the borehole. The higher the conductivity of the fluid contained within the total porosity the lower the bulk rock resistivity and hence the lower the radar range.

The main factor which effects the radar range is the resistivity of the rock matrix. Therefore, the geophysical wireline logs, specifically the laterologs are of principal importance in the estimation of radar ranges for Boreholes 2, 4 and 5 and this was shown by the correlation of the radar data with geophysical wireline logs.

To facilitate the estimation of radar range for the other boreholes the resistivity logs; laterologs and microspherically focused logs from Boreholes 7A, 2, 4 and 5 were studied. The boreholes were subdivided on the basis of DC resistivity into units which were then correlated with lithological units. Where available, core porosity data and fluid resistivity data obtained from laboratory analyses were also used to obtain a better understanding of the system influencing the radar range.

The available resistivity data (DC values) were used to derive anticipated AC values in order to calculate radar ranges. The resistivity values from Borehole 7A were correlated with the achieved radar ranges within the borehole, Table 8-1, and the corresponding 60 MHz radar frequency resistivity values were calculated using a quantitative radar wave attenuation equation for a point reflector model. The DC to AC conversion factor was estimated such that the AC resistivity values would be between 2 to 5 times less than the DC values. The conversion factor of 2 determines

the higher radar range whilst the conversion factor of 5 determines the lower radar range.

8.3 Estimates of Radar Range

Estimates of borehole radar range for Boreholes 2, 4 and 5 have been calculated based on Tables 8-2 to 8-4, AC conversion factors and a point reflection model. This model was used as it would not over estimate the range for other reflectors. Further a system sensitivity of 135 dB and a signal-to-noise detection limit of 5 dB were assumed. Estimated ranges of AC resistivity and calculated radar ranges are summarised in Table 8-5 and the radar ranges are presented graphically in Figures 8-1 to 8-3.

Within the BVG of Borehole 2, it has been estimated that two sections exist where reflection data may be obtained and these would be from 480 - 860 mbRT and from 1135 -1400 mbRT. Within the upper section the interval, 480 - 570 mbRT the estimated range is from 70m to 40m. Within the section between 570 - 660 mbRT a range of less than 20m may be expected whilst a moderate radar range between 25 - 40m could be attained between 600 - 860 mbRT. The section between 780 and 815 mbRT is a local very low resistivity zone and no results would be expected within this zone. Within the section of the borehole from 1135 to 1400 mbRT a radar range from 30m to 50m could be expected. Below 1400 mbRT to the bottom of the borehole the range is estimated to be approximately 10m. In this borehole low resistivity sections associated with higher core porosities may explain the estimated low radar ranges.

In Borehole 4 the situation is similar to upper part of Borehole 2. Radar reflection data is anticipated to be obtained between 410 - 840 mbRT. Within the sections 410 - 505 mbRT, 505 - 620 mbRT and 620 - 795 mbRT radar ranges are estimated to be 12 - 35m, 20 - 40m and 35 - 70m, respectively. However, below 840 mbRT where,

for example, a fault zone is encountered at 845 - 905m strong attenuation is predicted. In Borehole 4 low resistivity sections associated with higher core porosities similar to Borehole 2 may explain the estimated low radar ranges. Reflections from fault zone 845 - 905m may be recorded by the radar with measurements along the boreholes section between 620 - 795m.

From the resistivity logs it would appear that Borehole 5 is within very low resistivity rock formations and estimated radar ranges are consequently very limited. Measurable sections are estimated to be 490 - 630 mbRT having a range of 10 - 20m and 1170 - 1250 mbRT having a range of 12 - 25m. Within the fault zone at 575 - 605 mbRT the resistivities attain such low values that no recordable radar signal can be expected.

The predicted radar ranges for the three boreholes are summarised in Table 8-5.

Table 8-1. Radar evaluation parameters from Borehole 7A.

Depth section *Radar range*	**Lithology**	**Bulk resistivity values, Ωm**		**Core proosity, HGEVM %**	**Fluid resist. Ωm**	**Remarks**
		Laterologs	**Focused microresistivity**			
523.5-576.5 m *10m*	Limestone 565-576 Sandy LST, Sandstone	100-800	Up to 1500 Down to 15-50		0.22	
640-680 m	Andesite, Faults, Parataxitic Lapilli Tuff	30-60 <10 60-150	100-200 <10 Up to 600-700 Down to 60			Fault zones at 610-660m
680-770 m *7m*	Eutaxitic Lapilli Tuff	100-400	Up to ≈ 1000 Down to 100		0.12	Fault at 760 m
835-880 m *<5m*	Volcanic sediment	80-400	Up to 600 Down to 60-100 (Fault ≈ 5)			Fault at 855 m
895-925 m *<5m*	Andesite	50-300	Up to 1000 Down to 30		0.11	

Table 8-2. Radar evaluation parameters from Borehole 2.

Depth section	Lithology	Bulk resistivity values, Ωm		Core porosity, HGEVM %	Fluid resist. Ωm	Remarks
		Laterologs	Focused			
<467m	Sandstones	160-400 also <100	30-300 Ωm	5-18		
467m	BVG boundary					
480-570m	Parataxitic high grade tuff	1000-10000	(lab values from core 600-2000)	0.2-0.4	0.27	Casing shoe at 490m
570-660m	Parataxitic tuff, fault zone	200-2000	-1100	0.4	0.25	Fault at 630-655m, Dir. 335/75NE
660-780m	Parataxitic high grade tuff	400-10000	(300-600)	0.24-0.49	0.22	
780-815m	Parataxitic and Eutaxitic tuffs	80-500	-400	0.3	0.21	
815-860m	Tuffs & breccia	400-10000	(100-500)	0.3-0.6	0.21	
860-1135m	Eutaxitic lapilli tuff	200-800	(60-300)	0.3-1.8	0.20	Fault at 895-935m Dir. 315/50-60NE
1135-1400m	Eutaxitic lapilli tuff	700-10000	(200-2000)	0.1-0.55	0.18	
1400-1610m	Tuffs, sandstone & breccia	200-1000	(≈200)	0.3-2.0	0.15	

Table 8-3. Radar evaluation parameters from Borehole 4.

Depth section	Lithology	Bulk resistivity values, Ωm		Core porosity, HGEVM %	Fluid resist. Ωm	Remarks
		Laterologs	Focused			
410-505m	Tuff	200-10000		0.2-0.3	1.6	
505-620m	Lapilli tuff	300-20000		0.2-0.4		
620-795m	Lapilli tuff 620-685m, Tuff > 685m	1000-10000		0.2-1.7		
795-840m	Lapilli tuff	300-3000		0.3-1.1	0.28	
840-970m	Lapilli tuff with tuff & andesite	80-1000	(lab values from core 60-70)	2.3-3.1		Faults at 845-905m, Dir. 330/80NE
970-1100m	Lapilli tuff	90-1000	(lab values from core 60-150)	0.8-2.4		
1100-1250m	Lapilli tuff	200-1000	(lab values from core 100-200)	0.2-0.5	0.20 - 0.18	

Table 8-4. Radar evaluation parameters from Borehole 5.

Depth section	Lithology	Bulk resistivity values, Ωm		Core porosity, HGEVM %	Fluid resist. Ωm	Remarks
		Laterologs	Focused microresistivity			
490-630m	Parataxitic lapilli tuff	300-2000 (between 575-605m ≈ 100)				Fault at 575-605m Dir. 090/60S
630-770m	630-670m Tuff, 670-770m Volcanic Sediments and Tuff	60-600 (within fault 10-40)				Fault at 745-755m, Dir. 320/70NE
770-915m	Lapilli tuff	100-1000			0.27	Fault at 825-845m, Dir. 340/70NE
915-950m	Rhyolite tuff	70-200				
950-1170m	Eutaxitic lapilli tuff	100-1000				
1170-1250m	Eutaxitic lapilli tuff	≈ 1000				

Table 8-5. Borehole radar ranges for Borehole 2, Borehole 4 and Borehole 5.

Borehole 2		
Section (m)	AC resistivity (Ωm)	Estimated range (m)
480-570	1000-2000	40-70
570-660	200-400	12-20
660-780	500-1000	25-40
780-815	50-100	≈7
815-860	500-1000	25-40
860-1135	100-200	≈10
1135-1400	600-1500	30-50
1400-1610	150-300	10-12

Borehole 4		
Section (m)	AC resistivity (Ωm)	Estimated range (m)
410-505	300-700	12-35
505-620	400-1000	20-40
620-795	800-2000	35-70
795-840	150-400	10-20
840-970	70-150	5-10
970-1100	80-200	5-10
1100-1250	100-300	10-12

Table 8-5 cont. Borehole radar ranges for Borehole 2, Borehole 4 and Borehole 5.

Borehole 5		
Section (m)	AC resistivity (Ωm)	Estimated range (m)
490-630	150-400	10-20
630-770	50-90	≈7
770-915	80-200	5-10
915-950	30-50	no
950-1170	80-200	5-10
1170-1250	200-500	12-25

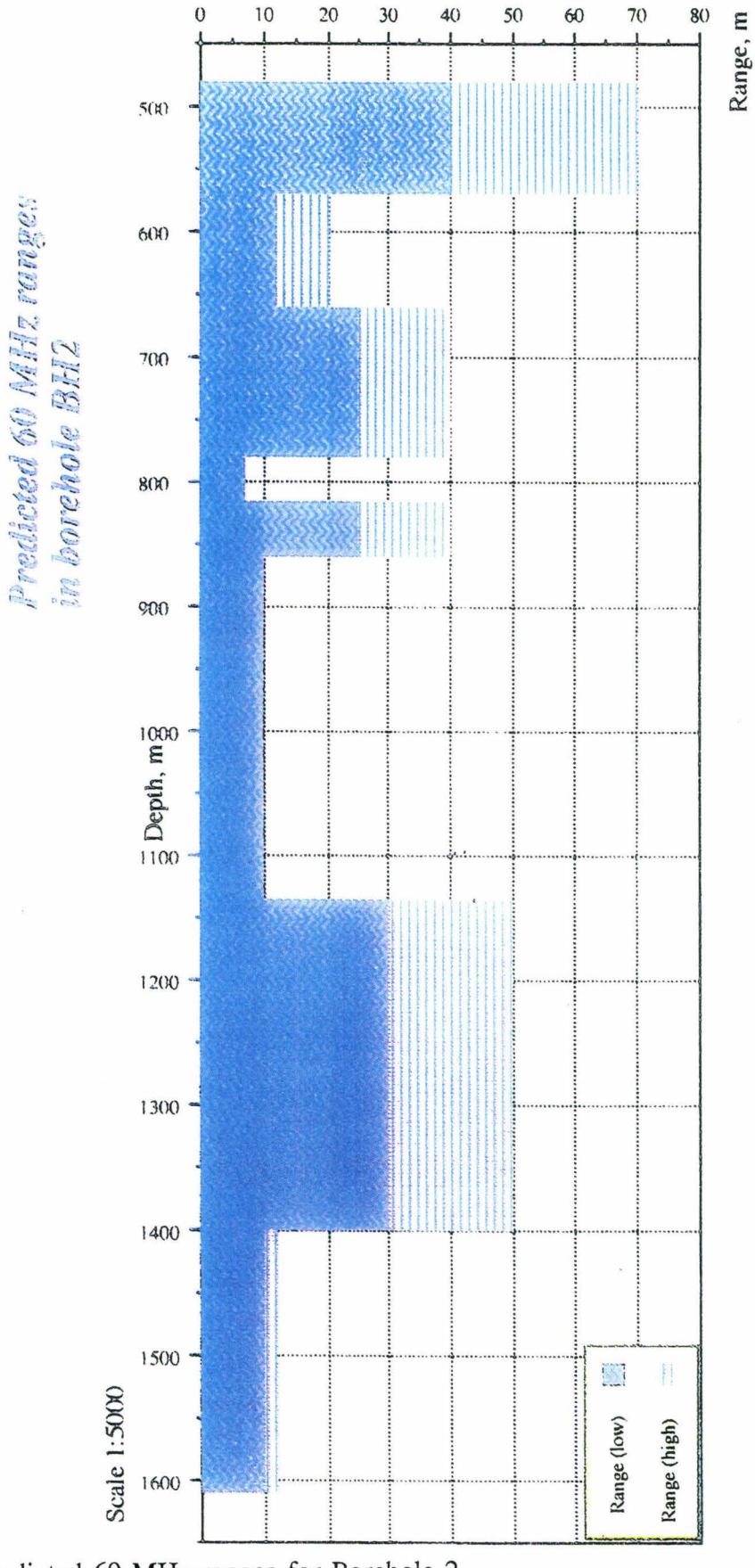

Figure 8-1 Predicted 60 MHz ranges for Borehole 2

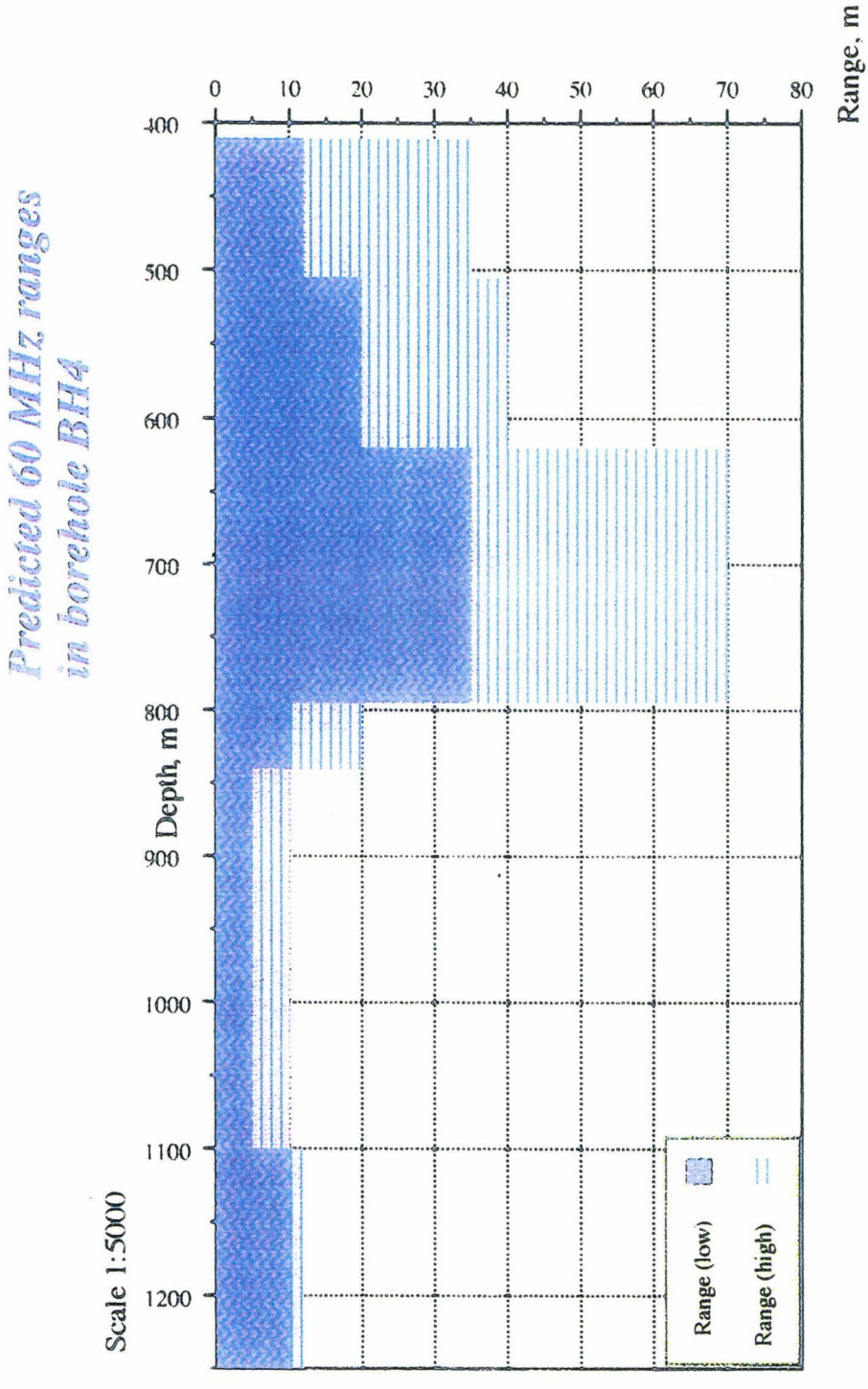

Figure 8-2 Predicted 60 MHz ranges for Borehole 4

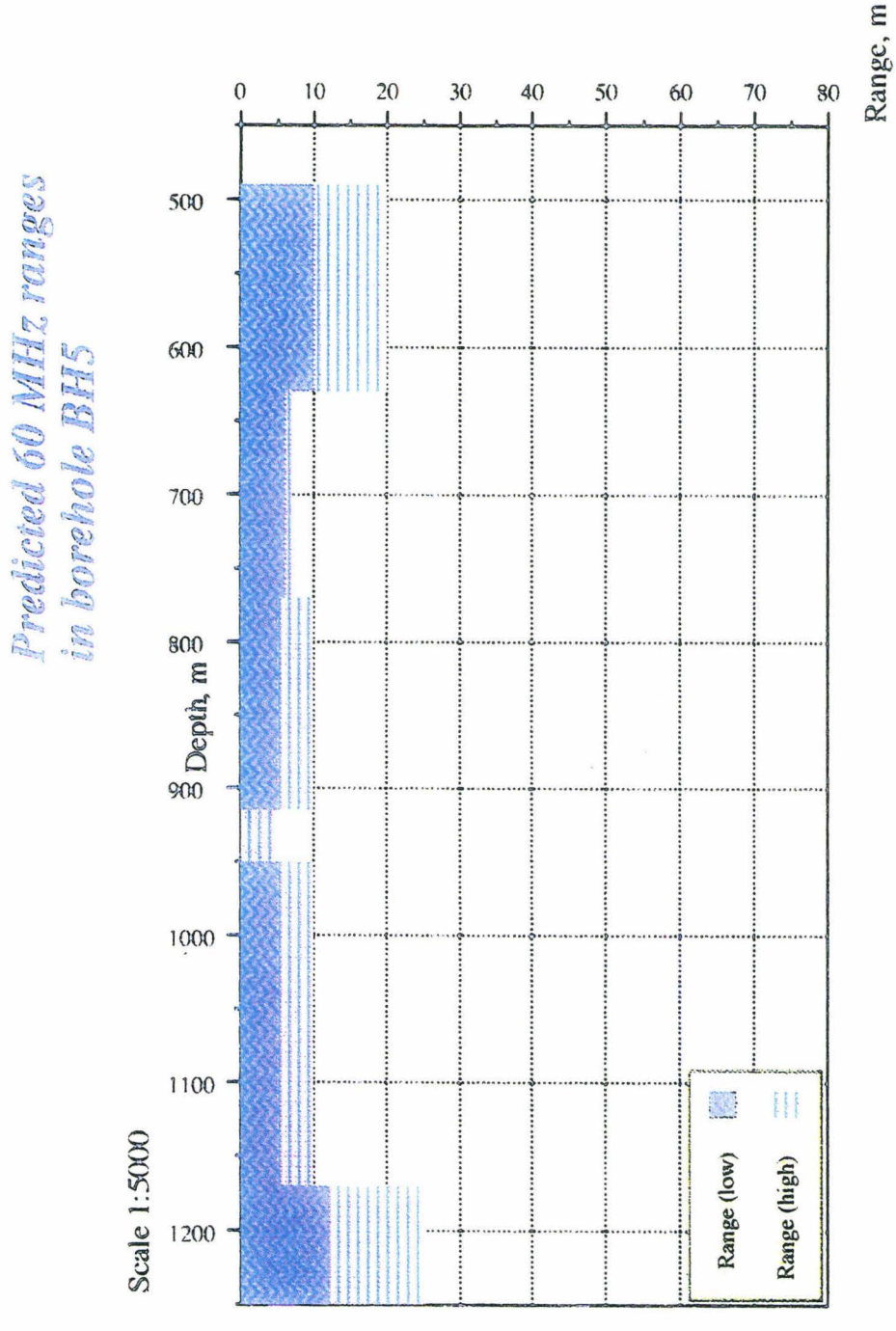

Figure 8-3 Predicted 60 MHz ranges for Borehole 5

9. DISCUSSION OF THE RESULTS OF THE RADAR TRIAL

A discussion of the results from the surveys conducted during the radar trials in Borehole 7A are presented in this Section, with the emphasis placed on the acquisition runs. Therefore only runs 3, 5, 6, and 9, 11 and 13 are considered in the summary and discussion of the results.

The discussion of the results of the borehole radar trial are also discussed in relation to the objectives of the survey and these are presented in Section 9.2.

9.1 Discussion of the Results

9.1.1 Run 3 - Velocity Determination Run

Whilst this run was not strictly an acquisition run of the survey it is briefly discussed in this section as it was used to evaluate the radar response in different stratigraphic units within the borehole.

This element of Run 3 was conducted from 508.14 - 608.14 mbRT and included the lower section of the Brockram (approximately 415 - 523.5 mbRT), the Carboniferous Limestone (523.5 - 576.5 mbRT) and an upper section of the Borrowdale Volcanic Group (BVG) (approximately 578 mbRT to TD).

Within the Brockram radar signals were not recorded over the interval 508.14 to ~ 516 mbRT, whilst a small amplitude direct wave was observed between ~ 516 to 523.5 mbRT. However, in the interval from 523.5 to 576.5 mbRT, the Carboniferous Limestone, a large amplitude direct wave was observed as were several reflections from discontinuities. Within the section represented by the BVG, 576.5 to 608.14 mbRT no signal was recorded.

9.1.2 Run 5 - 22 MHz Omni-directional Survey

The results from the 22 MHz omni-directional survey were dominated by a guided wave travelling within the borehole, which is considered to have resulted from the radar energy being reflected by discontinuities in the radar antenna array. This survey gave no information about any geological features, and the radar range can be considered to be zero.

9.1.3 Runs 6 and 9 - 60 MHz Omni-directional Survey

The data from this element of the survey was acquired in two runs, as a consequence of equipment malfunctions, and due to a greater transmitter to receiver separation, used during Run 9, the amplitudes of the radar waves are smaller for this run than for Run 6.

The real-time raw data plots showed that detectable radar signals were observed only in particular sections of the borehole interval surveyed and these are listed below:

BOREHOLE INTERVALS WHERE RADAR SIGNALS WERE OBSERVED	
From (mbRT)	To (mbRT)
517.64	579.64
647.64	773.08
833.08	878.08
890.08	920.08
943.08	955.08

In all other sections within the survey interval (517.64 - 956.08 mbRT) no radar signals were observed. Within the Carboniferous Limestone, 10 reflectors were

identified, which were qualitatively categorised as 'uncertain' through to 'strong'. The radar range within the Carboniferous Limestone was estimated to be between 10 and 15 metres. Radar signals were recorded for approximately 50% of the BVG, and within those zones where a signal was observed the radar range was between 5 and 10 metres but in general it did not exceed 8 metres. A total of 16 reflectors were identified within the BVG where signals were recorded, the majority of which were qualitatively described as 'weak' or 'uncertain' with the exception of one which was considered to be 'medium'.

The results from this survey element were used to design the 60 MHz directional survey intervals.

9.1.4 Runs 11 and 13 - 60 MHz Directional Survey

The 60 MHz directional survey was targeted on those zones where a radar signal was recorded during the 60 MHz omni-directional survey, although the precise intervals, surveyed were altered interactively during the survey, as discussed in Section 5.6. The range obtained within the Carboniferous Limestone was of the order of 5 - 10 metres and for those sections of the BVG which were surveyed the range was of the order of 5 metres.

The results of this survey element were used, where possible, to determine the azimuth of reflectors identified from the 60 MHz omni-directional survey data. From these data it was possible to determine the azimuth for 4 reflectors within the Carboniferous Limestone and only 1 reflector within the BVG.

9.2 Discussion of the Radar Trial in Relation to the Objectives

The results of the borehole radar trial are discussed in this section in relation to the objectives of the survey defined for the radar trial in Borehole 7A.

9.2.1 Objective 1 - Establish Radar Range in the BVG

The first objective was to establish the range of the radar in the Borrowdale Volcanic Group (BVG). The radar range was defined to encompass both the penetration and resolution of the survey.

The range, in terms of penetration, for the 22 MHz and 60 MHz omni-directional surveys varied and appeared to be dependent upon properties of the rock mass and fracture systems and/or fluid contained within the rock mass and fracture systems. The ranges obtained with the radar are summarised below.

		Range (metres)		
Stratigraphy	Borehole Interval (mbRT)	22 MHz omni-directional	60 MHz omni-directional	60 MHz directional
Carboniferous Limestone	523 - 578	0	10 - 15	5 - 10
Borrowdale Volcanic Group (BVG)	578 - 680 680 - 770 770 - 830 830 - 960	0 0 0 0	0 5 - 10 0 5	0 5 0 0

The radar range obtained with the 22 MHz omni-directional system was effectively 0 metres. It provided no information about geological features outside the borehole as the radar energy appeared to propagate as a guided borehole wave. The radar range within the Borrowdale Volcanic Group obtained with the 60 MHz omni-directional system was 5 - 10 metres and generally attained a maximum of 8 metres for approximately 50% of the interval surveyed whilst the range was effectively zero for the remainder of the interval.

The resolution of the radar is determined by the wavelength of the system and for the 60 MHz systems used during the trial the resolution was approximately 1 metre.

9.2.2 Objective 2 - Provide Information on Contrasts in Electrical Properties

The second objective of the radar trial was to provide information regarding the contrast in the electrical properties of the rock mass at distance from the borehole and with increasing depth in the borehole. Contrasts in electrical properties within the rock mass can be seen as radar reflectors and variations in the radar wave propagation velocity.

Within the Carboniferous Limestone (523.5-576.5 mbRT) 10 reflectors were identified from the 60 MHz omni-directional survey. Of these it was possible to determine the azimuth of 4 of the reflectors using the data obtained from the 60 MHz directional survey. A total of 16 reflectors were identified within the Borrowdale Volcanic Group (BVG) (576.5 mbRT - TD), however, data was only obtained for approximately 50% of this interval. Of the 16 reflectors it was possible to determine the azimuth of only 1 of the reflectors.

The velocity of propagation of the radar waves can be related to the dielectric permittivity and can therefore provide information about the change in electric properties of the rock mass with depth in the borehole. These are summarised below as average values for sections of the borehole.

Borehole Interval mbRT	**Velocity m/μs**	**Relative Dielectric Permittivity**
523 - 576	100	9.0
680 - 770	92	10.6
830 - 960	80	14.1

This can be considered to be a simplification as the velocity of propagation is frequency dependent and linked to dielectric permittivity and resistivity.

9.2.3 Objective 3 - Assess Whether the Results are Representative of other UK Nirex Ltd Boreholes at Sellafield.

The results from the correlation of radar data with geophysical wireline logs, discussed in Section 7, showed that the radar range was limited by the relatively low resistivities of the formation. The limit at which the radar begins to provide useful results is at resistivities of 200-300 ohmm for the 60MHz omni-directional system and 500-600 ohmm for the directional system. Therefore, at Sellafield, radar surveys should be restricted to those intervals of the borehole where the average resistivities exceed these values. The conductivity of the borehole fluid seems to be of limited importance, however, it is essential that the quantity of borehole fluid surrounding the borehole antennas is minimised.

The correlation of the radar results with the geophysical wireline logs can therefore be used as a basis for estimating the radar range which may be achieved in other UK Nirex Ltd boreholes at Sellafield.

Estimates of radar range were produced for Boreholes 2, 4 and 5 to assess whether and/or to what extent further single borehole radar reflection surveys would be successful. The ranges estimated have been used to assess whether the results obtained from the borehole trial are representative of other Boreholes at Sellafield.

The radar range determined from the radar trial in Borehole 7A are in general very similar to the ranges estimated for Borehole 5. Boreholes 2 and 4 radar range estimates are, in some sections of the boreholes, greater than the ranges attained in Borehole 7A. However, approximately 53% of the interval 480-1610 mbRT of Borehole 2 and approximately 65% of the interval 410-1250 mbRT are estimated to

be similar to the ranges measured in Borehole 7A. These comparisons have been made using the low end of the radar range estimates.

It may therefore be concluded that in general the results obtained from Borehole 7A are broadly representative of other UK Nirex Ltd boreholes at Sellafield. However, as can be seen from the discussion in Section 8 there are zones where estimated radar ranges may attain significantly greater values than those obtained in Borehole 7A.

9.2.4 Objective 4 - Assess the Feasibility of the Method and Equipment for Surveys in Boreholes 2 and 4.

The results from the borehole radar trial conducted in Borehole 7A illustrates that it would be feasible to acquire single hole borehole radar reflection data in Boreholes 2 and 4. However, the estimates of the radar range suggest that such a technique may only be effective over short sections of the boreholes comprising approximately 47% of Borehole 2 and approximately 35% of Borehole 4. Whilst it is generally feasible to acquire data by this methodology it was considered inappropriate for these boreholes due to the low resistivities of the formations encountered. Further the resolution of the radar system which is approximately 1 metre precluded the acquisition of detailed structural information required away from the borehole.

The equipment used for the survey is considered to be appropriate and could be used for surveys in Boreholes 2 and 4. However, modifications to the equipment to attempt to reduce coupling to the borehole fluid and to improve resolution close to the borehole and improve range in conductive formations, could be made to the radar system and these are briefly discussed in Section 9.2.5.

Further, additional antennas operating at different frequencies, both lower and higher than those used, may be appropriate for such surveys.

9.2.5 Objective 5 - Identify Equipment/Survey Parameters for Further Surveys

The fifth defined objective was to identify equipment/survey parameters for further single hole reflection surveys at Sellafield.

The results of the trial survey in Borehole 7A indicated that the equipment selected is appropriate for undertaking further surveys. However, minor modifications to the equipment may be required prior to any further survey work being undertaken.

The trial undertaken in Borehole 7A indicated that the 22 MHz omni-directional system did not operate as radar suggesting that the environment of the borehole and surrounding rock mass was too conductive causing dispersion and attenuation of the radar signals. Therefore for any further surveys conducted at Sellafield the 60 MHz omni-directional and directional systems should be used.

Minor modifications to the system which may be beneficial to the efficiency of any further survey work could include increasing the length of the plastic covers surrounding the antennas which should extend beyond the ends of antennas to reduce coupling to the borehole fluid. It may also be possible to increase the diameter of the covers, but this would have to be balanced against the increased risk of the radar system becoming stuck in the borehole. A further modification would be to reduce the separation between the transmitter and receiver in order to improve resolution close to the borehole and attempt to improve range in conductive formations. The latter modification would require redesign of the components of the borehole probes.

The parameters used for the trial survey in Borehole 7A, which include transmitter to receiver spacing, sampling frequency, number of samples and number of stacks, can be considered to be optimal for the system used for the survey. However, the parameters for further surveys cannot be defined prior to a survey or without testing in individual boreholes. The exception to this is the transmitter to receiver distance

which should be as short as possible to improve resolution close to the borehole wall and improve the range in conductive formations.

9.2.6 Objectives 6 and 7 - Correlate Reflectors with Fault/Fractures Already Identified

To address the sixth and seventh objectives, defined as additional objectives in Section 2, a comparison and correlation of the radar results with geophysical wireline logs has been undertaken, as discussed in Section 7. The correlation indicated that the propagation of the radar is dependent on the electric properties of the formation and consequently the resistivity logs could be used to predict radar performance and hence indicate where radar surveys should be performed.

The correlation between near borehole radar reflections and the location of resistivity anomalies was evaluated. A positive correlation existed between 17 of the 25 identified radar reflectors and resistivity anomalies. The difference in location was generally less than 1 metre which could be expected as the radar wavelength was approximately 2 metres. For some reflectors within the Carboniferous Limestone the difference in location between radar reflectors and resistivity anomalies is greater than within the BVG and this may be attributed to reflectors being oblique (30-45°) to the borehole resulting in geometrically poorly defined intersection depths. These discrepancies in depth caused some difficulties in assessing which feature intersecting the borehole caused the reflection.

The analysis shows that essentially all radar reflectors identified can be attributed to discontinuities in the formation and that the radar provides information on the orientation of these features over dimensions of the order of 10 metres.

However, the data obtained from the trial survey covers only approximately 50% of the BVG and further it must be bourne in mind that the resolution of the survey is approximately 1 metre and features narrower than this would probably not have been resolved.

10. CONCLUSIONS AND RECOMMENDATIONS

The results of the borehole radar trial suggested that the 22 MHz omni-directional system was not applicable or appropriate in the environment encountered within Borehole 7A. The survey gave no information about geological features in the formations surrounding the borehole and the range can therefore be considered to be zero. It is considered that this resulted from the radar energy propagating as a guided borehole wave. It is further considered that in the trial undertaken in Borehole 7A, under the conditions encountered, the 22 MHz omni-directional radar system did not perform as a radar system but can be considered to have performed more as a electromagnetic propagation tool.

The results from the 60 MHz omni-directional survey provided information about geological features in the formations surrounding the borehole and achieved a range of between 5-10 metres within the BVG. However, this only applied to approximately 50% of the BVG, whilst the range in the rest of the BVG was effectively 0 metres and no information on geological features was obtained. A total of 16 radar reflectors were identified within the BVG, which were weak or uncertain with the exception of one. Within the Carboniferous Limestone the radar range obtained was 10-15 metres. A total of 10 reflectors were identified within the Carboniferous Limestone section of the borehole (523.5 - 576.5 mbRT) which were stronger than those observed in the BVG.

The results obtained from the 60 MHz directional survey indicated the range attained in the BVG was approximately 5 metres although this was over a shorter overall length of BVG than for the omni-directional survey. Over the rest of the BVG the directional antenna provided no information. Within the Carboniferous Limestone the range attained was 5-10 metres. From the results obtained with the 60 MHz directional antenna it was only possible to determine the azimuth for one of the

reflectors in the BVG of the 16 identified and for four reflectors in the Carboniferous Limestone of the 10 identified.

The resolution of the radar system, is determined by the wavelength of the system, and for the 60 MHz systems this was approximately 1 metre.

Contrasts in electrical properties within the rock mass can be visualised by the presence of radar reflectors as discussed above. The variations in the velocity of propagation of the radar waves which can be related to the dielectric permittivity which also provides information about the variation of electrical properties. This is, however, a simplification as the velocity of propagation is frequency dependent and linked to the dielectric permittivity and resistivity.

The radar results from Borehole 7A have been correlated with geophysical wireline logs acquired in the borehole. The geophysical wireline logs used for correlation purposes were the Laterolog Deep LLD, Laterolog Groeningen LLG, Laterolog Shallow LLS and Microspherically Focused MSFL resistivity logs, the neutron porosity log (NPHI) and the fluid conductivity log (ACON).

The correlation of radar amplitude and the velocity of the direct wave propagating along the borehole shows good qualitative agreement between all logs except the fluid conductivity log. To facilitate a quantitative analysis of the correlation between the radar results and the geophysical wireline logs, the logs were resampled to 1 metre intervals to enable a comparison to be made of data having similar resolutions. The highest correlation coefficients were obtained between the radar amplitude and the LLS and MSFL resistivity logs. In addition good correlations were found between the radar velocity and neutron porosity log. The results of this correlation indicates that the resistivity logs can be used to predict the amplitude of the direct radar wave. Similarly the correlation between radar velocity and neutron porosity provides a means of using radar velocity to estimate porosity.

A further comparison was made between the average resistivity from the LLD resistivity logs for three borehole intervals and the estimated radar ranges for the same intervals to evaluate whether radar range could be estimated from resistivity data. The comparison showed that the radar range increased from approximately 4 metres for an average resistivity of 100 ohmm to approximately 15 metres for an average resistivity of 1000 ohmm.

Based on the quality of the radar maps and the number of reflectors identified within different sections of Borehole 7A it may be concluded that:

- the 60 MHz omni-directional system can provide useful information where the average LLD resistivity is in excess of 200-300 ohmm.

- the 60 MHz directional system can provide useful information where the average LLD resistivity is in excess of 500-600 ohmm.

The correlations undertaken showed that the resistivity logs can be used to estimate radar performance and hence indicate where radar surveys could be performed.

The correlation between predicted intersections of radar reflectors with the borehole and the location of resistivity anomalies was evaluated. This showed a positive correlation between 17 of the 26 radar reflectors identified and resistivity anomalies. The difference in location in practically all cases was 1 metre which would be expected with a resolution of 1 metre. The analysis shows that essentially all of the identified radar reflectors can be attributed to discontinuities in the formation and that the radar provides information on the orientation of these features over dimensions of the order of 10 metres.

The conductivity of the borehole fluid in the part of the borehole surveyed varies in the range 12 -18 mS/cm, whilst this variation is too small to have an apparent effect

on the radar range obtained with the 60 MHz systems it had an overall negative effect on the radar results, particularly for the 22 MHz system. The conductive borehole fluid tended to trap the radiated energy so that it propagated along the borehole as a guided wave. The plastic covers used in conjunction with the antennas were introduced in an attempt to reduce this and were reasonably successful for the 60 MHz systems. However the radiation from the 22 MHz antenna would appear to be better coupled to the conductive borehole fluid and this was possibly due to the greater relative length of the 22 MHz antennas relative to the total length of the plastic covers in terms of wavelength.

Another reason for the poor results obtained with the 22 MHz system is considered to be that the resistivity of the formation was so low that the radar did not work in the wave propagation mode.

The borehole radar trial in Borehole 7A at Sellafield and the subsequent analysis of the data have shown that single hole radar reflection range is limited by the relatively low resistivities of the formations. The low resistivities can be attributed to a combination of high porosity and conductive pore fluids. In low porosity regions the resistivities are sufficiently high for the radar to provide information on the location and orientation of discontinuities in the formation. The limit at which the radar commences to provide useful information is at 200-300 ohmm for the omni-directional system and 500-600 ohmm for the directional antenna. Hence, future radar surveys at Sellafield should be restricted to intervals of the boreholes where the average resistivities exceed these values. The conductivity of the borehole fluid seems to be of limited importance although it is essential that the annulus of borehole fluid surrounding the antennas is minimised.

The results of the borehole radar trial conducted in Borehole 7A were considered to have provided little further information than was already available from other geophysical surveys and geological information. The estimation of radar range which

may be attained in Boreholes 2 and 4 suggested that the technique may only be effective over short sections of the boreholes comprising approximately 47% of Borehole 2 and approximately 35% of Borehole 4. On this basis it was therefore decided not to conduct further surveys at this time. Furthermore, on the basis of the estimates of radar range it would not be possible to undertake cross-hole radar surveys.

However, the survey parameters used for the trial survey in Borehole 7A can be considered optimal for the system utilised and if further surveys were to be performed at Sellafield:

- the 60 MHz omni-directional and directional systems should be used and the use of higher frequencies should also be considered.

- the surveys should be confined to those parts of the boreholes where the formation is sufficiently resistive for the radar to provide useful results.

Minor modifications could also be made to the RAMAC system in an attempt to improve results of future surveys. The suggested modifications are:

- To increase the length of the plastic covers on the antennas. The plastic covers should not only surround the transmitter and receiver antennas but should surround the spacer rods between the two antennas and should also extend sufficiently far beyond the antenna ends to reduce the coupling of the antennas with the borehole fluid. It is also possible to increase the diameter of the plastic covers, but this would have to be balanced against the increased risk of getting the antenna array stuck in the borehole.

- To reduce the separation between transmitter and receiver in order to improve resolution close to the borehole and to improve range in conductive formations. This would require redesign of the mechanical components of the borehole probes.

REFERENCES

Almén, K.-E., Zellman, O., 1991. Äspö Hard Rock Laboratory, Field investigation methodology and instruments used in the preinvestigation phase, 1986-1990. SKB TR 91-21, SKB, Stockholm, Sweden.

Olsson, O., Falk, L., Forslund, O., Lundmark, L., Sandberg, E. 1987. Crosshole investigations - Results from borehole radar measurements. Stripa Project TR 87-11, SKB, Stockholm, Sweden.

Olsson, O., Falk, L., Forslund, O., Lundmark, L., Sandberg, E. 1992. Borehole radar applied to characterization of hydraulically conductive fracture zones in crystalline rock. Geophysical Prospecting, 40, 109-142.

Sandberg, E., Olsson, O., Falk, L. 1991. Combined interpretation of fracture zones in crystalline rock using single-hole, cross-hole tomography and directional borehole-radar data. The Log Analyst, 32(2), 108-119.

APPENDIX A

Run No.	Antenna Array Length (metres)	Antenna Separation (metres)	Measurement Point From Top of System (metres)	Survey Interval Depth below Top of Casing (metres) *		Depth Correction to Rotary Table (metres)	Corrected Depth of Survey Interval metres below RT (mbRT)		Trace No.		Comments
				Start	Stop		Start	Stop	Start	Stop	
1	N/A	N/A	N/A	N/A	N/A	N/A	N/A	N/A	1 6	5 11	Time Base Determination.
2	N/A	N/A	N/A	N/A	N/A	N/A	N/A	N/A	1 6 11	5 10 15	System Checks. 60 MHz Omni-direction antenna
3	9.27 9.27 9.27 15.27 11.27	5.9 5.9 5.9 11.9 7.9	3.6 3.6 3.6 6.6 4.6	435 500 700 700 700	444 600 725 724 724.5	8.14 8.14 8.14 11.14 9.14	443.14 508.14 708.14 711.14 709.14	452.14 608.14 733.14 735.14 733.64	1 21 250 301 351	19 223 300 350 400	Check of Depth Control Systems Radar Range Evaluation 1st Velocity Determination Run 2nd Velocity Determination Run 3rd Velocity Determination Run
4	N/A	N/A	N/A	N/A	N/A	N/A	N/A	N/A	1 6 11	5 10 15	System checks 22 MHz omni-directional antenna
5	12.25	7.39	5.24	510	949	9.78	519.78	958.78	1	440	22 MHz omni-directional survey

Run No.	Antenna Array Length (metres)	Antenna Separation (metres)	Measurement Point From Top of System (metres)	Survey Interval Depth below Top of Casing (metres) *		Depth Correction to Rotary Table (metres)	Corrected Depth of Survey Interval metres below RT (mbRT)		Trace No.		Comments
				Start	Stop		Start	Stop	Start	Stop	
6	N/A 8.26	N/A 4.89	N/A 3.10	N/A 510 741	N/A 746 N/A	N/A 7.64 7.64	N/A 517.64 748.64	N/A 753.64 N/A	1 11 486	5 485 N/A	Function checks. 60 MHz omni-directional survey Last trace 474; 749.14 mbRT Test, no transmitter pulse
7	N/A 8.26	N/A 4.89	N/A 3.10	N/A 735	N/A 855.5	N/A 7.64	N/A 742.64	N/A 863.14	1 11	5 251	Function checks. 60 MHz omni-directional survey. Transmitter failure approximately 862.64 mBRT
8	N/A 8.26	N/A 4.89	N/A 3.10	N/A 735	N/A 742	N/A 7.64	N/A 742.64	N/A 749.64	1 11 26	5 25 149	Function checks. 60 MHz omni-directional survey. Transmitter failure Test traces
9	N/A 9.75	N/A 5.78	N/A 3.54	N/A 735	N/A 948	N/A 8.08	N/A 743.08	N/A 956.08	1 6 11	5 10 438	Function checks. Test traces, downhole. 60 MHz omni-directional survey
10	N/A	N/A	N/A	N/A	N/A	N/A	N/A	N/A	1	55	System checks and Test traces
11	11.26	7.32	4.26	510	590	8.80	518.80	598.80	1	161	60 MHz directional survey
12	N/A	N/A	N/A	N/A	N/A	N/A	N/A	N/A	1	40	System checks

Run No.	Antenna Array Length (metres)	Antenna Separation (metres)	Measurement Point From Top of System (metres)	Survey Interval Depth below Top of Casing (metres) *		Depth Correction to Rotary Table (metres)	Corrected Depth of Survey Interval metres below RT (mbRT)		Trace No.		Comments
				Start	Stop		Start	Stop	Start	Stop	
13	11.26	7.32	4.26	N/A	N/A	8.80	N/A	N/A	1	N/A	Test above hole.
	11.26	7.32	4.26	445	N/A	8.80	453.80	N/A	2	N/A	Test trace.
	11.26	7.32	4.26	640	760	8.80	648.80	768.80	3	243	60 MHz directional survey
	11.26	7.32	4.26	832	867	8.80	840.80	875.80	250	320	60 MHz directional survey
	11.26	7.32	4.26	882	910	8.80	890.80	918.80	325	381	60 MHz directional survey
	11.26	7.32	4.26	935	946	8.80	943.80	954.80	385	406	60 MHz directional survey

Note * height of top of casing above ground level is 1.61 metres.
ground level is 46.97 maOD
Rotary Table is 53.06 maOD.

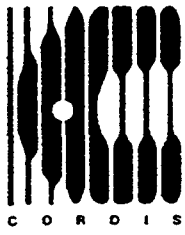

The Communities R & D Information Service

(Service d'information de recherche et développement des Communautés)

CORDIS

Un élément vital de votre stratégie de diffusion

CORDIS est un service d'information créé dans le cadre du programme VALUE afin de donner un accès rapide et facile à l'information sur les programmes de recherche de la Communauté européenne. Il s'agit d'un service en ligne gratuit accessible par le centre serveur de la Commission européenne (ECHO) et aussi d'un CD-ROM récemment mis à la disposition du public.

CORDIS offre à la Communauté de recherche et développement européenne:

— un aperçu détaillé et actualisé des activités RDT dans la Communauté européenne, grâce à un ensemble de bases de données et de services associés;

— un accès rapide et aisé à l'information sur les programmes et résultats de la recherche dans la Communauté européenne;

— un service de la Commission en évolution permanente adapté aux besoins de la communauté de recherche et de l'industrie;

— une assistance complète de l'utilisateur incluant la documentation, la formation et les services du bureau d'assistance CORDIS.

Bases de données CORDIS

RTD-Programmes — RTD-Projects — RTD-Partners — RTD-Results
RTD-Publications — RTD-Comdocuments — RTD-Acronyms — RTD-News

Pour que votre programme profite au maximum des services CORDIS:

— informez l'équipe CORDIS de vos initiatives en matière de programmes;

— communiquez régulièrement des informations aux bases de données CORDIS telles que RTD-News, RTD-Publications et RTD-Programmes;

— utilisez les bases de données CORDIS, telles que RTD-Partners, pour la mise en application de votre programme;

— consultez CORDIS pour obtenir les informations les plus récentes sur d'autres programmes proches de vos activités;

— informez vos partenaires des possibilités de CORDIS et de l'importance de leur contribution au service comme des bénéfices qu'ils pourront en retirer;

— contribuez à l'évolution de CORDIS en communiquant au bureau CORDIS vos commentaires sur le service.

Pour plus d'informations sur la communication avec CORDIS, contactez l'équipe CORDIS à la DG XIII:

Bruxelles
M^me^ I. Vounakis
Tél. (+32-2) 299 04 64
Fax (+32-2) 299 04 67

Luxembourg
M. B. Niessen
Tél. (+352) 43 01-33638
Fax (+352) 43 01-34989

Pour obtenir un accès en ligne à CORDIS, veuillez en faire la demande à l'adresse suivante:

Service de la clientèle ECHO
BP 2373
L-1023 Luxembourg
Tél. (+352) 34 98-1240
Fax (+352) 34 98-1248

Si vous êtes déjà un utilisateur ECHO, ayez l'amabilité d'indiquer votre numéro d'utilisateur.

European Commission

EUR 15974 — Borehole radar trial in Borehole 7A, Sellafield, Cumbria, UK

S. J. Emsley

Luxembourg: Office for Official Publications of the European Communities

1995 — XXIX, 298 pp., num. tab., fig. — 21.0 x 29.7 cm

Nuclear science and technology series

ISBN 92-826-9459-3

Price (excluding VAT) in Luxembourg: ECU 36.50

A trial borehole radar survey was conducted in UK NIREX Ltd Borehole 7A at Sellafield with the objectives of establishing the feasibility of the technique and determining the range and resolution of the system within the Borrowdale volcanic group (BVG).

The data acquired with the 22 MHz system provided no information on geological features in the BVG. However, a range of 5 to 10 metres was achieved with the 60 MHz omnidirectional system for 50% of the BVG, whilst a range of approximately five metres was obtained with the 60 MHz directional system; with resolutions of approximately one metre.

The correlation of the radar results with wireline logs indicated that the resistivity logs could be used to estimate radar ranges for other boreholes and showed a positive correlation between radar reflectors and resistivity anomalies. Further analysis showed that the radar range was limited by the relatively low resistivities of the formations and the conductivity of the borehole fluid seemed to be of limited importance. The estimates of radar range made on the basis of the correlations suggested that the technique would only be effective over short intervals of other boreholes at Sellafield and that it would not be possible to undertake a cross-hole radar survey.

Venta y suscripciones • Salg og abonnement • Verkauf und Abonnement • Πωλήσεις και συνδρομές
Sales and subscriptions • Vente et abonnements • Vendita e abbonamenti
Verkoop en abonnementen • Venda e assinaturas

BELGIQUE / BELGIË

Moniteur belge / Belgisch staatsblad

Rue de Louvain 42 / Leuvenseweg 42
1000 Bruxelles / 1000 Brussel
Tél. (02) 512 00 26
Fax (02) 511 01 84

Jean De Lannoy

Avenue du Roi 202 / Koningslaan 202
1060 Bruxelles / 1060 Brussel
Tél. (02) 538 51 69
Télex 63220 UNBOOK B
Fax (02) 538 08 41

Autres distributeurs/
Overige verkooppunten:

Librairie européenne/ Europese boekhandel

Rue de la Loi 244/Wetstraat 244
1040 Bruxelles / 1040 Brussel
Tél. (02) 231 04 35
Fax (02) 735 08 60

DANMARK

J. H. Schultz Information A/S

Herstedvang 10-12
2620 Albertslund
Tlf. 43 63 23 00
Fax (Sales) 43 63 19 69
Fax (Management) 43 63 19 49

DEUTSCHLAND

Bundesanzeiger Verlag

Breite Straße 78-80
Postfach 10 05 34
50445 Köln
Tel. (02 21) 20 29-0
Fax (02 21) 202 92 78

GREECE/ΕΛΛΑΔΑ

G.C. Eleftheroudakis SA

International Bookstore
Nikis Street 4
10563 Athens
Tel. (01) 322 63 23
Telex 219410 ELEF
Fax 323 98 21

ESPAÑA

Boletín Oficial del Estado

Trafalgar, 27-29
28071 Madrid
Tel. (91) 538 22 95
Fax (91) 538 23 49

Mundi-Prensa Libros, SA

Castelló, 37
28001 Madrid
Tel. (91) 431 33 99 (Libros)
431 32 22 (Suscripciones)
435 36 37 (Dirección)
Télex 49370-MPLI-E
Fax (91) 575 39 98

Sucursal:

Librería Internacional AEDOS

Consejo de Ciento, 391
08009 Barcelona
Tel. (93) 488 34 92
Fax (93) 487 76 59

Llibreria de la Generalitat de Catalunya

Rambla dels Estudis, 118 (Palau Moja)
08002 Barcelona
Tel. (93) 302 68 35
Tel. (93) 302 64 62
Fax (93) 302 12 99

FRANCE

Journal officiel
Service des publications des Communautés européennes

26, rue Desaix
75727 Paris Cedex 15
Tél. (1) 40 58 77 01/31
Fax (1) 40 58 77 00

IRELAND

Government Supplies Agency

4-5 Harcourt Road
Dublin 2
Tel. (1) 66 13 111
Fax (1) 47 80 645

ITALIA

Licosa SpA

Via Duca di Calabria 1/1
Casella postale 552
50125 Firenze
Tel. (055) 64 54 15
Fax 64 12 57
Telex 570466 LICOSA I

GRAND-DUCHÉ DE LUXEMBOURG

Messageries du livre

5, rue Raiffeisen
2411 Luxembourg
Tél. 40 10 20
Fax 49 06 61

NEDERLAND

SDU Overheidsinformatie

Externe Fondsen
Postbus 20014
2500 EA 's-Gravenhage
Tel. (070) 37 89 880
Fax (070) 37 89 783

PORTUGAL

Imprensa Nacional

Casa da Moeda, EP
Rua D. Francisco Manuel de Melo, 5
1092 Lisboa Codex
Tel. (01) 387 30 02/385 83 25
Fax (01) 384 01 32

Distribuidora de Livros Bertrand, Ld.ª

Grupo Bertrand, SA

Rua das Terras dos Vales, 4-A
Apartado 37
2700 Amadora Codex
Tel. (01) 49 59 050
Telex 15798 BERDIS
Fax 49 60 255

UNITED KINGDOM

HMSO Books (Agency section)

HMSO Publications Centre
51 Nine Elms Lane
London SW8 5DR
Tel. (071) 873 9090
Fax 873 8463
Telex 29 71 138

ÖSTERREICH

Manz'sche Verlags- und Universitätsbuchhandlung

Kohlmarkt 16
1014 Wien
Tel. (1) 531 610
Telex 112 500 BOX A
Fax (1) 531 61-181

SUOMI/FINLAND

Akateeminen Kirjakauppa

Keskuskatu 1
PO Box 218
00381 Helsinki
Tel. (0) 121 41
Fax (0) 121 44 41

NORGE

Narvesen Info Center

Bertrand Narvesens vei 2
PO Box 6125 Etterstad
0602 Oslo 6
Tel. (22) 57 33 00
Telex 79668 NIC N
Fax (22) 68 19 01

SVERIGE

BTJ AB

Traktorvgen 13
22100 Lund
Tel. (046) 18 00 00
Fax (046) 18 01 25
30 79 47

ICELAND

BOKABUD LARUSAR BLÖNDAL

Skólavördustíg, 2
101 Reykjavik
Tel. 11 56 50
Fax 12 55 60

SCHWEIZ / SUISSE / SVIZZERA

OSEC

Stampfenbachstraße 85
8035 Zürich
Tel. (01) 365 54 49
Fax (01) 365 54 11

BĂLGARIJA

Europress Klassica BK Ltd

66, bd Vitosha
1463 Sofia
Tel./Fax 2 52 74 75

ČESKÁ REPUBLIKA

NIS ČR

Havelkova 22
130 00 Praha 3
Tel. (2) 24 22 94 33
Fax (2) 24 22 14 84

HRVATSKA

Mediatrade

P. Hatza 1
4100 Zagreb
Tel. (041) 430 392

MAGYARORSZÁG

Euro-Info-Service

Honvéd Európá Ház
Margitsziget
1138 Budapest
Tel./Fax 1 111 60 61
1 111 62 16

POLSKA

Business Foundation

ul. Krucza 38/42
00-512 Warszawa
Tel. (2) 621 99 93, 628-28-82
International Fax&Phone
(0-39) 12-00-77

ROMÂNIA

Euromedia

65, Strada Dionisie Lupu
70184 Bucuresti
Tel./Fax 1-31 29 646

RUSSIA

CCEC

9,60-letiya Oktyabrya Avenue
117312 Moscow
Tel./Fax (095) 135 52 27

SLOVAKIA

Slovak Technical Library

Nm. slobody 19
812 23 Bratislava 1
Tel. (7) 5220 452
Fax : (7) 5295 785

CYPRUS

Cyprus Chamber of Commerce and Industry

Chamber Building
38 Grivas Dhigenis Ave
3 Deligiorgis Street
PO Box 1455
Nicosia
Tel. (2) 449500/462312
Fax (2) 458630

MALTA

Miller distributors Ltd

PO Box 25
Malta International Airport
LQA 05 Malta
Tel. 66 44 88
Fax 67 67 99

TÜRKIYE

Pres AS

Istiklal Caddesi 469
80050 Tünel-Istanbul
Tel. 0(212) 252 81 41 - 251 91 96
Fax 0(212) 251 91 97

ISRAEL

ROY International

PO Box 13056
41 Mishmar Hayarden Street
Tel Aviv 61130
Tel. 3 496 108
Fax 3 648 60 39

EGYPT/ MIDDLE EAST

Middle East Observer

41 Sherif St.
Cairo
Tel/Fax 39 39 732

UNITED STATES OF AMERICA / CANADA

UNIPUB

4611-F Assembly Drive
Lanham, MD 20706-4391
Tel. Toll Free (800) 274 4888
Fax (301) 459 0056

CANADA

Subscriptions only
Uniquement abonnements

Renouf Publishing Co. Ltd

1294 Algoma Road
Ottawa, Ontario K1B 3W8
Tel. (613) 741 43 33
Fax (613) 741 54 39
Telex 0534783

AUSTRALIA

Hunter Publications

58A Gipps Street
Collingwood
Victoria 3066
Tel. (3) 417 5361
Fax (3) 419 7154

JAPAN

Kinokuniya Company Ltd

17-7 Shinjuku 3-Chome
Shinjuku-ku
Tokyo 160-91
Tel. (03) 3439-0121

Journal Department

PO Box 55 Chitose
Tokyo 156
Tel. (03) 3439-0124

SOUTH-EAST ASIA

Legal Library Services Ltd

Orchard
PO Box 05523
Singapore 9123
Tel. 73 04 24 1
Fax 24 32 47 9

SOUTH AFRICA

Safto

5th Floor, Export House
Cnr Maude & West Streets
Sandton 2146
Tel. (011) 883-3737
Fax (011) 883-6569

AUTRES PAYS
OTHER COUNTRIES
ANDERE LÄNDER

Office des publications officielles des Communautés européennes

2, rue Mercier
2985 Luxembourg
Tél. 499 28-1
Télex PUBOF LU 1324 b
Fax 48 85 73/48 68 17

15

CD-NA-15974-EN-C

NOTICE TO THE READER

All scientific and technical reports published by the European Commission are announced in the monthly periodical **'euro abstracts'**. For subscription (1 year: ECU 63) please write to the address below.

Price (excluding VAT) in Luxembourg: ECU 36.50

OFFICE FOR OFFICIAL PUBLICATIONS
OF THE EUROPEAN COMMUNITIES

L-2985 Luxembourg

ISBN 92-826-9459-3